frontiers | Research Topics

Anesthetic-induced neurotoxicity and neurocognitive impairment of vulnerable brains

Edited by
Yingwei Wang, Zhongcong Xie and Jiaqiang Zhang

Published in
Frontiers in Aging Neuroscience
Frontiers in Neuroscience
Frontiers in Pharmacology

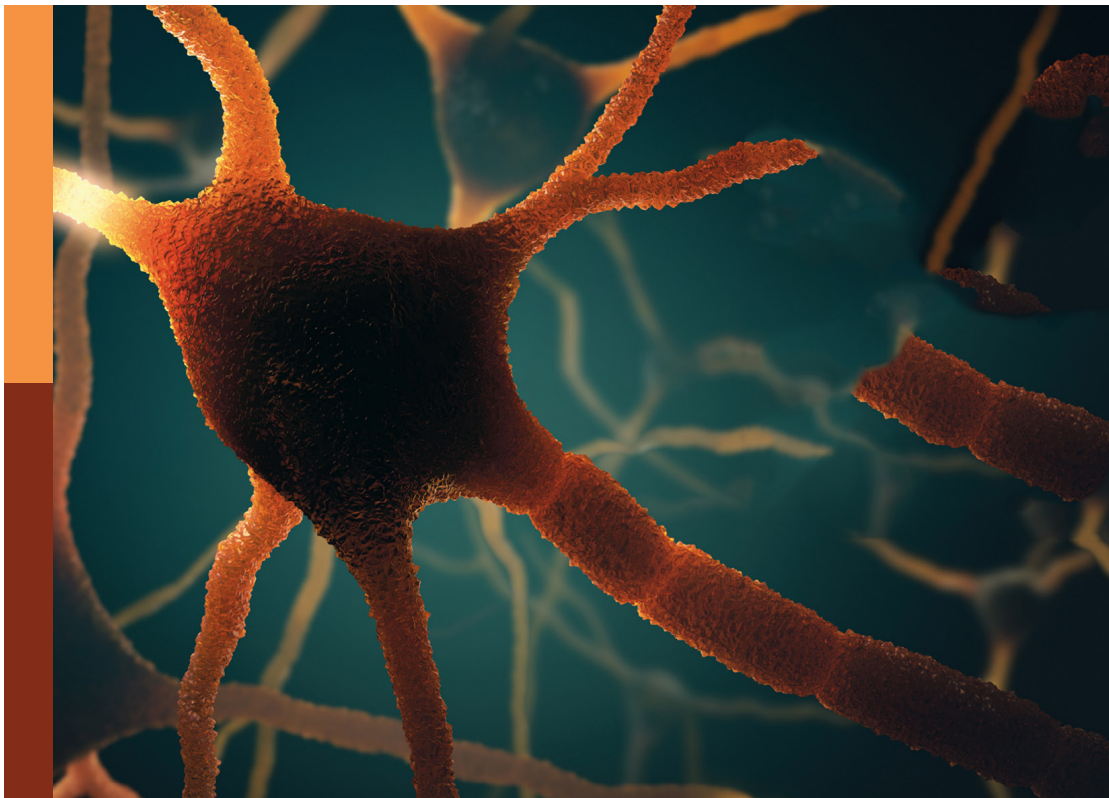

ISSN 1664-8714
ISBN 978-2-8325-3585-1
DOI 10.3389/978-2-8325-3585-1

About Frontiers

Frontiers is more than just an open access publisher of scholarly articles: it is a pioneering approach to the world of academia, radically improving the way scholarly research is managed. The grand vision of Frontiers is a world where all people have an equal opportunity to seek, share and generate knowledge. Frontiers provides immediate and permanent online open access to all its publications, but this alone is not enough to realize our grand goals.

Frontiers journal series

The Frontiers journal series is a multi-tier and interdisciplinary set of open-access, online journals, promising a paradigm shift from the current review, selection and dissemination processes in academic publishing. All Frontiers journals are driven by researchers for researchers; therefore, they constitute a service to the scholarly community. At the same time, the *Frontiers journal series* operates on a revolutionary invention, the tiered publishing system, initially addressing specific communities of scholars, and gradually climbing up to broader public understanding, thus serving the interests of the lay society, too.

Dedication to quality

Each Frontiers article is a landmark of the highest quality, thanks to genuinely collaborative interactions between authors and review editors, who include some of the world's best academicians. Research must be certified by peers before entering a stream of knowledge that may eventually reach the public - and shape society; therefore, Frontiers only applies the most rigorous and unbiased reviews. Frontiers revolutionizes research publishing by freely delivering the most outstanding research, evaluated with no bias from both the academic and social point of view. By applying the most advanced information technologies, Frontiers is catapulting scholarly publishing into a new generation.

What are Frontiers Research Topics?

Frontiers Research Topics are very popular trademarks of the *Frontiers journals series*: they are collections of at least ten articles, all centered on a particular subject. With their unique mix of varied contributions from Original Research to Review Articles, Frontiers Research Topics unify the most influential researchers, the latest key findings and historical advances in a hot research area.

Find out more on how to host your own Frontiers Research Topic or contribute to one as an author by contacting the Frontiers editorial office: frontiersin.org/about/contact

Anesthetic-induced neurotoxicity and neurocognitive impairment of vulnerable brains

Topic editors

Yingwei Wang — Fudan University, China

Zhongcong Xie — Massachusetts General Hospital, Harvard Medical School, United States

Jiaqiang Zhang — Zhengzhou University, China

Citation

Wang, Y., Xie, Z., Zhang, J., eds. (2023). *Anesthetic-induced neurotoxicity and neurocognitive impairment of vulnerable brains*. Lausanne: Frontiers Media SA. doi: 10.3389/978-2-8325-3585-1

Table of contents

frontiers | Frontiers in Aging Neuroscience

TYPE Editorial
PUBLISHED 10 October 2023
DOI 10.3389/fnagi.2023.1293491

OPEN ACCESS

EDITED AND REVIEWED BY
Kristy A. Nielson,
Marquette University, United States

*CORRESPONDENCE
Jiaqiang Zhang
✉ zhangjiq@zzu.edu.cn

RECEIVED 13 September 2023
ACCEPTED 22 September 2023
PUBLISHED 10 October 2023

CITATION
Zeng S and Zhang J (2023) Editorial: Anesthetic-induced neurotoxicity and neurocognitive impairment of vulnerable brains. *Front. Aging Neurosci.* 15:1293491. doi: 10.3389/fnagi.2023.1293491

Editorial: Anesthetic-induced neurotoxicity and neurocognitive impairment of vulnerable brains

Shuang Zeng and Jiaqiang Zhang*

Department of Anesthesiology and Perioperative Medicine, People's Hospital of Zhengzhou University, Henan Provincial People's Hospital, Zhengzhou, Henan, China

KEYWORDS

sevoflurane, apoptosis, neurodegeneration, calcium, tau

Editorial on the Research Topic
Anesthetic-induced neurotoxicity and neurocognitive impairment of vulnerable brains

With the development of technology, more and more infants are undergoing general anesthesia for surgery, other interventions, or clinical examinations in the early stages of life. However, whether general anesthesia affects the function and structure of the developing infant brain remains an important, complex, and controversial issue. Sevoflurane is the most commonly used anesthetic for infants, but this drug has potential neurotoxicity. Short term or single exposure to sevoflurane has a weaker impact on cognitive function, while long-term or repeated exposure to general anesthetics may lead to cognitive dysfunction. However, the underlying mechanisms are still being debated, and preventive measures need to be further explored. To provide an overview of this topic, we have selected six original research and review articles that delineate sevoflurane and developmental neurotoxicity.

Apoptosis is the main pathway leading to the death of nerve cells, and most preclinical studies of sevoflurane have regarded apoptosis as the main cause of neurotoxicity. This type of programmed cell death is normal during development, but long-term exposure to sevoflurane in young animals can lead to a 50-fold increase in nerve cell apoptosis rates (McCann and de Graaf, 2017). Hu et al. (2019) found that sevoflurane induces apoptosis of nerve cells in the developing brain of young rats through a cascade of apoptosis regulated by brain-derived neurotrophic factor (BDNF), which also led to a decrease in the anti-apoptotic/pro-apoptotic ratio, and induced intrinsic apoptosis.

Neurodegeneration is the foundation of many cognitive disorders. In some studies, exposure to sevoflurane can cause neurodegenerative changes. In a study by Wu et al. (2020) sevoflurane significantly up-regulates SIRT-2 in newborn rat hippocampus, promotes the expression of pro-inflammatory/M1-related markers in microglia, and activates microglia. Microglial activation has also been implicated in neurodegenerative diseases (Yeh et al., 2017). Iron is essential for normal neuronal function. However, excess iron has been linked to several neurodegenerative diseases. Sevoflurane exposure disrupts iron homeostasis and leads to hippocampal iron overload, which leads to neurodegenerative disease (Wu et al., 2020). Repeated exposure of neonatal mice to 3% sevoflurane induces tau phosphorylation Yu et al. (2020), leading to tau accumulation and the formation of neurofibrillary tangles, a signature pathology of the neurodegenerative brain, suggesting tau plays a key role in the neurodegenerative brain (Pirscoveanu et al., 2017; Yang and Wang, 2018). The neurodegenerative changes caused by neonatal sevoflurane exposure may involve multiple pathways, but the exact mechanisms are unknown and require further study.

Calcium imbalance can lead to nerve cell damage. Calcium plays a crucial role in human physiology, especially in the central nervous system (CNS). The precise maintenance of Ca^{2+}levels is crucial for normal cell function, and dysregulation of calcium homeostasis can lead to neuronal cell damage. Sevoflurane exposure leads to a significant decrease in calcium concentration in the ER, followed by a significant increase in Ca^{2+} in the cytoplasm and mitochondria through overactivation of the IP3 receptor (Yang et al., 2008). Mitochondrial Ca^{2+}overload leads to mitochondrial respiratory injury, ROS activation, ATP reduction, and MOMP, thereby inducing neuronal damage and apoptosis (Danese et al., 2017; Yang and Wei, 2017). Neonatal exposure to 2% sevoflurane upregulates CA1 region Ca^{2+} activated potassium channel type 2 (SK2s), which has persistent detrimental effects on long-term depression (LTD) and long-term enhancement (LTP) (Yu et al., 2018). Calcium homeostasis is an important mechanism of neurotoxicity induced by sevoflurane anesthesia, which is related to mitochondrial dysfunction, astrocyte dysfunction and neuronal dysfunction. Maintaining intracellular calcium homeostasis may be an effective intervention for sevoflurane induced developmental neurotoxicity.

Sevoflurane exposure in the developing brain reduces intermediates in glucose metabolic pathways, including lactic acid, significantly lower levels of succinic acid, and significantly reduced total creatine pools, including high-energy creatine phosphate and creatine (Liu et al., 2015). Alterations in amino acid metabolism in the neonatal brain may also play a key role in sevoflurane induced neurotoxicity. Exposure to sevoflurane during rapid brain development in monkeys also promotes microglial activation, which can be detected by upregulated transporter (TSPO) expression (Zhang et al., 2016). Activated microglia are a major source of cytokines in the central nervous system and release a range of pro-inflammatory cytokines and chemokines, such as monocyte chemokine-1, interleukin, macrophage colony-stimulating factor, tumor necrosis factor (TNF)-α, and macrophage inflammatory protein-1 α/β. Maternal exposure to sevoflurane directly affects fetal glial cells and enhances IL-6 through phosphorylated erk signaling (Hirotsu et al., 2019). Neuroinflammation is involved in sevoflurane-induced developmental neurotoxicity, which may be an important target for further study of sevoflurane-induced developmental neurotoxicity.

Tau protein is a microtubule-associated protein, and excessive tau phosphorylation promotes the formation of insoluble tau aggregates. Tau phosphorylation leads to cognitive dysfunction in mice (Faraco et al., 2019). Tao et al. (2014) found that Mice 6 days after birth were exposed to 3% sevoflurane for 2 h per day to induce tau phosphorylation through GSK-3β activation multiple times (rather than single), thereby increasing levels of IL-6 in the hippocampus and decreasing levels of PSD-95, leading to cognitive impairment. While these effects of sevoflurane did not occur in the tau KO mice, suggesting that tau plays a role in sevoflurane induced neuroinflammation and synaptic defects in mice.

In summary, the aim of the present Research Topic was to explore the potential mechanisms of sevoflurane and developmental neurotoxicity and the potential measures to prevent its occurrence in preclinical and clinical settings. These manuscripts provide important new insights on the topic. In the future, we hope that more studies will be performed to examine the association between sevoflurane and developmental neurotoxicity.

Author contributions

SZ: Writing—original draft. JZ: Writing—review and editing.

Funding

This work was supported by the National Natural Science Foundation of China (Nos. 82071217 and 82271288).

Acknowledgments

We appreciate all the editors, reviewers, and authors who contributed to this Research Topic.

Conflict of interest

The authors declare that the research was conducted in the absence of any commercial or financial relationships that could be construed as a potential conflict of interest.

Publisher's note

References

Danese, A., Patergnani, S., Bonora, M., Wieckowski, M. R., Previati, M., Giorgi, C., et al. (2017). Calcium regulates cell death in cancer: roles of the mitochondria and mitochondria-associated membranes (MAMs). *Biochim. Biophys. Acta Bioenerg.* 1858, 615–627. doi: 10.1016/j.bbabio.2017.01.003

Faraco, G., Hochrainer, K., Segarra, S. G., and Schaefer, S. (2019). Dietary salt promotes cognitive impairment through tau phosphorylation. *Nature* 574, 686–690. doi: 10.1038/s41586-019-1688-z

Hirotsu, A., Iwata, Y., Tatsumi, K., Miyai, Y., Matsuyama, T., and Tanaka, T. (2019). Maternal exposure to volatile anesthetics induces IL-6 in fetal brains and affects neuronal development. *Eur. J. Pharmacol.* 863, 172682. doi: 10.1016/j.ejphar.2019.172682

Hu, X., Hu, X., and Huang, G. (2019). LncRNA MALAT1 is involved in sevoflurane-induced neurotoxicity in developing rats. *J. Cell. Biochem.* 120, 18209–18218. doi: 10.1002/jcb.29127

Liu, B., Gu, Y., Xiao, H., Lei, X., Liang, W., Zhang, J., et al. (2015). Altered metabolomic profles may be associated with sevofuraneinduced neurotoxicity in neonatal rats. *Neurochem. Res.* 40, 788–799. doi: 10.1007/s11064-015-1529-x

McCann, M. E., and de Graaf, J. (2017). Current thinking regarding potential neurotoxicity of general anesthesia in infants. *Curr Opin Urol.* 27, 27–33. doi: 10.1097/MOU.0000000000000351

Pirscoveanu, D. F. V., Pirici, I., Tudorica, V., Balseanu, T. A., Albu, V. C., Bondari, S., et al. (2017). Tau protein in neurodegenerative diseases – a review. *Rom. J. Morphol. Embryol.* 58, 1141–1150.

Tao, G., Zhang, J., Zhang, L., Dong, Y., Yu, B., Crosby, G., et al. (2014). Sevoflurane induces tau phosphorylation and glycogen synthase kinase 3β activation in young mice. *Anesthesiology* 121, 510–527. doi: 10.1097/ALN.0000000000000278

Wu, Z., Zhang, Y., Zhang, Y., and Zhao, P. (2020). Sirtuin 2 inhibition attenuates sevofurane-induced learning and memory defcits in developing rats via modulating microglial activation. *Cell Mol. Neurobiol.* 40, 437–446. doi: 10.1007/s10571-019-00746-9

Yang, H., Liang, G., Hawkins, B. J., Madesh, M., Pierwola, A., Wei, H., et al. (2008). Inhalational anesthetics induce cell damage by disruption of intracellular calcium homeostasis with diferent potencies. *Anesthesiology* 109, 243–250. doi: 10.1097/ALN.0b013e31817f5c47

Yang, M., and Wei, H. (2017). Anesthetic neurotoxicity: apoptosis and autophagic cell death mediated by calcium dysregulation. *Neurotoxicol. Teratol.* 60, 59–62. doi: 10.1016/j.ntt.2016.11.004

Yang, Y., and Wang, J. Z. (2018). Nature of tau-associated neurodegeneration and the molecular mechanisms. *J Alzheimers Dis.* 62, 1305–1317. doi: 10.3233/JAD-170788

Yeh, F. L., Hansen, D. V., and Sheng, M. (2017). TREM2, Microglia, and neurodegenerative diseases. *Trends Mol Med.* 23, 512–533. doi: 10.1016/j.molmed.2017.03.008

Yu, X., Zhang, F., and Shi, J. (2018). Neonatal exposure to sevoflurane caused cognitive deficits by dysregulating SK2 channels and GluA2-lacking AMPA receptors in juvenile rat hippocampus. *Neuropharmacology* 141, 66–75. doi: 10.1016/j.neuropharm.2018.08.014

Yu, Y., Yang, Y., Tan, H., Boukhali, M., Khatri, A., Yu, Y., et al. (2020). Tau contributes to sevoflurane-induced neurocognitive impairment in neonatal mice. *Anesthesiology* 133, 595–610. doi: 10.1097/ALN.0000000000003452

Zhang, X., Liu, S., Newport, G. D., Paule, M. G., Callicott, R., Thompson, J., et al. (2016). *In vivo* monitoring of sevofurane-induced adverse efects in neonatal nonhuman primates using small animal positron emission tomography. *Anesthesiology* 125, 133–146. doi: 10.1097/ALN.0000000000001154

frontiers | Frontiers in Aging Neuroscience

ORIGINAL RESEARCH
published: 29 June 2022
doi: 10.3389/fnagi.2022.934230

Sevoflurane Exposure in the Developing Brain Induces Hyperactivity, Anxiety–Free, and Enhancement of Memory Consolidation in Mice

Rui Li[1†], Bei Wang[2†], Xiaohong Cao[1,3], Chao Li[1,4], Yuhan Hu[5], Dandan Yan[1], Yanchang Yang[1], Liqing Wang[1], Lingzhong Meng[1] and Zhiyong Hu[1]*

[1] Department of Anesthesiology, The First Affiliated Hospital, Zhejiang University School of Medicine, Hangzhou, China, [2] Department of Anesthesiology, The Children Hospital, Zhejiang University School of Medicine, Hangzhou, China, [3] Department of Anesthesiology, Jiaxing Hospital of Traditional China Medicine, Jiaxing, China, [4] Department of Anesthesiology, Lishui Municipal Central Hospital, Lishui, China, [5] Cell Biology Department, Yale University, New Haven, CT, United States

Background: Sevoflurane exposure at brain developmental stages has been reported to induce neurotoxicity and, subsequently, results in learning deficits at the juvenile age. In this study, we aimed to investigate the effects of prior early-age sevoflurane exposure on locomotor activity, anxiety, CA1-dependent learning, and spatial memory, as well as synapse changes in mice.

Methods: Totally, 3% sevoflurane was given to neonatal mice at postnatal day 7 for 4 h. These sevoflurane-treated mice were later subjected to open field and Morris water maze tests at their adult age (postnatal days 60–90) to assess their motor activity and spatial learning ability, respectively. The brain slices of sevoflurane-treated and control mice were examined for dendritic spine density and long-term potentiation (LTP) features following behavior tests (postnatal day 60). Protein levels of N-methyl-D-aspartate (NMDA) receptor subtypes and PSD95 in brain lysate were measured by using immunoblotting at the same age (postnatal day 60).

Results: Prior early-age sevoflurane exposure increased the overall moving distance, prolonged the central-area lingering time, and increased the central-area entries of adult mice. Sevoflurane-treated mice spent more time in the target quadrant during the probe test. An increase of the spine density of pyramidal neurons in the CA1 region was observed in sevoflurane-treated mice. NMDA receptor GluN2A subunit, but not the GluN2B or PSD95, was increased in the brain lysate of sevoflurane-treated mice compared with that of control mice. LTP in the hippocampus did not significantly differ between sevoflurane-treated and control mice.

OPEN ACCESS

Edited by:
Jiaqiang Zhang,
Zhengzhou University, China

Reviewed by:
Jian-Jun Yang,
Zhengzhou University, China
Ragu Varman Durairaj,
Virginia Commonwealth University, United States
Qingsheng Xue,
Shanghai Jiao Tong University, China
Yilin Zhao,
Huazhong University of Science and Technology, China

***Correspondence:**
Zhiyong Hu
huzhiyong777@zju.edu.cn

† These authors have contributed equally to this work

Specialty section:
This article was submitted to Neurocognitive Aging and Behavior, a section of the journal Frontiers in Aging Neuroscience

Received: *02 May 2022*
Accepted: *06 June 2022*
Published: *29 June 2022*

Citation:
Li R, Wang B, Cao X, Li C, Hu Y, Yan D, Yang Y, Wang L, Meng L and Hu Z (2022) Sevoflurane Exposure in the Developing Brain Induces Hyperactivity, Anxiety–Free, and Enhancement of Memory Consolidation in Mice. Front. Aging Neurosci. 14:934230. doi: 10.3389/fnagi.2022.934230

Conclusion: Exposure to sevoflurane for mice during an early brain developmental stage (P7) induces later-on hyperactivity, anxiety-free, and enhancement of memory retention. These observations shed light on future investigations on the underlying mechanisms of sevoflurane's effect on neuronal development.

Keywords: pediatric anesthesia, neurotoxicity, sevoflurane, hippocampus, cognition, synapse plasticity

INTRODUCTION

The emergence and development of modern anesthesiology have enabled tens of thousands of patients to tolerate some diagnostic treatments and surgical procedures, which is undoubtedly one of the great achievements in the history of human medicine. Although the sedation of the brain induced by anesthetics was thought to be reversible in the early days, some patients showed delirium, memory loss, and a long period of cognitive decline after anesthesia exposure. The critical period of human neurodevelopment is late pregnancy and infancy, and for rodents, it is within 2 days before birth and within 2 weeks after birth. Therefore, the pharmacological interference of anesthetics is particularly significant and persistent at this stage. In summary, related researchers quickly realized that anesthetic drugs may have a related effect on the neurodevelopment of the immature brain.

Many clinical retrospective cohort studies have shown that the exposure to anesthetics in childhood increases the risk of neurodevelopmental abnormalities, such as learning, cognitive, and behavioral abnormalities, through academic performance or some intelligence and behavioral development scale assessments (Hu et al., 2017; Zaccariello et al., 2019; Ing et al., 2020). Inconsistently, some studies suggested that exposure to anesthesia in early childhood had no significant effect on neurodevelopment. Clinical research cannot rule out the effects of many confounding factors, such as the instability of perioperative vital signs, the variation of anesthetic drugs, and technology, postoperative care, intellectual development education, and so on (Hu et al., 2017; Ing et al., 2020). The establishment of anesthesia animal models allowed researchers to better focus on anesthesia. Some animal studies have confirmed that anesthetics can cause neuronal apoptosis and cognitive dysfunction in the developing brain; however, other reports suggested that anesthetic exposure could even promote brain development (Chen et al., 2015; Hansen, 2015; Sun et al., 2016). These discrepancies may likely due to the differences in the experimental settings (Xu et al., 2016; Chen et al., 2018; Ing et al., 2020), such as the dosage of anesthetic drugs, the exposure time, and the combination.

Animal models have also facilitated the research on effects of anesthetics. The development of the brain involves many complex and time-specific and persistent cellular processes, including the neurogenesis, neuronal differentiation, and neuronal migration. There are many types of anesthetic drugs commonly used in clinical practice, including barbiturates, benzodiazepines, ketamine, and inhaled drugs, such as fluoroether and nitric oxide. The chemical composition of these drugs was diversified, but their neural mechanism of reversible depression was nearly identical: inhibiting neurotransmitter transmission by the N-methyl-D-aspartate (NMDA) receptors or activating neurotransmitter transmission by the gamma-aminobutyric acid (GABA) receptors (Buggy et al., 2000). The formation and stability of synapses are the key factors to ensure the transmission of electrochemical neurotransmitters. Both NMDA and GABA receptors are highly expressed in the hippocampus, which is essential for learning and memory formation. Activation of NMDA receptors is necessary for the formation of long-term memory, whereas activation of GABA receptors inhibits memory formation (Korotkova et al., 2010; Roncacé et al., 2017). Another key feature of brain development is that neurons form functional neural networks through synaptic refinement. Therefore, the interference caused by anesthetic drugs on the occurrence of synapses and the formation of neural circuits may play an important role in developmental disorders. NMDA and GABA receptor signaling pathways have been shown to regulate neuronal proliferation, differentiation, and the formation of neural circuits.

As an inhibitor of NMDA receptors, sevoflurane was the most commonly used inhaled anesthetics for induction and maintenance of pediatric anesthesia due to its quick onset and less airway irritation. More evidence is needed to understand whether and how sevoflurane acts on the central nervous system and the underlying molecular mechanism for neuronal development. To simulate the long-term effects of clinical exposure to anesthesia in infants and young children, herein, we used postnatal 7-day mice exposed to sevoflurane at clinically relevant doses and times. Then, we reared these mice to adulthood and observed behavioral changes by the open field test and Morris water maze; the former observes the motor activity and emotion of mice and the latter measures the spatial memory ability. Based on behavioral results, we further explored the NMDA receptor pathway interrelated long-term effects of sevoflurane on hippocampal functioning, including components changes of NMDA receptor subunits, morphological changes of the synapse, and electrophysiological changes.

Abbreviations: ACSF, artificial cerebrospinal fluid; ADHD, attention deficit hyperactivity disorder; fEPSP, field excitatory postsynaptic potential; HFS, high-frequency stimulation; GABA, gamma aminobutyric acid; LTP, long-term potentiation; mACSF, modified artificial cerebrospinal fluid; NMDA, N-methyl-D-aspartic acid; PSD95, postsynaptic density 95; WT, wild type.

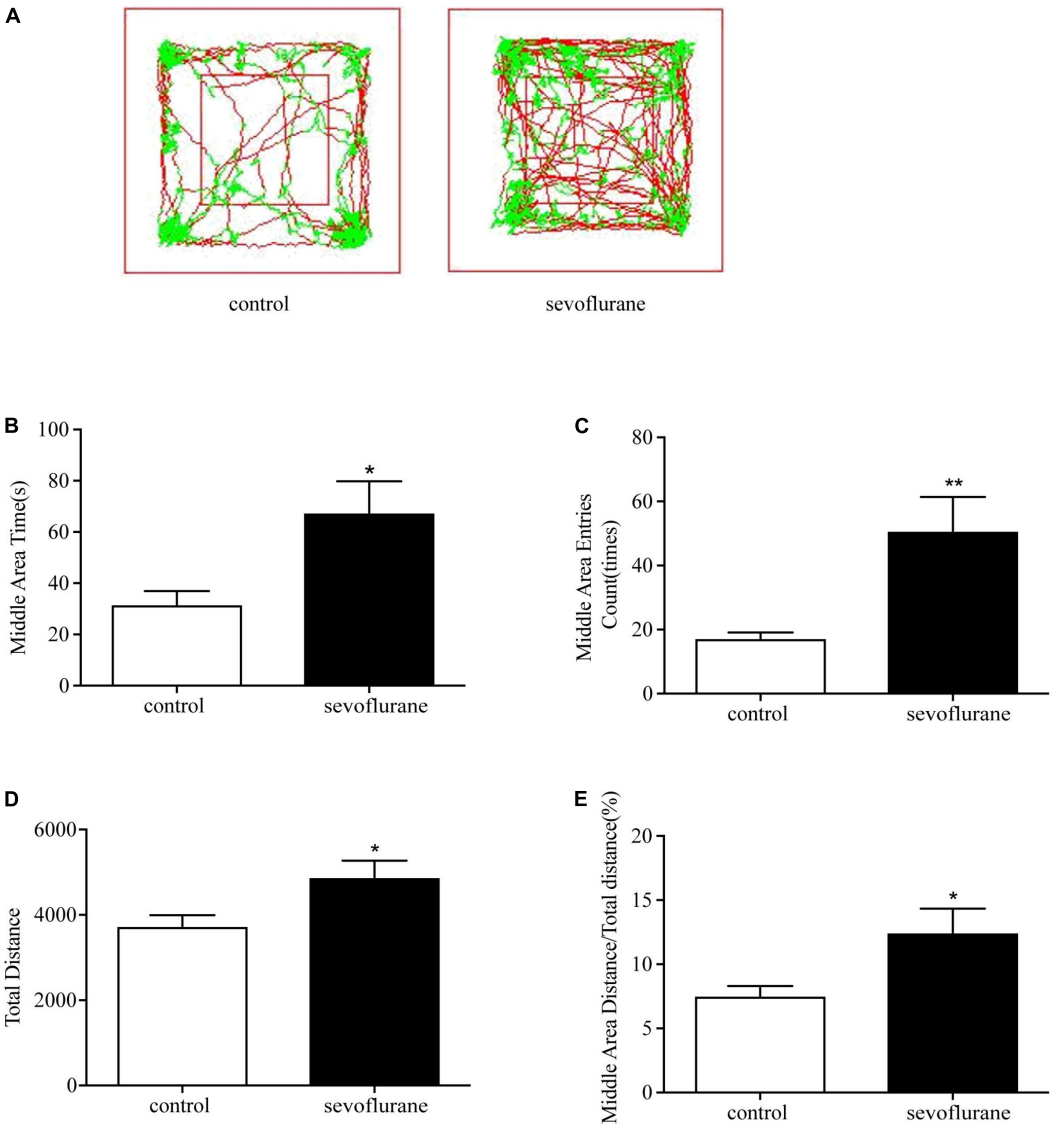

FIGURE 1 | Sevoflurane exposure changed movements in the open field test. Seven-day-old pups were exposed to 3% sevoflurane for 4 h and then allowed to grow up to 2 months. They were then subjected to the open field test. **(A)** The representative movement traces showing the locations of control and sevoflurane mice in the open field test. **(B)** The traveling total distance; **(C)** the crossing times in the central area; **(D)** the time spent in the central area; **(E)** and the traveling distance in the central area. Data are presented as mean ± SEM (n = 11). $^{*}P < 0.05$; $^{**}P < 0.01$. sevo, sevoflurane.

METHODS

Animals

All procedures were carried out in accordance with the National Institutes of Health Guidelines for the Care and Use of Laboratory Animals and were approved by the Animal Advisory Committee at Zhejiang University, Hangzhou, China (Laboratory Animal Management Regulations (2017 Revision)]. The experimental procedure has been reported previously (Shen et al., 2016). Wild-type C57BL/6 mice were purchased from the Jackson Laboratory (Bar Harbor, ME, United States). All mice were housed at the Animal Facility of Zhejiang University where constant temperature and humidity, standard light intensity, and dark/bright rhythm were maintained. A total of 9 L of 46 mice participated in the experiment without accidental casualties.

Exposure to Sevoflurane

Postnatal 7-day mice were randomly and equally divided into anesthesia group and control group. The anesthesia group was placed in a transparent plastic chamber (length, 20 cm; width, 10 cm; and height, 10 cm) that was wrapped around by the electric blanket to prevent hypothermia during anesthesia. The chamber was continuously flushed with a carrier gas mixture of oxygen and nitrogen (FIO_2 = 0.6) at 2 L/min. This relative high concentration of oxygen was given during gas exposure to allow spontaneous breath and to avoid hypoxemia (Satomoto et al.,

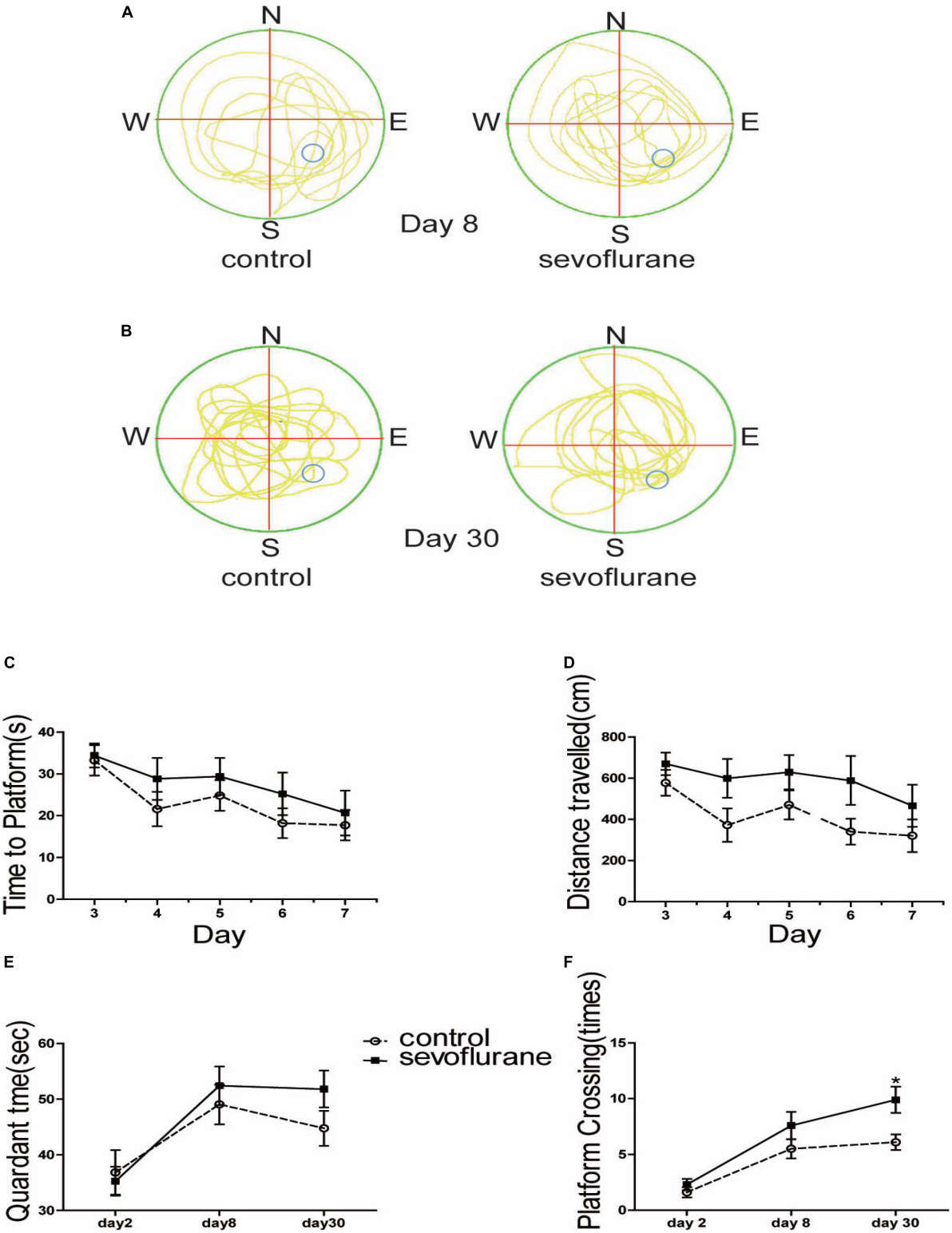

FIGURE 2 | Sevoflurane exposure changed spatial memory in the water maze test. Seven-day-old pups were exposed to 3% sevoflurane for 4 h and then allowed to grow up to 2 months. They were then subjected to the water maze test. **(A)** The trajectory path of day 8; **(B)** the trajectory path of day 30; **(C)** time spent to locate the platform during the 5-day course of the test after the 1st day for acclimatization and 2-day training; **(D)** the distance of swimming path; **(E)** the time spent in the platform region; and **(F)** the platform crossing times. Data are presented as mean ± SEM (n = 10). *P < 0.05.

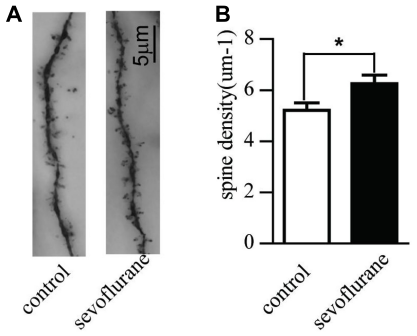

FIGURE 3 | Sevoflurane promoted the development of the pyramidal neurons in the hippocampal CA1 region with Golgi staining. Seven-day-old pups were exposed to 3% sevoflurane for 4 h and then allowed to grow up to 2 months. They were then subjected to the open field and water maze test. After which, their brain was removed for Golgi staining. **(A)** An example of Golgi staining dendritic spine morphology of the tertiary neurons from a Sham-treated or sevoflurane exposed mice; **(B)** the quantitative data of Golgi staining of the dendritic spine density of tertiary neurons. Data are presented as mean ± SEM (n = 20 neurons from 3 mice); *$P < 0.05$.

2009). The mice were exposed to 3% sevoflurane for 4 h (Fang et al., 2012). For the control group, one mouse at a time was placed in a plastic chamber flushed with the same carrier gas without sevoflurane for the same period of time. At the end of the gas exposure, the mice from both groups were allowed to grow up to 2 months. A total of 11 men from each group were allocated for the following behavioral experiments due to their constant hormone levels. The other 24 men and women from both cohorts were sacrificed under termination anesthesia, and their brains were collected for the *ex vivo* analysis. The mice that were subjected for brain tissue collection were anesthetized with a small amount of ether before being decapitated to avoid pain, while the mice that performed behavioral experiments were euthanized by excessive inhalation of ether.

Behavioral Testing

Open Field

The open field (45 cm × 45 cm × 45 cm) was made of opaque plastic material. Each mouse was placed individually into the center of the open field and allowed to explore the arena for 10 min. The entry times into the central area, time spent in the central portion (25% of total area), and locomotor activity of the whole field or central area were determined for each mouse. Time spent in the center area was used as an index of thigmotaxis, a measurement often being used for evaluating general anxiety in rodents.

Morris Water Maze

One week after the open field test, the mice were subjected to the Morris water maze test. This test was conducted in a closed, quiet, light-controlled environment in the Animal Experiment Center, Zhejiang University. On the first day, each mouse was placed in a 200 cm diameter black plastic pool filled with a depth of 50 cm with opaque water maintained at 23 ± 1°C for acclimatization. On the second day, each mouse was allowed to swim for 3 min to exclude the directionality of the mice and to evaluate the baseline of the number of times they crossed the platform and the time spent in each quadrant. Furthermore, mice were required to locate a 10-cm diameter platform that was submerged 1 cm below the surface of the water by using visual cues around the edges of the pool. In each trial, each mouse was gently put into the pool at one of four randomly assigned positions and allowed to locate the platform. The position of the platform remains the same throughout all training sessions. If the mouse was able to successfully find the platform and stayed on it for 10 s within 60 s, the experiment ended automatically; otherwise, the mouse was gently guided to the platform for 10 s. At the end of each trial, every mouse was gently removed from the water and dried using a paper towel. Each mouse was subjected to four trials per day, each time from one location, and each trial was intermittent for more than half an hour. Then, the formal test was started and lasted for 5 consecutive days (1st–5th test day). This test was videotaped, and the swimming route was tracked and recorded. The averaged latency to reach the platform and swimming path distance of each mouse were calculated daily. Once the water maze test was completed, all mice were allowed to live up to another 30 days for the probe test of water maze test. On the 6th and 30th day (90 days age) of the formal water maze test, the platform was removed, and mice were allowed to swim and the platform crossing times were accounted to assess their long-term memory retention.

Golgi Staining

Golgi staining was performed according to the manufacturer's instructions of the FD Rapid GolgiStain Kit (PK401, FD NeuroTechnologies). In brief, after gas exposure, fresh mice brains were dissected out, immediately immersed in impregnation solution for 2 weeks and then transferred to "Solution C" for 2 days. The 200-μm thick frozen sections were continuously cut off using a microtome (CM30503, Leica, Solms, GER). The sections were then mounted on glass slides coated with 3% gelatin and dried for 2 weeks. The sections were stained with silver nitrate solution "Solutions D and E" and then dehydrated by a series of decreasing concentrations of alcohol. They were finally installed by Permount. Olympus BX53 microscope acquired the images, and the NIH ImageJ software analyzed the neuronal morphology. The investigator was blinded to the control or experimental groups. At least five pyramidal neurons in the hippocampal CA1 region were randomly selected from each mouse. The neurons were then reconstructed by using a camera lucida and a 40 × objective lens (numerical aperture 0.95). The density of apical dendritic spines of a distinct branch was counted by using a 100 × oil-immersion objective lens (NA 1.3). The mean number of spines per micrometer was calculated using the spines from the both sides of dendritic segments.

Western Blotting

After gas exposure, pups were allowed to grow up to 2 months, and their hippocampi were obtained and homogenized using a chilled Vibrahomogenizer (Vibra cell, SONICS) containing 2 ml of radio immunoprecipitation assay (RIPA) buffer [1% Triton X-100, 0.1% SDS, 150 mM NaCl, 2 mM ethylene diamine tetraacetic acid (EDTA), 50 mM NaF, 10 mM sodium pyrophosphate,

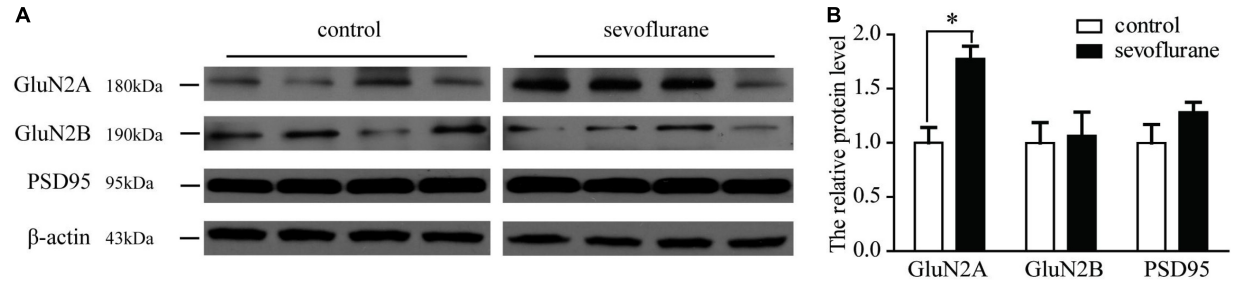

FIGURE 4 | (A) Western blotting of GluN2A, GluN2B, and PSD95 in mice of following group: control, sevoflurane. **(B)** Quantification of GluN2A, GluN2B, and PSD95 in mice of the following groups: control and sevoflurane-treated. Sevoflurane increased the GluN2A expression. Seven-day-old pups were exposed to 3% sevoflurane for 4 h and then allowed to grow up to 2 months. They were then subjected to the open field and water maze test. Then, their hippocampus was immediately removed for Western blot analysis. GluN2A expression was significantly increased by sevoflurane exposure. Data are presented as mean ± SEM (n = 4); $^*P < 0.05$.

1.0 mM Na_3VO_4, and 1.0 mM Phenylmethylsulfonyl fluoride (PMSF)]. The lysate was then centrifuged at 12,000 *g* for 20 min at 4°C. The supernatant was collected for protein concentration measurement [Pierce™ BCA Protein Assay Kit (Thermo Fisher Scientific, MA, United States)] and was then used for the Western blot analysis. After electrophoresis with 10% polyacrylamide gel electrophoresis (SDS-PAGE), proteins were transferred to polyvinylidene fluoride (PVDF) membranes (Millipore, MA, United States) using a constant voltage of 300 mV for 90 min. The membranes were then blocked in 5% milk in tris buffered saline, Tween (TBST) (25 mM Tris-HCl, 150 mM NaCl, and 0.1% Tween 20, pH 7.4) on a rocker for half an hour at room temperature and then incubated in the primary antibody solution on a rocker overnight at 4°C. Primary antibodies were diluted in blocking buffer solution (5% milk in TBST) with mouse anti-PSD95 (1:1,000; Millipore MAB1596), rabbit anti-GluN2A (1:1,000; Abcam ab133265), or mouse anti-GluN2B (1:1,000; a kindly gift from Jianhong Luo laboratory, the Department of Neurobiology, Zhejiang University). Subsequently, the membranes were washed in TBST for three times before being incubated with horseradish peroxidase (HRP)-conjugated antimouse secondary antibody (1:20,000 dilution in 5% milk in TBST; Thermo Fisher Scientific 31430) and HRP-conjugated antirabbit secondary antibody (1:20,000; Thermo Fisher Scientific 31460) on a rocker for 1 h at room temperature. After being rinsed again with TBST three times, protein bands were visualized using ECL Western blotting detection agentia (Thermo Fisher Scientific). The loading control was detected with mouse anti-β-actin (1:10,000; Sigma-Aldrich A5441) followed by corresponding antimouse secondary antibody. The intensity of the protein bands was quantified with the NIH ImageJ software, and the results were normalized to the corresponding β -actin bands.

Slice Recording

Two months after gas exposure, mice (2 months old) were anesthetized with terminated anesthesia of diethyl ether, and their brains were then removed after decapitation. The transverse brain slices (300 μm) containing the hippocampus were obtained rapidly by a tissue slicer (VT 1200S, Leica, GRE); the operation was carried out in oxygenated (95% O_2/5% CO_2) and ice-cold modified artificial cerebrospinal fluid (mACSF; in mM: 234 sucrose, 2.5 KCl, 1.25 NaH_2PO_4, 0.5 $CaCl_2$, 10 $MgCl_2$, 26 $NaHCO_3$, 11 D-glucose, pH 7.4, 300 mOsm). Furthermore, the brain slices were transferred to a chamber filled with oxygenated ACSF (in mM: 126 NaCl, 2.5 KCl, 1.25 KH_2PO_4, 1 $MgCl_2$, 2 $CaCl_2$, 26 $NaHCO_3$, and 10 D-glucose, pH 7.4, 300 mOsm), allowed to recover for 25 min at 32°C, and subsequently for 1 h at room temperature. During the signal recording process, the preoxygenated ASCF liquid was also continuously perfused on the brain slice to ensure the oxygenation requirement of the neurons. Electrode placement was identified based on the location and morphology of the brain slices under infrared differential interference contrast (IR-DIC) optics. ACSF-filled borosilicate glass (A-M system) pipettes (3–6 MΩ) were attached to the headstage of a Heka EPC 1024 amplifier (Heka Elektronik) and carefully adjusted for fast and slow capacitance and series resistance compensation. In the dendritic region of CA1, fEPSPs were evoked by stimulating the Schaffer collateral-commissural pathway (Sccp) by test stimuli (0.066 Hz, 4–5 V, 20 ms) delivered *via* a bipolar tungsten electrode insulated to the tip (tip diameter 50 mm). The slope of field excitatory postsynaptic potential (fEPSPs) measured between the time at which peak amplitude was observed and 1 ms after the application of the stimulus. Extracellular fEPSPs were monitored for 20 min before the evoking stimuli to confirm the stability of the baseline potential. Each slice received evoking stimuli at a high-frequency stimulus (HFS, 100 Hz, 2 trains of stimulation for 1 s applied 20 s apart). The averaged fEPSP slopes at 0, 20, 40, and 60 min after the delivery of evoking stimuli were normalized against the averaged value of fEPSP slopes for 20 min immediately before the delivery of evoking stimuli, and then they were statistically analyzed. Amplified fEPSPs using a laboratory interface board (ITC-16, Instrutech Corp., NY, United States) and stored to disk on a Power Macintosh G3 computer with the acquisition program Pulse, version 8.5 (Heka electronic GmbH, Lambrecht, GER).

Statistical Analysis

Data are presented as mean ± standard error of the mean (SEM). ANOVA followed by a *post-hoc* Newman-Keul's test for comparison was used for data analysis of Morris water maze experiments. Unpaired Student's *t*-test was used for data

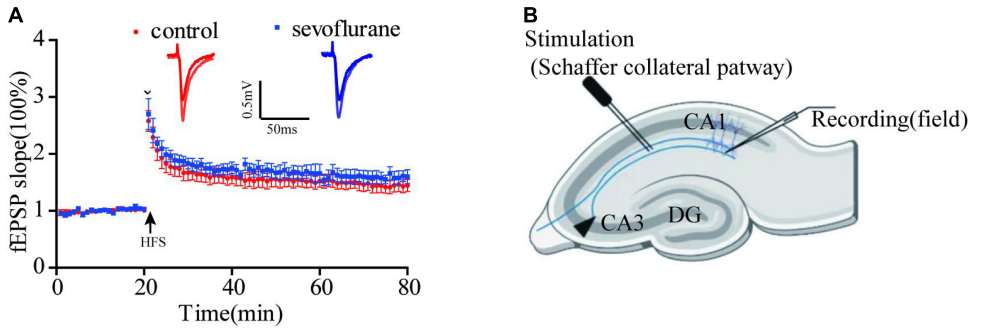

FIGURE 5 | Sevoflurane did not significantly change long-term potentiation (LTP). **(A)** We tested 0, 20, 40, and 60 min after high-frequency stimulation, and the response of sevoflurane exposure group to HFS has a mild increase than that of control group, but it was not statistically significant. **(B)** The position of stimulating and recording electrode in CA1 region. Data are presented as mean ± SEM (n = 6 slices from 5 mice for control group and n = 5 slices from 5 mice for sevoflurane group).

analysis of all other experiments. All of the data were appreciate with GraphPad Prism (Graph-Pad Software Inc.) and SPSS 22.0 (Chicago, IL, United States). $P < 0.05$ was considered to be a statistical significance.

RESULTS

Early Postnatal Sevoflurane Exposure Increased Motor Activity and Deceased Anxiety of Adult Mice

Open field experiment is one of the most commonly used experimental methods to detect psychological and motor functions. To detect the effect of sevoflurane on the basic motor activity, the open field test was performed to record the moving distance of adult mice during a certain period of time (see section "Methods" for details). We presented a 10-min motor path map of two groups of mice in the openfield (**Figure 1A**). Results showed that postnatal exposure to sevoflurane increased the overall moving distance (sevoflurane: 4,882 ± 1,031 cm vs. control: 3,736 ± 856 cm; $P = 0.026$; **Figure 1B**), suggesting that sevoflurane exposure in childhood causes hyperactivity in adulthood. Interestingly, compared with the control group, sevoflurane exposed mice also increased the number of times of entering the central area (sevoflurane: 50.8 ± 35.1 vs. control: 17.3 ± 6.0; $P = 0.01$; **Figure 1C**), and spent more time in the central area (sevoflurane: 67.6 ± 38.7 s vs. control: 31.7 ± 16.7 s; $P = 0.018$; **Figure 1D**). These differences were not merely due to the increased motor activity because the ratio of the locomotion distance in the central area over the total was also increased (sevoflurane: 12.5 ± 6.2 vs. control: 7.5 ± 2.6%; $P = 0.03$; **Figure 1E**), suggesting that sevoflurane exposure during childhood could reduce anxiety-like emotions in unfamiliar environments in mice after adulthood.

Sevoflurane-Enhanced Consolidate Space Memory in the Morris Water Maze

To investigate the effect of sevoflurane on cognition, the Morris water maze test was performed to assess spatial learning and memory. We showed the map of the swimming path of the mouse in the maze just after training (**Figure 2A**), and the path map of the re-entry into the water maze after a one-month rest period (**Figure 2B**). We found no statistically significant difference between sevoflurane-treated mice and the control group at 2 months old ($P > 0.05$; **Figure 2C**). Both swimming distance ($P > 0.05$; **Figure 2D**) and the time spent in the platform quadrant ($P > 0.05$; **Figure 2E**) were similar between the treated and control groups. However, the probe test showed significant difference between the anesthesia and control group on the 30th day (sevoflurane: 9.9 ± 3.7 vs. control: 6.1 ± 2.2; $P = 0.014$; **Figure 2F**) but not on the 6th day ($P > 0.05$; **Figure 2E**), suggesting that sevoflurane not only interfered with the learning ability of the spatial memory but also enhanced the ability of the mice to consolidate the acquired spatial memory.

Sevoflurane Increased the Dendritic Spine Density of Pyramidal Neurons

The formation and stability of synapses are the key factors to ensure the transmission of electrochemical neurotransmitters. To study long-term effects of sevoflurane on neuronal development, we observed synaptic morphology of hippocampal cognitive-related neurons. We counted the numbers of dendritic spines of the pyramidal neurons in the hippocampal CA1 region of 2-month-old mice. Contrary to the control group, early postnatal sevoflurane exposure induced an increase of the spine density of pyramidal neurons (sevoflurane: 6.3 ± 1.8 vs. control: 5.2 ± 1.5; $P = 0.028$) (**Figures 3A,B**), suggesting sevoflurane promoted the formation of dendritic spines.

Sevoflurane Increases the N-Methyl-D-Aspartate Receptor GluN2A Subunit in the Hippocampus

During the process of brain development and maturation, there is a conversion of NMDA receptors from GluN2B to GluN2A. The higher the ratio of GluN2A/GluN2B, the higher the maturity of neurons. To explore whether sevoflurane interfere with this conversion process, the hippocampus from 2-month-old mice

was harvested and subjected to Western blot analysis to compare the changes in protein content. Immunoblotting of GluN2A, GluN2B, or PSD95 showed that there was an increase of the levels of GluN2A subunit of NMDA receptor in the hippocampus of the mice after the sevoflurane exposure comparing with the control mice (152 vs. 100%, $P = 0.01$). There was no significant difference in the levels of GluN2B or PSD95 between the sevoflurane-treated mice and the control mice (**Figure 4**). This indicates that sevoflurane either promotes the above-mentioned conversion process or promotes the expression of GluN2A.

Sevoflurane Had No Effect on Long-Term Potentiation

Long-term potentiation (LTP) of synaptic transmission has been considered as one of the neural foundations of learning and memory, a functional indicator of synaptic plasticity. To evaluate the possibility that sevoflurane exposure may affect neuronal excitability, evoked potentials and synapse plasticity were studied in the hippocampal slices of anesthetized and control group in 2 months after gas exposure. In the control group, 0, 20, 40, and 60 min after HFS delivery, field excitatory postsynaptic potential (fEPSP) were no significant difference between two groups ($P > 0.05$; **Figure 5**). It seems that sevoflurane does not affect synaptic plasticity.

DISCUSSION

In our study, we found that 3% sevoflurane exposure for 4 h increased motor activity and promoted anxiety-free and consolidated space memory. Accordingly, compared with the control group, dendritic spine density of pyramidal neurons and the expression of GluN2A subunit were increased in the hippocampus of the sevoflurane group. However, we failed to identify any changes in LTP between the control and sevoflurane-treated group.

In line with our findings, previous studies also showed that neonates exposed to sevoflurane resulted in ADHD-like hyperactivity behaviors (Hu et al., 2017; Liang et al., 2017; Andropoulos, 2018). Although the underlying mechanisms behind these changes remain elusive, it has been reported that general anesthetics can induce dopaminergic receptors (DRs) subtype imbalance, glutamatergic receptors of N-methyl-D-aspartic acid receptor (NMDAR) subtype changes, and brain-derived neurotrophic factor (BDNF) reduction. All these changes, in turn, ultimately resulted in neurobehavioral changes due to various mechanisms including affecting neuronal development, interfering neurotransmitter transmission (Xu et al., 2019), and interrupting connections between the neurons. However, clinically, the GAS study showed no evidence for an increased risk of ADHD after anesthesia (McCann et al., 2019), but other studies indicated that there is an association of anesthetic exposure within the first few years of life and the development of ADHD (Chen et al., 2018). One can argue that neurotoxicity of general anesthetics can occur immediately after exposure and neurological dysfunction can be developed in a few years later. In our previous study, we found that repeated sevoflurane exposure at neonates can lead to impulsive behavior in adulthood (Xie et al., 2020). Moreover, research shows that general anesthesia can lead to hyperactivity behaviors (Xie et al., 2021). It is true that the synaptogenesis in 7-day-old rats is extremely sensitive to external factors, and the toxic effects from anesthetic agents can cause brain functional abnormalities that persist into adulthood. Clinically, ADHD normally appears in old-age children although the pathogenic damage to their brain happens in their early life *per se* (McCann et al., 2019).

Interestingly, the hyperactive and anxiety-like behaviors shown in the open field were not shown in the mirrors water maze experiment. This may be due to the fact that the open field anxiety-like behavior triggered by two main factors, namely, deviated from the original social groups and agoraphobia. In other words, the subject's response to different experiments is different and will affect the specific experimental results. Besides, previous studies also show that hippocampal damage enhanced spontaneous exercise activity (Yu et al., 2018). But damage to different regions within the hippocampus, such as the ventral and dorsal sides, can also have different effects. There is even an explanation that the anxiety behavior of the ventral hippocampus damage is thought to exist only at the more moderate pressure. Moreover, sometimes, the local area of the hippocampus damage only affects the anxiety-like emotions but not spatial memory capacity (Ju et al., 2019). Therefore, sevoflurane causes many types of behavioral changes, which may be caused by different brain regions and even different substructures. Perhaps, we need to promote mechanisms investigation by separating the above behaviors into related sub-brain regions. Previous studies found that anesthetic exposure in late postnatal life influenced dendritic spine formation and development in mice (De Roo et al., 2009). Indeed, volatile anesthetics of isoflurane, sevoflurane, or desflurane were reported to increase dendritic spine density in the rat medial prefrontal cortex (Briner et al., 2010). This was the case in this study showing that sevoflurane exposure increased dendritic spine density of pyramidal neurons in the hippocampal brain regions. Since excitatory synapses mostly form on dendritic spines (Ju et al., 2019), this may logically lead to change the excitatory synaptic transmission. This may explain our findings that sevoflurane treated mice have higher motor activities and better memory retention. Animal studies had indicated the developmental neurotoxicity of volatile anesthetics, but this study showed that sevoflurane exposure reduces anxiety and enhances memory consolidation in mice, which are accordant with others (Chen et al., 2015). The difference may be mainly due to the different dosage and duration of anesthesia in the established animal models.

In this study, we found that sevoflurane increased the expression of GluN2A but not GluN2B subunit in the whole hippocampus in the adult age after exposure (**Figure 4**). However, the exposure did not induce any changes of PSD95 and LTP in the CA1 region of the hippocampus. Previous experimental results showed that anesthetics regulate cognitive function mainly by changing the GluN2B content (Dumas, 2005), while the increase in GluN2A content is considered to be a manifestation of long-term memory deficits (Kopp et al., 2007). Moreover, pharmacological evidence indicated that GluN2A

are essential mediators of many forms of activity-dependent synaptic plasticity that are thought to underlie higher cognitive functions, such as learning and memory (Paoletti et al., 2013). Increasing the expression of GluN2A did not affect the LTP induced by 100 Hz in CA1 region. Instead, it only affected the LTD induced by fixed range of frequency (Lu et al., 2016). Also, there are still articles notion that the first hour and expression of LTP is still indeterminacy (Nicoll, 2017). Previous studies have shown that in anesthetized mice, neither cognitive performance nor long-term potentiation was impaired 24 h after anesthesia (Haseneder et al., 2013). This is consistent with our electrophysiology. We must point out that this test only detected the CA1 region of the LTP only used a stimulus protocol. Thus, overexpression of GluN2A may be associated with LTP with other induction patterns or other brain regions of long-term memory. Interestingly, sevoflurane anesthesia induced even an improvement of cognitive performance and an elevation of the expression levels of NMDA receptor type 1 and 2B subunits in the hippocampus (Haseneder et al., 2013). In addition, is there a correlation between the increase in GluN2A content and the improvement of memory consolidation ability? These conjectures need to examine in future experiments. This may reflect a regional specific pattern changes but may also indicate that early-life anesthetic exposure can induce differentiating changes in the brain. All these need to be verified in the future study.

This study has several limitations. First, both experimental and control mice the mice pups were maintained under spontaneous ventilation during sevoflurane anesthesia. Sevoflurane suppresses cardiorespiratory function, and, therefore, hypercapnia, hypoxemia, and hypotension likely may occur in this study. Due to technical difficulties, blood gases and blood pressure were not measured and if so, what impact they might have on our current study is unknown. However, it has been reported that previous research demonstrated that there was no significant difference in the rate of hypercapnia during 6 h exposure of sevoflurane at 3% (Goyagi, 2018). Second, only an open field test and the Morris water maze test were used in our study; more behavioral tests should be introduced in our future study. Third, we only selected male mice for behavioral testing, while they do not have the physiological cycle of female mice; we cannot rule out that sex selection may cause gender bias in the behavioral results. Finally, regional specific related molecular mechanisms and their association with behavioral changes are not investigated and warrant further study.

CONCLUSION

Totally, 3% sevoflurane exposure for 4 h at the brain development stage increased motor activity and promoted anxiety-free and consolidated space memory in the adult age. Accordingly, the dendritic spine density of pyramidal neurons in the CA1 region and the expression of GluN2A subunit were increased in the hippocampus. However, sevoflurane treatment did not induce any changes in LTP in the hippocampus. Conclusively, this study only describes some of the changes caused by sevoflurane acting on immature brains and raised related questions and directions for subsequent research. The implication of our study may call more studies to further verify the long-term effects of neurotoxicity of general anesthetics.

DATA AVAILABILITY STATEMENT

The raw data supporting the conclusions of this article will be made available by the authors, without undue reservation.

ETHICS STATEMENT

The animal study was reviewed and approved by the Tab of Animal Experimental Ethical Inspection of the First Affiliated Hospital, Zhejiang University School of Medicine.

AUTHOR CONTRIBUTIONS

ZH conceived and designed the study. RL and BW were involved in the study design, experimental operation, data review, data analysis, and writing article. XC and YH analyzed the data and modified the manuscript. CL, DY, YY, and LW contributed for the animal feeding and experimental operation. LM modified the manuscript. All authors read and approved the final manuscript.

FUNDING

This study was supported by the grant from the National Natural Science Funds of China (82171260, 81641042, and 81471240) and the Zhejiang Provincial Natural Science Foundation of China (LZ22H090002 and 2014C33170). The above funds provide financial support for our projects, including the purchase and breeding of mice, experimental consumables, rental of experimental instruments, living allowances for experimental personnel, and so on.

ACKNOWLEDGMENTS

We thank Yudong Zhou and Yi Shen, Zhejiang University, for their help and advice during the course of study. They also thank Daqing Ma, Imperial College London, United Kingdom, for his critical comments during manuscript preparation.

REFERENCES

Andropoulos, D. B. (2018). Effect of anesthesia on the developing brain: infant and fetus. *Fetal. Diagn. Ther.* 43, 1–11. doi: 10.1159/000475928

Briner, A., De Roo, M., Dayer, A., Muller, D., Habre, W., and Vutskits, L. (2010). Volatile anesthetics rapidly increase dendritic spine density in the rat medial prefrontal cortex during synaptogenesis. *Anesthesiology* 112, 546–556. doi: 10.1097/ALN.0b013e3181cd7942

Buggy, D. J., Nicol, B., Rowbotham, D. J., and Lambert, D. G. (2000). Effects of intravenous anesthetic agents on glutamate release. *Anesthesiology* 92, 1067–1073. doi: 10.1097/00000542-200004000-00025

Chen, C., Shen, F.-Y., Zhao, X., Zhou, T., Xu, D.-J., Wang, Z.-R., et al. (2015). Low-dose sevoflurane promotes hippocampal neurogenesis and facilitates the development of dentate gyrus-dependent learning in neonatal rats. *ASN Neuro* 7:175909141557584. doi: 10.1177/1759091415575845

Chen, X., Zhou, X., Yang, L., Miao, X., Lu, D.-H., Yang, X.-Y., et al. (2018). Neonatal exposure to low-dose (1.2%) sevoflurane increases rats' hippocampal neurogenesis and synaptic plasticity in later life. *Neurotox. Res.* 34, 188–197. doi: 10.1007/s12640-018-9877-3

De Roo, M., Klauser, P., Briner, A., Nikonenko, I., Mendez, P., Dayer, A., et al. (2009). Anesthetics rapidly promote synaptogenesis during a critical period of brain development. *PLoS One* 4:e7043. doi: 10.1371/journal.pone.0007043

Dumas, T. C. (2005). Developmental regulation of cognitive abilities: modified composition of a molecular switch turns on associative learning. *Prog. Neurobiol.* 76, 189–211. doi: 10.1016/j.pneurobio.2005.08.002

Fang, F., Xue, Z., and Cang, J. (2012). Sevoflurane exposure in 7-day-old rats affects neurogenesis, neurodegeneration and neurocognitive function. *Neurosci. Bull.* 28, 499–508. doi: 10.1007/s12264-012-1260-4

Goyagi, T. (2018). The additional oxygen as a carrier gas during long-duration sevoflurane exposure ameliorate the neuronal apoptosis and improve the long-term cognitive function in neonatal rats. *Brain Res.* 1678, 220–230. doi: 10.1016/j.brainres.2017.10.014

Hansen, T. G. (2015). Anesthesia-related neurotoxicity and the developing animal brain is not a significant problem in children. *Paediatr. Anaesth.* 25, 65–72. doi: 10.1111/pan.12548

Haseneder, R., Starker, L., Berkmann, J., Kellermann, K., Jungwirth, B., Blobner, M., et al. (2013). Sevoflurane anesthesia improves cognitive performance in mice, but does not influence in vitro long-term potentation in hippocampus CA1 stratum radiatum. *PLoS One* 8:e64732. doi: 10.1371/journal.pone.0064732

Hu, D., Flick, R. P., Zaccariello, M. J., Colligan, R. C., Katusic, S. K., Schroeder, D. R., et al. (2017). Association between exposure of young children to procedures requiring general anesthesia and learning and behavioral outcomes in a population-based birth cohort. *Anesthesiology* 127, 227–240. doi: 10.1097/ALN.0000000000001735

Ing, C., Ma, X., Sun, M., Lu, Y., Wall, M. M., Olfson, M., et al. (2020). Exposure to surgery and anesthesia in early childhood and subsequent use of attention deficit hyperactivity disorder medications. *Anesth. Analg.* 131, 723–733. doi: 10.1213/ANE.0000000000004619

Ju, X., Jang, Y., Heo, J. Y., Park, J., Yun, S., Park, S., et al. (2019). Anesthesia affects excitatory/inhibitory synapses during the critical synaptogenic period in the hippocampus of young mice: importance of sex as a biological variable. *Neurotoxicology* 70, 146–153. doi: 10.1016/j.neuro.2018.11.014

Kopp, C., Longordo, F., and Lüthi, A. (2007). Experience-dependent changes in NMDA receptor composition at mature central synapses. *Neuropharmacology* 53, 1–9. doi: 10.1016/j.neuropharm.2007.03.014

Korotkova, T., Fuchs, E. C., Ponomarenko, A., von Engelhardt, J., and Monyer, H. (2010). NMDA receptor ablation on parvalbumin-positive interneurons impairs hippocampal synchrony, spatial representations, and working memory. *Neuron* 68, 557–569. doi: 10.1016/j.neuron.2010.09.017

Liang, P., Li, F., Liu, J., Liao, D., Huang, H., and Zhou, C. (2017). Sevoflurane activates hippocampal CA3 kainate receptors (Gluk2) to induce hyperactivity during induction and recovery in a mouse model. *Br. J. Anaesth.* 119, 1047–1054. doi: 10.1093/bja/aex043

Lu, Y., Huang, Y., Jiang, J., Hu, R., Yang, Y., Jiang, H., et al. (2016). Neuronal apoptosis may not contribute to the long-term cognitive dysfunction induced by a brief exposure to 2% sevoflurane in developing rats. *Biomed. Pharmacother.* 78, 322–328. doi: 10.1016/j.biopha.2016.01.034

McCann, M. E., de Graaff, J. C., Dorris, L., Disma, N., Withington, D., Bell, G., et al. (2019). Neurodevelopmental outcome at 5 years of age after general anaesthesia or awake-regional anaesthesia in infancy (GAS): an international, multicentre, randomised, controlled equivalence trial. *Lancet* 393, 664–677. doi: 10.1016/S0140-6736(18)32485-1

Nicoll, R. A. (2017). A brief history of long-term potentiation. *Neuron* 93, 281–290. doi: 10.1016/j.neuron.2016.12.015

Paoletti, P., Bellone, C., and Zhou, Q. (2013). NMDA receptor subunit diversity: impact on receptor properties, synaptic plasticity and disease. *Nat. Rev. Neurosci.* 14, 383–400. doi: 10.1038/nrn3504

Roncacé, V., Burattini, C., Stagni, F., Guidi, S., Giacomini, A., Emili, M., et al. (2017). Neuroanatomical alterations and synaptic plasticity impairment in the perirhinal cortex of the Ts65Dn mouse model of Down syndrome. *Neurobiol. Dis.* 106, 89–100. doi: 10.1016/j.nbd.2017.06.017

Satomoto, M., Satoh, Y., Terui, K., Miyao, H., Takishima, K., Ito, M., et al. (2009). Neonatal exposure to sevoflurane induces abnormal social behaviors and deficits in fear conditioning in mice. *Anesthesiology* 110, 628–637. doi: 10.1097/ALN.0b013e3181974fa2

Shen, Y., Qin, H., Chen, J., Mou, L., He, Y., Yan, Y., et al. (2016). Postnatal activation of TLR4 in astrocytes promotes excitatory synaptogenesis in hippocampal neurons. *J. Cell Biol.* 215, 719–734. doi: 10.1083/jcb.201605046

Sun, L. S., Li, G., Miller, T. L. K., Salorio, C., Byrne, M. W., Bellinger, D. C., et al. (2016). Association between a single general anesthesia exposure before age 36 months and neurocognitive outcomes in later childhood. *JAMA* 315, 2312–2320. doi: 10.1001/jama.2016.6967

Xie, L., Hu, Y., Yan, D., McQuillan, P., Liu, Y., Zhu, S., et al. (2021). The relationship between exposure to general anesthetic agents and the risk of developing an impulse control disorder. *Pharmacol. Res.* 165, 105440. doi: 10.1016/j.phrs.2021.105440

Xie, L., Liu, Y., Hu, Y., Wang, B., Zhu, Z., Jiang, Y., et al. (2020). Neonatal sevoflurane exposure induces impulsive behavioral deficit through disrupting excitatory neurons in the medial prefrontal cortex in mice. *Transl. Psychiatry* 10:202. doi: 10.1038/s41398-020-00884-5

Xu, C., Seubert, C. N., Gravenstein, N., and Martynyuk, A. E. (2016). Propofol, but not etomidate, increases corticosterone levels and induces long-term alteration in hippocampal synaptic activity in neonatal rats. *Neurosci. Lett.* 618, 1–5. doi: 10.1016/j.neulet.2016.02.045

Xu, L., Hu, Y., Huang, L., Liu, Y., Wang, B., Xie, L., et al. (2019). The association between attention deficit hyperactivity disorder and general anaesthesia - a narrative review. *Anaesthesia* 74, 57–63. doi: 10.1111/anae.14496

Yu, X., Zhang, F., and Shi, J. (2018). Neonatal exposure to sevoflurane caused cognitive deficits by dysregulating SK2 channels and GluA2-lacking AMPA receptors in juvenile rat hippocampus. *Neuropharmacology* 141, 66–75. doi: 10.1016/j.neuropharm.2018.08.014

Zaccariello, M. J., Frank, R. D., Lee, M., Kirsch, A. C., Schroeder, D. R., Hanson, A. C., et al. (2019). Patterns of neuropsychological changes after general anaesthesia in young children: secondary analysis of the mayo anesthesia safety in kids study. *Br. J. Anaesth.* 122, 671–681. doi: 10.1016/j.bja.2019.01.022

Conflict of Interest: The authors declare that the research was conducted in the absence of any commercial or financial relationships that could be construed as a potential conflict of interest.

Publisher's Note: All claims expressed in this article are solely those of the authors and do not necessarily represent those of their affiliated organizations, or those of the publisher, the editors and the reviewers. Any product that may be evaluated in this article, or claim that may be made by its manufacturer, is not guaranteed or endorsed by the publisher.

frontiers | Frontiers in Aging Neuroscience

SYSTEMATIC REVIEW
published: 30 June 2022
doi: 10.3389/fnagi.2022.939848

Effects of Glucocorticoids on Postoperative Neurocognitive Disorders in Adult Patients: A Systematic Review and Meta-Analysis

Xiaoyu Xie[1,2†], *Rui Gao*[1,2†], *Hai Chen*[3,4], *Xueying Zhang*[1,2], *Xingwei Cai*[1,2], *Changteng Zhang*[1,2], *Changliang Liu*[1,2], *Tao Zhu*[1,2*] and *Chan Chen*[1,2*]

[1] *Department of Anesthesiology and National Clinical Research Center for Geriatrics, West China Hospital, Sichuan University and the Research Units of West China (2018RU012), Chinese Academy of Medical Sciences, Chengdu, China,* [2] *Laboratory of Anesthesia and Critical Care Medicine, National-Local Joint Engineering Research Centre of Translational Medicine of Anesthesiology, West China Hospital, Sichuan University, Chengdu, China,* [3] *Department of Respiratory and Critical Care Medicine, West China Medical School/West China Hospital, Sichuan University, Chengdu, China,* [4] *Department of Targeted Tracer Research and Development Laboratory, West China Hospital, Sichuan University, Chengdu, China*

OPEN ACCESS

Edited by:
Yingwei Wang,
Fudan University, China

Reviewed by:
Hao Wang,
Shanghai Jiao Tong University, China
Tian-Long Wang,
Capital Medical University, China

***Correspondence:**
Tao Zhu
xwtao.zhu@foxmail.com
Chan Chen
xychenchan@gmail.com

[†] *These authors have contributed equally to this work and share first authorship*

Specialty section:
This article was submitted to Neurocognitive Aging and Behavior, a section of the journal Frontiers in Aging Neuroscience

Received: *09 May 2022*
Accepted: *13 June 2022*
Published: *30 June 2022*

Citation:
Xie X, Gao R, Chen H, Zhang X, Cai X, Zhang C, Liu C, Zhu T and Chen C (2022) Effects of Glucocorticoids on Postoperative Neurocognitive Disorders in Adult Patients: A Systematic Review and Meta-Analysis. Front. Aging Neurosci. 14:939848. doi: 10.3389/fnagi.2022.939848

Background: Postoperative neurocognitive disorders (PNDs) is common among surgical patients, however, the effect of glucocorticoids for preventing PNDs is not clear. This review aims to evaluate the effect of glucocorticoids on the incidence of PNDs in adult patients undergoing surgery.

Methods: The databases of PubMed/Medline, Embase, the Cochrane Library, and Web of science were searched for all available randomized controlled trials (RCTs) from inception to April 30, 2022. RCTs comparing the effect of glucocorticoids with placebo on the incidence of PNDs in adult surgical patients (≥18 years old) were eligible. Subgroup analyses and meta-regressions were performed to evaluate sources of clinical heterogeneity. The level of certainty for main outcomes were assessed by the Grading of Recommendations Assessment, Development and Evaluation (GRADE) methodology.

Results: Eleven trials with a total of 10,703 patients were identified. Compared with the control group, glucocorticoids did not reduce the incidence of PNDs (RR: 0.84, 95% CI: 0.67 to 1.06, $P = 0.13$, GRADE = moderate). Secondary analyses for primary outcome did not change the result. In addition, the length of ICU stay was decreased in glucocorticoids group (RR: −13.58, 95% CI: −26.37 to −0.80, $P = 0.04$, GRADE = low). However, there were no significant differences between groups with regards to the incidence of postoperative infection (RR: 0.94, 95% CI: 0.84 to 1.06, $P = 0.30$, GRADE = moderate), blood glucose level (RR: 1.05, 95% CI: −0.09 to 2.19, $P = 0.07$, GRADE = low), duration of mechanical ventilation (RR: −2.44, 95% CI: −5.47 to 0.59, $P = 0.14$, GRADE = low), length of hospital stay (RR: −0.09, 95% CI: −0.27 to 0.09, $P = 0.33$, GRADE = moderate) and 30-day mortality (RR: 0.86, 95% CI: 0.70 to 1.06, $P = 0.16$, GRADE = moderate).

Conclusions: This meta-analysis suggests that perioperative administration of glucocorticoids may not reduce the incidence of PNDs after surgery. The effect of glucocorticoids on decreased length of ICU stay needs further researches. Future high-quality trials using acknowledged criteria and validated diagnostic tools are needed to determine the influence of glucocorticoids on long-term PNDs.

Systematic Review Registration: https://www.crd.york.ac.uk/prospero/display_record.php?ID=CRD42022302262, identifier: CRD42022302262.

Keywords: glucocorticoids, postoperative neurocognitive disorders, adult patients, surgery, meta-analysis

INTRODUCTION

Postoperative neurocognitive disorders (PNDs) is an overarching term that includes postoperative delirium and postoperative cognitive dysfunction (POCD) (Vacas et al., 2021). According to the Perioperative Cognition Nomenclature Working Group in 2018 (Evered et al., 2018), postoperative delirium is an acute state of cognitive impairment occurring within days after surgery and up to 1 week or until discharge, while POCD is a prolonged cognitive decline usually detected between 30 days and 12 months postoperatively. It has been reported that postoperative delirium occurred in 10–60% of elderly surgical patients, varying by surgical procedures (American Geriatrics Society Expert Panel on Postoperative Delirium in Older Adults, 2015), and the incidence of POCD is approximately 25–40% (Wei et al., 2019). Old age, low educational levels, poor preoperative cognitive function, perioperative pain and complicated surgery process are thought to be risk factors of PNDs (Xie and Shen, 2018; Evered et al., 2020; O'Gara et al., 2021). PNDs are the very common and severe postoperative neurological complications with poor outcomes, including increasing the length of hospital stay, mortality, and the risk of long-term cognitive impairment. These would cause significant clinical, social, and financial burdens on the patients and their communities (Monk et al., 2008; Inouye et al., 2014; Boone et al., 2020).

Improving cognitive outcome after surgery, therefore, is an important objective for anesthesiologists and surgeons. To date, there have been no compelling pharmacologic interventions to limit the incidence or severity of PNDs (Mahanna-Gabrielli et al., 2019; Deemer et al., 2020). Dexmedetomidine, an anesthetic agent with neural anti-inflammatory effects, has been found to show promise for PNDs prevention (Lee et al., 2018; Likhvantsev et al., 2021). However, it has common side effects such as bradycardia and hypotension (Wu et al., 2018; Shi et al., 2020; Zhao et al., 2020), and the evidence to support this effect is limited (Sanders et al., 2021). For non-pharmacologic approaches, cognitive prehabilitation, physical activity, and management of hypertension and diabetes seem to be effective to improve cognitive function (Wang et al., 2020; Humeidan et al., 2021), but there is still a gap in their integration into pathways of care for patients (Vlisides et al., 2019; Deiner et al., 2020).

Proposed potential mechanisms for PNDs, including mitochondrial dysfunction, oxidative stress (Netto et al., 2018), synaptic damage (Xiao et al., 2018), and neurotrophic support impairment (Fan et al., 2016) are speculative, among which neuroinflammation is the most significantly concerned (Luo et al., 2019). It has been reported that surgery and anesthesia could lead the peripheral immune system to produce pro-inflammatory signals (Balusu et al., 2016; Noll et al., 2017). These inflammatory mediators could transfer into the brain through paraventricular areas of the blood-brain barrier (BBB) and stimulate microglia to produce proinflammatory factors, destroying synapses and neurons, thus causing neurotoxic symptoms and cognitive disorders (Lim et al., 2013; Liu and Yin, 2018).

Glucocorticoids are commonly used in the perioperative period to attenuate the inflammatory response (Holte and Kehlet, 2002; Lunn and Kehlet, 2013). And they can alleviate the inflammation by inhibiting prostaglandin production (Rhen and Cidlowski, 2005), activating endothelial nitric oxide synthetase (Hafezi-Moghadam et al., 2002), and decreasing the stability of mRNA for genes for inflammatory proteins (Gille et al., 2001; Lasa et al., 2002; Saklatvala et al., 2003). Evaluating whether the perioperative administration of glucocorticoids is helpful in preventing cognitive decline could promote targeted preventive and therapeutic interventions. Therefore, in recent years several studies have investigated the efficacy of glucocorticoids on cognitive disorders after anesthesia and surgery. However, their conclusions have been inconsistent. Qiao et al. (2015) and Valentin et al. (2016) investigated the effect of glucocorticoids on PNDs in elderly patients undergoing non-cardiac surgery. They found that the preventive administration of glucocorticoids could effectively reduce POCD. In contrast, Sauër et al. (2014) demonstrated the opposite result, showing that intraoperative administration of glucocorticoids did not reduce the incidence of delirium after cardiac surgery. Besides, Fang et al. (2014) studied the effect of glucocorticoids in patients suffering from facial spasms requiring microvascular decompression. They found that administering a higher dose of glucocorticoids increased the incidence of POCD in the early postoperative period. Therefore, we applied a systematic review and meta-analysis to explore the effect of perioperative glucocorticoids administration on the incidence of PNDs.

METHODS

This meta-analysis was conducted following the recommendations of Preferred Reporting Items for Systematic Reviews and Meta-Analyses (PRISMA) (Page et al., 2021). This study protocol was registered in PROSPERO database (CRD42022302262).

Search Strategy

The databases of Pubmed/Medline, Embase, the Cochrane Library/Central, and Web of science were systematically searched for all relevant studies from inception to April 30, 2022. The references of included researches were also examined. According to the search strategy, both MeSH terms and free terms were used. The following keyword search terms were used: *glucocorticoids, cognitive disorders,*

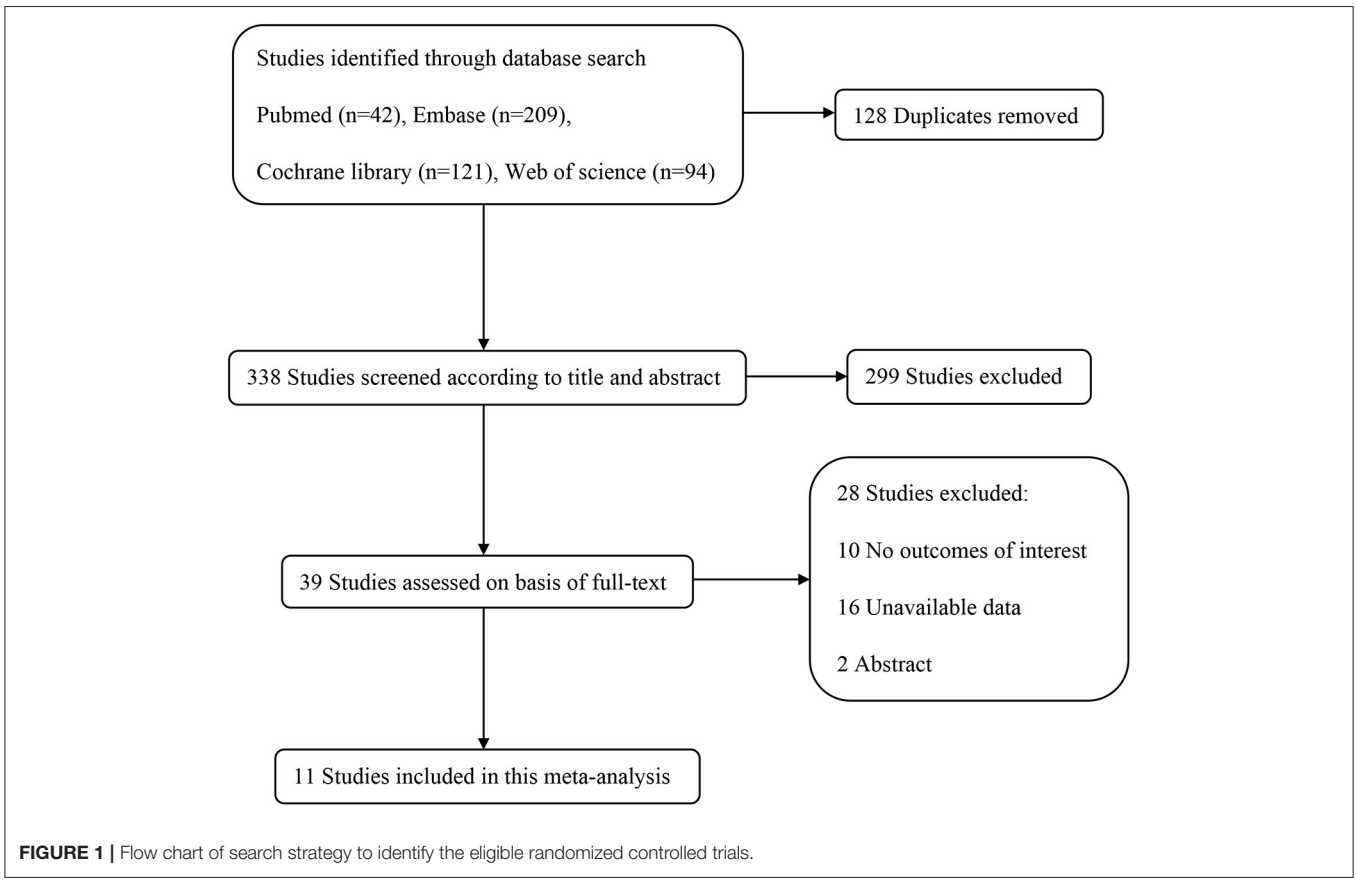

FIGURE 1 | Flow chart of search strategy to identify the eligible randomized controlled trials.

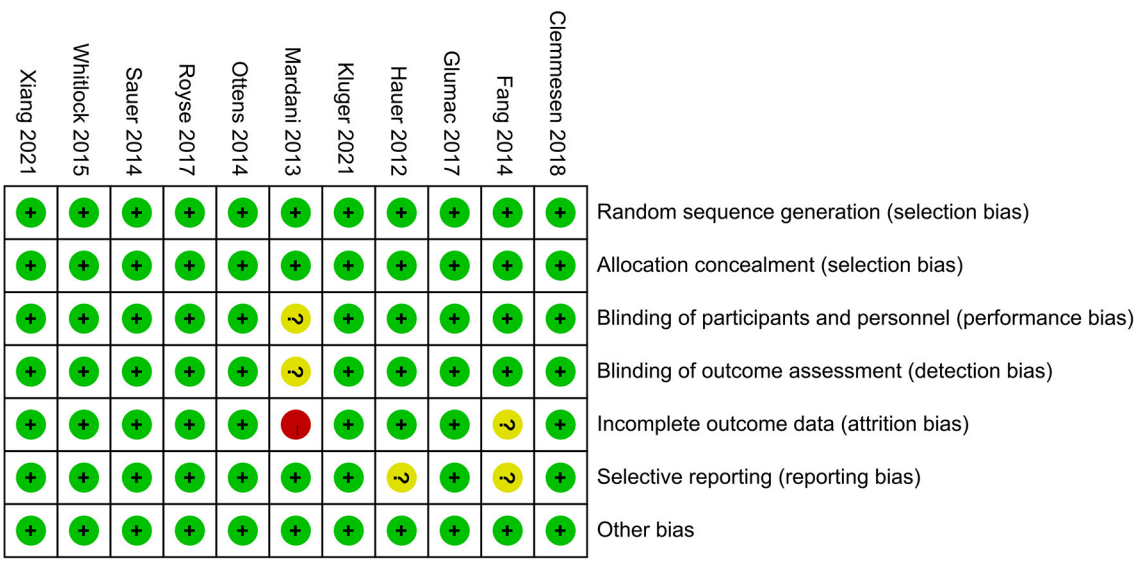

FIGURE 2 | Risk of bias assessment was undertaken for each included trial according to the Cochrane Risk of Bias Methods.

TABLE 1 | Characteristics of the 11 included trails.

First author	Year	Number of people (*n*)	Age (Y)	Surgery type	Glucocorticoids type	Doses, time and duration of intervention	Control	PNDs type	Assessment time	Assessment methods
Mardani	2013	DEX: 43	DEX: 64.55 ± 11.10	Cardiac surgery	DEX	8 mg before surgery and 8 mg every 8 h for the first three POD	NS	Delirium	PROD and POD1–3	MMSE
		NS: 50	NS: 60.04 ± 12.77							
Sauer	2014	DEX: 367	DEX: 67 ± 12	Cardiac surgery	DEX	1 mg/kg (maximum 100 mg) at anesthetic induction	NS	Delirium	POD1–4	CAM-ICU, CAM
		NS: 370	NS: 66 ± 12							
Kluger	2021	DEX: 40	DEX: 81.4 ± 7.2	Hip fracture	DEX	20 mg before surgery	NS	Delirium	POD1–3	4AT
		NS: 39	NS: 81.4 ± 8.9							
Fang	2014	DEX-1: 320	DEX-1: 48.9 ± 5.35	Microvascular decompression	DEX	0.1 mg/kg or 0.2 mg/kg before anesthesia	NS	POCD	PROD1 and POD5	A battery of tests
		DEX-2: 315	DEX-2: 48.0 ± 5.60							
		NS: 319	NS: 48.0 ± 5.77							
Ottens	2014	DEX: 140	DEX: 63.4 ± 12.3	Cardiac surgery	DEX	1 mg/kg (maximum 100 mg) after anesthetic induction	NS	POCD	PROD1 and POD30 and 12 months	A battery of tests
		NS: 138	NS: 65.4 ± 11.5							
Glumac	2017	DEX: 80	DEX: 63.7 ± 9.0	Cardiac surgery	DEX	0.1 mg/kg 10 h before surgery	NS	POCD	PROD2 and POD6	A battery of tests
		NS: 81	NS: 64.2 ± 9.4							
Whitlock	2015	MET: 3755	MET: 67.5 ± 13.6	Cardiac surgery	MET	250 mg at anesthetic induction and 250 mg at initiation of CPB	NS	Delirium	POD3	CAM
		NS: 3752	NS: 67.3 ± 13.8							
Royse	2017	MET: 250	MET: 73.4 ± 10.5	Cardiac surgery	MET	250 mg at anesthetic induction and 250 mg at initiation of CPB	NS	Delirium	POD1–3	CAM-ICU
		NS: 248	NS: 74.3 ± 9.3							
Clemmesen	2018	MET: 59	MET: 79 ± 8	Hip fracture	MET	125mg before surgery	NS	Delirium	POD1–3	CAM-S
		NS: 58	NS: 81 ± 9							
Xiang	2021	MET: 84	MET: 71 (68–74)	Laparoscopic gastrointestinal surgery	MET	2 mg/kg of before surgery	NS	Delirium	POD1–5	CAM
		NS: 84	NS: 70 (68–73)							
Hauer	2012	HYD: 56	HYD: 69.3 ± 8.9	Cardiac surgery	HYD	100 mg over 10 min before anesthesia, and 10 mg/h on POD 1, 5 mg/h on POD 2, 3 × 20 mg on POD 3, 3 × 10 mg on POD 4	NS	ACD/delirium	POD1	DSM-IV
		NS: 55	NS: 68.0 ± 8.3							

Date presented as mean ± SD or median (interquartile range).

DEX, dexamethasone; MET, methylprednisolone; HYD, hydrocortisone; NS, normal saline; CPB, cardiopulmonary bypass; POCD, postoperative cognitive dysfunction; PROD, pre-operative day; POD, post-operative day; MMSE, mini-mental state examination; CAM, confusion assessment method; CAM-ICU, CAM for intensive care unit; CAM-S, confusion assessment method-short; 4AT, arousal, attention, abbreviated Mental Test–4, acute change; ACD, acute postoperative cognitive dysfunction; DSM-IV, Diagnostic and Statistical Manual of Mental Disorders, Fourth Revision.

delirium, and surgery. The search strategy was given in the **Supplementary Material**.

Study Selection Criteria

Studies restricted to randomized controlled trials (RCTs) in adult surgical patients (≥18 years old). All published full-article RCTs compared the effect of glucocorticoids with placebo or equal volume of normal saline (NS) on the incidence of PNDs were eligible for inclusion. Language restriction was not applied.

Pediatric surgery, non-intravenous administration of glucocorticoids, no available assessment tools, and animal experiments were excluded from this meta-analysis.

Data Extraction

Data extraction and quality assessment were completed by two authors (XX and RG) independently. One author (XX) entered the information into the table and checked for consistency and completeness. Disagreements on data extraction and quality assessment were handled by discussion or reviewed by the third author (CC). The extracted data and information were as follows: first author, year of publication, surgery type, patient age, glucocorticoids type, timing and dose, control group, PNDs type, and cognitive assessment timing and methods. In addition, the following adverse events were extracted as well, including PNDs, infection, blood glucose level, duration of mechanical ventilation, length of ICU and hospital stay, and 30-day mortality.

Quality Assessment

Quality assessment of included RCTs was performed according to the second version of the Cochrane risk-of-bias tool for RCTs (RoB 2.0) (Sterne et al., 2019). There are seven sections of this assessment, random sequence generation, allocation concealment, blinding of participants and personnel, blinding of outcome assessment, incomplete outcome data, selective reporting, and other biases. Each section was classified into the low, high, or unclear risk of bias.

Endpoints

The primary endpoint of this meta-analysis was the incidence of PNDs. The secondary outcomes were the incidence of postoperative infection, blood glucose level, duration of mechanical ventilation, the length of ICU and hospital stay, and postoperative 30-day mortality.

Statistical Analysis

For dichotomous data (incidence of PNDs, postoperative infection, and 30-day mortality), the Mantel-Haenszel method was used to combine outcomes and risk ratio (RR) with 95% confidence intervals (CI) were calculated. Concerning continuous variables (blood glucose level, duration of mechanical ventilation, and the length of ICU and hospital stay), the Inverse-Variance method was used, and mean difference (MD) or standardized mean difference (SMD) with 95% CI were calculated. The I^2 statistics used to evaluate heterogeneity were divided into the following three levels (Melsen et al., 2014): low ($I^2 < 50\%$), moderate ($I^2 = 50$–75%) and high ($I^2 > 75\%$). When the heterogeneity was low, we used fixed effects model to pooled the data; otherwise, we chose random effects model.

To find sources of heterogeneity, subgroup analyses were conducted according to the type of PNDs (postoperative delirium and POCD), the type of glucocorticoids, surgery, dose, and age. In subgroup analysis for the dose of glucocorticoids, the trials were stratified into three broad dose groups: low dose group if the total dose of glucocorticoid used was ≤30 mg prednisolone or equivalent, medium dose group if the total dose used was between 30 and 100 mg prednisolone or equivalent, and high dose group if the total dose used was >100 mg prednisolone or equivalent. These cut points were chosen according to clinical practice (Czock et al., 2005). For studies that used dexamethasone, methylprednisolone, or hydrocortisone, the total dose of glucocorticoid used was converted to an equivalent dose of prednisolone with similar glucocorticoid effect. The dose conversion factors for dexamethasone, methylprednisolone, and hydrocortisone to prednisolone were 6, 1.25, and 0.25,

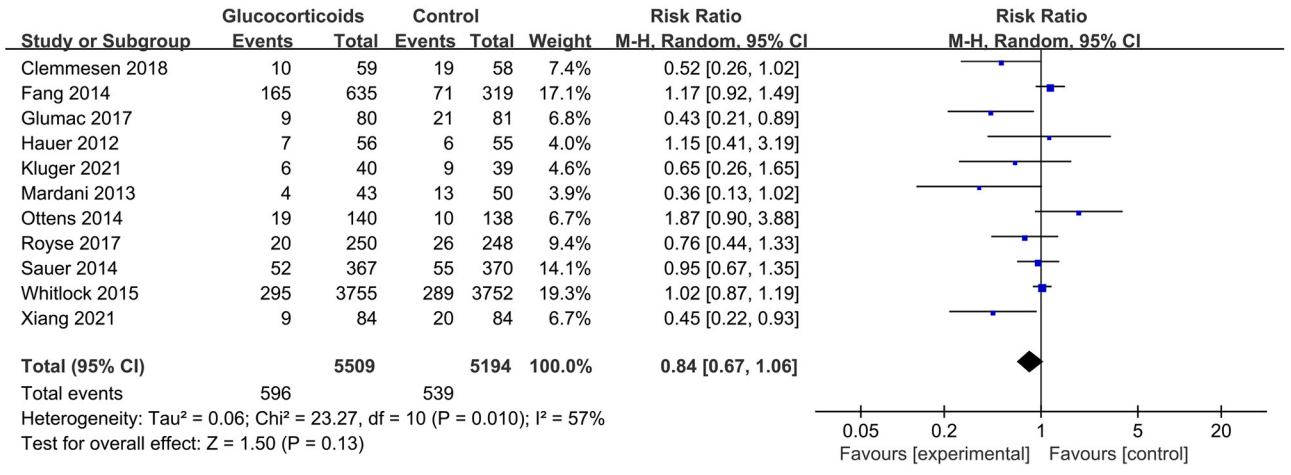

FIGURE 3 | Forest plot for the incidence of PNDs.

respectively (https://clincalc.com/corticosteroids/). In subgroup analysis for patient age, we calculated the mean age of the study population as the basis of classification. Besides, Hartung-Knapp adjusted meta-regressions were performed to find interactions between variables if subgroup analyses could not explain sources of heterogeneity.

Publication bias was assessed through visual inspection of funnel plots and Egger's test to evaluate the small-study effects. The influence of a potential publication bias on findings was explored by using the Duval and Tweedie trim-and-fill procedure. Sensitivity analyses were performed by excluding high-risk studies evaluated by RoB 2.0 or omitting one study each time to detect robustness of the pooled results. Finally, the level of certainty for main outcomes were assessed by the Grading of Recommendations Assessment, Development and Evaluation (GRADE) methodology (Langendam et al., 2013). $P < 0.05$ was considered statistically significant for all tests. All data analyses were performed by Revman 5.3. and Stata 16.

RESULTS

Study Characteristics

According to the search strategy, a total of 466 trials were identified. Among them, 128 studies were removed due to duplication, and the other 327 studies were excluded based on inclusion and exclusion criteria. Ultimately, 11 RCTs, including 10,703 patients, were included in this meta-analysis. The selection process flow chart was shown in **Figure 1**, and methodological quality assessment was conducted according to the RoB 2.0, and the result was summarized in **Figure 2**. The major characters of these eligible studies were extracted and presented in **Table 1**. Seven trials were cardiac surgery (Hauer et al., 2012; Mardani and Bigdelian, 2013; Ottens et al., 2014; Sauër et al., 2014; Whitlock et al., 2015; Glumac et al., 2017; Royse et al., 2017), one trial was neurologic surgery (Fang et al., 2014), and three trials were non-cardiac, non-neurologic surgery, including one laparoscopic gastrointestinal surgery (Xiang et al., 2022) and two hip fracture surgery (Clemmesen et al., 2018; Kluger et al., 2021). Furthermore, six studies used dexamethasone as intervention (Mardani and Bigdelian, 2013; Fang et al., 2014; Ottens et al., 2014; Sauër et al., 2014; Glumac et al., 2017; Kluger et al., 2021), four studies used methylprednisolone (Whitlock et al., 2015; Royse et al., 2017; Clemmesen et al., 2018; Xiang et al., 2022), and one study used hydrocortisone (Hauer et al., 2012). All of the included studies used normal saline as a placebo. Besides, eight studies investigated postoperative delirium (Hauer et al., 2012; Mardani and Bigdelian, 2013; Sauër et al., 2014; Whitlock et al., 2015; Royse et al., 2017; Clemmesen et al., 2018; Kluger et al., 2021; Xiang et al., 2022) while the other three trials investigated POCD (Fang et al., 2014; Ottens et al., 2014; Glumac et al., 2017). The timing and dose of glucocorticoids administration and cognitive assessment methods were varied between included studies.

Primary Outcome

The overall pooled result showed that glucocorticoids did not decrease the incidence of PNDs compared to the controls (RR: 0.84, 95% CI: 0.67 to 1.06, $P = 0.13$, $I^2 = 57\%$) (**Figure 3**). Sensitivity analyses were performed by excluding the high-risk study (Mardani and Bigdelian, 2013) or omitting one study each time from included studies, and the pooled result was still robust (**Supplementary Figure 1**). Meanwhile, no significant publication bias was evidenced by visual inspection of funnel plot (**Figure 4**) and Egger's test (**Supplementary Table 1**) for the effect of glucocorticoid administration on PNDs.

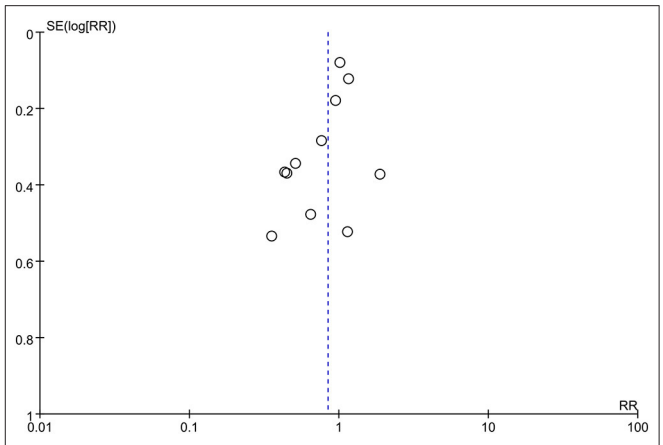

FIGURE 4 | Funnel plot of the primary outcome (the incidence of PNDs).

Similarly, the finding was consistent in subgroup analyses between postoperative delirium (RR: 0.78, 95% CI: 0.61 to 1.01, $P = 0.05$, $I^2 = 44\%$) and POCD (RR: 1.00, 95% CI: 0.51 to 1.96, $P = 1.00$, $I^2 = 77\%$) (**Figure 5**), between dexamethasone (RR: 0.87, 95% CI: 0.59 to 1.27, $P = 0.46$, $I^2 = 65\%$), methylprednisolone (RR: 0.72, 95% CI: 0.47 to 1.09, $P = 0.12$, $I^2 = 65\%$) and hydrocortisone (**Figure 6**). However, subgroup analyses for glucocorticoids dose, surgery type and patient age showed the inconsistent results. There were significant differences in medium dose group (RR: 0.49, 95% CI: 0.33 to 0.73, $P = 0.0005$, $I^2 = 0\%$) (**Supplementary Figure 2**), non-cardiac, non-neurologic surgery group (RR: 0.52, 95% CI: 0.33 to 0.80, $P = 0.003$, $I^2 = 0\%$) (**Supplementary Figure 3**) and mean age ≥70 years group (RR: 0.60, 95% CI: 0.43 to 0.85, $P = 0.004$, $I^2 = 0\%$) (**Supplementary Figure 4**). However, further meta-regressions showed that when glucocorticoids type, surgery type, patient age, and their interactions were entered as covariates in models, there were no significant differences between glucocorticoid group and placebo group on the incidence of PNDs (**Supplementary Table 2**).

Secondary Outcomes

Of the 11 studies included in this meta-analysis, four studies (Hauer et al., 2012; Mardani and Bigdelian, 2013; Whitlock et al., 2015; Glumac et al., 2017) compared the length of ICU stay between groups and the glucocorticoid group significantly reduced the length stay in ICU (RR: −13.58, 95% CI: −26.37 to −0.80, $P = 0.04$, $I^2 = 86\%$) (**Figure 7**). However, there were no significant differences in postoperative infection [five trials (Mardani and Bigdelian, 2013; Whitlock et al., 2015; Clemmesen et al., 2018; Kluger et al., 2021; Xiang et al., 2022); RR: 0.94, 95%

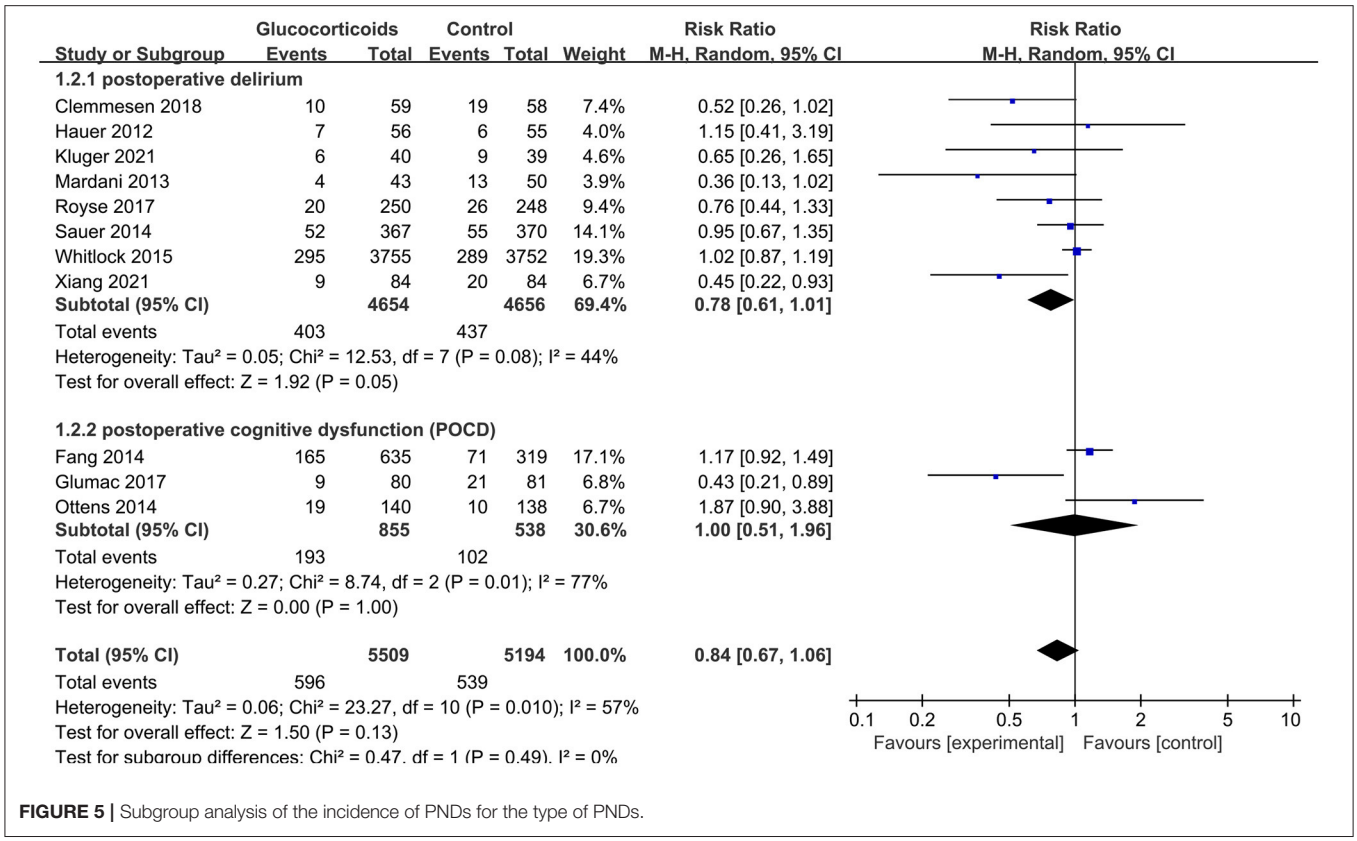

FIGURE 5 | Subgroup analysis of the incidence of PNDs for the type of PNDs.

CI: 0.84 to 1.06, $P = 0.30$, $I^2 = 26\%$] (**Figure 8**), blood glucose level [two trials (Mardani and Bigdelian, 2013; Whitlock et al., 2015); RR: 1.05, 95% CI: −0.09 to 2.19, $P = 0.07$, $I^2 = 61\%$] (**Figure 9**), duration of mechanical ventilation [two trials (Hauer et al., 2012; Glumac et al., 2017); RR: −2.44, 95% CI: −5.47 to 0.59, $P = 0.14$, $I^2 = 0\%$] (**Figure 10**), length of hospital stay [six trials (Mardani and Bigdelian, 2013; Whitlock et al., 2015; Glumac et al., 2017; Clemmesen et al., 2018; Kluger et al., 2021; Xiang et al., 2022); RR: −0.09, 95% CI: −0.27 to 0.09, $P = 0.33$, $I^2 = 11\%$] (**Figure 11**) and 30-day mortality [four trials (Whitlock et al., 2015; Clemmesen et al., 2018; Kluger et al., 2021; Xiang et al., 2022); RR: 0.86, 95% CI: 0.70 to 1.06, $P = 0.16$, $I^2 = 0\%$] (**Figure 12**).

Level of Certainty for Outcomes (GRADE)

Basing on GRADE framework, we evaluated the level of certainty for our main outcomes. The quality of these outcomes varied from low to moderate and the detailed information were shown in **Table 2**.

DISCUSSION

This meta-analysis suggests that perioperative glucocorticoids administration does not reduce the incidence of PNDs. Subgroup analyses and meta-regressions considering potential variables such as PNDs type, glucocorticoids type, dose, surgery type and patient age remained no difference in the outcome. Besides, glucocorticoids infusion was associated with a shorter length of ICU stay, while the incidence of postoperative infection, blood glucose level, duration of mechanical ventilation, length of hospital stay, and 30-day mortality did not differ significantly between groups.

Neuroinflammation has become a key hallmark of neurological complications including PNDs (Subramaniyan and Terrando, 2019). Perioperative glucocorticoid administration has been used in different surgical settings to counter the detrimental effect of inflammation induced by surgery and anesthesia (Awada et al., 2022). Several studies have shown that the preoperative administration of glucocorticoids reduces peripheral inflammatory markers in hepatic surgery (Orci et al., 2013; Richardson et al., 2014). However, the effect of glucocorticoids on PNDs was not observed despite pooling data for more than 10,000 randomized participants, with overall low risk of bias across studies in our review. Several reasons may account for this result. First, although excessive neuroinflammation leads to injury and death of neural elements, a large body of literatures have demonstrated that proper neuroinflammatory response can benefit outcomes of central nerve system (Yong et al., 2019). For example, neuroinflammation can promote neurogenesis (Ziv et al., 2006), facilitate axonal regeneration (David et al., 1990), and is critical for remyelination (Goldstein et al., 2016). It's crucial to suppress the excessive inflammation that mediates damage without

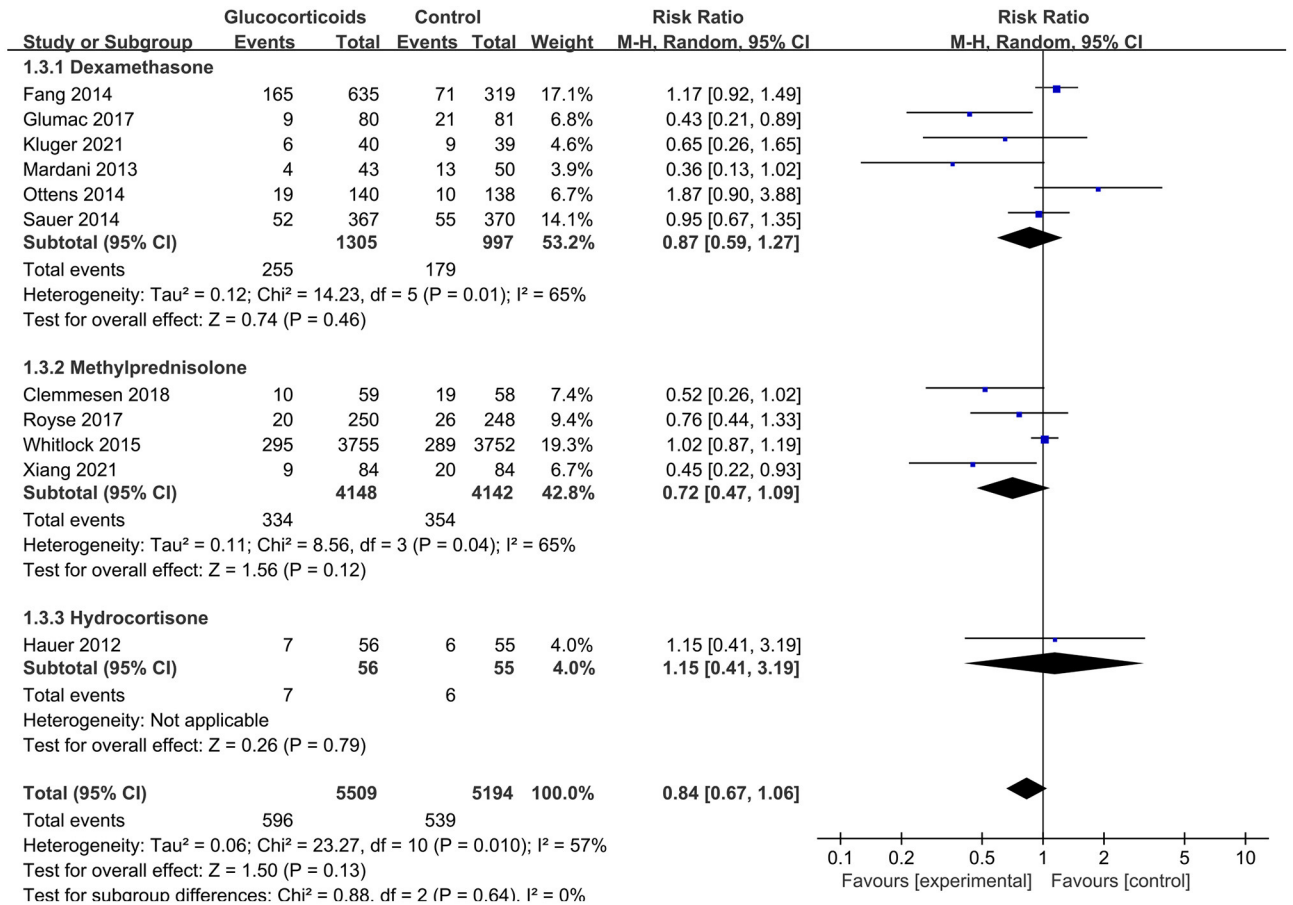

FIGURE 6 | Subgroup analysis of the incidence of PNDs for the type of glucocorticoids.

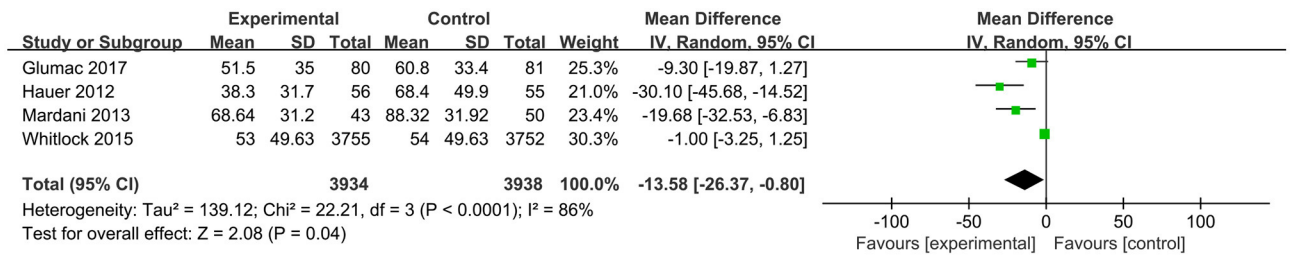

FIGURE 7 | Forest plot of length of ICU stay.

inhibiting the repairment effect from preventing PNDs. Second, the genesis of PNDs is multifactorial that other factors except for neuroinflammation may play great roles in the development of neurocognitive deficit (Siddiqi et al., 2016). Third, prolonged exposure to high concentrations of glucocorticoids can be toxic to neural structures, especially the glucocorticoid receptor–rich hippocampus (Sapolsky, 2000).

To explore sources of heterogeneity, we performed subgroup analyses based on PNDs type and glucocorticoids type, and the outcome remained no difference. Although subgroup analyses about glucocorticoids dose, surgery type and patient age seemed significantly different, meta-regressions were further conducted to understand the interactions between these variables on our outcomes and the results changed to no difference. Here what should be noted was that the subgroup of age was classified according to the mean age values in studies, which might induce some misclassification of accurate age. In general, these secondary analyses suggest that the genesis of PNDs is multifactorial that only administration of glucocorticoids may not significantly reduce the incidence of neurocognitive

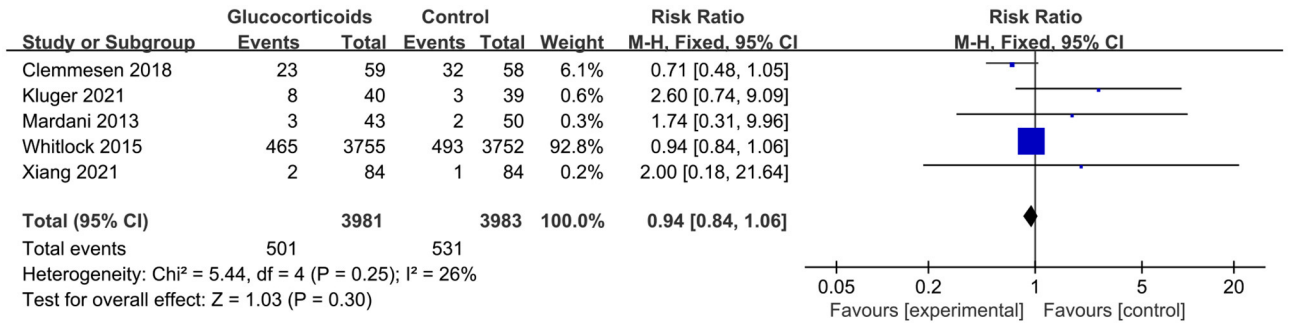

FIGURE 8 | Forest plot of postoperative injection.

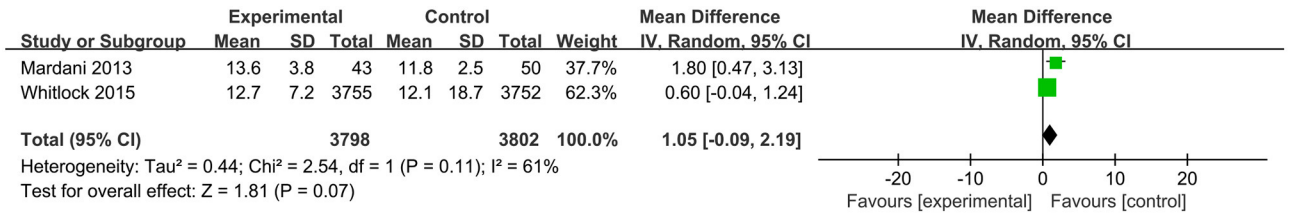

FIGURE 9 | Forest plot of postoperative blood glucose level.

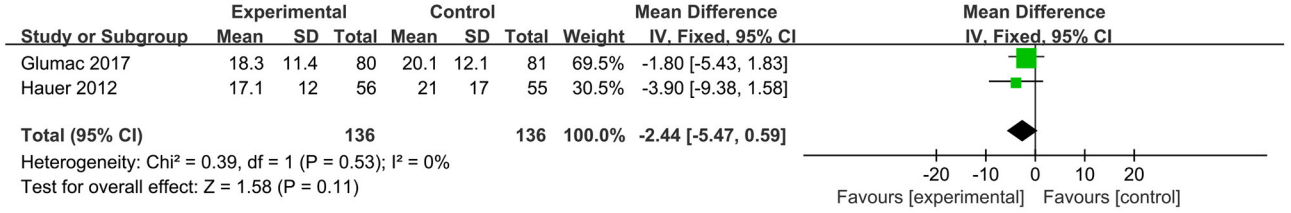

FIGURE 10 | Forest plot of duration of mechanical ventilation.

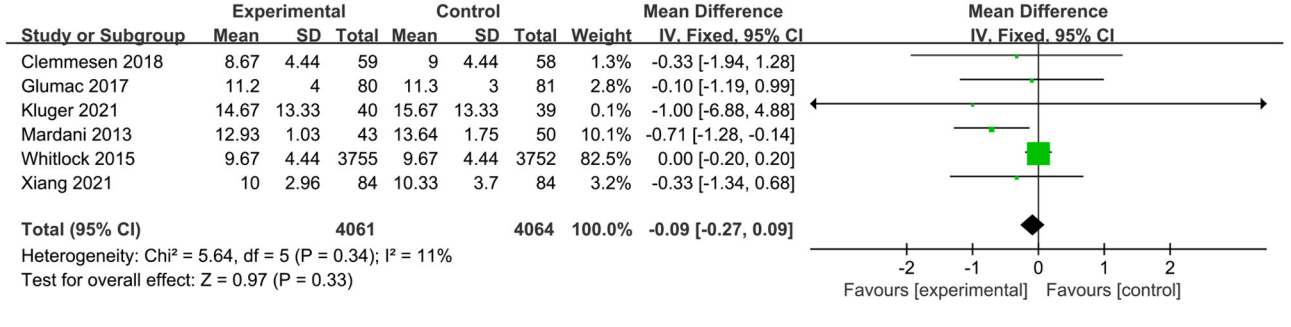

FIGURE 11 | Forest plot of length of hospital stay.

disorders after surgery. Besides, the impact of patient, surgery, or other variables, both measured and unmeasured, on the PNDs development likely far outweighs the impact of glucocorticoids.

PNDs is a summarized term encompassing postoperative delirium, a most pronounced and acute postoperative form, and POCD which is described as a long-term neurocognitive impairment (Evered et al., 2018). Delirium and POCD previously were considered distinct entities, but recent data has suggested an underlying relationship between them (Olotu, 2020). Several risk factors are common to both postoperative delirium and POCD,

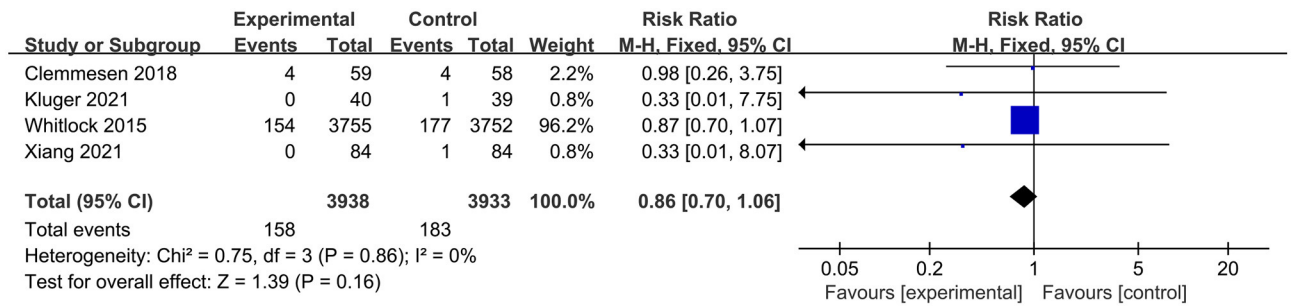

FIGURE 12 | Forest plot of postoperative 30-day mortality.

TABLE 2 | GRADE evidence for main outcomes.

Outcomes (N RCTs)	Risk of bias	Inconsistency	Indirectness	Imprecision	Publication bias	Quality
PNDs (11)	Not serious	No serious	Not serious	Serious[b]	Not detected	Moderate
Infection (5)	Not serious	Not serious	Not serious	Not serious	Strongly suspected[f]	Moderate
Blood glucose level (2)	Not serious	Not serious	Not serious	Serious[c]	Strongly suspected[f]	Low
Duration of mechanical ventilation (2)	Not serious	Not serious	Not serious	Serious[d]	Strongly suspected[f]	Low
Length of ICU stay (4)	Not serious	Serious[a]	Not serious	Not serious	Strongly suspected[f]	Low
Length of hospital stay (6)	Not serious	Not serious	Not serious	Not serious	Strongly suspected[f]	Moderate
30-day mortality (4)	Not serious	Not serious	Not serious	Serious[e]	Not detected	Moderate

PNDs, postoperative neurocognitive disorders.

[a] *Inconsistency due to significant statistical heterogeneity.*

[b] *Confidence intervals range from showing reduced incidence of PNDs associated with use of glucocorticoids to showing no clinically significant difference.*

[c] *Confidence intervals range from showing increased blood glucose level associated with use of glucocorticoids to showing no clinically significant difference.*

[d] *The number of patients included in this outcome was less than the optimal information size (OIS).*

[e] *Confidence intervals range from showing decreased 30-day mortality associated with use of glucocorticoids to showing no clinically significant difference.*

[f] *Publication bias was suspected because the outcomes in the Dexamethasone for Cardiac Surgery (DECS) trial (Dieleman et al., 2012) were different and not included here.*

and animal studies raise the possibility that neuroinflammation may play a role in both of these states (Berger et al., 2018; Devinney et al., 2018; Daiello et al., 2019). Therefore, in this meta-analysis we choose PNDs as the endpoint which in other words, combining postoperative delirium and POCD in the composite outcome, is acceptable from perspective of pathogenesis.

The diagnosis of PNDs, especially POCD, is complex requiring neuropsychological tests which are varied in studies. A recent systematic review noted that in 274 existing studies of POCD, diagnosis was based on 259 different cognitive assessment tools (Borchers et al., 2021). Moreover, neuropsychological tests have been undertaken at variable time intervals after anesthesia and surgery. In 2018, Evered et al. (2018) clarified that postoperative delirium was defined as occurring in hospital and up to 1 week post-procedure or until discharge, while POCD persisted for more than 30 days but <12 months following anesthesia and surgery. However, in trials included in this meta-analysis, Fang et al. (2014) and Glumac et al. (2017) examined POCD in postoperative day 5 and 6, respectively, in which delirium is usually to be assessed; while only Ottens et al. (2014) examined POCD at 1 month after surgery. In summary, heterogeneities of assessment tools, diagnostic criteria, and follow-up time limit the interpretation of existing data surrounding PNDs. Besides, there were only three studies (Fang et al., 2014; Ottens et al., 2014; Glumac et al., 2017) examining POCD in our meta-analysis, and two of them (Fang et al., 2014; Glumac et al., 2017) assessing this entity in the early postoperative day. Thus, the effect of glucocorticoids on long-term PNDs is still unclear. PNDs is associated with long-term sequelae including ongoing impaired cognition, increased risk of dementia, increased mortality, and premature retirement from work (Steinmetz et al., 2009). Interventions to mitigate these sequelae may therefore provide clinical and economic benefit in the long run. Further trials are needed to assess POCD using uniform criteria and validated diagnostic tools and then evaluate the effects of glucocorticoids on the incidence of long-term PNDs.

In our meta-analysis, glucocorticoids significantly reduced the length of ICU stay. However, there were only four studies examining this outcome with high heterogeneity. Besides, it is still obscure whether administration of glucocorticoids could impact the risk of postoperative infection, blood glucose level, length of hospital stay, duration of mechanical ventilation, and 30-day mortality. In the Dexamethasone for Cardiac Surgery (DECS) trial, Dieleman et al. (2012) reported that intraoperative administration of dexamethasone for cardiac surgery was associated with higher postoperative glucose level, lower infection rate, decreased duration of mechanical ventilation, and reduced length of hospital stay. Because of high heterogeneity

and limited studies in this meta-analysis, future high-quality researches are still needed to confirm these outcomes.

To our knowledge, this is the first systematic review and meta-analysis to comprehensively evaluate effects of glucocorticoids on PNDs. A meta-analysis by Li et al. (2019) studied effects of dexamethasone on postoperative cognitive dysfunction and delirium in adults following general anesthesia, which did not take other types of glucocorticoids into consideration. Another systematic review and meta-analysis performed by Liu et al. (2021) was about effects of glucocorticoids on postoperative delirium in adult patients undergoing cardiac surgery. Similarly, POCD, another form of PNDs mentioned above, and non-cardiac surgery patients were not included in this study. In our review, we thought through PNDs type, glucocorticoids type, and surgery type to make conclusions as rigorous as possible.

There are still several potential limitations in this meta-analysis. First, we studied three types of glucocorticoids and two types of PNDs in cardiac, neurologic, and non-cardiac non-neurologic surgery, so there was potential heterogeneity such as methods of diagnosis and dosages of glucocorticoids, which may affect the precision and reliability of the results. Second, most of these included studies excluded patients with pre-existing cognitive impairment, and children were also excluded from this meta-analysis. Therefore, the extrapolation of this meta-analysis was limited. Third, some studies that contained our interested second outcomes, but not PNDs data, were excluded, thus influencing this meta-analysis's completeness of secondary outcomes. Further, more structured and standardized perioperative glucocorticoids protocols and uniform definition and assessment tools of PNDs may be necessary to accurately evaluate the effect of glucocorticoids on PNDs.

CONCLUSION

In summary, our findings suggest that perioperative administration of glucocorticoids does not reduce the incidence of PNDs, regardless of PNDs type, glucocorticoids type, dose, surgery type and patient age. The effect of glucocorticoids on decreased length of ICU stay needs further researches. Future high-quality trials using acknowledged criteria and validated diagnostic tools are needed to determine the influence of glucocorticoids on long-term PNDs.

DATA AVAILABILITY STATEMENT

The original contributions presented in the study are included in the article/**Supplementary Material**, further inquiries can be directed to the corresponding author/s.

AUTHOR CONTRIBUTIONS

XX and RG wrote the manuscript and collected the data. XX, RG, TZ, and CC chose the topic. HC, XZ, and XC contributed to the conception. CZ and CL searched the literature. XX, RG, HC, XZ, and XC analyzed the data. TZ and CC made final decisions. All authors have read and approved the final manuscript.

FUNDING

This work was supported by the National Natural Science Foundation of China (Nos. 82171185 and 81870858 to CC); The National Key R&D Program of China (No. 2018YFC2001800 to TZ) and the National Natural Science Foundation of China (No. 81671062 to TZ); China Postdoctoral Science Foundation (Grant No. 2020M673234 to RG), Post-doctoral Research Project, West China Hospital, Sichuan University (Grant No. 2020HXBH022 to RG).

ACKNOWLEDGMENTS

We thank the authors of the primary studies for providing their data and other critical information. Additionally, we thank all participants for their valuable contributions to this article.

SUPPLEMENTARY MATERIAL

The Supplementary Material for this article can be found online at: https://www.frontiersin.org/articles/10.3389/fnagi.2022.939848/full#supplementary-material

Supplementary Material | Search strategy.

Supplementary Figure 1 | Sensitivity analysis of the incidence of PNDs by excluding each study individually.

Supplementary Figure 2 | Subgroup analysis of the incidence of PNDs for the dose of glucocorticoids.

Supplementary Figure 3 | Subgroup analysis of the incidence of PNDs for the type of surgery.

Supplementary Figure 4 | Subgroup analysis of the incidence of PNDs based on age classification.

Supplementary Table 1 | Tests for publication bias.

Supplementary Table 2 | Meta-regressions for the incidence of PNDs.

REFERENCES

American Geriatrics Society Expert Panel on Postoperative Delirium in Older Adults (2015). Postoperative delirium in older adults: best practice statement from the American Geriatrics Society. *J. Am. Coll. Surg.* 220, 136–148.e131. doi: 10.1016/j.jamcollsurg.2014.10.019

Awada, H. N., Steinthorsdottir, K. J., Schultz, N. A., Hillings,ø, J. G., Larsen, P. N., Jans, Ø., et al. (2022). High-dose preoperative glucocorticoid for prevention of emergence and postoperative delirium in liver resection: a double-blinded randomized clinical trial substudy. *Acta Anaesthesiol. Scand.* doi: 10.1111/aas.14057. [Epub ahead of print].

Balusu, S., Van Wonterghem, E., De Rycke, R., Raemdonck, K., Stremersch, S., Gevaert, K., et al. (2016). Identification of a novel mechanism of blood-brain communication during peripheral inflammation via choroid plexus-derived extracellular vesicles. *EMBO Mol. Med.* 8, 1162–1183. doi: 10.15252/emmm.201606271

Berger, M., Terrando, N., Smith, S. K., Browndyke, J. N., Newman, M. F., and Mathew, J. P. (2018). Neurocognitive function after cardiac surgery: from phenotypes to mechanisms. *Anesthesiology* 129, 829–851. doi: 10.1097/aln.0000000000002194

Boone, M. D., Sites, B., von Recklinghausen, F. M., Mueller, A., Taenzer, A. H., and Shaefi, S. (2020). Economic burden of postoperative neurocognitive disorders among US medicare patients. *JAMA Netw. Open* 3, e208931. doi: 10.1001/jamanetworkopen.2020.8931

Borchers, F., Spies, C. D., Feinkohl, I., Brockhaus, W. R., Kraft, A., Kozma, P., et al. (2021). Methodology of measuring postoperative cognitive dysfunction: a systematic review. *Br. J. Anaesth.* 126, 1119–1127. doi: 10.1016/j.bja.2021.01.035

Clemmesen, C. G., Lunn, T. H., Kristensen, M. T., Palm, H., and Foss, N. B. (2018). Effect of a single pre-operative 125 mg dose of methylprednisolone on postoperative delirium in hip fracture patients; a randomised, double-blind, placebo-controlled trial. *Anaesthesia* 73, 1353–1360. doi: 10.1111/anae.14406

Czock, D., Keller, F., Rasche, F. M., and Häussler, U. (2005). Pharmacokinetics and pharmacodynamics of systemically administered glucocorticoids. *Clin. Pharmacokinet.* 44, 61–98. doi: 10.2165/00003088-200544010-00003

Daiello, L. A., Racine, A. M., Yun Gou, R., Marcantonio, E. R., Xie, Z., Kunze, L. J., et al. (2019). Postoperative delirium and postoperative cognitive dysfunction: overlap and divergence. *Anesthesiology* 131, 477–491. doi: 10.1097/aln.0000000000002729

David, S., Bouchard, C., Tsatas, O., and Giftochristos, N. (1990). Macrophages can modify the nonpermissive nature of the adult mammalian central nervous system. *Neuron* 5, 463–469. doi: 10.1016/0896-6273(90)90085-t

Deemer, K., Zjadewicz, K., Fiest, K., Oviatt, S., Parsons, M., Myhre, B., et al. (2020). Effect of early cognitive interventions on delirium in critically ill patients: a systematic review. *Can. J. Anaesth.* 67, 1016–1034. doi: 10.1007/s12630-020-01670-z

Deiner, S., Fleisher, L. A., Leung, J. M., Peden, C., Miller, T., and Neuman, M. D. (2020). Adherence to recommended practices for perioperative anesthesia care for older adults among US anesthesiologists: results from the ASA Committee on Geriatric Anesthesia-Perioperative Brain Health Initiative ASA member survey. *Perioper. Med.* 9, 6. doi: 10.1186/s13741-020-0136-9

Devinney, M. J., Mathew, J. P., and Berger, M. (2018). Postoperative delirium and postoperative cognitive dysfunction: two sides of the same coin? *Anesthesiology* 129, 389–391. doi: 10.1097/aln.0000000000002338

Dieleman, J. M., Nierich, A. P., Rosseel, P. M., van der Maaten, J. M., Hofland, J., Diephuis, J. C., et al. (2012). Intraoperative high-dose dexamethasone for cardiac surgery: a randomized controlled trial. *JAMA* 308, 1761–1767. doi: 10.1001/jama.2012.14144

Evered, L., Silbert, B., Knopman, D. S., Scott, D. A., DeKosky, S. T., Rasmussen, L. S., et al. (2018). Recommendations for the nomenclature of cognitive change associated with anaesthesia and surgery-2018. *Br. J. Anaesth.* 121, 1005–1012. doi: 10.1016/j.bja.2017.11.087

Evered, L. A., Vitug, S., Scott, D. A., and Silbert, B. (2020). Preoperative frailty predicts postoperative neurocognitive disorders after total hip joint replacement surgery. *Anesth. Analg.* 131, 1582–1588. doi: 10.1213/ane.0000000000004893

Fan, D., Li, J., Zheng, B., Hua, L., and Zuo, Z. (2016). Enriched environment attenuates surgery-induced impairment of learning, memory, and neurogenesis possibly by preserving BDNF expression. *Mol. Neurobiol.* 53, 344–354. doi: 10.1007/s12035-014-9013-1

Fang, Q., Qian, X., An, J., Wen, H., Cope, D. K., and Williams, J. P. (2014). Higher dose dexamethasone increases early postoperative cognitive dysfunction. *J. Neurosurg. Anesthesiol.* 26, 220–225. doi: 10.1097/ana.0000000000000024

Gille, J., Reisinger, K., Westphal-Varghese, B., and Kaufmann, R. (2001). Decreased mRNA stability as a mechanism of glucocorticoid-mediated inhibition of vascular endothelial growth factor gene expression by cultured keratinocytes. *J. Invest. Dermatol.* 117, 1581–1587. doi: 10.1046/j.0022-202x.2001.01573.x

Glumac, S., Kardum, G., Sodic, L., Supe-Domic, D., and Karanovic, N. (2017). Effects of dexamethasone on early cognitive decline after cardiac surgery: a randomised controlled trial. *Eur. J. Anaesthesiol.* 34, 776–784. doi: 10.1097/eja.0000000000000647

Goldstein, E. Z., Church, J. S., Hesp, Z. C., Popovich, P. G., and McTigue, D. M. (2016). A silver lining of neuroinflammation: Beneficial effects on myelination. *Exp. Neurol.* 283(Pt B), 550–559. doi: 10.1016/j.expneurol.2016.05.001

Hafezi-Moghadam, A., Simoncini, T., Yang, Z., Limbourg, F. P., Plumier, J. C., Rebsamen, M. C., et al. (2002). Acute cardiovascular protective effects of corticosteroids are mediated by non-transcriptional activation of endothelial nitric oxide synthase. *Nat. Med.* 8, 473–479. doi: 10.1038/nm0502-473

Hauer, D., Weis, F., Campolongo, P., Schopp, M., Beiras-Fernandez, A., Strewe, C., et al. (2012). Glucocorticoid-endocannabinoid interaction in cardiac surgical patients: relationship to early cognitive dysfunction and late depression. *Rev. Neurosci.* 23, 681–690. doi: 10.1515/revneuro-2012-0058

Holte, K., and Kehlet, H. (2002). Perioperative single-dose glucocorticoid administration: pathophysiologic effects and clinical implications. *J. Am. Coll. Surg.* 195, 694–712. doi: 10.1016/s1072-7515(02)01491-6

Humeidan, M. L., Reyes, J. C., Mavarez-Martinez, A., Roeth, C., Nguyen, C. M., Sheridan, E., et al. (2021). Effect of cognitive prehabilitation on the incidence of postoperative delirium among older adults undergoing major noncardiac surgery: the neurobics randomized clinical trial. *JAMA Surg.* 156, 148–156. doi: 10.1001/jamasurg.2020.4371

Inouye, S. K., Westendorp, R. G., and Saczynski, J. S. (2014). Delirium in elderly people. *Lancet* 383, 911–922. doi: 10.1016/s0140-6736(13)60688-1

Kluger, M. T., Skarin, M., Collier, J., Rice, D. A., McNair, P. J., Seow, M. Y., et al. (2021). Steroids to reduce the impact on delirium (STRIDE): a double-blind, randomised, placebo-controlled feasibility trial of pre-operative dexamethasone in people with hip fracture. *Anaesthesia* 76, 1031–1041. doi: 10.1111/anae.15465

Langendam, M. W., Akl, E. A., Dahm, P., Glasziou, P., Guyatt, G., and Schünemann, H. J. (2013). Assessing and presenting summaries of evidence in Cochrane reviews. *Syst. Rev.* 2, 81. doi: 10.1186/2046-4053-2-81

Lasa, M., Abraham, S. M., Boucheron, C., Saklatvala, J., and Clark, A. R. (2002). Dexamethasone causes sustained expression of mitogen-activated protein kinase (MAPK) phosphatase 1 and phosphatase-mediated inhibition of MAPK p38. *Mol. Cell. Biol.* 22, 7802–7811. doi: 10.1128/mcb.22.22.7802-7811.2002

Lee, C., Lee, C. H., Lee, G., Lee, M., and Hwang, J. (2018). The effect of the timing and dose of dexmedetomidine on postoperative delirium in elderly patients after laparoscopic major non-cardiac surgery: a double blind randomized controlled study. *J. Clin. Anesth.* 47, 27–32. doi: 10.1016/j.jclinane.2018.03.007

Li, L. Q., Wang, C., Fang, M. D., Xu, H. Y., Lu, H. L., and Zhang, H. Z. (2019). Effects of dexamethasone on post-operative cognitive dysfunction and delirium in adults following general anaesthesia: a meta-analysis of randomised controlled trials. *BMC Anesthesiol.* 19:113. doi: 10.1186/s12871-019-0783-x

Likhvantsev, V. V., Landoni, G., Grebenchikov, O. A., Ovezov, A. M., Skripkin, Y. V., Lembo, R., et al. (2021). Perioperative dexmedetomidine supplement decreases delirium incidence after adult cardiac surgery: a randomized, double-blind, controlled study. *J. Cardiothorac. Vasc. Anesth.* 35, 449–457. doi: 10.1053/j.jvca.2020.02.035

Lim, A., Krajina, K., and Marsland, A. L. (2013). Peripheral inflammation and cognitive aging. *Mod Trends Pharmacopsychiatry* 28, 175–187. doi: 10.1159/000346362

Liu, W., Wang, Y., Wang, J., Shi, J., Pan, J., and Wang, D. (2021). Effects of glucocorticoids on postoperative delirium in adult patients undergoing cardiac surgery: a systematic review and meta-analysis. *Clin. Ther.* 43, 1608–1621. doi: 10.1016/j.clinthera.2021.07.021

Liu, Y., and Yin, Y. (2018). Emerging roles of immune cells in postoperative cognitive dysfunction. *Mediators Inflamm.* 2018, 6215350. doi: 10.1155/2018/6215350

Lunn, T. H., and Kehlet, H. (2013). Perioperative glucocorticoids in hip and knee surgery – benefit vs. harm? A review of randomized clinical trials. *Acta Anaesthesiol. Scand.* 57, 823–834. doi: 10.1111/aas.12115

Luo, A., Yan, J., Tang, X., Zhao, Y., Zhou, B., and Li, S. (2019). Postoperative cognitive dysfunction in the aged: the collision of neuroinflammaging with perioperative neuroinflammation. *Inflammopharmacology* 27, 27–37. doi: 10.1007/s10787-018-00559-0

Mahanna-Gabrielli, E., Schenning, K. J., Eriksson, L. I., Browndyke, J. N., Wright, C. B., Culley, D. J., et al. (2019). State of the clinical science of perioperative brain health: report from the American Society of Anesthesiologists Brain Health Initiative Summit 2018. *Br. J. Anaesth.* 123, 464–478. doi: 10.1016/j.bja.2019.07.004

Mardani, D., and Bigdelian, H. (2013). Prophylaxis of dexamethasone protects patients from further post-operative delirium after cardiac surgery: a randomized trial. *J. Res. Med. Sci.* 18, 137–143.

Melsen, W. G., Bootsma, M. C., Rovers, M. M., and Bonten, M. J. (2014). The effects of clinical and statistical heterogeneity on the predictive values of results from meta-analyses. *Clin. Microbiol. Infect.* 20, 123–129. doi: 10.1111/1469-0691.12494

Monk, T. G., Weldon, B. C., Garvan, C. W., Dede, D. E., van der Aa, M. T., Heilman, K. M., et al. (2008). Predictors of cognitive dysfunction after major noncardiac surgery. *Anesthesiology* 108, 18–30. doi: 10.1097/01.anes.0000296071.19434.1e

Netto, M. B., de Oliveira Junior, A. N., Goldim, M., Mathias, K., Fileti, M. E., da Rosa, N., et al. (2018). Oxidative stress and mitochondrial dysfunction contributes to postoperative cognitive dysfunction in elderly rats. *Brain Behav. Immun.* 73, 661–669. doi: 10.1016/j.bbi.2018.07.016

Noll, F., Behnke, J., Leiting, S., Troidl, K., Alves, G. T., Müller-Redetzky, H., et al. (2017). Self-extracellular RNA acts in synergy with exogenous danger signals to promote inflammation. *PLoS ONE* 12:e0190002. doi: 10.1371/journal.pone.0190002

O'Gara, B. P., Gao, L., Marcantonio, E. R., and Subramaniam, B. (2021). Sleep, pain, and cognition: modifiable targets for optimal perioperative brain health. *Anesthesiology* 135, 1132–1152. doi: 10.1097/aln.0000000000004046

Olotu, C. (2020). Postoperative neurocognitive disorders. *Curr. Opin. Anaesthesiol.* 33, 101–108. doi: 10.1097/aco.0000000000000812

Orci, L. A., Toso, C., Mentha, G., Morel, P., and Majno, P. E. (2013). Systematic review and meta-analysis of the effect of perioperative steroids on ischaemia-reperfusion injury and surgical stress response in patients undergoing liver resection. *Br. J. Surg.* 100, 600–609. doi: 10.1002/bjs.9035

Ottens, T. H., Dieleman, J. M., Sauër, A. M., Peelen, L. M., Nierich, A. P., de Groot, W. J., et al. (2014). Effects of dexamethasone on cognitive decline after cardiac surgery: a randomized clinical trial. *Anesthesiology* 121, 492–500. doi: 10.1097/aln.0000000000000336

Page, M. J., Moher, D., Bossuyt, P. M., Boutron, I., Hoffmann, T. C., Mulrow, C. D., et al. (2021). PRISMA 2020 explanation and elaboration: updated guidance and exemplars for reporting systematic reviews. *BMJ* 372, n160. doi: 10.1136/bmj.n160

Qiao, Y., Feng, H., Zhao, T., Yan, H., Zhang, H., and Zhao, X. (2015). Postoperative cognitive dysfunction after inhalational anesthesia in elderly patients undergoing major surgery: the influence of anesthetic technique, cerebral injury and systemic inflammation. *BMC Anesthesiol.* 15:154. doi: 10.1186/s12871-015-0130-9

Rhen, T., and Cidlowski, J. A. (2005). Antiinflammatory action of glucocorticoids–new mechanisms for old drugs. *N. Engl. J. Med.* 353, 1711–1723. doi: 10.1056/NEJMra050541

Richardson, A. J., Laurence, J. M., and Lam, V. W. (2014). Use of pre-operative steroids in liver resection: a systematic review and meta-analysis. *HPB* 16, 12–19. doi: 10.1111/hpb.12066

Royse, C. F., Saager, L., Whitlock, R., Ou-Young, J., Royse, A., Vincent, J., et al. (2017). Impact of methylprednisolone on postoperative quality of recovery and delirium in the steroids in cardiac surgery trial: a randomized, double-blind, placebo-controlled substudy. *Anesthesiology* 126, 223–233. doi: 10.1097/aln.0000000000001433

Saklatvala, J., Dean, J., and Clark, A. (2003). Control of the expression of inflammatory response genes. *Biochem. Soc. Symp.* 70, 95–106. doi: 10.1042/bss0700095

Sanders, R. D., Wehrman, J., Irons, J., Dieleman, J., Scott, D., and Shehabi, Y. (2021). Meta-analysis of randomised controlled trials of perioperative dexmedetomidine to reduce delirium and mortality after cardiac surgery. *Br. J. Anaesth.* 127, e168–e170. doi: 10.1016/j.bja.2021.08.009

Sapolsky, R. M. (2000). Glucocorticoids and hippocampal atrophy in neuropsychiatric disorders. *Arch. Gen. Psychiatry* 57, 925–935. doi: 10.1001/archpsyc.57.10.925

Sauër, A. M., Slooter, A. J., Veldhuijzen, D. S., van Eijk, M. M., Devlin, J. W., and van Dijk, D. (2014). Intraoperative dexamethasone and delirium after cardiac surgery: a randomized clinical trial. *Anesth Analg* 119, 1046–1052. doi: 10.1213/ane.0000000000000248

Shi, H., Du, X., Wu, F., Hu, Y., Xv, Z., and Mi, W. (2020). Dexmedetomidine improves early postoperative neurocognitive disorder in elderly male patients undergoing thoracoscopic lobectomy. *Exp. Ther. Med.* 20, 3868–3877. doi: 10.3892/etm.2020.9113

Siddiqi, N., Harrison, J. K., Clegg, A., Teale, E. A., Young, J., Taylor, J., et al. (2016). Interventions for preventing delirium in hospitalised non-ICU patients. *Cochrane Database Syst. Rev.* 3, Cd005563. doi: 10.1002/14651858.CD005563.pub3

Steinmetz, J., Christensen, K. B., Lund, T., Lohse, N., and Rasmussen, L. S. (2009). Long-term consequences of postoperative cognitive dysfunction. *Anesthesiology* 110, 548–555. doi: 10.1097/ALN.0b013e318195b569

Sterne, J. A. C., Savović, J., Page, M. J., Elbers, R. G., Blencowe, N. S., Boutron, I., et al. (2019). RoB 2: a revised tool for assessing risk of bias in randomised trials. *BMJ* 366, l4898. doi: 10.1136/bmj.l4898

Subramaniyan, S., and Terrando, N. (2019). Neuroinflammation and perioperative neurocognitive disorders. *Anesth. Analg.* 128, 781–788. doi: 10.1213/ane.0000000000004053

Vacas, S., Cole, D. J., and Cannesson, M. (2021). Cognitive decline associated with anesthesia and surgery in older patients. *JAMA*. doi: 10.1001/jama.2021.4773. [Epub ahead of print].

Valentin, L. S., Pereira, V. F., Pietrobon, R. S., Schmidt, A. P., Oses, J. P., Portela, L. V., et al. (2016). Effects of single low dose of dexamethasone before noncardiac and nonneurologic surgery and general anesthesia on postoperative cognitive dysfunction – a phase III double blind, randomized clinical trial. *PLoS ONE* 11:e0152308. doi: 10.1371/journal.pone.0152308

Vlisides, P. E., Das, A. R., Thompson, A. M., Kunkler, B., Zierau, M., Cantley, M. J., et al. (2019). Home-based cognitive prehabilitation in older surgical patients: a feasibility study. *J. Neurosurg. Anesthesiol.* 31, 212–217. doi: 10.1097/ana.0000000000000569

Wang, Y. Y., Yue, J. R., Xie, D. M., Carter, P., Li, Q. L., Gartaganis, S. L., et al. (2020). Effect of the tailored, family-involved hospital elder life program on postoperative delirium and function in older adults: a randomized clinical trial. *JAMA Intern. Med.* 180, 17–25. doi: 10.1001/jamainternmed.2019.4446

Wei, P., Yang, F., Zheng, Q., Tang, W., and Li, J. (2019). The potential role of the NLRP3 inflammasome activation as a link between mitochondria ROS generation and neuroinflammation in postoperative cognitive dysfunction. *Front. Cell. Neurosci.* 13:73. doi: 10.3389/fncel.2019.00073

Whitlock, R. P., Devereaux, P. J., Teoh, K. H., Lamy, A., Vincent, J., Pogue, J., et al. (2015). Methylprednisolone in patients undergoing cardiopulmonary bypass (SIRS): a randomised, double-blind, placebo-controlled trial. *Lancet* 386, 1243–1253. doi: 10.1016/s0140-6736(15)00273-1

Wu, M., Liang, Y., Dai, Z., and Wang, S. (2018). Perioperative dexmedetomidine reduces delirium after cardiac surgery: a meta-analysis of randomized controlled trials. *J. Clin. Anesth.* 50, 33–42. doi: 10.1016/j.jclinane.2018.06.045

Xiang, X. B., Chen, H., Wu, Y. L., Wang, K., Yue, X., and Cheng, X. Q. (2022). The effect of preoperative methylprednisolone on postoperative delirium in older patients undergoing gastrointestinal surgery: a randomized, double-blind, placebo-controlled trial. *J. Gerontol. A Biol. Sci. Med. Sci.* 77, 517–523. doi: 10.1093/gerona/glab248

Xiao, J. Y., Xiong, B. R., Zhang, W., Zhou, W. C., Yang, H., Gao, F., et al. (2018). PGE2-EP3 signaling exacerbates hippocampus-dependent cognitive impairment after laparotomy by reducing expression levels of hippocampal synaptic plasticity-related proteins in aged mice. *CNS Neurosci. Ther.* 24, 917–929. doi: 10.1111/cns.12832

Xie, Z., and Shen, Y. (2018). New biomarkers of postoperative neurocognitive disorders. *Nat. Rev. Neurol.* 14, 320–321. doi: 10.1038/s41582-018-0001-3

Yong, H. Y. F., Rawji, K. S., Ghorbani, S., Xue, M., and Yong, V. W. (2019). The benefits of neuroinflammation for the repair of the injured central nervous system. *Cell. Mol. Immunol.* 16, 540–546. doi: 10.1038/s41423-019-0223-3

Zhao, W., Hu, Y., Chen, H., Wang, X., Wang, L., Wang, Y., et al. (2020). The effect and optimal dosage of dexmedetomidine plus sufentanil for postoperative analgesia in elderly patients with postoperative delirium and early postoperative cognitive dysfunction: a single-center, prospective, randomized, double-blind, controlled trial. *Front. Neurosci.* 14:549516. doi: 10.3389/fnins.2020.549516

Ziv, Y., Ron, N., Butovsky, O., Landa, G., Sudai, E., Greenberg, N., et al. (2006). Immune cells contribute to the maintenance of neurogenesis and spatial learning abilities in adulthood. *Nat. Neurosci.* 9, 268–275. doi: 10.1038/nn1629

Conflict of Interest: The authors declare that the research was conducted in the absence of any commercial or financial relationships that could be construed as a potential conflict of interest.

Publisher's Note: All claims expressed in this article are solely those of the authors and do not necessarily represent those of their affiliated organizations, or those of the publisher, the editors and the reviewers. Any product that may be evaluated in this article, or claim that may be made by its manufacturer, is not guaranteed or endorsed by the publisher.

frontiers | Frontiers in Aging Neuroscience

BRIEF RESEARCH REPORT
published: 30 June 2022
doi: 10.3389/fnagi.2022.918640

The Effect of Sevoflurane Anesthesia on the Biomarkers of Neural Injury in the Prefrontal Cortex of Aged Marmosets

Yanyong Cheng[1†], *Lingling Shi*[1†], *Haoli Mao*[1], *Zhenyu Xue*[1], *Siyu Liu*[1], *Zilong Qiu*[2*], *Lei Zhang*[1*] *and Hong Jiang*[1*]

[1] Department of Anesthesiology, Shanghai Ninth People's Hospital, Shanghai Jiao Tong University School of Medicine, Shanghai, China, [2] State Key Laboratory of Neuroscience, CAS Center for Excellence in Brain Science and Intelligence Technology, Shanghai Center for Brain Science and Brain-Inspired Intelligence Technology, Institute of Neuroscience, Chinese Academy of Sciences, University of Chinese Academy of Sciences, Shanghai, China

OPEN ACCESS

Edited by:
Jiaqiang Zhang,
Zhengzhou University, China

Reviewed by:
Jun Zhang,
Fudan University, China
Hui Zheng,
Chinese Academy of Medical Sciences and Peking Union Medical College, China

***Correspondence:**
Zilong Qiu
zqiu@ion.ac.cn
Lei Zhang
weiymzhl@126.com
Hong Jiang
jianghongjiuyuan@163.com

[†] These authors have contributed equally to this work

Specialty section:
This article was submitted to Neurocognitive Aging and Behavior, a section of the journal Frontiers in Aging Neuroscience

Received: 12 April 2022
Accepted: 16 May 2022
Published: 30 June 2022

Citation:
Cheng Y, Shi L, Mao H, Xue Z, Liu S, Qiu Z, Zhang L and Jiang H (2022) The Effect of Sevoflurane Anesthesia on the Biomarkers of Neural Injury in the Prefrontal Cortex of Aged Marmosets. Front. Aging Neurosci. 14:918640. doi: 10.3389/fnagi.2022.918640

Background: Surgery under general anesthesia leads to neural injury, especially in older patients. Sevoflurane anesthesia without surgery for 2 h does not induce neural injury, however, whether prolonger sevoflurane anesthesia without surgery has the same consequence is still unknown.

Methods: In the present study, aged marmosets were exposed to a clinical concentration of sevoflurane (1.5–2%) for 6 h to access the effects of prolonged sevoflurane anesthesia on the levels of interleukin-6 (IL-6) and tumor necrosis factor-α (TNF-α), Caspase3 activity and myelin formation in the brain.

Results: Sevoflurane anesthesia did not alter the expression of IL-6 (120.1 ± 2.21 vs. 120.8 ± 2.25, $p = 0.74$), TNF-α (189.3 ± 31.35 vs. 218.7 ± 21.47, $p = 0.25$) and Caspase3 (57.35 ± 1.54 vs. 58.67 ± 1.19, $p = 0.53$) in the prefrontal cortex (PFC) of aged marmosets. The amount of MBP expression (60.99 ± 6.21 vs. 58.91 ± 2.71, $p = 0.77$) did not change following sevoflurane exposure.

Conclusion: Sevoflurane anesthesia did not increase the levels of IL-6 and TNF-α, activated the the expression of Caspase3, and induced myelination deficits in the PFC of aged marmosets.

Keywords: general anesthetic, sevoflurane, neural injury, cytokine, primate

INTRODUCTION

The increase of interleukin-6 (IL-6) and tumor necrosis factor-α (TNF-α) during the perioperative period has been associated with postoperative complications and prolonged hospitalization in patients after surgery (O'bryan et al., 2022). However, the contribution of general anesthesia and surgery can hardly be differentiated in clinical settings, as patients receive general anesthesia only when they undergo surgery. In a recent prospective cohort study, 59 elderly volunteers received sevoflurane general anesthesia without surgery for 2 h, and the result showed no increase in

IL-6 and TNF-α in their blood (Deiner et al., 2020). However, due to the more complex disease presentation in the elderly, surgical procedures take longer than in younger people. A previous study revealed that sevoflurane exposure for 5 h in aged rats induced apoptosis of the neurons, which led to learning and memory deficits (Chen et al., 2013). We consider whether IL-6 and TNF-α, as well as other injury markers such as the markers of apoptosis and myelination deficits, are altered in the brain with prolonged sevoflurane general anesthesia. As it is not feasible to take these measurements in the human brain, Marmosets (*Callithrix jacchus*) are increasingly used as an alternative primate model in biomedical research because their genetic and neuroanatomical features are closer to those of humans. However, no study identified the effects of sevoflurane anesthesia on inflammation factors and other neuroinjury markers in aged marmosets.

The activation of neuroinflammation and apoptosis are mutually reinforcing. Recent studies have suggested that the inflammation and apoptosis process were not limited to neurons and that it can also be found in non-neuron cells, such as oligodendrocytes (OLs). The myelin sheath which constructed of OLs was concerned in this study simultaneously.

The present study assessed the effects of acute sevoflurane anesthesia, without surgery, on the amounts of IL-6 and TNF-α as well as the markers of apoptosis (Caspase3) and myelination deficits via Elisa, immunohistochemistry, and transmission electron microscopy in the PFC of aged marmosets.

METHODS AND MATERIALS

Marmoset Anesthesia

The processes of the animal study were performed according to the guidelines of the Animal Care Committee of the Center for Excellence in Brain Science and Intelligence Technology (CEBSIT, China) and were approved by the Institutional Animal Care and Use Committee (Protocol number CEBSIT-2021035). Sexually mature common marmosets aged 18–24 months were purchased from CEBSIT. They were considered to be "aged" when they were >8 years old.

Two male and one female marmoset (6 marmosets in total) were involved in each group (the control and anesthesia group). Efforts were made to minimize the number of marmosets. In consideration of the restricted number of marmosets in this study, we did not take the potential sex difference of the anesthesia in marmosets into account. The marmosets received induction (2–4 min) under 6–8% sevoflurane with 100% oxygen. For the maintenance of general anesthesia, then they received 1.5–2% sevoflurane and 100% oxygen without endotracheal intubation for 6 h. Spontaneous respirations were retained during the general anesthesia.

The temperatures of the marmosets were maintained at 37°C by an animal warming placing system (AHM06, Reptizoo, China). The heart rate, electrocardiograph, respiratory rate, peripheral capillary oxygen saturation (SpO_2), and rectal temperature were monitored by Patient Monitors (BeneVision M12, Mindray, China) (**Supplementary Video**). The arterial blood gas determinations were monitored by cardiac puncture using a portable clinical analyzer (i-STAT; Abbott Laboratories Inc., East Windsor, NJ, USA) at the end of the anesthetic. An infusion of 5 mL stroke-physiological saline solution was applied every 2 h to prevent dehydration.

For the sampling stage, in the control group, marmosets received high concentrations (6–8%) of anesthetic sevoflurane (about 1 min) for quick entering a sufficient depth of anesthesia. Then they were decapitated and under 5% sevoflurane for about 1–2 min. No body movements and reflexes were observed during the execution. Marmosets in the sevoflurane group were decapitated under 3% sevoflurane anesthesia for 5 min with a complete loss of all reflexes. The PFC of all marmosets was harvested.

Elisa

Marmoset brain tissues were lysed using RIPA buffer with a protease inhibitor cocktail. The TNF-α or IL-6 standards were re-suspended by adding 500 μL Sample Diluent NS. It was put at room temperature for 10 min and mixed gently. This is the 5,000 pg/mL Stock Standard Solution. Label eight tubes, Standards 1 to 8. We added 320 μL Sample Diluent NS into tube number 1 and 150 μL of Sample Diluent NS into numbers 2 to 8.

TNF-α and IL-6 ELISA kits were used (# ab252354, ab242233, abcam, USA). We added 50 μL of all samples or standard to appropriate wells and then 50 μL of the Antibody Cocktail to each well. Wells were incubated for 1 h at room temperature on a plate shaker which was set to 400 rpm and washed 3 times by Wash Buffer PT. Wash Buffer PT should remain in wells for at least 10 s. We added 100 μL of TMB Development Solution to each well and incubated it for 20 min in the dark on a plate shaker set to 400 rpm. Then we halted reactions with 100 μL of Stop Solution and shacked for 1 min to mix. We determined the optical density of each well using a Fluorescence Plate Reader (Medical Device, San Jose, CA, USA) at 450 nm. Next, we created a standard curve by plotting the average blank control subtracted absorbance value for each standard concentration (y-axis) against the target protein concentration (x-axis) of the standard. We draw the best smooth curve through these points to construct the standard curve by Graphing software. We determined the concentration of the target protein in the sample by interpolating the blank control subtracted absorbance values against the standard curve. The resulting value was multiplied by the appropriate sample dilution factor to obtain the concentration of the target protein in the sample.

Immunohistochemistry

After prolonged sevoflurane inhalation, marmosets were euthanized and brains were immersed in 4% paraformaldehyde fixed over days. Prefrontal cortex paraffin slices were deparaffinized with xylene and washed with anhydrous ethanol, 95 and 75% alcohol by volume. After being blocked with 10% donkey serum albumen and 0.3% Triton for 2 h, the slices were stained with primary antibodies and secondary antibodies (anti-MBP #NB600-717, 1:200 dilution, Novus Biologicals, USA; anti-Caspase 3 #NB600-1235,1:200 dilution, Novus Biologicals, USA) at 4°C overnight; Goat Anti-Rabbit IgG H&L (#ab150077, 1:1000 dilution, abcam, USA) for 2 h at room temperature. Nuclei were visualized with DAPI and images were taken with

upright fluorescence microscopy (Nikon, Japan). Antibody-positive cells were counted by manual counting. The number of target channels was normalized to DAPI. Three animals for each group and 5 to 7 brain slices from each animal were used. We calculated the number of antibody-positive cells within a certain area (2,500 μm^2) of each slice. Each contained at least 100 cells.

Transmission Electron Microscopy

Marmosets were euthanized and perfused with PBS for preparing tissue samples for transmission electron microscopy. Issues were fixed in 2.5% glutaraldehyde and then postfixed in 1% osmium tetroxide. They were dehydrated and embedded in araldite resin. Ultrathin sections (60 nm) were stained in uranyl acetate and lead citrate. A transmission electron microscope (H-7650, hitachi, Japan) at 80 kV was used.

Statistical Analysis

An unpaired *t*-test was used to compare the mean of the two groups, and $p < 0.05$ were considered statistically significant. We used the software Prism 6 (GraphPad, USA) to evaluate all of the data in the studies.

RESULTS

In the present study, we used marmosets aged 8–9 years to evaluate the contribution of anesthetics to neural injury. Marmosets older than 8 years old were considered aged marmosets (Abbott et al., 2003). The characteristics of the aged marmosets in both the control and sevoflurane anesthesia groups are shown in **Supplementary Table 1**. Several biomarkers of neural injury were documented in this study from various aspects, such as cytokine, the critical enzyme of apoptosis, and indicator of the myelin sheath.

We first assessed the effects of sevoflurane without surgery on the level of IL-6 and TNF-α in the PFC of aged marmosets by ELISA. The result suggested that prolonged sevoflurane anesthesia for 6 h without surgery did not alter the expression of IL-6 (120.1 ± 2.21 vs. 120.8 ± 2.25, $p = 0.74$, **Figure 1A**) and TNF-α (189.3 ± 31.35 vs. 218.7 ± 21.47, $p = 0.25$, **Figure 1B**) in the PFC of aged marmosets.

Secondly, to investigate whether the activation of Caspase3, a critical enzyme of apoptosis, was affected by sevoflurane anesthesia, immunofluorescence was employed to detect the Caspase3 activation in the PFC of aged marmosets. Caspase3 showed no significant changes in protein levels (57.35 ± 1.54 vs. 58.67 ± 1.19, $p = 0.53$, **Figures 1C,D**).

Finally, immunofluorescence staining was used to explore the structure and status of the myelin sheath following sevoflurane anesthesia. The expression level of myelin basic protein (MBP) was insusceptible to the sevoflurane exposure (60.99 ± 6.21 vs. 58.91 ± 2.71, $p = 0.77$, **Figures 1E,F**). The formation of ultrastructure in marmosets' PFC was also illustrated by electron microscopy. Myelin sheath was followed with interest. Although we observed degeneration of the myelin sheath, mainly as lamellae loosening, splits and other myelin distortions, in both groups of aged marmosets, the sevoflurane group did not show significant changes compared with the control group (**Figures 1G,H**).

DISCUSSION

To explore whether general anesthesia without surgery induces the process of neural injury (neuroinflammatory, apoptosis, and myelination deficits), we assessed the altered expression of IL-6 and TNF-α, Caspase3 activation, levels of MBP, and the ultrastructure of myelin sheath in the PFC of aged marmosets. The sevoflurane anesthesia with a duration of 6 h was applied based on previous studies (Schenning et al., 2017; Lai et al., 2021). Five to six hours of exposure to inhalation anesthetics were commonly used in the study of perioperative neural disorders. As a result, prolonged sevoflurane anesthesia did not increase the levels of IL-6 and TNF-α, activated the expression of Caspase3, and induced myelination deficits in the PFC of aged marmosets.

The results of the neuroinflammatory process are consistent with previous studies. Isoflurane anesthesia for 6 h did not increase IL-6 and interleukin-1β (IL-1β) in blood, spleen, and hippocampus in 18-month-old mice (Lai et al., 2021). Also, in adult rhesus macaques (16–17 years of age), an 8-hour-exposure to sevoflurane anesthesia did not induce microglial activation (Walters et al., 2019). Consistently, 59 elderly volunteers received sevoflurane general anesthesia without surgery for 2 h, with no increase in the level of IL-6 and TNF-α in their blood (Deiner et al., 2020). Our results from aged marmosets also suggested that sevoflurane anesthesia for 6 h has no impact on the expression of IL-6 and TNF-α. Surgical trauma, but not anesthesia, could be the critical factor in increasing the levels of inflammation factors.

Existing evidence demonstrates increased apoptotic death in the brains of young rhesus macaques by anesthetic sevoflurane (5h) (Rosado-Mendez et al., 2019). Our previous findings also supported the conclusion that sevoflurane exposure induced developmental toxicity to the myelin sheath in young rhesus macaques (Zhang et al., 2019). These findings suggested that anesthesia leads to neuroinflammation and apoptosis in young non-human primates, however, whether sevoflurane anesthesia without surgery causes the same consequence in aged non-human primates is still unknown. Notably, in the present study, sevoflurane did not induce Caspase3 activation and myelination deficits in the PFC of aged marmosets. In general, there was no significant difference in caspase3 in aged marmosets after sevoflurane exposure, while neural apoptosis was found in young rhesus macaques. As brain structure and functions differ with age (Zhao et al., 2019), anesthetic management of the aged requires different approaches compared with that of the young (Purdon et al., 2015). In the young brain, nerve cells are mainly in the process of proliferation and development. The cells can always assist in the maintenance of normal brain function. They rarely undergo apoptosis under normal conditions. Cellular stress or drugs could cause abnormal changes and apoptosis in nerve cells. After sevoflurane exposure, significant differences could be found more easily. While age-related neuronal apoptosis is obvious in the aged brain. After sevoflurane exposure, the process

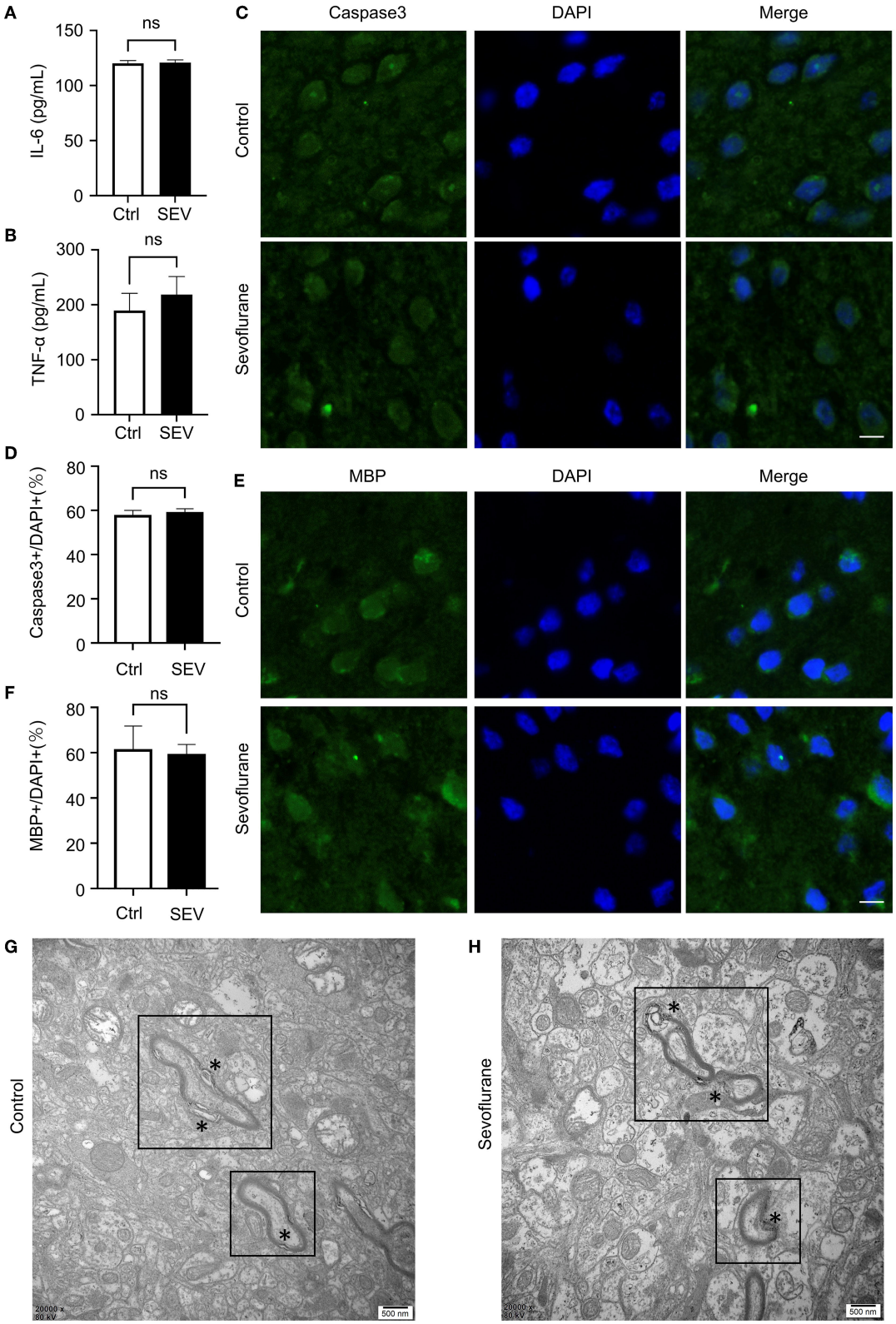

FIGURE 1 | The effect of sevoflurane anesthesia on the biomarkers of neural injury in the prefrontal cortex (PFC) of aged marmosets. **(A,B)** Elisa analysis indicated the amounts of IL-6 ($n = 3$, 120.1 ± 2.21 vs. 120.8 ± 2.25, $p = 0.74$, one-way ANOVA) and TNF-α ($n = 3$, 189.3 ± 31.35 vs. 218.7 ± 21.47, $p = 0.25$, one-way ANOVA) *(Continued)*

FIGURE 1 | in the PFC of the marmosets in Ctrl and SEV groups. **(C)** Immunofluorescence staining showed that Caspase3 protein level did not alter in aged marmosets' PFC upon sevoflurane exposure as quantified by the number of Caspase3+ cells. The scale bar indicates 50 μm. **(D)** The number of target channels (Caspase3) was normalized to the number of DAPI+ cells in marmosets' PFC. Sevoflurane did not alter Caspase3 expression in marmosets' prefrontal cortical compared to control condition (n = 3, 57.35 ± 1.54 vs. 58.67 ± 1.19, $p = 0.53$, one-way ANOVA). **(E)** Immunofluorescence staining exhibited that MBP protein level did not alter in aged marmosets' PFC upon sevoflurane exposure as quantified by the number of MBP+ cells. The scale bar indicates 50 μm. **(F)** The number of MBP+ cells was normalized to the number of DAPI+ cells in marmosets' PFC. Sevoflurane did not alter MBP expression in marmosets' prefrontal cortical compared to control condition (n = 3, 60.99 ± 6.21 vs. 58.91 ± 2.71, $p = 0.77$, one-way ANOVA). **(G,H)** Electron microscopy showed the loosening and splits (*) in adjacent membrane layers and myelin distortions in both Ctrl group **(G)** and SEV group **(H)**. The myelination deficits in the sevoflurane group looked no more serious than that in the control group. The scale bar indicates 0.5 μm.

of apoptosis may be accelerated, but not easy to be detected. The immediate injury might be masked over in the original state of chronic age-related injury. The age difference was exactly a complication to the effect of sevoflurane exposure. The different effects of sevoflurane on the age and the young is also a potential direction of study that requires further research.

There were some limitations in our study. Firstly, we harvested the brain tissue immediately after sevoflurane anesthesia, and the myelination deficits may not be reflected at this point. This study only examined acute sevoflurane exposure. If we want to focus on the long-term effect of sevoflurane exposure, the sampling time should be appropriately extended. Secondly, we did not assess enough neuroinflammation and apoptosis factors. These three markers are commonly used and important in neuroscience research. Due to this unusual species, it was difficult to find the appropriate Elisa kits and the antibody for marmosets. The sample size might also be insufficient for this current study. Due to the scarcity and high cost of laboratory primates, efforts were made to minimize the number of marmosets. Though the sample size of three in each group usually satisfies the bottom line, it is not large enough to draw a persuasive conclusion. Here we found this phenomenon and presented some clues of the sevoflurane's effect on aged primates by restricted sample sizes. It is feasible to carry out experiments under the direction of the findings in this preliminary study.

DATA AVAILABILITY STATEMENT

The raw data supporting the conclusions of this article will be made available by the authors, without undue reservation.

ETHICS STATEMENT

The process of the animal study was performed according to the guidelines of the Animal Care Committee of Center for Excellence in Brain Science and Intelligence Technology (CEBSIT, China) and was approved by the Institutional Animal Care and Use Committee (Protocol number CEBSIT-2021035). The marmosets were purchased from CEBSIT.

AUTHOR CONTRIBUTIONS

LZ and HJ: conceptualization. YC, HM, ZX, SL, and LS: methodology. YC, LS, and LZ: writing—original draft preparation. LZ, ZQ, and HJ: writing—review and editing. All authors contributed to the article and approved the submitted version.

FUNDING

This work was supported by NSFC Grants (#81970990, #82071177, and #82171173), the Shanghai Jiao Tong University School of Medicine Two-hundred Talent (20191818), the Cross Disciplinary Research Fund of Shanghai Ninth People's Hospital (JYJC202002), and the Science and Technology Commission of Shanghai Municipality (STCSM) (22YF1422500 and JYHX2021012).

ACKNOWLEDGMENTS

We thank Dr. Cheng Li from Shanghai Fourth People's Hospital for assistance with a portable clinical analyzer for arterial blood gases.

SUPPLEMENTARY MATERIAL

The Supplementary Material for this article can be found online at: https://www.frontiersin.org/articles/10.3389/fnagi.2022.918640/full#supplementary-material

Supplementary Table 1 | The characteristics of the aged marmosets.

Supplementary Video | The process of sevoflurane anesthesia.

REFERENCES

Abbott, D. H., Barnett, D. K., Colman, R. J., Yamamoto, M. E., and Schultz-Darken, N. J. (2003). Aspects of common marmoset basic biology and life history important for biomedical research. *Comp. Med.* 53, 339–350.

Chen, G., Gong, M., Yan, M., and Zhang, X. (2013). Sevoflurane induces endoplasmic reticulum stress mediated apoptosis in hippocampal neurons of aging rats. *PLoS ONE* 8, e57870. doi: 10.1371/journal.pone.0057870

Deiner, S., Baxter, M. G., Mincer, J. S., Sano, M., Hall, J., Mohammed, I., et al. (2020). Human plasma biomarker responses to inhalational general anaesthesia without surgery. *Br. J. Anaesth.* 125, 282–290. doi: 10.1016/j.bja.2020.04.085

Lai, Z., Min, J., Li, J., Shan, W., Yu, W., and Zuo, Z. (2021). Surgery trauma severity but not anesthesia length contributes to postoperative cognitive dysfunction in mice. *J. Alzheimers Dis.* 80, 245–257. doi: 10.3233/JAD-201232

O'bryan, L. J., Atkins, K. J., Lipszyc, A., Scott, D. A., Silbert, B. S., and Evered, L. A. (2022). Inflammatory biomarker levels after propofol

or sevoflurane anesthesia: a meta-analysis. *Anesth. Analg.* 134, 69–81. doi: 10.1213/ANE.0000000000005671

Purdon, P. L., Pavone, K. J., Akeju, O., Smith, A. C., Sampson, A. L., Lee, J., et al. (2015). The Ageing Brain: Age-dependent changes in the electroencephalogram during propofol and sevoflurane general anaesthesia. *Br. J. Anaesth.* 115 (Suppl 1), i46–i57. doi: 10.1093/bja/aev213

Rosado-Mendez, I. M., Noguchi, K. K., Castaneda-Martinez, L., Kirvassilis, G., Wang, S. H., Manzella, F., et al. (2019). Quantitative ultrasound and apoptotic death in the neonatal primate brain. *Neurobiol. Dis.* 127, 554–562. doi: 10.1016/j.nbd.2019.03.032

Schenning, K. J., Noguchi, K. K., Martin, L. D., Manzella, F. M., Cabrera, O. H., Dissen, G. A., et al. (2017). Isoflurane exposure leads to apoptosis of neurons and oligodendrocytes in 20- and 40-day old rhesus macaques. *Neurotoxicol. Teratol.* 60, 63–68. doi: 10.1016/j.ntt.2016.11.006

Walters, J. L., Zhang, X., Talpos, J. C., Fogle, C. M., Li, M., Chelonis, J. J., et al. (2019). Sevoflurane exposure has minimal effect on cognitive function and does not alter microglial activation in adult monkeys. *Neurotoxicology* 71, 159–167. doi: 10.1016/j.neuro.2018.12.008

Zhang, L., Xue, Z., Liu, Q., Liu, Y., Xi, S., Cheng, Y., et al. (2019). Disrupted folate metabolism with anesthesia leads to myelination deficits mediated by epigenetic regulation of ERMN. *EBioMed.* 43, 473–486. doi: 10.1016/j.ebiom.2019.04.048

Zhao, L., Matloff, W., Ning, K., Kim, H., Dinov, I. D., and Toga, A. W. (2019). Age-related differences in brain morphology and the modifiers in middle-aged and older adults. *Cereb Cortex* 29, 4169–4193. doi: 10.1093/cercor/bhy300

Conflict of Interest: The authors declare that the research was conducted in the absence of any commercial or financial relationships that could be construed as a potential conflict of interest.

Publisher's Note: All claims expressed in this article are solely those of the authors and do not necessarily represent those of their affiliated organizations, or those of the publisher, the editors and the reviewers. Any product that may be evaluated in this article, or claim that may be made by its manufacturer, is not guaranteed or endorsed by the publisher.

frontiers | Frontiers in Aging Neuroscience

TYPE Original Research
PUBLISHED 27 July 2022
DOI 10.3389/fnagi.2022.925728

OPEN ACCESS

EDITED BY
Yingwei Wang,
Huashan Hospital of Fudan University, China

REVIEWED BY
Stephan Krähenbühl,
University of Basel, Switzerland
Qianbo Chen,
Eastern Hepatobiliary Surgery Hospital, China
Xude Sun,
The Second Affiliated Hospital of Air Force Medical University, China

*CORRESPONDENCE
Xia Feng
fengxia@mail.sysu.edu.cn
Ming Wei
weiming@mail.sysu.edu.cn

†These authors have contributed equally to this work

SPECIALTY SECTION
This article was submitted to Neurocognitive Aging and Behavior, a section of the journal Frontiers in Aging Neuroscience

RECEIVED 21 April 2022
ACCEPTED 28 June 2022
PUBLISHED 27 July 2022

CITATION
Chen K, Lu D, Yang X, Zhou R, Lan L, Wu Y, Wang C, Xu X, Jiang MH, Wei M and Feng X (2022) Enhanced hippocampal neurogenesis mediated by PGC-1α-activated OXPHOS after neonatal low-dose Propofol exposure. *Front. Aging Neurosci.* 14:925728. doi: 10.3389/fnagi.2022.925728

Enhanced hippocampal neurogenesis mediated by PGC-1α-activated OXPHOS after neonatal low-dose Propofol exposure

Keyu Chen[1,2†], Dihan Lu[1,2†], Xiaoyu Yang[1†], Rui Zhou[3], Liangtian Lan[1], Yan Wu[1], Chen Wang[1], Xuanxian Xu[1], Mei Hua Jiang[2,4,5,6], Ming Wei[1*] and Xia Feng[1*]

[1]Department of Anesthesiology, First Affiliated Hospital, Sun Yat-sen University, Guangzhou, China, [2]Key Laboratory for Stem Cells and Tissue Engineering, Center for Stem Cell Biology and Tissue Engineering, Ministry of Education, Zhongshan School of Medicine, Sun Yat-sen University, Guangzhou, China, [3]Department of Hepatobiliary Surgery, Sun Yat-Sen Memorial Hospital, Sun Yat-sen University, Guangzhou, China, [4]Department of Anatomy, Zhongshan School of Medicine, Sun Yat-sen University, Guangzhou, China, [5]Guangdong Key Laboratory of Reproductive Medicine, Guangzhou, China, [6]Program of Stem Cells and Regenerative Medicine, Affiliated Guangzhou Women and Children's Hospital, Zhongshan School of Medicine, Sun Yat-sen University, Guangzhou, China

Background: Developing brain is highly plastic and can be easily affected. Growing pediatric usage of anesthetics during painless procedures has raised concerns about the effect of low-dose anesthetics on neurodevelopment. It is urgent to ascertain the neuronal effect of low-dose Propofol, a widely used anesthetic in pediatrics, on developing brains.

Methods: The behavioral tests after neonatal exposure to low-dose/high-dose Propofol in mice were conducted to clarify the cognitive effect. The nascent cells undergoing proliferation and differentiation stage in the hippocampus and cultured neural stem cells (NSCs) were further identified. In addition, single-nuclei RNA sequencing (snRNA-seq), NSCs bulk RNA-seq, and metabolism trials were performed for pathway investigation. Furthermore, small interfering RNA and stereotactic adenovirus injection were, respectively, used in NSCs and hippocampal to confirm the underlying mechanism.

Results: Behavioral tests in mice showed enhanced spatial cognitive ability after being exposed to low-dose Propofol. Activated neurogenesis was observed both in hippocampal and cultured NSCs. Moreover, transcriptome analysis of snRNA-seq, bulk RNA-seq, and metabolism trials revealed a significantly enhanced oxidative phosphorylation (OXPHOS) level in NSCs. Furthermore, PGC-1α, a master regulator in mitochondria metabolism, was found upregulated after Propofol exposure both *in vivo* and *in vitro*. Importantly, downregulation of PGC-1α remarkably prevented the effects of low-dose Propofol in activating OXPHOS and neurogenesis.

Conclusions: Taken together, this study demonstrates a novel alteration of mitochondrial function in hippocampal neurogenesis after low-dose Propofol exposure, suggesting the safety, even potentially beneficial effect, of low-dose Propofol in pediatric use.

KEYWORDS

Propofol, hippocampal neurogenesis, neural stem cell, OXPHOS, PGC-1α

Introduction

The early stage of life is believed to be the vulnerable period of brain development. Early life events can exert a powerful influence on both the pattern of brain architecture and behavioral development (Jevtovic-Todorovic and Brambrick, 2018). With the growing number of infants and children exposed to general anesthesia or sedation for surgery or examinations, the effect of anesthetics on brain development remains controversial. Anesthesia-induced neurotoxicity in the developing brain has been revealed in numerous studies (Vutskits and Xie, 2016; Zhou et al., 2021; Ing et al., 2022), while the neuroprotective property of general anesthetics, especially low-dose anesthetics, is increasingly recognized (Li et al., 2016; Wu et al., 2019; Zhao et al., 2022). As previously described, the application of low-dose ketamine could enhance neurogenesis in mice in the depression model (Deyama and Duman, 2020) and showed significant antidepression effects in human studies (Colla et al., 2021). Besides, a low dose of sevoflurane has been reported to stimulate neurogenesis and promote learning and memory ability in neonatal rats (Chen et al., 2015). However, the effects of low-dose Propofol, which has been commonly used in sedation for non-invasive procedures, on neurodevelopment and cognitive function in the developing brain remain uncovered.

Hippocampal neurogenesis is the crucial process of neurodevelopment, which is well known involved in determining emotion and cognitive function (Anacker and Hen, 2017). This includes the process of neural stem cells (NSCs) proliferation, differentiation into neuronal progenitor cells (NPCs), and giving rise to granule neurons (GCs) in the dentate gyrus (DG) (Toda et al., 2019). Highly activated neurogenesis in the young mammalian brain could be affected by specific factors, such as epigenetic changes, metabolic shift in NSCs, extracellular matrix signaling, neuropeptides, and other neurogenesis-related transcription factors (Vieira et al., 2018; Niklison-Chirou et al., 2020). Mitochondrial metabolism, including oxidative phosphorylation (OXPHOS), has been reported to mediate neurogenesis and NSCs fate decision (Khacho et al., 2019). It had been reported that efforts to enhance mitochondrial function can improve impaired neurogenesis and behavioral deficits in young mice after neonatal hypoxia exposure (Sun et al., 2020).

In this study, we aimed to determine the effects of neonatal exposure to low-dose Propofol on cognitive function as well as altered neurogenesis state. Furthermore, single-nuclei RNA-seq (snRNA-seq) and NSCs bulk RNA-seq analysis were used for mechanism investigation and further experiments were conducted to verify the pathway. This study might suggest the effect and mechanisms of low-dose Propofol on neurodevelopment, and its potential benefits in clinical pediatrics sedation.

Materials and methods

Animals

C57BL/6N mice were purchased from the Beijing Vital River Laboratory Animal Technology Co., Ltd. (Beijing, China). Homozygous Nestin-GFP transgenic mice that express enhanced GFP under the control of the Nestin promoter (Nes-GFP), which were on the C57BL/6J genetic background, were kindly provided by Yamaguchi et al. (2000) as previously reported. All the mice were housed in a room at 23°C under a 12-h (h) light/dark cycle and were given food and water *ad libitum*. All animal protocols were reviewed and approved by the Sun Yat-Sen University Institutional Animal Care and Use Committee. Newborn mice from the maternal mouse, both male and female mice, would be included in the experiment and divided into groups randomly with an online randomization tool: http://www.randomizer.org. Mice injured severely would be excluded.

Drug administration and EdU labeling *in vivo*

Wild-type C57BL/6N mice or Nestin-GFP mice at postnatal day (PND) 7 were randomly allocated to different groups and administrated 4 $mg.kg^{-1}$ (L-Propofol group) and 50 $mg.kg^{-1}$ (H-Propofol group) Propofol (Diprivan;

AstraZeneca; Cambridge, England) by i.p. injection. EdU (5-ethynyl-2'-deoxyuridine; A10044; Invitrogen; California, USA) was first given i.p. 30 min after drug injection at a dose of 50 mg kg^{-1} in 0.9% saline and the same dosage was administrated per 12 h for six times within 3 days.

Tissue processing

Tissues were obtained from mice sacrificed on the 3-day post-injection (dpi), 7 dpi, and 28 dpi of Propofol injection for immunofluorescent staining. For positive cell counting, at least three hippocampal sections from three different individuals were calculated. Sections were paired with the same location of the hippocampus among groups. For 10× Genomics snRNA-seq, hippocampus were dissociated freshly from PND10 mice brain 3 dpi of propofol.

Primary NSCs separation, culture, and induction

NSCs were obtained from cortical tissues collected from C57BL/6N mouse fetuses on embryonic day 14.5. The dissociated cells were seeded in the NSCs medium, DMEM/F12 (SH30023.01; HyClone; Logan, Utah, USA) supplemented with epidermal growth factor (EGF) and basic fibroblast growth factor (bFGF) (both at 20 ng ml^{-1}; 100-47, 100-18B; Peprotech; Cranbury, NJ, USA), B27 (2%; 17504-044; Gibco), N2 (1%; 17502-048; Gibco; Grand Island, NewYork, USA), and 100 IU/ml penicillin/streptomycin (SV30010; HyClone) to form primary neurospheres and grown in 5% CO2 in the air, at 37°C. NSCs differentiation was induced by plating cells onto 24-well plates in DMEM/F12 medium supplemented with 2% FBS (10099; Invitrogen), 2% B27, and 100 $IU.ml^{-1}$ penicillin/streptomycin.

Treatment of the primary NSCs

NSCs in passages 4 to 6 were seeded into cell culture plates with PLL (poly-L-lysine; P4707; Sigma) and incubated overnight. About 10 μM Propofol (1.78 $\mu g.ml^{-1}$, deemed as low-dose Propofol) was added to the cells for 24 h as previously described (Qiao et al., 2017). For proliferation tests, the cell numbers were counted once daily for consecutive 6 days in 24-well plates. For differentiation tests, the cells were maintained in a differentiation medium for 10 days before being analyzed by Tuj-1 (neuron) and GFAP (astrocyte) staining. The antibodies used are shown in the Supplementary material. For NSCs bulk RNA-seq, cells were harvested 24 h after 10 μM Propofol treatment.

10× genomics snRNA-seq

Nucleus dissociation

Hippocampus nucleus was isolated at 4°C. The tissue was homogenized using a douncer with Nuclei EZ Lysis Buffer (Nuc101, Sigma) in the tube. After incubated with Nuclei EZ Lysis Buffer on ice, the homogenate was filtered with a 70-μm strainer mesh. The sample was centrifuged at 500 g for 5 min and was resuspended pellet with another EZ Lysis buffer. After incubated for 5 min on ice, the sample was centrifuged at 500 g for 5 min. Nuclei Wash and Resuspension Buffer were added to the pellet and incubate for 5 min. After incubation, another Nuclei Wash and Resuspension Buffer are added and the nucleus was resuspended. Centrifuged the nucleus at 500 g for 5 min and resuspended with Nuclei Wash and Resuspension Buffer supplemented with DAPI. Collected all nuclei by filtering with a 35-μm strainer. The number of nuclei was assessed under a microscope and counted with a cell counter. Sorted nucleus into 10× RT Buffer prepared without the RT Enzyme Mix and proceeded with the 10× Genomics Single Cell Protocol.

cDNA library construction and sequencing

Gel Beads-In-Emulsions (GEMs) were performed by loading onto the Chromium Controller (10× Genomics) following the manufacturer's instruction (Chromium Single Cell 3' Library & Gel Bead Kit v2). The amplified cDNA was optimized by enzymatic fragmentation and size selection before library construction. The single-cell libraries were sequenced on a HiSeq4000 system (Illumina).

snRNA-seq data analysis

Bioinformatic analysis of snRNA-seq was conducted by LC-bio (Hangzhou, China). The data were post-processed and quality controlled using the 10× Cell Ranger package (v1.2.0; 10× Genomics). Reads were demultiplexed, aligned, and quantified by the 10× Cell Ranger (version 6.1.1). Aggregate options were analyzed with the R package Seurat (version 3.0) with default parameters. Cells were considered valid only when genes were more than 200 and <2,500 as well as containing <5% mitochondrial genes. A correlation analysis was performed by employing the RunPCA function of the Seurat package. Clustering analysis was carried out with standard Seurat package procedures with a resolution of 1.2. Data visualization was performed using Uniform Manifold Approximation and Projection (UMAP) of the principal components in Seurat. Pseudotime analysis was used to illustrate the transition of neurogenic lineage cells during neurogenesis by importing the data to Monocle2 to perform cell trajectory analysis. To investigate the potential effect of low-dose Propofol on cell clusters, we calculated gene expression. Differentially expressed genes (DEGs) were identified by the Seurat bimod test

(Seurat2.3.4) according to the literature (Ximerakis et al., 2019) [p-value < 0.05 and log2-fold change (log2FC) ≥ 0.138].

Bulk RNA-seq

Total RNA from the NSCs was isolated using the TRIzol reagent. The purity and quantity of the total RNA were evaluated using a NanoDrop1000 spectrophotometer (Thermo Fisher Scientific Inc.). The absorbance ratio of OD260/280 was between 1.8 and 2.0 for all samples, and RNA integrity was assessed by electrophoresis analysis on a standard denaturing agarose gel. The library for transcriptome sequencing was conducted by NovelBio Co., Ltd (Shanghai, China). DEGs were screened by the principles: log2FC > 0.585 or < -0.585, FDR < 0.05. GO analysis was applied to analyze the main function of the differential expression genes according to the Gene Ontology from NCBI. Generally, Fisher's exact test was applied in this study to identify the significant GO pathways and the false discovery rate (FDR) was used to correct the p-values. Thus, based on the FDR value, the top 10 pathways were included for evaluation. GO pathways presentation was based on the ratio of the upregulated DEGs in total different genes.

siRNA transfection of NSCs

PGC-1α siRNA and control siRNA were obtained from the RiboBio company (Guangzhou, China). The PGC-1α-specific siRNAs were 5′ -CUGCGAACAUAUUUGAGAA dTdT-3′ (sense) and 5′ -UUCUCAAAUAUGUUCGCAG dTdT-3′ (antisense). About 50 μM siRNA diluted in Opti-MEM medium (Invitrogen, 13778075, Carlsbad, CA) and Lipofectamine RNAimax transfection reagent (Invitrogen, 11058021, Carlsbad, CA) were used according to the manufacturer's protocol for transfection. After seeding for 24 h, the cells were transfected with siRNA and cultured in an NSC medium for 8 h. Cells were cultured in an NSCs differentiation medium for 1 and 4 days for qPCR and staining, respectively.

Stereotactic virus injection

The PGC-1α shRNA and control shRNA ligated into adenovirus vector expressing EGFP were obtained from WZ Biosciences Inc. (Shandong, China). PGC-1α-specific shRNA were CTGCGAACATATTTGAGAATTCAAGAGATTCT-CAAATATGTTCGCAGTTTTTT. We made a tailored stage for stereotactic injection according to the literature (Mathon et al., 2015). After anesthetized by a freeze, PND3 mice were placed into the tailored stage on a stereotactic frame (KOPF, KD Scientific) for injection. Scissors were used to make a 5-mm incision to make the skull visible. After determining the lambda, find the coordinate position (anterior-posterior, +1.1 mm, mediolateral, ±0.9 mm, dorsoventral, −2.0 mm referring to lambda) and directly pinch with the Hamilton syringe (Hamilton Medical, Reno, NV, USA). The virus was injected into the hippocampus with 0.12 μl of viral titer (1.2×10^9 vg. ml^{-1}) at an injection speed of 0.12 μl min^{-1}. The injections were conducted in PND3 mice and immunofluorescence staining was performed on PND10 by calculating infected cells and PGC-1α intensity in DG to evaluate the efficiency.

Other methods

Procedures related to the behavioral test, immunofluorescent staining, apoptosis analysis, western blot analysis, qRT-PCR analysis, HPLC analysis, and seahorse metabolism analysis are provided in the Supplementary material.

Statistical analysis

All results were obtained from at least three independent experiments and expressed as mean ± SD. Student's t-test was used to compare the means between two groups, while one-way ANOVA was performed for comparisons of three or more groups, followed by an LSD test for multiple comparisons. One-way ANOVA repeated measurement analysis was used to compare repeated assessments. The $p < 0.05$ was considered significant. Data of snRNA-seq was analyzed on the website: https://www.omicstudio.cn. Statistical analysis and graphs generation were performed using SPSS Statistics 26 (Armonk, New York, U.S.), GraphPad Prism software 9 (San Diego, CA, USA), and website: https://app.biorender.com.

Results

Low-dose Propofol enhanced spatial cognitive ability in neonatal mice

To uncover the effect of different doses of Propofol on cognitive function, 4 $mg.kg^{-1}$ (L-Propofol, sub-anesthesia dose reported) (Chen et al., 2021) and 50 $mg.kg^{-1}$ (H-Propofol, anesthesia dose used previously) (Jiang et al., 2018) of Propofol were delivered by intraperitoneal (i.p.) injection on PND 7 C57BL/6N mice, and behavioral tests were conducted according to the workflow (Figure 1A).

Morris water maze (MWM) was performed to clarify the effect on spatial learning and memory ability since PND35. There was no motor deficit for the similar velocity of swimming among groups during the training session (Figure 1B). Curiously, improved spatial cognitive function

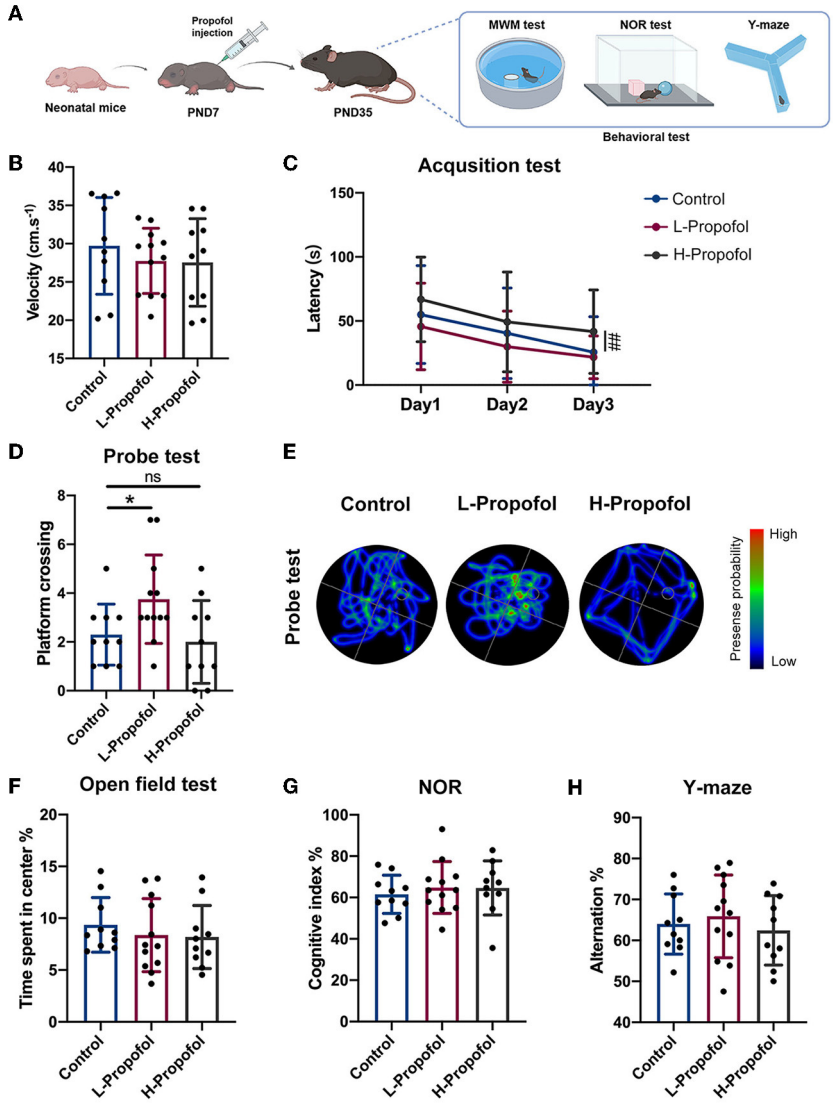

FIGURE 1
Early low-dose Propofol administration promoted spatial cognitive ability in mice. **(A)** Workflow of Propofol treatment and behavior tests in C57BL/6N. **(B)** Velocity of mice among groups showing similarity on day 1 of acquisition test. **(C)** Acquisition test showing a trend that L-Propofol mice spent less time on the hidden platform compared with the Control group, while H-Propofol mice exhibited increased escape latency (H-Propofol vs. Control: $p = 0.009$) relative to the other two groups during day 1–3. **(D)** Platform crossing in probe test showing that L-Propofol mice significantly increased the number of platform crossing (L-Propofol vs. Control: $p = 0.046$). **(E)** Typical swimming path in the probe test. **(F)** Time spend exploring the center in OFT. **(G)** The cognitive index in NOR. **(H)** The percentage of spontaneous alternation in Y-maze. Three groups performed similarly in OFT, NOR, and Y-maze. $N = 10$ (Control), 12 (L-Propofol), 10 (H-Propofol). Error bars means ± SD. * (L-Propofol vs Control), $p < 0.05$; ## (H-Propofol vs Control), $p < 0.01$, ns, no significant. One-way repeated measures ANOVA, one-way ANOVA, and LSD test for multiple comparisons were used for analysis.

was observed in the L-Propofol group with a shortening trend of escape latency during the acquisition trial as well as significantly more platform crossing in the probe test (1.6-fold) (Figures 1C–E). Besides, plasma concentrations of mice in the L-Propofol group were measured and verified as clinically sedative concentrations (Supplementary Figure 1, 1.36 $\mu g.ml^{-1}$) (Kim, 2007). Nevertheless, impaired learning ability was confirmed in the H-Propofol group for significantly longer escape latency (Figures 1C–E). In addition, we further assessed the effects of Propofol on anxiety emotion with an open field test (OFT), recognition memory *via* novel object recognition test (NOR), and working memory by Y-maze. No significant difference was observed among the three groups in these tests (Figures 1F–H). Taken together, these results implicated that low-dose Propofol

improved spatial cognitive function specifically, with no obvious change in object recognition memory, working memory, or emotion-related performance. Thus, the L-Propofol group was adopted for the following experiments.

Low-dose Propofol-treatment activated hippocampal neurogenesis process both *in vivo* and *in vitro*

Since hippocampal neurogenesis contributes to specific spatial cognitive function (Goncalves et al., 2016), lineage tracing with EdU labeling was used to assess the proliferation and differentiation of NSCs (Figure 2A). Quantitative analysis showed significantly expanded EdU^+ cells (1.2-fold) in DG 3 dpi of Propofol (Figures 2B,C), suggesting increased hippocampal newborn cells in neonatal mice after exposure to low-dose Propofol. Further analysis revealed increased $EdU^+/Nestin^+$ cells (1.4-fold) at 3 dpi indicating NSCs expansion in the L-Propofol group (Figures 2D,E). To clarify the fate of the expanded cells, we next assessed EdU^+/DCX^+ cells representing newborn neurons at 7 dpi and $EdU^+/NeuN^+$ cells representing mature neurons at 28 dpi. Consequently, significantly elevated neuronal fate (1.4-fold and 1.2-fold) was found in the L-Propofol group (Figures 2F–I). All of these data demonstrated the activated hippocampal neurogenesis after low-dose Propofol administration, which might be involved in enhanced spatial cognitive capability.

To elucidate the explicit change in NSCs after low-dose Propofol treatment, primary-cultured NSCs were obtained and an overall activation was observed with 1 to 100 μM Propofol (Supplementary Figure S2). We adopted the clinical-related concentration of 10 μM (Schraag et al., 2019) and deemed it as low-dose Propofol for our following study. Similar to the effect *in vivo*, low-dose Propofol treatment markedly increased the number of viable cells (Figure 2J) and EdU-incorporating cells (1.5-fold) (Figures 2K,L) and without resulting in apoptosis level alternation (Supplementary Figure 3), indicating the promoted NSCs proliferation after low-dose Propofol treatment. Besides, treatment with low-dose Propofol significantly increased the number of $Tuj\text{-}1^+$ cells (4.7-fold) in the NSCs differentiation assay (Figures 2M,N). In summary, the results suggested that low-dose Propofol might simultaneously enhance both proliferation and neuronal differentiation of NSCs *in vitro*.

In addition, we further assessed adult neurogenesis in 18-month-old mice in Control and L-Propofol groups to verify whether L-Propofol-activated hippocampal neurogenesis results in diminished NSCs pool with aging (Ceccarelli et al., 2020). The number of NSCs storage was examined by immunohistological staining with Sox2, a transcription factor important for controlling NSCs maintenance (Favaro et al., 2009). Similar Sox2 expression was observed in both Control and L-Propofol groups, implying no obvious persistent hazard during aging after neonatal low-dose Propofol exposure (Supplementary Figure 4).

snRNA-seq showed enhanced hippocampal neurogenesis in 3-day post-treatment neonatal mice

To characterize the variation of neurogenesis-related cell types affected by low-dose Propofol precisely and illustrate the molecular signatures, we carried out snRNA-seq, which is particularly suited to investigate neuronal development (Armand et al., 2021), in the hippocampus at 3 dpi in neonatal mice. A total of 22,457 (11,347 in Control and 11,110 in L-Propofol) nuclei were isolated and a 10× Genomics platform was used for single-nuclei transcriptomes (Figure 3A). UMAP was used to separate the dataset into 26 clusters (Figure 3B) and subsequently classified the major clusters into 12 cell types (Figures 3C–E): astrocytes and NSCs (expressing Hopx, Notch2, and Aqp4), NPCs (expressing Igfbpl1 and Sox11), GCs (expressing Prox1), mossy cells (expressing Tm4sf1 and Calb2), pyramidal cells (expressing Meis2 and Spock1), interneurons (expressing Gad1, Gad2, and Slc17a6), oligodendrocyte precursor cells (OPCs, expressing Pdgfra), oligodendrocytes (expressing Mbp), microglia (expressing Cx3cr1), endothelial cells (expressing Flt1), vascular and leptomeningeal cells (VLMCs, expressing Slc6a13), and ependymocytes (expressing Enkur), consistent with previous studies (Cembrowski et al., 2016; Artegiani et al., 2017; Hochgerner et al., 2018; Rosenberg et al., 2018; Zywitza et al., 2018; Mizrak et al., 2019).

To assess the overall effect of low-dose Propofol on cell fate specification, we regrouped neurogenesis-related cells for the difficulty in differing astrocytes and NSCs in the primary classification as the similar phenotype with sharing markers (Artegiani et al., 2017). Thus, neurogenesis-related cell types including astrocytes and NSCs, NPCs, and GCs were re-separated into five clusters (Figures 4A–C): astrocytes (expressing Aqp4), NSCs (expressing Notch2), NPCs (expressing Top2a and Eomes) (Hochgerner et al., 2018), immature GCs (expressing Prox1), and mature GCs (expressing Dock10). Pseudotime analysis suggested that the development of neurogenesis-related cells between groups was similar (Figure 4D). In addition, the ratios of cells in each cluster over total cells in the hippocampus were calculated, and the result showed an increasing trend in the percentages of neurogenesis-related cells in the L-Propofol group, including an 8% increase in NSCs, 48% increase in NPCs, 23% increase in immature GCs, and 28% increase in mature GCs (Figure 4E).

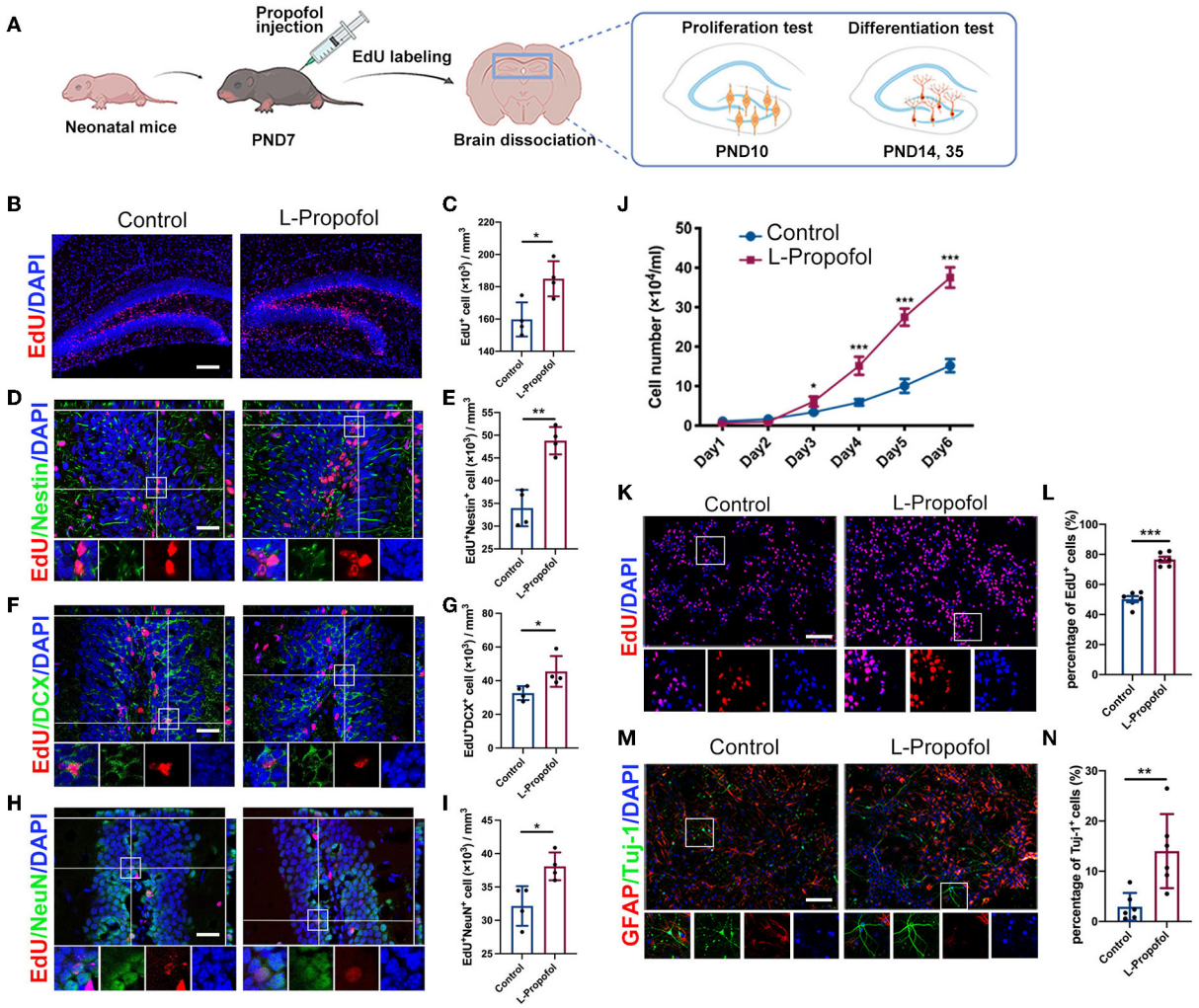

FIGURE 2
Long-term tracing showed boosted hippocampal neurogenesis after low-dose Propofol treatment. **(A)** Timeline for treatment for hippocampal neurogenesis. **(B,C)** Images of maximum intensity projection **(B)** and quantification **(C)** showing the increased EdU$^+$(red) cells ($p = 0.016$) in DG of mice at PND 10 in the L-Propofol group. $N = 4$. Scale bars, 200 μm. **(D,E)** Images with z-plane projections **(D)** and quantification **(E)** showing the increased Nestin$^+$ (green)/EdU$^+$ (red) newborn NSCs ($p = 0.001$) in DG of mice at PND 10 in the L-Propofol group. $N = 4$. **(F,G)** Images with z-plane projections **(F)** and quantification **(G)** showing an increased DCX$^+$ (green)/EdU$^+$ (red) newborn neurons ($p = 0.043$) in the DG of mice at PND 14 in the L-Propofol group. $N = 4$. **(G,I)** Images with z-plane projections **(H)** and quantification **(I)** showing an increased NeuN$^+$ (green)/EdU$^+$ (red) mature neurons ($p = 0.017$) in the DG of mice at PND 28 in the L-Propofol group. $N = 4$. For **(D–I)**, Scale bars, 50 μm. Bottom panels: higher-magnification views of selected regions. **(J)** Growth curves of NSCs as assessed by direct counting for consecutive 6 days after treatment ($p < 0.001$). $N = 3$. **(K,L)** Fluorescence images **(K)** and quantification analysis **(L)** showing significantly increased EdU$^+$ cells in NSCs ($p < 0.001$) at 4 days after treatment. Scale bar: 50 μm. $N = 6$. **(M,N)** Fluorescence staining **(M)** and quantification **(N)** showing an increased proportion of Tuj-1$^+$ newborn neurons ($p = 0.006$) at 10 days after differentiated induction in the L-Propofol group. $N = 6$. Scale bar: 20 μm. Error bars, mean ± SD, Bottom panels: higher-magnification views of selected regions. $^*p < 0.05$, $^{**}p < 0.01$, $^{***}p < 0.001$. Repeated measurement and Student's *t*-test were used for analysis.

Transcriptome analysis revealed mitochondrial metabolism enhancement in hippocampal NSCs after low-dose Propofol treatment

To further study the dynamic change of hippocampal NSCs after low-dose Propofol administration, significantly differential genes and transcriptome analysis were performed in early neurogenesis-related cell types including NSCs and NPCs according to the clusters revealed by snRNA-seq. A total of 1,975 total genes were detected and 865 were identified as significantly affected in the L-Propofol group at least in one cell type. Further analysis of significantly upregulated genes revealed that low-dose

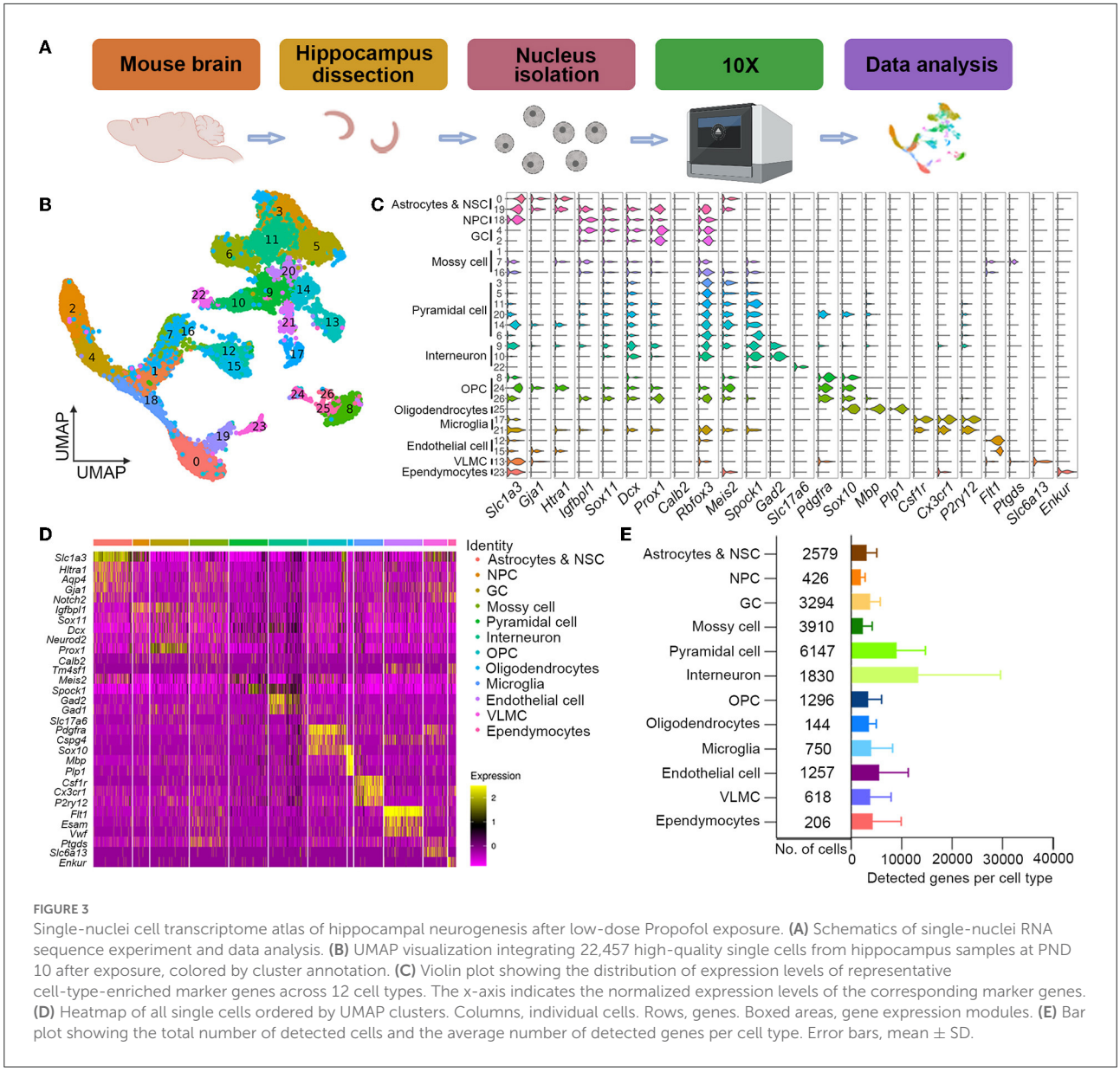

FIGURE 3
Single-nuclei cell transcriptome atlas of hippocampal neurogenesis after low-dose Propofol exposure. **(A)** Schematics of single-nuclei RNA sequence experiment and data analysis. **(B)** UMAP visualization integrating 22,457 high-quality single cells from hippocampus samples at PND 10 after exposure, colored by cluster annotation. **(C)** Violin plot showing the distribution of expression levels of representative cell-type-enriched marker genes across 12 cell types. The x-axis indicates the normalized expression levels of the corresponding marker genes. **(D)** Heatmap of all single cells ordered by UMAP clusters. Columns, individual cells. Rows, genes. Boxed areas, gene expression modules. **(E)** Bar plot showing the total number of detected cells and the average number of detected genes per cell type. Error bars, mean ± SD.

Propofol exposed NSCs and NPCs presented higher expression (1.1 to 2.4-fold) of neurogenesis promotion-related genes such as Meg3, Ttr, Baz1b, Ddx17, and so on (Kapoor et al., 2015; Lalli et al., 2016; Gao et al., 2019; Suthapot et al., 2022), and mitochondrial metabolism-related genes such as Atp1a2, mt-Rnr2, Atp11c, Atp5o, Etfa, Atp6ap2, and so on (Figure 4F). Besides, GO analysis of NSCs bulk RNA-seq obtained 24 h after low-dose Propofol administration revealed the enrichment in mitochondrial metabolism (Figure 4G). The results suggested that low-dose Propofol might promote mitochondrial metabolism in hippocampal NSCs.

Emerging evidence reveals that mitochondria are the key master regulators in neurogenesis, while the neuronal lineage differentiation of NSCs is highly dependent on mitochondrial OXPHOS (Iwata and Vanderhaeghen, 2021). As the difficulty of metabolism trials performed specifically in hippocampal NSCs *in vivo*, Seahorse XF assays were performed *in vitro* and showed a significant sustained enhancement (2-fold) in oxygen consumption rate (OCR) including basal respiration, maximal respiration, ATP production, spare respiration (Figures 5A–E), and no change in extracellular acidification rate (ECAR; Figure 5F) after low-dose Propofol treatment, verified the activation of OXPHOS in NSCs post-Propofol exposure.

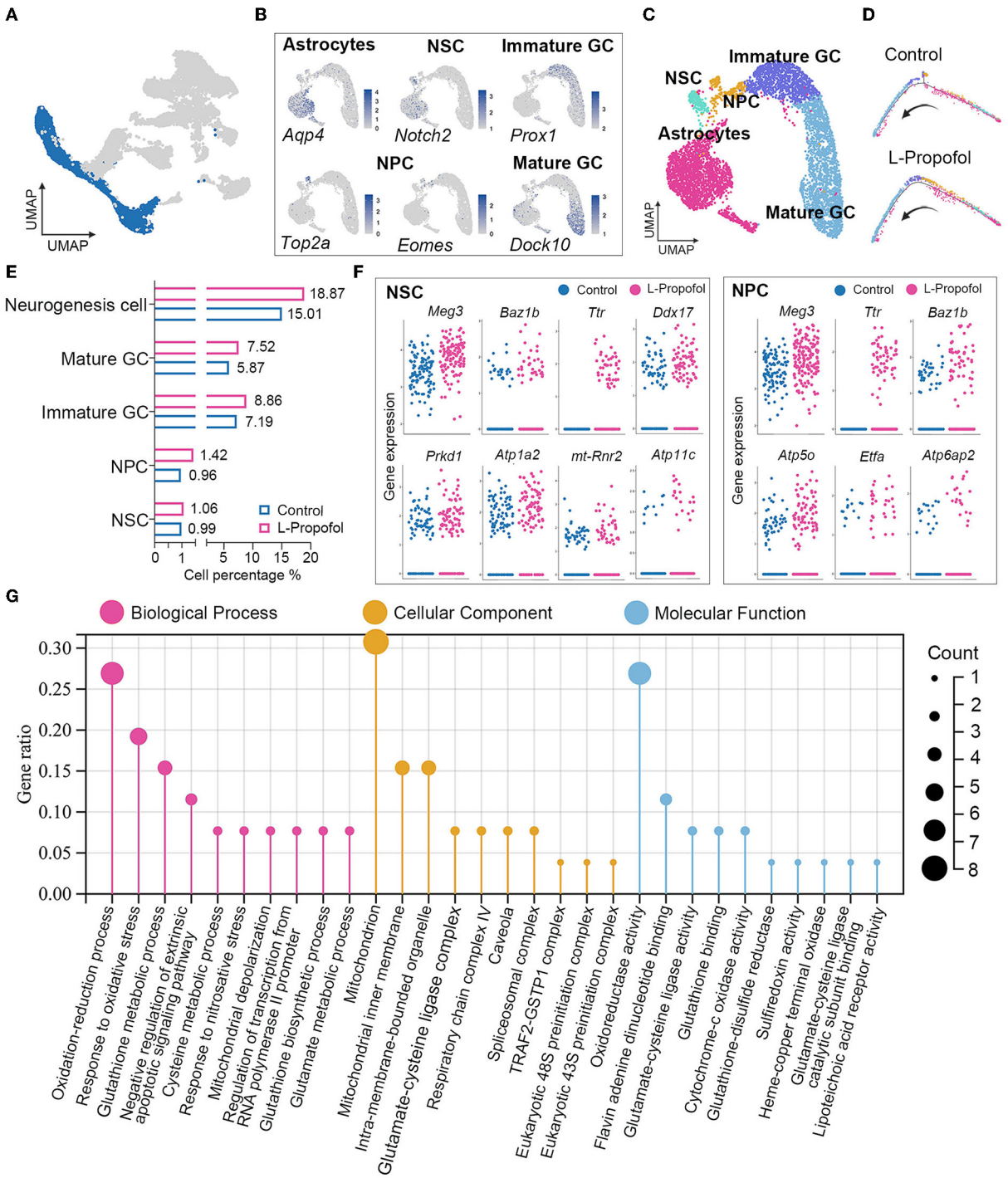

FIGURE 4
Enhancement of mitochondria metabolism in NSCs post-treatment revealed by transcriptome analysis. **(A)** Target clusters of neurogenesis-related cell types for cell regrouping. **(B)** Expression of representative markers for each cell type. Cells were colored according to their expression levels, ranging from "not detected" (gray) to "highest detected" (blue). **(C)** Distribution for neurogenesis-related cell types in UMAP analysis in which clusters were separated by colors. **(D)** Pseudotime analysis of neurogenesis in Control group and L-Propofol group, respectively. **(E)** Quantification of the percentage of NSCs, NPCs, immature GCs, mature GCs, and overall neurogenesis cells among all cells showing overall activated neurogenesis in the L-Propofol group. **(F)** Level of gene expression showing the enhancement of neurogenesis and mitochondrial metabolism-related genes in NSCs (Meg3: $p < 0.001$, Ttr: $p < 0.001$, Baz1b: $p = 0.01$, Ddx17: $p = 0.03$, Atp1a2: $p < 0.001$, Prkd: $p = 0.04$, mt-Rnr2: $p < 0.001$, Atp11c: $p = 0.04$) and NPCs (Meg3: $p < 0.001$, Ttr: $p < 0.001$, Baz1b: $p < 0.001$, Atp5o: $p = 0.01$, Etfa: $p = 0.03$, Atp6ap2: $p < 0.001$) between Control and L-Propofol. **(G)** GO analysis showing the mitochondrial metabolism pathway enrichment in NSCs in the L-Propofol group compared with the Control group.

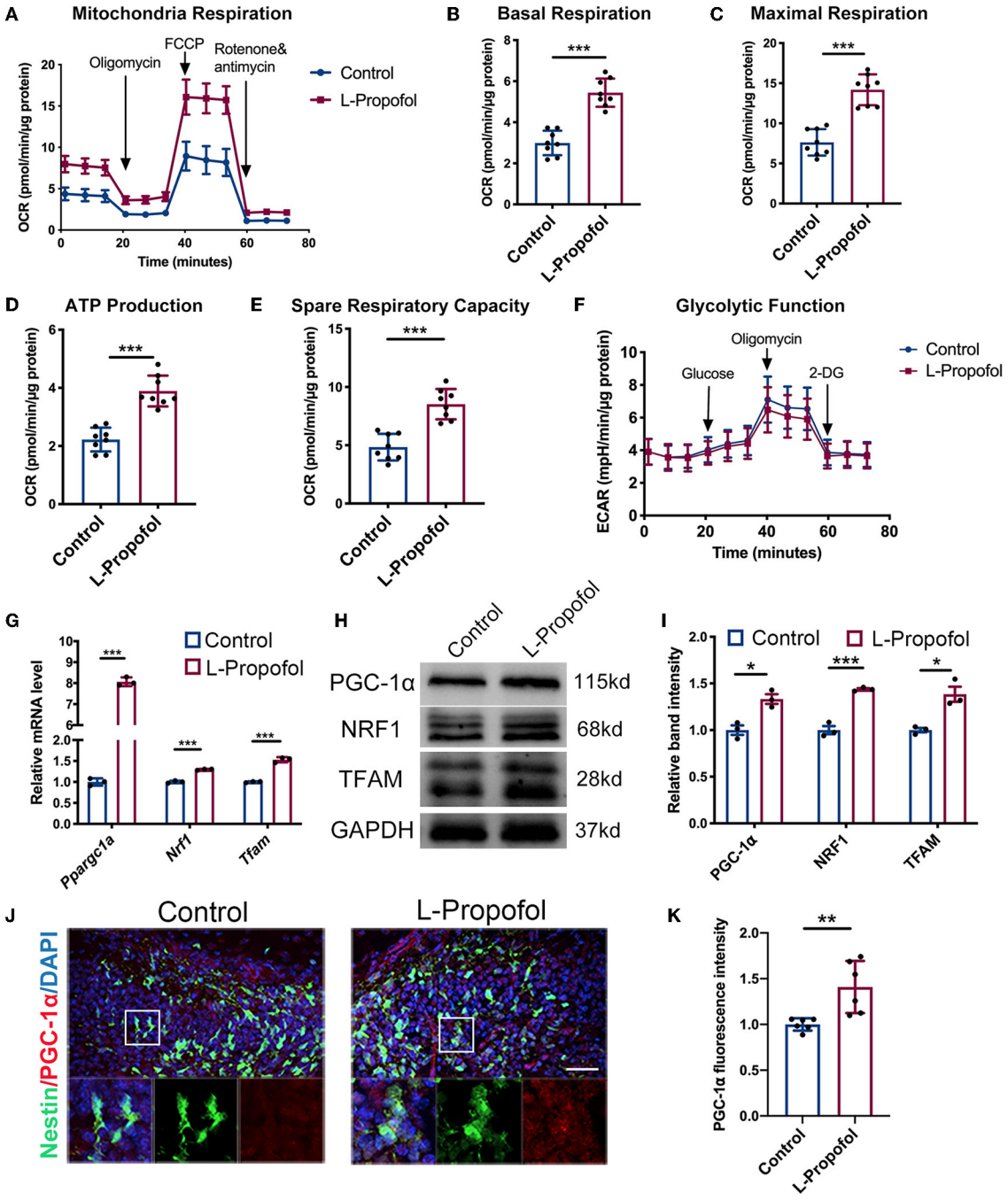

FIGURE 5
Metabolic shift and activated PGC-1α/NRF1/TFAM pathway in NSCs were confirmed after Propofol treatment. **(A–E)** Low-dose Propofol enhanced OXPHOS level in primary NSCs measured by the **(A)** oxygen consumption rate (OCR) normalized by protein content (μg) including OXPHOS parameters **(B)** basal respiration ($p < 0.001$), **(C)** maximal respiration ($p < 0.001$), **(D)** ATP-linked respiration ($p < 0.001$), and **(E)** spare respiratory capacity ($p < 0.001$). $N = 8$. **(F)** Glycolytic function showed a similar result in normalized extracellular acidification rate (ECAR). $N = 8$. **(G–I)** Relative mRNA **(G)** (Ppargc1a: $p < 0.001$; Nrf1: $p < 0.001$; Tfam: $p < 0.001$) and protein **(H,I)** levels (PGC-1α: $p = 0.010$; NRF1: $p < 0.001$; TFAM: $p = 0.011$) showing activated mitochondrial biogenesis mediated by PGC-1α/NRF1/TFAM pathway after low-dose Propofol treatment. $N = 3$. **(J,K)** Confocal images of PGC-1α (red) staining **(J)** and quantification **(K)** showing an increased intensity of PGC-1α in NSCs in the DG of Nestin-GFP mice 6 h after low-dose Propofol administration at PND 7 in L-Propofol group ($p = 0.007$). $N = 6$. Scale bar, 40 μm. $^*p < 0.05$; $^{**}p < 0.01$; $^{***}p < 0.001$. Error bars, mean ± SD. The Student's *t*-test was used for analysis.

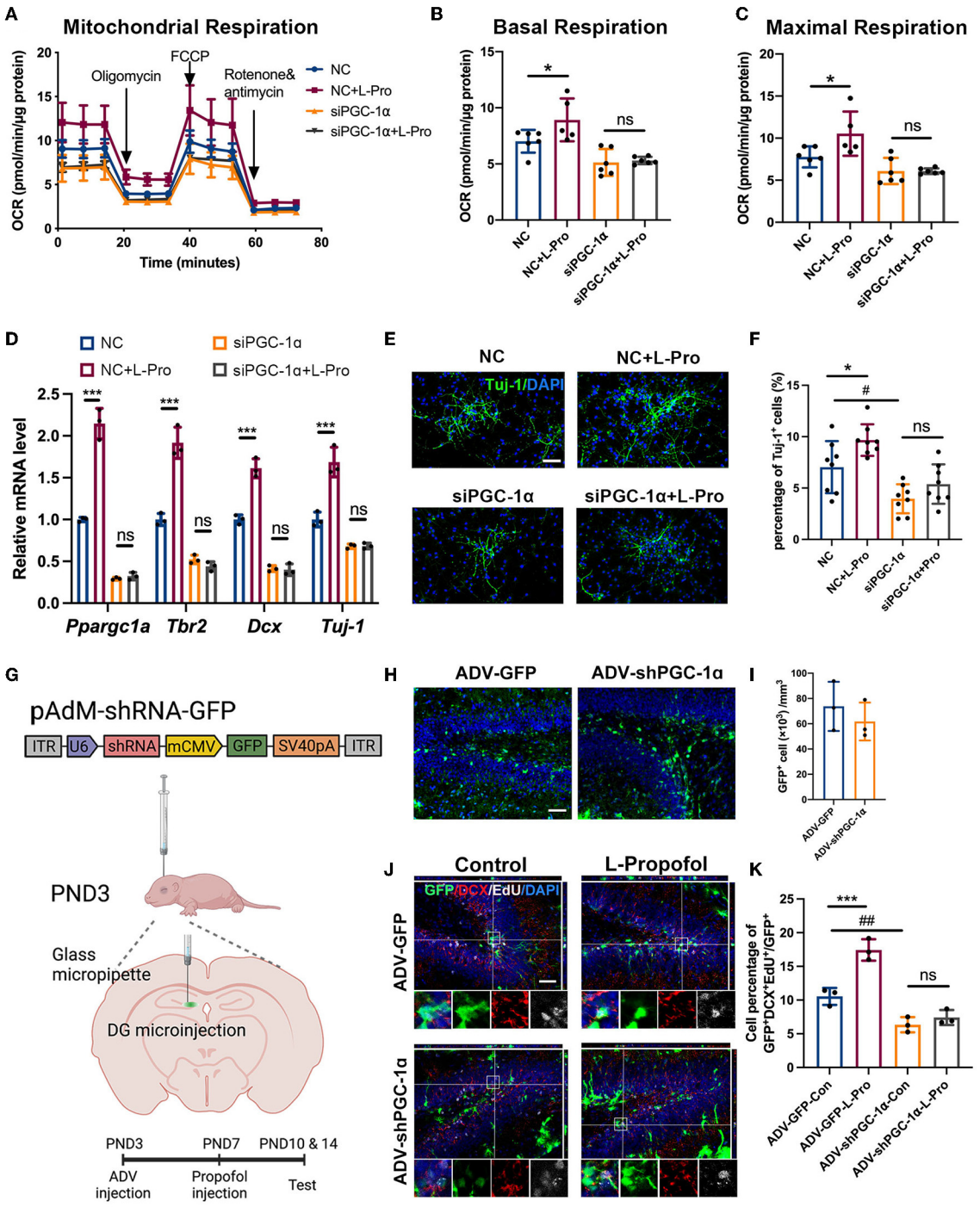

FIGURE 6
Low-dose Propofol promoted neurogenesis *via* activating PGC-1α-induced mitochondrial OXPHOS. **(A–C)** Administration of siPGC-1α prevented low-dose Propofol-induced mitochondrial OXPHOS promotion in primary NSCs measured by the **(A)** normalized OCR; including **(B)** basal respiration (NC vs. NC+L-Pro: $p = 0.017$, siPGC-1α vs. siPGC-1α+L-Pro: $p = 0.803$) and **(C)** maximal respiration (NC vs. NC+L-Pro: $p = 0.010$, siPGC-1α vs. siPGC-1α+L-Pro, $p = 0.996$), suggesting the dominant role of PGC-1α in Propofol-induced OXPHOS. $N = 5–6$. **(D–F)** siPGC-1α abolished neurogenesis elevation in primary NSCs differentiation determined by **(D)** relative mRNA level (Ppargc1a: NC vs. NC+L-Pro: $p < 0.001$, siPGC-1α vs. siPGC-1α+L-Pro: $p = 0.979$; Tbr2: $p < 0.001$, $p = 0.776$; Dcx: $p < 0.001$, $p = 0.996$), and Tuj-1: $p < 0.001$, $p > 0.999$. $N = 3$) and staining with Tuj-1(green) **(E,F)** (NC vs. NC+L-Pro: $p = 0.047$, siPGC-1α vs. siPGC-1α+L-Pro: $p = 0.444$, NC vs. siPGC-1α: $p = 0.015$. $N = 8$). Scale bar, 50 μm. Error bars, mean ± SD. *(NC vs. NC+L-Pro): $p < 0.05$; *** $p < 0.001$; # (NC vs. siPGC-1α): $p < 0.05$. **(G)** Schematic diagram of stereotactic virus injection. **(H,I)** Confocal images of maximum intensity projection **(H)** and quantification **(I)** of adenovirus infection cell (green) after microinjection in DG in PND10. Scale bar, 50 μm. **(J,K)** Confocal image of EdU (gray) and DCX (red) staining with z-plane projections **(J)** and quantification **(K)** of the percentage of GFP⁺/DCX⁺/EdU⁺ (showing newborn neurons) in GFP⁺ infected cells in the

(Continued)

FIGURE 6
DG of mice at PND 14 after adenovirus injection (ADV-GFP-Con vs. ADV-GFP-L-Pro, $p < 0.001$, ADV-shPGC-1α-Con vs. ADV-shPGC-1α-L-Pro, $p = 0.334$. ADV-GFP-Con vs. ADV-shPGC-1α-Con, $p = 0.004$. $N = 3$). Scale bar, 50 μm. Error bars, mean ± SD. ***(ADV-GFP-Con vs ADV-GFP-L-Pro): $p < 0.001$; ## (ADV-GFP-Con vs. ADV-shPGC-1α-Con): $p < 0.01$. One-way ANOVA followed by an LSD test was used for analysis.

Low-dose Propofol promoted neurogenesis *via* PGC-1α/NRF1/TFAM pathway

It has been reported that Peroxisome proliferator-activated receptor gamma coactivator 1-alpha (Ppargc1a/PGC-1α) is the central regulator of mitochondrial biogenesis and respiration including OXPHOS and OCR (LeBleu et al., 2014). PGC-1α has been shown to affect neuronal differentiation (Uittenbogaard and Chiaramello, 2014). Therefore, the PGC-1α pathway was investigated after low-dose Propofol treatment. Consequently, increased mRNA level of Ppargc1a was observed to be most pronounced at 6 h post-Propofol treatment both in cultured NSCs (8-fold) (Supplementary Figure 5A) and hippocampus (1.6-fold) (Supplementary Figure 5B). Besides, PGC-1α and its downstream genes including Nuclear Respiratory Factor 1 (NRF1) and mitochondrial transcription factor A (TFAM) (Fanibunda et al., 2019; McMeekin et al., 2021) were all found to be elevated (1.3- to 1.5-fold) by low-dose Propofol at this timepoint *in vitro* (Figures 5G–I). In addition, PGC-1α was also found elevated (1.4-fold) in Nestin$^+$ cells of PND7 mice at 6 h-post-Propofol exposure (Figures 5J,K). These data indicated that low-dose Propofol activated PGC-1α-mediated mitochondrial biogenesis, which may exert an important regulatory control on OXPHOS and differentiation in NSCs.

To substantiate the association between PGC-1α and activated neurogenesis mediated by low-dose Propofol, downregulation of PGC-1α with associated small interfering RNA (siPGC-1α) was conducted in cultured NSCs. Inhibitory effects were evaluated *via* qPCR (70%) *in vitro* (Figure 6D). We found that siPGC-1α significantly prevented the OXPHOS promotion effect of low-dose Propofol (40%) (Figures 6A–C, S6). Besides, siPGC-1α also decreased the expression of neurogenesis markers (Tbr2, Dcx, and Tuj-1) at mRNA level (50–75%) (Figure 6D) and prevented the percentage of Tuj-1$^+$ cells (50%) (Figures 6E,F) increased by low-dose Propofol in NSCs differentiation 24 h- and 96 h-induction trials, respectively. We subsequently downregulated PGC-1α using adenovirus (ADV-shPGC-1α) in DG (Figure 6G). The efficiency was evaluated by confirming the infected level (Figures 6H,I) and calculating the downregulated level (57%) of PGC-1α (Supplementary Figure S7) by immunofluorescence staining *in vivo*. As expected, ADV-shPGC-1α injection in DG significantly prevented the elevated newborn neurons (64%) caused by low-dose Propofol (Figures 6J,K). These results provide direct evidence that the PGC-1α pathway participated in low-dose Propofol-activated OXPHOS and neuronal differentiation in NSCs both *in vitro* and *in vivo*.

Taken together, these results indicated the participation of PGC-1α-mediated OXPHOS in neuronal fate commitment preference in NSCs caused by low-dose Propofol.

Discussion

To explore the effect of Propofol applied in sedation or anesthesia in pediatrics on brain development, we first tested the sub-anesthesia dosage, 4 mg.kg^{-1} (L-Propofol) (Chen et al., 2021) along with the frequently used dosage in mice and 50 mg.kg^{-1} (H-Propofol) in cognitive function of neonatal mice (Jiang et al., 2018). As reported before, under 50 mg.kg^{-1}, slightly impaired spatial learning function in the acquisition test was observed (Zhong et al., 2018). Under 4 mg.kg^{-1}, mice were sedated but still responding to painful stimuli, and the plasma Propofol concentration was verified as a clinically sedative concentration. Surprisingly, our study demonstrated that mice exhibited a trend of shortened escape latency, and significantly increased platform crossing after low-dose Propofol treatment in the MWM test, suggesting the enhanced spatial cognitive ability. Moreover, we further explored other memory capabilities, including object recognition memory and working memory, as well as the anxiety emotion in mice after Propofol treatment. As no significant difference was found in NOR, Y maze, and OFT, specifically enhanced spatial cognitive abilities after 4 mg.kg^{-1} Propofol treatment was confirmed. Previous studies have reported that low doses of anesthetics presented positive effects on neurodevelopment, such as sevoflurane could promote the learning ability in neonatal rats (Chen et al., 2018). Besides, Propofol at doses of 10–50 mg.kg^{-1} has been reported to protect neurological function in ischemia and hypoxia models (Shi et al., 2014; Yang et al., 2018), but the underlying mechanism has not been fully elucidated. There are still no studies investigating the effects of single low-dose Propofol, which exerts sedative effects, on the developing brain. In this study, 4 mg.kg^{-1} Propofol, which produced the sedative effect in neonatal mice, was used to clarify the effect of low-dose Propofol on children's brain development when undergoing invasive procedures clinically. Our behavioral results demonstrated a new perspective on anesthetics for pediatric brain development: 4 mg.kg^{-1} Propofol promoted cognitive function in neonatal brains.

One of the important factors influencing emotion and spatial cognitive function lies in hippocampal neurogenesis. Decreased neurogenesis in childhood is accompanied by a decline in learning and memory (Doi et al., 2021), while the increase in hippocampal neurons in neonatal mice contributes to the preservation of cognitive function (Martin et al., 2012). In our study, 4 mg.kg^{-1} Propofol increased the overall EdU^{+} newborn cells in the developing hippocampal DG, while lineage tracing also showed significantly increased NSCs expansion and neuronal differentiation. *In vitro*, 10 μM Propofol, closely to plasma concentrations *in vivo* (8 μM) measured in this study (Supplementary Figure 1), was selected and found to significantly increase NSC proliferation and neuronal differentiation. The result was consistent with the conclusion in a previous study that 10 μM Propofol was used to treat human-derived NPC cell lines (Qiao et al., 2017), suggesting that a sedative dose of Propofol promoted NSCs proliferation and neuronal fate decision.

To understand the effect of 4 mg.kg^{-1} Propofol on the hippocampal neurogenesis pool more accurately, an snRNA-seq was adopted to deeply analyze the specific changes in neurogenesis-related cell groups. First, pseudotime analysis suggested a similar pattern of neurogenesis after low-dose Propofol exposure. An increased trend in the proportion of neurons in all differentiation stages was found, especially NPCs (48%), after low-dose Propofol exposure. One possible explanation is that low-dose Propofol not only acted on neurons in a particular stage but might affect neurons at all stages, especially in neuronal differentiation. Another possibility is that Propofol inhibited the apoptosis of newborn neurons, but a previous study showed that apoptosis was not the main factor that Propofol affects the viability of NSCs (Tao et al., 2013), which we confirmed the result in our research (Supplementary Figure 3). Moreover, to observe the safety of Propofol usage in promoting neurogenesis, hippocampal neurogenesis in aged mice after treatment was further evaluated. There was no significant difference in the amount of NSCs in DG after neonatal 4 mg.kg^{-1} Propofol exposure, suggesting the safety of 4 mg.kg^{-1} Propofol exposure in childhood as it would not later cause NSCs pool depletion due to the promotion of neurogenesis. Our study drew consistent conclusions from three aspects: *in vivo* lineage tracing, *in vitro* NSCs experiments, and snRNA-seq, that low-dose Propofol could promote hippocampal neurogenesis in neonatal mice, without causing a significant long-term negative effect.

Mitochondria function plays an essential role in neurogenesis. In healthy PND 3-14 rat brain, PGC-1α, the master regulator of mitochondrial respiration, specifically highly expressed in DG, has been indicated to be important in brain development (Cowell et al., 2007; Finck and Kelly, 2007). By downregulating PGC-1α both *in vitro* and *in vivo*, we found that the promotion of neurogenesis after low-dose Propofol treatment was prevented, implying that PGC-1α-mediated mitochondrial metabolism was of great significance in Propofol-induced neurogenesis. Previous studies have shown that PGC-1α, as a key molecule in mitochondrial biogenesis, is significantly upregulated during NPCs differentiation (Zheng et al., 2016). Besides, it has been reported that overexpression of PGC-1α in NSCs from aged mice affected the proliferation of NSCs *in vitro*, while overexpression of PGC-1α in SVZ of aged mice regulated neural regeneration by increasing DCX^{+} and DA^{+} neurons (Stoll et al., 2015), verifying that PGC-1α could mediate the fate of NSCs. In this study, by downregulating PGC-1α in NSCs, a reduction in the proportion of Tuj-1^{+} cells *in vitro* and a decrease in newborn neurons *in vivo* were observed. Thus, our results suggested that low-dose Propofol could regulate the expression of PGC-1α which could be involved in NSCs neuronal differentiation. However, we did not verify whether overexpression of PGC-1α in NSCs could mimic the pro-neurogenesis phenomenon of low-dose Propofol in this study, which remains to be further explored. Taken together, our results suggested that PGC-1α-mediated mitochondrial metabolism was involved in the effect of low-dose Propofol on hippocampal neurogenesis in neonatal mice.

Propofol is one of the most commonly used drugs for sedation in children. In this study, we explored the effect of 4 mg.kg^{-1} Propofol, as a clinically sedative dosage, on brain development. Our study found that 4 mg.kg^{-1} Propofol promoted hippocampal neurogenesis and spatial cognitive function in neonatal mice. Meanwhile, the crucial role of PGC-1α-mediated mitochondrial metabolism in neurogenesis was further revealed, especially in NSCs' fate decisions. Increasing evidence has shown that mitochondria function contributed to neuronal function protection and neurogenesis regulation. Pharmacological upregulation of PGC-1α expression restores neuronal morphogenesis in mitochondrial dysfunctional cerebral organoids (Inak et al., 2021), while a large number of studies have suggested that PGC-1α is a potential therapeutic target for neurodegenerative diseases (Panes et al., 2022). Thus, our work provides new clues for the usage of low-dose Propofol in pediatrics examinations as a potential benefit for neurodevelopment in the vulnerable period.

Data availability statement

The datasets in the current study are available from the corresponding author on reasonable request. Raw data and processed data of snRNA-seq are available at the Gene Expression Omnibus (GEO) database with accession number "GEO: GSE186216". Raw data and processed data of bulk RNA-seq are available at the GEO database with accession number "GEO: GSE200968".

Ethics statement

The animal study was reviewed and approved by Ethical Committee of Sun Yat-sen University.

Author contributions

XF and MW: study supervision. KC, DL, and XY: study design/planning. KC, DL, XY, RZ, LL, YW, XX, CW, and MHJ: study conduct. All authors contributed to the article and approved the submitted version.

Funding

This study was supported by the National Natural Science Foundation of China [Grant Numbers: 81770290 (MHJ), 81870829 (XF), 82071224 (XF), and 31972894 (MHJ)], the Science and Technology Program of Guangzhou, China (201804010492, XF), and the Major Project of Basic and Applied Basic Research Foundation of Guangdong Province (2019B1515120054, XF).

Acknowledgments

We want to thank Prof. Weiwei Su and Dr. Taobin Chen, for the kindly help in accessing the drug concentration *via* HPLC and thank Prof. Yibo Qu and Prof. Li Zhang for the valuable advice on study design.

Conflict of interest

The authors declare that the research was conducted in the absence of any commercial or financial relationships that could be construed as a potential conflict of interest.

Publisher's note

Supplementary material

The Supplementary Material for this article can be found online at: https://www.frontiersin.org/articles/10.3389/fnagi.2022.925728/full#supplementary-material

References

Anacker, C., and Hen, R. (2017). Adult hippocampal neurogenesis and cognitive flexibility - linking memory and mood. *Nat. Rev. Neurosci.* 18, 335–346. doi: 10.1038/nrn.2017.45

Armand, E. J., Li, J., Xie, F., Luo, C., and Mukamel, E. A. (2021). Single-cell sequencing of brain cell transcriptomes and epigenomes. *Neuron* 109, 11–26. doi: 10.1016/j.neuron.2020.12.010

Artegiani, B., Lyubimova, A., Muraro, M., van Es, J. H., van Oudenaarden, A., and Clevers, H. (2017). A single-cell RNA sequencing study reveals cellular and molecular dynamics of the hippocampal neurogenic niche. *Cell Rep.* 21, 3271–3284. doi: 10.1016/j.celrep.2017.11.050

Ceccarelli, M., D'Andrea, G., Micheli, L., and Tirone, F. (2020). Interaction between neurogenic stimuli and the gene network controlling the activation of stem cells of the adult neurogenic niches, in physiological and pathological conditions. *Front. Cell. Dev. Biol.* 8, 211. doi: 10.3389/fcell.2020.00211

Cembrowski, M. S., Wang, L., Sugino, K., Shields, B. C., and Spruston, N. (2016). Hipposeq: a comprehensive RNA-seq database of gene expression in hippocampal principal neurons. *Elife* 5, e14997. doi: 10.7554/eLife.14997.028

Chen, C., Shen, F. Y., Zhao, X., Zhou, T., Xu, D. J., Wang, Z. R., et al. (2015). Low-dose sevoflurane promotes hippocampal neurogenesis and facilitates the development of dentate gyrus-dependent learning in neonatal rats. *ASN Neuro* 7, 1759091415575845. doi: 10.1177/1759091415575845

Chen, H., Xu, D., Zhang, Y., Yan, Y., Liu, J., Liu, C., et al. (2021). Neurons in the locus coeruleus modulate the hedonic effects of sub-anesthetic dose of propofol. *Front. Neurosci.* 15, 636901. doi: 10.3389/fnins.2021.636901

Chen, X., Zhou, X., Yang, L., Miao, X., Lu, D.H., Yang, X.Y., et al. (2018). Neonatal exposure to low-dose (1.2%) sevoflurane increases rats' hippocampal neurogenesis and synaptic plasticity in later life. *Neurotox. Res.* 34, 188–197. doi: 10.1007/s12640-018-9877-3

Colla, M., Scheerer, H., Weidt, S., Seifritz, E., and Kronenberg, G. (2021). Novel insights into the neurobiology of the antidepressant response from ketamine research: a mini review. *Front. Behav. Neurosci.* 15, 759466. doi: 10.3389/fnbeh.2021.759466

Cowell, R. M., Blake, K. R., and Russell, J. W. (2007). Localization of the transcriptional coactivator PGC-1alpha to GABAergic neurons during maturation of the rat brain. *J. Comp. Neurol.* 502, 1–18. doi: 10.1002/cne.21211

Deyama, S., and Duman, R. S. (2020). Neurotrophic mechanisms underlying the rapid and sustained antidepressant actions of ketamine. *Pharmacol. Biochem. Behav.* 188, 172837. doi: 10.1016/j.pbb.2019.172837

Doi, H., Matsuda, T., Sakai, A., Matsubara, S., Hoka, S., Yamaura, K., et al. (2021). Early-life midazolam exposure persistently changes chromatin accessibility to impair adult hippocampal neurogenesis and cognition. *Proc. Natl. Acad. Sci. U. S. A.* 118, e2107596118. doi: 10.1073/pnas.2107596118

Fanibunda, S. E., Deb, S., Maniyadath, B., Tiwari, P., Ghai, U., Gupta, S., et al. (2019). Serotonin regulates mitochondrial biogenesis and function in rodent cortical neurons via the 5-HT2A receptor and SIRT1-PGC-1alpha axis. *Proc. Natl. Acad. Sci. U. S. A.* 116, 11028–11037. doi: 10.1073/pnas.1821332116

Favaro, R., Valotta, M., Ferri, A. L., Latorre, E., Mariani, J., Giachino, C., et al. (2009). Hippocampal development and neural stem cell maintenance require Sox2-dependent regulation of Shh. *Nat. Neurosci.* 12, 1248–1256. doi: 10.1038/nn.2397

Finck, B. N., and Kelly, D. P. (2007). Peroxisome proliferator-activated receptor gamma coactivator-1 (PGC-1) regulatory cascade in cardiac physiology and disease. *Circulation* 115, 2540–2548. doi: 10.1161/CIRCULATIONAHA.107.670588

Gao, Y., Zhang, R., Wei, G., Dai, S., Zhang, X., Yang, W., et al. (2019). Long non-coding RNA maternally expressed 3 increases the expression of neuron-specific genes by targeting miR-128-3p in all-trans retinoic acid-induced neurogenic differentiation from amniotic epithelial cells. *Front. Cell Dev. Biol.* 7, 342. doi: 10.3389/fcell.2019.00342

Goncalves, J. T., Schafer, S. T., and Gage, F. H. (2016). Adult neurogenesis in the hippocampus: from stem cells to behavior. *Cell* 167, 897–914. doi: 10.1016/j.cell.2016.10.021

Hochgerner, H., Zeisel, A., Lonnerberg, P., and Linnarsson, S. (2018). Conserved properties of dentate gyrus neurogenesis across postnatal development revealed by single-cell RNA sequencing. *Nat. Neurosci.* 21, 290–299. doi: 10.1038/s41593-017-0056-2

Inak, G., Rybak-Wolf, A., Lisowski, P., Pentimalli, T. M., Juttner, R., Glazar, P., et al. (2021). Defective metabolic programming impairs early neuronal morphogenesis in neural cultures and an organoid model of Leigh syndrome. *Nat. Commun.* 12, 1929. doi: 10.1038/s41467-021-22117-z

Ing, C., Warner, D. O., Sun, L. S., Flick, R. P., Davidson, A. J., Vutskits, L., et al. (2022). Anesthesia and developing brains: unanswered questions and proposed paths forward. *Anesthesiology* 136, 500–512. doi: 10.1097/ALN.0000000000004116

Iwata, R., and Vanderhaeghen, P. (2021). Regulatory roles of mitochondria and metabolism in neurogenesis. *Curr. Opin. Neurobiol.* 69, 231–240. doi: 10.1016/j.conb.2021.05.003

Jevtovic-Todorovic, V., and Brambrick, A. (2018). General anesthesia and young brain: what is new? *J. Neurosurg. Anesthesiol.* 30, 217–222. doi: 10.1097/ANA.0000000000000432

Jiang, C., Logan, S., Yan, Y., Inagaki, Y., Arzua, T., Ma, P., et al. (2018). Signaling network between the dysregulated expression of microRNAs and mRNAs in propofol-induced developmental neurotoxicity in mice. *Sci. Rep.* 8, 14172. doi: 10.1038/s41598-018-32474-3

Kapoor, R., Fanibunda, S. E., Desouza, L. A., Guha, S. K., and Vaidya, V. A. (2015). Perspectives on thyroid hormone action in adult neurogenesis. *J. Neurochem.* 133, 599–616. doi: 10.1111/jnc.13093

Khacho, M., Harris, R., and Slack, R. S. (2019). Mitochondria as central regulators of neural stem cell fate and cognitive function. *Nat. Rev. Neurosci.* 20, 34–48. doi: 10.1038/s41583-018-0091-3

Kim, I. T. (2007). Adjustable strabismus surgery under intravenous anesthesia with propofol and fentanyl. *J. Korean Ophthalmol. Soc.* 48, 1522–1526. doi: 10.3341/jkos.2007.48.11.1522

Lalli, M. A., Jang, J., Park, J. H. C., Wang, Y., Guzman, E., Zhou, H., et al. (2016). Haploinsufficiency of BAZ1B contributes to Williams syndrome through transcriptional dysregulation of neurodevelopmental pathways. *Hum. Mol. Genet.* 25, 1294–1306. doi: 10.1093/hmg/ddw010

LeBleu, V. S., O'Connell, J. T., Gonzalez Herrera, K. N., Wikman, H., Pantel, K., Haigis, M. C., et al. (2014). PGC-1alpha mediates mitochondrial biogenesis and oxidative phosphorylation in cancer cells to promote metastasis. *Nat. Cell Biol.* 16 992–1003, 1001–1015. doi: 10.1038/ncb3039

Li, C. T., Chen, M. H., Lin, W. C., Hong, C. J., Yang, B. H., Liu, R. S., et al. (2016). The effects of low-dose ketamine on the prefrontal cortex and amygdala in treatment-resistant depression: a randomized controlled study. *Hum. Brain Mapp.* 37, 1080–1090. doi: 10.1002/hbm.23085Images with z-plane projections

Martin, N., Bossenmeyer-Pourie, C., Koziel, V., Jazi, R., Audonnet, S., Vert, P., et al. (2012). Non-injurious neonatal hypoxia confers resistance to brain senescence in aged male rats. *PLoS ONE* 7, e48828. doi: 10.1371/journal.pone.0048828

Mathon, B., Nassar, M., Simonnet, J., Le Duigou, C., Clemenceau, S., Miles, R., et al. (2015). Increasing the effectiveness of intracerebral injections in adult and neonatal mice: a neurosurgical point of view. *Neurosci. Bull.* 31, 685–696. doi: 10.1007/s12264-015-1558-0

McMeekin, L. J., Fox, S. N., Boas, S. M., and Cowell, R. M. (2021). Dysregulation of PGC-1alpha-dependent transcriptional programs in neurological and developmental disorders: therapeutic challenges and opportunities. *Cells* 10, 352. doi: 10.3390/cells10020352

Mizrak, D., Levitin, H. M., Delgado, A. C., Crotet, V., Yuan, J., Chaker, Z., et al. (2019). Single-cell analysis of regional differences in adult V-SVZ neural stem cell lineages. *Cell Rep* 26, 394–406.e395. doi: 10.1016/j.celrep.2018.12.044

Niklison-Chirou, M. V., Agostini, M., Amelio, I., and Melino, G. (2020). Regulation of adult neurogenesis in mammalian brain. *Int. J. Mol. Sci.* 21. doi: 10.3390/ijms21144869

Panes, J. D., Wendt, A., Ramirez-Molina, O., Castro, P. A., and Fuentealba, J. (2022). Deciphering the role of PGC-1alpha in neurological disorders: from mitochondrial dysfunction to synaptic failure. *Neural Regen. Res.* 17, 237–245. doi: 10.4103/1673-5374.317957

Qiao, H., Li, Y., Xu, Z., Li, W., Fu, Z., Wang, Y., et al. (2017). Propofol affects neurodegeneration and neurogenesis by regulation of autophagy via effects on intracellular calcium homeostasis. *Anesthesiology* 127, 490–501. doi: 10.1097/ALN.0000000000001730

Rosenberg, A. B., Roco, C. M., Muscat, R. A., Kuchina, A., Sample, P., Yao, Z., et al. (2018). Single-cell profiling of the developing mouse brain and spinal cord with split-pool barcoding. *Science* 360, 176–182. doi: 10.1126/science.aam8999

Schraag, S., Petscher, M., Wachter, U., Kreuer, S., Kenny, G., and Wagner, F. (2019). Performance of target-controlled infusion of propofol in plasma versus effect-site control during induction in elderly patients: a letter to the editor. *J. Clin. Anesth.* 58, 9–11. doi: 10.1016/j.jclinane.2019.04.013

Shi, S. S., Yang, W. Z., Chen, Y., Chen, J. P., and Tu, X. K. (2014). Propofol reduces inflammatory reaction and ischemic brain damage in cerebral ischemia in rats. *Neurochem. Res.* 39, 793–799. doi: 10.1007/s11064-014-1272-8

Stoll, E. A., Makin, R., Sweet, I. R., Trevelyan, A. J., Miwa, S., Horner, P. J., et al. (2015). Neural stem cells in the adult subventricular zone oxidize fatty acids to produce energy and support neurogenic activity. *Stem Cells* 33, 2306–2319. doi: 10.1002/stem.2042

Sun, L., Ye, R., Liang, R., and Xing, F. (2020). Treadmill running attenuates neonatal hypoxia induced adult depressive symptoms and promoted hippocampal neural stem cell differentiation via modulating AMPK-mediated mitochondrial functions. *Biochem. Biophys. Res. Commun.* 523, 514–521. doi: 10.1016/j.bbrc.2019.12.036

Suthapot, P., Xiao, T., Felsenfeld, G., Hongeng, S., and Wongtrakoongate, P. (2022). The RNA helicases DDX5 and DDX17 facilitate neural differentiation of human pluripotent stem cells NTERA2. *Life Sci.* 291, 120298. doi: 10.1016/j.lfs.2021.120298

Tao, T., Zhao, Z., Hao, L., Gu, M., Chen, L., and Tang, J. (2013). Propofol promotes proliferation of cultured adult rat hippocampal neural stem cells. *J. Neurosurg. Anesthesiol.* 25, 299–305. doi: 10.1097/ANA.0b013e31828baa93

Toda, T., Parylak, S. L., Linker, S. B., and Gage, F. H. (2019). The role of adult hippocampal neurogenesis in brain health and disease. *Mol. Psychiatry* 24, 67–87. doi: 10.1038/s41380-018-0036-2

Uittenbogaard, M., and Chiaramello, A. (2014). Mitochondrial biogenesis: a therapeutic target for neurodevelopmental disorders and neurodegenerative diseases. *Curr. Pharm. Des.* 20, 5574–5593. doi: 10.2174/1381612820666140305224906

Vieira, M. S., Santos, A. K., Vasconcellos, R., Goulart, V. A. M., Parreira, R. C., Kihara, A. H., et al. (2018). Neural stem cell differentiation into mature neurons: mechanisms of regulation and biotechnological applications. *Biotechnol. Adv.* 36, 1946–1970. doi: 10.1016/j.biotechadv.2018.08.002

Vutskits, L., and Xie, Z. (2016). Lasting impact of general anaesthesia on the brain: mechanisms and relevance. *Nat. Rev. Neurosci.* 17, 705–717. doi: 10.1038/nrn.2016.128

Wu, L., Zhao, H., Weng, H., and Ma, D. (2019). Lasting effects of general anesthetics on the brain in the young and elderly: "mixed picture" of neurotoxicity, neuroprotection and cognitive impairment. *J. Anesth.* 33, 321–335. doi: 10.1007/s00540-019-02623-7

Ximerakis, M., Lipnick, S. L., Innes, B. T., Simmons, S. K., Adiconis, X., Dionne, D., et al. (2019). Single-cell transcriptomic profiling of the aging mouse brain. *Nat. Neurosci.* 22, 1696–1708. doi: 10.1038/s41593-019-0491-3

Yamaguchi, M., Saito, H., Suzuki, M., and Mori, K. (2000). Visualization of neurogenesis in the central nervous system using nestin promoter-GFP transgenic mice. *Neuroreport* 11, 1991–1996. doi: 10.1097/00001756-200006260-00037

Yang, C. Y., Liu, S. Y., Wang, H. Y., Li, Y. L., Guo, D., Wang, X. Y., et al. (2018). Neuroprotection by propofol post-conditioning: focus on PKMzeta/KCC2 pathway activity. *Cell. Mol. Neurobiol.* 38, 691–701. doi: 10.1007/s10571-017-0530-0

Zhao, T., Ziwen, S., Ling, N., Xu, Y., Qin, J., Zhou, Q., et al. (2022). Sevoflurane ameliorates schizophrenia in a mouse model and patients: pre-clinical and clinical feasibility study. *Curr. Neuropharmacol.* doi: 10.2174/1570159X20666220310115846. [Epub ahead of print].

Zheng, X., Boyer, L., Jin, M., Mertens, J., Kim, Y., Ma, L., et al. (2016). Metabolic reprogramming during neuronal differentiation from aerobic glycolysis to neuronal oxidative phosphorylation. *Elife* 5, e13374. doi: 10.7554/eLife.13374.034

Zhong, Y., Chen, J., Li, L., Qin, Y., Wei, Y., Pan, S., et al. (2018). PKA-CREB-BDNF signaling pathway mediates propofol-induced long-term learning and memory impairment in hippocampus of rats. *Brain Res.* 1691, 64–74. doi: 10.1016/j.brainres.2018.04.022

Zhou, H., Xie, Z., Brambrink, A. M., and Yang, G. (2021). Behavioural impairments after exposure of neonatal mice to propofol are accompanied by reductions in neuronal activity in cortical circuitry. *Br. J. Anaesth.* 126, 1141–1156. doi: 10.1016/j.bja.2021.01.017

Zywitza, V., Misios, A., Bunatyan, L., Willnow, T. E., and Rajewsky, N. (2018). Single-cell transcriptomics characterizes cell types in the subventricular zone and uncovers molecular defects impairing adult neurogenesis. *Cell Rep.* 25, 2457–2469.e2458. doi: 10.1016/j.celrep.2018.11.003

frontiers | Frontiers in Neuroscience

TYPE Original Research
PUBLISHED 18 August 2022
DOI 10.3389/fnins.2022.925300

OPEN ACCESS

EDITED BY
Yingwei Wang,
Independent Researcher, Shanghai, China

REVIEWED BY
Gu Hanwen,
First Affiliated Hospital of Zhengzhou University, China
Muhuo Ji,
Nanjing Medical University, China

*CORRESPONDENCE
Chan Chen
chenchan@scu.edu.cn;
xychenchan@gmail.com

†These authors have contributed equally to this work

SPECIALTY SECTION
This article was submitted to Neuropharmacology, a section of the journal Frontiers in Neuroscience

RECEIVED 31 May 2022
ACCEPTED 14 July 2022
PUBLISHED 18 August 2022

CITATION
Liu C, Gao R, Tang Y, Chen H, Zhang X, Sun Y, Zhao Q, Lv P, Wang H, Ye-Lehmann S, Liu J and Chen C (2022) Identification of potential key circular RNAs related to cognitive impairment after chronic constriction injury of the sciatic nerve. *Front. Neurosci.* 16:925300. doi: 10.3389/fnins.2022.925300

Identification of potential key circular RNAs related to cognitive impairment after chronic constriction injury of the sciatic nerve

Changliang Liu [1,2,3†], Rui Gao[1,2,3†], Yidan Tang[1,2,3], Hai Chen[4], Xueying Zhang[1,2,3], Yalan Sun[1,2,3], Qi Zhao[1,2,3], Peilin Lv[1,2,3], Haiyang Wang[5], Shixin Ye-Lehmann[6], Jin Liu[1,2,3] and Chan Chen[1,2,3*]

[1]Department of Anesthesiology, National Clinical Research Center for Geriatrics, West China Hospital, Sichuan University, Chengdu, China, [2]Laboratory of Anesthesia and Critical Care Medicine, National-Local Joint Engineering Research Center of Translational Medicine of Anesthesiology, West China Hospital, Sichuan University, Chengdu, China, [3]The Research Units of West China, Chinese Academy of Medical Sciences, Chengdu, China, [4]Targeted Tracer Research and Development Laboratory, Department of Respiratory and Critical Care Medicine, West China Hospital, Sichuan University, Chengdu, China, [5]Department of Otolaryngology, Head and Neck Surgery, West China Hospital, Sichuan University, Chengdu, China, [6]Unité INSERM U1195, Hôpital de Bicêtre, Université Paris-Saclay, Paris, France

Chronic neuropathic pain is commonly accompanied by cognitive impairment. However, the underlying mechanism in the occurrence of cognitive deficits under constant nociceptive irritation remains elusive. Herein, we established a chronic neuropathic pain model by chronic constriction injury (CCI) of the unilateral sciatic nerve in rats. Behavioral tests indicated that CCI rats with long-term nociceptive threshold decline developed significant dysfunction of working memory and recognitive memory starting at 14 days and lasting for at least 21 days. Afterward, circRNA expression profiles in the hippocampus of CCI and sham rats were analyzed *via* high-throughput sequencing to explore the potential key factors associated with cognitive impairment induced by ongoing nociception, which showed 76 differentially expressed circRNAs, 39 upregulated and 37 downregulated, in the CCI group. These differentially expressed circRNA host genes were validated to be primarily associated with inflammation and apoptotic signaling pathways according to GO/KEGG analysis and the circRNA-miRNA-mRNA network, which was also confirmed through the analysis of neuroinflammation and neuronal apoptosis. Consequently, we assumed that enhanced neuroinflammation and neuronal apoptosis might act as potential regulators of cognitive impairment induced by chronic

neuropathic pain. The identification of the regulatory mechanism would provide promising clinical biomarkers or therapeutic targets in the diagnostic prediction and intervention treatment of memory deficits under neuropathic pain conditions.

KEYWORDS

chronic neuropathic pain, cognitive impairment, chronic constriction injury, neuroinflammation, neuronal apoptosis

Introduction

Chronic pain, characterized by persistent pain and typical sensory, cognitive, and affective abnormalities, impacts 20∼30% of the adult population (Ta Dinh et al., 2019). Increasing clinical evidence has also demonstrated that patients with chronic pain suffer from objective adverse effects on cognition, including learning memory, decision-making, attention, processing speed, and psychomotor speed (Zhang et al., 2021). Among these, the memory processes associated with attention and working are the most likely to be affected under chronic pain conditions (Mazza et al., 2018), which may substantially influence quality of life in patients with chronic pain. Meanwhile, preclinical research has revealed that rodents with chronic neuropathic pain also develop significant damage in working memory and recognitive memory (You et al., 2018). Despite the clinical and preclinical evidence confirming that memory impairment is a frequent comorbidity in chronic pain, the underlying mechanisms remain unclear.

Alterations in mRNA expression have been validated to be correlated with a variety of diseases by regulating protein expression, including cancer, cardiovascular disease, and neurodegenerative disorders (Lee and Young, 2013). In comparison, non-coding RNAs (ncRNAs) are crucial classes of untranslated transcripts that have been proven to be a significant part of human transcriptomes and are involved in almost all physiological and pathological processes (Li et al., 2017). Circular RNAs (circRNAs), a well-established class of ncRNAs characterized by a covalently based circular structure formed by non-linear splicing, are highly expressed in mammalian brain tissues (Hanan et al., 2017). Increasing studies have revealed that circRNAs play essential roles in inhibiting the function of microRNAs, regulating the activity of RNA polymerase, and modulating the expression of corresponding genes by binding to promoters (Jens, 2014; Xiao et al., 2015). Of note, a growing number of studies have further confirmed that circRNAs are essential regulators of inflammation and apoptotic processes (Liu J. et al., 2021; Zhu et al., 2021), which are closely associated with the development of neuropsychiatric disorders. In addition, the dysregulation of circRNA expression in the dorsal root ganglion or brain could contribute to nociceptive threshold reduction and nociceptive hypersensitivity (Xin et al., 2021; Xu et al., 2021). Meanwhile, circRNAs also play substantial roles in the occurrence of cognitive impairment with different neuropathologies (Lu et al., 2019; Cao et al., 2020). However, the potential vital regulatory factors related to cognitive deficits under chronic pain conditions are extremely unclear.

Insights into the potential mechanism of long-lasting nociceptive threshold decline-induced cognitive decline promise to advance the understanding of the underlying pathophysiology and benefit from developing biomarkers and therapeutic strategies. Therefore, we fabricated a chronic neuropathic pain model by CCI on the left sciatic nerve. Behavioral tests demonstrated that the ongoing chronic pain condition of the CCI rats exhibited apparent deficits in working and recognition memory. Then, we performed transcriptome sequencing analysis to investigate the differential expression profiles of circRNAs in the hippocampus between the CCI and sham groups. The results revealed that the genes related to inflammation and apoptosis were significantly disturbed in the hippocampus of CCI rats, which indicated a possible mechanism of chronic pain-induced cognitive impairment. These results might help provide insights for clinical biomarkers and therapeutic targets for cognitive dysfunction under chronic pain conditions.

Materials and methods

Animals

Adult male Sprague Dawley rats (5–8 weeks, 180–220 g) were obtained from Dossy Experimental Animals Co., Ltd. (Chengdu, China) and raised under controlled conditions with a 12-h alternate circadian rhythm, a room temperature of 22–25°C, a relative humidity of 40∼70%, and food and water provided *ad libitum*. The rats were housed 2–6 per cage and allowed 1 week to acclimate to the surroundings before the beginning of experiments. All animal experiments in this study were approved by the Ethics Committee of Sichuan University and performed in strict compliance with the guidelines accepted by the International Association for the Study of Pain and the National Institute of Health Guidelines for the Care and Use of Laboratory Animals.

Establishment of the chronic neuropathic pain model

A chronic neuropathic pain model was constructed through chronic constriction injury (CCI) of the sciatic nerve as described previously (Bao et al., 2021). Briefly, rats were anesthetized with sodium pentobarbital (50 mg/kg), and an incision was made in the left thigh to expose the sciatic nerve with almost transverse running, which was visible between the anterior and posterior groups of muscles. Four ligatures were tied loosely by chromic gut sutures 4–0 around the sciatic nerve with a 1.0∼1.5 mm interval between each ligature. The sham group was operated on by exposing only the sciatic nerve without ligation.

Pain-related behaviors

Machinal allodynia and thermal hyperalgesia of all animals were assessed at days –1, 1, 3, 7, 14, and 21 after CCI according to previous reports (Zhang et al., 2021). Machinal allodynia was investigated by detecting the paw withdrawal thresholds (PWTs) with von Frey filaments through the up and down method. Briefly, the rats were allowed to acclimatize for 30 min in suspended cages with wire mesh floors before the test. A series of von Frey filaments weighing 0.008∼300 g was applied. The filaments were in ascending order of strength and perpendicular to the plantar surface with sufficient force to cause slight bending against the paw. Paw withdrawal, flinching, or paw licking was recorded as a positive response. Afterward, the filament of the next lower force was applied to press the plantar surface until a negative response appeared. Then, the filament of the next greater force was applied. This up-down method was repeated until five behavioral changes were determined, and the pattern of positive and negative responses was recorded. Thermal hyperalgesia was determined by detecting paw withdrawal latency (PWL) on a thermal testing apparatus (Ugo Basile plantar test, 37370, Italy). Rats were kept in transparent cages on an elevated glass plate and allowed to acclimatize for 30 min before the experiment. After that, an infrared radiant thermal stimulator was focused on the plantar surface of the hind paw through the glass plate. The time of the nociceptive endpoint was considered the PWL when the characteristic lifting or licking of the hind paw appeared. A cutoff time of 20 s was used to avoid tissue damage.

Assessment of cognitive behavior

The cognitive function of rats after CCI was investigated through the Y maze and novel object recognition according to the literature reports (Xiong et al., 2020; Zhang et al., 2021). Prior to the cognitive behavior test, the locomotor activity of the rats was investigated through an open field test (OFT) in a large black arena of 120 × 120 × 60 cm. The total traveled distance in 5 min was recorded using a camera mounted above the arena and analyzed by the data analysis system. The OFT arena was cleaned with 75% v/v ethanol between each rat. Afterward, the Y maze spontaneous alternation test was performed to investigate exploratory behavior based on the willingness of the rats to visit a new arm rather than a familiar arm in the maze. The Y maze consists of three enclosed arms with an angle of 120 degrees, and each arm was 50 cm in length, 10 cm in width, and 25 cm in height. Each rat was gently placed in the same position of the maze and traced using a video-tracking system for an 8 min period in a caliginous and quiet room. The sequence and number of arm entries were carefully recorded, and a spontaneous alternation was defined as a rat entering all three arms on consecutive choices (ABC, ACB, BCA, BAC, CAB or CBA). The percentage of spontaneous alternation was calculated according to the formula:% spontaneous alternation = number of spontaneous alternations/(total arm entries—2) × 100%. Additionally, the novel object recognition test was performed in a box of 60 × 60 × 50 cm. The rats were placed into the box for 10 min on the first day without objects. After 2 h, two identical objects were placed into the testing box, and the rats were allowed to explore the objects for 5 min of training. After a 24 h intertrial interval in the home cage, the rats were allowed to explore the objects freely for 5 min in the same arena with one of the familiar objects and a novel object. The total time spent investigating each object within 1.5 cm using sniffing or touching the object with the nose was recorded. The longer exploration duration of a novel object was defined as evidence for intact recognition memory. The recognition index was calculated by (novel object investigation time)/(total investigation time of both objects) × 100% to compare the memory retention of each group of rats.

Tissue collection and total RNA isolation

The rats were sacrificed at day 21 after CCI, and the hippocampus was excised quickly and stored in liquid nitrogen. Total RNA was extracted using the FastPure Cell/Tissue Total RNA Isolation Kit (Vazyme), and RNA integrity was investigated on an Agilent 2100 Bioanalyzer (Santa Clara, CA, United States). The samples with an RNA integrity number (RIN) ≥ 7 were stored at –80℃ for further usage.

RNA sequencing and analysis

Total transcriptome sequencing of six samples containing three hippocampal samples from the CCI group and three from the sham group was carried out by Shanghai OE Biotech.

Co. Ltd. (China). Clean data were obtained by removing reads containing poly-N, adapters, and low-quality reads, and then the average GC content (48.51%) and Q30 base distribution (93.01∼93.4%) were analyzed. Each sample's genome alignment was obtained with an alignment rate of 96.24∼96.63% by comparing reads to the reference genome. Afterward, the circRNA sequencing (RNA-seq) libraries were acquired, and the fold change (ratio of the average expression in each group) and *P*-value were calculated. CircRNAs with fold change ≥ 2 or ≤ 0.5 and *P*-value ≤ 0.05 were screened as the significant differentially expressed genes for further analysis. Of note, the genes undetected either in the sham groups or CCI groups were not screened in the further investigation.

Western blot assay

When obvious cognitive impairment was exhibited at 21 days after CCI, the rats were sacrificed, and the hippocampus was excised immediately on ice. Total protein was collected from the hippocampus by homogenizing the tissues in RIPA lysis buffer supplemented with proteinase (Solarbio, Beijing, China) and phosphatase inhibitors (Solarbio). After incubation for 1 h, the protein fractions were harvested by centrifugation at 13,000 rpm for 10 min at 4℃. The protein concentrations were identified using a BCA relative protein quantification kit (Beyotime, Shanghai, China). Next, the proteins were separated in SDS-PAGE gels and transferred to poly(vinylidene difluoride) membranes (0.22 or 0.45 μm, Millipore, Bedford, MA, United States). The membranes were blocked with 5% non-fat milk (Beyotime) in Tris-buffered saline with 0.1% Tween-20 (TBST) for 1 h at room temperature. Afterward, the membranes were incubated with rabbit anti-Bax antibody (Proteintech, 50599-2), rabbit anti-Bcl2 antibody (Proteintech, 26593-1), rabbit anti-TGF-β1 antibody (Proteintech, 21898-1), rabbit anti-Cleaved Caspase3 antibody (CST, 9661), and mouse anti-α-tubulin antibody (Proteintech, 66031) overnight at 4℃. After that, the membranes were incubated with horseradish peroxidase-conjugated secondary antibodies for another 1 h at room temperature in TBST buffer containing 5% non-fat milk. Finally, the membranes were washed three times with TBST, and the blots were developed using a BeyoECL Plus Chemiluminescence Kit (Beyotime) and visualized on an Amersham Imager 600 (Cytiva, Germany). The differential expression of proteins after CCI was quantified by ImageJ software using α-tubulin as a control.

Quantitative real-time polymerase chain reaction

Furthermore, quantification of cytokine mRNA expression and determination of the identified circRNAs in the hippocampus were investigated by quantitative real-time polymerase chain reaction (qRT-PCR). In brief, total RNA was extracted from hippocampal tissue through the TRIzol method and reverse transcribed by HiScript$^{\bigcirc eR}$ III RT SuperMix (Vazyme, Nanjing, China) according to the manufacturer's instructions. Afterward, the templates were amplified by qRT-PCR using primers for rat genes *IL-6*, *IL-1β*, *TNF-α*, *CCL2*, *CXCR4*, *CXCL12*, *Chr6:136059672_136091144, Chr11:87902732_87908586, Chr2:104882050_104908155, Chr 17:84219927_84249246, Chr1:255706980_255774681, Chr6: 76491315_76492176, Chr8:126307382_126317853, Chr12:9 292180_9313769, Chr7:134659946_134667817, Chr10:182 18676_18238682* listed in **Table 1**. Each sample was run in a 20 μL reaction system of the Taq Pro Universal SYBR qPCR Master Mix kit (Vazyme). qRT-PCR was performed on a CFX96 Real-Time System (Bio-Rad, Hercules, CA, United States). Next, the relative quantification of the sample transcripts was calculated through the $^{\Delta\Delta}$Cq method with 18S as an internal reference.

Prediction of circular RNA-miRNA-mRNA association

CircRNA-miRNA interactions were predicted using circAtlas 2.0 and miRanda. The top five miRNAs were identified for each differentially expressed circRNA according to the score. Then, the network of the top five highest miRNAs connecting to one circRNA was constructed. Furthermore, we used TargetScan and miRanda databases to predict the targete genes of the miRNAs. We generally accept the overlapping genes of the two databases with the cumulative weight context++ score ≤ -0.4 and the target score ≥ 80. Then, OmicStudio tools[1] were used to construct the circRNA-miRNA-mRNA network for the ten typical differentially expressed circRNAs that we validated as well as their predicted target genes.

Enzyme-linked immunosorbent assay

Changes in neuroinflammation in the hippocampus after CCI were detected by Enzyme-linked immunosorbent assay (ELISA). Briefly, the hippocampi of the CCI groups and sham group at 21 days were collected on ice and homogenized in PBS. Then, the supernatant was harvested by centrifugation at 13,000 rpm for 10 min at 4℃. Thereafter, the concentrations of IL-6, IL-1β, and TNF-α in the hippocampal extract were determined with a rat IL-6 ELISA kit (ABclonal, Wuhan, China), rat IL-1β ELISA kit (ABclonal, Wuhan, China), and rat TNF-α ELISA kit (Dogesce, Beijing, China) following the manufacturer's instructions.

1 https://www.omicstudio.cn/tool/56

TABLE 1 List of polymerase chain reaction primers for real-time qRT-PCR analysis.

Genes	Forward primers (5′~3′)	Reverse primers (5′~3′)
IL-6	TCTTGGAAATGAGAAAAGAGTTGTG	AGTGAGGAATGTCCACAAACTGA
IL-1β	AGCAGCTTTCGACAGTGAGG	AGGCCACAGGGATTTTGTCG
TNF-α	AGCACAGAAAGCATGATCCGA	GAAGTGGCAAATCGGCTGAC
CCL2	CTGTCTCAGCCAGATGCAGT	TGGATCTACATCTTGCATTTAAGGA
CXCR4	GCCATGGCTGACTGGTACTT	CGATGCTGATCCCCACGTAA
CXCL12	TGCCCTTCAGATTGTTGCAAGG	AGAAGCTCCAAAGCAAACCG
18S	GACACGGACAGGATTGACAG	GCTCCACCAACTAAGAACGG
Chr6:136059672_136091144	ACCCAAACATAGGTGAAGTATT	GTCTGTAGTTTCCAATATGAGG
Chr11:87902732_87908586	GCAGAATTGGCTCCATGACCT	TGTGGATGAGCTGTTGATGAAC
Chr2:104882050_104908155	AGAGGATCAGTGCTTTGACCGA	GCCTTTCATTTTCTGGGACAGT
Chr17:84219927_84249246	CCAGAAAGTGCACCGAGCT	AGCTCCATGCTTAGGTCTTCAA
Chr1:255706980_255774681	CTCGGTGCAAGCGTTGATAGAC	GCCACTGGGAGGGTAGTGTTTA
Chr6:76491315_76492176	CTCAGAACAAGATGAACCAACA	ACTCGTTAGCATAGCAGGACCA
Chr8:126307382_126317853	GTACAGGAGCCCACGGCAA	GCTGCAGCATTTTCTCCAGTTC
Chr12:9292180_9313769	ATCCAAGGCACGAAAAGCAAAG	TTTGTTTCTACCGGGCTTCCAA
Chr7:134659946_134667817	AAGAAACTGCTGACGAACTTGA	CGGCACCCTTATTTATTGACCA
Chr10:18218676_18238682	GGCAAGAGATCTTCGAGGGATT	TACCATGAGAAGGCGAGTGAGG

Terminal deoxynucleotidyl transferase-mediated dUTP nick-end labeling

Cell apoptosis in the central nervous system was studied through a Terminal deoxynucleotidyl transferase-mediated dUTP nick-end labeling (TUNEL) assay. Briefly, the brain tissues of the CCI and sham groups at 21 days were collected after transcardiac perfusion with 1 × PBS for 10 min and 4% paraformaldehyde for 30 min, successively. Then, the brains were excised and fixed in 4% paraformaldehyde for 48 h, followed by dehydration using sucrose containing 0.5% NaN_3 for another 48 h. Afterward, the tissues were dissected into 10 μm thick sections and stained with a One Step TUNEL Apoptosis Assay Kit (Beyotime) following the instruction manual. Nuclei were stained with 4, 6-diamidino-2-phenylindole, dihydrochloride (DAPI) and sealed with anti-fluorescence quenching sealing solution. Apoptotic cells were observed by fluorescence microscopy (Olympus, Tokyo, Japan) at excitation wavelengths of 405 and 488 nm.

Statistical analysis

Quantitative data are displayed as the means ± standard deviations and were analyzed using GraphPad Prism version 8.0.2 software. Student's *t*-test was utilized as a *post hoc* test. $P < 0.05$ was identified to be statistically significant. The counts of circRNA in each sample were standardized using DESeq software, and the expression quantity was reckoned through BaseMean (Anders and Huber, 2012). Differences in circRNA expression between the sham and CCI groups were obtained by analyzing the counts of circRNAs with a negative binomial distribution test.

Results

Nociceptive hypersensitivity and cognitive decline after chronic constriction injury

As described in Figure 1A, nociceptive threshold tests were performed to evaluate allodynia in the evoked nociceptive models at 1, 3, 7, 14, and 21 days after CCI. The nociceptive thresholds were measured at 1 day before CCI as the baseline. As expected, the CCI rats exhibited a significant reduction in both PWT (Figure 1B, $P = 0.6381$ CCI vs. sham on day −1, $P = 0.2531$ CCI vs. sham on day 1, $P = 0.0024$ CCI vs. sham on day 3, $P < 0.0001$ CCI vs. sham on day 7, day 14, and day 21) and PWL (Figure 1C, $P = 0.1755$ CCI vs. sham on day −1, $P = 0.3497$ CCI vs. sham on day 1, $P = 0.0002$ CCI vs. sham on day 3, $P < 0.0001$ CCI vs. sham on day 7, day 14, and day 21) from the third day to the 21st day after surgery compared with the sham group, which demonstrated the successful establishment of a chronic neuropathic pain model in rats. Next, cognitive function was detected in the CCI and sham groups at 7, 14, and 21 days after surgery through the spontaneous alternation of rats in the Y maze (Figure 1A). Prior to the cognitive behavior test, the locomotor function of the rats after surgery was investigated through an OFT. No difference in exercise distance in this open field

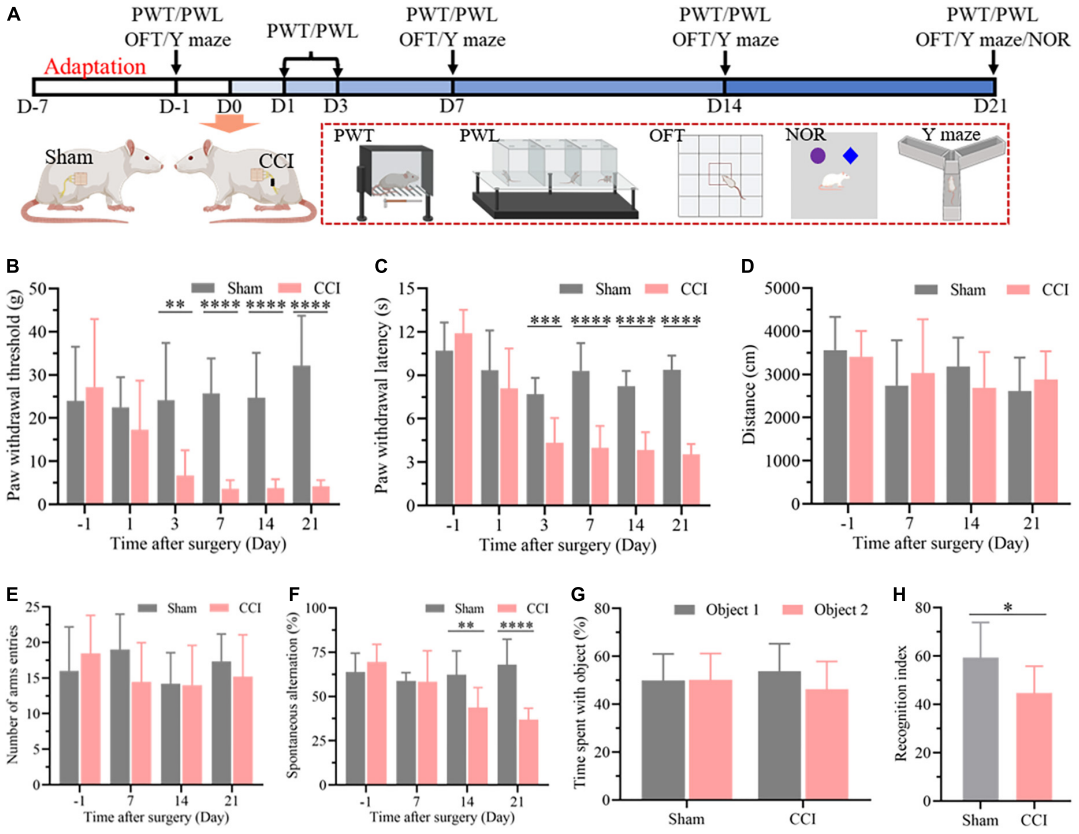

FIGURE 1
CCI contributes to nociceptive hypersensitivity and cognitive impairment. **(A)** Flowchart diagrams show the timeline of the experimental procedures. PWT represent paw withdrawal threshold; PWL represent paw withdrawal latency; OFT represent open field test; NOR represent novel object recognition. **(B)** The PWT was determined by the von Frey method. **(C)** The PWL was tested on a thermal testing apparatus within 20 s. **(D)** Locomotor activity of the rats after surgery was detected by the total travel distance in the open field. **(E)** The number of arm entries and **(F)** spontaneous alternation were detected in each group through the Y maze. Data of **(B–F)** are presented as the mean ± SD (n = 9), and the statistical analysis was conducted *via* unpaired Student's t-test. $^{**}P < 0.01$, $^{***}P < 0.001$, $^{****}P < 0.0001$. **(G,H)** In the NOR test, investigation time of objects was recorded in the training and test periods, and the discrimination index was calculated in the test period. Data are presented as the mean ± SD (n = 12), and the statistical analysis was conducted *via* unpaired Student's t-test. $^{*}P < 0.05$.

demonstrated the negligible influence of CCI on locomotor function (Figure 1D, P = 0.6520 CCI vs. sham on day −1, P = 0.5998 CCI vs. sham on day 7, P = 0.1833 CCI vs. sham on day 14, P = 0.4456 CCI vs. sham on day 21), which was also confirmed by the total number of arm entries without significant difference in the Y maze (Figure 1E, P = 0.3837 CCI vs. sham on day −1, P = 0.0847 CCI vs. sham on day 7, P = 0.9258 CCI vs. sham on day 14, P = 0.3787 CCI vs. sham on day 21). However, the spontaneous alternation in the Y maze was significantly decreased 14 days after CCI and until at least 21 days in comparison with the sham group at the corresponding time points (Figure 1F, P = 0.2590 CCI vs. sham on day −1, P = 0.9320 CCI vs. sham on day 7, P = 0.0061 CCI vs. sham on day 14, $P < 0.0001$ CCI vs. sham on day 21), indicating cognitive deficits in the CCI rats. We next performed a novel object recognition test 21 days after surgery to evaluate each group's hippocampus-dependent memory function. In the training session, no significant difference was observed in the time spent exploring each identical object between the sham and CCI groups (Figure 1G, P = 0.9625 Object 2 vs. Object 1 in sham group, P = 0.1313 Object 2 vs. Object 1 in CCI group). In contrast, the recognition index, defined as the proportion of the amount of time spent exploring the novel object and the total time spent exploring objects, was significantly decreased in the CCI group compared with the sham group, demonstrating significant cognitive decline (Figure 1H, P = 0.0113 CCI vs. sham group).

Bioinformatics analysis of differentially expressed circular RNAs in the hippocampus of chronic constriction injury rats

In this study, high-throughput RNA-seq was performed to profile circRNAs with differential expression in the

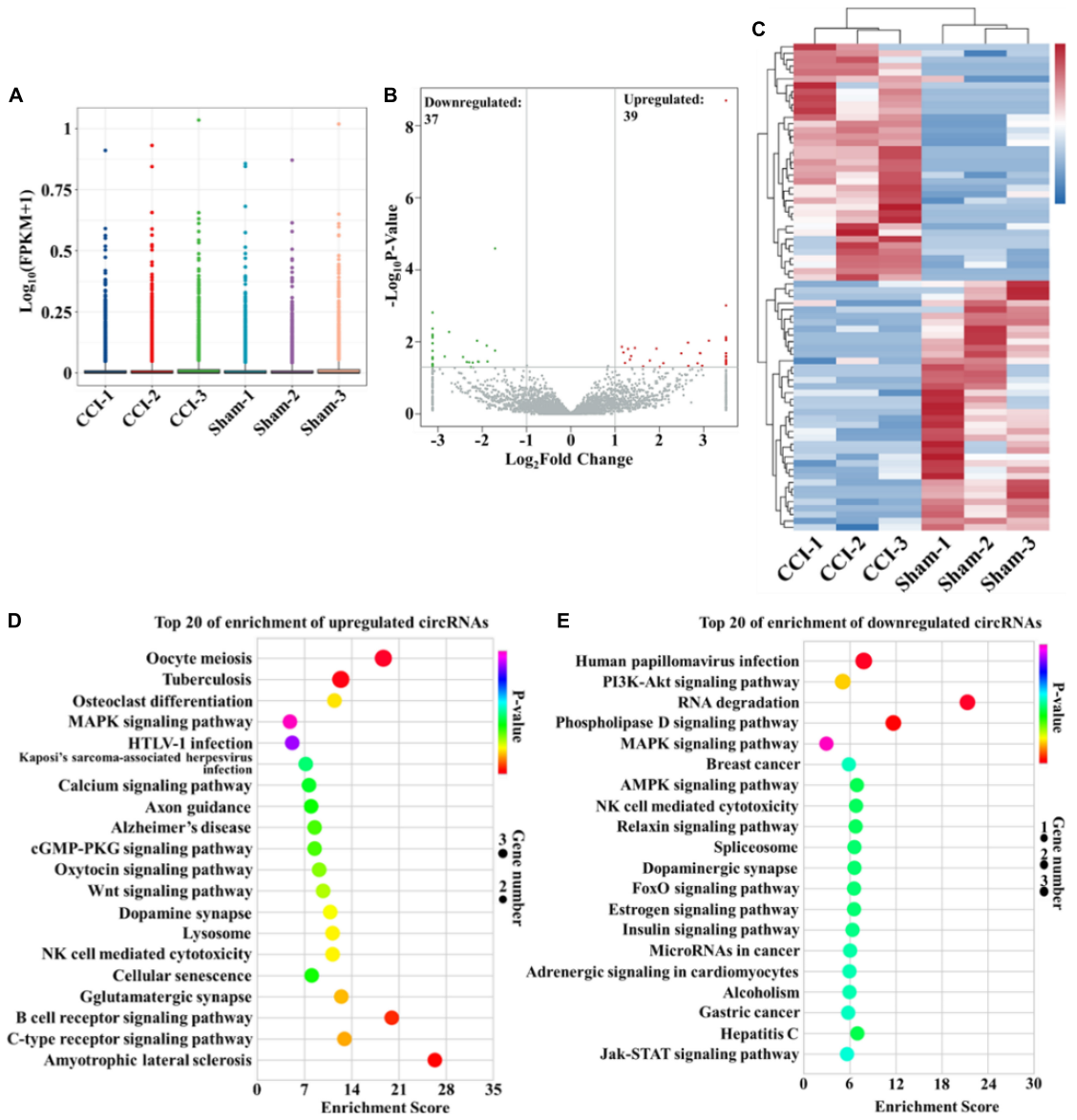

FIGURE 2
Bioinformatic analysis of differentially expressed circRNAs in the hippocampus after CCI. **(A)** Box-whisker plot showing the symmetry and distribution of data. Statistical analysis was conducted based on the minimum, first quartile (25%), median (50%), third quartile (75%), and maximum. **(B)** Volcano plots displaying the differentially expressed circRNAs with | log2(fold change)| > 1 and P-value < 0.05. Statistical analysis was conducted *via* a negative binomial distribution test. **(C)** Hierarchical clustering plot displaying the differentially expressed circRNA profile in the hippocampus after CCI. **(D,E)** KEGG pathway analysis showed the top 20 significantly enriched pathways and their scores for the upregulated and downregulated circRNAs. Statistical analysis was conducted *via* a hypergeometric test.

hippocampus after CCI. The box-whisker plot was first obtained by analyzing the rat circRNA microarray, which demonstrated the good symmetry and distribution of the data (Figure 2A). Analysis of circRNA category distribution showed that the type of the identified circRNAs was mainly sense-overlapping (87.56%). In addition, antisense (1.76%), exonic (4.28%), intergenic (5.38%) and intronic (1.02%) circRNAs were also identified (Supplementary Figure 1A). Volcano plots were generated to visualize the significant differences between the sham and CCI groups with fold change ≥ 2.0 and P-value ≤ 0.05. According to the volcano plots, we identified 76 differentially expressed circRNAs in the two groups, including 39 upregulated and 37 downregulated circRNAs (Figure 2B and Supplementary Table 1). These differentially expressed circRNAs also primarily belonged to the sense-overlapping type with a ratio of 89.47% (Supplementary Figure 1B). Next, hierarchical cluster analysis was performed to analyze the distinguishable circRNA profiles from the

hippocampal samples based on their expression levels, which indicated the different expression patterns of circRNAs in the hippocampus of CCI rats compared with those in sham rats (**Figure 2C**). Additionally, GO and KEGG analyses were performed using a network tool[2] to investigate the function and signaling pathway of differentially expressed circRNA host genes. The GO analysis revealed that the significantly differentially expressed circRNAs were enriched in terms of biological process, cellular components and molecular function. These results suggested that the upregulated circRNAs had a strong relationship with the negative regulation of transcription by RNA polymerase II, cytoplasm and metal ion binding (**Supplementary Figure 2A**). Meanwhile, the downregulated circRNAs were associated with signal transduction, cytoplasm and ATP binding (**Supplementary Figure 2B**). The KEGG pathway enrichment demonstrated that the upregulated circRNAs were primarily enriched in the MAPK, cGMP-PKG and Wnt signaling pathways (**Figure 2D**). The downregulated circRNAs were mainly enriched in the PI3K-Akt, MAPK, AMPK, and Jak-STAT signaling pathways (**Figure 2E**). Of note, these processes and pathways were reported to be associated with inflammation and apoptosis in the development of cognitive deficits (Suo et al., 2018; Chen et al., 2019; Sun Q. Y. et al., 2019; Feng et al., 2020; Li et al., 2020; Liu X. Y. et al., 2021).

2 https://cloud.oebiotech.cn/task/

Identification of differentially expressed circular RNAs

Among all the differentially expressed circRNAs, ten typical differentially expressed circRNAs were screened and detected by qRT-PCR assay, which included *Chr6:136059672_136091144, Chr11:87902732_87908586, Chr2:104882050_104908155, Chr17:84219927_84249246, Chr1:255706980_255774681, Chr 6:76491315_76492176, Chr8:126307382_126317853, Chr12: 9292180_9313769, Chr7:134659946_134667817,* and *Chr 10:18218676_18238682.* We found that the expression of *Chr6:76491315_76492176* (**Figure 3A**, $P = 0.0109$), *Chr8: 126307382_126317853* (**Figure 3B**, $P = 0.0284$), *Chr12: 9292180_9313769* (**Figure 3C**, $P = 0.0111$), *Chr7: 134659946_134667817* (**Figure 3D**, $P = 0.0207$), and *Chr10: 18218676_18238682* (**Figure 3E**, $P = 0.0268$) was substantially upregulated in the hippocampus of CCI rats with cognitive dysfunction, while the expression of *Chr6:136059672_136091144* (**Figure 3F**, $P = 0.0008$), *Chr11:87902732_87908586* (**Figure 3G**, $P = 0.0376$), *Chr2:104882050_104908155* (**Figure 3H**, $P = 0.0011$), *Chr17:84219927_84249246* (**Figure 3I**, $P = 0.0081$), and *Chr1:255706980_255774681* (**Figure 3J**, $P = 0.0079$) was significantly decreased. The expression levels of the abovementioned circRNAs were associated with the microarray analysis results, suggesting the reliability of the microarray data.

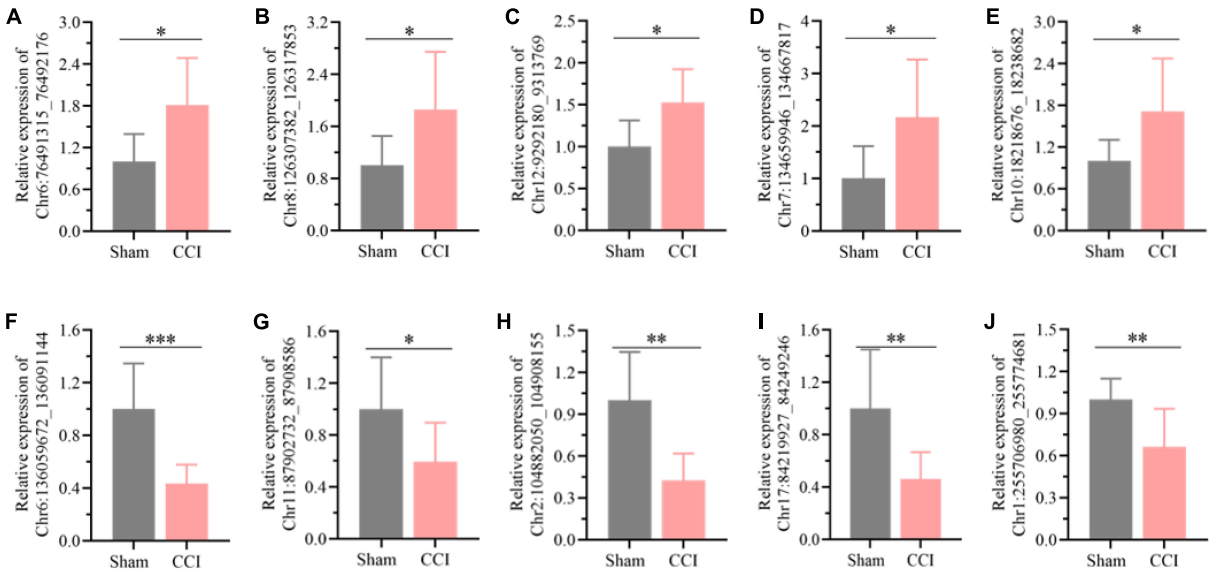

FIGURE 3
Detection of the typical differentially expressed circRNAs by qRT-PCR. **(A)** *Chr6:76491315_76492176*, **(B)** Chr8:126307382_126317853, **(C)** Chr12:9292180_9313769, **(D)** Chr7:134659946_134667817, **(E)** Chr10:18218676_18238682, **(F)** *Chr6:136059672_136091144*, **(G)** *Chr11:87902732_87908586*, **(H)** *Chr2:104882050_104908155*, **(I)** *Chr17:84219927_84249246*, **(J)** *Chr1: 255706980_255774681*. Error bars represent the mean ± SD ($n = 8$), and the statistical analysis was conducted *via* unpaired Student's *t*-test. $^{*}P < 0.05$, $^{**}P < 0.01$, $^{***}P < 0.001$.

Circular RNA-miRNA-mRNA co-expression network for the differentially expressed circRNAs

CircRNAs can interact with miRNAs *via* miRNA response elements due to the specific binding sites of miRNAs in circRNA sequences. Five miRNAs with the highest scores among the ten typical circRNAs were predicted and are shown in **Table 2**. Considering that circRNAs act as miRNA sponges to regulate the circRNA-miRNA-mRNA network, we further predicted the target genes of the top five miRNAs utilizing TargetScan and miRanda. Based on the overlapping results of TargetScan and miRanda, a total of 440 target genes for the five upregulated circRNAs and 533 target genes for the five downregulated circRNAs were identified. Furthermore, the circRNA-miRNA-mRNA interaction network was constructed as shown in **Figure 4**.

Evaluation of neuroinflammation in the hippocampus post chronic constriction injury

The results of the functional analysis revealed that neuroinflammation and neuronal apoptosis might play essential roles in the occurrence of cognitive impairment after CCI for 21 days. Thus, the key factors involved in neuroinflammation in the hippocampus of CCI and sham rats were first determined through qRT-PCR and ELISA. As expected, the expression of proinflammatory cytokines, including IL-6, IL-1β, and TNF-α, was higher in the hippocampus of CCI rats than in the sham group (**Figure 5A**, $P = 0.0005$ CCI vs. sham of IL-6, $P = 0.0061$ CCI vs. sham of IL-1β, $P = 0.0275$ CCI vs. sham of TNF-α), which was also validated by ELISA as shown in **Figure 5B** ($P = 0.0015$ CCI vs. sham of IL-6, $P = 0.0169$ CCI vs. sham of IL-1β, $P = 0.0279$ CCI vs. sham of TNF-α). In addition, in contrast with the sham group, the inflammatory chemokine C-C ligand 2 (CCL2) levels were substantially upregulated in CCI rats (**Figure 5C**, $P = 0.0757$ CCI vs. sham). Meanwhile, the expression of chemokine (C-X-C) receptor 4 (CXCR4) and CXCL12 was also dramatically increased with significance in the hippocampus after CCI for 21 days (**Figure 5C**, $P = 0.002$ CCI vs. sham of CXCL12, $P = 0.0175$ CCI vs. sham of CXCR4).

Evaluation of neuronal apoptosis in the hippocampus post chronic constriction injury

Furthermore, the expression of Bcl-2 was significantly decreased in the hippocampus of CCI rats at 21 days (**Figures 6A,C**, $P = 0.0116$ CCI vs. sham), while Bax in the hippocampus was upregulated substantially (**Figures 6A,B**, $P = 0.0275$ CCI vs. sham), and the proportion of Bcl-2 and Bax further declined significantly (**Figure 6D**, $P = 0.0002$ CCI vs. sham). Meanwhile, western blotting results demonstrated that ongoing chronic neuropathic pain stimuli resulted in the upregulation of TGF-β (**Figures 6A,E**, $P = 0.0160$ CCI vs. sham) and cleavage of caspase-3 (**Figures 6A,F**, $P = 0.0339$ CCI vs. sham). Additionally, the ratio of apoptotic neurons in the hippocampal CA1 region of CCI rats was markedly improved compared to that of sham rats according to the TUNEL staining assay (**Figure 6G**, $P = 0.0016$ CCI vs. sham).

Discussion

Cognitive impairment is one of the most common complications associated with chronic pain, which was also validated in preclinical observations of chronic neuropathic pain in rodents (Mazza et al., 2018; Zhang et al., 2021). However, the underlying mechanisms of chronic pain-induced memory dysfunction are still indistinct. In the present work, we established chronic neuropathic pain models by CCI of the sciatic nerve. Behavioral test results indicated that CCI rats with long-term nociceptive threshold reduction developed typical cognitive deficits in working memory and recognition memory. There was no substantial difference in the total traveled distance in the OFTs after surgery, which demonstrated that recognitive impairment was unlikely to be connected with deficits in locomotor function and exploratory activities during recognitive test periods. Previous reports have validated that nociceptive hypersensitivity induced by CCI always occurs 2 days after surgery, reaches a plateau at 6∼7 days and is constantly sustained for at least 30 days (Bridges et al., 2001), which is consistent with our results. Additionally, our results also suggested that the cognitive function of CCI rats decreased significantly 14 days after surgery and lasted until 21 days. Thus, we collected hippocampal tissues on day 21 for further transcriptome sequencing and identified the potential key factors associated with cognitive impairment.

CircRNAs are endogenous non-coding RNAs with covalently closed loops that endow them with higher stability than linear RNAs and sequence conservatism among species (Zhang et al., 2019). Most circRNAs have been determined to be more abundant in the mammalian brain than in other tissues, demonstrating that circRNAs may play a vital role in the pathological process of some neurological disorders (Hanan et al., 2017). For instance, circRNA has been confirmed to mediate synaptic and amyloid precursor protein processing deficits through the circHDAC9/mi-138/sirtuin-1 pathway in Alzheimer's disease (Lu et al., 2019). Aerobic exercise could improve vascular cognitive impairment through circRIMS2/miR-186/BDNF-mediated neuronal apoptosis (Niu et al., 2021). Moreover, increasing evidence has suggested

TABLE 2 Predicted miRNA response elements of the ten typical differentially expressed circRNAs.

CircRNA ID	Predicted miRNA response elements (MREs)				
2-6	MRE1	MRE2	MRE3	MRE4	MRE5
Chr6:136059672_136091144	rno-miR-141-5p	rno-miR-205	rno-miR-3551-5p	–	–
Chr11:87902732_87908586	rno-miR-3594-5p	rno-miR-6321	rno-miR-149-5p	rno-let-7b-3p	rno-miR-17-2-3p
Chr2:104882050_104908155	rno-miR-330-3p	rno-miR-30e-3p	rno-miR-30a-3p	rno-miR-185-3p	–
Chr17:84219927_84249246	–	–	–	–	–
Chr1:255706980_255774681	rno-miR-130a-3p	rno-miR-5132-5p	rno-miR-3588	rno-miR-433-3p	rno-miR-15a-3p
Chr6:76491315_76492176	rno-miR-329-5p	rno-miR-106b-5p	rno-miR-137-3p	rno-miR-93-5p	rno-miR-6321
Chr8:126307382_126317853	rno-miR-145-5p	rno-miR-666-3p	rno-miR-3557-5p	rno-miR-3550	rno-miR-486
Chr12:9292180_9313769	rno-miR-880-3p	rno-miR-125a-3p	rno-miR-298-3p	rno-miR-138-5p	rno-miR-320-3p
Chr7:134659946_134667817	rno-miR-876	rno-miR-93-3p	rno-miR-127-3p	rno-miR-370-3p	rno-miR-23a-5p
Chr10:18218676_18238682	rno-miR-106b-3p	rno-miR-301b-3p	rno-miR-3573-5p	rno-miR-452-5p	–

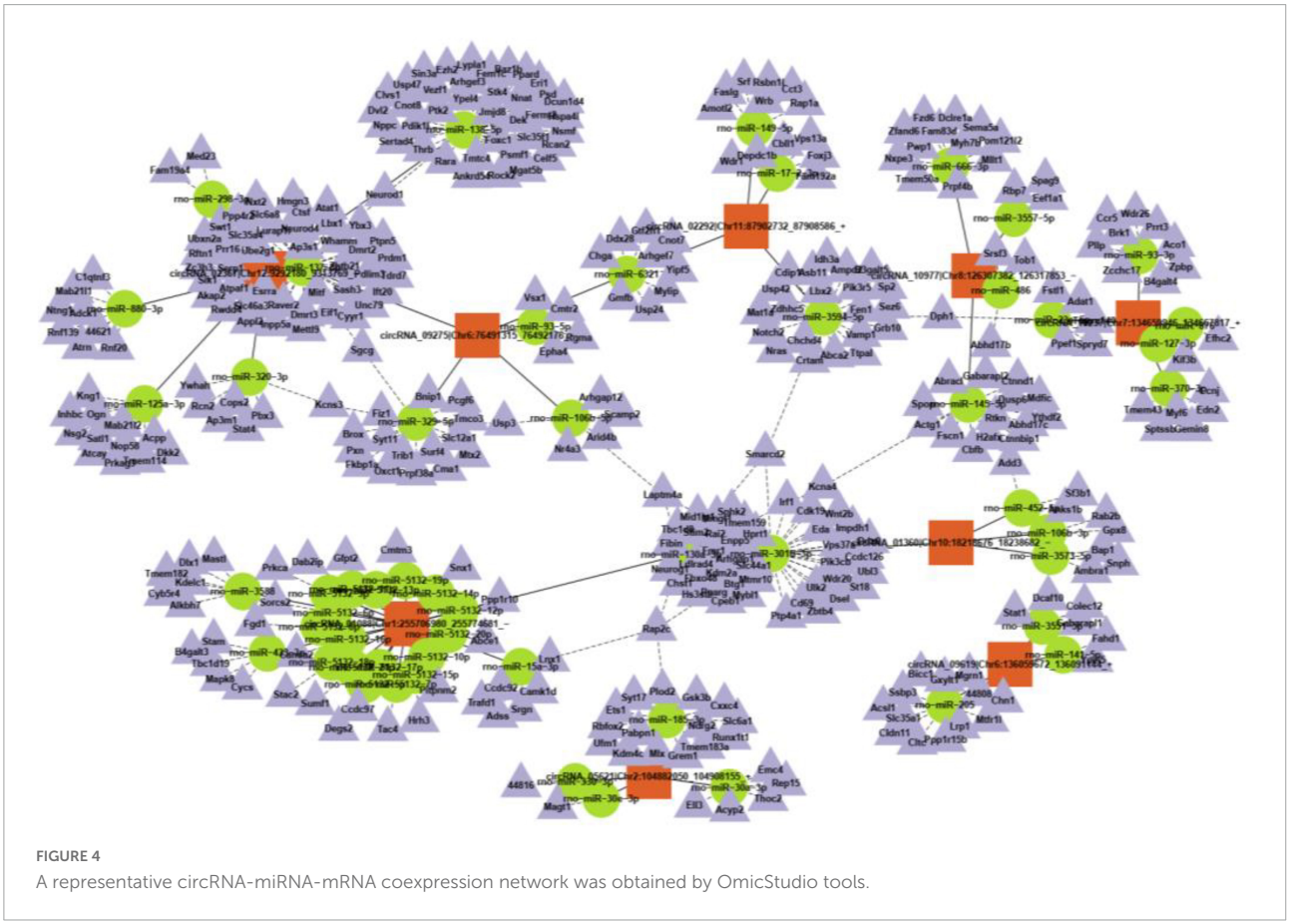

FIGURE 4
A representative circRNA-miRNA-mRNA coexpression network was obtained by OmicStudio tools.

that neuropsychiatric disorder-associated circRNAs in the blood and CSF are promising non-invasive biomarkers for the diagnosis of complex neuropsychiatric disorders (Zhuo et al., 2020). However, the clinical value and roles of circRNAs in neuropathic pain-induced cognitive impairment are still unclear. Therefore, we performed microarray analysis for circRNAs in the hippocampus of CCI and sham rats to explore the potential key circRNAs with a significant connection to cognitive impairment. A total of 76 differentially expressed circRNAs were identified in the hippocampus between CCI and sham rats, including 39 upregulated and 37 downregulated circRNAs. Afterward, we verified ten circRNAs during the validation process, which are all consistent with the microarray results. Notably, the pathogenesis of cognitive impairment is complicated, and one signaling pathway might be regulated by a series of upstream molecules, such as RNAs. Thus, the function

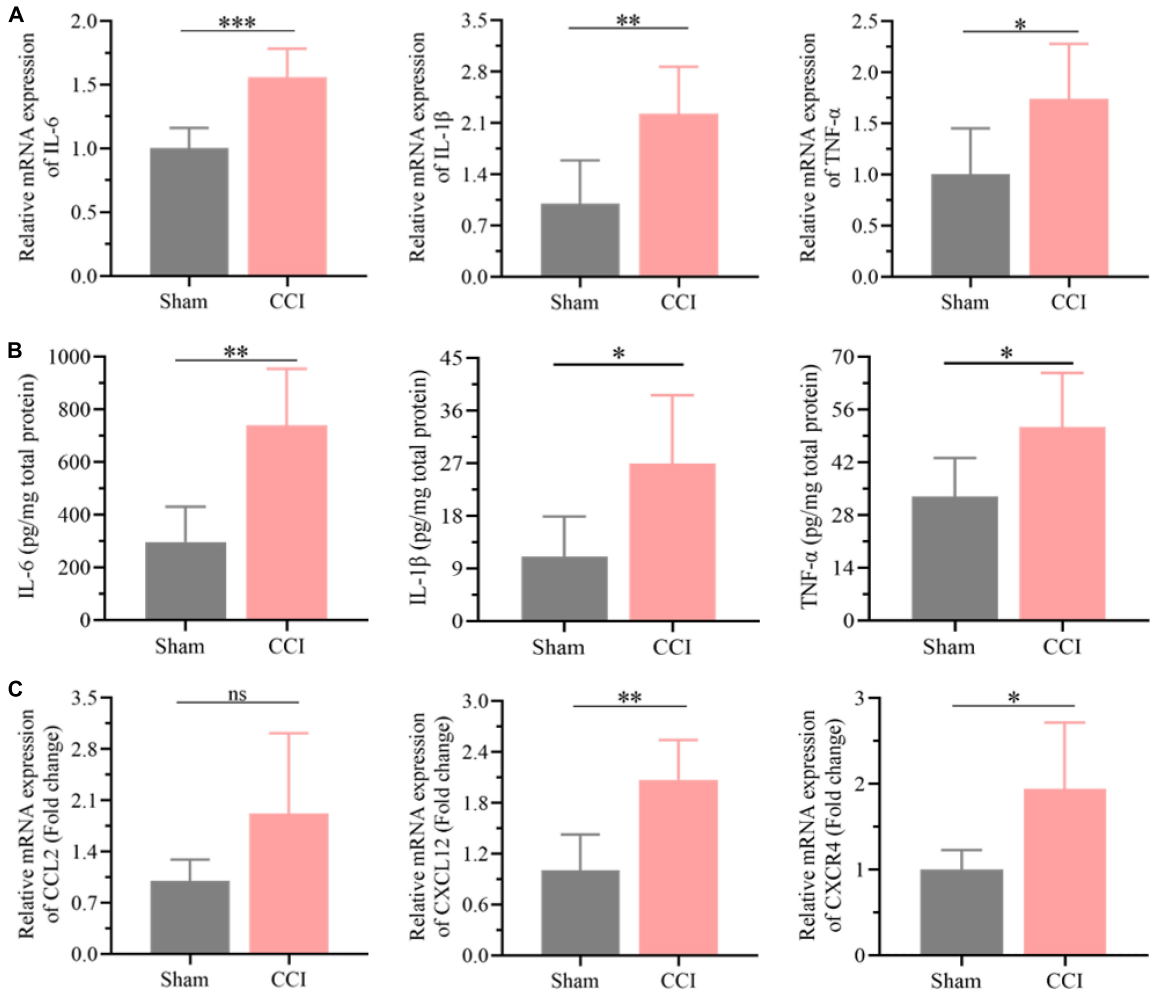

FIGURE 5
Neuroinflammation was substantially elevated in the hippocampus post CCI. **(A)** The expression levels of proinflammatory cytokines, including *IL-6*, *IL-1β* and *TNF-α*, in the hippocampus of CCI and sham rats were detected by qRT-PCR. **(B)** CCI induced upregulation of these proinflammatory cytokines in the hippocampus as detected by ELISA. **(C)** The expression levels of inflammation-related proteins, including *CCL2*, *CXCR4,* and *CXCL12,* in the hippocampus of CCI and sham rats were detected by qRT-PCR. Error bars represent the mean ± SD (n = 6), and the statistical analysis was conducted *via* unpaired Student's t-test. $^{*}P < 0.05$, $^{**}P < 0.01$, $^{***}P < 0.001$, ns represent no significance.

of the differentially expressed circRNAs was further investigated in the present work.

Generally, circRNAs serve functions through competing endogenous RNAs or miRNA sponges, interacting with RNA binding proteins, modulating the stability of mRNAs, regulating gene transcription and translating proteins (Meng et al., 2017). Therefore, the functions and associated signaling pathways were further analyzed through GO and KEGG enrichment. The GO analysis showed that the differentially expressed circRNAs were involved in dendritic spines in terms of cellular comments. Dendritic spines are post-synaptic structures at a majority of excitatory synapses in the mammalian brain, whose number and size are closely related to cognitive function in different neurological diseases (Herms and Dorostkar, 2016; Zhang et al., 2020). Moreover, transcription and ATP-associated functions in terms of biological processes and molecular functions were also enriched in GO analysis and are also involved in cognitive impairment by regulating inflammatory and apoptotic reactions (Sun X. Y. et al., 2019; Velasquez et al., 2019). Meanwhile, the KEGG enrichment analysis indicated that the upregulated circRNAs were mainly enriched in the MAPK, cGMP-PKG and Wnt signaling pathways, and the downregulated circRNAs were primarily enriched in the PI3K-Akt, MAPK and AMPK signaling pathways. These signaling pathways have been validated to be closely related to inflammation and apoptosis (Suo et al., 2018; Chen et al., 2019; Gabbouj et al., 2019; Sun Q. Y. et al., 2019; Li et al., 2020; Yue and Lopez, 2020; Liu X. Y. et al., 2021), further indicating that neuroinflammation and apoptosis might play vital roles in the development of cognitive deficits after CCI.

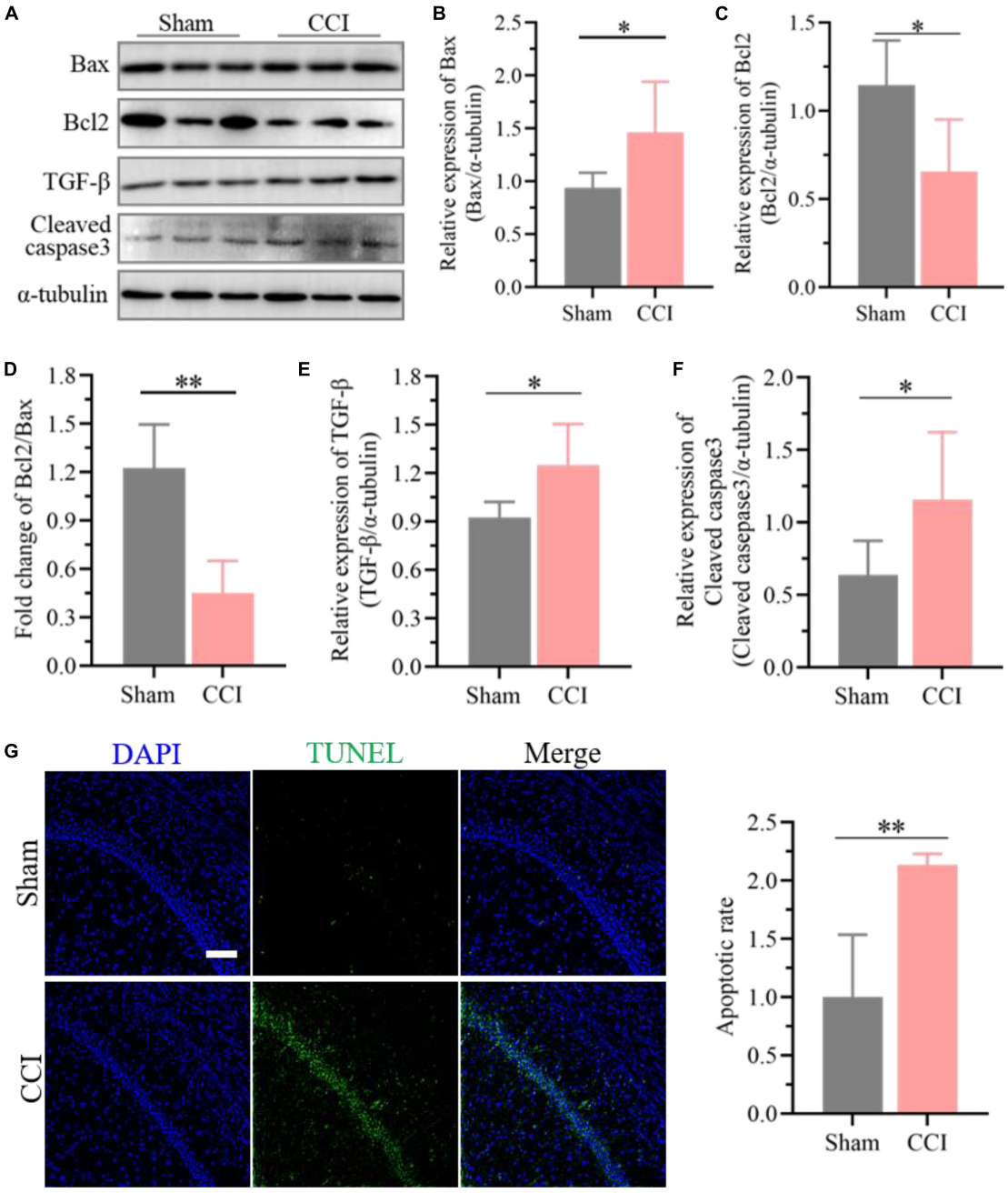

FIGURE 6
Enhanced neuronal apoptosis after CCI plays essential roles in cognitive deficits. **(A)** Representative images of western blotting showing the expression levels of Bcl-2, Bax, TGF-β and cleaved caspase-3 in the hippocampus of CCI and sham rats. **(B,C)** Quantitative analysis of **(B)** Bax and **(C)** Bcl-2 expression after CCI using ImageJ software. **(D)** The proportion of Bcl2 and Bax was calculated. **(E,F)** Quantitative analysis of **(E)** TGF-β and **(F)** cleaved caspase-3 expression after CCI using ImageJ software. Data of **(B–F)** are presented as the mean ± SD (n = 6), and the statistical analysis was conducted *via* unpaired Student's t-test. $^{*}P < 0.05$, $^{**}P < 0.01$. **(G)** Representative images for TUNEL detection in the hippocampal CA1 region after CCI, and the percentage of apoptotic ratio was quantified. Error bars represent the mean ± SD (n = 5), and the statistical analysis was conducted *via* unpaired Student's t-test. $^{**}P < 0.01$. Scale bar: 100 μm.

Additionally, the miRNAs and targeted genes associated with the typical upregulated and downregulated circRNAs were further identified. Further analysis of the circRNA-miRNA-mRNA network also demonstrated that several miRNAs and target genes were closely related to inflammation and apoptosis in the development of neurodegenerative disease.

As expected, the expression of proinflammatory cytokines such as IL-6, IL-1β, and TNF-α and the inflammatory

chemokine CCL2 in the hippocampus increased dramatically after CCI, suggesting elevated neuroinflammation in the hippocampus. A previous study reported that overexpressed CXCL12 could lead to memory dysfunction in neuropathic pain by recruiting inflammatory monocytes into the perivascular space (Mai et al., 2021). Interestingly, the expression of CXCR4 and CXCL12 was also higher in the hippocampus of CCI rats than in sham rats, which further demonstrated improved inflammation in the hippocampus. Bcl-2 and Bax have been proven to play essential roles in the process of apoptosis (Opferman and Kothari, 2018) and are extremely disturbed in the hippocampus after CCI. Meanwhile, the expression of activated caspase-3 and TGF-β was also increased substantially, further indicating that neuronal apoptosis occurring in the hippocampus was associated with the development of cognitive dysfunction after CCI. Consequently, improved neuronal apoptosis might be a key potential factor in neuropathic pain-induced cognitive dysfunction, which was also confirmed by TUNEL staining. Therefore, it could be hypothesized that the dysregulation of circRNA expression in the hippocampus after CCI-induced long-lasting nociceptive threshold reduction may contribute to cognitive dysfunction by improving neuroinflammation and neuronal apoptosis.

Our study also has several potential limitations. In the present work, we provide an expanded perspective on possible circRNAs and a potential mechanism promoting cognitive deficits induced by chronic neuropathic pain. However, the expression of the differentially expressed circRNAs was only detected in the hippocampus at one time point after CCI when learning and memory dysfunction was observed. Further verification of these screened circRNAs at several time points in CCI and other chronic neuropathic pain models need to be performed to provide more clinical significance for diagnosis or prediction. Additionally, the possible roles of circRNA in CCI-induced cognitive impairment were based on bioinformatics prediction. Therefore, further *in vivo* investigation should be performed to identify how these differentially expressed circRNAs initiate cognitive deficits in CCI. Meanwhile, more experiments should be carried out to determine the changes in the potential key circRNAs in different structures, including the dorsal root ganglion and dorsal root of the spinal cord, and to further explore the association of the identified circRNAs between cognitive impairment and chronic neuropathic pain. Besides, the association between the differentially expressed circRNAs and cognitive impairment induced by chronic pain might be a concomitant phenomenon. These differentially expressed circRNAs might be involved in the regulation of some other pathophysiological processes. In addition to cognitive dysfunction, affective disorders such as anxiety and depression are serious adverse consequences of chronic pain (Haanpaa et al., 2011; Radat et al., 2013). Previous evidence has demonstrated that more than 60% of chronic pain patients suffer from anxiety or depression (Kremer et al., 2021), which has also been observed in different rodent models of chronic pain (Mogil, 2009). Moreover, increasing evidence has also confirmed that inflammation and apoptosis in the hippocampus play vital roles in the development of mood disorders (Zhou et al., 2018). Thus, further studies are needed to identify the potential regulatory effects of the differentially expressed circRNAs in the hippocampus in the occurrence of mood disorders.

Conclusion

In conclusion, our study confirmed the significant differentially expressed circRNAs and predicted miRNAs and genes involved in the development of cognitive impairment induced by chronic neuropathic pain. This study provides a preliminary perspective for circRNAs with different expression levels and predicts their potential participation mechanisms in cognitive deficits. Indeed, further studies are still needed to investigate how these circRNAs function on genes regulating cognitive dysfunction and become novel potential peripheral clinical biomarkers and therapeutic targets for constant nociceptive irritation-triggered cognitive impairment.

Data availability statement

The datasets presented in this study can be found in online repositories. The names of the repository/repositories and accession number(s) can be found below: NCBI BioProject, and the NCBI accession number is PRJNA796160.

Ethics statement

The animal study was reviewed and approved by the Ethics Committee of Sichuan University.

Author contributions

CL proposed the project, designed and performed the major experiments, and wrote the manuscript. JL and CC supervised the project and provided funding. RG, YT, HC, XZ, SY-L, QZ, PL, HW, and YS participated in some experiments and data analysis. All authors listed have made a substantial, direct, and intellectual contribution to the work, and approved it for publication.

Funding

This work was supported by the National Natural Science Foundation of China (Nos. 82171185 and 81870858 to CC, No.

82101259 to CL, and No. 81801117 to PL), the fellowship of China Postdoctoral Science Foundation (No. 2020M683314 to CL), and the Post-Doctor Research Project, West China Hospital, Sichuan University (No. 2020HXBH097 to CL).

Acknowledgments

The authors are very grateful to Prof. Tao Zhu for his funding support in this study.

Conflict of interest

The authors declare that the research was conducted in the absence of any commercial or financial relationships that could be construed as a potential conflict of interest.

Publisher's note

Supplementary material

The Supplementary Material for this article can be found online at: https://www.frontiersin.org/articles/10.3389/fnins.2022.925300/full#supplementary-material

References

Anders, S., and Huber, W. (2012). *Differential Expression of RNA-Seq Data at the Gene Level–the DESeq Package*. Heidelberg: European Molecular Biology Laboratory (EMBL).

Bao, Y. N., Dai, W. L., Fan, J. F., Ma, B., Li, S. S., Zhao, W. L., et al. (2021). The dopamine D1-D2DR complex in the rat spinal cord promotes neuropathic pain by increasing neuronal excitability after chronic constriction injury. *Exp. Mol. Med.* 53, 235–249. doi: 10.1038/s12276-021-00563-5

Bridges, D., Thompson, S. W. N., and Rice, A. S. C. (2001). Mechanisms of neuropathic pain. *Br. J. Anesth.* 87, 12–26. doi: 10.1093/bja/87.1.12

Cao, C., Deng, F., and Hu, Y. (2020). Dexmedetomidine alleviates postoperative cognitive dysfunction through circular RNA in aged rats. *3 Biotech* 10:176. doi: 10.1007/s13205-020-2163-0

Chen, C., Zhou, F., Zeng, L., Jiang, Z., and Hu, Z. (2019). Methylene blue offers neuroprotection after intracerebral hemorrhage in rats through the PI3K/Akt/GSK3beta signaling pathway. *J. Cell. Physiol.* 234, 5304–5318. doi: 10.1002/jcp.27339

Feng, C., Wan, H., Zhang, Y., Yu, L., Shao, C., He, Y., et al. (2020). Neuroprotective effect of danhong injection on cerebral ischemia reperfusion injury in rats by activation of the PI3K-Akt pathway. *Front. Pharmacol* 11:298. doi: 10.3389/fphar.2020.00298

Gabbouj, S., Ryhanen, S., Marttinen, M., Wittrahm, R., Takalo, M., Kemppainen, S., et al. (2019). Altered insulin signaling in Alzheimer's disease brain-special emphasis on PI3K-Akt pathway. *Front. Neurosci.* 13:629. doi: 10.3389/fnins.2019.00629

Haanpaa, M., Attal, N., Backonja, M., Baron, R., Bennett, M., Bouhassira, D., et al. (2011). NeuPSIG guidelines on neuropathic pain assessment. *Pain* 152, 14–27. doi: 10.1016/j.pain.2010.07.031

Hanan, M., Soreq, H., and Kadener, S. (2017). CircRNAs in the brain. *RNA Biol.* 14, 1028–1034. doi: 10.1080/15476286.2016.1255398

Herms, J., and Dorostkar, M. M. (2016). Dendritic spine pathology in neurodegenerative diseases. *Annu. Rev. Pathol. Mech.* 11, 221–250. doi: 10.1146/annurev-pathol-012615-044216

Jens, M. (2014). Circular RNAs are a Large Class of Animal RNAs With Regulatory Potency. Springer Theses. 69–80. doi: 10.1007/978-3-319-07082-7_5

Kremer, M., Becker, L. J., Barrot, M., and Yalcin, I. (2021). How to study anxiety and depression in rodent models of chronic pain? *Eur. J. Neurosci.* 53, 236–270. doi: 10.1111/EJN.14686

Lee, T. I., and Young, R. A. (2013). Transcriptional regulation and its misregulation in disease. *Cell* 152, 1237–1251. doi: 10.1016/j.cell.2013.02.014

Li, D., Xu, D., Zou, Y., Xu, Y., Fu, L., Xu, X., et al. (2017). Noncoding RNAs and ovarian diseases (review). *Mol. Med. Rep.* 15, 1435–1440. doi: 10.3892/mmr.2017.6176

Li, Y. J., Yang, L. P., Hou, J. L., Li, X. M., Chen, L., Zhu, J. H., et al. (2020). Prenatal stress impairs postnatal learning and memory development *via* disturbance of the cGMP-PKG pathway and oxidative phosphorylation in the hippocampus of rats. *Front. Mol. Neurosci.* 13:158. doi: 10.3389/fnmol.2020.00158

Liu, J., Duan, P., Xu, C., Xu, D., Liu, Y., and Jiang, J. (2021). CircRNA circ-ITCH improves renal inflammation and fibrosis in streptozotocin-induced diabetic mice by regulating the miR-33a-5p/SIRT6 axis. *Inflamm. Res.* 70, 835–846. doi: 10.1007/s00011-021-01485-8

Liu, X. Y., Xu, Y. L., Cheng, S. B., Zhou, X. H., Zhou, F. H., He, P. K., et al. (2021). Geniposide combined with notoginsenoside R1 attenuates inflammation and apoptosis in atherosclerosis *via* the AMPK/mTOR/Nrf2 signaling pathway. *Front. Pharmacol.* 12:687394. doi: 10.3389/fphar.2021.687394

Lu, Y., Tan, L., and Wang, X. (2019). Circular HDAC9/microRNA-138/sirtuin-1 pathway mediates synaptic and amyloid precursor protein processing deficits in Alzheimer's disease. *Neurosci. Bull.* 35, 877–888. doi: 10.1007/s12264-019-00361-0

Mai, C. L., Tan, Z., Xu, Y. N., Zhang, J. J., Huang, Z. H., Wang, D., et al. (2021). CXCL12-mediated monocyte transmigration into brain perivascular space leads to neuroinflammation and memory deficit in neuropathic pain. *Theranostics* 11, 1059–1078. doi: 10.7150/thno.44364

Mazza, S., Frot, M., and Rey, A. E. (2018). A comprehensive literature review of chronic pain and memory. *Prog. Neuropsychopharmacol. Biol. Psychiatry* 87(Pt B), 183–192. doi: 10.1016/j.pnpbp.2017.08.006

Meng, S., Zhou, H., Feng, Z., Xu, Z., Tang, Y., Li, P., et al. (2017). CircRNA: functions and properties of a novel potential biomarker for cancer. *Mol. Cancer* 16:94. doi: 10.1186/s12943-017-0663-2

Mogil, J. S. (2009). Animal models of pain: progress and challenges. *Nat. Rev. Neurosci.* 10, 283–294. doi: 10.1038/nrn2606

Niu, Y., Wan, C., Zhang, J., Zhang, S., Zhao, Z., Zhu, L., et al. (2021). Aerobic exercise improves VCI through circRIMS2/miR-186/BDNF-mediated neuronal apoptosis. *Mol. Med.* 27:4. doi: 10.1186/s10020-020-00258-z

Opferman, J. T., and Kothari, A. (2018). Anti-apoptotic BCL-2 family members in development. *Cell Death Differ.* 25, 37–45. doi: 10.1038/cdd.2017.170

Radat, F., Margot-Duclot, A., and Attal, N. (2013). Psychiatric co-morbidities in patients with chronic peripheral neuropathic pain: a multicentre cohort study. *Eur. J. Pain* 17, 1547–1557. doi: 10.1002/j.1532-2149.2013.00334.x

Sun, Q. Y., Ding, L. W., Johnson, K., Zhou, S., Tyner, J. W., Yang, H., et al. (2019). SOX7 regulates MAPK/ERK-BIM mediated apoptosis in cancer cells. *Oncogene* 38, 6196–6210. doi: 10.1038/s41388-019-0865-8

Sun, X. Y., Zheng, T., Yang, X., Liu, L., Gao, S. S., Xu, H. B., et al. (2019). HDAC2 hyperexpression alters hippocampal neuronal transcription and microglial activity in neuroinflammation-induced cognitive dysfunction. *J. Neuroinflamm.* 16:249. doi: 10.1186/s12974-019-1640-z

Suo, T., Chen, G. Z., Huang, Y., Zhao, K. C., Wang, T., and Hu, K. (2018). miRNA-1246 suppresses acute lung injury-induced inflammation and apoptosis *via* the NF-κNB and Wnt/β-catenin signal pathways. *Biomed. Pharmacother.* 108, 783–791. doi: 10.1016/j.biopha.2018.09.046

Ta Dinh, S., Nickel, M. M., Tiemann, L., May, E. S., Heitmann, H., Hohn, V. D., et al. (2019). Brain dysfunction in chronic pain patients assessed by resting-state electroencephalography. *Pain* 160, 2751–2765. doi: 10.1097/j.pain.0000000000001666

Velasquez, S., Prevedel, L., Valdebenito, S., Gorska, A. M., Golovko, M., Khan, N., et al. (2019). Circulating levels of ATP is a biomarker of HIV cognitive impairment. *EBioMedicine* 51:102503. doi: 10.1016/j.ebiom.2019.10.029

Xiao, X., Wong, D. T. W., Kim, Y., Lin, X., Chan, T. M., Li, F., et al. (2015). The landscape of microRNA, piwi-interacting RNA, and circular RNA in human saliva. *Clin. Chem.* 61, 221–230. doi: 10.1373/clinchem.2014.230433

Xin, Y., Song, X., and Ge, Q. (2021). Circular RNA SMEK1 promotes neuropathic pain in rats through targeting microRNA-216a-5p to mediate Thioredoxin Interacting Protein (TXNIP) expression. *Bioengineered* 12, 5540–5551. doi: 10.1080/21655979.2021.1965811

Xiong, B., Zhang, W., Zhang, L., Huang, X., Zhou, W., Zou, Q., et al. (2020). Hippocampal glutamatergic synapses impairment mediated novel-object recognition dysfunction in rats with neuropathic pain. *Pain* 161, 1824–1836. doi: 10.1097/j.pain.0000000000001878

Xu, D., Ma, X., Sun, C., Han, J., Zhou, C., Chan, M. T. V., et al. (2021). Emerging roles of circular RNAs in neuropathic pain. *Cell Proliferat.* 54:e13139. doi: 10.1111/cpr.13139

You, Z., Zhang, S., Shen, S., Yang, J., Ding, W., Yang, L., et al. (2018). Cognitive impairment in a rat model of neuropathic pain: role of hippocampal microtubule stability. *Pain* 159, 1518–1528. doi: 10.1097/j.pain.0000000000001233

Yue, J., and Lopez, J. M. (2020). Understanding MAPK signaling pathways in apoptosis. *Int. J. Mol. Sci.* 21:2346. doi: 10.3390/ijms21072346

Zhang, C., Zhu, Z. L., Gao, J. X., Yang, L. T., Dang, E. L., Fang, H., et al. (2020). Plasma exosomal miR-375-3p regulates mitochondria-dependent keratinocyte apoptosis by targeting XIAP in serve drug-induced skin reactions. *Sci. Transl. Med.* 12:eaaw6142. doi: 10.1126/scitranslmed.aaw6142

Zhang, G. F., Zhou, Z. Q., Guo, J., Gu, H. W., Su, M. Z., Yu, B. C., et al. (2021). Histone deacetylase 3 in hippocampus contributes to memory impairment after chronic constriction injury of sciatic nerve in mice. *Pain* 162, 382–395. doi: 10.1097/j.pain.0000000000002056

Zhang, S. B., Lin, S. Y., Liu, M., Liu, C. C., Ding, H. H., Sun, Y., et al. (2019). CircAnks1a in the spinal cord regulates hypersensitivity in a rodent model of neuropathic pain. *Nat. Commun.* 10:4119. doi: 10.1038/s41467-019-12049-0

Zhou, X., Gan, T., Fang, G., Wang, S., Mao, Y., and Ying, C. (2018). Zeaxanthin improved diabetes-induced anxiety and depression through inhibiting inflammation in hippocampus. *Metab. Brain Dis.* 33, 705–711. doi: 10.1007/s11011-017-0179-x

Zhu, Y., Zhao, P., Sun, L., Lu, Y., Zhu, W., Zhang, J., et al. (2021). Overexpression of circRNA SNRK targets miR-103-3p to reduce apoptosis and promote cardiac repair through GSK3beta/beta-catenin pathway in rats with myocardial infarction. *Cell Death Discov.* 7:84. doi: 10.1038/s41420-021-00467-3

Zhuo, C. J., Hou, W. H., Jiang, D. G., Tian, H. J., Wang, L. N., Jia, F., et al. (2020). Circular RNAs in early brain development and their influence and clinical significance in neuropsychiatric disorders. *Neural Regen. Res.* 15, 817–823. doi: 10.4103/1673-5374.268969

frontiers | Frontiers in Aging Neuroscience

TYPE Original Research
PUBLISHED 20 September 2022
DOI 10.3389/fnagi.2022.978768

OPEN ACCESS

EDITED BY
Zhongcong Xie,
Massachusetts General Hospital and Harvard Medical School, United States

REVIEWED BY
Heinrich S. Gompf,
University of Massachusetts Medical School, United States
Nobuyuki Kimura,
Okayama University of Science, Japan

*CORRESPONDENCE
E. Wang
ewang324@csu.edu.cn

SPECIALTY SECTION
This article was submitted to Neurocognitive Aging and Behavior, a section of the journal Frontiers in Aging Neuroscience

RECEIVED 26 June 2022
ACCEPTED 29 August 2022
PUBLISHED 20 September 2022

CITATION
Luo S-m, Li L-y, Guo L-z, Wang L, Wang Y-f, Chen N and Wang E (2022) Dexmedetomidine exerts an anti-inflammatory effect via α2 adrenoceptors to alleviate cognitive dysfunction in 5xFAD mice. Front. Aging Neurosci. 14:978768. doi: 10.3389/fnagi.2022.978768

Dexmedetomidine exerts an anti-inflammatory effect *via* α2 adrenoceptors to alleviate cognitive dysfunction in 5xFAD mice

Su-mei Luo[1], Long-yan Li[1,2], Li-zhe Guo[1], Lu Wang[1], Yan-feng Wang[1], Na Chen[1] and E. Wang[1,2]*

[1]Department of Anesthesiology, Xiangya Hospital Central South University, Changsha, China, [2]National Clinical Research Center for Geriatric Disorders (Xiangya Hospital), Changsha, China

Background: Inflammation promotes the progression of Alzheimer's disease (AD). In this study, we explored the effect of dexmedetomidine on inflammation and cognitive function in a mouse model of AD.

Methods: 5xFAD mice were intragastrically administered saline, dexmedetomidine, or dexmedetomidine and yohimbine for 14 days. The effects of dexmedetomidine on the acquisition and retention of memory in the Morris water-maze test and Y maze were evaluated. The deposition of amyloid beta protein (Abeta) and cytokine levels in the hippocampus were assessed. The expression of Bace1 protein and NFκB-p65 protein was assessed by Western blotting.

Results: Compared with WT mice, 5xFAD mice exhibited cognitive impairment in the Morris water maze test and Y maze test. Cognitive decline was alleviated by dexmedetomidine and this was reversed by the α2 adrenoceptor antagonist yohimbine. Compared with saline treatment, dexmedetomidine led to a reduction in the Abeta deposition area ($p < 0.05$) and in the mean gray value ($p < 0.01$) in the hippocampus of 5xFAD mice. Compared with saline treatment, dexmedetomidine inhibited the activation of astrocytes and microglia in the hippocampal DG of 5xFAD mice and reduced the area of GFAP ($p < 0.01$) and IBA1 ($p < 0.01$). The level of IL-1β in the hippocampus decreased significantly after dexmedetomidine treatment compared with saline treatment in 5xFAD mice ($p < 0.01$). Yohimbine neutralized the effects of dexmedetomidine. Dexmedetomidine inhibited the expression of BACE1 and NF-κB p65 ($p < 0.01$), and these changes were reversed by yohimbine treatment.

Conclusion: Dexmedetomidine alleviates cognitive decline, inhibits neuroinflammation, and prevents the deposition of Abeta in 5xFAD mice. The effect is mediated by the α2 adrenoceptor-mediated anti-inflammatory pathway. Dexmedetomidine may be effective for the treatment of AD and a better choice for the sedation of AD.

KEYWORDS

Alzheimer's disease, dexmedetomidine, yohimbine, amyloid plaques, neuroinflammation

Introduction

Alzheimer's disease (AD) results in memory impairment and cognitive decline (Thies and Bleiler, 2012). AD is characterized by the pathogenesis of extracellular amyloid plaques, neurofibrillary tangles, hyperphosphorylated tau protein, reductions in synaptic density, and neuroimmune activation (Bertram and Tanzi, 2008). Neuroinflammation is an important factor in AD (Parhizkar and Holtzman, 2022), persistent neuroinflammation induces amyloid-beta (Aβ), and neurofibrillary tangle production and death of neurons (Rajesh and Kanneganti, 2022; Weng et al., 2022), activated microglia and astrocytes cause the release of inflammatory factors, such as IL-6, IL-1β, and NF-κB (Bales et al., 1998). Many studies revealed that inflammatory factors involve the Aβ deposition and tau protein phosphorylation and direct toxic effects on neurons and synapses (Heneka et al., 2015; Hong et al., 2016; Sung et al., 2020), leading to the decline of cognitive function. Thus far, therapeutic options for AD are very limited.

Dexmedetomidine is an α2-adrenergic receptor agonist that is commonly used clinically for sedation and analgesia. In recent years, it has been reported that dexmedetomidine can protect neurocognition by reducing interleukin (IL)-6 and IL-1β in the hippocampus (Wang et al., 2019; Mei et al., 2021), it also can reduce the inflammatory response by reducing IL-1β and NF-κB levels *via* α2 adrenoceptors (Li et al., 2020). In addition, Chen's report indicates that NF-κB overexpression leads to upregulated β-secretase cleavage and Abeta production (Chen et al., 2012). We hypothesized that dexmedetomidine can delay cognitive decline in 5xFAD mice and explored its mechanism.

Materials and methods

Animals and ethics statement

All animal experimental procedures were approved by the Ethics Committee for Animal Research of Central South University and were performed in accordance with guidelines for treating laboratory animals. Furthermore, the study conformed with the National Institutes of Health Guide for the Care and Use of Laboratory Animals (NIH Publication No. 8023, revised 1978). For this study, we used the transgenic mouse line 5xFAD, which expresses five human mutations in APP and PS1 [B6SJL-Tg (APP*K670N*M671L*I716V*V717I, PSEN1*M146*L286V) 6799Vas/J], through a neuron-specific element in the Thy1 promoter. 5xFAD mice were originally gifted from the Shen Laboratory (School of Life Science, University of Science and Technology of China). The animals were housed with free access to food and water in a colony room under the following conditions: a temperature of 19°C–22°C humidity level of 40%–60%, and a 12 h/12 h cycle of automatic lighting. For genotyping of 5xFAD mice by PCR, the following primer pairs were used: forward primer (5'-AGG ACT GAC CAC TCG ACC AG-3') and reverse primer (5'-CGG GGG TCT AGT TCT GCA T-3').

Treatment of 5xFAD mice with dexmedetomidine

Forty-eight male 22-week-old wild-type and 5xFAD mice were divided into four groups: the wild-type treated with normal saline group (WT+NS), 5xFAD treated with normal saline group (AD+NS), 5xFAD treated with dexmedetomidine group (AD+Dex), and 5xFAD treated with dexmedetomidine and yohimbine group (AD+Dex+Y). The mice in the dexmedetomidine group were given dexmedetomidine (Hengrui Pharmaceutical Co. Ltd, Jiangsu, China) intragastrically at a dosage of 100 μg/kg once a day for 14 days. The mice in the dexmedetomidine and yohimbine groups were given the same dosage of dexmedetomidine and a dose of 0.5 mg/kg yohimbine hydrochloride (Abmole, Houston, TX), yohimbine was given 10 min before dexmedetomidine. An equal volume of saline was given intragastrically to mice in the control groups.

Morris water maze behavioral tests

After 14 days of continuous feeding, the mice were brought to the testing room to adapt to the environment for 30 min before the behavioral test. The Morris water maze (MWM) test was performed with minor adjustments as previously described. The test consisted of 5 days of learning trials and a 1-day probe test. The mice were given 1 min to find the platform. If a mouse found the platform within 1 min and stayed for 3 s, we considered the mouse to have successfully found the platform and ended the experiment. Otherwise, something was used to guide the mouse to the platform and stay for 20 s. In the probe test, the platform was removed, and the mice were allowed to swim for 1 min. All mouse movements were recorded and analyzed by Smart v3.0 (Panlab, Spain), a computerized tracking system.

Y-maze behavioral tests

Mice were brought to the testing room to adapt to the environment for 30 min before the test and then subjected to the Y-maze test, as previously described (Dinel et al., 2014; Jeon et al., 2018). The Y-maze consists of three arms and a center, which together form a Y shape. Before the test, one arm of the maze was closed, and then the mice were placed in one open arm facing the wall. Mice were allowed 8 min to explore the two open arms of the maze. Thirty minutes later, the mice were returned to the Y-maze with all arms open for 5 min. The time spent in the novel arm and the new arm entries were recorded.

Real time RT-PCR analysis

After behavioral testing, the mice were euthanized by cervical dislocation, and the hippocampus was immediately harvested. RNA was extracted from the hippocampus using TranZol Up (TRANS, China) according to the manufacturer's instructions. A NanoDrop (Thermo, Wilmington, DE) was used to quantify RNA, and the SureScript First-Strand cDNA synthesis kit (Genecopoeia, Rockville, MD) was used to reverse transcribe cDNA. Real-time RT-PCR was performed using a 96-well microfluidic card, and gene expression was assessed by performing SYBR-green reagent assays (Applied Biosystems, Thermo Fisher Scientific, Wilmington, DE). The β-actin gene was used to normalize the expression of target genes. The primer sets for RT-qPCR analysis were as follows: β-actin: forward primer (sequence 5'−3') (TGCTCTCCCTCACGCCATCC); reverse primer (sequence 5'−3') (GTCACGCACGATTTCCCTCTCAG); Bace1: forward primer (sequence 5'−3') (CAGTGGAAGGTCCGTTTGTT); reverse primer (sequence 5'−3') (CTAAAGGATGCTGGGCAGAG).

Immunofluorescence staining assay

Immunofluorescence staining was performed on frozen coronal sections of the mouse brain. The brain sections were washed with PBS and incubated with Immunol Staining Blocking Buffer (Beyotime Biotechnology, China) to block nonspecific reactions for 2 h at room temperature. After blocking, the sections were incubated overnight at 4°C in Immunol Staining Primary Antibody Dilution Buffer (Beyotime Biotechnology, China), which contained rabbit anti-β-amyloid antibody (1:1,000, Cell Signaling Technology, Boston, MA). The next day, sections were incubated for 2 h at room temperature in PBS containing Alexa Fluor 488 (1:500, green, Invitrogen, CA). Finally, the sections were photographed using a Nikon fluorescence microscope. The results were analyzed with ImageJ software.

Western blot

Tissues were homogenized in RIPA buffer supplemented with protease and phosphatase inhibitors (NCM Biotech, China), sonicated to shear DNA, and centrifuged at 14,000× *g* for 20 min at 4°C. Equal amounts of protein sample (50 μg) were resolved by SDS-PAGE. The following primary antibodies were used: rabbit anti-β-actin antibody (1:10,000; Affinity, Cincinnati, OH), rabbit anti-bace1 antibody (1:1,000; Cell Signaling Technology, Boston, MA), rabbit anti-NF-KB antibody (1:1,000; Cell Signaling Technology, Boston, MA), and goat anti-rabbit IgG (H+L) HRP (1:5,000; Affinity, Cincinnati, OH). Quantification of immunoreactive bands is reported as a ratio against β-actin using ImageJ software.

Enzyme-linked immunosorbent assay

Hippocampal samples were collected from each group for use in assessing the effects of dexmedetomidine on the hippocampal levels of inflammatory factors. An IL-6 ELISA kit (Cusabio Biotech Co., Ltd, Hubei, China) and IL-1β ELISA kit (Proteintech Group Inc., Rosemont, PA) were used, and the ELISA protocol for IL-6 and IL-1β was performed according to the respective instructions.

Statistical analysis

All data are expressed as the means ± SD or means ± SEM and were analyzed with GraphPad Prism 8.0. One-way ANOVA or two-way ANOVA was used for comparisons with three groups or more. $P < 0.05$ was considered indicative of statistical significance.

Results

Dexmedetomidine protects against cognitive impairment in 5xFAD mice

In the Morris water maze, mice in the 5xFAD treated with normal saline (AD+NS) group spent more time finding the escape platform than mice in the WT+NS group ($p < 0.05$). There is no statistically significant difference between the AD+NS group and the AD+Dex group, nor between the AD+Dex group and the AD+Dex+Y group. But the trends can be seen as follows, mice in the AD+NS group spent more time finding the platform than mice in the 5xFAD treated with dexmedetomidine (AD+Dex) group, and mice in the 5xFAD treated with dexmedetomidine and yohimbine (AD+Dex+Y) group spent more time finding the platform than mice in the AD+Dex group (**Figure 1A**). In the probe test, mice in the wild-type treated with normal saline (WT+NS) group crossed the platform more often than mice in the AD+NS group (WT+NS vs. AD+NS, 3.25 ± 0.43 vs. 1.17 ± 0.24, $p < 0.001$). Mice in the AD+Dex group crossed the platform more often than those in the AD+NS group and AD+Dex+Y group (AD+Dex vs. AD+NS, 2.75 ± 0.43 vs. 1.17 ± 0.24, $p = 0.01$), (AD+Dex vs. AD+Dex+Y, 2.75 ± 0.43 vs. 1.25 ± 0.25, $p = 0.02$, $n = 12$ in each group; **Figure 1B**). There was no significant difference in swimming speed among the four groups (**Figure 1C**). Video tracks of the probe trial can be seen in **Figure 1D**.

In the Y maze, mice in the WT+NS group spent more time in the new arm than mice in the AD+NS group (WT+NS vs. AD+NS, 91.67 ± 5.51 vs. 38.79 ± 3.11 s, $p < 0.001$). Mice in the AD+Dex group spent more time in the new arm than mice in the AD+NS group (AD+Dex vs. AD+NS, 74.95 ± 4.72 vs. 38.79 ± 3.11 s, $p < 0.001$). Furthermore, mice in the AD+Dex group spent more time in the new arm than mice in the AD+Dex+Y group (AD+Dex vs. AD+Dex+Y, 74.95 ± 4.72 vs. 45.46 ± 3.25 s, $p < 0.001$, $n = 12$ in each group; **Figure 1E**). There was no significant difference in new arm entries among the four groups (**Figure 1F**).

Dexmedetomidine alleviates the deposition of Abeta in the hippocampus of 5xFAD Mice

Abeta deposition was detected in the four groups of mice with an immunofluorescence staining assay (**Figure 2A**). There

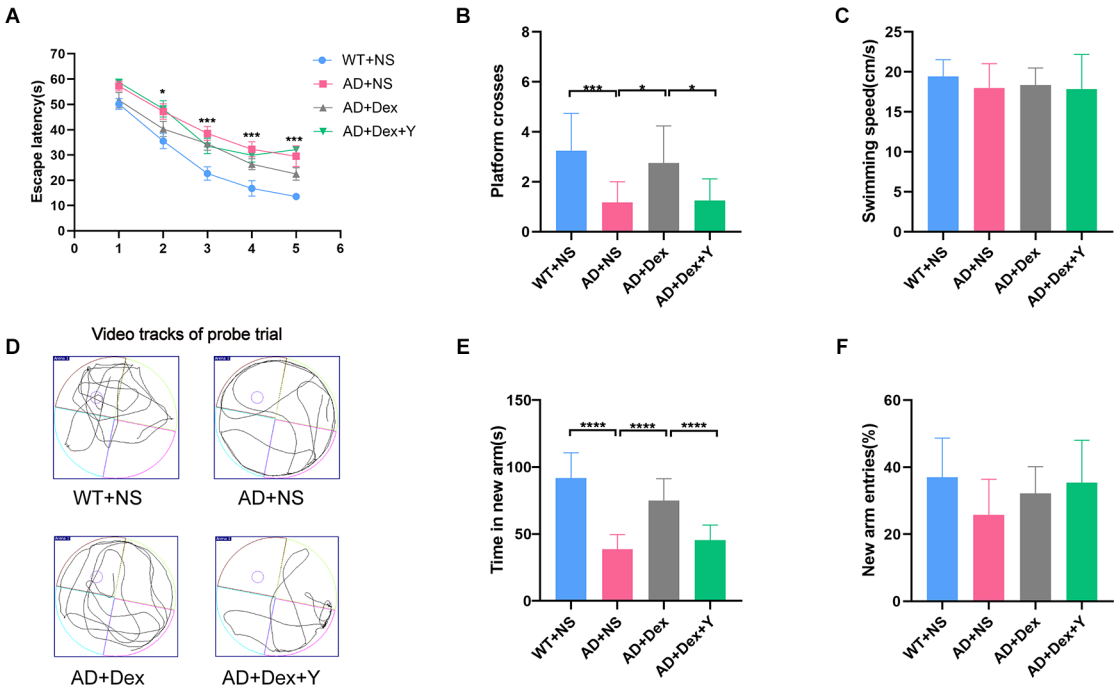

FIGURE 1
Dexmedetomidine improves learning and memory ability in 5xFAD mice. The data from the Morris water maze **(A–D)** and Y maze **(E,F)** were recorded and statistically analyzed. Panel **(A)** represents latency during the acquisition phase (means ± SEM, two-way repeated measures ANOVA and Bonferroni *post-hoc* test, $*p < 0.05$, AD+NC compared to the WT+NC group). Panel **(B)** represents the number of animals crossing the platform. Panel **(C)** represents swimming speed by mice in the target quadrant during the probe trial. Panel **(D)** represents video tracks of the probe trial. Panel **(E)** represents time spent in the new arm of the Y maze. Panel **(F)** represents the percentage of new arm entries in the Y maze (means ± SEM, ANOVA, Tukey's test, $*p < 0.05$, $***p < 0.001$, $****p < 0.0001$). $n = 12$ in each group.

10.3389/fnagi.2022.978768

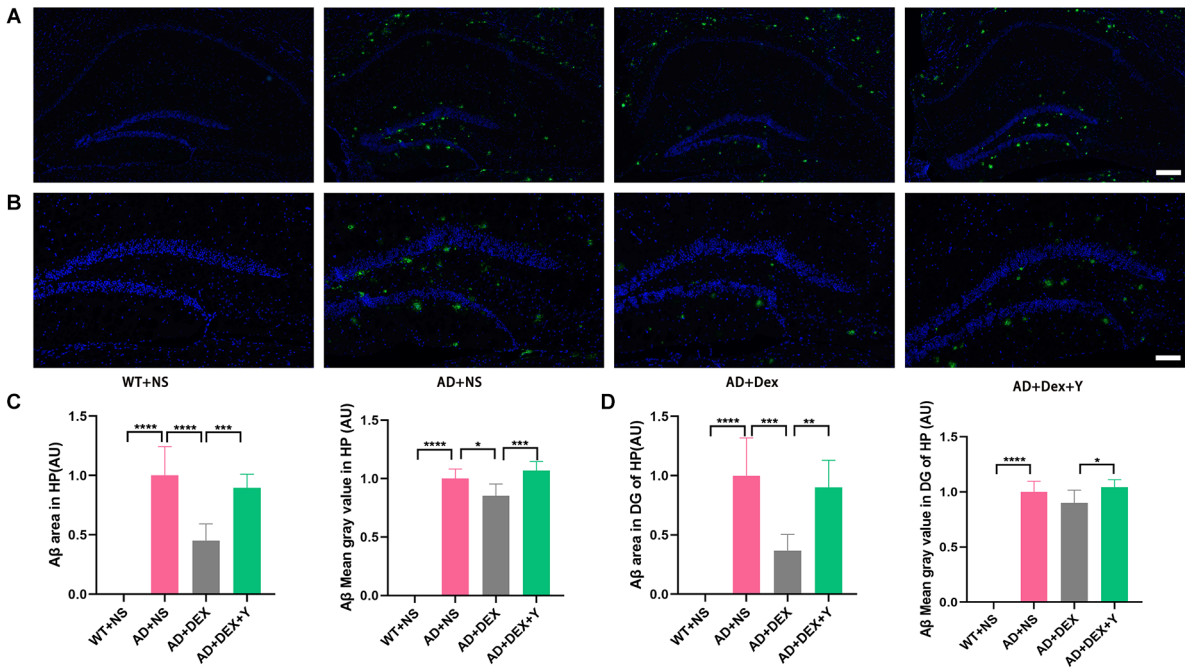

FIGURE 2
Dexmedetomidine alleviates the deposition of Aβ **(A,B,C,D)** (means ± SD, ANOVA, *$p < 0.05$, **$p < 0.01$, ***$p < 0.001$, ****$p < 0.0001$). **(A)** Immunofluorescence staining of hippocampal sections from WT and 5xFAD mice, scale bars, 200 μm. **(B)** Immunofluorescence staining of the hippocampal DG sections from WT and 5xFAD mice, scale bars, 100 μm. **(C)** Bar graph represents Abeta expression levels in the hippocampus. **(D)** The bar graph represents Abeta expression levels in the hippocampus DG.

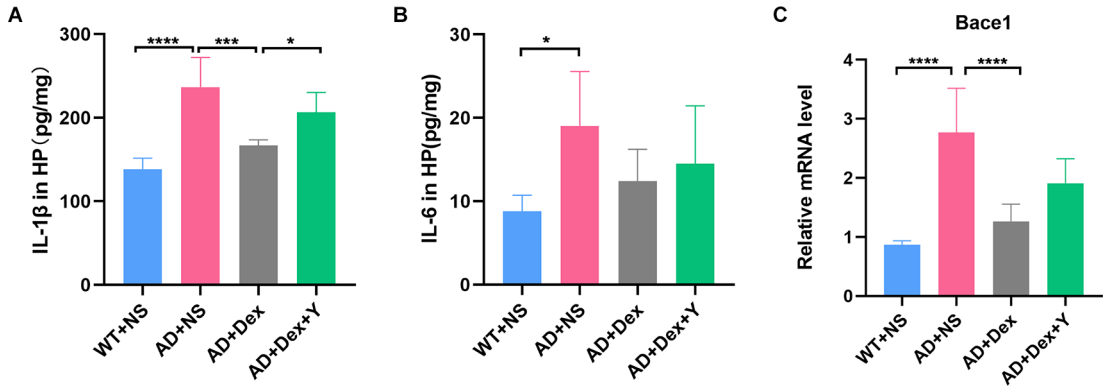

FIGURE 3
Panels **(A,B)** show ELISA data of IL-1β and IL-6 expression levels in the hippocampus ($n = 6$ in each group). **(C)** The expression level of Bace1 in qRT-PCR ($n = 6$ in each group). *$p < 0.05$, ***$p < 0.001$, ****$p < 0.0001$.

was no Abeta deposition in the hippocampus of the WT+NS group. Mice in the AD+NS group and AD+Dex+Y group had larger areas of Abeta deposition in the hippocampus, especially in the hippocampal dentate gyrus (DG; Figure 2B) than mice in the AD+Dex group. The Abeta deposition areas in the hippocampus in different groups were as follows: AD+NS vs. AD+Dex, 1.00 ± 0.24 vs. 0.45 ± 0.14 AU, $p < 0.001$; AD+Dex vs. AD+Dex+Y, 0.45 ± 0.14 vs. 0.89 ± 0.11, $p < 0.001$. The mean gray values of Abeta deposition were AD+NS vs. AD+Dex, 1.0 ± 0.08 vs. 0.85 ± 0.10 AU, $p = 0.02$, and AD+Dex vs. AD+Dex+Y, 0.85 ± 0.10 vs. 1.07 ± 0.08 AU, $p < 0.001$ (Figure 2C). The Abeta deposition areas in the hippocampus DG in different groups were as follows: AD+NS vs. AD+Dex, 1.00 ± 0.32 vs. 0.37 ± 0.14 AU, $p < 0.001$; AD+Dex vs. AD+Dex+Y, 0.37 ± 0.14 vs. 0.90 ± 0.23, $p = 0.001$. The mean gray values of Abeta deposition were AD+Dex vs. AD+Dex+Y,

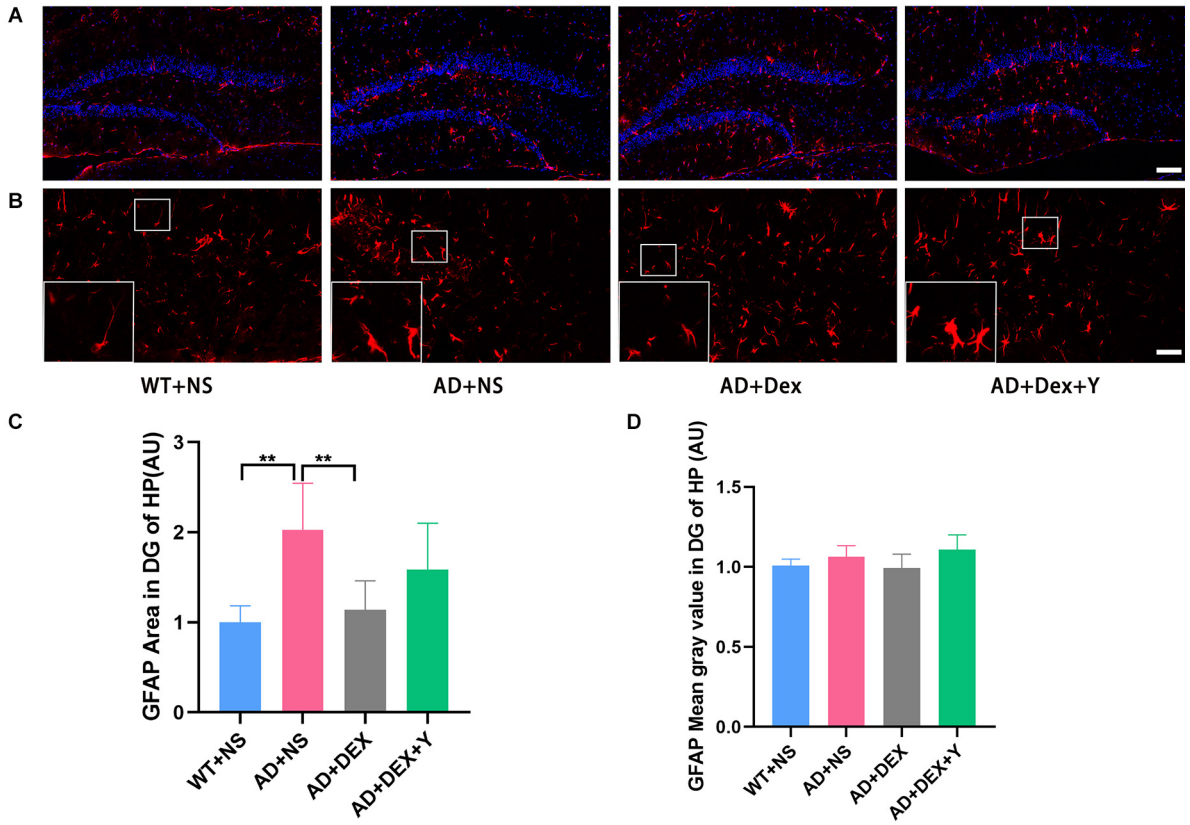

FIGURE 4
Dexmedetomidine inhibited glial cell activation in the hippocampus DG of 5xFADmice (means ± SD, ANOVA, $^{**}p < 0.01$). **(A)** Representative images of GFAP-positive staining in the hippocampus DG from WT and 5xFAD mice, scale bars, 100 μm. **(B)** High magnification images of GFAP-positive staining in the hippocampus DG from WT and 5xFAD mice, scale bars, 50 μm. **(C,D)** The bar graph represents GFAP expression levels in the hippocampus DG.

0.90 ± 0.11 vs. 1.05 ± 0.07 AU, $p = 0.03$, $n = 6$ in each group (Figure 2D). This finding reveals that dexmedetomidine delays hippocampal Abeta deposition in 5xFAD mice through an α2 receptor-dependent mechanism.

Dexmedetomidine reduces 5xFAD mouse hippocampal inflammatory responses

Enzyme-linked immunosorbent assay showed that the levels of IL-6 and IL-1β in 5xFAD mice were significantly higher than those in their littermate WT mice when they were administered NS (IL-6, 8.82 ± 1.89 pg/mg vs. 19.04 ± 6.51 pg/mg, $p = 0.01$; IL-1β, 138.70 ± 12.92 pg/mg vs. 237.00 ± 35.07 pg/mg, $p < 0.0001$; Figures 3A,B). Administration of dexmedetomidine reduced the level of IL-1β in hippocampal tissue (237.00 ± 35.07 pg/mg vs. 167.20 ± 6.50 pg/mg, $p = 0.0002$). The α_2 receptor antagonist yohimbine counteracted the anti-inflammatory effect of dexmedetomidine (IL-1β: 167.20 ± 6.50 pg/mg vs. 206.30 ± 23.96 pg/mg, $p = 0.03$, $n = 6$ in each group; Figure 3A). IL-6 levels were not different in the three 5xFAD groups (Figure 3B).

DG is more heavily regulated by various environmental and neurotrophic factors than other areas of the hippocampus (Yamashima et al., 2004; Lee and Son, 2009). So, we assessed the activation of astrocytes and microglia in hippocampus and area DG by immunostaining respectively using glial fibrillary acidic protein (GFAP) and ionized calcium-binding adapter molecule 1 (Iba-1). In the experiment, we found the level of GFAP was increased in the 5xFAD group of animals than that in littermate wild-type mice, and the administration of dexmedetomidine reduced the level of GFAP in the hippocampus DG (Figures 4A,B). The GFAP areas in the hippocampus DG in different groups were as follows: WT+NS vs. AD+NS, 1.00 ± 0.18 vs. 2.03 ± 0.52, $p = 0.002$; AD+NS vs. AD+Dex, 2.03 ± 0.52 vs. 1.14 ± 0.32 AU, $p = 0.006$. The GFAP areas of hippocampus DG in the AD+Dex+Y group increased compared with that in the AD+Dex group, although not statistically significant (Figures 4C,D). A significant increase

10.3389/fnagi.2022.978768

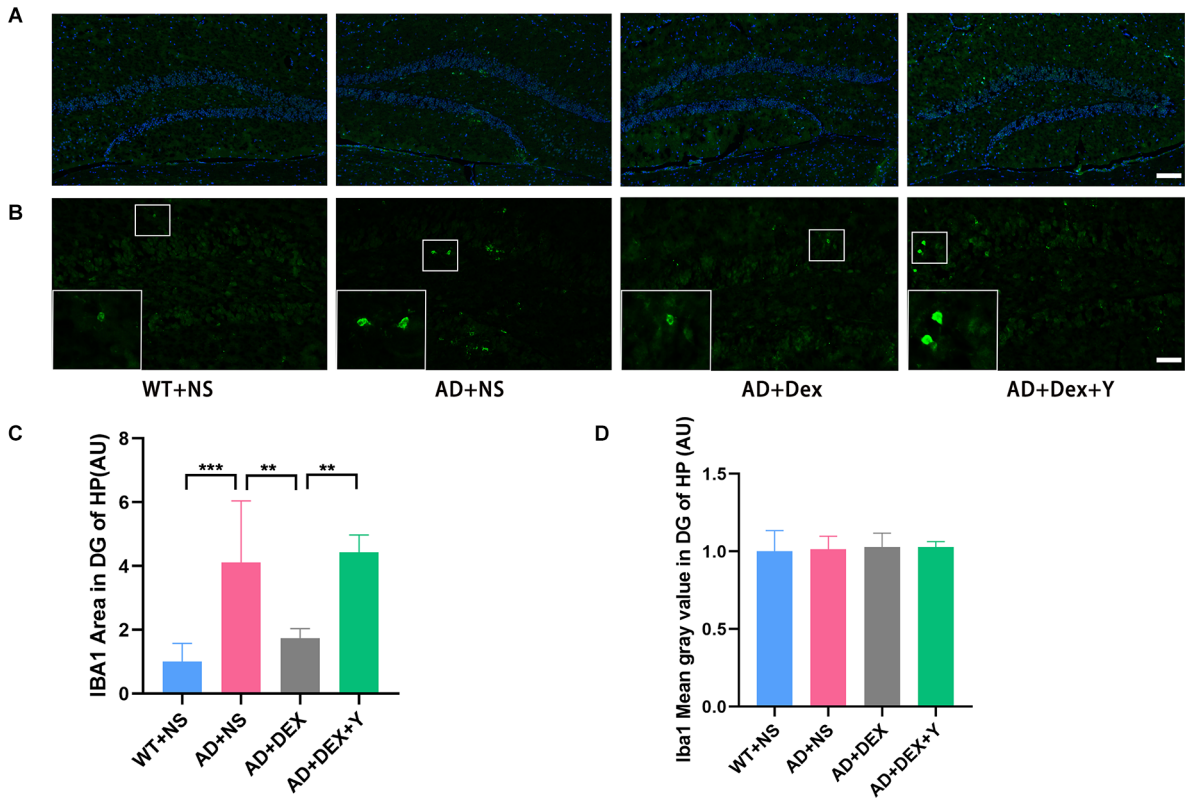

FIGURE 5
Dexmedetomidine inhibited glial cell activation in the hippocampus DG of 5xFAD mice (means ± SD, ANOVA, $^{**}p < 0.01$, $^{***}p < 0.001$). **(A)** Representative images of IBA1-positive staining in the hippocampus DG from WT and 5xFAD mice, scale bars, 100 μm. **(B)** High magnification images of IBA1-positive staining in the hippocampus DG from WT and 5xFAD mice, scale bars, 50 μm. **(C,D)** The bar graph represents IBA1 expression levels in the hippocampus DG ($n = 6$ in each group).

of Iba1-positive microglial cells was detected in AD mice than that in littermate wild-type mice, administration of dexmedetomidine reduced the Iba1-positive microglial cells in the hippocampus DG (Figures 5A,B). The Iba1 areas in the hippocampus DG in different groups were as follows: WT+NS vs. AD+NS, 1.00 ± 0.58 vs. 4.12 ± 1.93, $p < 0.001$; AD+NS vs. AD+Dex, 4.12 ± 1.93 vs. 1.73 ± 0.31 AU, $p = 0.004$; AD+Dex vs. AD+Dex+Y, 1.73 ± 0.31 vs. 4.43 ± 0.55 AU, $p = 0.001$, $n = 6$ in each group. The GFAP areas of hippocampus DG in the AD+Dex+Y group increased compared with that in the AD+Dex group, although not statistically significant (Figures 5C,D).

Dexmedetomidine reverses 5xFAD mouse hippocampal NfκB-P65 phosphorylation and prevents the production of bace1

In the qRT-PCR experiment, we found that the level of bace1 mRNA expression in 5xFAD mice was significantly higher than that in littermate wild-type mice (WT+NS vs. AD+NS, 0.86 ± 0.07 vs. 2.77 ± 0.75, $p < 0.0001$; Figure 3C). Administration of dexmedetomidine reduced the level of bace1 expression in the hippocampus (AD+NS vs. AD+Dex, 2.77 ± 0.75 vs. 1.26 ± 0.30, $p < 0.0001$). Western blot analysis showed that the expression of bace1 in the AD+NS group was significantly increased compared with that in the WT+NS group (WT+NS vs. AD+NS, 1.00 ± 0.22 vs. 1.65 ± 0.24, $p = 0.003$); the expression of bace1 in the AD+Dex group was significantly decreased compared with that in the AD+NS group (AD+Dex vs. AD+NS, 1.11 ± 0.30 vs. 1.65 ± 0.24, $p = 0.03$, $n = 6$ in each group; Figures 6A,C).

There was a significant difference in the expression of NF-κB-p65 between the WT+NS group and the AD+NS group (WT+NS vs. AD+NS, 1.00 ± 0.36 vs. 1.80 ± 0.45, $p = 0.004$ (Figure 4D). The expression of NF-κB-p65 in the AD+Dex+Y group increased significantly compared with that in the AD+Dex group (AD+Dex vs. AD+Dex+Y, 1.27 ± 0.28 vs. 1.83 ± 0.45, $p = 0.04$, $n = 6$ in each group; Figures 6B,D). This finding reveals that dexmedetomidine acts on bace1 through the NF-κB signaling pathway in the hippocampus of 5xFAD mice through an α2 receptor-dependent mechanism.

10.3389/fnagi.2022.978768

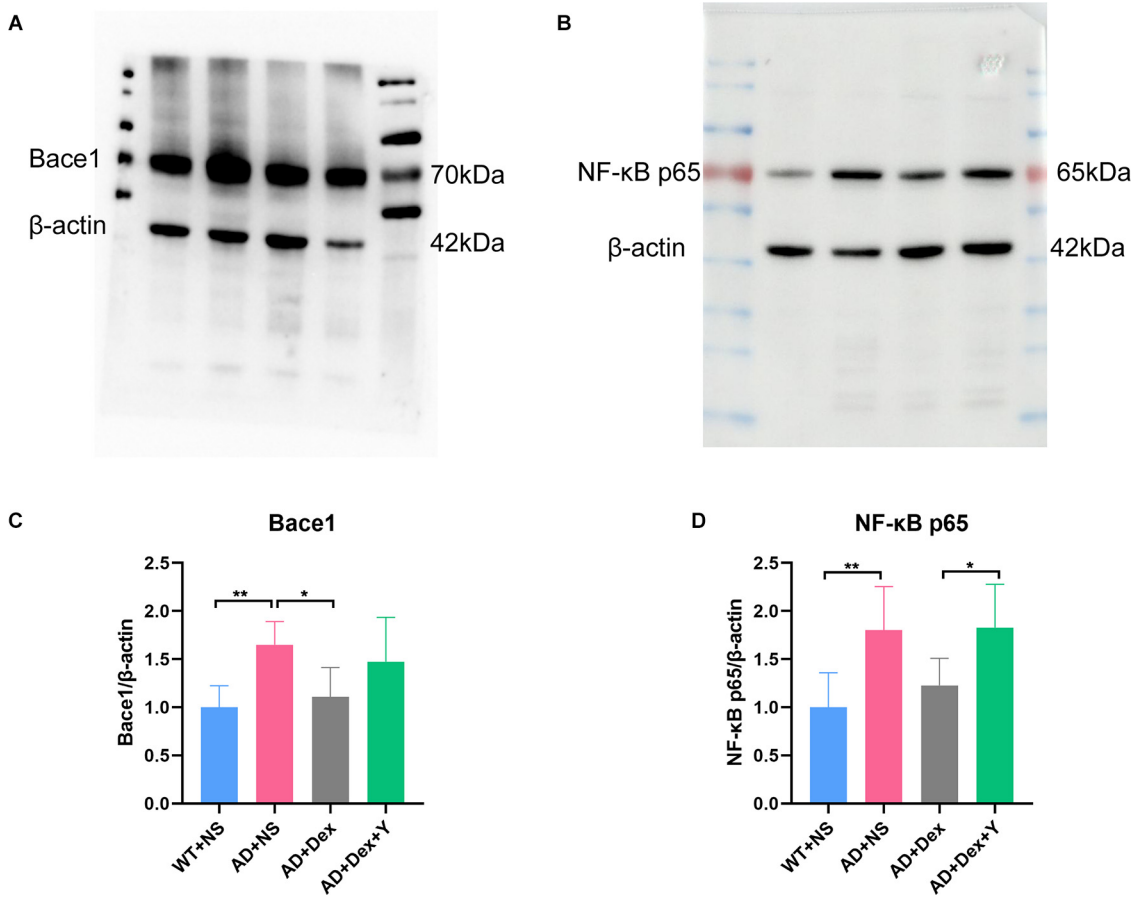

FIGURE 6
Dexmedetomidine downregulates the expression of Bace1 **(A,C)** and NF-κB p65 (**B,D**; means ± SD, ANOVA, $*p < 0.05$, $**p < 0.01$). **(A)** Western blotting data showing Bace1 expression levels in the hippocampus. **(B)** Western blotting data of NF-κB p65 expression levels in the hippocampus. **(C)** The bar graph represents Bace1 expression levels in the hippocampus. **(D)** The bar graph represents NF-κB p65 expression levels in the hippocampus ($n = 6$ in each group).

Discussion

5xFAD mice are a classic model of AD and express human APP under the control of the murine Thy-1 promoter (Oakley et al., 2006). Extracellular amyloid plaques can be detected as early as 2 months in the hippocampus, and amyloid plaques and cognitive decline worsen with age (Richard et al., 2015). In this study, we found that WT mice performed better than 5xFAD mice in the Y-maze and Morris water maze. Dexmedetomidine treatment improved the spatial and learning memory performance of 5xFAD mice. Biochemical experiments showed that 5xFAD mice treated with dexmedetomidine had less Abeta deposition than those treated with NS. The expression levels of GFAP, IBA1, bace1, NF-κB p65, and IL-1β were downregulated. However, yohimbine neutralized the effects of dexmedetomidine. The present study demonstrated that dexmedetomidine exerts an anti-inflammatory effect *via* the α_2 adrenoceptor to alleviate cognitive function decline in 5xFAD mice.

AD is a complex neurodegenerative disease with two main pathological features, amyloid plaques, and neurofibrillary tangles. In recent years, an increasing number of studies have started to focus on neuroinflammation in AD (Howard et al., 2020; Zhang F. et al., 2021), and many studies have pointed out the important role of inflammation in the progression of AD (Holmes, 2013; McAlpine et al., 2021; Milner et al., 2021). Inflammation in the brains of AD patients is a typical double-edged sword, and activation of microglia and astrocytes can eliminate debris and protein aggregates; in contrast, over-activated glia produces inflammatory factors leading to neuronal system damage (Schwartz and Deczkowska, 2016). Pascoal's team proposed that amyloid plaques, neurofibrillary tangles, and neuroinflammation interact with each other and together promote the development of AD (Pascoal et al., 2021). Persistently activated microglia have been found in the AD brain

and are associated with overexpression of IL-6, IL-1β, and NF-κB (Bales et al., 1998). It was reported that IL-6 is involved in dementia (Koyama et al., 2013). Griffin et al. (1998) found that IL-1β promotes the synthesis of β-amyloid precursor protein and induces the production of Aβ. Furthermore, Chen's report indicates that NF-κB p65 overexpression leads to upregulated β-secretase cleavage and Abeta production (Chen et al., 2012). Hence, anti-inflammatory effects have therapeutic potential.

Dexmedetomidine not only has anti-inflammatory effects (Li et al., 2018) but also can improve cognitive impairment caused by various reasons (Deiner et al., 2017; Alam et al., 2018). Animal experiments have shown that dexmedetomidine can reduce the inflammatory response by reducing IL-1β and NF-κB levels *via* α2 adrenoceptors, thereby improving the cognitive decline caused by inflammation (Li et al., 2020). In addition, dexmedetomidine can protect against $A\beta_{1-42}$-induced hippocampal neuronal apoptosis and cognitive impairment in mice (Sun et al., 2020). Furthermore, dexmedetomidine could also improve cognitive function in aged rats, and it may be associated with Abeta (Zhang et al., 2018). Some clinical trials have shown that reducing amyloid plaques fails to improve cognition, leading some studies to conclude that Abeta has little effect on AD (Cummings et al., 2019; Egan et al., 2019). There is growing evidence that Abeta may influence synaptic activity, tau pathology, and neuroinflammation (Pereira et al., 2021).

The effect of dexmedetomidine on cognitive function and Abeta deposition in AD is still unknown, so we investigated the efficacy of dexmedetomidine in 5xFAD mice and explored the possible mechanism. Alzheimer's disease is a chronic progressive disease, so we need to choose a long-term administration time to affect the course of the disease. European Medicines Agency revealed that no accumulation in patients when dexmedetomidine was infused for 14 days (Keating, 2015), therefore, by administrating dexmedetomidine for 14 days not only the action time of the drug is guaranteed, but also there is no accumulation in mice in subsequent behavioral experiments. Our study shows that dexmedetomidine can prevent Abeta deposition by regulating NF-κB-bace1, reduce neuroinflammation resulting from Abeta, and prevent cognitive decline in 5xFAD mice.

Dexmedetomidine is a highly selective α2 adrenergic receptor agonist, and α2 adrenoceptors are distributed on circulating and tissue immunocytes, so dexmedetomidine can affect the innate immune response through α2 adrenergic receptors (Quatrini et al., 2018). In ischemia-reperfusion injury in the heart, dexmedetomidine activation of α2 adrenoceptors downregulates toll-like receptor 4 (TLR4) expression and then regulates NF-κB (Sun et al., 2020); therefore, α2 adrenoceptors may regulate bace1 through the TLR4-NF-κB signaling pathway, affecting Abeta deposition. Yohimbine has an extremely high affinity for α2 adrenoceptors and can counteract the effect of dexmedetomidine through α2 adrenoceptors (Gao et al., 2019).

Our study has limitations. Our results indicate dexmedetomidine inhibits neuroinflammation in 5xFAD mice, but the mechanism is not investigated. Reports reveal that dexmedetomidine can improve sleep disorders (Zhang Y. et al., 2021), and sleep disorders play an important role in AD (Irwin and Vitiello, 2019), maybe dexmedetomidine can alleviate AD by improving sleep disorders.

In conclusion, dexmedetomidine alleviates cognitive decline, prevents the production of Abeta, and inhibits neuroinflammation in 5xFAD mice. These findings demonstrated that dexmedetomidine may be a potential drug for the treatment of AD. This conclusion may benefit the clinical use of the drug in patients at risk for cognitive impairment.

Data availability statement

The original contributions presented in the study are included in the article, further inquiries can be directed to the corresponding author.

Ethics statement

The animal study was reviewed and approved by Ethics Committee for Animal Research of Central South University.

Author contributions

EW designed and supervised the study. S-mL, L-yL, L-zG, NC, and Y-fW performed the experiments. S-mL and LW wrote the manuscript draft. All authors contributed to the article and approved the submitted version.

Funding

This work was financially supported by the National Key Research and Development Program of China (No: 2020YFC2005300) and the Youth Program of National Natural Science Foundation of China (grant number 81601728).

Conflict of interest

The authors declare that the research was conducted in the absence of any commercial or financial relationships that could be construed as a potential conflict of interest.

Publisher's note

References

Alam, A., Hana, Z., Jin, Z., Suen, K. C., and Ma, D. (2018). Surgery, neuroinflammation and cognitive impairment. *EBioMedicine* 37, 547–556. doi: 10.1016/j.ebiom.2018.10.021

Bales, K. R., Du, Y., Dodel, R. C., Yan, G. M., Hamilton-Byrd, E., Paul, S. M., et al. (1998). The NF-κB/Rel family of proteins mediates Aβ-induced neurotoxicity and glial activation. *Brain Res. Mol. Brain Res.* 57, 63–72. doi: 10.1016/s0169-328x(98)00066-7

Bertram, L., and Tanzi, R. E. (2008). Thirty years of Alzheimer's disease genetics: the implications of systematic meta-analyses. *Nat. Rev. Neurosci.* 9, 768–778. doi: 10.1038/nrn2494

Chen, C. H., Zhou, W., Liu, S., Deng, Y., Cai, F., Tone, M., et al. (2012). Increased NF-κB signalling up-regulates BACE1 expression and its therapeutic potential in Alzheimer's disease. *Int. J. Neuropsychopharmacol.* 15, 77–90. doi: 10.1017/S1461145711000149

Cummings, J., Lee, G., Ritter, A., and Sabbagh, M, Zhong, K. (2019). Alzheimer's disease drug development pipeline: 2019. *Alzheimers Dement. (N Y)* 5, 272–293. doi: 10.1016/j.trci.2019.05.008

Deiner, S., Luo, X., Lin, H. M., Sessler, D. I., Saager, L., Sieber, F. E., et al. (2017). Intraoperative infusion of dexmedetomidine for prevention of postoperative delirium and cognitive dysfunction in elderly patients undergoing major elective noncardiac surgery: a randomized clinical trial. *JAMA Surg.* 152:e171505. doi: 10.1001/jamasurg.2017.1505

Dinel, A. L., Joffre, C., Trifilieff, P., Aubert, A., Foury, A., Le Ruyet, P., et al. (2014). Inflammation early in life is a vulnerability factor for emotional behavior at adolescence and for lipopolysaccharide-induced spatial memory and neurogenesis alteration at adulthood. *J. Neuroinflammation* 11:155. doi: 10.1186/s12974-014-0155-x

Egan, M. F., Kost, J., Voss, T., Mukai, Y., Aisen, P. S., Cummings, J. L., et al. (2019). Randomized trial of verubecestat for prodromal Alzheimer's disease. *N. Engl. J. Med.* 380, 1408–1420. doi: 10.1056/NEJMoa1812840

Gao, J., Sun, Z., Xiao, Z., Du, Q., Niu, X., Wang, G., et al. (2019). Dexmedetomidine modulates neuroinflammation and improves outcome via alpha2-adrenergic receptor signaling after rat spinal cord injury. *Br. J. Anaesth.* 123, 827–838. doi: 10.1016/j.bja.2019.08.026

Griffin, W. S., Sheng, J. G., Royston, M. C., Gentleman, S. M., McKenzie, J. E., Graham, D. I., et al. (1998). Glial-neuronal interactions in Alzheimer's disease: the potential role of a 'cytokine cycle' in disease progression. *Brain Pathol.* 8, 65–72. doi: 10.1111/j.1750-3639.1998.tb00136.x

Heneka, M. T., Carson, M. J., El Khoury, J., Landreth, G. E., Brosseron, F., Feinstein, D. L., et al. (2015). Neuroinflammation in Alzheimer's disease. *Lancet Neurol.* 14, 388–405. doi: 10.1016/S1474-4422(15)70016-5

Holmes, C. (2013). Review: systemic inflammation and Alzheimer's disease. *Neuropathol. Appl. Neurobiol.* 39, 51–68. doi: 10.1111/j.1365-2990.2012.01307.x

Hong, S., Beja-Glasser, V. F., Nfonoyim, B. M., Frouin, A., Li, S., Ramakrishnan, S., et al. (2016). Complement and microglia mediate early synapse loss in Alzheimer mouse models. *Science* 352, 712–716. doi: 10.1126/science.aad8373

Howard, R., Zubko, O., Bradley, R., Harper, E., Pank, L., O'Brien, J., et al. (2020). Minocycline at 2 different dosages vs. placebo for patients with mild Alzheimer disease: a randomized clinical trial. *JAMA Neurol.* 77, 164–174. doi: 10.1001/jamaneurol.2019.3762

Irwin, M. R., and Vitiello, M. V. (2019). Implications of sleep disturbance and inflammation for Alzheimer's disease dementia. *Lancet Neurol.* 18, 296–306. doi: 10.1016/S1474-4422(18)30450-2

Jeon, S. G., Kang, M., Kim, Y. S., Kim, D. H., Nam, D. W., Song, E. J., et al. (2018). Intrahippocampal injection of a lentiviral vector expressing neurogranin enhances cognitive function in 5XFAD mice. *Exp. Mol. Med.* 50:e461. doi: 10.1038/emm.2017.302

Keating, G. M. (2015). Dexmedetomidine: a review of its use for sedation in the intensive care setting. *Drugs* 75, 1119–1130. doi: 10.1007/s40265-015-0419-5

Koyama, A., O'Brien, J., Weuve, J., Blacker, D., Metti, A. L., Yaffe, K., et al. (2013). The role of peripheral inflammatory markers in dementia and Alzheimer's disease: a meta-analysis. *J. Gerontol. A. Biol. Sci. Med. Sci.* 68, 433–440. doi: 10.1093/gerona/gls187

Lee, E., and Son, H. (2009). Adult hippocampal neurogenesis and related neurotrophic factors. *BMB Rep.* 42, 239–244. doi: 10.5483/bmbrep.2009.42.5.239

Li, H., Zhang, X., Chen, M., Chen, J., Gao, T., and Yao, S. (2018). Dexmedetomidine inhibits inflammation in microglia cells under stimulation of LPS and ATP by c-Fos/NLRP3/caspase-1 cascades. *Excli. J.* 17, 302–311. doi: 10.17179/excli2017-1018

Li, R., Lai, I. K., Pan, J. Z., Zhang, P., and Maze, M. (2020). Dexmedetomidine exerts an anti-inflammatory effect via α2 adrenoceptors to prevent lipopolysaccharide-induced cognitive decline in mice. *Anesthesiology* 133, 393–407. doi: 10.1097/ALN.0000000000003390

McAlpine, C. S., Park, J., Griciuc, A., Kim, E., Choi, S. H., Iwamoto, Y., et al. (2021). Astrocytic interleukin-3 programs microglia and limits Alzheimer's disease. *Nature* 595, 701–706. doi: 10.1038/s41586-021-03734-6

Mei, B., Li, J., and Zuo, Z. (2021). Dexmedetomidine attenuates sepsis-associated inflammation and encephalopathy via central α2A adrenoceptor. *Brain Behav. Immun.* 91, 296–314. doi: 10.1016/j.bbi.2020.10.008

Milner, M. T., Maddugoda, M., Götz, J., Burgener, S. S., and Schroder, K. (2021). The NLRP3 inflammasome triggers sterile neuroinflammation and Alzheimer's disease. *Curr. Opin. Immunol.* 68, 116–124. doi: 10.1016/j.coi.2020.10.011

Oakley, H., Cole, S. L., Logan, S., Maus, E., Shao, P., Craft, J., et al. (2006). Intraneuronal β-amyloid aggregates, neurodegeneration and neuron loss in transgenic mice with five familial Alzheimer's disease mutations: potential factors in amyloid plaque formation. *J. Neurosci.* 26, 10129–10140. doi: 10.1523/JNEUROSCI.1202-06.2006

Parhizkar, S., and Holtzman, D. M. (2022). APOE mediated neuroinflammation and neurodegeneration in Alzheimer's disease. *Semin. Immunol.* 26:101594. doi: 10.1016/j.smim.2022.101594

Pascoal, T. A., Benedet, A. L., Ashton, N. J., Kang, M. S., Therriault, J., Chamoun, M., et al. (2021). Microglial activation and tau propagate jointly across braak stages. *Nat. Med.* 27, 1592–1599. doi: 10.1038/s41591-021-01456-w

Pereira, J. B., Janelidze, S., Ossenkoppele, R., Kvartsberg, H., Brinkmalm, A., Mattsson-Carlgren, N., et al. (2021). Untangling the association of amyloid-β and tau with synaptic and axonal loss in Alzheimer's disease. *Brain* 144, 310–324. doi: 10.1093/brain/awaa395

Quatrini, L., Vivier, E., and Ugolini, S. (2018). Neuroendocrine regulation of innate lymphoid cells. *Immunol. Rev.* 286, 120–136. doi: 10.1111/imr.12707

Rajesh, Y., and Kanneganti, T. D. (2022). Innate immune cell death in neuroinflammation and Alzheimer's disease. *Cells* 11:e121885. doi: 10.3390/cells11121885

Richard, B. C., Kurdakova, A., Baches, S., Bayer, T. A., Weggen, S., Wirths, O., et al. (2015). Gene dosage dependent aggravation of the neurological phenotype in the 5XFAD mouse model of Alzheimer's disease. *J. Alzheimers Dis.* 45, 1223–1236. doi: 10.3233/JAD-143120

Schwartz, M., and Deczkowska, A. (2016). Neurological disease as a failure of brain-immune crosstalk: the multiple faces of neuroinflammation. *Trends Immunol.* 37, 668–679. doi: 10.1016/j.it.2016.08.001

Sun, W., Zhao, J., and Li, C. (2020). Dexmedetomidine provides protection against hippocampal neuron apoptosis and cognitive impairment in mice with Alzheimer's disease by mediating the miR-129/YAP1/JAG1 axis. *Mol. Neurobiol.* 57, 5044–5055. doi: 10.1007/s12035-020-02069-z

Sung, P. S., Lin, P. Y., Liu, C. H., Su, H. C., and Tsai, K. J. (2020). Neuroinflammation and neurogenesis in Alzheimer's disease and potential therapeutic approaches. *Int. J. Mol. Sci.* 21:701. doi: 10.3390/ijms21030701

Thies, W., and Bleiler, L. (2012). Alzheimer's disease facts and figures. *Alzheimers Dement.* 8, 131–168. doi: 10.1016/j.jalz.2012.02.001

Wang, K., Wu, M., Xu, J., Wu, C., Zhang, B., Wang, G., et al. (2019). Effects of dexmedetomidine on perioperative stress, inflammation and immune function: systematic review and meta-analysis. *Br. J. Anaesth.* 123, 777–794. doi: 10.1016/j.bja.2019.07.027

Weng, S., Lai, Q. L., Wang, J., Zhuang, L., Cheng, L., Mo, Y., et al. (2022). The role of exosomes as mediators of neuroinflammation in the pathogenesis and treatment of Alzheimer's disease. *Front. Aging Neurosci.* 14:899944. doi: 10.3389/fnagi.2022.899944

Yamashima, T., Tonchev, A. B., Vachkov, I. H., Popivanova, B. K., Seki, T., Sawamoto, K., et al. (2004). Vascular adventitia generates neuronal progenitors in the monkey hippocampus after ischemia. *Hippocampus* 14, 861–875. doi: 10.1002/hipo.20001

Zhang, F., Zhong, R. J., Cheng, C., Li, S., and Le, W. D. (2021). New therapeutics beyond amyloid-β and tau for the treatment of Alzheimer's disease. *Acta Pharmacol. Sin.* 42, 1382–1389. doi: 10.1038/s41401-020-00565-5

Zhang, Y., Lin, Y., Liu, Q., Yuan, X., Mao, A., Liu, Y., et al. (2018). The effect of dexmedetomidine on cognitive function and protein expression of Aβ, p-Tau and PSD95 after extracorporeal circulation operation in aged rats. *Biomed. Res. Int.* 2018:4014021. doi: 10.1155/2018/4014021

Zhang, Y., Tan, S. L., Du, J., Chen, Y., Jia, J., Feng, J. G., et al. (2021). Dexmedetomidine alleviates neuroinflammation, restores sleep disorders and neurobehavioral abnormalities in rats with minimal hepatic encephalopathy. *Int. Immunopharmacol.* 96:107795. doi: 10.1016/j.intimp.2021.107795

frontiers | Frontiers in Aging Neuroscience

TYPE Original Research
PUBLISHED 26 September 2022
DOI 10.3389/fnagi.2022.982154

OPEN ACCESS

EDITED BY
Yingwei Wang,
Fudan University, China

REVIEWED BY
Yunfei Hou,
Peking University People's Hospital, China
Nan Lin,
Capital Medical University, China

*CORRESPONDENCE
Huihui Miao
miaohuihui@bjsjth.cn
Tianzuo Li
litz@bjsjth.cn

SPECIALTY SECTION
This article was submitted to Neurocognitive Aging and Behavior, a section of the journal Frontiers in Aging Neuroscience

RECEIVED 30 June 2022
ACCEPTED 08 September 2022
PUBLISHED 26 September 2022

CITATION
Lin X, Cao Y, Liu X, Yu K, Miao H and Li T (2022) The hotspots and publication trends in postoperative delirium: A bibliometric analysis from 2000 to 2020.
Front. Aging Neurosci. 14:982154.
doi: 10.3389/fnagi.2022.982154

The hotspots and publication trends in postoperative delirium: A bibliometric analysis from 2000 to 2020

Xiaowan Lin, Ying Cao, Xiao Liu, Kang Yu, Huihui Miao* and Tianzuo Li*

Department of Anesthesiology, Beijing Shijitan Hospital, Capital Medical University, Beijing, China

Background: Postoperative delirium (POD) is a common aging-associated postoperative complication that has received increasing attention in the context of the aging global population and the number of articles published on POD is gradually increasing. This study aimed to quantify the basic information of scholarly publications on POD and identify the most impactful literature, trends, and hotspots in POD research.

Materials and methods: We searched articles on POD through the Science Citation Index Expanded databases published from 2000 to 2020. Bibliographic information, including year, country, authorship, type, journal, funding, affiliations, subject areas, and hotspots, was collected for further analysis.

Results: A total of 2,114 articles on POD from 2000 to 2020 were identified. The highest number of studies (n = 748) were published in the United States, comprising the most total citations (13,928), followed by China (n = 278), and Germany (n = 209). Inouye, Sharon K. was the most productive author, with 66 publications on POD. The *Journal of the American Geriatrics Society* published the highest number of articles (n = 80), with the most total citations (4,561) and average (57.01), followed by *Anesthesia and Analgesia* (n = 52), and the *British Journal of Anaesthesia* (n = 43). Harvard University was the most productive institute, with the highest H-index (n = 46) and highest degree centrality (n = 191). The top hotspots in the field of POD during this period were "elderly," "cardiac surgery," "cognitive impairment," "hip fracture," and "intensive care unit."

Conclusion: This study provides an overview of developments in the field of POD over the past 20 years using bibliometric analysis. Overall, research on POD has flourished worldwide. The United States (US) has a relatively high academic impact owing to its productive expertise and institutions in this field. Despite much research illustrating the diagnosis and management of POD in clinical practice, more basic research is needed.

KEYWORDS

POD, elderly, bibliometric, hotspots, publication trends

Introduction

Postoperative delirium (POD) is a common complication that is characterized by acute and fluctuating changes in mental status, attention, and level of consciousness after surgeries and anesthesia (Aldecoa et al., 2017). According to the recommendations for the nomenclature of cognitive change associated with anesthesia and surgery in 2018, by the nomenclature consensus working group, POD was included in perioperative neurocognitive disorder (PND); however, should be recognized as a specific category that is consistent with the diagnostic criteria (Diagnostic and Statistical Manual for Mental Disorders, fifth edition, DSM-5) (Evered et al., 2018). Before the nomenclature, POD was always studied as an independent concept since the acute clinical symptoms were different from those of postoperative cognitive dysfunction (POCD). The incidence of POD ranges from 5 to 50% and can occur at any age; however, mostly in the elderly (American Geriatrics Society Expert Panel on Postoperative Delirium in Older Adults, 2015). It has been demonstrated that POD was associated with adverse outcomes, such as increased mortality, prolonged hospitalization, increased incidence of POCD, and higher medical cost (Bai et al., 2020; Hughes et al., 2020). Numerous studies have aimed to identify the risk factors for POD, including advanced age, multiple comorbidities, preoperative cognitive impairment, poor vision or hearing, and presence of infection (American Geriatrics Society Expert Panel on Postoperative Delirium in Older Adults, 2015; Raats et al., 2015; Yang et al., 2017). However, the pathogenesis of POD has not been fully elucidated, and the research for more effective treatments is ongoing. Meanwhile, with the trend of global aging, POD, being an aging-associated disease, has attracted increasing attention from researchers. Therefore, we analyzed publications and hotspots in the field of POD in this study.

Bibliometric analysis is a method of analyzing books, articles, and other documents using mathematical and statistical techniques (Roldan-Valadez et al., 2019), allowing researchers to gain a general understanding of the frontier area and hotspots in a certain field. Bibliometric analysis also provides a reference for accurately reading the literature and for selecting research directions. It has been widely applied in many fields (Hong et al., 2019; Mi et al., 2021), including hotspots in POCD and the hundred most cited articles in PND (Chen et al., 2020; Mi et al., 2021); however, few bibliometric studies have been performed on POD. This study aimed to quantify the basic information of scholarly publications and identify the most impactful literature, trends, and hotspots, thereby providing a comprehensive overview of the current status of POD research.

Materials and methods

Search strategy

An online literature search was performed on May 19, 2021, using the Science Citation Index Expanded databases. Articles and reviews published between 2000 and 2020 were included in this analysis. The requirement for written informed consent was waived by the Institutional Review Board. This manuscript reports results of an observational bibliometric study, and therefore follows the applicable Enhancing the QUAlity and Transparency Of health Research EQUATOR guidelines (PRISMA and STROBE). The terms used in the search were SU = (POD) and Language = English. **Figure 1** showed the detail of the search flow. A total of 2,551 records were found, excluded publications were meeting abstract (n = 162), editorial material (n = 138), letter (n = 119), proceedings paper (n = 47), correction (n = 9), news item (n = 4), retracted publication (n = 1), early access (n = 1), and publication with expression of concern (n = 1). Then, duplicates removal (n = 0) was performed. Finally, The retained publications (n = 2114) with 1,702 articles and 412 reviews were employed for bibliometric analysis. The following information was collected: year, country, authorship, type, journal, funding, affiliations, subject areas, and

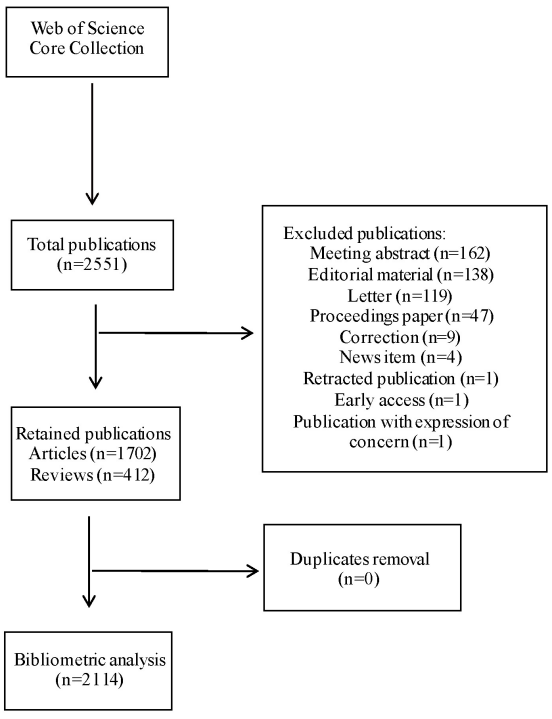

FIGURE 1
Flowchart for the publication selection included in this study.

hotspots. Figure 1 shows the search flow for this bibliometric-analysis.

Statistical analysis

The CiteSpace software was used for bibliometric analysis (co-citation, co−occurrence, hotspots, and cluster analysis). Statistical analyses were performed using SPSS version 23 (IBM SPSS, Inc., Chicago, IL, USA). Data were expressed as numbers or percentages. Correlation analysis was performed using a two-tailed Pearson's correlation. Statistical significance was set at $P < 0.05$.

Results

Analysis of years and countries

A total of 2,114 articles were employed in our search strategy. The United States (US) was top-ranked with the highest number of publications on POD (n = 748), followed by China (n = 278), Germany (n = 209), and Canada (n = 148). The US also had the highest total citations (13,928), followed by Germany (3,660), England (3,616), Canada (3,591), and the Netherlands (3,546). Inconsistent with the number of articles, Denmark had the highest mean number of citations per paper (32.38), followed by Belgium (31.96), Netherlands (29.07), Sweden (29.00), and Ireland (27.42; Table 1).

TABLE 1 The top 20 countries with the highest number of publications on postoperative delirium (POD).

Rank	Country	Number of papers	Total citations	Mean citations/ Paper
1	USA	748	13,928	18.62
2	China	278	2,563	9.22
3	Germany	209	3,660	17.51
4	Canada	148	3,591	24.26
5	Japan	141	1,635	11.60
6	England	137	3,616	26.39
7	Netherlands	122	3,546	29.07
8	Australia	91	1,718	18.88
9	South Korea	78	739	9.47
10	Italy	79	1,523	19.28
11	Switzerland	51	1,372	26.90
12	Sweden	43	1,247	29.00
13	Denmark	42	1,360	32.38
14	Poland	36	529	14.69
15	France	34	497	14.62
16	Spain	33	664	20.12
17	Belgium	26	831	31.96
18	Ireland	26	713	27.42
19	Turkey	26	357	13.73
20	Norway	24	494	20.58

The total number of articles from the top 10 countries increased annually from 2000 to 2020, and the growth rate increased year by year, with a substantial increase of approximately 70 articles in 2017. Additionally, the number of articles from China and Germany exhibited remarkable growth compared with those from other countries (Figure 2A). Figure 2B shows the network visualization map for a total of 64 countries/regions collaborations, where the size of the circle represents the number of publications and the thickness of the connecting lines indicates the extent of collaboration between the countries/regions. The top collaborative countries/regions in the field of POD can be observed visually. The US was located at the core of the network and cooperated frequently with China, Germany, Canada, England, Japan, and other countries.

Analysis of authors and institutions

The top 20 authors with the highest number of publications on POD from 2000 to 2020 are listed in Table 2. Among them, Inouye, Sharon K. was listed on top with the largest number of studies (n = 66) and the highest H-index (34) and proved to be the most influential professor in the field of POD. Marcantonio Edward was second, with 63 articles, followed by Jones Richard (n = 36), Fong Tamara (n = 23), and Xie, Zhongcong (n = 22). Interestingly, the top five ranked authors aforementioned and eight authors out of the top 20 shared the same affiliation, Harvard University; thus, it was likely the most influential institution in terms of research on POD.

Harvard University appeared to be the most influential institution in the field of POD, which was further proven by its having the largest number of studies (n = 171), highest H-index (n = 46), and highest degree centrality (n = 191) among the top 20 most productive institutions (Table 3). Second, the University of California System, whose number of studies (n = 77) was less than half that of Harvard University, followed by Johns Hopkins University (n = 76). Overall, most institutions were based in the US (n = 12), while the rest were based in Netherlands (n = 2), China (n = 2), Canada (n = 2), England (n = 1), and Germany (n = 1).

Visually, the publication profile of the institutions is illustrated in Figure 3A. The number of studies from Harvard University clearly stands out among institutions making variation between other institutions looks like very small whose number of studies ranged from 20 to 77. Unlike the number of studies, the University of Pennsylvania ranked the highest in terms of the average number of citations (n = 94.97), followed by the University of Manitoba (n = 51.55), which

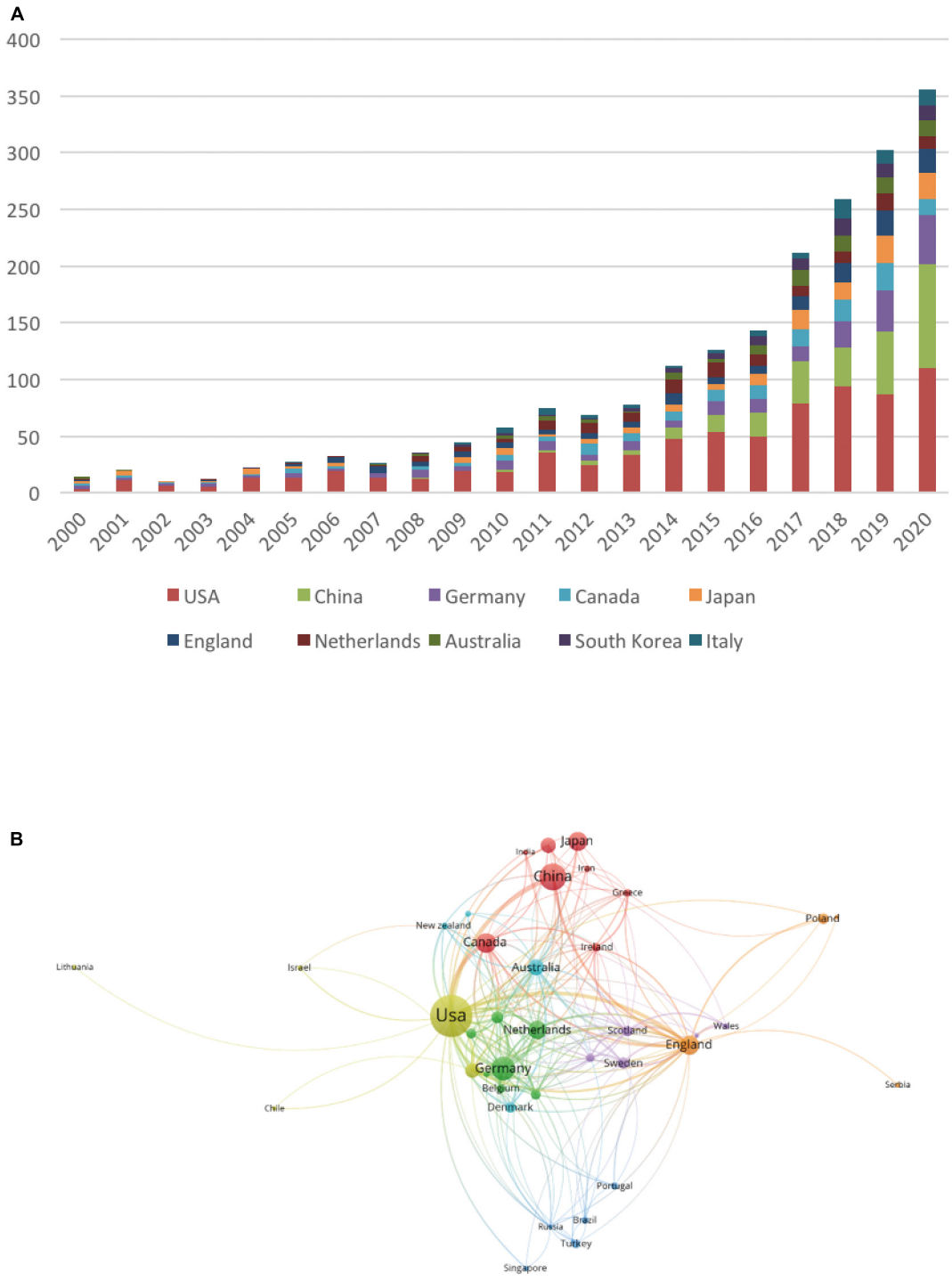

FIGURE 2
The effect of changes in years and countries on the number of postoperative delirium (POD) articles. **(A)** The number of POD articles from the top 10 countries per year. **(B)** The network visualization map indicating collaborations between countries.

ranked 10 and 18 out of 20, respectively. Next, we explored the cooperative relationships between institutions. As illustrated in Figure 3B, institutions worked closely with each other and were divided into several clusters according to their cooperation; however, no obvious boundaries were identifiable between these clusters, suggesting extensive collaboration worldwide. Moreover, Harvard University occupies the most important position in collaborative network.

TABLE 2 The top 20 authors with the highest number of publications on postoperative delirium (POD).

Name	Affiliations	Number of papers	H-index
Inouye, Sharon K.	Harvard University	66	34
Marcantonio, Edward R.	Harvard University	63	29
Jones, Richard N.	Harvard University	36	21
Fong, Tamara G.	Harvard University	23	16
Xie, Zhongcong	Harvard University	22	12
Neufeld, Karin J.	Johns Hopkins University	20	14
Leung, Jacqueline M.	University of California San Francisco	19	15
Avidan, Michael S.	Washington University	18	11
Ely, E. Wesley	Vanderbilt University	17	17
Schmitt, Eva M.	Harvard University	17	13
Brown, Charles H.	Johns Hopkins University	17	12
Sieber, Frederick E.	Johns Hopkins University	16	10
Alsop, David C.	Harvard University	15	11
Travison, Thomas G.	Harvard University	15	10
Spies, Claudia D.	Charite Medical University of Berlin	15	6
MacLullich, Alasdair M. J.	University of Edinburgh	14	9
Wang, Dong-Xin	Peking University	14	9
de Rooij, Sophia E.	University of Groningen	14	9
Pandharipande, Pratik P.	Vanderbilt University	13	10
Bellelli, Giuseppe	University of Milano-Bicocca	13	10

Analysis of journals

By analyzing the distribution of journals in the field of POD, we discovered that the *Journal of the American Geriatrics Society* published more articles (n = 80) than any other journal from 2000 to 2020, which were the most frequently cited, with 4,561 total citations and the highest average of 57.01; however, it only ranked sixth in terms of impact factor (IF) among the top 20 most productive journals (Table 4). Further, *Anesthesia and Analgesia* and the *British Journal of Anaesthesia* ranked second and third, with 52 and 43 publications, respectively, and their total and average citations were high among the top 20 journals. The top three journals belonged to Q1, a classification by Journal Citation Reports (JCR), representing their high status in their respective domains. Q1 journals had a higher rate of citations, such as the *International Journal of Geriatric Psychiatry* (average citation 28.09), *Anesthesiology* (average citation 37.94), the *American Journal of Geriatric Psychiatry* (average citation 41.93), and *Critical Care Medicine* (average citation 55.74).

The number of studies published in the top 10 journals exhibited an overall growing trend, particularly in 2011, 2014, and 2017 (Figure 4). Notably, there was a visible increase in the number of papers published in *Anesthesia and Analgesia* in 2020.

Analysis of funding agency and subject areas

Studies were supported by various funding agencies, which significantly motivated the development of POD research. The top 10 funding bodies are listed in Table 5, with the first three being the US Department of Health Human Services, National Institutes of Health (NIH), and NIH National Institute on Aging. The top three funding agencies funded 73.7% of the publications, and the number of funded papers exceeded 200. Among the remaining seven funding agencies, the National Natural Science Foundation of China listed the fourth with 67 founded articles. Overall, among these agencies, six were based in the US, two in Japan, one in China, and one in Europe.

As aforementioned, POD is a complication associated with surgeries and anesthesia with a high incidence in the elderly, representing altered mental status; hence, the subject areas in the POD research field include *anesthesiology* (n = 471, 14%), *geriatrics and gerontology* (n = 431, 13%), *surgery* (n = 322, 10%), and *psychiatry* (n = 265, 8%), contributing to nearly half (45%) of the total articles (Figure 5). POD is highly prevalent after cardiac surgery and requires multidisciplinary management; therefore, other relevant subjects include *clinical neurology, critical care medicine, cardiac and cardiovascular systems, neuroscience, and nursing.*

Analysis of the most frequently cited articles

The top 20 cited articles on POD are listed in Table 6, with citation counts ranging from 256 to 1,531. The classification of these publications is shown in Figure 6A. Of these, 12 articles were original research, all of which were clinical trials (n = 12, 60%), primarily cohort studies (n = 7, 35%), and randomized controlled trials (n = 5, 25%), and the remaining eight were reviews (systematic or literature reviews were defined as reviews) (n = 8, 40%), and the most cited article was written by *Ely, EW* et al., published by *JAMA-Journal of the American Medical Association* in 2001, and titled "Delirium in mechanically ventilated patients - Validity and reliability of the Confusion Assessment Method for the intensive care unit (CAM-ICU)." This prospective cohort study tested the validity and reliability of the CAM-ICU, which turned out to be "rapid, valid, and reliable for diagnosing delirium in the ICU setting (Ely et al., 2001b)." Another article published by the same author was ranked fourth (cited 606 times) out of the top 20. The second and third -most cited papers (cited 1,215 and 851 times) were published by the same author, Inouye et al. (2014b), both were reviews, entitled "Delirium in elderly people" and "Geriatric syndromes: Clinical, research, and policy implications of a core geriatric concept (Inouye et al., 2007)." Additionally, another article by *Inouye, Sharon K.* was included

in the top 20. From the perspective of publication years, there were more articles published in the preceding decade, from 2000 to 2010 (n = 13). We then analyzed the association between the number of citations and the year of publication. However, the number of citations did not correlate with the year of publication (R^2 = 0.0457, p = 0.366; Figure 6B). Additionally, not all articles were published in journals with high IFs, and most were from the US.

Analysis of keywords and hotspots

Hotspots in the field of POD can be inferred by keyword co-occurrence analysis, which refers to the frequency of two keywords appearing together in the same article. Likewise, the size of the circles and the thickness of the line represent the frequency of occurrence and co-occurrence of keywords. As shown in Figure 7, "elderly" was the most frequently encountered keyword, indicating that studies of POD focus on the elderly, which is consistent with the high incidence of POD in the elderly. Second, the most frequent keywords co-occurring with "elderly" were "cardiac surgery," "cognitive impairment," "hip fracture," and "intensive care unit." Some sub-clusters were distinguished by different colors, which can be roughly divided into five groups: "anesthesia-related," "drug-related," "inflammation-related," "prognosis-related," and "cardiovascular surgery-related." More specific research points are shown in Figure 7.

Discussion

Delirium is an acute altered mental status, also be thought of as "acute brain failure," with high incidence rates observed in the intensive care unit (Inouye et al., 2014b; Mattison, 2020). POD specifically refers to delirium that occurs during the postoperative period and is associated with poor clinical outcomes (Schenning and Deiner, 2015). Many studies have indicated that increasing age (>65 years) is a significant risk factor for POD (Steiner, 2011; Berger et al., 2018; Zhu et al., 2020), making POD a major concern in the context of global population aging, and an increasing number of articles about POD have been published. Here, we provide an overview of the developments in the field of POD over the past 20 years by applying bibliometric analysis, and 2,114 papers were identified and recruited from the Science Citation Index Expanded databases.

Overall, the number of papers on POD from various countries increased yearly, and frequent collaboration between countries suggested POD as a global issue. Among the countries, the US contributed the most due to having the most productive experts and institutions in the field of POD. And the core position of the US is mainly supported by several experts including Inouye, Sharon K., Marcantonio, Edward R., Jones, Richard N., Fong, Tamara G., and Xie, Zhongcong. Of these, Inouye appeared to be the most influential person with the highest number of publications and H-index. The first relevant study on delirium by Inouye et al. (1990)

TABLE 3 The top 20 institutes with the highest number of publications in postoperative delirium (POD).

Rank	Affiliations	Number of papers	Total citations	Mean citations/Paper	H-index	Degree centrality
1	Harvard Univ	171	6,042	35.33	46	191
2	UNIV of California System	77	2,341	30.40	27	50
3	Johns Hopkins Univ	76	2,223	29.25	32	91
4	Vanderbilt Univ	54	998	18.48	25	44
5	Duke Univ	54	1,167	21.61	19	80
6	Charite Univ Med Berlin	49	618	12.61	17	13
7	Univ Toronto	42	1,166	27.76	20	14
8	Yale Univ	39	988	25.33	20	32
9	Brown Univ	37	868	23.46	18	52
10	Univ Penn	34	3,229	94.97	16	63
11	Washington Univ	30	1,460	48.67	12	33
12	Univ Med Ctr Utrecht	29	611	21.07	18	8
13	Univ Amsterdam	28	1,278	45.64	18	8
14	Peking Univ	25	1,092	43.68	10	7
15	Purdue Univ	24	670	27.92	19	21
16	Univ Edinburgh	23	223	9.70	14	10
17	Capital Med Univ	23	677	29.43	5	10
18	Univ Manitoba	22	1,134	51.55	13	18
19	Mayo Clin	21	574	27.33	13	38
20	Univ Groningen	20	344	17.20	11	5

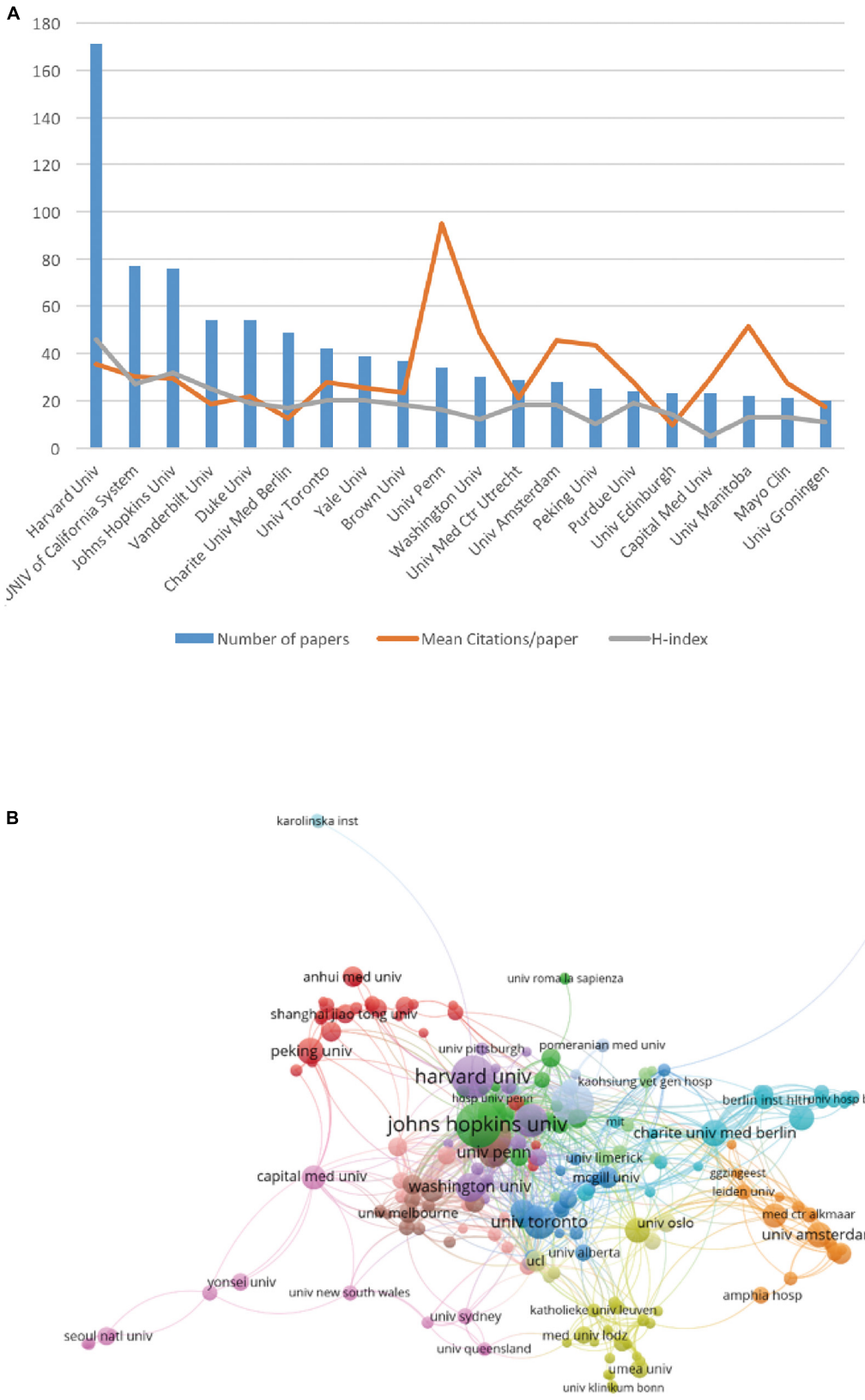

FIGURE 3
The articles on postoperative delirium (POD) published by different research institutions. **(A)** The top 20 most productive institutes. The blue bar graph represents the number of articles published by each institution, the red line represents the average number of citations per article, and the green line represents the H-index of each institution. **(B)** The network visualization map indicating collaborations between institutions.

10.3389/fnagi.2022.982154

TABLE 4 The top 20 journals with the highest number of publications on postoperative delirium (POD).

Rank	Journal	Number of papers	Total citations	Mean citations/ Paper	Impact factor (IF)	Journal Citation Reports (JCR)
1	Journal of the American Geriatrics Society	80	4,561	57.01	4.18	Q1
2	Anesthesia and Analgesia	52	1,807	34.75	4.305	Q1
3	British Journal of Anaesthesia	43	1,543	35.88	6.88	Q1
4	PLoS One	38	599	15.76	2.74	Q2
5	Journal of Cardiothoracic and Vascular Anesthesia	37	636	17.19	2.258	Q3
6	BMJ Open	36	433	12.03	2.496	Q2
7	International Journal of Geriatric Psychiatry	34	955	28.09	2.675	Q1
8	Anesthesiology	32	1,214	37.94	7.067	Q1
9	Current Opinion in Anesthesiology	32	337	10.53	2.276	Q3
10	American Journal of Geriatric Psychiatry	27	1,132	41.93	3.393	Q1
11	Journal of Clinical Anesthesia	25	194	7.76	6.039	Q1
12	Canadian Journal of Anesthesia-Journal Canadien D Anesthesie	24	373	15.54	3.779	Q2
13	Psychosomatics	23	727	31.61	2	Q2
14	Clinical Interventions in Aging	23	563	24.48	3.023	Q2
15	BMC Anesthesiology	23	159	6.91	1.695	Q4
16	General Hospital Psychiatry	22	769	34.95	2.86	Q2
17	Aging Clinical and Experimental Research	22	373	16.95	2.697	Q3
18	Medicine	22	64	2.91	1.552	Q3
19	Critical Care Medicine	19	1,059	55.74	7.414	Q1
20	Minerva Anestesiologica	19	387	20.37	2.498	Q3
21	Trials	19	143	7.53	1.883	Q3

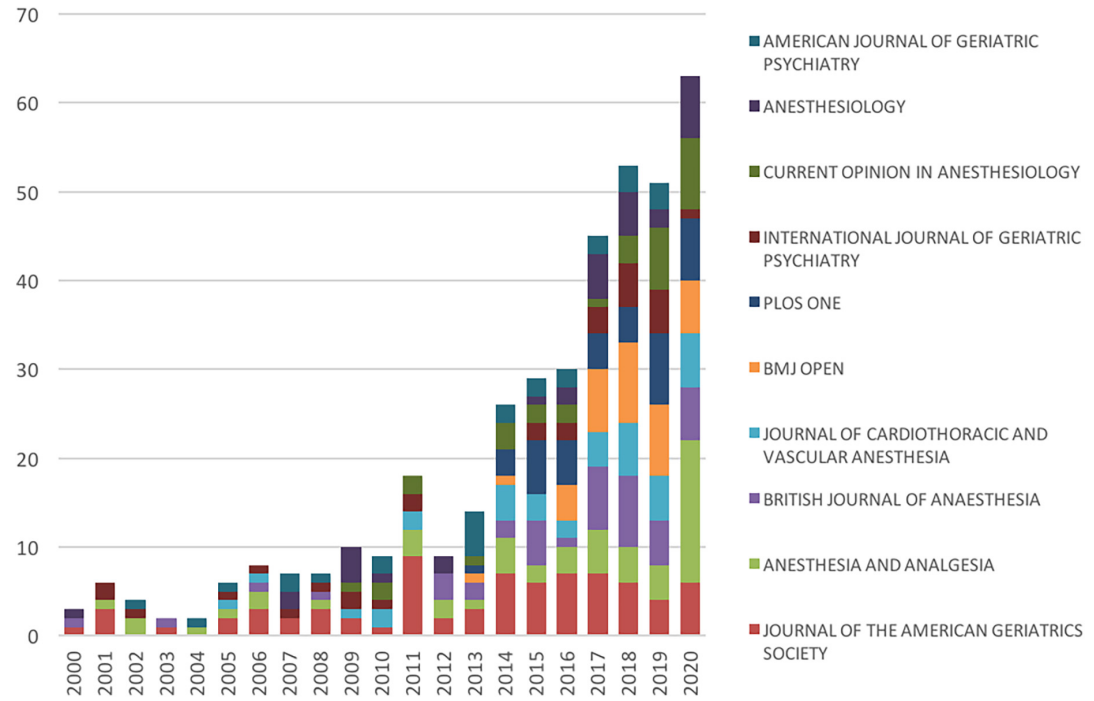

FIGURE 4
The number of articles on postoperative delirium (POD) published in the top 10 journals each year.

TABLE 5 The top 10 funding agencies with the highest number of publications on postoperative delirium (POD).

Rank	Funding agency	Number of papers
1	United States Department of Health Human Services	333
2	National Institutes of Health NIH USA	327
3	NIH National Institute on Aging NIA	237
4	National Natural Science Foundation of China NSFC	67
5	NIH National Heart Lung Blood Institute NHLBI	53
6	NIH National Center for Advancing Translational Sciences NCATS	49
7	European Commission	42
8	Ministry of Education Culture Sports Science and Technology Japan MEXT	38
9	NIH National Institute of General Medical Sciences NIGMS	38
10	Japan Society for the Promotion of Science	32

was published in 1990, after which he and his colleagues published many high-quality papers related to delirium or POD (Vasunilashorn et al., 2018) and developed a new delirium severity assessment, the Confusion Assessment Method-Severity (CAM-S) (Inouye et al., 2014a), which is widely used in clinical practice.

In terms of journals, the *Journal of the American Geriatrics Society* possessed both high quantity and quality of articles and is considered the most influential journal in the POD area indicating a good choice to publish researchers' POD-related work or follow the frontier. While hotspot analysis results roughly reflect the different research branches at present, like elderly age, different anesthetics (sevoflurane, propofol, and dexmedetomidine) and different types of surgeries (cardiac surgery, non-cardiac surgery, hip fracture surgery, total knee arthroplasty, spine surgery, and vascular surgery). And inflammation, cytokines, and C-reactive protein, which are related to the biomarkers or mechanisms of POD, need to be explored in the future.

Assessment tools

The top one and six highest-cited article were about the assessment tool for POD. CAM is the classical and the

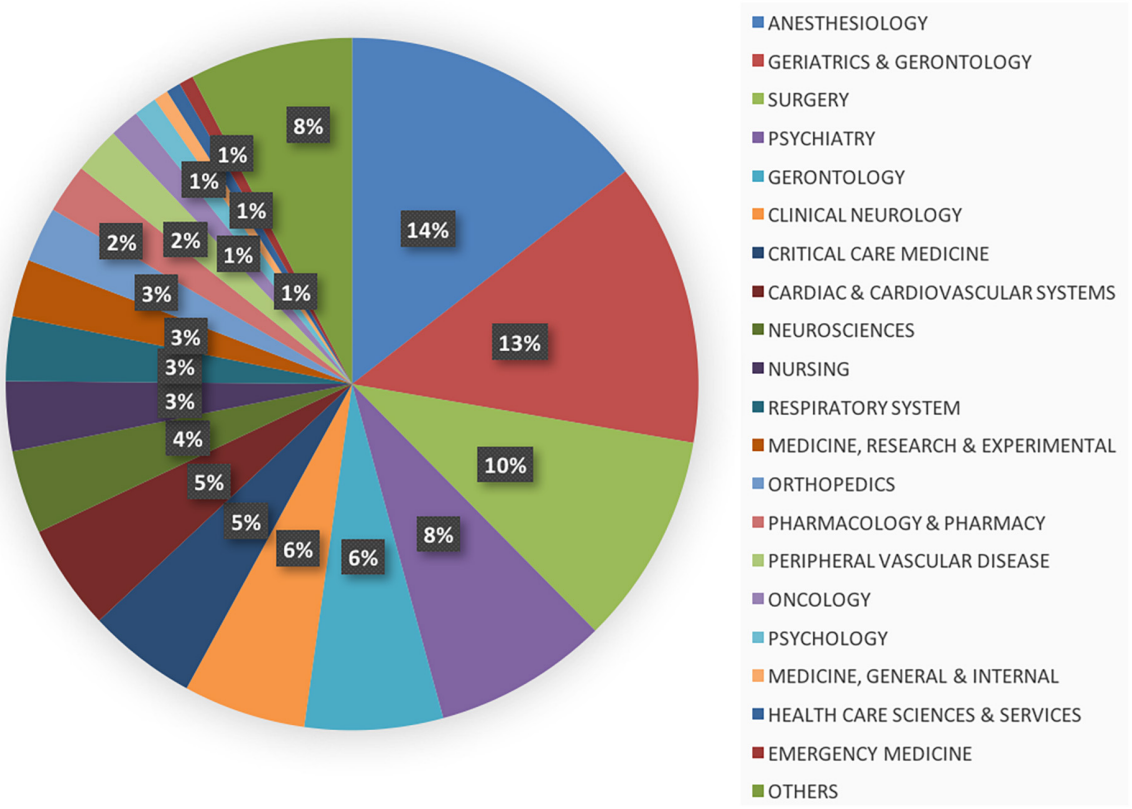

FIGURE 5
The distribution of top 20 subjects associated with the field of postoperative delirium (POD).

TABLE 6 The top 20 highest-cited articles on postoperative delirium (POD).

Rank	Title	Corresponding author	Affiliation	Source title	Year of publication	Cited by
1	Delirium in mechanically ventilated patients - validity and reliability of the confusion assessment method for the intensive care unit (CAM-ICU)	Ely, EW	Vanderbilt Univ	Jama-Journal of the American Medical Association	2001	1531
2	Delirium in elderly people	Inouye, Sharon K.	Univ Harvard Hebrew SeniorLife	Lancet	2014	1215
3	Geriatric syndromes: Clinical, research, and policy implications of a core geriatric concept	Inouye, Sharon K.;	Univ Harvard Hebrew SeniorLife	Journal of the American Geriatrics Society	2007	851
4	The impact of delirium in the intensive care unit on hospital length of stay	Ely, EW;	Vanderbilt Univ	Intensive Care Medicine	2001	606
5	Cognitive trajectories after postoperative delirium	Saczynski, Jane S.	Univ Massachusetts	New England Journal of Medicine	2012	542
6	The confusion assessment method: A systematic review of current usage	Inouye, Sharon K.	Univ Harvard Hebrew SeniorLife	Journal of the American Geriatrics Society	2008	406
7	Delirium in elderly adults: diagnosis, prevention and treatment	Fong, Tamara G.	Univ Harvard Hebrew SeniorLife	Nature Reviews Neurology	2009	396
8	Relationship between pain and opioid analgesics on the development of delirium following hip fracture	Morrison, RS	Mt Sinai Sch Med	Journals of Gerontology Series A-Biological Sciences and Medical Sciences	2003	394
9	A multicenter trial of remote ischemic preconditioning for heart surgery	Meybohm, P.	Univ Hosp Frankfurt	New England Journal of Medicine	2015	379
10	Haloperidol prophylaxis for elderly hip-surgery patients at risk for delirium: A randomized placebo-controlled study	Kalisvaart, KJ	Med Ctr Alkmaar	Journal of the American Geriatrics Society	2005	375
11	BIS-guided Anesthesia decreases postoperative delirium and cognitive decline	Chan, Matthew T. V.;	Chinese Univ Hong Kong	Journal of Neurosurgical Anesthesiology	2013	322
12	Postoperative delirium in the elderly risk factors and Outcomes	Robinson, Thomas N.	Univ of Colorado Denver Sch Med	Annals of Surgery	2009	320
13	European society of Anaesthesiology evidence-based and consensus-based guideline on postoperative delirium	Spies, Claudia D.	Charite Univ Med Berlin	European Journal of Anaesthesiology	2017	277
14	Use of medications with anticholinergic effect predicts clinical severity of delirium symptoms in older medical inpatients	Han, L	St Marys Hosp Ctr	Archives of Internal Medicine	2001	274
15	Derivation and validation of a preoperative prediction rule for delirium after cardiac surgery	Rudolph, James L.	VA Boston Healthcare Syst	Circulation	2009	272
16	Dexmedetomidine for prevention of delirium in elderly patients after non-cardiac surgery: a randomised, double-blind, placebo-controlled trial	Wang, Dong-Xin	Peking Univ, Hosp	Lancet	2016	270
17	The cognitive impact of anticholinergics: A clinical review	Boustani, Malaz;	Regenstrief Inst Inc.	Clinical Interventions in Aging	2009	268
18	The association between delirium and cognitive decline: A review of the empirical literature	Jackson, JC	Vanderbilt Univ	Neuropsychology Review	2004	260
19	Monitoring depth of anaesthesia in a randomized trial decreases the rate of postoperative delirium but not postoperative cognitive dysfunction	Spies, C. D.	Charite	British Journal of Anaesthesia	2013	257
20	Preoperative risk assessment for delirium after non-cardiac surgery: A systematic review	Dasgupta, Mondipa	St Joseph's Htlh Care	Journal of the American Geriatrics Society	2006	256

most widely used assessment tool for identification of POD, originally established in 1990 by Inouye et al. (1990). Also, there are other tools, such as the four "A"s Test (Shenkin et al., 2019), CAM-ICU13, EECHAM confusion scale (Van Rompaey et al., 2007), and intensive care delirium screening checklist (ICDSC) (Gusmao-Flores et al., 2012). Wilson et al. (2020) have summarized several common delirium screening tools which can provide reference for future studies.

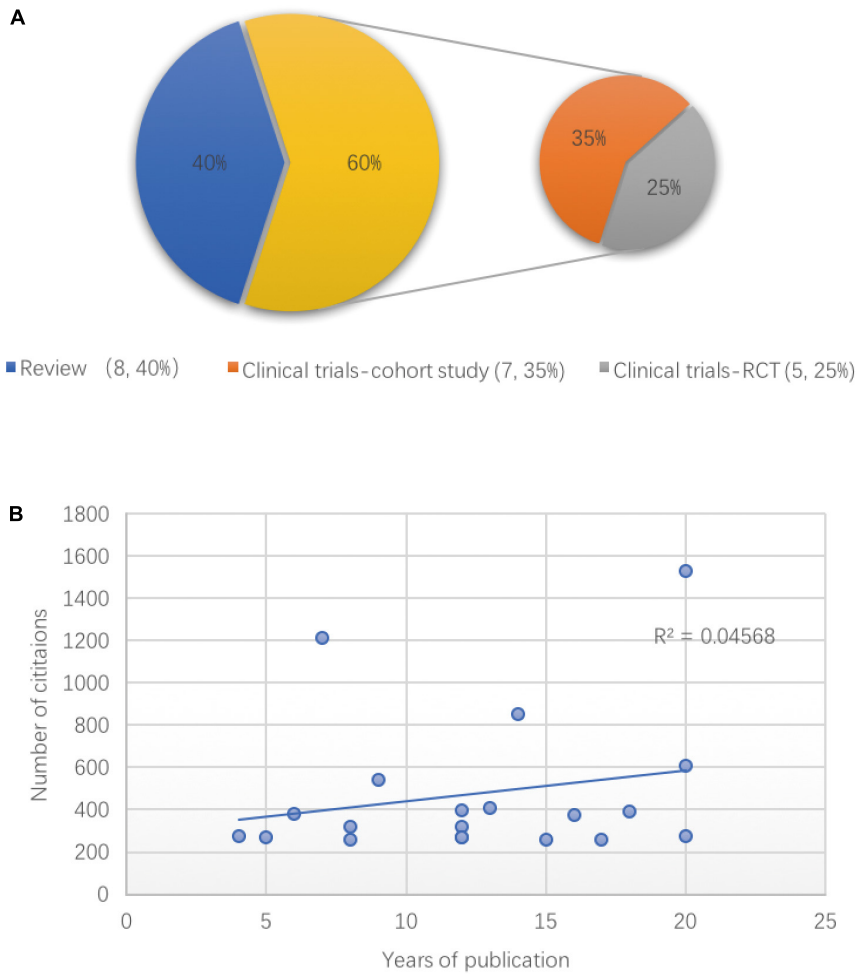

FIGURE 6
The classification and correlation analysis of the top 20 cited articles on postoperative delirium (POD). **(A)** The article types of the top 20 cited articles on POD, randomized controlled trial (RCT). **(B)** Linear correlation between the years of publication and numbers of citations among the top 20 POD articles.

Epidemiology and identification of risk factors

Now we are aware that POD is a common global disease and is prevalent worldwide. But the incidence of POD varies greatly across different studies. In a 1-day point-prevalence study undertaken in 104 ICUs, the prevalence of POD was 32.3% (Salluh et al., 2010). And the overall incidence of POD was 22.9% in the Perioperative Neurocognitive Disorder and Biomarker Lifestyle (PNDABLE) study, which also showed that the higher the vascular risk score, the higher the incidence of POD (Wang et al., 2022). Likewise, in a meta-analysis, the top 20 cited article, the incidence of POD in included twenty-five studies ranged from 5.1 to 52.2%, especially those who have received hip fracture or aortic surgeries tend to have a higher rate (Dasgupta and Dumbrell, 2006). Consistent with findings in analysis of keywords and hotspots, older age (Robinson et al., 2009), cardiac surgery (Rudolph et al., 2009), hip fracture (Kalisvaart et al., 2005), etc., appear to be risk factors for POD, and the incidence of POD in intensive care unit was as high as 81.3% (Ely et al., 2001a), besides POD was associated with prolonged cognitive impairment (Jackson et al., 2004; Saczynski et al., 2012). In addition to the above−mentioned risk factors, there were other potential variables associated with the development of POD, including hypoalbuminemia, pre-existing dementia (Robinson et al., 2009), undertreated pain (Morrison et al., 2003), comorbidities (Yang et al., 2017), and etc.

Prevention and therapy

Base on the identification of risk factors, targeted preventive measures can significantly reduce the incidence rate of

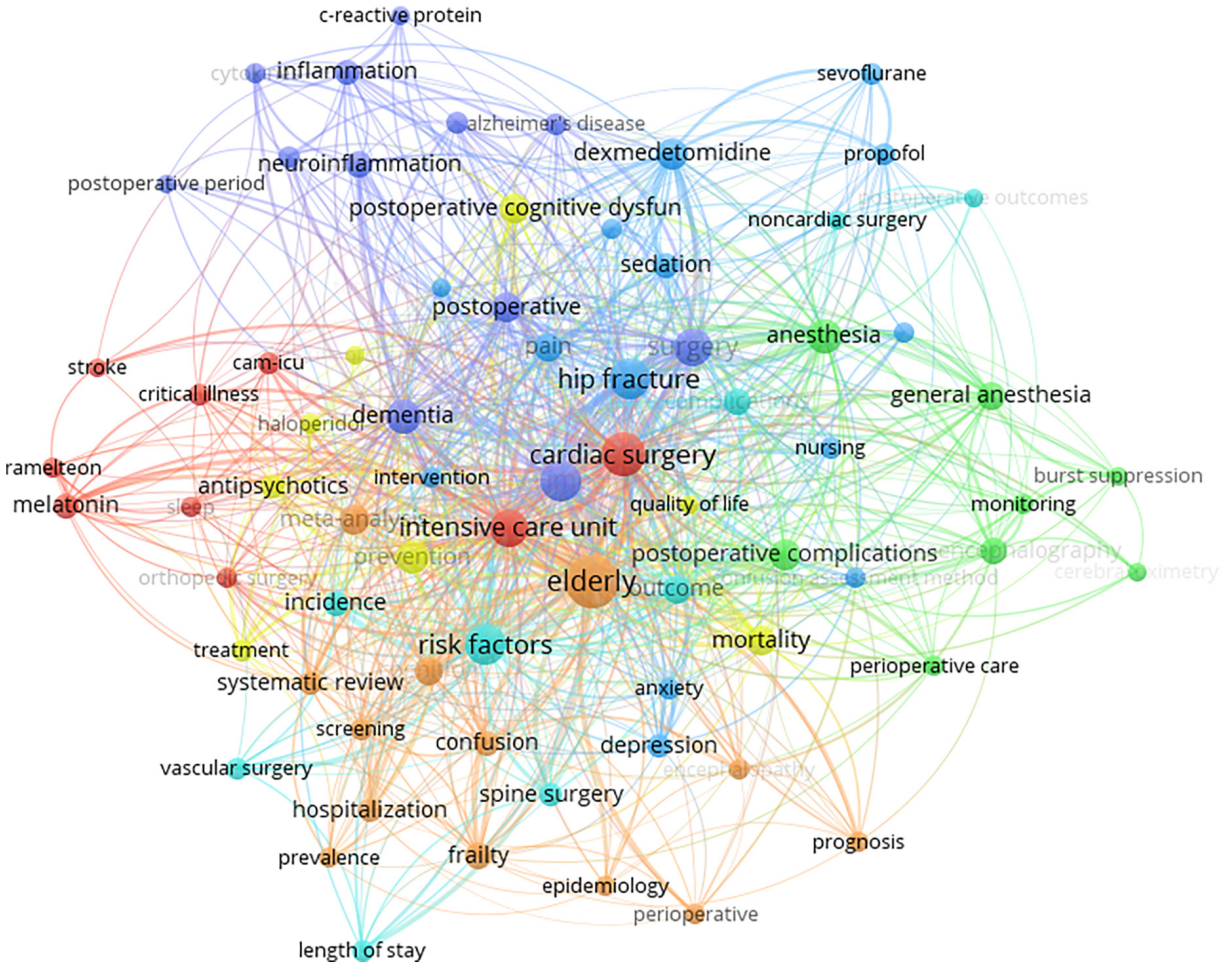

FIGURE 7
Map of hotspots and keyword co-occurrence analysis regarding postoperative delirium (POD).

POD. Several reviews (Fong et al., 2009; Janssen et al., 2019) have summarized some feasible interventions which can be broadly divided into preoperative (administration of melatonin, pre-operative multidisciplinary evaluation), intraoperative (infusion of dexmedetomidine, use of bispectral index (BIS)-guidance, varying tidal volumes during mechanical ventilation, choice of anesthetic regimen), postoperative (reducing postoperative pain, improving sleep, music therapy, orientation, oral and nutritional assistance,and early mobilization), or perioperative (multimodal intervention program), besides, there was no certain pharmacological therapy proved to be effective in improving POD except for Haloperidol. In short, identifying risk factors thereby adopt targeted measures for prevention was important for POD, and more effective medication should be explored in the future. We truly recommend the top 13 highest-cited article "European Society of Anaesthesiology evidence-based and consensus-based guideline on POD" (Aldecoa et al., 2017) published in 2017, which provides a comprehensive presentation of POD and practical recommendations in clinical practice.

Basic research of postoperative delirium

From the analysis of the most frequently cited articles, it can be seen that basic research of POD is relatively sparse, partly due to the lack of suitable animal models. Some performed orthopedic surgery using aged Alzheimer's disease transgenic mice to establish POD model (Wang et al., 2020), some performed abdominal surgery under isoflurane in old mice (Liufu et al., 2020). Basic research is undeniably important in obtaining a comprehensive understanding of the pathogenesis of POD, for example neuroinflammation (Velagapudi et al., 2019) and mitochondrial dysfunction (Lu et al., 2020) were reported to be involved in the development of POD, but the underlying mechanism of POD still remains to be elucidated.

Our study has some limitations. As aforementioned, POD is now included in PND; thus, our search strategy might not have been sufficiently comprehensive, and might have been insufficiently sensitive to find all relevant articles. Moreover, the earlier the articles published, the greater the number of citations. It is better to consider the time factor, although a correlation analysis between the years of publication of articles in the top 20 list and their number of citations suggested that the citation of articles was mainly dependent on the quality of the articles themselves, studies with larger sample sizes are needed to confirm this.

Finally, we conclude that research on POD is flourishing worldwide. The US has a relatively high academic impact because of its productive expertise and institutions in this field. Despite much research illustrating the diagnosis and management of POD in clinical practice, more basic research for the mechanism study of POD is needed.

Data availability statement

The original contributions presented in this study are included in the article/supplementary material, further inquiries can be directed to the corresponding authors.

Author contributions

XWL and YC helped perform the literature search and data acquisition. XWL and HM helped perform the manuscript preparation. XL and KY helped perform the data and statistical analysis. HM helped perform the secure funding. TL helped conceive and design the structure of this manuscript and revise the manuscript. All authors contributed to the article and approved the submitted version.

Funding

This study was funded by the Natural Science Foundation of Beijing (7212023), National Natural Science Foundation of China (82071180), and the Beijing Municipal Administration of Hospitals' Youth Programme (QML20200102) to HM.

Conflict of interest

The authors declare that the research was conducted in the absence of any commercial or financial relationships that could be construed as a potential conflict of interest.

The reviewer NL declared a shared parent affiliation with the authors to the handling editor at the time of review.

Publisher's note

All claims expressed in this article are solely those of the authors and do not necessarily represent those of their affiliated organizations, or those of the publisher, the editors and the reviewers. Any product that may be evaluated in this article, or claim that may be made by its manufacturer, is not guaranteed or endorsed by the publisher.

References

Aldecoa, C., Bettelli, G., Bilotta, F., Sanders, R. D., Audisio, R., Borozdina, A., et al. (2017). European society of anaesthesiology evidence-based and consensus-based guideline on postoperative delirium. *Eur. J. Anaesthesiol.* 34, 192–214. doi: 10.1097/EJA.0000000000000594

American Geriatrics Society Expert Panel on Postoperative Delirium in Older Adults (2015). Postoperative delirium in older adults: Best practice statement from the American Geriatrics Society. *J. Am. Coll. Surg.* 220, 136–148.e1.

Bai, J., Liang, Y., Zhang, P., Liang, X., He, J., Wang, J., et al. (2020). Association between postoperative delirium and mortality in elderly patients undergoing hip fractures surgery: A meta-analysis. *Osteoporos. Int.* 31, 317–326. doi: 10.1007/s00198-019-05172-7

Berger, M., Schenning, K. J., Brown, C. H. IV, Deiner, S. G., Whittington, R. A., Eckenhoff, R. G., et al. (2018). Best practices for postoperative brain health: Recommendations from the fifth international perioperative neurotoxicity working group. *Anesth. Analg.* 127, 1406–1413. doi: 10.1213/ANE.0000000000003841

Chen, S., Zhang, Y., Dai, W., Qi, S., Tian, W., Gu, X., et al. (2020). Publication trends and hot spots in postoperative cognitive dysfunction research: A 20-year bibliometric analysis. *J. Clin. Anesth.* 67:110012. doi: 10.1016/j.jclinane.2020.110012

Dasgupta, M., and Dumbrell, A. C. (2006). Preoperative risk assessment for delirium after noncardiac surgery: A systematic review. *J. Am. Geriatr. Soc.* 54, 1578–1589. doi: 10.1111/j.1532-5415.2006.00893.x

Ely, E. W., Gautam, S., Margolin, R., Francis, J., May, L., Speroff, T., et al. (2001a). The impact of delirium in the intensive care unit on hospital length of stay. *Intens. Care Med.* 27, 1892–1900. doi: 10.1007/s00134-001-1132-2

Ely, E. W., Inouye, S. K., Bernard, G. R., Gordon, S., Francis, J., May, L., et al. (2001b). Delirium in mechanically ventilated patients: Validity and reliability of the confusion assessment method for the intensive care unit (CAM-ICU). *JAMA* 286, 2703–2710. doi: 10.1001/jama.286.21.2703

Evered, L., Silbert, B., Knopman, D. S., Scott, D. A., DeKosky, S. T., Rasmussen, L. S., et al. (2018). Recommendations for the nomenclature of cognitive change associated with anaesthesia and surgery-2018. *Br. J. Anaesth.* 121, 1005–1012. doi: 10.1016/j.bja.2017.11.087

Fong, T. G., Tulebaev, S. R., and Inouye, S. K. (2009). Delirium in elderly adults: Diagnosis, prevention and treatment. *Nat. Rev. Neurol.* 5, 210–220. doi: 10.1038/nrneurol.2009.24

Gusmao-Flores, D., Salluh, J. I., Chalhub, R., and Quarantini, L. C. (2012). The confusion assessment method for the intensive care unit (CAM-ICU) and intensive care delirium screening checklist (ICDSC) for the diagnosis of delirium: A systematic review and meta-analysis of clinical studies. *Crit. Care* 16:R115. doi: 10.1186/cc11407

Hong, T., Feng, X., Tong, W., and Xu, W. (2019). Bibliometric analysis of research on the trends in autophagy. *PeerJ* 7:e7103. doi: 10.7717/peerj.7103

Hughes, C. G., Boncyk, C. S., Culley, D. J., Fleisher, L. A., Leung, J. M., McDonagh, D. L., et al. (2020). American society for enhanced

recovery and perioperative quality initiative joint consensus statement on postoperative delirium prevention. *Anesth. Analg.* 130, 1572–1590. doi: 10.1213/ANE.0000000000004641

Inouye, S. K., Kosar, C. M., Tommet, D., Schmitt, E. M., Puelle, M. R., Saczynski, J. S., et al. (2014a). The CAM-S: Development and validation of a new scoring system for delirium severity in 2 cohorts. *Ann. Intern. Med.* 160, 526–533. doi: 10.7326/M13-1927

Inouye, S. K., Studenski, S., Tinetti, M. E., and Kuchel, G. A. (2007). Geriatric syndromes: Clinical, research, and policy implications of a core geriatric concept. *J. Am. Geriatr. Soc.* 55, 780–791. doi: 10.1111/j.1532-5415.2007.01156.x

Inouye, S. K., van Dyck, C. H., Alessi, C. A., Balkin, S., Siegal, A. P., and Horwitz, R. I. (1990). Clarifying confusion: The confusion assessment method. A new method for detection of delirium. *Ann. Intern. Med.* 113, 941–948. doi: 10.7326/0003-4819-113-12-941

Inouye, S. K., Westendorp, R. G., and Saczynski, J. S. (2014b). Delirium in elderly people. *Lancet* 383, 911–922. doi: 10.1016/S0140-6736(13)60688-1

Jackson, J. C., Gordon, S. M., Hart, R. P., Hopkins, R. O., and Ely, E. W. (2004). The association between delirium and cognitive decline: A review of the empirical literature. *Neuropsychol. Rev.* 14, 87–98. doi: 10.1023/B:NERV.0000028080.39602.17

Janssen, T. L., Alberts, A. R., Hooft, L., Mattace-Raso, F., Mosk, C. A., and van der Laan, L. (2019). Prevention of postoperative delirium in elderly patients planned for elective surgery: Systematic review and meta-analysis. *Clin. Interv. Aging* 14, 1095–1117. doi: 10.2147/CIA.S201323

Kalisvaart, K. J., de Jonghe, J. F., Bogaards, M. J., Vreeswijk, R., Egberts, T. C., Burger, B. J., et al. (2005). Haloperidol prophylaxis for elderly hip-surgery patients at risk for delirium: A randomized placebo-controlled study. *J. Am. Geriatr. Soc.* 53, 1658–1666. doi: 10.1111/j.1532-5415.2005.53503.x

Liufu, N., Liu, L., Shen, S., Jiang, Z., Dong, Y., Wang, Y., et al. (2020). Anesthesia and surgery induce age-dependent changes in behaviors and microbiota. *Aging* 12, 1965–1986. doi: 10.18632/aging.102736

Lu, Y., Chen, L., Ye, J., Chen, C., Zhou, Y., Li, K., et al. (2020). Surgery/Anesthesia disturbs mitochondrial fission/fusion dynamics in the brain of aged mice with postoperative delirium. *Aging* 12, 844–865. doi: 10.18632/aging.102659

Mattison, M. L. P. (2020). Delirium. *Ann Intern Med* 173, Itc49–Itc64. doi: 10.7326/AITC202010060

Mi, X., Wang, X., Yang, N., Han, Y., Li, Y., Liu, T., et al. (2021). Hundred most cited articles in perioperative neurocognitive disorder: A bibliometric analysis. *BMC Anesthesiol.* 21:186. doi: 10.1186/s12871-021-01408-4

Morrison, R. S., Magaziner, J., Gilbert, M., Koval, K. J., McLaughlin, M. A., Orosz, G., et al. (2003). Relationship between pain and opioid analgesics on the development of delirium following hip fracture. *J. gerontol. Ser. A Biol. Sci. Med. Sci.* 58, 76–81. doi: 10.1093/gerona/58.1.M76

Raats, J. W., van Eijsden, W. A., Crolla, R. M., Steyerberg, E. W., and van der Laan, L. (2015). Risk factors and outcomes for postoperative delirium after major surgery in elderly patients. *PLoS One* 10:e0136071. doi: 10.1371/journal.pone.0136071

Robinson, T. N., Raeburn, C. D., Tran, Z. V., Angles, E. M., Brenner, L. A., and Moss, M. (2009). Postoperative delirium in the elderly: Risk factors and outcomes. *Ann. Surg.* 249, 173–178. doi: 10.1097/SLA.0b013e31818e4776

Roldan-Valadez, E., Salazar-Ruiz, S. Y., Ibarra-Contreras, R., and Rios, C. (2019). Current concepts on bibliometrics: A brief review about impact factor, Eigenfactor score, CiteScore, SCImago Journal Rank, Source-Normalised Impact per Paper, H-index, and alternative metrics. *Ir. J. Med. Sci.* 188, 939–951. doi: 10.1007/s11845-018-1936-5

Rudolph, J. L., Jones, R. N., Levkoff, S. E., Rockett, C., Inouye, S. K., Sellke, F. W., et al. (2009). Derivation and validation of a preoperative prediction rule for delirium after cardiac surgery. *Circulation* 119, 229–236. doi: 10.1161/CIRCULATIONAHA.108.795260

Saczynski, J. S., Marcantonio, E. R., Quach, L., Fong, T. G., Gross, A., Inouye, S. K., et al. (2012). Cognitive trajectories after postoperative delirium. *N. Engl. J. Med.* 367, 30–39. doi: 10.1056/NEJMoa1112923

Salluh, J. I., Soares, M., Teles, J. M., Ceraso, D., Raimondi, N., Nava, V. S., et al. (2010). Delirium epidemiology in critical care (DECCA): An international study. *Crit. Care* 14:R210. doi: 10.1186/cc9333

Schenning, K. J., and Deiner, S. G. (2015). Postoperative delirium in the geriatric patient. *Anesthesiol. Clin.* 33, 505–516. doi: 10.1016/j.anclin.2015.05.007

Shenkin, S. D., Fox, C., Godfrey, M., Siddiqi, N., Goodacre, S., Young, J., et al. (2019). Delirium detection in older acute medical inpatients: A multicentre prospective comparative diagnostic test accuracy study of the 4AT and the confusion assessment method. *BMC Med.* 17:138. doi: 10.1186/s12916-019-1367-9

Steiner, L. A. (2011). Postoperative delirium. Part 1: Pathophysiology and risk factors. *Eur. J. Anaesthesiol.* 28, 628–636. doi: 10.1097/EJA.0b013e328349b7f5

Van Rompaey, B., Bossaert, L., Shortridge-Bagett, L., Schuurmans, M., and Truijen, S. (2007). A comparison of the confusion assessment method for the intensive care unit and the NEECHAM confusion scale in intensive care delirium assessment. *Crit. Care* 11(Suppl 2):419. doi: 10.1186/cc5579

Vasunilashorn, S. M., Fong, T. G., Albuquerque, A., Marcantonio, E. R., Schmitt, E. M., Tommet, D., et al. (2018). Delirium severity post-surgery and its relationship with long-term cognitive decline in a cohort of patients without dementia. *J. Alzheimers Dis.* 61, 347–358. doi: 10.3233/JAD-170288

Velagapudi, R., Subramaniyan, S., Xiong, C., Porkka, F., Rodriguiz, R. M., Wetsel, W. C., et al. (2019). Orthopedic surgery triggers attention deficits in a delirium-like mouse model. *Front. Immunol.* 10:2675. doi: 10.3389/fimmu.2019.02675

Wang, J., Wang, L., Tang, X., Wang, F., Liu, S., Wu, X., et al. (2022). The relationship between cardiovascular disease risk score and postoperative delirium: The PNDABLE Study. *Front. Aging Neurosci.* 14:851372. doi: 10.3389/fnagi.2022.851372

Wang, P., Velagapudi, R., Kong, C., Rodriguiz, R. M., Wetsel, W. C., Yang, T., et al. (2020). Neurovascular and immune mechanisms that regulate postoperative delirium superimposed on dementia. *Alzheimers Dement.* 16, 734–749. doi: 10.1002/alz.12064

Wilson, J. E., Mart, M. F., Cunningham, C., Shehabi, Y., Girard, T. D., MacLullich, A. M. J., et al. (2020). Delirium. *Nat. Rev. Dis. Primers* 6:90. doi: 10.1038/s41572-020-00223-4

Yang, Y., Zhao, X., Dong, T., Yang, Z., Zhang, Q., and Zhang, Y. (2017). Risk factors for postoperative delirium following hip fracture repair in elderly patients: A systematic review and meta-analysis. *Aging Clin. Exp. Res.* 29, 115–126. doi: 10.1007/s40520-016-0541-6

Zhu, C., Wang, B., Yin, J., Xue, Q., Gao, S., Xing, L., et al. (2020). Risk factors for postoperative delirium after spinal surgery: A systematic review and meta-analysis. *Aging Clin. Exp. Res.* 32, 1417–1434. doi: 10.1007/s40520-019-01319-y

frontiers | Frontiers in Neuroscience

TYPE Original Research
PUBLISHED 28 September 2022
DOI 10.3389/fnins.2022.1006175

OPEN ACCESS

EDITED BY
Zhongcong Xie,
Massachusetts General Hospital and Harvard Medical School, United States

REVIEWED BY
Shiyong Li,
Huazhong University of Science and Technology, China
Jianhui Liu,
Tongji Hospital Affiliated to Tongji University, China
Yuanlin Dong,
Mass General Brigham, United States

*CORRESPONDENCE
Jia Yan
mzkyanj@163.com
Hong Jiang
jianghongjiuyuan@163.com

†These authors have contributed equally to this work

SPECIALTY SECTION
This article was submitted to Neuropharmacology, a section of the journal Frontiers in Neuroscience

RECEIVED 11 August 2022
ACCEPTED 08 September 2022
PUBLISHED 28 September 2022

CITATION
Zhong L, Ma X, Niu Y, Zhang L, Xue Z, Yan J and Jiang H (2022) Sevoflurane exposure may cause dysplasia of dendritic spines and result in fine motor dysfunction in developing mouse through the PI3K/AKT/mTOR pathway.
Front. Neurosci. 16:1006175.
doi: 10.3389/fnins.2022.1006175

Sevoflurane exposure may cause dysplasia of dendritic spines and result in fine motor dysfunction in developing mouse through the PI3K/AKT/mTOR pathway

Linhong Zhong†, Xiaofan Ma†, Yixuan Niu, Lei Zhang, Zhenyu Xue, Jia Yan* and Hong Jiang*

Department of Anesthesiology, Shanghai Ninth People's Hospital, Shanghai Jiao Tong University School of Medicine, Shanghai, China

Sevoflurane has become one of the most widely used volatile anesthetics in pediatric surgery. However, sevoflurane exposure may interfere with dendritic development and synaptogenesis, resulting in brain function impairment. The PI3K/AKT/mTOR pathway plays an important role in dendritic development and synaptic plasticity. Here we investigated whether sevoflurane exposure would affect the morphological proportions of dendritic spines in developing mouse and explored the role of the change of plasticity of dendritic spines in sevoflurane-induced neurodevelopmental toxicity. The related signaling pathway was also examined. C57BL/6 mice at postnatal day (PND) 7 were exposed to 2% sevoflurane for 3 h. The PI3k/AKT/mTOR agonist IGF-1 or the mTOR phosphorylation inhibitor KU0063794 was intraperitoneally injected 30 min before sevoflurane or O_2 exposure at PND7. Hippocampi were harvested 6 h after sevoflurane exposure. Western blotting was applied to measure the protein expression of PI3K/AKT/mTOR pathway phosphorylation. At PND14, brains from all groups were harvested for Golgi staining, and the morphology of dendritic spines of hippocampal neurons was observed by an oil immersion lens. When the mice grew to adolescence (PND48), fine motor function was measured by the Beam walking test. Here we showed that exposure to 2% sevoflurane for 3 h decreased the proportion of thin dendritic spines and increased the proportion of mushroom dendritic spines, but not changed the density of the dendritic spines. Sevoflurane exposure also suppressed the phosphorylation of the PI3K/AKT/mTOR pathway in immature mice hippocampi, and eventually led to long-term fine motor dysfunction. Meanwhile, IGF-1 pretreatment could rescue and KU0063794 pretreatment could aggravate the impairment induced by sevoflurane. In

conclusion, sevoflurane exposure may cause a change of proportions of the types of dendritic spines through impacting the phosphorylation expression of the PI3K/AKT/mTOR pathway, and eventually led to long-term fine motor dysfunction in developing mouse.

KEYWORDS

sevoflurane, dendritic spine, PI3k/AKT/mTOR pathway, fine motor dysfunction, developing brain

Introduction

Every year, millions of infants and children receive surgery under anesthesia. The safety of brain development under anesthesia is directly related to the quality of the population and is one of the public health issues concerned by the whole society (Psaty et al., 2015). A recent U.S. Food and Drug Administration (FDA) warning advised that exposure to general anesthetics may affect neurodevelopment in children (Davidson and Sun, 2018). Unfortunately, to date, no effective strategies exist to avoid to this problem.

Sevoflurane is one of the most widely used volatile anesthetics in pediatric anesthesia. In developing animals particularly in rodents and monkeys, receiving prolonged sevoflurane exposure induces neuronal apoptosis (He et al., 2018; Zhao et al., 2020; Zhu et al., 2021), abnormal development of the dendritic spine (Briner et al., 2010) and synapse formation and loss (Vutskits and Xie, 2016). Increasing evidence demonstrate that sevoflurane exposure induces neuronal apoptosis and subsequently leads to motor and cognitive dysfunction (Kalkman et al., 2009; Wilder et al., 2009; Sun, 2010; Flick et al., 2011; Sprung et al., 2012; Stratmann et al., 2014). Clinically, exposure to low concentration (2%) of sevoflurane for 3 h is closer to the practical approach to pediatric anesthesia (Zou et al., 2009). It was found that exposure to 2% sevoflurane for 3 h did not induce neuroapoptosis, but could cause long-term abnormal behavior (Lu et al., 2016). It suggests the mechanisms of immature brain injury induced by sevoflurane anesthesia are various.

Neurogenesis, especially dendritic spine morphogenesis, is a key step in brain circuits during the development of the central nervous system (Liao et al., 2021). During the peak period of brain development, the development of the dendritic spine also reaches its peak. In this period, the abnormal morphological plasticity of dendritic spines will trigger disturbances in synapse formation, which will lead to long-term neurodevelopmental dysfunction (Bian et al., 2015). Dendritic spines can be divided into four types: mushroom, thin, stubby and branched (Harris et al., 1992). Studies have confirmed that a change in the proportions of the types of dendritic spines would predict a decrease in learning ability (Bello-Medina et al., 2016). The morphological plasticity of dendritic spines is not only related to learning and memory function, but also closely related to motor coordination. Previous studies have found that neuroplasticity is the basis of the brain's restorative response to environmental factors that impair neurobiological processes. Neuropathological lesions resulting in motor dysfunction are usually accompanied with neuroplasticity change (Gonzalez-Burgos et al., 2011).

The phosphatidylinositol 3-hydroxy kinase/protein kinase B/mammalian target of the rapamycin (PI3K/AKT/mTOR) pathway plays an important role in different neuronal functions (Gilbert and Man, 2017; Sharma and Mehan, 2021). Several studies have shown that the phosphorylation expression of the PI3K/AKT/mTOR pathway involved in different neuronal functions mainly involves synaptogenesis, corticogenesis, and related neuronal cerebral processes, especially in the hippocampus (Sharma and Mehan, 2021). As the key component of the pathways, the importance of mTOR is self-evident. PI3K/AKT, the upstream signal of mTOR, plays an important regulatory role in the activation of mTOR (Kim et al., 2017).

In this study, we investigated whether exposure to 2% sevoflurane for 3 h would affect the morphological plasticity of dendritic spines in developing mouse, and explored whether PI3K/AKT/mTOR pathway played a key role in sevoflurane-induced immature neurotoxicity.

Materials and methods

Animals and animal treatments

This study was approved by the Animal Ethics Committee of Shanghai Ninth People's Hospital, Shanghai Jiao Tong University School of Medicine and was performed in compliance with the Guide for the Care and Use of Laboratory Animals of the institution. C57BL/6 mouse pups with the age of postnatal day 7 (PND7), provided by the Animal Center of Shanghai Jiao Tong University School of Medicine (Shanghai, China), were used. The animals were housed on a 12 h light/dark cycle and with free access to food and water.

Mouse pups were separated from their mothers for acclimatization before sevoflurane exposure. Mouse pups were exposed to 2% sevoflurane for 3 h or 100% oxygen for 3 h in a chamber. The concentration of sevoflurane in the chamber was monitored and maintained by a vaporizer. The gas flow to the chamber was 2 L/min. Other studies have shown that PND7 C57BL/6 mice can be exposed to up to 3% sevoflurane for 6 h without any detrimental effect on cerebral perfusion, arterial blood gas, or glucose values (Satomoto et al., 2009). After exposure, the mouse pups were returned to the cages of mothers for further experiments.

In the brain, the time to reach the effective concentration of IGF-1 (a phosphorylated activator for PI3K/AKT/mTOR) was from 30 min to 2 h (Guan et al., 2015) and that of KU0063794 (a second generation mTOR inhibitor targeting mTORC1 and mTORC2) was from 10 min to 4 h after intraperitoneal (i.p.) injection (Garcia-Martinez et al., 2009). Therefore, to ensure the effectiveness of these drugs during anesthesia, the mice received IGF-1 or KU0063794 i.p. 30 min before exposure to sevoflurane or O_2. IGF-1 was dissolved in saline, which possesses the ability to cross the blood brain barrier (BBB) according to the previous report (Nishijima et al., 2010). KU0063794 was dissolved in DMSO. We used 240 μg/kg IGF-1 (Yuan et al., 2020) or 5 mg/kg KU-0063794 (Cordaro et al., 2017; Campolo et al., 2021) as previously reported. As the solute group, the mice received the equivalent amount of saline or DMSO with i.p. injection 30 min before exposure to sevoflurane or O_2. The overall experimental procedures were shown in **Figure 1**.

Western blotting

The mouse hippocampus was isolated immediately on ice after being sacrificed by decapitation 6 h after exposure to sevoflurane for western blotting. In brief, tissues were lysed and homogenized in a buffer containing a protease inhibitor and phosphatase inhibitor cocktail (Epizyme, Shanghai, China). The homogenate was centrifuged and the supernatant was collected for further analysis. The protein concentrations of samples were determined using the BCA protein assay (Beyotime, Shanghai, China). Equal amounts of protein were boiled in loading buffer (Sangon Biotech, Shanghai, China) and separated by 8% polyacrylamide gel electrophoresis, and transferred onto PVDF membranes (Millipore, Burlington, MA, USA). The membranes were incubated at room temperature for 2 h in a blocking buffer. Protein sample were subjected to western blot analysis using the following primary antibodies: anti-mTOR (1:10,000, Abcam), anti-phospho-mTOR (1:1,000, Abcam), anti-PI3K (1:1,000, Abcam), anti- phospho-PI3K (1:1,000, Abcam), anti-AKT (1:500, Abcam), anti-phospho-AKT (1:1,000, Abcam), and anti-β-actin (1:1,000, Cell Signaling Technology). The secondary antibodies were goat-anti-rabbit IgG or mouse-anti-goat IgG (1:3,000, Cell Signaling Technology). All blots were detected using the enhanced chemiluminescence (ECL) detection system (Millipore, MA, USA). The scanned images were quantified with Image J. We used β-actin concentrations to standardize amounts of protein.

Golgi staining and dendritic spines counting

To observe the morphology of the dendritic spines, Golgi staining was performed after sevoflurane exposure. The brains were harvested at the age of postnatal day 14 (PND14). At PND14, dendritic spines have reached the peak development in mice (Fiala et al., 1998). Golgi staining was performed on 120 μm thick cryosectioned brain slices, using the FD Rapid Golgi Stain kit (FD NeuroTechnologies, Inc., Columbia, CA, USA) according to the manufacturer's protocol (Du, 2019). For each hippocampal region, ten pyramidal neurons that were well-impregnated and separated from others were scanned with a confocal microscope (Nikon A1). To analysis the morphology of dendritic spines, five segments of 50 μm (or longer) dendrites were randomly chosen from each neuron with clearly trace of origin and well separated from neighboring dendrites and imaged with 100× oil immersion lens. Spine density was calculated as the number of spines per 10 μm of dendritic length.

The data on the morphology of the dendritic spine were analyzed by using the NeuroStudio® Software (version 0.9.92; Computational Neurobiology and Imaging Center Mount Sinai School of Medicine, New York, NY, USA). The software can classify spines according to a default classification scheme. Morphological criteria based on the spine length (SL), neck diameter (ND), head diameter (HD), and the number of protrusions from a single stalk were used to classify the spines in thin (when HD/ND $<$ 1.1 and SL/HD $>$ 2.5), mushroom (when HD $>$ 0.35 μm), branch (with a single stalk with two or more spine heads), and stubby (others) (Dall'oglio et al., 2015; Zancan et al., 2018). The data on the dendritic spine density were also collected. Dendritic spines density was calculated as the total number of spines divided by the length of the dendrite studied (Rasia-Filho et al., 2004). All the analysis was completed by two independent investigators who were blinded to the condition.

Beam walking test

A protocol for behavioral assessment showed that mice could be tested for motor function, balance and coordination at 1 month of age (Rogers et al., 2001). Beam walking test was performed for testing fine motor coordination and balance of mice reaching PND 48 from all groups, as described before

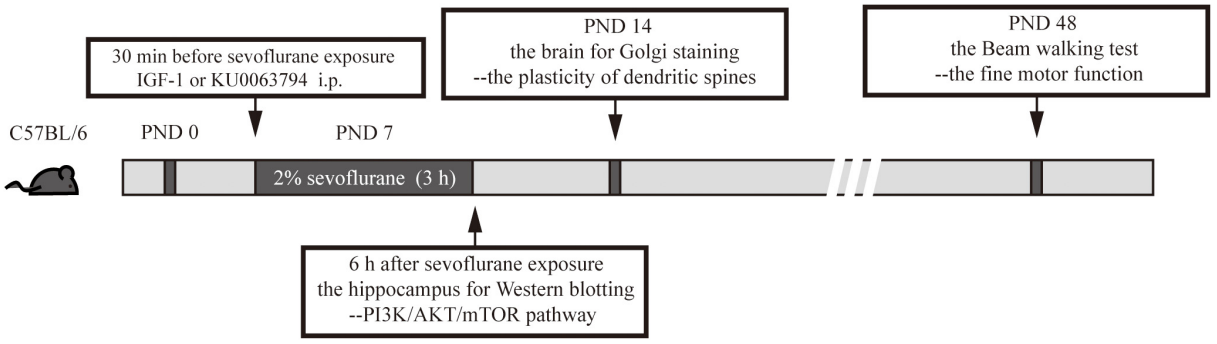

FIGURE 1
The overall experimental procedures in this study.

(Luong et al., 2011). Briefly, the beam apparatus consists of 1 m beams with a flat surface of 12 mm, resting 50 cm above the table top on two poles. A black box was placed at the end of the beam as the finish point. The time and performance to cross the center 80 cm were measured by a video camera. Mice were placed at one end of a beam and the time required to cross the escape box at the other end (80 cm away) was measured by a timer. The timer was started with the nose of the mice entering the center 80 cm, and stopped when the animal reached the end. This test takes place over three consecutive days. A slip was defined as the foot coming off the top of the beam. The times of their foot slipping off the beam were recorded. The beam was cleaned with 75% alcohol to avoid olfactory cues between two tests.

Statistical analysis

All values are presented as means ± standard deviation. All the data were analyzed by one-way ANOVA analysis of variance followed by the Tukey's test. The GraphPad Prism 9.0 (GraphPad, USA) software were used to conduct the statistical analysis. Statistical significance was accepted as $P < 0.05$.

Results

Exposure to sevoflurane in the neonatal period can alter the proportions of the types of dendritic spines, but not the density of the dendritic spines in young mice

To explore the possible effect of sevoflurane on the plasticity of dendritic spines, we first examined the morphology of dendritic spines in the hippocampus from PND14 after exposure to sevoflurane using Golgi staining (Figure 2A). There was no significant change in dendritic spine density ($P > 0.05$, Figure 2B). Notably, the proportion of mushroom dendritic spines increased in the sevoflurane (SEV) group ($P < 0.05$), and the proportion of thin dendritic spines decreased ($P < 0.05$), but the proportion of other types of dendritic spines had no significant change ($P > 0.05$), compared with the control (Ctrl) group (Figure 2C). These results suggested that sevoflurane could induce morphological change of dendritic spines in the hippocampus of young mice.

Exposure to sevoflurane can suppress the phosphorylation of the PI3K/AKT/mTOR pathway in the hippocampus in neonatal mice

To study whether the phosphorylation of the PI3K/AKT/mTOR pathway is involved in sevoflurane-induced morphological abnormality of dendritic spines, the expressions of the proteins were detected by western blot (Figure 3A). Compared with the Ctrl group, the phosphorylation of PI3K ($P < 0.05$, Figure 3B), AKT ($P < 0.05$, Figure 3C), and mTOR ($P < 0.05$, Figure 3D) were suppressed by the SEV group. These results indicated that exposure to 2% sevoflurane for 3 h could inhibit the phosphorylation of the PI3K/AKT/mTOR pathway.

IGF-1 can alleviate the inhibition of PI3K/AKT/mTOR phosphorylation and rescue the morphological abnormality of dendritic spines induced by sevoflurane

To define the role of the pathway in sevoflurane-induced morphological change of dendritic spines in the

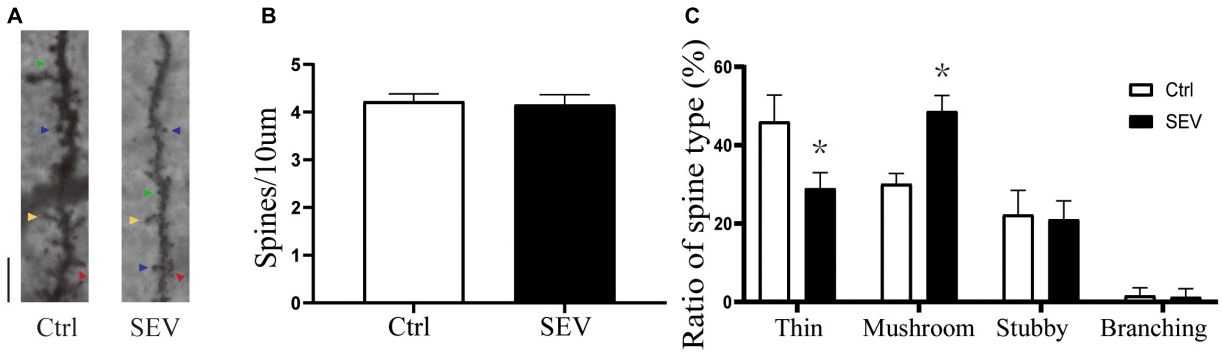

FIGURE 2
Sevoflurane can alert the proportions of the dendritic spines. **(A)** Representative images of Golgi staining of dendritic spines in the hippocampi of PND 14 mice. Different spine types are indicated by relevant color arrowheads: thin spine (yellow), mushroom spine (blue), stubby spine (green), branching spine (red). Scale bar = 10 μm. **(B,C)** The quantitative analysis of spine density and proportions of spine types by one-way ANOVA. Results are the means ± SD, n = 6 mice per group. *$P < 0.05$ vs. Ctrl.

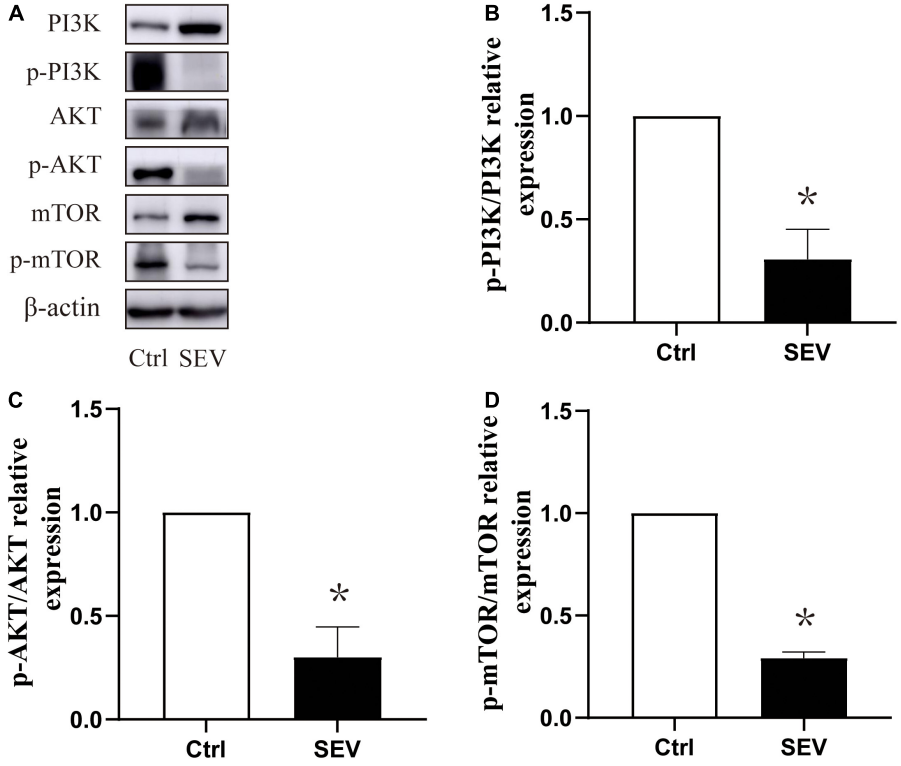

FIGURE 3
Sevoflurane can suppress the phosphorylation expression of the PI3K/AKT/mTOR pathway in the hippocampus in neonatal mice.
(A) Representative Western blots of PI3K, AKT, and mTOR. **(B–D)** Bars represent normalization of target proteins were ratio of phosphorylated and non-phosphorylated forms. The quantitative analysis of PI3K, AKT and mTOR when exposure to sevoflurane after 6 h by one-way ANOVA. Results are the means ± SD. n = 6 in each group. *$P < 0.05$ vs. Ctrl.

hippocampus in young mice. We used the agonists of PI3K/AKT/mTOR pathway for stimulating signaling cascades. Compared with the control (NS) group, the phosphorylation of PI3K ($P < 0.05$, Figures 4A,B), AKT ($P < 0.01$, Figures 4A,C) and mTOR ($P < 0.01$, Figures 4A,D) was suppressed in the sevoflurane (SEV + NS) group. Treatment with IGF-1 before sevoflurane (SEV + IGF-1) group showed no significant difference in phosphorylation of PI3K/AKT/mTOR pathway,

compared with the NS group ($P > 0.05$). However, the expression of phosphorylation of PI3K ($P < 0.05$, Figure 4B), AKT ($P < 0.05$, Figure 4C) and mTOR ($P < 0.05$, Figure 4D) was increased, compared with the SEV + NS group. It indicated that IGF-1 could rescue the inhibition of PI3K/AKT/mTOR phosphorylation pathway induced by sevoflurane.

In Golgi staining analysis (Figure 4E), there was no significant change in density of dendritic spines in each group ($P > 0.05$, Figure 4F). However, compared with the NS group, the proportion of mushroom dendritic spines increased ($P < 0.05$) and the proportion of thin dendritic spines decreased ($P < 0.05$), but the proportion of other types of dendritic spines had no significant change ($P > 0.05$) in the SEV + NS group (Figure 4G). Surprisingly, the decrease of the proportion of thin dendritic spines and increase of the proportion of mushroom dendritic spines were rescued by IGF-1 ($P > 0.05$, Figure 4G). These results suggested that sevoflurane-induced change of the proportions of the types of dendritic spines was mediated by the PI3K/AKT/mTOR phosphorylation pathway.

KU0063794 can aggravate sevoflurane-induced morphological abnormality of dendritic spines

We used the inhibitor of mTOR to suppress the PI3K/AKT/mTOR signaling pathway (Figure 5A). Compared with the control (DMSO) group, the phosphorylation of PI3K ($P < 0.01$, Figure 5B), AKT ($P < 0.01$, Figure 5C), and mTOR ($P < 0.01$, Figure 5D) were suppressed in sevoflurane (SEV + DMSO) group. Moreover, the mTOR inhibitor administration before exposure to sevoflurane (SEV + KU group) could aggravate the inhibition of the phosphorylation of mTOR, compared with the SEV + DMSO group ($P < 0.05$, Figure 5D). Using the inhibitor of mTOR alone (KU group) significantly also reduced the phosphorylation of mTOR ($P < 0.05$, Figure 5D) and barely changed the phosphorylation of PI3K and AKT ($P > 0.05$, Figures 5B,C). In Golgi staining experiment (Figure 5E), although there was no significant change in density of dendritic spines in each group ($P > 0.05$, Figure 5F), the proportion of mushroom dendritic spines increased ($P < 0.05$) and the proportion of thin dendritic spines decreased ($P < 0.05$) in the SEV + DMSO group, compared with the DMSO group (Figure 5G). Compared with the SEV + DMSO group, the increase of proportion of mushroom dendritic spines ($P < 0.05$) and the decrease of proportion of thin dendritic spines were aggravated ($P < 0.05$) in the SEV + KU group, but the proportions of other types of dendritic spines had no significant change ($P > 0.05$) (Figure 5G). In addition, compared with the DMSO group, the proportion of mushroom dendritic spines increased ($P < 0.05$) and the proportion of thin dendritic spines ($P < 0.05$) deceased in the KU group (Figure 5G). Taken together, these results indicated that sevoflurane-induced morphological abnormality of dendritic spines was mediated by the inhibition of the phosphorylation of PI3K/AKT/mTOR pathway.

Exposure to sevoflurane in neonatal period can induce long-term fine motor dysfunction which can be rescued by IGF-1 and KU0063794 can induce fine motor impairment which is similar as sevoflurane-induced

Beam walking test is performed to detect fine motor coordination and balance function when the mice grew up (Figure 6A). Compared with the NS group, the number of slips significantly increased in the SEV + NS group ($P < 0.01$). The number of slips in the SEV + IGF-1 group was less than the SEV + NS group on the third day ($P < 0.01$, Figure 6B). Furthermore, compared with the DMSO group, both of the numbers of slips in the SEV + DMSO and SEV + KU group significantly increased on the third day ($P < 0.05$). Similar as SEV + DMSO group, the number of slips increased in the KU group at the third day ($P < 0.05$, Figure 6C). These results indicated that exposure to 2% sevoflurane for 3 h in the neonatal period could induce long-term fine motor dysfunction, which could be rescued by IGF-1. The inhibitor of mTOR also could induce similar impact as sevoflurane-induced.

Discussion

Recent studies have found that a brief exposure to anesthesia in childhood do not damage the subsequent intellectual development (Ing et al., 2014; Sun et al., 2016). However, there are still evidence suggesting that exposure to anesthesia during infants and young children is associated with impaired motor skills and lower processing speed (Ing et al., 2014; Zaccariello et al., 2019). In the present study, we performed a series of experiments in a mouse model of exposure to 2% sevoflurane for 3 h to analyze the underlying mechanisms of sevoflurane-induced neurodevelopmental impairment. The result showed that exposure to 2% sevoflurane for 3 h could alter the proportions of the types of dendritic spines, but not the density of the dendritic spines. Also, sevoflurane exposure suppressed the phosphorylation expression of the PI3K/AKT/mTOR pathway in immature mouse hippocampus resulting in subsequent long-term fine motor dysfunction. IGF-1, which is the agonist of this

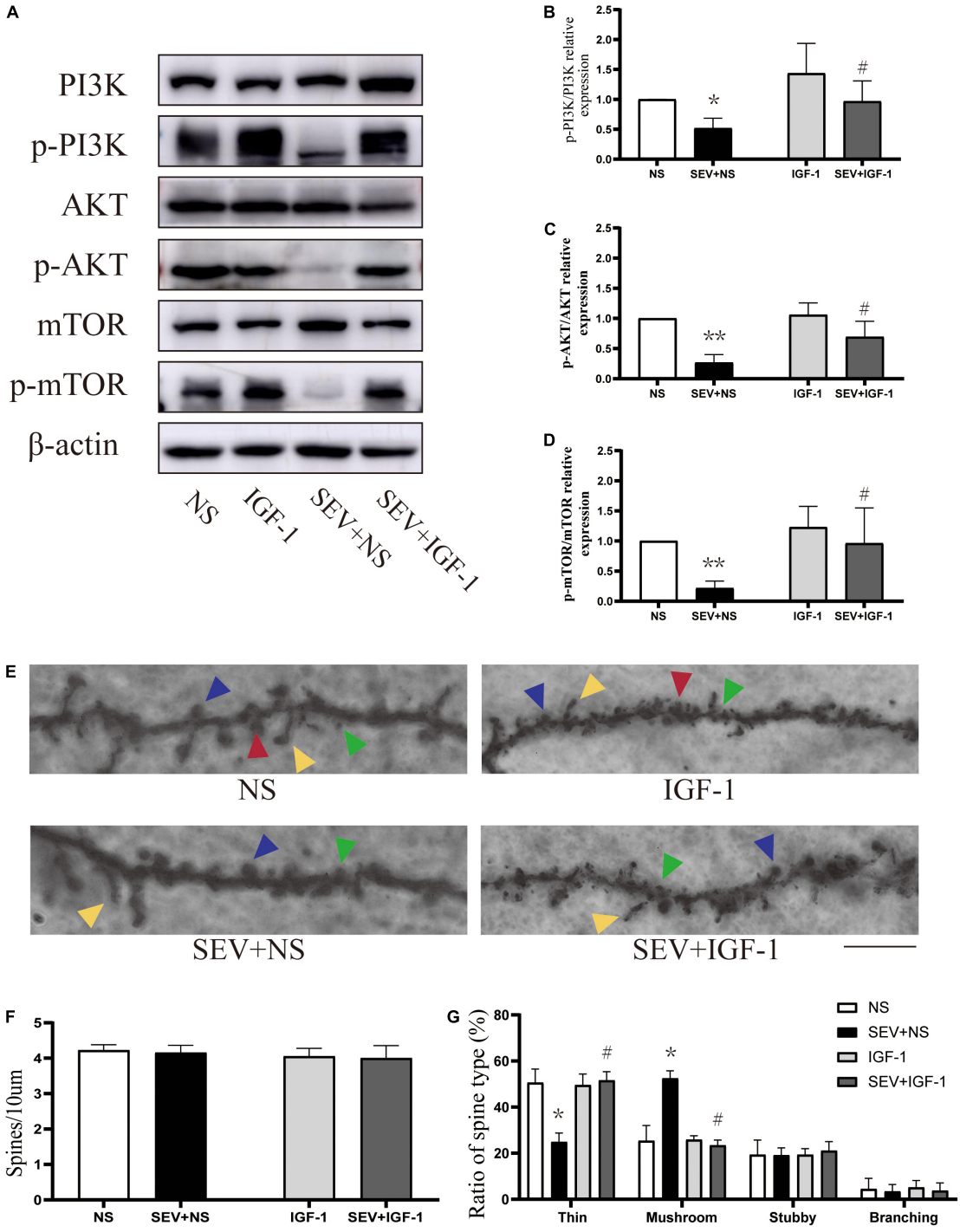

FIGURE 4
IGF-1 can alleviate the inhibition of PI3K/AKT/mTOR phosphorylation and rescue sevoflurane-induced morphological abnormality of dendritic spines. **(A)** Representative Western blot of PI3K, AKT, mTOR, and phosphor-PI3K, phosphor-AKT, phosphor-mTOR for different groups. β-actin was used as reference. **(B–D)** Bars represent normalization of target proteins were ratios of phosphorylated and non-phosphorylated forms. Results of one-way ANOVA and significance are shown inside graphs: data were presented as mean ± SD, $n = 6$ for per group. **(E)** Representative images of Golgi staining of dendritic spines in the hippocampi of PND 14 mice for different groups. Different spine types are indicated by relevant color arrowheads: thin spine (yellow), mushroom spine (blue), stubby spine (green), branching spine (red). Scale bar = 10 μm. **(F)** The density of the dendritic spines in different groups. **(G)** The proportions of dendritic spine types in different groups. Data were presented as mean ± SD by one-way ANOVA, $n = 6$ mice per group. $^{*}P < 0.05$, $^{**}P < 0.01$ vs. NS; $^{\#}P < 0.05$ vs. SEV + NS.

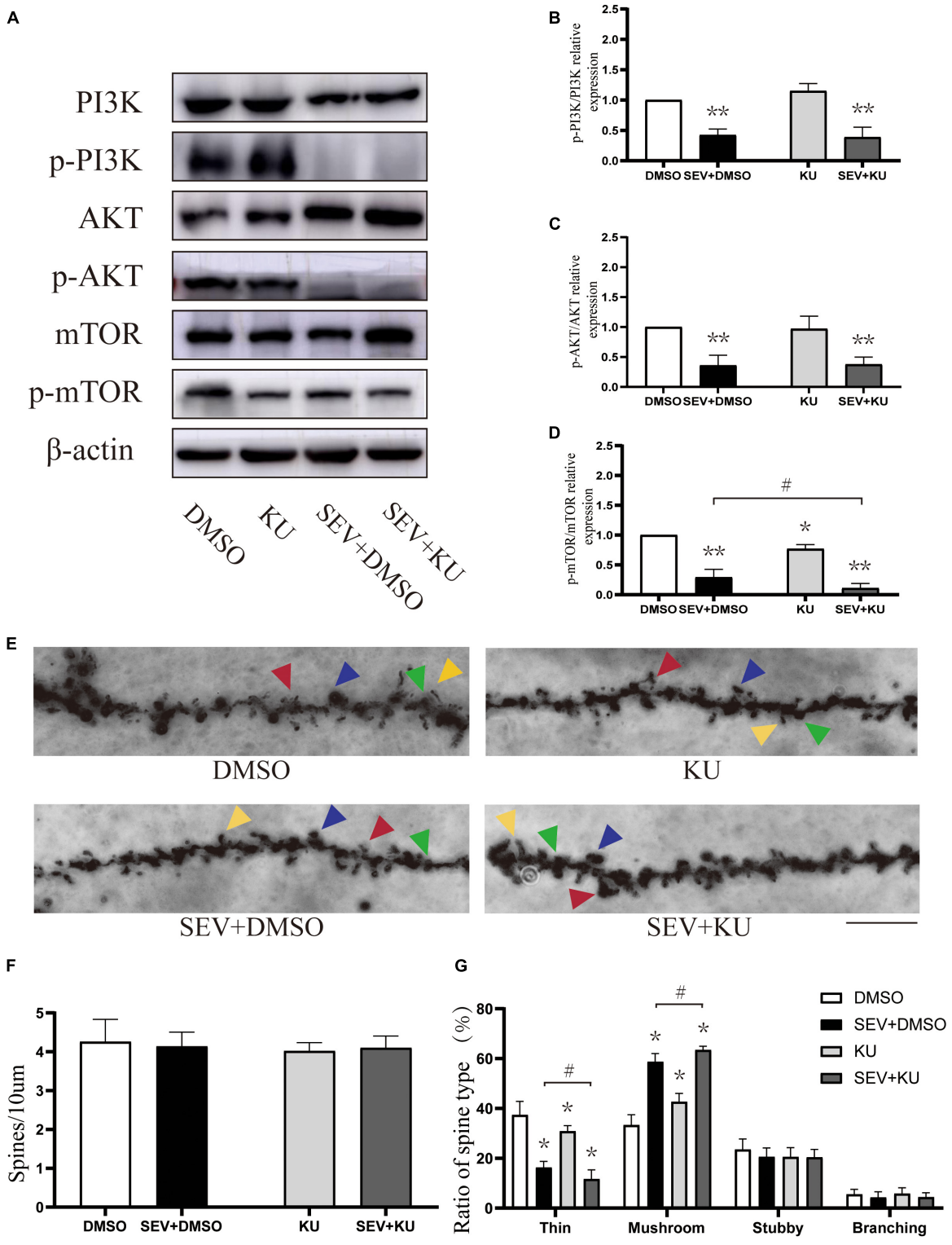

FIGURE 5
KU0063794 can aggravate sevoflurane-induced morphological abnormality of dendritic spines. **(A)** Representative Western blot of phosphorylated and non-phosphorylated proteins for different groups. β-actin was used as reference. **(B–D)** Normalization of phosphorylated and non-phosphorylated forms. Results of one-way ANOVA and significance are shown inside graphs: data were presented as mean ± SD, $n = 6$ for per group. **(E)** Representative images of Golgi staining of dendritic spines in the hippocampi of PND 14 mice in different groups. Different spine types are indicated by relevant color arrowheads: thin spine (yellow), mushroom spine (blue), stubby spine (green), branching spine (red). Scale bar = 10 μm. **(F)** The density of the dendritic spine in different groups. **(G)** The proportion of dendritic spine types in different groups. Data were presented as mean ± SD by one-way ANOVA, $n = 6$ mice per group. $^{*}P < 0.05$, $^{**}P < 0.01$ vs. DMSO; $^{\#}P < 0.05$ vs. SEV + DMSO.

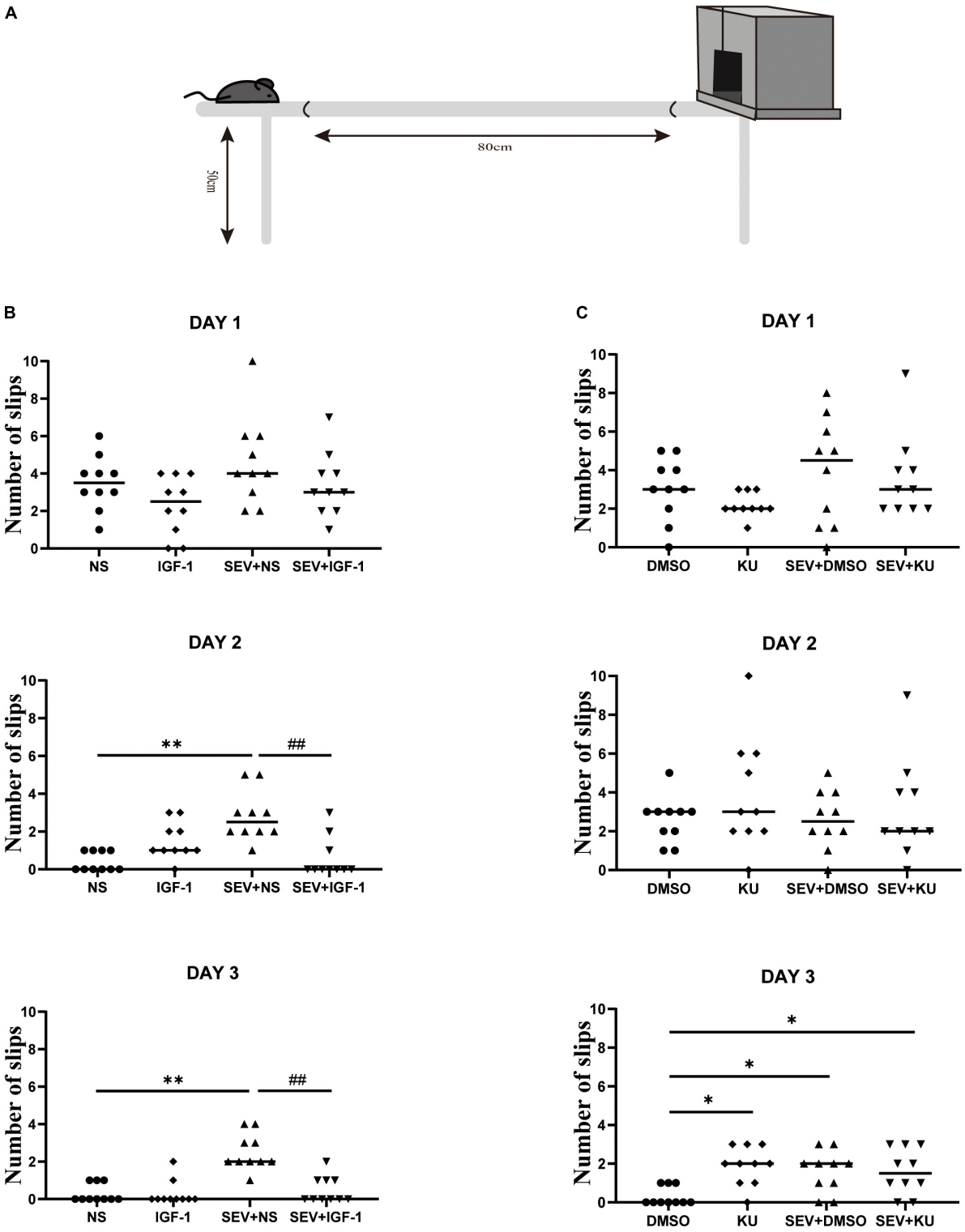

FIGURE 6
IGF-1 can rescue sevoflurane-induced deficits in fine motor function, and KU0063794 can induce fine motor impairment which is similar as sevoflurane-induced. **(A)** Schematic diagram of the beam walking test. **(B,C)** The numbers of slips of beam walking test at PND 48 over three consecutive days in all groups by one-way ANOVA, $n = 10$ for each group. $^{*}P < 0.05$, $^{**}P < 0.01$ vs. NS or DMSO; $^{\#}P < 0.05$, $^{\#\#}P < 0.01$ vs. SEV + NS.

pathway, can alleviate the inhibition of PI3K/AKT/mTOR phosphorylation and rescue the morphological abnormality of dendritic spines together with the fine motor dysfunction induced by sevoflurane. Moreover, the use of the inhibitor of mTOR phosphorylation aggravated the proportion alteration of the types of dendritic spines induced by sevoflurane, and finally led to long-term fine motor disorders as well.

Previous studies reported that in rodents' early-life, long duration (6–9 h) exposure to high concentrations (3–4%) of sevoflurane could impair cognitive functions through apoptosis (Wang et al., 2013; Zhou et al., 2013). Meanwhile, it has also been shown in non-human primates that exposure to 2.5–3.5% sevoflurane for 5 h in neonatal rhesus monkey caused widespread apoptotic death of neurons and oligodendrocytes in the brain (Ikonomidou et al., 2019). Clinically, exposure to the lower concentration (2%) of sevoflurane for 3 h is closer to the practical approach to pediatric anesthesia (Zou et al., 2009). However, it was found that exposure to 2% sevoflurane for 3 h did not induce neuroapoptosis but could also cause long-term dysfunction in brain development (Lu et al., 2016). It suggests the mechanisms of immature brain injury induced by different concentrations and exposure durations of sevoflurane are not the same.

According to the function of spines, mushroom spines have larger spines, corresponding to stable and mature synapses, and are called "memory dendritic spines." The thin spines, known as the "learning dendritic spines," are more plastic and can be transformed into "memory dendritic spines" under the condition of long-term enhancement (LTP) caused by learning and other behaviors (Bourne and Harris, 2007). Dendritic spines show highly dynamic changes in morphology and number during development and adulthood (Yuste and Majewska, 2001). Under normal circumstances, the proportions of thin and mushroom spines keep a certain balance (Bourne and Harris, 2007). The decrease of "learning dendritic spines" and increase of "memory dendritic spines" predicted the impairment of neurodevelopment (Bello-Medina et al., 2016). Our data showed that although the total number of dendritic spines remained stable after exposure to sevoflurane, the proportions of thin and mushroom dendritic spines changed significantly, companying with fine motor dysfunction when the mice grew up. In the missing in metastasis (a protein initiates new dendritic spines) knockout mice, the decreased proportion of thin dendritic spines is associated with observed behavioral defects in motor-coordination (Minkeviciene et al., 2019). Therefore, we consider that sevoflurane exposure may alter the morphology of dendritic spines during neurodevelopment, and lead to long-term fine motor dysfunction.

The PI3K/AKT/mTOR pathway plays an important role in maintaining the plasticity of dendritic spines in the normal nervous system (Kumar et al., 2005). The general relevance of the PI3K/AKT/mTOR pathway in the regulation of dendritic growth and spine formation has been reported recently. It has been shown previously that the activation of the PI3K/AKT/mTOR pathway is required for the insulin action on the spine and synapse formation in hippocampal neurons (Lee et al., 2011). Our results suggested that sevoflurane-induced morphological abnormality of dendritic spines was dependent on the phosphorylation of the PI3k/AKT/mTOR pathway. Moreover, the results are consistent with the fact that mTOR is important in maintaining dendritic spine stability (Jaworski and Sheng, 2006; Tang et al., 2014; Chen et al., 2020). Although the density of dendritic spines is associated with dendritic growth and neurological diseases (Liu et al., 2019), our data showed that exposure to 2% sevoflurane for 3 h had no effect on the density of dendritic spines in the developing hippocampus which is consistent with Qiu et al. (2016).

Although the results suggested that the PI3K/AKT/mTOR pathway played an important role in the regulation of dendritic spines morphology in sevoflurane-induced neurotoxicity, how the PI3K/AKT/mTOR pathway trigger the morphological changes of dendritic spines remains unclear. In fact, Tau protein has been implicated as the PI3K/AKT/mTOR pathway downstream effector to control neurite outgrowth, and its hyperphosphorylation is considered to be the basis of neuronal degeneration in Alzheimer's disease (Tao et al., 2014; Yang et al., 2020). A study has reported that Glutamate (Glu) can induce Tau phosphorylation in the postsynaptic structure by activating NMDA receptors under physiological conditions, thus promoting dendritic spines maturation (Pallas-Bazarra et al., 2016). Thus, we expect that further work will be performed to assess the role of Tau phosphorylation and NMDA receptor in the PI3K/AKT/mTOR pathway-mediating sevoflurane-induced dysplasia of dendritic spines.

In summary, our data showed that exposure to 2% sevoflurane for 3 h induces abnormal morphological proportions, but not density, of dendritic spines by impacting the phosphorylation of PI3K/AKT/mTOR pathway, which may be effect on developmental brain injury. It is expected to be of great significance and good application prospect in improving the safety of infant brain development during anesthesia.

Data availability statement

The raw data supporting the conclusions of this article will be made available by the authors, without undue reservation.

Ethics statement

The animal study was approved by the Animal Ethics Committee of Shanghai Ninth People's Hospital, Shanghai Jiao Tong University School of Medicine (Shanghai, China) and was performed in compliance with the Guide for the Care and Use of Laboratory Animals of the institution.

Author contributions

JY, HJ, and LZ: conceptualization. LZ, XM, YN, and ZX: methodology. LHZ: writing-original draft preparation. JY and HJ: writing-review and editing. All authors contributed to the article and approved the submitted version.

Funding

This work was supported by the National Natural Science Foundation of China (Grant No. 81870818) and the Natural Science Foundation of Shanghai (Grant No. 22ZR1437200).

Acknowledgments

We would like to thank Dr. Jian Yu for providing the tool of the beam walking test and Dr. Liu Yang for guiding the confocal microscopy shooting technique.

Conflict of interest

The authors declare that the research was conducted in the absence of any commercial or financial relationships that could be construed as a potential conflict of interest.

Publisher's note

All claims expressed in this article are solely those of the authors and do not necessarily represent those of their affiliated organizations, or those of the publisher, the editors and the reviewers. Any product that may be evaluated in this article, or claim that may be made by its manufacturer, is not guaranteed or endorsed by the publisher.

References

Bello-Medina, P. C., Flores, G., Quirarte, G. L., Mcgaugh, J. L., and Prado Alcala, R. A. (2016). Mushroom spine dynamics in medium spiny neurons of dorsal striatum associated with memory of moderate and intense training. *Proc. Natl. Acad. Sci. U.S.A.* 113, E6516–E6525. doi: 10.1073/pnas.1613680113

Bian, W. J., Miao, W. Y., He, S. J., Qiu, Z., and Yu, X. (2015). Coordinated spine pruning and maturation mediated by inter-spine competition for cadherin/catenin complexes. *Cell* 162, 808–822. doi: 10.1016/j.cell.2015.07.018

Bourne, J., and Harris, K. M. (2007). Do thin spines learn to be mushroom spines that remember? *Curr. Opin. Neurobiol.* 17, 381–386. doi: 10.1016/j.conb.2007.04.009

Briner, A., De Roo, M., Dayer, A., Muller, D., Habre, W., and Vutskits, L. (2010). Volatile anesthetics rapidly increase dendritic spine density in the rat medial prefrontal cortex during synaptogenesis. *Anesthesiology* 112, 546–556. doi: 10.1097/ALN.0b013e3181cd7942

Campolo, M., Casili, G., Lanza, M., Filippone, A., Cordaro, M., Ardizzone, A., et al. (2021). The inhibition of mammalian target of rapamycin (mtor) in improving inflammatory response after traumatic brain injury. *J. Cell. Mol. Med.* 25, 7855–7866.

Chen, K., Zhu, L., Guo, L., Pan, Y. B., and Feng, D. F. (2020). Maf1 regulates dendritic morphogenesis and influences learning and memory. *Cell Death Dis.* 11:606. doi: 10.1038/s41419-020-02809-y

Cordaro, M., Paterniti, I., Siracusa, R., Impellizzeri, D., Esposito, E., and Cuzzocrea, S. (2017). Ku0063794, a dual mtorc1 and mtorc2 inhibitor, reduces neural tissue damage and locomotor impairment after spinal cord injury in mice. *Mol. Neurobiol.* 54, 2415–2427. doi: 10.1007/s12035-016-9827-0

Dall'oglio, A., Dutra, A. C., Moreira, J. E., and Rasia-Filho, A. A. (2015). The human medial amygdala: Structure, diversity, and complexity of dendritic spines. *J. Anat.* 227, 440–459. doi: 10.1111/joa.12358

Davidson, A. J., and Sun, L. S. (2018). Clinical evidence for any effect of anesthesia on the developing brain. *Anesthesiology* 128, 840–853.

Du, F. (2019). Golgi-cox staining of neuronal dendrites and dendritic spines with FD rapid golgiStain kit. *Curr. Protoc. Neurosci.* 88:e69.

Fiala, J. C., Feinberg, M., Popov, V., and Harris, K. M. (1998). Synaptogenesis via dendritic filopodia in developing hippocampal area Ca1. *J. Neurosci.* 18, 8900–8911. doi: 10.1523/JNEUROSCI.18-21-08900.1998

Flick, R. P., Katusic, S. K., Colligan, R. C., Wilder, R. T., Voigt, R. G., Olson, M. D., et al. (2011). Cognitive and behavioral outcomes after early exposure to anesthesia and surgery. *Pediatrics* 128, e1053–e1061.

Garcia-Martinez, J. M., Moran, J., Clarke, R. G., Gray, A., Cosulich, S. C., Chresta, C. M., et al. (2009). Ku-0063794 is a specific inhibitor of the mammalian target of rapamycin (mtor). *Biochem. J.* 421, 29–42.

Gilbert, J., and Man, H. Y. (2017). Fundamental elements in autism: From neurogenesis and neurite growth to synaptic plasticity. *Front. Cell. Neurosci.* 11:359. doi: 10.3389/fncel.2017.00359

Gonzalez-Burgos, I., Gonzalez-Tapia, D., Zamora, D. A., Feria-Velasco, A., and Beas-Zarate, C. (2011). Guided motor training induces dendritic spine plastic changes in adult rat cerebellar purkinje cells. *Neurosci. Lett.* 491, 216–220. doi: 10.1016/j.neulet.2011.01.043

Guan, J., Harris, P., Brimble, M., Lei, Y., Lu, J., Yang, Y., et al. (2015). The role for Igf-1-derived small neuropeptides as a therapeutic target for neurological disorders. *Expert Opin. Ther. Targets* 19, 785–793. doi: 10.1517/14728222.2015.1010514

Harris, K. M., Jensen, F. E., and Tsao, B. (1992). Three-dimensional structure of dendritic spines and synapses in rat hippocampus (Ca1) at postnatal day 15 and adult ages: Implications for the maturation of synaptic physiology and long-term potentiation. *J. Neurosci.* 12, 2685–2705. doi: 10.1523/JNEUROSCI.12-07-02685.1992

He, H., Liu, W., Zhou, Y., Liu, Y., Weng, P., Li, Y., et al. (2018). Sevoflurane post-conditioning attenuates traumatic brain injury-induced neuronal apoptosis by promoting autophagy via the Pi3K/Akt signaling pathway. *Drug Des. Dev. Ther.* 12, 629–638. doi: 10.2147/DDDT.S158313

Ikonomidou, C., Kirvassilis, G., Swiney, B. S., Wang, S. H., Huffman, J. N., Williams, S. L., et al. (2019). Mild hypothermia ameliorates anesthesia toxicity in the neonatal macaque brain. *Neurobiol. Dis.* 130:104489. doi: 10.1016/j.nbd.2019.104489

Ing, C. H., Dimaggio, C. J., Whitehouse, A. J., Hegarty, M. K., Sun, M., Von Ungern-Sternberg, B. S., et al. (2014). Neurodevelopmental outcomes after initial childhood anesthetic exposure between ages 3 and 10 years. *J. Neurosurg. Anesthesiol.* 26, 377–386. doi: 10.1097/ANA.0000000000000121

Jaworski, J., and Sheng, M. (2006). The growing role of mtor in neuronal development and plasticity. *Mol. Neurobiol.* 34, 205–219.

Kalkman, C. J., Peelen, L., Moons, K. G., Veenhuizen, M., Bruens, M., Sinnema, G., et al. (2009). Behavior and development in children and age at the time of first anesthetic exposure. *Anesthesiology* 110, 805–812.

Kim, K. Y., Park, K. I., Kim, S. H., Yu, S. N., Park, S. G., Kim, Y. W., et al. (2017). Inhibition of autophagy promotes salinomycin-induced apoptosis via reactive oxygen species-mediated Pi3K/Akt/mtor and Erk/p38 Mapk-dependent signaling in human prostate cancer cells. *Int. J. Mol. Sci.* 18:1088. doi: 10.3390/ijms18051088

Kumar, V., Zhang, M. X., Swank, M. W., Kunz, J., and Wu, G. Y. (2005). Regulation of dendritic morphogenesis by Ras-Pi3K-Akt-mtor and Ras-Mapk signaling pathways. *J. Neurosci.* 25, 11288–11299. doi: 10.1523/JNEUROSCI.2284-05.2005

Lee, C. C., Huang, C. C., and Hsu, K. S. (2011). Insulin promotes dendritic spine and synapse formation by the Pi3K/Akt/mtor and Rac1 signaling pathways. *Neuropharmacology* 61, 867–879. doi: 10.1016/j.neuropharm.2011.06.003

Liao, Z., Huang, Z., Li, J., Li, H., Miao, L., Liu, Y., et al. (2021). Regulation of Crmp2 by Cdk5 and Gsk-3beta participates in sevoflurane-induced dendritic development abnormalities and cognitive dysfunction in developing rats. *Toxicol. Lett.* 341, 68–79. doi: 10.1016/j.toxlet.2021.01.023

Liu, B., Ou, G., Chen, Y., and Zhang, J. (2019). Inhibition of protein tyrosine phosphatase 1B protects against sevoflurane-induced neurotoxicity mediated by ER stress in developing brain. *Brain Res. Bull.* 146, 28–39. doi: 10.1016/j.brainresbull.2018.12.006

Lu, Y., Huang, Y., Jiang, J., Hu, R., Yang, Y., Jiang, H., et al. (2016). Neuronal apoptosis may not contribute to the long-term cognitive dysfunction induced by a brief exposure to 2% sevoflurane in developing rats. *Biomed. Pharmacother.* 78, 322–328.

Luong, T. N., Carlisle, H. J., Southwell, A., and Patterson, P. H. (2011). Assessment of motor balance and coordination in mice using the balance beam. *J. Vis. Exp.* 10:2376.

Minkeviciene, R., Hlushchenko, I., Virenque, A., Lahti, L., Khanal, P., Rauramaa, T., et al. (2019). Mim-deficient mice exhibit anatomical changes in dendritic spines, cortex volume and brain ventricles, and functional changes in motor coordination and learning. *Front. Mol. Neurosci.* 12:276. doi: 10.3389/fnmol.2019.00276

Nishijima, T., Piriz, J., Duflot, S., Fernandez, A. M., Gaitan, G., Gomez-Pinedo, U., et al. (2010). Neuronal activity drives localized blood-brain-barrier transport of serum insulin-like growth factor-I into the Cns. *Neuron* 67, 834–846. doi: 10.1016/j.neuron.2010.08.007

Pallas-Bazarra, N., Jurado-Arjona, J., Navarrete, M., Esteban, J. A., Hernandez, F., Avila, J., et al. (2016). Novel function of Tau in regulating the effects of external stimuli on adult hippocampal neurogenesis. *EMBO J.* 35, 1417–1436. doi: 10.15252/embj.201593518

Psaty, B. M., Platt, R., and Altman, R. B. (2015). Neurotoxicity of generic anesthesia agents in infants and children: An orphan research question in search of a sponsor. *JAMA* 313, 1515–1516. doi: 10.1001/jama.2015.1149

Qiu, L., Zhu, C., Bodogan, T., Gomez-Galan, M., Zhang, Y., Zhou, K., et al. (2016). Acute and long-term effects of brief sevoflurane anesthesia during the early postnatal period in rats. *Toxicol. Sci.* 149, 121–133. doi: 10.1093/toxsci/kfv219

Rasia-Filho, A. A., Fabian, C., Rigoti, K. M., and Achaval, M. (2004). Influence of sex, estrous cycle and motherhood on dendritic spine density in the rat medial amygdala revealed by the Golgi method. *Neuroscience* 126, 839–847. doi: 10.1016/j.neuroscience.2004.04.009

Rogers, D. C., Peters, J., Martin, J. E., Ball, S., Nicholson, S. J., Witherden, A. S., et al. (2001). Shirpa, a protocol for behavioral assessment: Validation for longitudinal study of neurological dysfunction in mice. *Neurosci. Lett.* 306, 89–92. doi: 10.1016/s0304-3940(01)01885-7

Satomoto, M., Satoh, Y., Terui, K., Miyao, H., Takishima, K., Ito, M., et al. (2009). Neonatal exposure to sevoflurane induces abnormal social behaviors and deficits in fear conditioning in mice. *Anesthesiology* 110, 628–637.

Sharma, A., and Mehan, S. (2021). Targeting Pi3K-Akt/mtor signaling in the prevention of autism. *Neurochem. Int.* 147:105067.

Sprung, J., Flick, R. P., Katusic, S. K., Colligan, R. C., Barbaresi, W. J., Bojanic, K., et al. (2012). Attention-deficit/hyperactivity disorder after early exposure to procedures requiring general anesthesia. *Mayo Clin. Proc.* 87, 120–129. doi: 10.1016/j.mayocp.2011.11.008

Stratmann, G., Lee, J., Sall, J. W., Lee, B. H., Alvi, R. S., Shih, J., et al. (2014). Effect of general anesthesia in infancy on long-term recognition memory in humans and rats. *Neuropsychopharmacology* 39, 2275–2287. doi: 10.1038/npp.2014.134

Sun, L. (2010). Early childhood general anaesthesia exposure and neurocognitive development. *Br. J. Anaesth.* 105(Suppl. 1), i61–i68.

Sun, L. S., Li, G., Miller, T. L., Salorio, C., Byrne, M. W., Bellinger, D. C., et al. (2016). Association between a single general anesthesia exposure before age 36 months and neurocognitive outcomes in later childhood. *JAMA* 315, 2312–2320. doi: 10.1001/jama.2016.6967

Tang, G., Gudsnuk, K., Kuo, S. H., Cotrina, M. L., Rosoklija, G., Sosunov, A., et al. (2014). Loss of mtor-dependent macroautophagy causes autistic-like synaptic pruning deficits. *Neuron* 83, 1131–1143. doi: 10.1016/j.neuron.2014.07.040

Tao, G., Zhang, J., Zhang, L., Dong, Y., Yu, B., Crosby, G., et al. (2014). Sevoflurane induces tau phosphorylation and glycogen synthase kinase 3beta activation in young mice. *Anesthesiology* 121, 510–527. doi: 10.1097/ALN.0000000000000278

Vutskits, L., and Xie, Z. (2016). Lasting impact of general anaesthesia on the brain: Mechanisms and relevance. *Nat. Rev. Neurosci.* 17, 705–717. doi: 10.1038/nrn.2016.128

Wang, W. Y., Yang, R., Hu, S. F., Wang, H., Ma, Z. W., and Lu, Y. (2013). N-stearoyl-L-tyrosine ameliorates sevoflurane induced neuroapoptosis via Mek/Erk1/2 Mapk signaling pathway in the developing brain. *Neurosci. Lett.* 541, 167–172. doi: 10.1016/j.neulet.2013.02.041

Wilder, R. T., Flick, R. P., Sprung, J., Katusic, S. K., Barbaresi, W. J., Mickelson, C., et al. (2009). Early exposure to anesthesia and learning disabilities in a population-based birth cohort. *Anesthesiology* 110, 796–804. doi: 10.1097/01.anes.0000344728.34332.5d

Yang, W., Liu, Y., Xu, Q. Q., Xian, Y. F., and Lin, Z. X. (2020). Sulforaphene ameliorates neuroinflammation and hyperphosphorylated tau protein via regulating the Pi3K/Akt/Gsk-3beta pathway in experimental models of Alzheimer's disease. *Oxid. Med. Cell. Longev.* 2020:4754195. doi: 10.1155/2020/4754195

Yuan, Z. F., Mao, S. S., Shen, J., Jiang, L. H., Xu, L., Xu, J. L., et al. (2020). Insulin-like growth factor-1 down-regulates the phosphorylation of Fxyd1 and rescues behavioral deficits in a mouse model of rett syndrome. *Front. Neurosci.* 14:20. doi: 10.3389/fnins.2020.00020

Yuste, R., and Majewska, A. (2001). On the function of dendritic spines. *Neuroscientist* 7, 387–395.

Zaccariello, M. J., Frank, R. D., Lee, M., Kirsch, A. C., Schroeder, D. R., Hanson, A. C., et al. (2019). Patterns of neuropsychological changes after general anaesthesia in young children: Secondary analysis of the mayo anesthesia safety in kids study. *Br. J. Anaesth.* 122, 671–681. doi: 10.1016/j.bja.2019.01.022

Zancan, M., Da Cunha, R. S. R., Schroeder, F., Xavier, L. L., and Rasia-Filho, A. A. (2018). Remodeling of the number and structure of dendritic spines in the medial amygdala: From prepubertal sexual dimorphism to puberty and effect of sexual experience in male rats. *Eur. J. Neurosci.* 48, 1851–1865. doi: 10.1111/ejn.14052

Zhao, S., Fan, Z., Hu, J., Zhu, Y., Lin, C., Shen, T., et al. (2020). The differential effects of isoflurane and sevoflurane on neonatal mice. *Sci. Rep.* 10:19345. doi: 10.1038/s41598-020-76147-6

Zhou, H., Li, S., Niu, X., Wang, P., Wang, J., and Zhang, M. (2013). Protective effect of Fty720 against sevoflurane-induced developmental neurotoxicity in rats. *Cell Biochem. Biophys.* 67, 591–598. doi: 10.1007/s12013-013-9546-3

Zhu, X., Yao, Y., Guo, M., Li, J., Yang, P., Xu, H., et al. (2021). Sevoflurane increases intracellular calcium to induce mitochondrial injury and neuroapoptosis. *Toxicol. Lett.* 336, 11–20. doi: 10.1016/j.toxlet.2020.11.002

Zou, X., Patterson, T. A., Sadovova, N., Twaddle, N. C., Doerge, D. R., Zhang, X., et al. (2009). Potential neurotoxicity of ketamine in the developing rat brain. *Toxicol. Sci.* 108, 149–158.

frontiers | Frontiers in Aging Neuroscience

TYPE Original Research
PUBLISHED 20 October 2022
DOI 10.3389/fnagi.2022.990679

OPEN ACCESS

EDITED BY
Yingwei Wang,
Huashan Hospital of Fudan University, China

REVIEWED BY
Fuzhou Hua,
Second Affiliated Hospital of Nanchang University, China
Lei Zhang,
Shanghai Jiao Tong University, China

*CORRESPONDENCE
Qiujun Wang
wangqiujunsy@163.com

SPECIALTY SECTION
This article was submitted to Neurocognitive Aging and Behavior, a section of the Frontiers in Aging Neuroscience

RECEIVED 10 July 2022
ACCEPTED 07 October 2022
PUBLISHED 20 October 2022

CITATION
Zhang Q, Li Y, Wang X, Yin C, Zhou Q, Guo J, Zhao J, Xian X, Hou Z and Wang Q (2022) Sevoflurane exposure causes neuronal apoptosis and cognitive dysfunction by inducing ER stress *via* activation of the inositol 1, 4, 5-trisphosphate receptor. *Front. Aging Neurosci.* 14:990679. doi: 10.3389/fnagi.2022.990679

Sevoflurane exposure causes neuronal apoptosis and cognitive dysfunction by inducing ER stress *via* activation of the inositol 1, 4, 5-trisphosphate receptor

Qi Zhang[1], Yanan Li[2], Xupeng Wang[2], Chunping Yin[2], Qi Zhou[2], Junfei Guo[3], Juan Zhao[4], Xiaohui Xian[5], Zhiyong Hou[3] and Qiujun Wang[2]*

[1]Department of Anesthesiology, Children's Hospital of Hebei Province Affiliated to Hebei Medical University, Shijiazhuang, China, [2]Department of Anesthesiology, The Third Hospital of Hebei Medical University, Shijiazhuang, China, [3]Department of Orthopaedics, The Third Hospital of Hebei Medical University, Shijiazhuang, China, [4]Experimental Centre for Teaching, Hebei Medical University, Shijiazhuang, China, [5]Department of Pathophysiology, Hebei Medical University, Shijiazhuang, China

The role of the inositol 1, 4, 5-trisphosphate receptor (IP3R) in hippocampal neuronal apoptosis and cognitive dysfunction induced by sevoflurane is currently unclear. Therefore, in this study, we investigated the role of the IP3R in endoplasmic reticulum (ER) stress and hippocampal neuronal apoptosis induced by sevoflurane in aged rats and isolated hippocampal neurons using both *in vivo* and *in vitro* experiments, including bioinformatics, functional enrichment analysis, gene set enrichment analysis, hematoxylin, and eosin staining, TUNEL assay, flow cytometry, western blot analysis and transmission electron microscopy. Furthermore, behavioral assessment was performed with the Morris water maze test. We identified 232 differentially expressed genes induced by sevoflurane exposure, including 126 upregulated genes and 106 downregulated genes. Sevoflurane exposure caused cognitive impairment and neuronal injury, and increased p-IP3R levels and ER stress. An IP3R inhibitor, 2-APB, suppressed these changes, while an IP3R agonist, FK-506, aggravated these changes. Together, these findings suggest that sevoflurane exposure causes marked cognitive dysfunction in aged rats and neuronal injury in isolated hippocampal neurons by activating the IP3R and inducing cytoplasmic calcium overload, thereby resulting in ER stress and hippocampal neuronal apoptosis.

KEYWORDS

sevoflurane, cognitive dysfunction, IP3R, neuroapoptosis, calcium

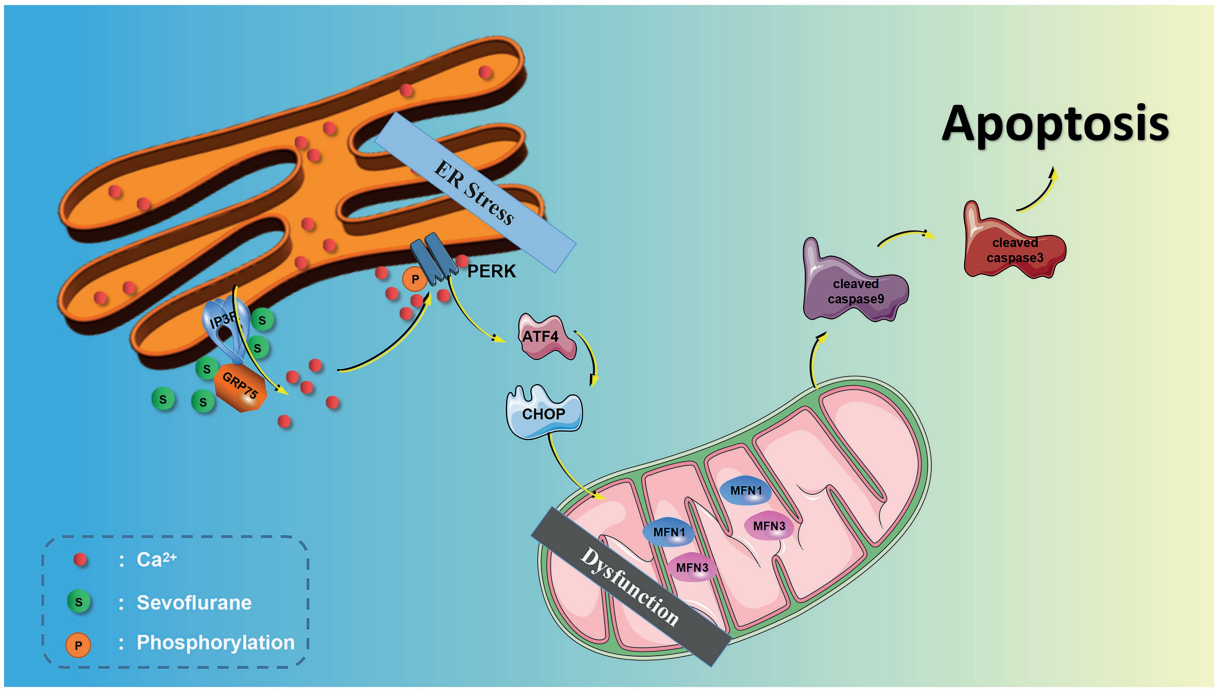

GRAPHICAL ABSTRACT

Introduction

Postoperative cognitive dysfunction (POCD) refers to the postoperative impairment in cognition, learning, memory, orientation, and psychomotor behavior in patients without preoperative mental disorder after anesthesia and surgery (Gold and Forryan, 2018). The incidence of POCD 7 days after non-cardiac surgery can be as high as 9.1–17% (Evered et al., 2011; Krenk et al., 2014) and it can reduce the quality of life of patients and even increase mortality (Silbert et al., 2014). Accumulating evidence indicates that POCD is associated with two main risk factors: anesthesia and aging and sevoflurane inhalation could induce neurotoxicity and neurocognitive decline in elderly patients with POCD (Miller et al., 2018; Wang et al., 2018). POCD, however, still lacks a clear understanding of its underlying mechanisms (Chen et al., 2020; Ge et al., 2021; Wang et al., 2021). Therefore, a better understanding of the molecular mechanisms of POCD caused by sevoflurane is urgently needed.

Although the mechanisms underlying sevoflurane neurotoxicity are unclear, numerous studies have shown that neuroinflammation, calcium imbalance, neuronal apoptosis, and an increase in oxidative stress are closely related to sevoflurane-induced cognitive impairment (Ma et al., 2016; Chen et al., 2020; Wang et al., 2021). As a major intracellular messenger, calcium is involved in regulating the physiological activities of many cells and tissues, including muscle contraction, metabolism and cell division. In the resting physiological state, calcium ions are maintained at relatively high concentrations outside the cell and low concentrations inside the cell through homeostatic flux (Kumar, 2020; Sahu and Turner, 2021). When cells are stimulated, this calcium homeostasis is broken, and cytoplasmic calcium ($[Ca^{2+}]c$) levels increase instantaneously, inducing cell damage or death, such as apoptosis and necroptosis under certain circumstances (Cheng et al., 2022; Matuz-Mares et al., 2022). Qiu LL et al. (Qiu et al., 2020) showed dysregulation of BDNF/TrkB signaling mediated by NMDAR/Ca^{2+}/calpain caused by anesthesia/surgery might contribute to POCD in aging mice. Our previous studies showed that sevoflurane causes learning and memory deficits in rats by inducing neuroapoptosis by increasing $[Ca^{2+}]c$ and calcium pathway proteins such as calcineurin and calpain. Furthermore, we showed that inhibition of calcium overload alleviates the cognitive impairment induced by sevoflurane (Liu et al., 2016; Wang et al., 2021).

The endoplasmic reticulum (ER) is extremely sensitive to alterations in the intracellular environment, and cytoplasmic Ca^{2+} overload and oxidative stress caused by external stimuli will lead to ER dysfunction and trigger ER stress processes (Hotamisligil and Davis, 2016; Di Conza and Ho, 2020). The ER stress response can be accompanied by the activation of downstream double-stranded RNA-activated protein kinase-like ER kinase (PERK) and inositol-requiring enzyme-1 (IRE1). The activation of PERK and IRE1 promotes cellular apoptosis. Sevoflurane exposure can induce ER stress and hippocampal neuroapoptosis and cause cognitive impairment in aged and neonatal rats (Liu et al., 2017; Shen et al., 2018). The research from Yang et al. (2008) also suggested Inhalational anesthetics may induce cell damage by

causing abnormal calcium release from the ER *via* excessive activation of IP3 receptors. Isoflurane has greater potency than sevoflurane or desflurane to cause calcium release from the ER and to induce cell damage.

The inositol 1, 4, 5-trisphosphate receptor (IP3R) is one of two calcium channels located on the ER membrane that play an important physiological role in normal cells. IP3R channel activity is regulated by redox status and by phosphorylation by various kinases, such as cAMP-dependent protein kinase (PKA), cGMP-dependent protein kinase (PKG), Ca^{2+}/calmodulin-dependent protein kinase II (CaMKII) and different tyrosine kinases (Berridge, 2016). However, abnormal calcium release from the ER through overactivation of IP3R on the ER membrane may lead to abnormally elevated $[Ca^{2+}]c$, mitochondrial calcium overload, and ER calcium depletion, all of which may lead to cell death (Egorova and Bezprozvanny, 2018; Mangla et al., 2020). We previously showed in isolated hippocampal neurons that the inhaled anesthetics sevoflurane and isoflurane can activate IP3R, increase hippocampal $[Ca^{2+}]c$, and induce neuroapoptosis (Liu et al., 2016). Similarly, some studies have shown that activation of IP3R leads to calcium homeostatic imbalance, which can cause ER stress and induce apoptosis (Li et al., 2009; Yang et al., 2021). However, whether ER stress is involved in IP3R-activation-mediated cytoplasmic calcium disorder and neuroapoptosis induced by sevoflurane remains unknown.

The current evidence suggests that there is an intimate connection between ER stress and perturbed calcium homeostasis caused by IP3R activation in the neurotoxicity of sevoflurane in aged rats. Thus, we hypothesize that sevoflurane first activates IP3 receptors, causing calcium overload in the cytoplasm of hippocampal neurons, and then induces ER stress, causing hippocampal apoptosis and neurotoxicity. In this study, we test this hypothesis using bioinformatics analysis, behavioral experiments and molecular biology experiments, with the aim of clarifying the mechanisms underlying the clinical neurotoxicity of sevoflurane.

Materials and methods

Bioinformatics analysis

From the GENE EXPRESSION OMNIBUS (GEO) database[1], we downloaded the postoperative cognitive impairment-related gene expression dataset (GSE95426). We used the R language limma package for quantile RNA-seq data standardization and to analyze differences in gene expression ($|logFC| < 2$, *value of* $p < 1$). The ggplot2 software package was used to process the GSE95426 dataset to generate a volcano map of differentially expressed genes (DEGs) in R software, and the R software package pheatmap was used to draw the cluster analysis heatmap of the DEGs.

Functional enrichment analysis

The gene ontology (GO) and Kyoto Encyclopedia of Genes and Genomes (KEGG) analyses of the DEGs was conducted for the dataset GSE95426. Using the DAVID online database tools[2], the level of biological processes for DEGs were analyzed by integrating the GO term and network to create the DEGs for a biological process. Ggplot2 and GOplot packages were used to map the GO pathway and enrichment analysis diagram of the KEGG pathway of DEGs in the R linguistic environment.

Gene set enrichment analysis

GSEA[3] was used for enrichment analysis of all genes, and the GSEA pathway was mapped.

Animals and model preparation

Seventy-five healthy male Sprague–Dawley rats, 18 months of age, weighing 550–650 g, were purchased from the Experimental Animal Center of Hebei Medical University (License Number:SCXK2018-004). All animals were placed in a room maintained at a constant temperature and allowed free access to water and food. After a week of adaptive feeding, all rats were randomly divided into the following three groups ($n = 25$ each): Control, Sev, and Sev + 2-APB. Rats in the Sev and Sev + 2-APB groups were placed in an acrylic anesthetizing chamber with two interfaces; one was connected to a sevoflurane vaporizer (Drager, Germany) and the other was connected to a multi-gas monitor (Datex-Ohmeda, United States). The rats were exposed to 2% sevoflurane (Maruishi Pharmaceutical Co., Ltd. Japan) delivered in humidified 30% O_2 carrier gas for 5 h according to our previous study (Yin et al., 2022). Rats in the Control group were exposed to humidified 30% O_2 balanced by N_2 in an acrylic anesthetizing chamber without sevoflurane. 2-APB (Cat# D9754; Sigma-Aldrich, United States), a IP3 receptor antagonist, were dissolved in 10% DMSO. Before anesthesia, 3 mg/kg 2-APB was injected intraperitoneally in Sev + 2-APB group, and the same amount of 10% DMSO was injected into the other two groups according to the previous research (Vaidya et al., 2022; Figure 1). The protocols were approved by the Animal Review Board of Hebei Medical University (Ethical code: 2017–026-1).

1 https://www.ncbi.nlm. nih.gov/gds/

2 https://david.ncifcrf.gov/

3 http://www.gsea-msigdb.org/

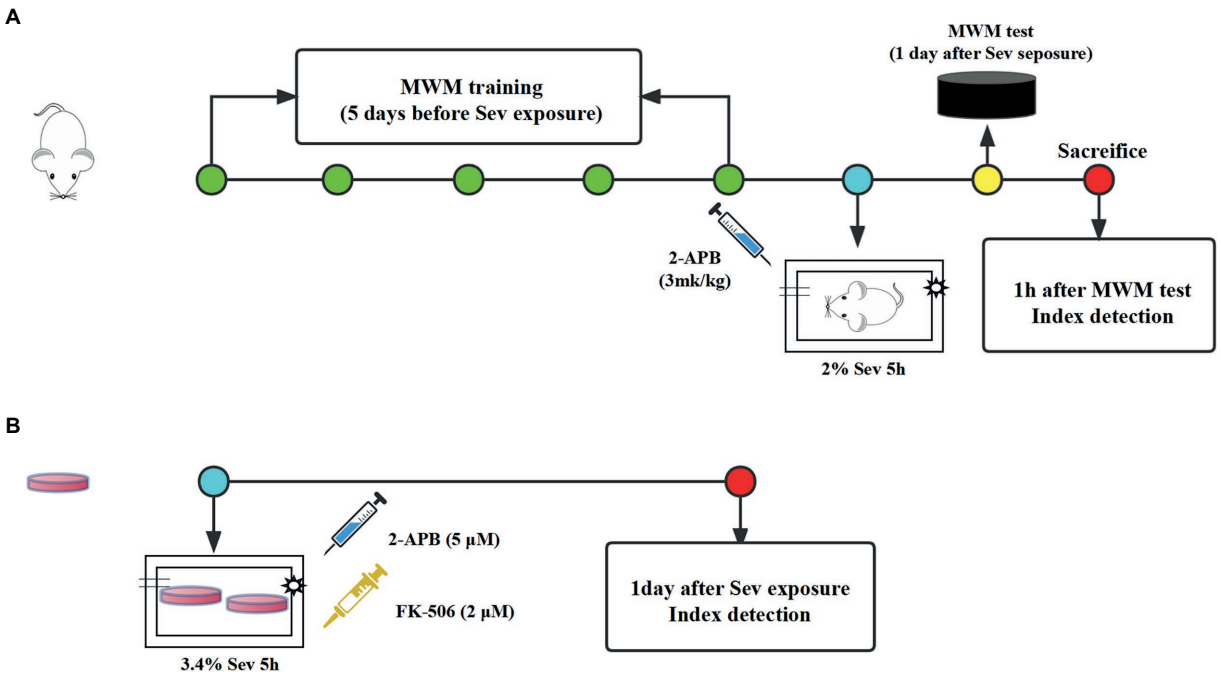

FIGURE1
The experimental schematic diagram. **(A)** Rats received MWM training once a day for 5 days and were exposed to 3% sevoflurane for 2 h at 1 day after the last MWM training. At 1 day after sevoflurane exposure, MWM tests was established to evaluate cognitive function of aged rats, then 1 h after MWM tests, rats were sacrificed for index detection. **(B)** All dishes of hippocampal neurons were exposed to 3.4% sevoflurane for 5 h. At 1day after sevoflurane exposure, all index were detected. MWM, Morris water maze, Sev, sevflurane.

Cell culture and processing

Primary rat hippocampal neurons were obtained from fetal rats for *in vitro* experiments, according to the method described by Patrich et al. (2016). Pregnant rats (16–18 days of gestation) were purchased from the Experimental Animal Center of Hebei Medical University (License Number: SCXK2018-2-003), and the fetal rats were taken by laparotomy immediately after deep anesthesia. The fetuses were placed in precooled equilibrium solution, decapitated, and the brain tissue was removed and placed in an ice-cold petri dish containing DMEM/F12. The hippocampal tissue was separated under an anatomical microscope, cut into 1 × 1 × 1 mm pieces, placed in a centrifuge tube, topped with 0.25% trypsin (HyClone, United States) of equal volume, and placed in a CO_2 incubator at a constant temperature of 37°C. The centrifuge tube was shaken once every 3 min. After digestion for 10 min, an equal volume of DMEM containing 20% fetal bovine serum (Gibco, United States) was added to the centrifuge tube to terminate the trypsin reaction. After centrifugation, the supernatant was removed, the pellet was resuspended and filtered to collect the cells, and the morphology of neurons was observed under an inverted microscope and analyzed with the EVOS imaging system (EVOS M7000, Thermo Fisher Scientific, United States). If the neuronal cell bodies were plump and distinct, and the processes formed a dense network, the cells were included in the study. Hippocampal neurons were plated onto culture dishes pre-coated with 5 μg/mL poly-L-lysine at a density of 5×10^5/mL, 2,000 μl/well. Then, 24 h later, the medium was replaced with medium for hippocampal neurons [Neurobasal +3% B27], and half of the medium was replaced twice a week. On day 7 of culture, histochemistry for the microtubule-associated protein MAP2 and DAPI was used to identify neurons. The neurons had plump cell bodies and processes that formed a dense network, with a purity of >95%, and therefore were used in subsequent experiments. All cultures of hippocampal neurons were divided into the following four groups: Control, Sev, Sev + 2APB, and Sev + FK-506. Each group of dishes was placed in an anesthesia induction chamber maintained at 37°C (RWD Life Science Co., Ltd., Shenzhen, China) containing fresh gas (21% O_2, 5% CO_2 and 69% N_2) (Control group) or with the addition of 3.4% sevoflurane for 5 h (Sev, Sev + 2APB, Sev + FK-506 group) according to the previous study (Xu et al., 2018). A steady level of 3.4% sevoflurane was maintained at a gas flow rate of 1 l/min, measured with a multi-gas monitor (Datex-Ohmeda). Then, 1 h before sevoflurane exposure, 2-APB (cell permeable IP3R inhibitor, 5 μM) and FK-506 (activator of IP3R, 2 μM) were added into the culture medium in the Sev + 2APB and Sev + FK-506 groups, respectively, according to the method described by Fujii (Fujii et al., 2016; Figure 1). 2-APB and FK-506 were obtained from Sigma-Aldrich.

Morris water maze test

The memory and learning ability were evaluated by MWM test. For the MWM experiment, we used an indoor stainless steel drum (1,500 mm in diameter and 500 mm in height), with a black inner surface, filled with warm water (24–26°C). The water in the pool was made opaque after adding nontoxic black ink, which was then divided into 4 quadrants: I, II III, and IV, and in the middle part of quadrant IV,a circular platform of 12 cm in diameter and 30 cm in height was positioned at 2 cm below the surface of the water. In addition, the reference substance and the room lights were maintained around the pool. The spatial acquisition experiment was conducted on all animals for 5 consecutive days before sevoflurane exposure. During training period, rats were dropped into the water at four different starting positions facing the wall, then guided to board the platform and remain on it for 15 s if they failed within 120 s. Cleaning the pool every day after training eliminated the smell prompt. The rats trained for four sessions per day. According to our previous study (Yin et al., 2022), 24 h after sevoflurane exposure, the learning and memory ability was tested using the positional navigation experiment. The time from entering the water to finding the hidden platform in the contralateral quadrant was recorded. Then, the platform was removed, and spatial memory ability was evaluated positioning navigation experiment and space exploration experiment. The number of crossings of the platform, the time spent in the target quadrant and swimming speed were recorded.

Hematoxylin and eosin staining

At 1 h after the MWM test, five mice from each group were sacrificed, and brain tissues were collected and rinsed with phosphate buffer solution. The tissues were then immersed in 4% paraformaldehyde for 24 h. Subsequently, the samples were dehydrated and embedded in paraffin wax. The paraffin-embedded coronal brain sections (5 μM) containing the hippocampus were cut and HE-stained. The pathological changes in the hippocampus were examined by optical microscopy.

TUNEL assay

At 1 h after the MWM test, five aged mice from each group were sacrificed, the brain tissues were removed and embedded in OCT medium, and then placed in the −80°C freezer. Frozen sections at a thickness of 10 μM were fixed with 4% paraformaldehyde for 30 min, rinsed with phosphate-buffered saline (PBS), fixed and treated with 3% BSA + 0.3% Triton X-100 for 1 h, and then TUNEL-stained. Briefly, after treatment with protease solution, the sections were incubated with equilibration buffer for 10 min, followed by incubation with the terminal DNA transferase reaction mixture containing fluorescent-labeled substrate at 37°C for 1 h in the dark. Finally, anti-fade solution containing DAPI was added. The number of apoptotic cells was counted with Image J software under the fluorescence microscope.

Measurement of hippocampal $[Ca^{2+}]_c$ and apoptosis rate

The hippocampus tissues from each group ($n = 5$) were harvested 1 h after the MWM test and prepared into cell suspensions, as previously described (Liu et al., 2016; Zhang et al., 2018). A 200-mesh nylon sieve was employed for filtration of the hippocampal tissues (1 g), followed by centrifugation at 1310 × g for 5 min at 4°C and removal of the supernatant (n = 5). The cells were then washed twice with PBS and centrifuged to prepare single cell suspensions at a concentration of 1 × 105/mL. Subsequently, the single cell suspension was incubated with 5 μmol/l Fura-3 AM (Solarbio, IF0150) at 37°C for 30 min. After washing twice, cells were re-suspended in PBS at 37°C for 15 min. Flow cytometry was performed to measure fluorescence intensity, with an excitation wavelength of 480 nm and an emission wavelength of 525 nm. The fluorescence intensity reflects the concentration of intracellular calcium.

The cell suspension was prepared by the same method as above, resuspending the cells in 500 μl of 1 × binding buffer after centrifugation. Subsequently, added 5 μL of 20 μg/mL Annexin V-FITC and 10 μL of 50 mg/mL PI (Invitrogen, 282,932–000), incubated at room temperature for 10 min in the dark. The cells were washed and analyzed by FACS Calibur (Becton, Dickinson Company, United States). The percentages of cells in each quadrant were analyzed by FACS Calibur (FC500; Beckman Coulter Inc.) using ModFit software (EXPO32 ADC v1.2; Beckman Coulter Inc.). The apoptosis rate was detected by calculating the (Annexin V-FITC)+/PI+ and (Annexin V-FITC)-/PI+ cells numbers.

Ultrastructure of hippocampal neurons

Hippocampal tissues from the CA1 region from each group ($n = 5$) were collected (approximately 1 mm × 1 mm × 3 mm), fixed with 4% glutaraldehyde and 1% osmium tetroxide, dehydrated through a series of ethanol solutions, and then embedded in epoxy resin and double stained with uranyl acetate and lead citrate. The ultrastructure of hippocampal neurons was observed under a transmission electron microscope (H-7500, Hitachi, Japan).

Western blot

Total protein extraction was performed using the Whole Cell and Tissue Protein Extraction Kit (Thermo Fisher Scientific, United States) according to the manufacturer's protocol ($n = 5$). Protein concentrations were measured using the BCA Protein Assay Kit (A53225, Thermo Fisher Scientific). The proteins were separated by 10% SDS-PAGE and transferred onto a PVDF membrane. After

blocking with 5% skim milk powder for 2 h, the membrane was incubated overnight with primary antibody [p-IP3R (ab111615), total-IP3R (ab264281), MFN1 (ab221661), MFN2 (ab260861), GRP75 (ab171089), p-PERK (ab192591), ATF4 (ab184909), CHOP (ab11419), cleaved caspase-3 (ab32042), cleaved caspase-9 (ab184786), Bax (ab32503) and Bcl-2 (ab32124) were purchased from Abcam and diluted to 1: 1,000 before use). In this study, β-actin (ab8226, 1: 2000) served as the internal reference protein. After washing, the membrane was incubated with secondary antibody for 2 h. The ultra-sensitive chemiluminescent liquid-based FujiFilm LAS 4000 imaging analyzer (FujiFilm, Tokyo, Japan) was used for visualization, and Image J (NIH, Bethesda, MD, United States) was used to analyze the relative intensities of individual bands.

Immunohistochemistry

The brain was prepared as described in Method 2.3, sliced into 15 mm sections on a cryostat, blocked in PBS containing 1% goat serum and 0.1% Triton-X 100, and incubated at 4°C overnight with anti-p-IP3R (ab111615). After washing, a streptavidin horseradish peroxidase (HRP) complex (1: 1000; Dako) was applied for 1 h. Color development was performed with a diaminobenzidine peroxidase substrate kit (Vector Labs, Burlingame, CA, United States). Sections were counterstained with hematoxylin or eosin. The sections were observed and photographed under an inverted light microscope, and the positive cell rate was calculated by Image Pro Plus 6.0 software (Media Cybernetics, Inc., Rockville, MD, United States).

Statistical analysis

SPSS 21.0 software was used for statistical analysis. The data meet normal distribution were expressed as mean ± standard deviation, and differences between groups were assessed by one-way analysis of variance (ANOVA), followed by the Turkey multiple comparison analysis. $p < 0.05$ indicated that the difference was statistically significant.

Results

Screening of differentially expressed genes

To analyze gene expression differences of sevoflurane's neurotoxicity, the dataset GSE95426 was downloaded from the GEO database, and quantile standardization was performed on the data. With *value of p* <0.05 and |logFC| <2 as criteria for screening GSE95426, a total of 232 DEGs were retrieved, among which 126 were upregulated and 106 were downregulated. The ggplot2 software package was used to construct the visual group DEG volcano map of GSE95426 in R software (Figure 2), and the R software package pheatmap was used to draw the cluster analysis heatmap of the DEGs (Figure 2).

Results of bioinformatics analysis

Functional enrichment analysis of DEGs were performed by GO and KEGG enrichment analyses. Using DAVID online database tools (see text footnote 2), thelevelofbiological processes for DEGs were analyzed by integrating the GO term and network to identify the DEGs in a biological process. Upregulated and downregulated GO pathway maps of DEGs (Figure 2) were drawn by R language (Figure 2). GO pathway diagram revealed PERK-mediated unfolded protein response and positive regulation of transcription from RNA polymerase II promoter, regulation of cardiac conduction are the top 3 enriched GO terms among the upregulated DEGs, DNA replication, G1/S transition of mitotic cell cycle and DNA replication initiation are the top 3 enriched GO terms among the downregulated DEGs.. DEGs were used to analyze and map the KEGG pathways (Figure 3). From the KEGG pathway map, we found that pathways such as Apoptosis and DNA replication were enriched. In addition, through GSEA, we found that UNFOLDED_PROTEIN_RESPONSE (enrichment score: 0.63, $p<0.001$), MITOCHONDRIAL_ RESPIRATORY_ CHAIN_ COMPLEX_ASSEMBLY (enrichment score: 0.47, $p<0.001$) and APOPTOSIS (enrichmeand nt score: 0.58 $p = 0.001$) were significantly enriched pathways (Figure 3).

Sevoflurane impairs spatial learning and memory abilities in aged rats

The Morris water maze test was carried out to evaluate the cognitive ability of aged rats after sevoflurane exposure. The trajectories of the animals, the number of crossings over the original platform location and the percent time spent in the target quadrant were evaluated in the spatial probe trial. Compared with the Control and Sev + 2-APB groups, the swimming trajectory of the Sev group was more complex, and the time to find the platform was increased (Figure 4A). The escape latency, number of platform crossings and time spent in the target quadrant were significantly decreased in the Sev group compared with the Control group. The escape latency, number of platform crossings and time spent in the target quadrant were increased in the Sev + 2-APB group compared with the Sev group (Figures 4B–D). However, there were no significant differences in swimming speed among the three groups (Figure 4E).

Sevoflurane causes neuronal injury in aged rats

We used HE staining to investigate the Pathological changes of hippocampus after sevoflurane exposure. The results revealed

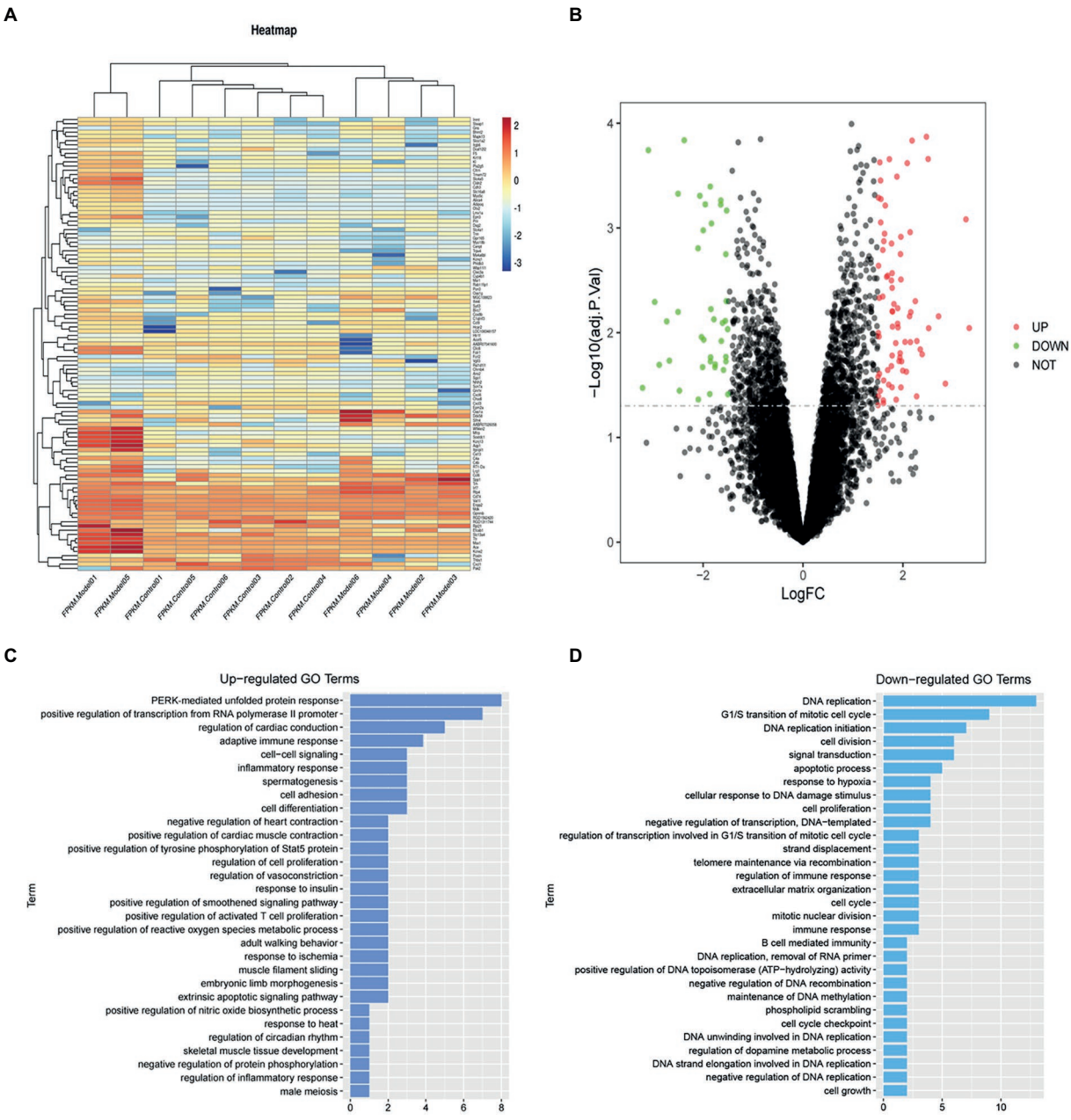

FIGURE 2
(A) Heatmap of differential gene cluster analysis. **(B)** Differential gene volcano map. **(C)** GO enrichment analysis upregulated pathways. **(D)** GO enrichment analysis downregulated pathways.

that neurons in the hippocampal CA1 region were arranged in an orderly manner, with normal morphology, a distinct cell membrane, round nucleus and clear nucleolus in the Control group. Neurons in the hippocampal CA1 region were arranged in a disordered manner, appeared shrunken and degenerated, the nuclear boundary was unclear, the nucleolus was undetectable, and showed signs of interstitial edema in the Sev group. Atrophy and degeneration of neurons and interstitial edema in the hippocampal CA1 region in the Sev+2-APB group were less pronounced compared with the Sev group (Figure 5A).

We used transmission electron microscopy to evaluate hippocampal ultrastructure in the different groups at magnifications of ×3,000 (Figure 5B) and ×8,000 (Figure 5C). The blue arrow shows that the mitochondrial ridge structure is complete, without fracture, indicating the viability of hippocampal neurons. The red arrow indicates that the mitochondrial ridge structure is broken or even absent, and that the mitochondria are pyknotic, indicating the apoptosis of hippocampal neurons. These results demonstrate that compared with the Control group, hippocampal apoptosis

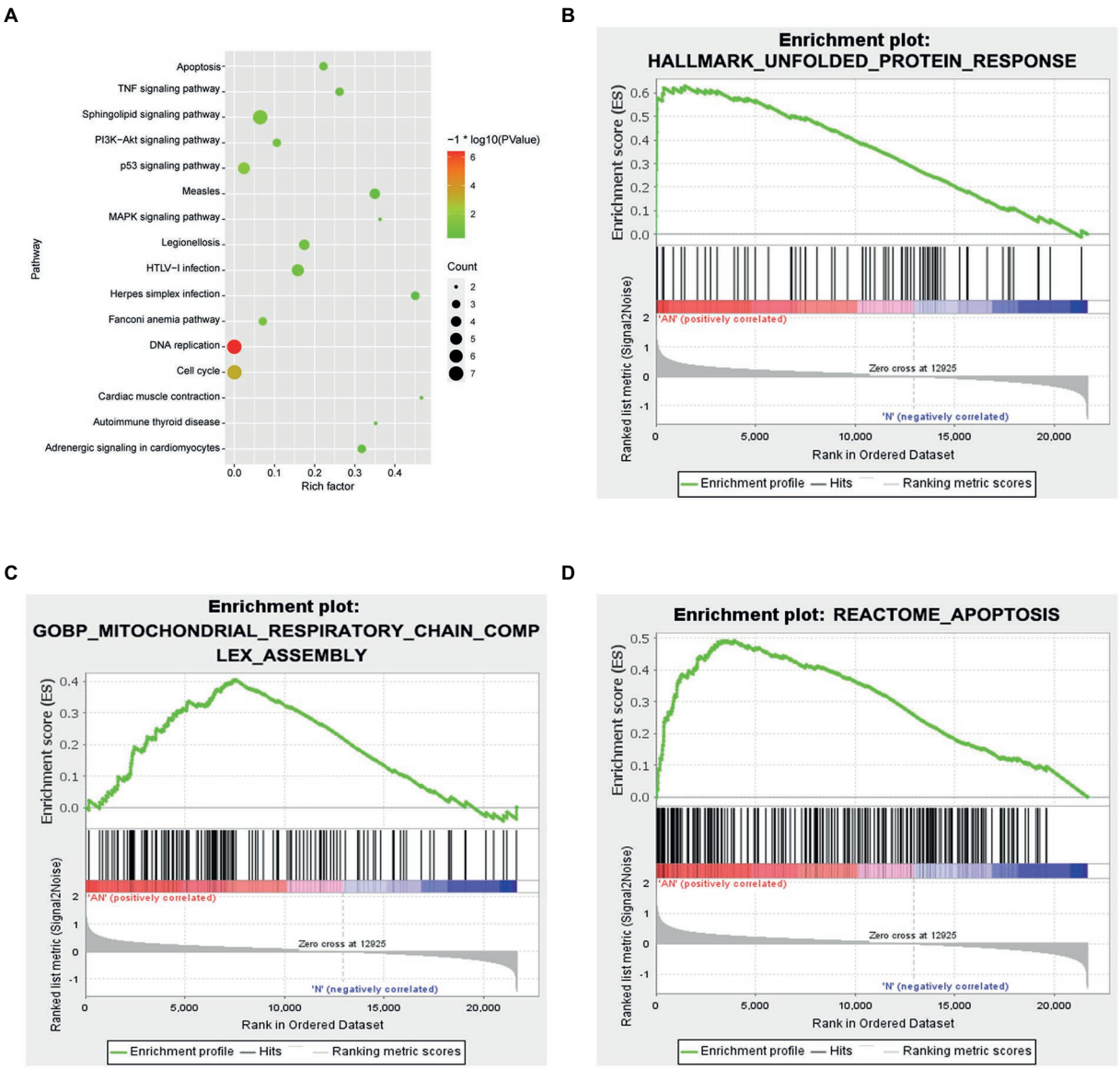

FIGURE 3
(A) KEGG enrichment analysis revealed that pathways such as Apoptosis and DNA replication were enriched. **(B–D)** GSEA gene enrichment analysis revealed that the unfolded protein response, mitochondrial respiratory chain complex assembly and apoptosis pathways were significantly enriched pathways.

caused by mitochondrial damage was significantly increased in the Sev group, and that these pathological changes were ameliorated (less severe) in the Sev + 2-APB group.

Sevoflurane promotes hippocampal neuroapoptosis in aged rats and isolated hippocampal neurons

We used TUNEL staining to assess hippocampal neuroapoptosis in aged rats and flow cytometry (annexin V and PI double staining) to detect apoptosis in isolated hippocampal neurons. The *in vivo* experiments revealed that TUNEL-positive neurons were increased in the Sev group compared with the Control group ($p < 0.01$). In comparison, in the Sev + 2-APB group, the IP3R inhibitor 2-APB decreased the number of TUNEL-positive neurons ($p < 0.01$) (Figures 6A,B). The *in vitro* experiments showed that the apoptosis rate in hippocampal neurons was increased after sevoflurane exposure in the Sev group, compared with the Control group ($p < 0.01$). Compared with the Sev group, hippocampal neurons exhibited a notably reduced rate of apoptosis in the Sev + 2-APB group and an increased apoptosis rate in the Sev + FK-506 group after FK-506 (activator of IP3R) exposure ($p < 0.01$, Figures 6C,D).

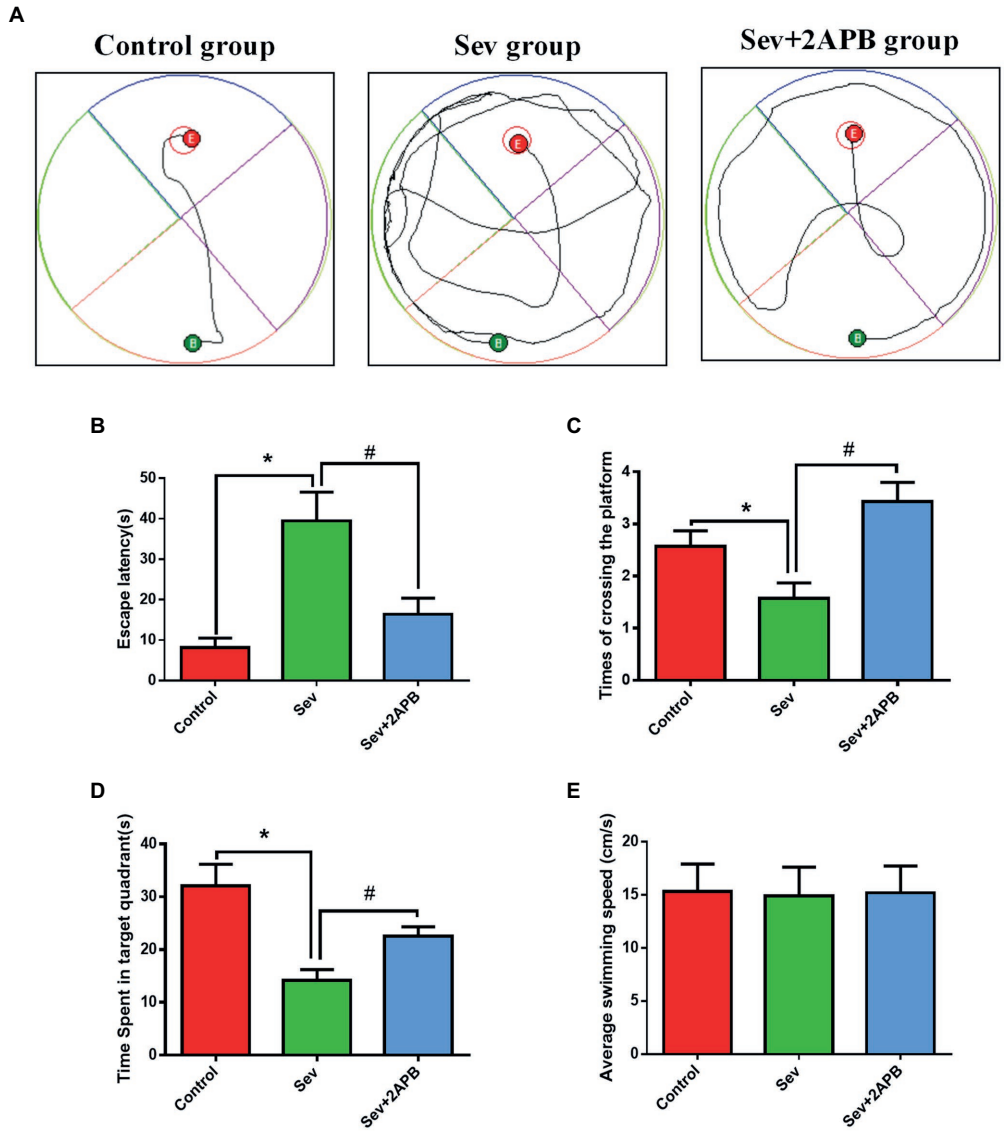

FIGURE 4
Sevoflurane impairs spatial learning and memory abilities in aged rats. (**A**) Swimming trajectory in the spatial exploration experiment. **(B)** Average escape latency. (**C**) Number of crossings of the platform area. (**D**) Time spent in the target quadrant. (**E**) Average swimming speed in the MWM test. Data are presented as mean±SD (n=25 in each group). Compared with Control group, *p<0.05; compared with Sev group, $^{\#}p$<0.05.

Sevoflurane elevates $[Ca^{2+}]_c$ in aged rats and isolated hippocampal neurons

To evaluate changes in intracellular calcium, we used the Ca^{2+} probe Fluo-3 AM and flow cytometry to measure $[Ca^{2+}]_c$. The *in vivo* experiments showed that $[Ca^{2+}]_c$ was significantly increased in the Sev group after sevoflurane exposure compared with the Control group ($p < 0.01$). In comparison, $[Ca^{2+}]_c$ was decreased in the Sev + 2-APB group ($p < 0.01$) (Figures 6A,C). The *in vitro* experiments showed that $[Ca^{2+}]_c$ was significantly increased after sevoflurane exposure in the Sev group, compared with the Control group ($p < 0.01$). Compared with the Sev group, the hippocampal neurons exhibited markedly reduced $[Ca^{2+}]_c$ in the Sev + 2-APB group and increased $[Ca^{2+}]_c$ in the Sev + FK-506 group ($p < 0.01$, Figures 7B,D).

Sevoflurane increases the expression of p-IP3R and activates endoplasmic reticulum stress in aged rats

To explore the potential mechanism of sevoflurane in reducing postoperative cognitive function in aged rats, we evaluated the expression of PERK-related ER stress markers in hippocampus by Western blot assay. The results revealed that sevoflurane exposure upregulated p-IP3R and PERK-related ER stress markers: MFN1,

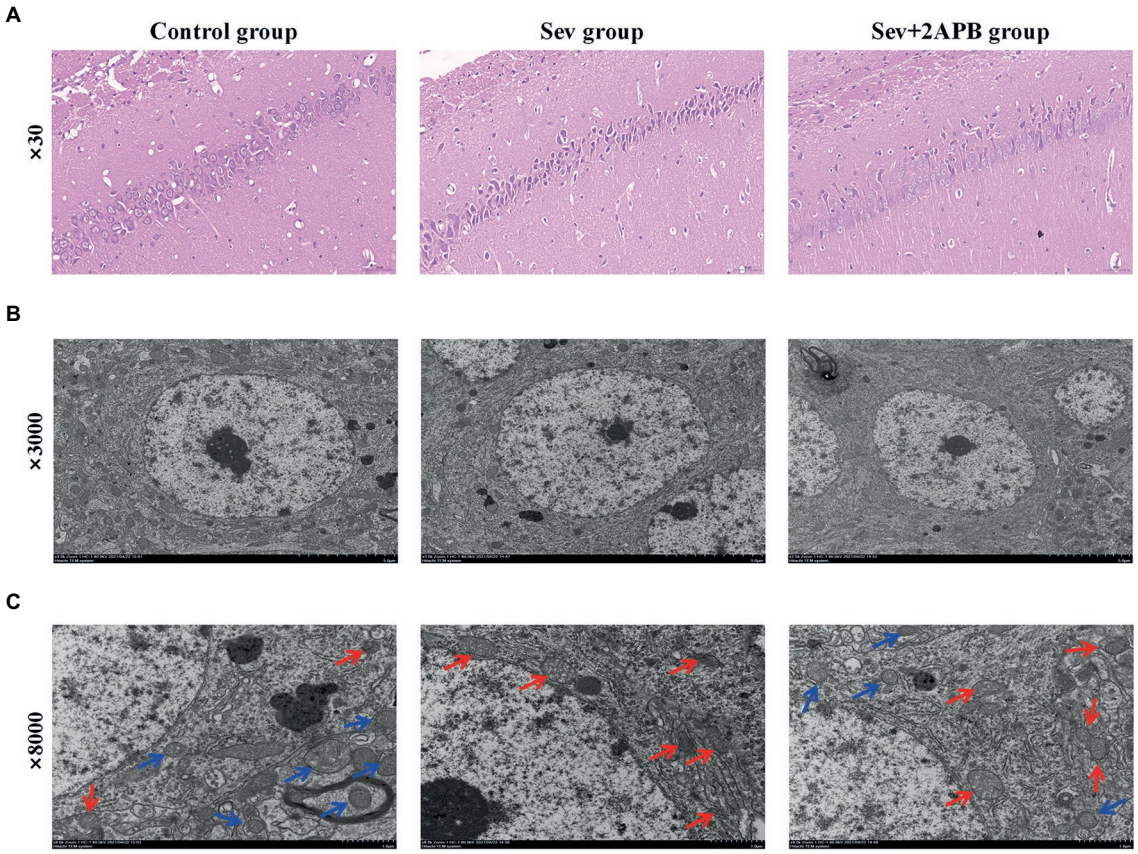

FIGURE 5
Sevoflurane promotes neuronal injury in aged rats. (A) Representative images of histopathological changes in the hippocampal CA1 region of aged rats (×30). **(B)** Representative images of hippocampal neurons in the CA1 region under the transmission electron microscope (×3,000). **(C)** Representative images of hippocampal neurons in the CA1 region under the transmission electron microscope (×8,000). *n*=5 in each group.

MFN2, GRP75, p-PERK, ATF4, and CHOP in the Sev group. In the Sev + 2-APB group, the IP3R inhibitor 2-APB suppressed the increase in these proteins induced by sevoflurane. There were no significant differences in total IP3R (t-IP3R) levels among the three groups (Figures 8A,B). To show activated IP3R in hippocampal neurons by sevflurane, we also performed immunohistochemistry of p-IP3R in CA1. The results showed the positive cell rate of p-IP3R was higher in group Sev than that in group C; moreover, the positive cell rate of p-IP3R was was lower in group Sev + 2APB than in group Sev (Figures 8C,D).

Sevoflurane upregulates IP3R, increases ER stress and activates the caspase-related apoptotic pathway in isolated hippocampal neurons

To corroborate the findings in aged rats, we performed Western blot on isolated hippocampal neurons to evaluate the expression levels of the above proteins. Expression of signaling pathway proteins and apoptosis-related proteins was assessed by western blot analysis, with β-actin as a loading control. Representative blots and bar graphs from four independent experiments are shown. The results showed sevoflurane increased p-IP3R levels and upregulated ER stress-related proteins, including PERK-related ER stress markers: MFN1, MFN2, GRP75, p-PERK, ATF4 and CHOP. Furthermore, sevoflurane increased levels of cleaved caspase-9, cleaved caspase-3 and Bax, but downregulated the anti-apoptotic protein Bcl-2 in the Sev group. In comparison, 2-APB reduced p-IP3R levels and downregulated ER stress-related proteins and proapoptotic proteins, but upregulated anti-apoptotic proteins in the Sev + 2-APB group. In contrast, the IP3R agonist FK-506 upregulated p-IP3R and ER stress-related proteins and proapoptotic proteins, but decreased anti-apoptotic proteins in the Sev + FK-506 group. There were no significant differences in t-IP3R among the four groups (Figures 9A,B).

Discussion

A large number of studies have shown that sevoflurane exposure is an important risk factor for POCD, and can result in increased mortality, delayed recovery, additional complications, longer hospital stays, and significantly higher medical costs (Ge et al., 2021; Wang et al., 2021). However, the mechanisms

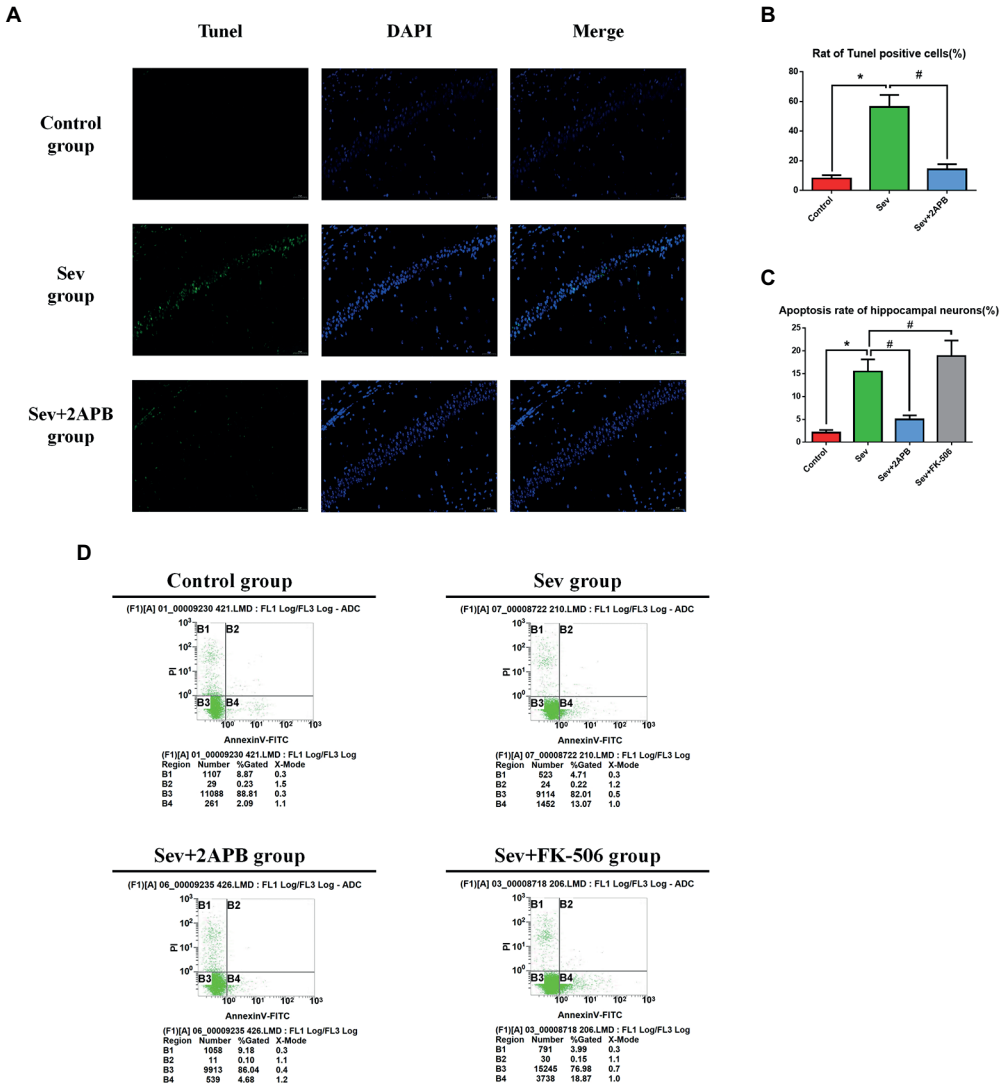

FIGURE 6
Sevoflurane promotes hippocampal neuroapoptosis in aged rats and isolated hippocampal neurons. **(A)** Representative images of TUNEL staining in the hippocampal CA1 region of aged rats (×30) (green: Tunel positive cells; blue: DAPI, scale bar=50 μM). **(B)** Numbers of TUNEL-positive cells. **(C)** Apoptosis rate of hippocampal neurons. **(D)** Representative flow cytometry of hippocampal apoptosis. Data are presented as mean±SD (n=5 in each group). Compared with Control group, *p<0.05; compared with Sev group, #p<0.05.

underlying sevoflurane-induced POCD are still unclear. The current findings provide new mechanistic insight into how sevoflurane exposure in aged rats induces cognitive impairment. Notably, the DEGs associated with cognitive dysfunction caused by sevoflurane were mainly concentrated in the PERK-mediated unfolded protein response and apoptosis pathways. The *in vivo* and *in vitro* experiments suggest that sevoflurane causes neuronal injury and cognitive dysfunction by activating IP3R and inducing ER stress, and by promoting apoptosis of hippocampal neurons through cytoplasmic calcium overload.

Medical bioinformatics is an interdisciplinary approach that uses computer science as a tool to store, retrieve, analyze, and interpret biological and medical data (Chattopadhyay et al., 2020). The rapid development of gene chip and high-throughput sequencing technologies has allowed researchers to quickly perform detailed analysis of the transcriptome and genome, which has promoted the rapid development and progress of the life sciences. In this study, we downloaded the rat sevoflurane expression-related dataset from the official GEO website, performed quantile standardization in R language, and analyzed the differential genes. The differential genes were analyzed by GO enrichment analysis, KEGG enrichment analysis and GSEA analysis. The analyses revealed that the ER stress and apoptosis pathways were the most markedly affected by sevoflurane exposure, laying the course for further *in vivo* and *in vitro* experiments.

Sevoflurane is the most commonly used halogen inhalation anesthetic in China. Sevoflurane anesthesia is closely related to cognitive decline, especially in elderly patients. Our previous study

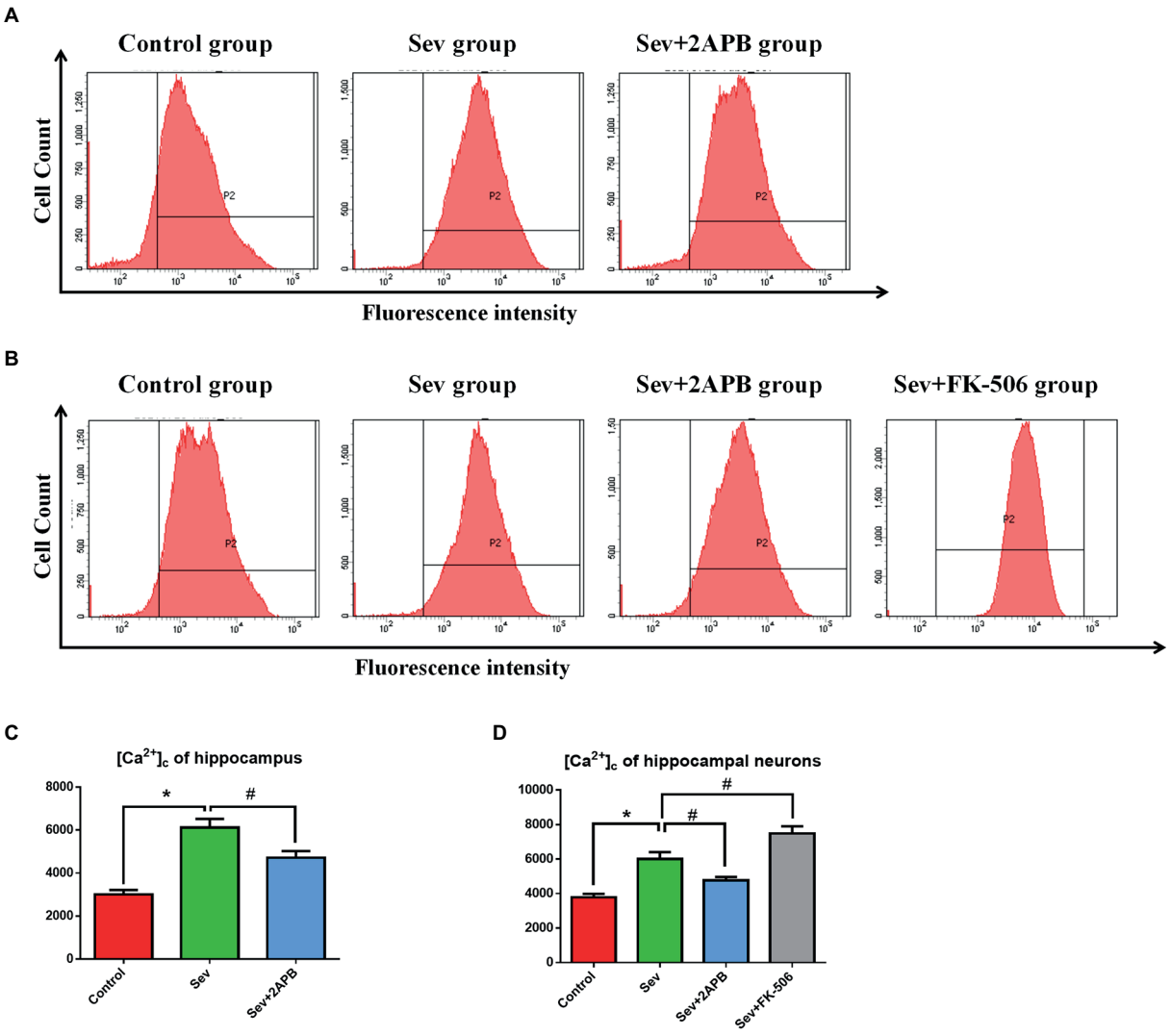

FIGURE 7
Sevoflurane elevates $[Ca^{2+}]_c$ in aged rats and isolated hippocampal neurons. **(A)** Intracellular $[Ca^{2+}]_c$ in hippocampal cells of aged rats. **(B)** Intracellular $[Ca^{2+}]_c$ in isolated hippocampal neurons. **(C)** Representative histograms of $[Ca^{2+}]_c$ by flow cytometry in the hippocampus of aged rats. **(D)** Representative histograms of $[Ca^{2+}]_c$ by flow cytometry of isolated hippocampal neurons. Data are presented as mean±SD (n=5 in each group). Compared with the Control group, $^{*}p<0.05$; compared with the Sev group, $^{\#}p<0.05$.

(Yin et al., 2022) showed that continuous exposure to 2% sevoflurane for 5 h significantly impairs cognitive function in aged rats. Therefore, using this animal model, we tested cognitive function with the MWM test 1 day after sevoflurane anesthesia, and we examined the morphology of hippocampal neurons by transmission electron microscopy and HE staining. The MWM is a common method for evaluating the spatial cognitive function of rodents. It is divided into a positional navigation experiment and a spatial exploration experiment. The position navigation experiment reflects the spatial learning ability of animals, while the spatial exploration experiment reflects spatial memory ability (Ravichandran et al., 2018). The shorter escape latency and the increase in the number of crossings of the original platform location indicate better learning and memory abilities. Our results revealed that the cognitive function of aged rats was significantly reduced and that hippocampal neurons were severely damaged after sevoflurane anesthesia, consistent with previous studies (Yin et al., 2022).

The ER, as the intracellular calcium store, plays an important role in maintaining intracellular calcium homeostasis. IP3R is an important calcium release channel located in the ER. The overactivation of IP3R can lead to the release of ER calcium into the cytoplasm, induce ER stress, and cause programmed cell death (such as apoptosis and necroptosis). A study by Yang found that sevoflurane may induce cell damage by causing abnormal calcium release from the ER *via* excessive activation of IP3 receptors (Yang et al., 2008), and IP3R knockout can prevent this damage. A study by Wang found that disruption of intracellular calcium balance by activation of IP3R results in hippocampal apoptosis, which underlies subsequent spatial memory impairment in mice (Wang et al., 2018). Previous studies found that 3.4% sevoflurane

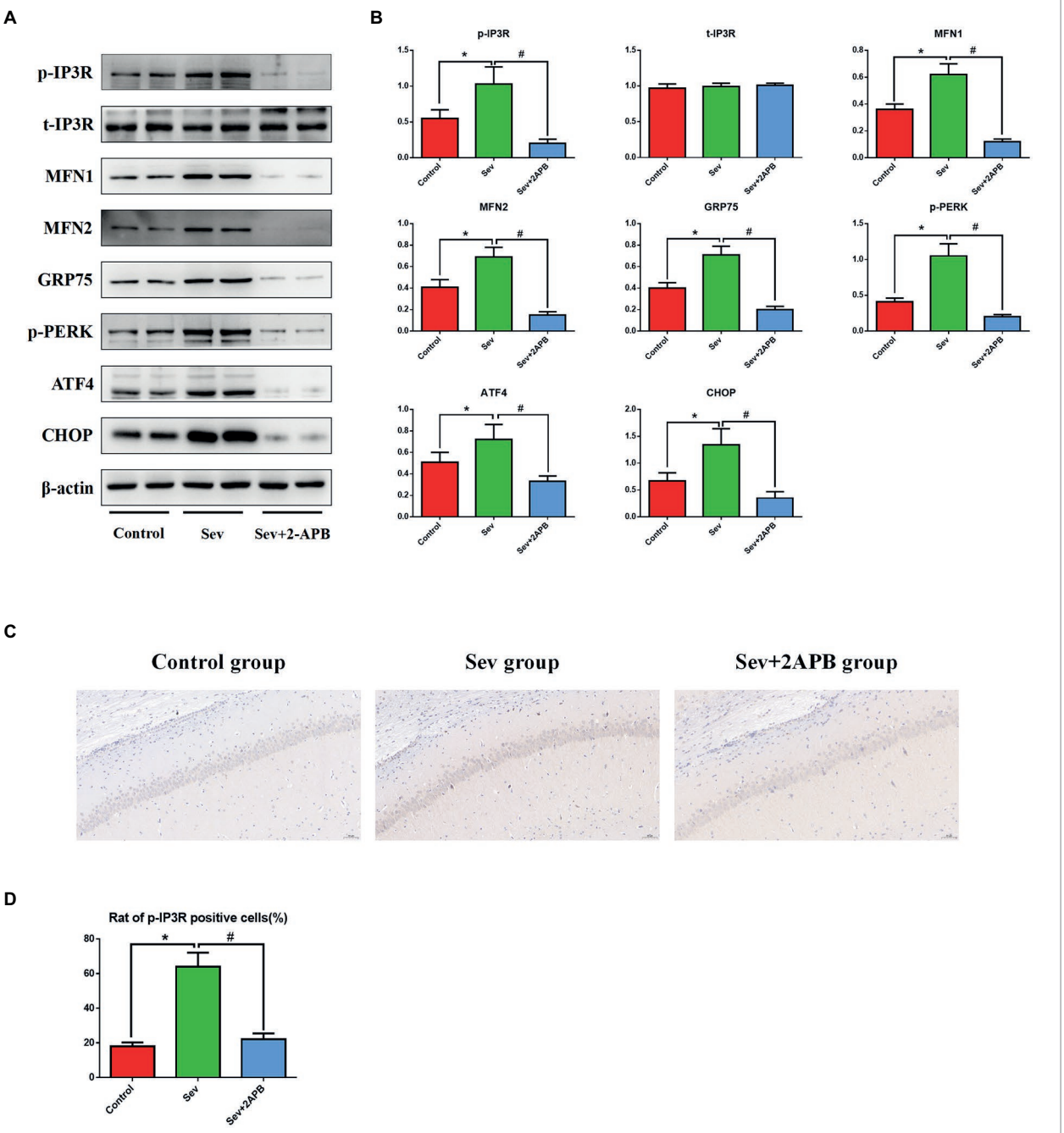

FIGURE 8
Sevoflurane upregulates p-IP3R and activates endoplasmic reticulum stress in aged rats. **(A)** Representative western blot of p-IP3R, t-IP3R, MFN1, MFN2, GRP75, p-PERK, ATF4 and CHOP. **(B)** Representative histogram of the relative expression of p-IP3R, t-IP3R, MFN1, MFN2, GRP75, p-PERK, ATF4, and CHOP. **(C)** Representative images of immunohistochemistry of p-IP3R in CA1 (scale bar=50 μM). **(D)** Representative histogram of positive cell rate of p-IP3R. Data are presented as mean±SD (n=5 in each group). Compared with the Control group, *p<0.05; compared with the Sev group, $^{\#}p$<0.05.

exposure for 5 h can significantly increase the apoptosis rate of isolated hippocampal neurons and cause nerve damage. Therefore, in this study, we chose 3.4% sevoflurane exposure for 5 h to explore the specific mechanism of sevoflurane neurotoxicity (Xu et al., 2018). In this study, we used FK-506 to activate IP3R, as in the study of Fujii (Fujii et al., 2016). FK-506 competes with IP3R for binding to FK506 binding protein (FKBP), and this process is irreversible. FK-506 allows IP3R to release FKBP, greatly increasing the activity of IP3R. Therefore, we used FK-506 as an agonist of IP3R (Mac Millan, 2013). Our current findings revealed that sevoflurane exposure activates IP3R and induces hippocampal apoptosis by disrupting intracellular calcium balance.

Apoptosis is a mechanism of programmed cell death caused by changes to the internal and external environments (Elmore, 2007).

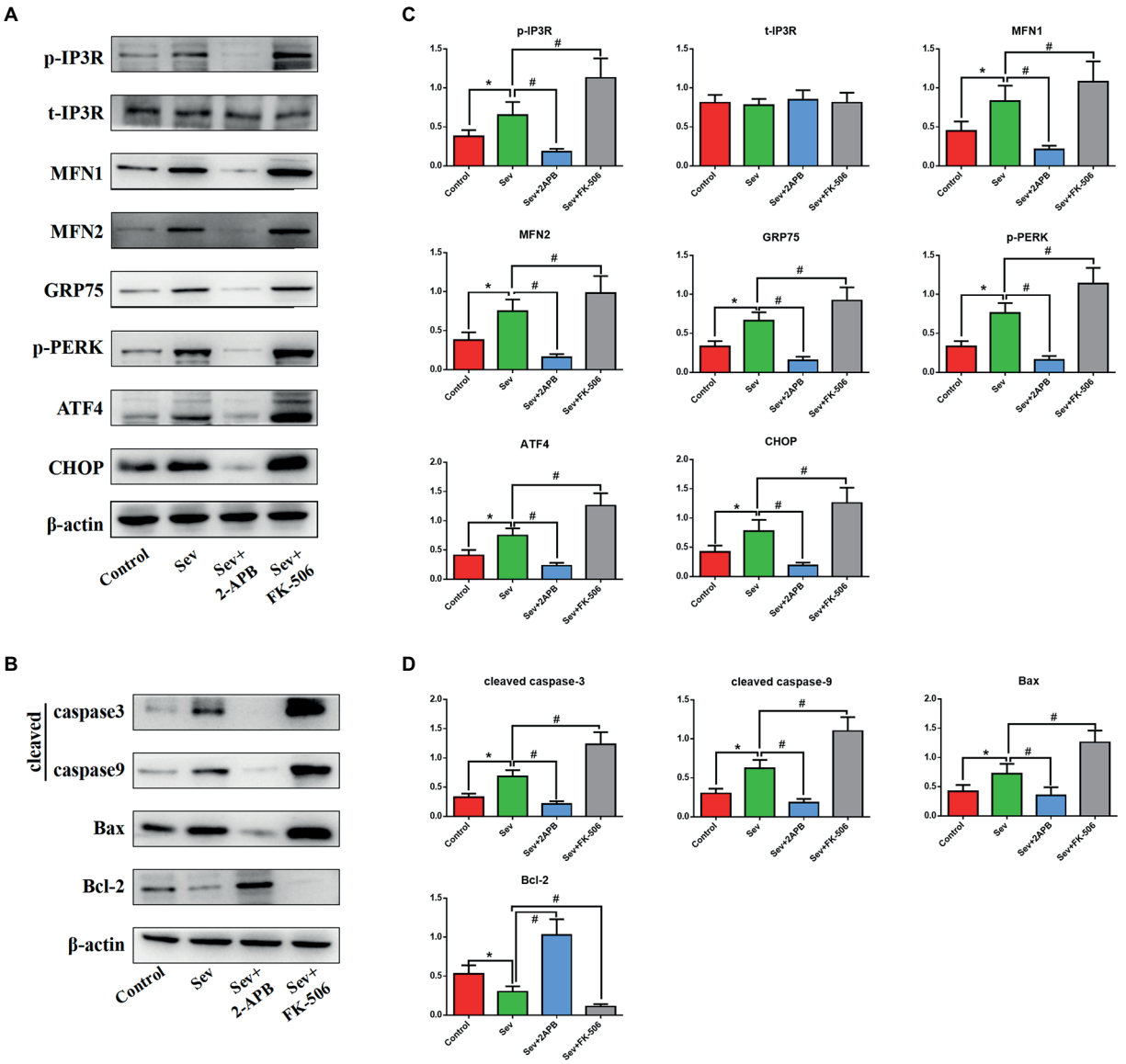

FIGURE 9
Sevoflurane upregulates IP3R and activates endoplasmic reticulum stress and the caspase-related apoptotic pathway in isolated hippocampal neurons. **(A)** Representative western blot of p-IP3R, t-IP3R, MFN1, MFN2, GRP75, p-PERK, ATF4, CHOP, cleaved caspase-9, cleaved caspase-3, Bcl-2, and Bax. **(B)** Representative histogram of the relative expression of p-IP3R, t-IP3R, MFN1, MFN2, GRP75, p-PERK, ATF4, CHOP, cleaved caspase-9, cleaved caspase-3, Bcl-2 and Bax. Data are presented as mean±SD (n=5 in each group). Compared with the Control group, *p<0.05; compared with the Sev group, #p<0.05.

There are two apoptotic pathways in mammalian cells—the exogenous caspase 8 pathway, involving tumor necrosis factor receptor family members, and the endogenous caspase 9 pathway, involving cytochrome C (CytC)(D'Arcy, 2019). The process of apoptosis is regulated by a variety of genes, among which the Bcl-2 gene family is an important regulatory factor and plays various roles in apoptosis, depending on the family member. Bax is the most important apoptosis-inducing gene in the Bcl-2 family. It releases CytC into the cytoplasm through mitochondrial permeability transformation channel protein, forming the CytC-Apaf-pro-caspase-9 apoptotic complexes, which inhibit Bcl-2 and initiate the apoptotic cascade. Activation of the upstream effector caspase-9 can also activate downstream caspases, leading to apoptosis. Our previous study showed that sevoflurane exposure activates the caspase-dependent apoptotic pathway by inducing cytoplasmic calcium overload in hippocampal neurons (Liu et al., 2016). However, it was unclear whether ER stress is involved in this process.

ER stress is a process in which cells activate signaling pathways such as the unfolded protein response, ER overload response and the caspase-12-mediated apoptotic pathway in response to protein misfolding and aggregation in the ER lumen and calcium imbalance. ER stress not only induces the expression of ER molecular chaperones of glucose regulatory proteins (GRP78, GRP94) to exert

protective effects, but also activates intrinsic apoptotic pathways. PERK is an important transmembrane sensor that senses and participates in the unfolded protein response in the mammalian ER. When the ER is stable, PERK and GRP75 are inactive. When the ER is stressed, PERK phosphorylates and catalyzes the phosphorylation of eIF2α through MFN1 and MFN2. Phosphorylated eIF2α selectively promotes the translation of ATF-4 and upregulates CHOP. CHOP increases the expression of the pro apoptotic protein Bax and cleaved-caspase-3/9 and downregulates the anti-apoptotic protein Bcl-2, thereby inducing apoptosis. Liu showed that sevoflurane exposure induces neuroapoptosis *via* the PERK-eIF2α-ATF4-CHOP axis of the ER stress signaling pathway (Liu et al., 2017). However, whether IP3R mediates cytoplasmic calcium remained unclear. In the current study, we found that after sevoflurane exposure, IP3R, $[Ca^{2+}]_c$ and neuronal apoptosis in the hippocampus were increased, and that the ER stress-related PERK pathway proteins and apoptotic proteins were increased, suggesting that sevoflurane exposure-induced neuroapoptosis is mediated by the activation of IP3R, which increases $[Ca^{2+}]_c$ and ER stress.

Although rigorous bioinformatics analysis and both *in vitro* and *in vivo* experiments were conducted in this study, there are some limitations. For example, no animal experiments with gene overexpression or knockout were conducted to further verify the findings. We plan on addressing this shortcoming in future studies. Additionally, the current study only evaluated the neurotoxic effects and related mechanisms of sevoflurane on aged male rats, and its effects on female and other age rats need to be further explored. Finally, we only explored PERK-induced ER stress, and the other two pathways (IRE1α-xbp1 and ATF6 signaling pathway) need to be further explored.

Conclusion

Our data show that sevoflurane exposure causes cognitive impairment in aged rats and cellular damage in isolated hippocampal neurons. The mechanisms underlying the neurotoxicity of sevoflurane involve in activating the IP3R and inducing cytoplasmic calcium overload, thereby resulting in endoplasmic reticulum stress and hippocampal neuronal apoptosis.

Data availability statement

The datasets presented in this study can be found in online repositories. The names of the repository/repositories and accession number(s) can be found in the article/Supplementary material.

Ethics statement

The animal study was reviewed and approved by the Animal Review Board of Hebei Medical University (Ethical code: 2017–026-1).

Author contributions

QZ, YL, CY, ZH, and QW: conception and design of study，bioinformatics analysis，and animal model construction. XW, QZ, JG, and JZ: acquisition of data, western blot, and cell culture experiment. XW, JG, and XX: analysis and/or interpretation of data, transmission electron microscope experiment. QZ and YL: drafting the manuscript. QZ, XW, and QW: revising the manuscript critically important intellectual content. All authors contributed to the article and approved the submitted version.

Funding

This work was supported by the Natural Science Foundation of Hebei Province (H2022316001), Graduate Innovation Funding Project of Degree Office of Hebei Provincial Department of Education (CXZZBS2022092), and National Natural Science Foundation of China (81771134). The Hebei Provincial government funded the specialty capacity building and specialty leader training program.

Acknowledgments

We thank Barry Patel from Liwen Bianji (Edanz) (www.liwenbianji.cn/), for editing the English text of a draft of this manuscript.

Conflict of interest

The authors declare that the research was conducted in the absence of any commercial or financial relationships that could be construed as a potential conflict of interest.

Publisher's note

Supplementary material

The Supplementary material for this article can be found online at: https://www.frontiersin.org/articles/10.3389/fnagi.2022.990679/full#supplementary-material

References

Berridge, M. J. (2016). The inositol Trisphosphate/calcium signaling pathway in health and disease. *Physiol. Rev.* 96, 1261–1296. doi: 10.1152/physrev.00006.2016

Chattopadhyay, A., Iwema, C. L., Epstein, B. A., Lee, A. V., and Levine, A. S. (2020). Molecular biology information service: an innovative medical library-based bioinformatics support service for biomedical researchers. *Brief. Bioinform.* 21, 876–884. doi: 10.1093/bib/bbz035

Chen, Y., Zhang, P., Lin, X., Zhang, H., Miao, J., Zhou, Y., et al. (2020). Mitophagy impairment is involved in sevoflurane-induced cognitive dysfunction in aged rats. *Aging* 12, 17235–17256. doi: 10.18632/aging.103673

Cheng, K. C., Huang, C. Y., Hsieh, T. C., and Chiang, H. C. (2022). Disrupted cellular calcium homeostasis is responsible for Aβ-induced Learning and memory damage and lifespan shortening in a model of Aβ transgenic fly. *IUBMB life* 74, 754–762. doi: 10.1002/iub.2621

D'Arcy, M. S. (2019). Cell death: a review of the major forms of apoptosis, necrosis and autophagy. *Cell Biol. Int.* 43, 582–592. doi: 10.1002/cbin.11137

Di Conza, G., and Ho, P. C. (2020). ER stress responses: an emerging modulator for innate immunity. *Cells* 9:695. doi: 10.3390/cells9030695

Egorova, P. A., and Bezprozvanny, I. B. (2018). Inositol 1,4,5-trisphosphate receptors and neurodegenerative disorders. *FEBS J.* 285, 3547–3565. doi: 10.1111/febs.14366

Elmore, S. (2007). Apoptosis: a review of programmed cell death. *Toxicol. Pathol.* 35, 495–516. doi: 10.1080/01926230701320337

Evered, L., Scott, D. A., Silbert, B., and Maruff, P. J. A. (2011). Postoperative cognitive dysfunction is independent of type of surgery and anesthetic. *Anesth. Analg.* 112, 1179–1185. doi: 10.1213/ANE.0b013e318215217e

Fujii, S., Yamazaki, Y., Goto, J., Fujiwara, H., and Mikoshiba, K. (2016). Prior activation of inositol 1,4,5-trisphosphate receptors suppresses the subsequent induction of long-term potentiation in hippocampal CA1 neurons. *Learn. Mem.* 23, 208–220. doi: 10.1101/lm.041053.115

Ge, X., Zuo, Y., Xie, J., Li, X., Li, Y., Thirupathi, A., et al. (2021). A new mechanism of POCD caused by sevoflurane in mice: cognitive impairment induced by cross-dysfunction of iron and glucose metabolism. *Aging* 13, 22375–22389. doi: 10.18632/aging.203544

Gold, S., and Forryan, S. (2018). Postoperative cognitive decline: a current problem with a wifficult future. *Trends Anaesth Crit.* 24, 49–58. doi: 10.1016/j.tacc.2018.04.002

Hotamisligil, G. S., and Davis, R. J. (2016). Cell Signaling and Stress Responses. *Cold Spring Harb. Perspect. Biol.* 8:a006072. doi: 10.1101/cshperspect.a006072

Krenk, L., Kehlet, H., Bæk Hansen, T., Solgaard, S., Soballe, K., Rasmussen, L. S. (2014). Cognitive dysfunction after fast-track hip and knee replacement. *Anesth. Analg.* 118, 1034–1040. doi: 10.1213/ANE.0000000000000194

Kumar, A. (2020). Calcium signaling during brain aging and its influence on the hippocampal synaptic plasticity. *Adv. Exp. Med. Biol.* 1131, 985–1012. doi: 10.1007/978-3-030-12457-1_39

Li, G., Mongillo, M., Chin, K. T., Harding, H., Ron, D., Marks, A. R., et al. (2009). Role of ERO1-alpha-mediated stimulation of inositol 1,4,5-triphosphate receptor activity in endoplasmic reticulum stress-induced apoptosis. *J. Cell Biol.* 186, 783–792. doi: 10.1083/jcb.200904060

Liu, X., Song, S., Wang, Q., Yuan, T., and He, J. (2016). A mutation in β-amyloid precursor protein renders SH-SY5Y cells vulnerable to isoflurane toxicity: the role of inositol 1,4,5-trisphosphate receptors. *Mol. Med. Rep.* 14, 5435–5442. doi: 10.3892/mmr.2016.5930

Liu, X., Song, X., Yuan, T., He, J., Wang, X., and Wang, Q. (2016). Effects of calpain on sevoflurane-induced aged rats hippocampal neuronal apoptosis. *Aging Clin. Exp. Res.* 28, 633–639. doi: 10.1007/s40520-015-0466-5

Liu, B., Xia, J., Chen, Y., and Zhang, J. (2017). Sevoflurane-induced endoplasmic reticulum stress contributes to Neuroapoptosis and BACE-1 expression in the developing brain: the role of eIF2α. *Neurotox. Res.* 31, 218–229. doi: 10.1007/s12640-016-9671-z

Ma, H., Yao, L., Pang, L., Li, X., and Yao, Q. (2016). Tetrandrine ameliorates sevoflurane-induced cognitive impairment via the suppression of inflammation and apoptosis in aged rats. *Mol. Med. Rep.* 13, 4814–4820. doi: 10.3892/mmr.2016.5132

Mac Millan, D. (2013). FK506 binding proteins: cellular regulators of intracellular Ca2+ signalling. *Eur. J. Pharmacol.* 700, 181–193. doi: 10.1016/j.ejphar.2012.12.029

Mangla, A., Guerra, M. T., and Nathanson, M. H. (2020). Type 3 inositol 1,4,5-trisphosphate receptor: a calcium channel for all seasons. *Cell Calcium* 85:102132. doi: 10.1016/j.ceca.2019.102132

Matuz-Mares, D., González-Andrade, M., Araiza-Villanueva, M. G., Vilchis-Landeros, M. M., and Vázquez-Meza, H. (2022). Mitochondrial calcium: effects of its imbalance in disease. *Antioxidants* 11:801. doi: 10.3390/antiox11050801

Miller, D., Lewis, S. R., Pritchard, M. W., Schofield-Robinson, O. J., Shelton, C. L., Alderson, P., et al. (2018). Intravenous versus inhalational maintenance of anaesthesia for postoperative cognitive outcomes in elderly people undergoing non-cardiac surgery. *Cochrane Database Syst. Rev.* 2018:Cd012317. doi: 10.1002/14651858.CD012317.pub2

Patrich, E., Piontkewitz, Y., Peretz, A., Weiner, I., and Attali, B. (2016). Maternal immune activation produces neonatal excitability defects in offspring hippocampal neurons from pregnant rats treated with poly I: C. *Sci. Rep.* 6:19106. doi: 10.1038/srep19106

Qiu, L. L., Pan, W., Luo, D., Zhang, G. F., Zhou, Z. Q., Sun, X. Y., et al. (2020). Dysregulation of BDNF/TrkB signaling mediated by NMDAR/Ca(2+)/calpain might contribute to postoperative cognitive dysfunction in aging mice. *J. Neuroinflam.* 17:23. doi: 10.1186/s12974-019-1695-x

Ravichandran, V. A., Kim, M., Han, S. K., and Cha, Y. S. (2018). Stachys sieboldii extract supplementation attenuates memory deficits by modulating BDNF-CREB and its downstream molecules, in animal models of memory impairment. *Nutrients* 10:917. doi: 10.3390/nu10070917

Sahu, G., and Turner, R. W. (2021). The molecular basis for the calcium-dependent slow Afterhyperpolarization in CA1 hippocampal pyramidal neurons. *Front. Physiol.* 12:759707. doi: 10.3389/fphys.2021.759707

Shen, F. Y., Song, Y. C., Guo, F., Xu, Z. D., Li, Q., Zhang, B., et al. (2018). Cognitive impairment and endoplasmic reticulum stress induced by repeated short-term Sevoflurane exposure in early life of rats. *Front. Psych.* 9:332. doi: 10.3389/fpsyt.2018.00332

Silbert, B. S., Evered, L. A., and Scott, D. (2014). Incidence of postoperative cognitive dysfunction after general or spinal anaesthesia for extracorporeal shock wave lithotripsy 113, 784–791. doi: 10.1093/bja/aeu163,

Vaidya, B., Kaur, H., Thapak, P., Sharma, S. S., and Singh, J. N. (2022). Pharmacological modulation of TRPM2 channels via PARP pathway leads to Neuroprotection in MPTP-induced Parkinson's disease in Sprague Dawley rats. *Mol. Neurobiol.* 59, 1528–1542. doi: 10.1007/s12035-021-02711-4

Wang, C. M., Chen, W. C., Zhang, Y., Lin, S., and He, H. F. (2021). Update on the mechanism and treatment of Sevoflurane-induced postoperative cognitive dysfunction. *Front. Aging Neurosci.* 13:702231. doi: 10.3389/fnagi.2021.702231

Wang, Z., Meng, S., Cao, L., Chen, Y., Zuo, Z., and Peng, S. (2018). Critical role of NLRP3-caspase-1 pathway in age-dependent isoflurane-induced microglial inflammatory response and cognitive impairment. *J. Neuroinflam.* 15:109. doi: 10.1186/s12974-018-1137-1

Wang, Y., Yin, C. P., Tai, Y. L., Zhao, Z. J., Hou, Z. Y., and Wang, Q. J. (2021). Apoptosis inhibition is involved in improvement of sevoflurane-induced cognitive impairment following normobaric hyperoxia preconditioning in aged rats. *Exp. Ther. Med.* 21:203. doi: 10.3892/etm.2021.9636

Wang, X., Yu, H., You, J., Wang, C., Feng, C., Liu, Z., et al. (2018). Memantine can improve chronic ethanol exposure-induced spatial memory impairment in male C57BL/6 mice by reducing hippocampal apoptosis. *Toxicology* 406–407, 21–32. doi: 10.1016/j.tox.2018.05.013

Xu, L., Shen, J., Yu, L., Sun, J., McQuillan, P. M., Hu, Z., et al. (2018). Role of autophagy in sevoflurane-induced neurotoxicity in neonatal rat hippocampal cells. *Brain Res. Bull.* 140, 291–298. doi: 10.1016/j.brainresbull.2018.05.020

Yang, H., Liang, G., Hawkins, B. J., Madesh, M., Pierwola, A., and Wei, H. (2008). Inhalational anesthetics induce cell damage by disruption of intracellular calcium homeostasis with different potencies. *Anesthesiology* 109, 243–250. doi: 10.1097/ALN.0b013e31817f5c47

Yang, F., Ma, H., Butler, M. R., and Ding, X. Q. (2021). Preservation of endoplasmic reticulum (ER) Ca(2+) stores by deletion of inositol-1,4,5-trisphosphate receptor type 1 promotes ER retrotranslocation, proteostasis, and protein outer segment localization in cyclic nucleotide-gated channel-deficient cone photoreceptors. *FASEB J.* 35:e21579. doi: 10.1096/fj.202002711R

Yin, C., Zhang, Q., Zhao, J., Li, Y., Yu, J., Li, W., et al. (2022). Necrostatin-1 against Sevoflurane-induced cognitive dysfunction involves activation of BDNF/TrkB pathway and inhibition of Necroptosis in aged rats. *Neurochem. Res.* 47, 1060–1072. doi: 10.1007/s11064-021-03505-9

Zhang, Q., Li, Y., Bao, Y., Yin, C., Xin, X., Guo, Y., et al. (2018). Pretreatment with nimodipine reduces incidence of POCD by decreasing calcineurin mediated hippocampal neuroapoptosis in aged rats. *BMC Anesthesiol.* 18:42. doi: 10.1186/s12871-018-0501-0

frontiers | Frontiers in Aging Neuroscience

TYPE Original Research
PUBLISHED 21 October 2022
DOI 10.3389/fnagi.2022.1034041

OPEN ACCESS

EDITED BY
Jiaqiang Zhang,
Zhengzhou University, China

REVIEWED BY
Hao Wang,
Shanghai Jiao Tong University, China
Heather M. Wilkins,
University of Kansas Medical Center Research Institute, United States

*CORRESPONDENCE
Haiyun Wang
why819@126.com

SPECIALTY SECTION
This article was submitted to Neurocognitive Aging and Behavior, a section of the journal Frontiers in Aging Neuroscience

RECEIVED 01 September 2022
ACCEPTED 03 October 2022
PUBLISHED 21 October 2022

CITATION
Xia T, Yang C, Wang X, Bai L, Ma J, Zhao M, Hua W and Wang H (2022) Heterogeneous nuclear ribonucleoprotein A2/B1 as a novel biomarker in elderly patients for the prediction of postoperative neurocognitive dysfunction: A prospective nested case-control study.
Front. Aging Neurosci. 14:1034041.
doi: 10.3389/fnagi.2022.1034041

Heterogeneous nuclear ribonucleoprotein A2/B1 as a novel biomarker in elderly patients for the prediction of postoperative neurocognitive dysfunction: A prospective nested case-control study

Tong Xia[1], Chenyi Yang[1,2,3,4,5], Xinyi Wang[1,2,3,4,5], Lili Bai[1], Ji Ma[1,2,3,4,5], Mingshu Zhao[1,2,3,4,5], Wei Hua[1,2,3,4,5] and Haiyun Wang[1,2,3,4,5]*

[1]Department of Anesthesiology, The Third Central Clinical College of Tianjin Medical University, Tianjin, China, [2]Department of Anesthesiology, Nankai University Affinity the Third Central Hospital, Tianjin, China, [3]Tianjin Key Laboratory of Extracorporeal Life Support for Critical Diseases, Tianjin, China, [4]Artificial Cell Engineering Technology Research Center, Tianjin, China, [5]Tianjin Institute of Hepatobiliary Disease, Tianjin, China

Background and objective: Postoperative neurocognitive dysfunction (PND) occurs in up to 54% of older patients, giving rise to the heavy psychological and economic burdens to patients and society. To date, the development of PND biomarkers remains a challenge. Heterogeneous nuclear ribonucleoprotein A2/B1 (hnRNPA2/B1) is an RNA-binding protein whose prion-like structure is prone to mutation and hence leads to neurodegenerative diseases, but its expression changes in PND remains unclear. Here, we detect the preoperative hnRNPA2/B1 level in patients with PND, and to explore its value in the prediction and diagnosis of PND.

Methods: The study included 161 elderly patients undergoing lumbar decompression and fusion in Nankai University Affinity the Third Central Hospital from September 2021 to July 2022. Neuropsychological and psychometric evaluations were performed before surgery, 1 week and 3 months after surgery to diagnose the occurrence of PND, then the peripheral blood was collected from patients before induction of anesthesia. The concentration in plasma of hnRNPA2/B1 and amyloid-β 42 were determined by enzyme-linked immunosorbent assay. The median fluorescence intensity and mRNA levels of hnRNPA2/B1 in peripheral blood mononuclear cells was detected by indirect intracellular staining flow cytometry and quantitative real-time PCR, respectively.

Results: The preoperative hnRNPA2/B1 level in patients with PND was higher both in short-time and long-time follow-up. We found significantly higher concentrations of hnRNPA2/B1 in PND at 7 days after surgery (median, 72.26

pg/mL vs. 54.95 pg/mL, p = 0.022) compared with patients without PND, and so as 3 months after surgery (median, 102.93 pg/mL vs. 56.38 pg/mL, p = 0.012). The area under the curve (AUC) was predicted to be 0.686 at 7 days after surgery and 0.735 at 3 months. In addition, when combining several clinical information, the diagnostic efficiency of hnRNPA2/B1 for PND could further increase (AUC, 0.707 at 7 days, 0.808 at 3 months).

Conclusion: Based on the findings reported here, hnRNPA2/B1 may serve as a new and powerful predictive biomarker to identify elderly patients with PND.

KEYWORDS

postoperative neurocognitive dysfunction, biomarker, lumbar decompression and fusion, HnRNPA2/B1, Aβ42

Introduction

Postoperative neurocognitive dysfunction (PND) is a cognition-related complication, whose incidence fluctuates from 20 to 54% and increases with age (Needham et al., 2017; Carr et al., 2018; Evered and Silbert, 2018). This postoperative outcome is also independently associated with some adverse effects, including increased surgical morbidity and mortality, length of hospital stay, hospitalization and out-of-hospital care costs and functional disability (Dijkstra et al., 1999; Steinmetz et al., 2009; O'Gara et al., 2020). Considering these outcomes caused by PND, it is, therefore, vital to recognize individuals prone to PND as early as possible.

Exploring PND biomarkers would help clinicians stratify patients by risk and conduct individualized management, and such biomarkers could also provide clues to help elucidate the mechanisms behind PND. Currently, the majority of the detected PND biomarkers are related to nerve damage, neurotoxicity, astrocyte injury or neurotrophic effect. One potential PND marker is neuron-specific enolase (NSE), though considered as a reliable indicator of neuronal and brain damage, but it works not very well in the early stage of brain injury (Ramlawi et al., 2006). Its diagnostic sensitivity could be reduced for its non-specificity to brain tissue, then causing a high prevalence of false-positive results and even a reverse gradient change (Rappold et al., 2016; Danielson et al., 2018). Glial fibrillary acidic protein (GFAP), a cytoskeletal protein in astrocytes and highly specific to brain, is associated with the incidence and severity of PND (Rappold et al., 2016), but Ballweg et al. (2021) found that the receiver operating characteristic (ROC) curve of GFAP to diagnose PND was only 0.49. Therefore, there remains no standard biomarkers for diagnosis and prognosis of PND.

Considering the accelerated aging of the population, incremental number of operations and consequent increasing incidence of PND, we urgently need accurate biomarkers to identify high-risk PND populations. Heterogeneous nuclear ribonucleoprotein (hnRNP) A2/B1 is an important RNA-binding protein that participate in various processes of nucleic acid metabolism, and its expression changes and mutations are closely related to neurodegenerative diseases (Zhang et al., 2021). Our previous studies have found the up-regulation of hnRNPA2/B1 in hippocampal neurons would induce the cognitive impairment of rats (Wang et al., 2020). Despite hnRNPA2/B1 has been confirmed as a significant role in the development of neurodegenerative disorders, especially amyotrophic lateral sclerosis (ALS) and Alzheimer's disease (AD), the relationship between hnRNPA2/B1 and PND remains unclear.

It's reported that PND shares several common molecular pathways with dementia, including neuroinflammation (Le et al., 2014; Luo et al., 2019), oxidative stress (Netto et al., 2018), impaired synaptic function (Xiao et al., 2018; Gao et al., 2021), and the microbiota–gut-brain axis (Yang et al., 2018; Jiang et al., 2019). These pathologic changes may provide physiological basis to the conversion from PND to AD (Steinmetz et al., 2009; Evered et al., 2016), the latter resulting much heavier economic burden. Therefore, we explored the hnRNPA2/B1 level in elderly patients and confirmed the potential predictive value of it to PND so that more high-risk population of PND could be identified.

Materials and methods

Sample size

Based on the results of hnRNPA2/B1 predictive to ALS and the reported incidence of PND, the ratio between the PND and non-PND arms was predefined in the range of 1:3 to make age and gender reveal no differences between groups, and 140 patients were presumably required for the study (α = 0.05; 1−β = 0.9). Allowing an attrition rate of 10–20%, we would recruit 161 participants finally.

Participants

After obtaining the approval from the Ethics Committee of Nankai University Affinity the Third Central Hospital and the written informed consents from all patients, 161 consecutively admitted patients, with the age of more than 65 years, undergoing lumbar decompression and fusion within 4 h from September 2021 to July 2022 were enrolled in the study [SZX-IRB-SOP-016(F)-002-02]. The exclusion criteria were as follows: critical illness (preoperative ASA $\geq$ IV); history of mental illness or neurological disorders; intake of tranquilizers or antidepressants; suspected dementia or memory impairment with a score on the mini-mental state examination (MMSE) < 17 or Montreal Cognitive Assessment (MoCA) < 15; cancer; unwilling to comply with the procedures; or hearing loss.

Regarding the intraoperative anesthetic management, routine electrocardiogram, pulse oximetry, invasive blood pressure and bispectral index (BIS) were continuously monitored after the patients admitted to the operating room. All patients undergoing lumbar decompression and fusion surgery received general anesthesia with midazolam (0.05 mg/kg), sufentanil (0.3 μg/kg), etomidate (0.3 mg/kg), Cisatracurium (0.2 mg/kg), and was maintained with continuous infusion of propofol (1.2 μg/ml) and remifentanil (0.1–0.4 μg/kg/min) + 0.7 MAC sevoflurane during surgery to maintain the BIS value within 40–60. Patients under poor hemodynamic conditions should be treated timely. Additionally, all patients received postoperative analgesia *via* a patient-controlled analgesia device for the initial 48 h after surgery.

Cognition assessment

Neuropsychological tests were assessed pre-operatively (the day before the operation), 7 days and 3 months after surgery. The battery primarily focused on memory, learning, attention, executive functions, and cognitive flexibility, and included the following tests: MMSE, MoCA, Instrumental Activities of Daily Living (IADL) as well as Clinical Dementia Rating (CDR). Mild cognitive impairment (MCI) was identified in terms of education-specific cutoff points of total scores of MMSE and MoCA, respectively. According to MMSE norms, 17∼27 for illiterate individuals, 20∼27 for participants with elementary school education, and 24∼27 for those with middle school education and above (Mitchell, 2009). MoCA score in the range of 15∼24 indicates no dementia and below the threshold for diagnosis of AD (Memoria et al., 2013) and CDR is equal to 0.5. Patients with MCI would be enrolled in the study and then followed for 3 months.

According to the definition of PND that the neurocognitive results drop over one SD from baseline when following up (Newman et al., 2001), participants were evaluated whether have PND or not and then divided into PND_1 or non-PND_1 according to the follow-up results of 1 week after surgery, and PND_2 or non-PND_2 at 3 months after surgery.

Sample preparation

The blood samples were collected in EDTA-K2 anti-coagulation vacuum tubes before the induction of anesthesia and divided into three parts, applied to FCM, ELISA, and qRT-PCR. After centrifuging at 3,000 × g for 10 min, the plasma samples were stored at −80°C until analysis. Furthermore, the PBMCs were extracted using Lymphocyte Separation Medium (Human) (P8610, Solarbio, Beijing, China), washed with 1 × PBS (FZ1258, Solarbio, Beijing, China) 3 times totally and then flow cytometry and qRT-PCR are conducted.

Flow cytometry

After harvesting and suspending the PBMCs, add cell fixation and permeabilization (00-5523-00, Thermo Fisher Scientific Inc., Waltham, MA, USA), anti-hnRNPA2/B1 primary antibody (ab259894, Abcam, Toronto, ON, Canada) or Rabbit Monoclonal IgG (ab172730, Abcam, Toronto, ON, Canada) as isotype control and Goat F(ab')2 Anti-Rabbit IgG (DyLight® 488, ab98507, Abcam, Toronto, ON, Canada) as the secondary antibody and incubate, respectively, at room temperature in the dark for about 30–60 min. Wash the cells 3 times by centrifugation at 400 × g for 5 min and resuspend after each incubation. Resuspend cells in 1% paraformaldehyde to prevent deterioration at last for extended storage as well as greater flexibility in planning time on the cytometer. When gating on cell populations by Flowjo data analysis software (TreeStar, USA), we would obtain the median fluorescence intensity of lymphocytes and monocytes to analyze the difference between groups.

Enzyme linked immunosorbent assay

Concentrations of hnRNPA2/B1 (SBJ-H2321, SenBeiJia, Jiangsu, China) and $A\beta_{42}$ (E-EL-H543c, Elabscience, Houston, USA) were examined by ELISA kit. The kit and plasma samples were balanced to room temperature half an hour before use, and the operation is fully carried out following the manufacturer's instructions. Notably, it should be detected within 15 min after adding the stop

solution. The absorbance was read on a spectrophotometer (PerklnElmer, Waltham, MA, USA) at a wavelength of 450 nm. The concentrations of hnRNPA2/B1 and $A\beta_{42}$ were calculated according to the standard curve and presented as pg/mg protein.

Quantitative real-time polymerase chain reaction

Total RNA was extracted from PBMC using the TRIzol reagent (15596026, Thermo Fisher Scientific Inc., Waltham, MA, USA) and its concentration was measured by spectrophotometer (Thermo Fisher Scientific, Waltham, MA, USA). The complementary DNA (cDNA) was obtained by the reverse transcription kit (RR036A, Takara, Japan) and then transcribed to mRNA using the SYBR Premix Ex Taq II (RR820A, Takara, Japan) on an ABI 7,500 instrument (Applied Biosystems, Foster City, CA, USA), with 3 duplicates set in each well. The mRNA levels were normalized to β-actin and the fold changes were calculated using the method of $2^{-\Delta\Delta Ct}$. The nucleotide sequences of the PCR primers (Sangon Biotech, Shanghai, China) are as follows:

β-actin mRNA: (forward 5′-CAC CAT TGG CAA TGA GCG GTT C -3′
reverse 5′-AGG TCT TTG CGG ATG TCC ACG T-3′)
hnRNPA2/B1 mRNA: (forward 5′- GCT TAA GCT TTG AAA CCA CAG A -3′
reverse 5′-CTT GAT CTT TTG CTT GCA GGA T-3′).

Statistical analysis

Descriptive results of continuous variables were presented as the means ± standard deviations (SD) if data follow a normal distribution and homogeneity of variance, otherwise median with interquartile range (IQR). Categorical data were expressed as a percentage or counts. Intergroup comparisons were compared by the independent sample *t*-test or Kruskal-Wallis H test. For comparisons of qualitative parameters, Chi-square or Fisher exact test was applied. Multivariate logistic regression analysis was used to determine the independent risk factors of PND based on the results of previous univariate analysis. Results were shown as odds ratio (OR) and 95% CI. Additionally, we built prediction models for the occurrence of PND and then evaluated its prediction effect by the ROC curve on the basis of the results of ELISA. All statistical analysis were performed using the SPSS 25.0 software (IBM Corp. Armonk, NY, USA), and $P < 0.05$ was considered to be statistically significant.

Results

Patients

Among the eligible 161 patients, 138 were included in the final data analyses (Figure 1). Postoperative short-term follow-up results showed that, no clinically statistical differences were observed with regard to the gender, BMI, ASA classification, hypertension, coronary artery heart disease, and duration of anesthesia, while patients with PND presented lower education level, longer duration of surgery and were subject to receive blood transfusion during surgery compared to those without PND. Postoperative results of long-term follow-up showed no difference in baseline information between two groups (Table 1, $P < 0.05$). Moreover, pre-/post-operative scores of neuropsychological tests also displayed difference between groups (Table 2, $P < 0.05$).

Preoperative heterogeneous nuclear ribonucleoprotein A2/B1 level increases in patients with postoperative neurocognitive dysfunction

Both the median fluorescence intensity and mRNA of preoperative hnRNPA2/B1 levels in the PND group were significantly higher than the other one. Besides, the median fluorescence intensity of hnRNPA2/B1 in monocytes was higher than that in lymphocytes (Figure 2). The preoperative hnRNPA2/B1 and $A\beta_{42}$ levels in the PND group were significantly higher than that in the non-PND group, except for preoperative $A\beta_{42}$ level at 7 days after surgery (Figure 3 and Table 3 $P < 0.05$). Moreover, we analyzed the sex differences of two biomarkers, hnRNPA2/B1 as well as $A\beta_{42}$, and found no sex differences in both plasma biomarkers (Supplementary Table).

Heterogeneous nuclear ribonucleoprotein A2/B1 is able to early predict the occurrence of postoperative neurocognitive dysfunction and has high diagnostic efficiency

As shown within Figure 4, univariate linear regression analysis showed that hnRNPA2/B1 had a stronger negative correlation with preoperative MoCA scores ($R = -0.72$, $p < 0.001$) than $A\beta_{42}$ ($R = -0.53$, $p < 0.001$). The similar results could also be found in the correlation with preoperative MMSE scores ($R = -0.50$ in hnRNPA2/B1, $R = -0.35$ in $A\beta_{42}$, $p < 0.001$).

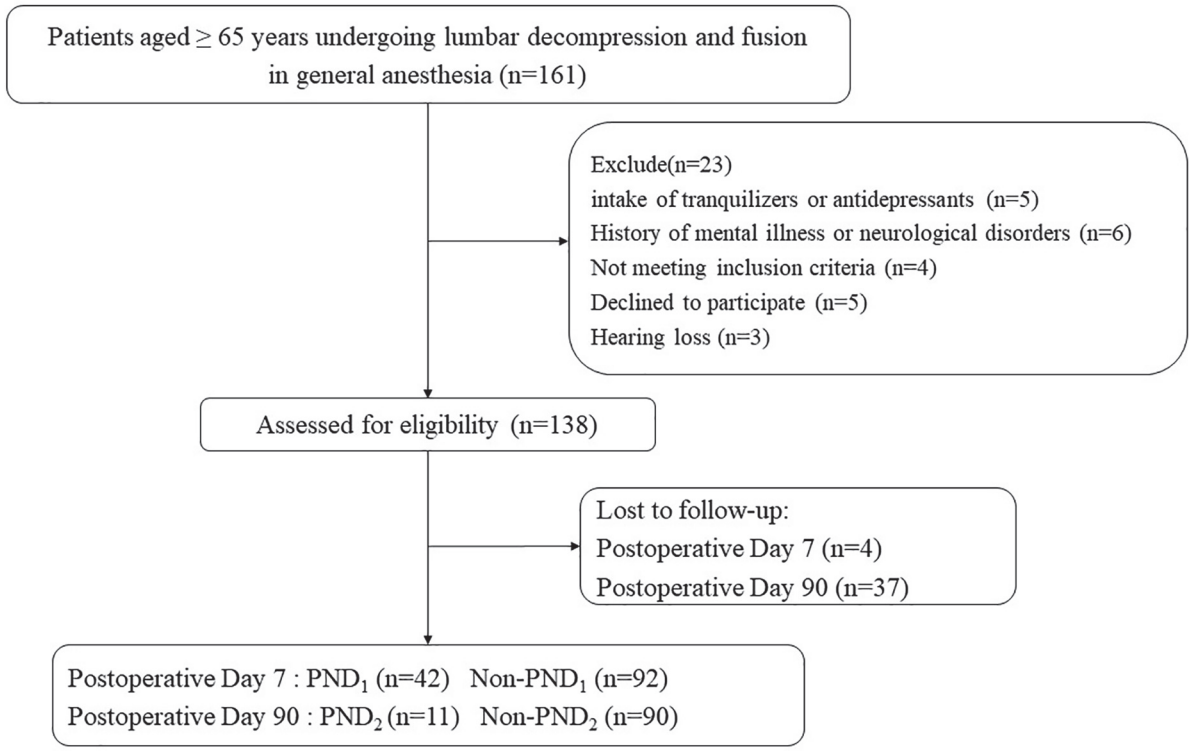

FIGURE 1
The CONSORT diagram showing patients' flow through the study.

TABLE 1 Demographic data at baseline for patients with/without PND.

	Postoperative day 7 (n = 134)			Postoperative day 90 (n = 101)		
	Non-PND$_1$ (n = 92)	PND$_1$ (n = 42)	P-value	Non-PND$_2$ (n = 90)	PND$_2$ (n = 11)	P-value
Preoperative data						
Male sex, n (%)	48.9% (n = 45)	40.5% (n = 17)	0.264	47.8% (n = 43)	18.2% (n = 2)	0.062
Age (year)	68.24 ± 4.43	68.50 ± 4.17	0.748	68.16 ± 4.36	68.27 ± 3.98	0.933
BMI (kg/m^2)	25.61 ± 3.12	24.96 ± 3.25	0.273	25.38 ± 2.87	24.24 ± 4.32	0.246
ASA (II/III), n	50/42	26/16	0.413	50/40	8/3	0.277
Education level (year)	9.01 ± 4.80	7.26 ± 4.58	0.049*	8.24 ± 4.90	6.27 ± 4.73	0.210
Comorbidity, before operation, n (%)						
Hypertension	53.3% (n = 49)	50.0% (n = 21)	0.726	52.2% (n = 47)	72.7% (n = 8)	0.197
Diabetes	20.7% (n = 19)	38.1% (n = 16)	0.033*	22.2% (n = 20)	36.4% (n = 4)	0.298
Coronary Artery Heart Disease	20.7% (n = 19)	9.5% (n = 4)	0.130	16.7% (n = 15)	9.1% (n = 1)	0.516
Intraoperative data						
Duration of surgery (min)	162.48 ± 51.35	182.29 ± 48.72	0.037*	168.39 ± 53.10	179.55 ± 63.74	0.521
Duration of anesthesia (min)	196.98 ± 55.24	215.88 ± 51.84	0.063	202.94 ± 56.44	217.00 ± 70.19	0.450
Blood loss (mL)	273.86 ± 165.21	324.52 ± 205.10	0.130	285.50 ± 184.74	281.82 ± 172.15	0.950
Blood transfusion	25.0% (n = 23)	42.9% (n = 18)	0.037*	31.1% (n = 28)	27.3% (n = 3)	0.794

Values are reported as mean ± standard deviation and numbers with percentages. The P-value is calculated by the independent-samples T-test, chi-square test, respectively. *$p < 0.05$ compared with group Non-PND$_1$. $^+p < 0.05$ compared with group Non-PND$_2$.
BMI, Body Mass Index; ASA, American Society of Anesthesiology.

10.3389/fnagi.2022.1034041

TABLE 2 Neuropsychological test results for patients with/without PND.

	Time	Non-PND	PND	*T*-value	*P*-value
MMSE	Preoperative day 1	25.20 ± 1.51	25.17 ± 1.08	0.112	0.911
	Postoperative day 7	25.27 ± 1.68	22.64 ± 1.27	9.041	0.000*
	Preoperative day 1	25.16 ± 1.45	25.00 ± 1.34	0.339	0.735
	Postoperative day 90	25.21 ± 1.43	23.00 ± 1.55	4.788	0.000^{+}
MoCA	Preoperative day 1	20.54 ± 3.23	20.12 ± 3.28	0.703	0.483
	Postoperative day 7	20.54 ± 3.39	18.50 ± 3.19	3.296	0.001*
	Preoperative day 1	20.13 ± 3.30	18.55 ± 3.59	1.493	0.139
	Postoperative day 90	20.48 ± 3.71	17.82 ± 3.97	2.227	0.028^{+}

Pre-/Post-operative MMSE and MoCA scores for patients with/without PND are presented as mean ± standard deviation. The *P*-value is calculated by independent-samples *T*-test. *$p < 0.05$ compared with group Non-PND$_1$. $^{+}p < 0.05$ compared with group Non-PND$_2$.

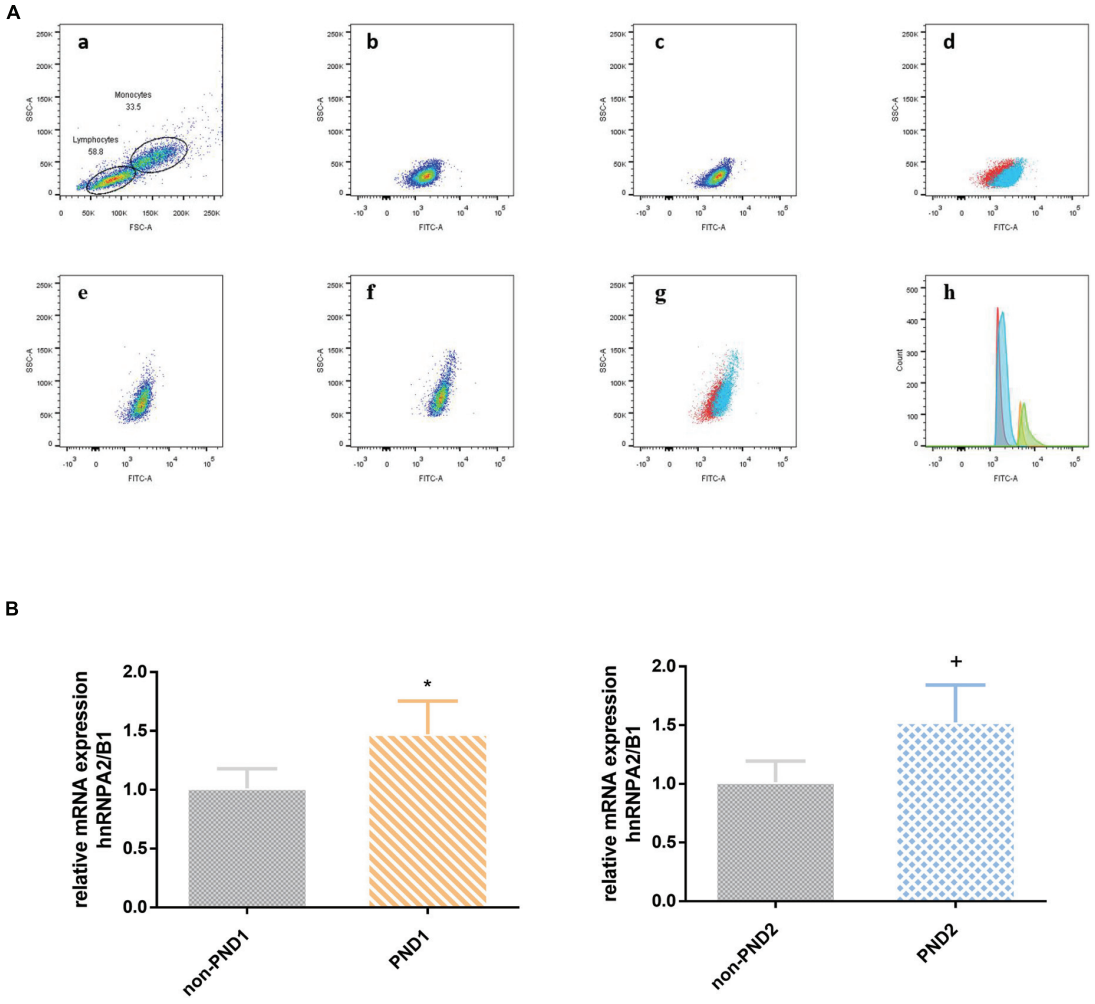

FIGURE 2
(A) The expression of hnRNPA2/B1 in PBMC was analyzed by FCM. The effect regions were created for FSC and SSC **(a)**; median fluorescence intensity of hnRNPA2/B1 in lymphocytes between PND and non-PND **(b,c)**, and the overlay of two groups (**d**; PND, blue; non-PND, red); median fluorescence intensity of hnRNPA2/B1 in monocytes between PND and non-PND **(e,f)**, and the overlay of two groups (**G**; PND, blue; non-PND, red); histogram overlay of hnRNP A2/B1 expression in patients with PND compared to patients without PND in different cell population (**h**; lymphocytes of non-PND, red; lymphocytes of PND, blue; monocytes of non-PND, orange; monocytes of PND, green). **(B)** mRNA level analysis of hnRNPA2/B1 in PBMCs. Data are expressed as the mean ± SD. Note that mRNA expression of hnRNPA2/B1 in patients with PND significantly increased compared with those without PND. *$p < 0.05$ compared with group Non-PND$_1$. $^{+}p < 0.05$ compared with group Non-PND$_2$.

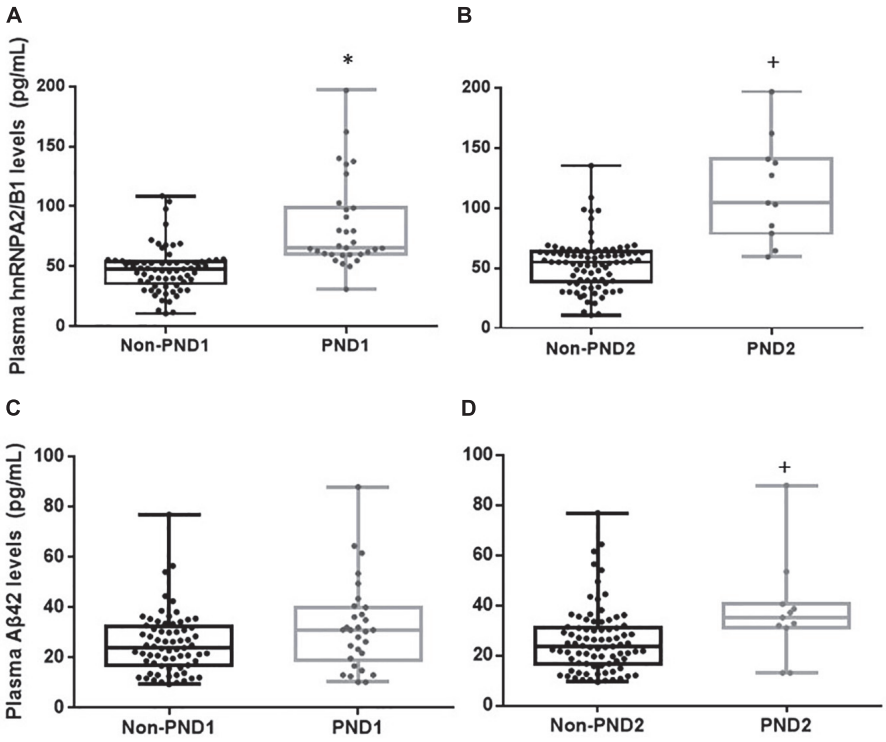

FIGURE 3
Plasma hnRNPA2/B1, $A\beta_{42}$. Concentrations of hnRNPA2/B1 or $A\beta_{42}$ in patients with or without PND at 7 days **(A,C)** and 3 months **(B,D)** after surgery. Boxes represent the median, the 25th and 75th percentiles, and bars indicate the range of data distribution. $^{*}p < 0.05$ compared with group Non-PND_1.$^{+}p < 0.05$ compared with group Non-PND_2.

According to the ROC curve of PND_1, the cut-off value (59.26 pg/mL, sen: 0.687, spe: 0.649) of preoperative hnRNPA2/B1 level was determined by Youden Index, and the AUC was 0.686 (95% CI 0.568∼0.804). The cut-off value (30.48 pg/mL, sen: 0.567, spe:0.714) of preoperative $A\beta_{42}$ level was determined by Youden Index, and the AUC was 0.616 (95% CI 0.489∼0.744). In PND_2, the cut-off value (75.53 pg/mL, sen:0.882, spe:0.636) of preoperative hnRNPA2/B1 level was determined by Youden Index, and the AUC was 0.735 (95% CI 0.525∼0.945). The cut-off value (31.10 pg/mL, sen:0.818, spe:0.747) of preoperative $A\beta_{42}$ level was determined by Youden Index, and the AUC was 0.728 (95% CI 0.554∼0.903). In addition, combination hnRNPA2/B1 and $A\beta_{42}$ could further increase the specificity of predictive value but the sensitivity of model did not improve. In the longer follow-up duration, the efficacy of these two biomarkers and their combination all increased a lot (Figure 5 and Table 4). To determine whether preoperative hnRNPA2/B1 level was an independent risk factor for PND, a multivariable logistic regression analysis was performed. The results showed that the preoperative hnRNPA2/B1 level was an independent risk factor of PND (Table 5). Finally, the model's predictive effect was examined by the ROC curve (Figure 6).

Conclusion

Preoperative higher level of hnRNPA2/B1 is relevant to a higher risk of PND in patients after lumbar decompression and fusion. Therefore, it seems that hnRNPA2/B1 could be a clinically valuable biomarker to predict PND and patients with a higher preoperative hnRNPA2/B1 should be placed more emphasis. Considering that the number of the elderly who need surgical therapy is growing, more extensive clinical and basic studies are urgently needed to ensure our findings as well as further clarify the potential mechanisms.

Discussion

We identified PND in 31.3% of patients at 7 days after lumbar decompression and fusion and 10.9% at 3 months after surgery. Patients with higher preoperative hnRNPA2/B1 level tend to present cognitive decline for a more extended time after operation (median, 72.26 pg/mL in PND_1, 102.93 pg/mL in PND_2). High hnRNPA2/B1 was a significant predictor of PND and the cut-off value for hnRNPA2/B1 was 75.53 pg/mL (AUC, 0.735; 95% CI

0.525∼0.945), whose predictive value could improve further with the consideration of individual demographic data at baseline. Therefore, hnRNPA2/B1 is expected to become a new and powerful predictive marker to identify elderly patients with PND.

Current theories on the etiology of PND now include surgery-related factors such as surgery time, patient position and postoperative infection; anesthesia-related factors such as anesthesia method and intraoperative hypotension; and patient-related factors such as age and physical state. By analyzing several basic characteristics of enrolled patients, we found that there was significant difference in history of intraoperative blood transfusion, educational attainment, preoperative comorbidity, and the duration of surgery and anesthesia.

It's generally believed that educational attainment can predict postoperative neurocognitive disorders to some degree, an effect that can be attributed to cognitive reserve as well as brain connectivity (Monk et al., 2008; Arenaza-Urquijo et al., 2013; Feinkohl et al., 2017b; Perry et al., 2017), which is in line with our findings. And we observed no clinically meaningful difference in age though there is no doubt that aging itself is the major independent risk factor for age-associated disorders. We think that's because the age distribution of patients enrolled in our study mainly concentrated in the narrow age group of 65∼70 years old, some survey about the shifting architecture of cognition across the adult life span shows that compared to other age groups, there is no significant decline in long-term memory and working memory between 60 and 70 years old (Park and Reuter-Lorenz, 2009).

We also investigated the association of some preoperative comorbidities with the risk of PND, such as hypertension, diabetes, coronary artery heart disease. We found significant association for diabetes but not for hypertension or coronary artery heart disease with PND risk, which is consistent with the results of some studies (Feinkohl et al., 2017a, 2018; Lachmann et al., 2018). Several lines of evidence suggest that its possible mechanism may be the changes in brain structure and function, such as impaired glucose metabolism, cerebral atrophy, cerebrovascular damage (Moran et al., 2019; van Sloten et al., 2020; Krell-Roesch et al., 2021). As for other preoperative complications, our findings differ from some research that a range of cardiovascular conditions, including hypertension and coronary artery heart disease, would attribute to cognitive dysfunction induced by cerebral small vessel lesions (Liu et al., 2018; Iadecola and Gottesman, 2019). We consider that is because majority of participants could take medicine punctually to monitor their blood pressure regularly, and antihypertensive agents are significantly associated with a lower risk of dementia or cognitive impairment (Hughes et al., 2020; de Menezes et al., 2021). Of course, there is another possibility that we should have assessed the severity of hypertension and duration of diagnosis which may be important to cognitive risk prediction.

In terms of surgical information, we analyzed the relationship of operative duration and history of intraoperative blood transfusion with PND. Lumbar decompression and fusion is a major operation with extensive trauma, long duration and large amount of intraoperative blood loss, resulting in various postoperative complications (Heemskerk et al., 2021). Blood transfusion is a lifesaving treatment, which can provide volume expansion and increase oxygen-carrying capacity. Nevertheless, transfusion of allogeneic blood products can also trigger enhanced acute inflammatory responses (Cata et al., 2013). We showed that history of intraoperative blood transfusion may contribute to short-term cognitive decline after surgery, while not to long-term cognitive performance. Several lines of findings show that some inflammatory factors would remarkably elevate due to blood transfusion, such as tumor necrosis factor (TNF)-α, interleukin (IL)-β, IL-6, and IL-8, and then lead to neurocognitive impairment (Urner et al., 2012; Ferraris et al., 2013). In addition, transfusion of old red blood cells (>14 days) frequently occurs in clinical practice, inducing neuroinflammation and the development of PND *via* cell-free hemoglobin (Zhu et al., 2014; Tan et al., 2015). Surgery-induced cognitive decline may be attributed to the microglial activation, and the latter would result the release of inflammatory factors and neuroendocrine hormone (Terrando et al., 2011; Subramaniyan and Terrando, 2019; Xiao et al., 2020). Therefore, longer duration of operation is associated with a stronger inflammatory response. Moreover, we found this perioperative stress doesn't seem to cause long-term cognitive deficit.

Apart from paying attention to the baseline information and clinical data, we also explored the biomarkers of PND, aiming to provide guidance for clinical perioperative brain protection, and even promote the screening of patients before admission to hospital and facilitate the process of brain health.

PND has been demonstrated to be associated with multiple factors, among which the theories of neuroinflammation and oxidative stress may be the mainstream. In recent years, there are mounting studies about the association between hnRNPA2/B1 and the exacerbation of cognitive performance (Mizukami et al., 2005; Shorter and Taylor, 2013; Lorente Pons et al., 2020). HnRNPA2/B1 could affect cognitive function through alternative splicing and hence lead to the over-expression of β-secretase 1, and which could increase the accumulation of amyloid precursor protein and soluble $A\beta_{1-42}$ in cytoplasm and promote the phosphorylation of tau protein (Kolisnyk et al., 2017; Zhang et al., 2021). These pathological changes not only damage the neurons directly, but also indirectly trigger neuroinflammation by interacting synergistically with glial cells, ultimately making neurodegenerative lesion stabile and irreversible. What's more, the prion-like domains (PrLD)

TABLE 3 Plasma hnRNPA2/B1 and $A\beta_{42}$ levels for patients with/without PND [pg/mL, M (Q1, Q3)].

Time	Variable	Non-PND	PND	*Z*-value	*P*-value
Postoperative day 7	hnRNPA2/B1	54.95 (37.23, 63.35)	72.26 (58.33, 133.32)	−2.292	0.022*
	$A\beta_{42}$	22.62 (12.94, 30.21)	30.78 (21.33, 45.77)	−1.230	0.219
Postoperative day 90	hnRNPA2/B1	56.38 (40.06, 64.99)	102.93 (59.46, 140.78)	−2.525	0.012^{+}
	$A\beta_{42}$	23.98 (16.80, 31.48)	35.23 (31.13, 40.61)	−2.453	0.014^{+}

Data are presented as median with inter-quartile range. The *P*-value is calculated by the Mann-Whitney *U*-test. $^{*}p < 0.05$ compared with group Non-PND_1. $^{+}p < 0.05$ compared with group Non-PND_2.

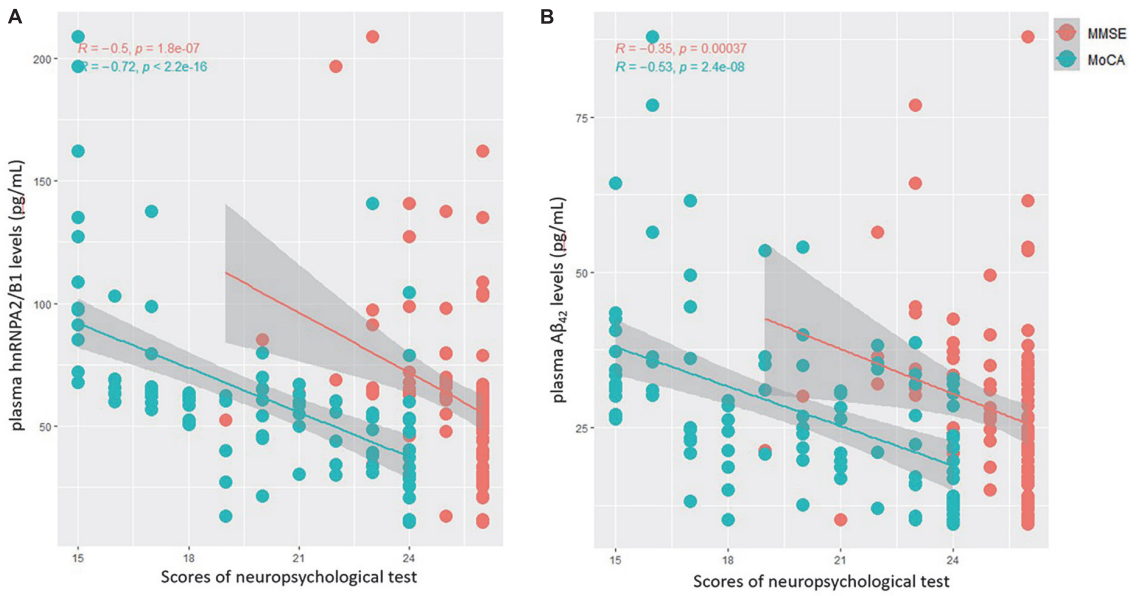

FIGURE 4
(A) Correlations between plasma hnRNPA2/B1 levels and MMSE(red) as well as MoCA(green) scores. **(B)** Correlations between plasma $A\beta_{42}$ levels and MMSE(red) as well as MoCA(green) scores.

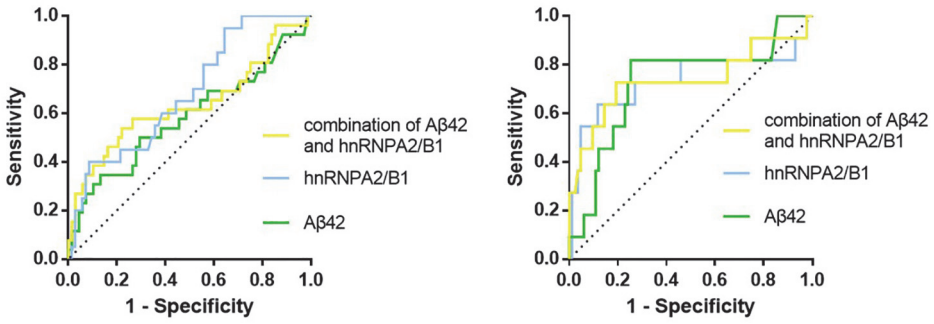

FIGURE 5
ROC curves for preoperative biomarkers. The figure showed the ROC curves for hnRNPA2/B1, $A\beta_{42}$ and their combination at 7 days **(Left)** and 3 months **(Right)** after surgery, respectively.

of hnRNPA2/B1 are the critical components that drive liquid–liquid phase separation (LLPS) and subsequently contribute stress granule (SG) to the hydrogel phase transition (Lee et al., 2016), while the latter is the key mechanism of conversion from neurodegeneration to dementia in the elderly (Lu et al., 2020; Rossi et al., 2020). Consistently, we found that the elderly with PND usually had a higher preoperative hnRNPA2/B1 level and this biomarker could

TABLE 4 ROC curve analysis results of plasma hnRNPA2/B1 and $A\beta_{42}$ levels.

Time	Variable	Sensitivity	Specificity	Youden index	AUC	95% CI
Postoperative day 7	hnRNPA2/B1	0.687	0.649	0.336	0.686	0.568∼0.804
	$A\beta_{42}$	0.567	0.714	0.281	0.616	0.489∼0.744
	hnRNPA2/B1 + $A\beta_{42}$	0.567	0.783	0.349	0.664	0.538∼0.791
Postoperative day 90	hnRNPA2/B1	0.882	0.636	0.519	0.735	0.525∼0.945
	$A\beta_{42}$	0.818	0.747	0.565	0.728	0.554∼0.903
	hnRNPA2/B1 + $A\beta_{42}$	0.727	0.807	0.535	0.738	0.535∼0.940

TABLE 5 Multivariate logistic regression analysis.

Factors	PND_1		PND_2	
	Odds ratio (95% CI)	*P*-value	Odds ratio (95% CI)	*P*-value
Blood transfusion	2.066 (0.747∼5.717)	0.162	0.899 (0.169∼4.796)	0.901
Education level	0.932 (0.837∼1.038)	0.200	0.948 (0.805∼1.117)	0.525
hnRNPA2/B1	1.018 (1.003∼1.034)	0.018*	1.023 (1.007∼1.039)	0.005*
$A\beta_{42}$	1.021 (0.987∼1.056)	0.237	1.033 (0.992∼1.077)	0.120
DM	1.139 (0.383∼3. 384)	0.815	2.039 (0.430∼9.680)	0.370
Duration of surgery	1.003 (0.994∼1.012)	0.475	1.003 (0.992∼1.077)	0.734
Age	1.031 (0.923∼1.152)	0.587	0.972 (0.812∼1.163)	0.755

*P means P-value < 0.05.
OR, Odds ratio; CI, Confidence interval.

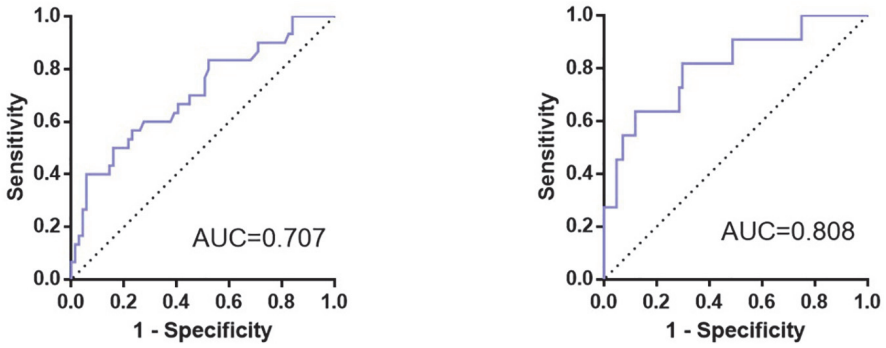

FIGURE 6
ROC curve for prediction model of occurrence of PND. The figure showed the ROC curves for the prediction model of PND at 7 days (Left) and 3 months (Right) after surgery, whose area under the curve (AUC) were 0.707 and 0.808, respectively.

provide preferable specificity and sensitivity to predict PND. In summary, our finding that hnRNPA2/B1 combined with $A\beta_{42}$ could further increase the predictive value is encouraging as it could accurately identify people at high risk of PND.

As for the logistic multivariable regression and the prediction model, we only took preoperative hnRNPA2/B1 and $A\beta_{42}$ level, intraoperative blood transfusion event, educational level, diabetes, duration of surgery and age into consideration due to the size of the sample, the former six factors are significantly different in our single variable analysis. While age has been reported as comorbidities of PND in previous literature (Monk et al., 2008; Wu et al., 2016). With the result, we built a prediction model for PND, and its AUC of the ROC curve was 0.707 in short-term follow-up and 0.808 in a longer time. As a result, this model is meaningful to predict PND after major orthopedic surgery at the early stage, guiding proper care for the patients at high-risk of PND much earlier. Though there is a prediction model of postoperative cognitive outcomes for elderly orthopedic patients, this model was based on postoperative delirium only at 1 day after

surgery (Wang et al., 2021). Therefore, our research is novel and profound with the consideration of long-term cognitive changes after surgery, while a larger scale of multicenter clinical researches need to be conducted in the future.

For the first time to explore the influence of hnRNPA2/B1 on the occurrence of PND after spinal surgery, our finding could give clinicians assistance to monitor and intervene the cognitive function in the elderly patients at the early stage. Sleep, pain, and cognition are three key intervenable targets in any multicomponent intervention designed to optimize perioperative brain (O'Gara et al., 2021). In consequence, we could reduce the occurrence and severity of PND by week-long cognitive training before surgery, relieving preoperative pain and tension, improving the sleeping conditions and so on (Ball et al., 2002; Sieber et al., 2011; Kamdar et al., 2013).

There are several limitations in our present study. Firstly, patients are usually discharged from hospital within 5 days, making it hard to collect blood samples in a longer follow-up period and investigate the dynamic changes of hnRNPA2/B1 in the development of disease as well as the severity of cognitive decline. Moreover, we only observed cognitive outcomes at 7 days and 3 months after surgery and did not perform longer follow-up. Therefore, longer-term impact of preoperative hnRNPA2/B1 level to AD conversion remains unknown. In the future, we will continue to follow up this population to clarify the relationship between hnRNPA2B1 and the outcome of PND and establish a complete perioperative warning system of MCI-PND-AD. A large-scale multicenter study will be carried out to further validate our findings as well. However, it should be noted that, we have indeed found some patients present a tendency to progress to dementia at the 3-month follow-up after surgery, whose neuropsychological performance is poorer than before and meet the criteria of dementia.

Briefly, our data expand the clinical value of hnRNPA2/B1 and suggest that patients occurring PND after lumbar decompression and fusion have higher hnRNPA2/B1 level as compared to controls. When taking baseline characteristics and biomarker signature of patients into account, we believe that increasing number of individuals at high risk of PND will be identified with high accuracy for they may benefit the most from timely interventions aimed at preventing pathological cognitive decline.

Data availability statement

The datasets presented in this study can be found in online repositories. The names of the repository/repositories and accession number(s) can be found in the article/**Supplementary material**.

Ethics statement

The studies involving human participants were reviewed and approved by the Medical Ethics Committee of Tianjin Third Central Hospital Nankai University Affinity the Third Central Hospital. The patients/participants provided their written informed consent to participate in this study.

Author contributions

HW: study design and manuscript revision. TX: data analysis and manuscript writing. CY: FCM. XW: follow-up of patients and post-operative data acquisition. LB: subjects' recruitment. JM: qRT-PCR. MZ: ELISA. WH: peri- and intra-operative data acquisition. All authors contributed to the article and approved the submitted version.

Funding

This work was supported by grants from the National Natural Science Foundation of China (82071220), the Natural Science Foundation of Tianjin (20JCYBJC01290), the Science and Technology Foundation of Tianjin Health Commission (MS20013), and the Tianjin key Medical Discipline (Specialty) Construction Project (TJYXZDXK-072C).

Conflict of interest

The authors declare that the research was conducted in the absence of any commercial or financial relationships that could be construed as a potential conflict of interest.

Publisher's note

Supplementary material

The Supplementary Material for this article can be found online at: https://www.frontiersin.org/articles/10.3389/fnagi.2022.1034041/full#supplementary-material

References

Arenaza-Urquijo, E. M., Landeau, B., La Joie, R., Mevel, K., Mezenge, F., Perrotin, A., et al. (2013). Relationships between years of education and gray matter volume, metabolism and functional connectivity in healthy elders. *Neuroimage* 83, 450–457. doi: 10.1016/j.neuroimage.2013.06.053

Ball, K., Berch, D. B., Helmers, K. F., Jobe, J. B., Leveck, M. D., Marsiske, M., et al. (2002). Effects of cognitive training interventions with older adults: A randomized controlled trial. *JAMA* 288, 2271–2281. doi: 10.1001/jama.288.18.2271

Ballweg, T., White, M., Parker, M., Casey, C., Bo, A., Farahbakhsh, Z., et al. (2021). Association between plasma tau and postoperative delirium incidence and severity: A prospective observational study. *Br. J. Anaesth.* 126, 458–466. doi: 10.1016/j.bja.2020.08.061

Carr, Z. J., Cios, T. J., Potter, K. F., and Swick, J. T. (2018). Does dexmedetomidine ameliorate postoperative cognitive dysfunction? A brief review of the recent literature. *Curr. Neurol. Neurosci. Rep.* 18:64. doi: 10.1007/s11910-018-0873-z

Cata, J. P., Wang, H., Gottumukkala, V., Reuben, J., and Sessler, D. I. (2013). Inflammatory response, immunosuppression, and cancer recurrence after perioperative blood transfusions. *Br. J. Anaesth.* 110, 690–701. doi: 10.1093/bja/aet068

Danielson, M., Reinsfelt, B., Westerlind, A., Zetterberg, H., Blennow, K., and Ricksten, S. E. (2018). Effects of methylprednisolone on blood-brain barrier and cerebral inflammation in cardiac surgery-a randomized trial. *J. Neuroinflammation* 15:283. doi: 10.1186/s12974-018-1318-y

de Menezes, S. T., Giatti, L., Brant, L. C. C., Griep, R. H., Schmidt, M. I., Duncan, B. B., et al. (2021). Hypertension, prehypertension, and hypertension control: Association with decline in cognitive performance in the ELSA-Brasil cohort. *Hypertension* 77, 672–681. doi: 10.1161/HYPERTENSIONAHA.120.16080

Dijkstra, J. B., Houx, P. J., and Jolles, J. (1999). Cognition after major surgery in the elderly: Test performance and complaints. *Br. J. Anaesth.* 82, 867–874. doi: 10.1093/bja/82.6.867

Evered, L., Silbert, B., Scott, D. A., Ames, D., Maruff, P., and Blennow, K. (2016). Cerebrospinal fluid biomarker for Alzheimer disease predicts postoperative cognitive dysfunction. *Anesthesiology* 124, 353–361. doi: 10.1097/ALN.0000000000000953

Evered, L. A., and Silbert, B. S. (2018). Postoperative cognitive dysfunction and noncardiac surgery. *Anesth. Analg.* 127, 496–505. doi: 10.1213/ANE.0000000000003514

Feinkohl, I., Winterer, G., and Pischon, T. (2017a). Diabetes is associated with risk of postoperative cognitive dysfunction: A meta-analysis. *Diabetes Metab. Res. Rev.* 33:e2884. doi: 10.1002/dmrr.2884

Feinkohl, I., Winterer, G., Spies, C. D., and Pischon, T. (2017b). Cognitive reserve and the risk of postoperative cognitive dysfunction. *Dtsch. Arztebl. Int.* 114, 110–117. doi: 10.3238/arztebl.2017.0110

Feinkohl, I., Winterer, G., and Pischon, T. (2018). Associations of dyslipidaemia and lipid-lowering treatment with risk of postoperative cognitive dysfunction: A systematic review and meta-analysis. *J. Epidemiol. Commun. Health* 72, 499–506. doi: 10.1136/jech-2017-210338

Ferraris, V. A., Ballert, E. Q., and Mahan, A. (2013). The relationship between intraoperative blood transfusion and postoperative systemic inflammatory response syndrome. *Am. J. Surg.* 205, 457–465. doi: 10.1016/j.amjsurg.2012.07.042

Gao, S., Zhang, S., Zhou, H., Tao, X., Ni, Y., Pei, D., et al. (2021). Role of mTOR-regulated autophagy in synaptic plasticity related proteins downregulation and the reference memory deficits induced by anesthesia/surgery in aged mice. *Front. Aging Neurosci.* 13:628541. doi: 10.3389/fnagi.2021.628541

Heemskerk, J. L., Oluwadara Akinduro, O., Clifton, W., Quinones-Hinojosa, A., and Abode-Iyamah, K. O. (2021). Long-term clinical outcome of minimally invasive versus open single-level transforaminal lumbar interbody fusion for degenerative lumbar diseases: A meta-analysis. *Spine J.* 21, 2049–2065. doi: 10.1016/j.spinee.2021.07.006

Hughes, D., Judge, C., Murphy, R., Loughlin, E., Costello, M., Whiteley, W., et al. (2020). Association of blood pressure lowering with incident dementia or cognitive impairment: A systematic review and meta-analysis. *JAMA* 323, 1934–1944. doi: 10.1001/jama.2020.4249

Iadecola, C., and Gottesman, R. F. (2019). Neurovascular and cognitive dysfunction in hypertension. *Circ. Res.* 124, 1025–1044. doi: 10.1161/CIRCRESAHA.118.313260

Jiang, X. L., Gu, X. Y., Zhou, X. X., Chen, X. M., Zhang, X., Yang, Y. T., et al. (2019). Intestinal dysbacteriosis mediates the reference memory deficit induced by anaesthesia/surgery in aged mice. *Brain Behav. Immun.* 80, 605–615. doi: 10.1016/j.bbi.2019.05.006

Kamdar, B. B., King, L. M., Collop, N. A., Sakamuri, S., Colantuoni, E., Neufeld, K. J., et al. (2013). The effect of a quality improvement intervention on perceived sleep quality and cognition in a medical ICU. *Crit. Care Med.* 41, 800–809. doi: 10.1097/CCM.0b013e3182746442

Kolisnyk, B., Al-Onaizi, M., Soreq, L., Barbash, S., Bekenstein, U., Haberman, N., et al. (2017). Cholinergic surveillance over hippocampal RNA metabolism and Alzheimer's-like pathology. *Cereb. Cortex* 27, 3553–3567. doi: 10.1093/cercor/bhw177

Krell-Roesch, J., Syrjanen, J. A., Vassilaki, M., Lowe, V. J., Vemuri, P., Mielke, M. M., et al. (2021). Brain regional glucose metabolism, neuropsychiatric symptoms, and the risk of incident mild cognitive impairment: The mayo clinic study of aging. *Am. J. Geriatr. Psychiatry* 29, 179–191. doi: 10.1016/j.jagp.2020.06.006

Lachmann, G., Feinkohl, I., Borchers, F., Ottens, T. H., Nathoe, H. M., Sauer, A. M., et al. (2018). Diabetes, but not hypertension and obesity, is associated with postoperative cognitive dysfunction. *Dement. Geriatr. Cogn. Disord.* 46, 193–206. doi: 10.1159/000492962

Le, Y., Liu, S., Peng, M., Tan, C., Liao, Q., Duan, K., et al. (2014). Aging differentially affects the loss of neuronal dendritic spine, neuroinflammation and memory impairment at rats after surgery. *PLoS One* 9:e106837. doi: 10.1371/journal.pone.0106837

Lee, K. H., Zhang, P., Kim, H. J., Mitrea, D. M., Sarkar, M., Freibaum, B. D., et al. (2016). C9orf72 dipeptide repeats impair the assembly, dynamics, and function of membrane-less organelles. *Cell* 167, 774–788.e17. doi: 10.1016/j.cell.2016.10.002

Liu, Y., Dong, Y. H., Lyu, P. Y., Chen, W. H., and Li, R. (2018). Hypertension-induced cerebral small vessel disease leading to cognitive impairment. *Chin. Med. J.* 131, 615–619. doi: 10.4103/0366-6999.226069

Lorente Pons, A., Higginbottom, A., Cooper-Knock, J., Alrafiah, A., Alofi, E., Kirby, J., et al. (2020). Oligodendrocyte pathology exceeds axonal pathology in white matter in human amyotrophic lateral sclerosis. *J. Pathol.* 251, 262–271. doi: 10.1002/path.5455

Lu, J., Cao, Q., Hughes, M. P., Sawaya, M. R., Boyer, D. R., Cascio, D., et al. (2020). CryoEM structure of the low-complexity domain of hnRNPA2 and its conversion to pathogenic amyloid. *Nat. Commun.* 11:4090. doi: 10.1038/s41467-020-17905-y

Luo, A., Yan, J., Tang, X., Zhao, Y., Zhou, B., and Li, S. (2019). Postoperative cognitive dysfunction in the aged: The collision of neuroinflammaging with perioperative neuroinflammation. *Inflammopharmacology* 27, 27–37. doi: 10.1007/s10787-018-00559-0

Memoria, C. M., Yassuda, M. S., Nakano, E. Y., and Forlenza, O. V. (2013). Brief screening for mild cognitive impairment: Validation of the Brazilian version of the Montreal cognitive assessment. *Int. J. Geriatr. Psychiatry* 28, 34–40. doi: 10.1002/gps.3787

Mitchell, A. J. (2009). A meta-analysis of the accuracy of the mini-mental state examination in the detection of dementia and mild cognitive impairment. *J. Psychiatr. Res.* 43, 411–431. doi: 10.1016/j.jpsychires.2008.04.014

Mizukami, K., Ishikawa, M., Iwakiri, M., Ikonomovic, M. D., Dekosky, S. T., Kamma, H., et al. (2005). Immunohistochemical study of the hnRNP A2 and B1 in the hippocampal formations of brains with Alzheimer's disease. *Neurosci. Lett.* 386, 111–115. doi: 10.1016/j.neulet.2005.05.070

Monk, T. G., Weldon, B. C., Garvan, C. W., Dede, D. E., Van Der Aa, M. T., Heilman, K. M., et al. (2008). Predictors of cognitive dysfunction after major noncardiac surgery. *Anesthesiology* 108, 18–30. doi: 10.1097/01.anes.0000296071.19434.1e

Moran, C., Beare, R., Wang, W., Callisaya, M., Srikanth, V., and Alzheimer's Disease Neuroimaging Initiative [ADNI]. (2019). Type 2 diabetes mellitus, brain atrophy, and cognitive decline. *Neurology* 92, e823–e830. doi: 10.1212/WNL.0000000000006955

Needham, M. J., Webb, C. E., and Bryden, D. C. (2017). Postoperative cognitive dysfunction and dementia: What we need to know and do. *Br. J. Anaesth.* 119, i115–i125. doi: 10.1093/bja/aex354

Netto, M. B., De Oliveira Junior, A. N., Goldim, M., Mathias, K., Fileti, M. E., Da Rosa, N., et al. (2018). Oxidative stress and mitochondrial dysfunction contributes to postoperative cognitive dysfunction in elderly rats. *Brain Behav. Immun.* 73, 661–669. doi: 10.1016/j.bbi.2018.07.016

Newman, M. F., Kirchner, J. L., Phillips-Bute, B., Gaver, V., Grocott, H., Jones, R. H., et al. (2001). Longitudinal assessment of neurocognitive function after coronary-artery bypass surgery. *N. Engl. J. Med.* 344, 395–402. doi: 10.1056/NEJM200102083440601

O'Gara, B. P., Gao, L., Marcantonio, E. R., and Subramaniam, B. (2021). Sleep, pain, and cognition: Modifiable targets for optimal perioperative brain health. *Anesthesiology* 135, 1132–1152. doi: 10.1097/ALN.0000000000004046

O'Gara, B. P., Mueller, A., Gasangwa, D. V. I., Patxot, M., Shaefi, S., Khabbaz, K., et al. (2020). Prevention of early postoperative decline: A randomized, controlled feasibility trial of perioperative cognitive training. *Anesth. Analg.* 130, 586–595. doi: 10.1213/ANE.0000000000004469

Park, D. C., and Reuter-Lorenz, P. (2009). The adaptive brain: Aging and neurocognitive scaffolding. *Annu. Rev. Psychol.* 60, 173–196. doi: 10.1146/annurev.psych.59.103006.093656

Perry, A., Wen, W., Kochan, N. A., Thalamuthu, A., Sachdev, P. S., and Breakspear, M. (2017). The independent influences of age and education on functional brain networks and cognition in healthy older adults. *Hum. Brain Mapp.* 38, 5094–5114. doi: 10.1002/hbm.23717

Ramlawi, B., Rudolph, J. L., Mieno, S., Khabbaz, K., Sodha, N. R., Boodhwani, M., et al. (2006). Serologic markers of brain injury and cognitive function after cardiopulmonary bypass. *Ann. Surg.* 244, 593–601. doi: 10.1097/01.sla.0000239087.00826.b4

Rappold, T., Laflam, A., Hori, D., Brown, C., Brandt, J., Mintz, C. D., et al. (2016). Evidence of an association between brain cellular injury and cognitive decline after non-cardiac surgery. *Br. J. Anaesth.* 116, 83–89. doi: 10.1093/bja/aev415

Rossi, S., Rompietti, V., Antonucci, Y., Giovannini, D., Scopa, C., Scaricamazza, S., et al. (2020). UsnRNP trafficking is regulated by stress granules and compromised by mutant ALS proteins. *Neurobiol. Dis.* 138:104792. doi: 10.1016/j.nbd.2020.104792

Shorter, J., and Taylor, J. P. (2013). Disease mutations in the prion-like domains of hnRNPA1 and hnRNPA2/B1 introduce potent steric zippers that drive excess RNP granule assembly. *Rare Dis.* 1:e25200. doi: 10.4161/rdis.25200

Sieber, F. E., Mears, S., Lee, H., and Gottschalk, A. (2011). Postoperative opioid consumption and its relationship to cognitive function in older adults with hip fracture. *J. Am. Geriatr. Soc.* 59, 2256–2262. doi: 10.1111/j.1532-5415.2011.03729.x

Steinmetz, J., Christensen, K. B., Lund, T., Lohse, N., Rasmussen, L. S., and Group, I. (2009). Long-term consequences of postoperative cognitive dysfunction. *Anesthesiology* 110, 548–555. doi: 10.1097/ALN.0b013e318195b569

Subramaniyan, S., and Terrando, N. (2019). Neuroinflammation and perioperative neurocognitive disorders. *Anesth. Analg.* 128, 781–788. doi: 10.1213/ANE.0000000000004053

Tan, H., Bi, J., Wang, Y., Zhang, J., and Zuo, Z. (2015). Transfusion of old RBCs induces neuroinflammation and cognitive impairment. *Crit. Care Med.* 43, e276–e286. doi: 10.1097/CCM.0000000000001023

Terrando, N., Eriksson, L. I., Ryu, J. K., Yang, T., Monaco, C., Feldmann, M., et al. (2011). Resolving postoperative neuroinflammation and cognitive decline. *Ann. Neurol.* 70, 986–995. doi: 10.1002/ana.22664

Urner, M., Herrmann, I. K., Buddeberg, F., Schuppli, C., Roth Z'graggen, B., Hasler, M., et al. (2012). Effects of blood products on inflammatory response in endothelial cells in vitro. *PLoS One* 7:e33403. doi: 10.1371/journal.pone.0033403

van Sloten, T. T., Sedaghat, S., Carnethon, M. R., Launer, L. J., and Stehouwer, C. D. A. (2020). Cerebral microvascular complications of type 2 diabetes: Stroke, cognitive dysfunction, and depression. *Lancet Diabetes Endocrinol.* 8, 325–336. doi: 10.1016/S2213-8587(19)30405-X

Wang, G., Zhang, L., Qi, Y., Chen, G., Zhou, J., Zhu, H., et al. (2021). Development and validation of a postoperative delirium prediction model for elderly orthopedic patients in the intensive care unit. *J. Healthc. Eng.* 2021:9959077. doi: 10.1155/2021/9959077

Wang, J., Yang, C., Wang, H., Li, D., Li, T., Sun, Y., et al. (2020). A new rat model of chronic cerebral hypoperfusion resulting in early-stage vascular cognitive impairment. *Front. Aging Neurosci.* 12:86. doi: 10.3389/fnagi.2020.00086

Wu, C., Wang, R., Li, X., and Chen, J. (2016). Preoperative serum MicroRNA-155 expression independently predicts postoperative cognitive dysfunction after laparoscopic surgery for colon cancer. *Med. Sci. Monit.* 22, 4503–4508. doi: 10.12659/MSM.898397

Xiao, J. Y., Xiong, B. R., Zhang, W., Zhou, W. C., Yang, H., Gao, F., et al. (2018). PGE2-EP3 signaling exacerbates hippocampus-dependent cognitive impairment after laparotomy by reducing expression levels of hippocampal synaptic plasticity-related proteins in aged mice. *CNS Neurosci. Ther.* 24, 917–929. doi: 10.1111/cns.12832

Xiao, Q. X., Liu, Q., Deng, R., Gao, Z. W., and Zhang, Y. (2020). Postoperative cognitive dysfunction in elderly patients undergoing hip arthroplasty. *Psychogeriatrics* 20, 501–509. doi: 10.1111/psyg.12516

Yang, X. D., Wang, L. K., Wu, H. Y., and Jiao, L. (2018). Effects of prebiotic galacto-oligosaccharide on postoperative cognitive dysfunction and neuroinflammation through targeting of the gut-brain axis. *BMC Anesthesiol.* 18:177. doi: 10.1186/s12871-018-0642-1

Zhang, Q., Zhang, J., Ye, J., Li, X., Liu, H., Ma, X., et al. (2021). Nuclear speckle specific hnRNP D-like prevents age- and AD-related cognitive decline by modulating RNA splicing. *Mol. Neurodegener.* 16:66. doi: 10.1186/s13024-021-00485-w

Zhu, S. H., Ji, M. H., Gao, D. P., Li, W. Y., and Yang, J. J. (2014). Association between perioperative blood transfusion and early postoperative cognitive dysfunction in aged patients following total hip replacement surgery. *Ups. J. Med. Sci.* 119, 262–267. doi: 10.3109/03009734.2013.873502

frontiers | Frontiers in Aging Neuroscience

TYPE Original Research
PUBLISHED 11 November 2022
DOI 10.3389/fnagi.2022.1040569

OPEN ACCESS

EDITED BY
Jiaqiang Zhang,
Zhengzhou University,
China

REVIEWED BY
Shanwu Feng,
Nanjing Medical University, China
Natalija Popovic,
University of Murcia,
Spain

*CORRESPONDENCE
Qiujun Wang
wangqiujunsy@163.com

SPECIALTY SECTION
This article was submitted to Neurocognitive Aging and Behavior, a section of the journal Neurocognitive Aging and Behavior

RECEIVED 09 September 2022
ACCEPTED 25 October 2022
PUBLISHED 11 November 2022

CITATION
Wang X, Li Y, Zhao J, Yu J, Zhang Q, Xu F, Zhang Y, Zhou Q, Yin C, Hou Z and Wang Q (2022) Activation of astrocyte Gq pathway in hippocampal CA1 region attenuates anesthesia/surgery induced cognitive dysfunction in aged mice. *Front. Aging Neurosci.* 14:1040569. doi: 10.3389/fnagi.2022.1040569

Activation of astrocyte Gq pathway in hippocampal CA1 region attenuates anesthesia/surgery induced cognitive dysfunction in aged mice

Xupeng Wang[1], Yanan Li[1], Juan Zhao[2], Jiaxu Yu[1], Qi Zhang[1,3], Fang Xu[1], Yahui Zhang[1], Qi Zhou[1], Chunping Yin[1], Zhiyong Hou[4,5] and Qiujun Wang[1]*

[1]Department of Anesthesiology, Third Hospital of Hebei Medical University, Shijiazhuang, Hebei, China, [2]Teaching Experiment Center, Hebei Medical University, Shijiazhuang, Hebei, China, [3]Department of Anesthesiology, Hebei Children's Hospital Affiliated to Hebei Medical University, Shijiazhuang, Hebei, China, [4]Department of Orthopedics, The Third Hospital of Hebei Medical University, Shijiazhuang, Hebei, China, [5]NHC Key Laboratory of Intelligent Orthopaedic Equipment, The Third Hospital of Hebei Medical University, Shijiazhuang, Hebei, China

The elderly are particularly vulnerable to brain dysfunction after fracture surgery, but the mechanism underlying the cognitive decline due to anesthesia/surgery is not well understood. In this study, we observed hippocampus-dependent cognitive impairment in aged mice undergoing anesthesia and tibial fracture surgery, a common model of postoperative cognitive dysfunction in aged mice. We used Golgi staining and neuroelectrophysiological techniques to detect structurally and functionally impaired synaptic plasticity in hippocampal CA1 region of Postoperative cognitive dysfunction aged mice, respectively. Based on the 'third party synapse' hypothesis of astrocytes, we used glial fibrillary acidic protein to label astrocytes and found an increase in abnormal activation of astrocytes in the CA1 region of hippocampus. We hypothesize that abnormal astrocyte function is the driving force for impaired synaptic plasticity. So we used chemogenetic methods to intervene astrocytes. Injection of adeno-associated virus into the CA1 region of the hippocampus bilateral to aged mice resulted in the specific expression of the Gq receptor, a receptor specially designed to be activated only by certain drugs, within astrocytes. The results of novel object recognition and conditioned fear experiments showed that CNO activation of astrocyte Gq pathway could improve the learning and memory ability and the synaptic plasticity of Postoperative cognitive dysfunction aged mice was also improved. The results of this study suggest that activation of the Gq pathway in astrocytes alleviates Postoperative cognitive dysfunction induced by anesthesia and surgery in aged mice.

KEYWORDS

POCD, astrocyte, synaptic plasticity, chemical genetics, aged mice

Introduction

With the continuous improvement and development of the economy and medical system, the quality of life has been improved and the life expectancy has been extended (Kontis et al., 2017). Aging is a common phenomenon in our society, and the number of fractures in this population is increasing every year due to the deterioration of physical abilities, weakness and osteoporosis (Gallagher, 2004; Frisoli et al., 2021). The incidence of postoperative cognitive dysfunction (POCD) is very high in elderly patients after fracture, surgery and anesthesia (Papadopoulos et al., 2014; Beishuizen et al., 2017; Kristek et al., 2019). POCD is one of the most common postoperative complications in elderly patients, manifested by cognitive decline, anxiety, reduced attention, impaired memory, impaired language comprehension and social integration. A growing body of evidence from clinical studies suggests that POCD may lead to longer hospital stays, reduced quality of life, and increased mortality (Holmgaard et al., 2019; Lin et al., 2020). However, the mechanism of POCD in elderly patients remains unclear. How to provide a stable perioperative period for elderly patients and protect their cognitive function from being impaired has become an urgent clinical problem. Numerous studies have shown that the hippocampal CA1 region is critical for recent memory and that the occurrence of POCD is associated with altered synaptic plasticity of neurons in the hippocampal CA1 region (Tian et al., 2015; Xiao et al., 2018; Liu et al., 2021). The exact mechanism is subject to different opinions. Astrocytes are the most numerous non-neural cells in the brain and are known to provide structural and metabolic support for neuronal networks, but there is growing evidence that they also play an active role in regulating neuronal activity (Suzuki et al., 2011; Zhou et al., 2021). Recent studies have shown that astrocytes are required for synaptic plasticity and normal memory capacity, and have even proposed the hypothesis of "tripartite synapses"-that astrocytes not only wrap, support, and insulate synapses, but also sense and actively modify synaptic structures (Durkee and Araque, 2019). Chemical genetic techniques based on engineered proteins are a powerful approach featuring chemical genetic techniques for designing receptors exclusively activated by designer drugs (DEARD; Gomez et al., 2017). Many recent studies have used astrocyte-specific chemogenetic techniques to confirm the importance of activation of astrocytes in memory formation. For example, Adamsky et al. (2018) demonstrated that activation of astrocytes led to increased spontaneous vesicle release and NMDA-mediated *de novo* synaptic potentiation. Suzuki et al. (2011) reported a key role of astrocytes in the transition from short-term to long-term memory. However, most studies on astrocytes have focused on their positive role in normal memory, and relatively few studies have been conducted on the role of astrocytes in POCD. In the present study, we found abnormal activation of astrocytes in the hippocampal CA1 region of POCD-aged mice. By injecting adeno-associated virus expressing specially designed receptor hM3D under the control of glial fibrillary acidic protein promoter in the hippocampal CA1 region, the cognitive decline in aged mice could be improved, revealing that abnormal astrocyte function may be one of the causes of POCD in aged mice, and activation of astrocyte Gq-GPCR signaling in the hippocampal CA1 region could improve postoperative cognitive dysfunction.

Materials and methods

Animals

A total of 55 18-month-old, weighing 25–32 g, specific pathogen-free (SPF)-grade male C57BL/6 J mice purchased from Hebei Ex&InVivo Biotechnology Co., Ltd. [License No.: SCXK(J)2020–002] were used in this experiment. Two mice were excluded because anatomical repositioning was not achieved, and another three were excluded because the cerebral cortex was damaged during cranial drilling. All excluded mice were replenished afterwards, resulting in 10 mice per group (n = 10). All mice were housed in an animal room with temperature maintained at (25 ± 1) °C, humidity at (55 ± 5) %, and a light/dark cycle of 12 h/12 h. The Ethics Committee of the Third Hospital of Hebei Medical University has approved the experimental design and protocol [GA2017-026-1]. All mice were habituated in separate cages for 1 week prior to surgery, and all mice received human care during the experiments with reference to the recommendations of the Guide for the Care and Use of Laboratory Animals published by the National Institutes of Health.

Anesthesia/surgical model

Anesthesia/surgery model was established by performing right tibial fracture surgery on mice under sevoflurane anesthesia as described in other studies (Liu et al., 2021). In the first experiment, mice were randomly divided into two groups ($n = 10$): the control group (C) and the tibial fracture surgery group (TF). Mice in group C did not receive anesthesia or any surgical stimulation. Older mice in the TF group were placed in an anesthesia-inducing chamber pre-filled with 5% sevoflurane (21,070,531, Shanghai Hengrui Pharmaceutical Co., Ltd., China, Shanghai) and removed after the righting reflex disappeared. They were then fixed in the left lateral position on a heated blanket-lined operating table and maintained under anesthesia with 3% sevoflurane. To provide good intra-and postoperative analgesia, the incision site was infiltrated anesthesia with 0.5% lidocaine after disinfecting and removing the hair of the surgical site. A longitudinal incision of approximately 1 cm was subsequently made along the medial surface of the tibia to fully expose the tibial plateau. An 8-mm long needle with an internal diameter of 0.3 mm was inserted vertically into the tibial plateau and along the longitudinal axis of the tibial marrow cavity, and then the upper middle part of the tibia was cut with a scalpel. Finally, the incision

was sutured, and the mice were kept warm and allowed to awaken naturally. The total time was about 20 min (Figure 1A).

Stereotactic injection of virus

In the interventional study, mice were randomly divided into 3 groups (n = 10): the TF + rAAV5-GfaABC1D-mCherry + CNO group (AAV-mCherry/CNO), the TF + rAAV5-GfaABC1D-hM3D(Gq)-mCherry + saline group (AAV-hM3D/Saline), and the TF + rAAV5-GfaABC1D-hM3D(Gq)-mCherry + CNO group (AAV-hM3D/CNO). The experimental procedure is shown in a schematic diagram (Figure 1B). Brifely, the mice were placed in an anesthesia induction chamber (Beijing Zhongshi Di Chuang Development Technology Co., Ltd., Beijing, China) pre-filled with 5% sevoflurane, and then removed when the reflexes disappeared, and fixed in prone position on a single-arm digital stereotaxic apparatus (Beijing Zhongshi Di Chuang Development Technology Co., Ltd., Beijing, China) To keep both eyes moist, vitamin A palmitate ophthalmic gel (Lot No.: 220101, Shenyang Xingqi Pharmaceutical CO., LTD., Shenyang, China) was applied to both eyes of the mice. Subsequently, the skin was prepared, disinfected, and the scalp was locally infiltrated with 0.5% lidocaine. The scalp was cut longitudinally and the periosteum was removed to expose the skull, followed by drilling a tiny hole 1.8 mm posterior to bregma at 1.2 mm on each side. The CA1 area of the hippocampus is reached by inserting glass electrodes along the small holes to a depth of 1.8 mm from the cortex. Subsequently 500 nl of rAAV5-GfaABC1D-hM3D(Gq)-mCherry (Titer: 3.05E + 12 VG/ml, BC-0476, Brain Case, China, Shenzhen) or rAAV5-GfaABC1D-mCherry (Titer: 3.25E + 12 VG/ml, BC-0908, Brain Case, China, Shenzhen) was injected at 50 nl/min. The needle was left in place for 10 min after injection, and the glass electrode was slowly withdrawn. Finally, the skull notch was closed with bone wax and the incision was sutured.

Preparation of clozapine N-oxide

Clozapine N-oxide (CNO, S6887, Selleck Chemicals, USA) 50 mg was dissolved in 10 ml of dimethyl sulfoxide (DMSO, ST038, Beyotime, Shanghai, China) solution to prepare a CNO master mix at a concentration of 5 mg/ml. For intraperitoneal injection, CNO was diluted to 0.25 mg/ml working solution using saline. A dose of 2.5 mg/kg CNO was administered intraperitoneally 30 min before the behavioral test. The control solvent was saline containing the same dose of DMSO (subsequently referred to collectively as saline).

Open field test

The open field tests were performed on mice in tibial fracture and control groups on postoperative day 7 to compare the locomotion of the mice ($n = 10$). The bottom surface of the open field box (40 cm × 40 cm × 40 cm) is equally divided by 16 quadrants, the middle 4 quadrants are the central area and the remaining 12 quadrants are the border area including the 4 corner quadrants that were are analyzed as the corner area. We cleaned the open field boxes with 75% alcohol before testing to avoid foreign smells that might influence mice behavior. After 10 s of adaptation, the behavior of mice was recorded for 5 min. Computerized tracking systems (Labmaze V3.0, Beijing Zhongshi Di Chuang Development Technology Co., Ltd., Beijing, China) were used to analyze the distance and speed of movements in mice and time they spent in specific regions.

Elevated plus maze test

The elevated plus maze consisted of two relative open arms (25 cm long and 6 cm wide) and two relative closed arms (25 cm

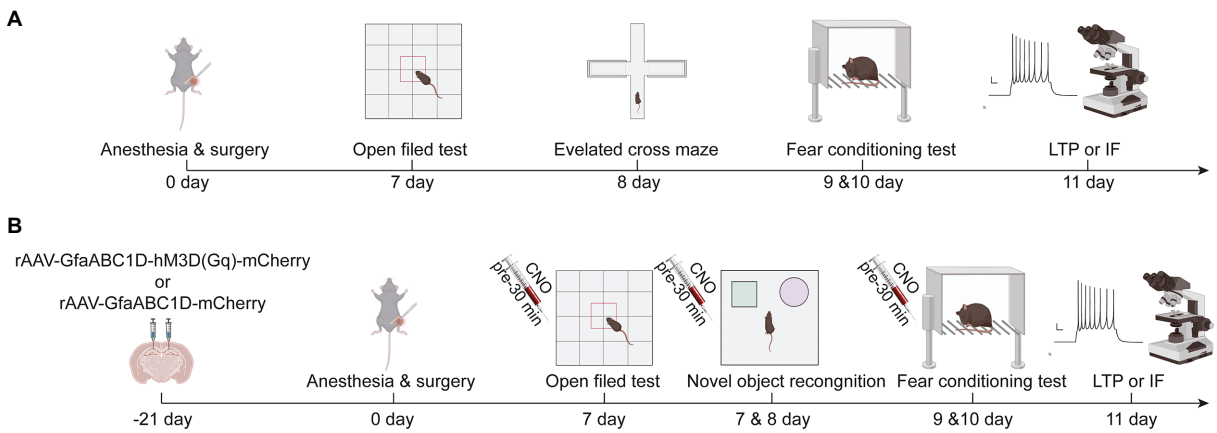

FIGURE 1
(A) Schematic diagram of experimental procedure of aging mice in group C and TF, **(B)** Schematic diagram of experimental procedure of aging mice in AAV mCherry/CNO group, AAV hM3D/Saline group and AAV hM3D/CNO group. Images were created on the BioRender web platform.

long, 6 cm wide and 20 cm high) and a central area (6 cm × 6 cm) connected. Mice were gently stroked in a quiet room for 5 min and then placed with their heads facing the open arm in the central area of the elevated maze. The number of times the mice entered the open arm and the residence time within 5 min were recorded using the animal behavior video analysis system (Labmaze V3.0, Beijing Zhongshi Di Chuang Development Technology Co., Ltd., Beijing, China), and the proportion of residence time in the open arm was calculated.

Novel object recognition test

Mice were trained in novel object recognition on the 7th postoperative day (n = 10). Briefly, two identical, odorless, non-smooth, non-movable objects A and B were placed in symmetrical positions and the mice were allowed to explore them for 10 min for familiarization. Memory tests were performed on postoperative day 8. The familiar object B was replaced with a novel object C of a different shape, and then the mice were placed in a behavioral test chamber and their exploratory behavior was recorded for 5 min by a behavioral analysis system (Labmaze V3.0, Beijing Zhongshi Di Chuang Development Technology Co., Ltd., Beijing, China). Percentage of novel object exploration = novel object exploration time/(novel object exploration time + familiar object exploration time) × 100%; discrimination index = (novel object exploration time – familiar object exploration time)/(novel object exploration time + familiar object exploration time) × 100%.

Fear conditioning test

Aging mice on day 10 post-anesthesia/surgery were subjected to 3 cycles of conditioned fear memory training with context-cue-electric shock pairing (n = 10). Briefly, mice were placed in a square test chamber with a white background for 180 s, then conditioned sound (70 dB, 3 kHz) was added for 30 s, followed by an electric shock (0.75 mA) for 2 s. The entire procedure was repeated three times. The freezing time for the first 180 s of placement in the conditioned fear box was recorded as a baseline. The chamber was wiped with 75% alcohol between each experiment to prevent residual odor from affecting the next experiment. The context association experiment and the cue association experiment were conducted separately on the second day. The context association test was performed as follows: the mice were placed in the same background test chamber for 180 s without adding sound stimuli, and the freezing time of the mice was recorded using the animal behavior analysis software (Labmaze V3.0, Beijing Zhongshi Di Chuang Development Technology Co., Ltd., Beijing, China). Two hours later, the cue association test was performed. The procedure was as follows: the test chamber was modified from a white background to a blue background, and the square activity space was modified to a triangular shape. Mice were placed in the modified new contextual chamber for 180 s. Mice were then subjected to a 180 s sound spike (70 dB, 3 kHz) and their freezing time during this period was recorded. The percentage of freezing time associated with context or with sound was compared between groups of mice to assess fear memory function.

Golgi-cox staining

Three mice in each group were randomly selected for Golgi staining on day 10 after tibial fracture surgery ($n = 3$). Mice were executed under deep anesthesia with 8% sevoflurane, and brain tissues were fixed in 4% paraformaldehyde (G1101, Wuhan servicebio technology CO., Ltd., Wuhan, China) for 48 h. The brain tissues were cut into 2 mm thick pieces, gently rinsed several times with saline, and then placed in Golgi staining solution (G1069, Wuhan servicebio technology CO., Ltd., Wuhan, China) and changed to new staining solution every 3 days for 14 days in a cool and ventilated place. The brain tissue was then washed 3 times with double distilled water (ddH_2O) and incubated overnight in 80% glacial acetic acid (10,000,218, Sinopharm Chemical Reagent Co., Ltd., Shanghai, China). The brain tissue was then rinsed with ddH_2O and dehydrated in 30% sucrose. The brain tissue was cut into 100 μm sections using an oscillating microtome (CRYOSTAR NX50, Thermo, America) and then attached to gelatin slides. The air-dried tissue slides were treated with concentrated ammonia for 15 min, followed by ddH_2O rinsing for 1 min and then treated with acidic firm film fixative for 15 min, ddH_2O rinsing for 3 min and air-drying, and sealed with glycerol gelatin. Two microscopic fields were taken from each mouse in the hippocampus bilaterally and quantitative analysis was performed using Image-Pro Plus 6.0 software. The number and length of dendritic spines in the 30 ~ 90 μm length range on the second or third branch of the neuron were measured, and the density of dendritic spines per 10 μm was calculated according to the following formula: density = number of dendritic spines/dendritic length × 10. Ten concentric circles with 10 μm spacing centered were drawn on the cell body using the Sholl analysis plug-in, and the number of intersections between the dendrites and the concentric circles was calculated.

Long-term potential recording

On day 11 after tibial fracture surgery, three mice per group were randomly selected for neurophysiological testing ($n = 3$). Briefly, 0.2% sodium pentobarbital 50 mg/kg was injected intraperitoneally and the mice were immobilized on a stereotaxic apparatus when the bracing reflex disappeared, then the head hair was removed after sterilization and the scalp was incised medially to expose the skull. Stimulating and receiving electrodes (Kedou Brain-Computer Technology, China, Suzhou) were implanted

after drilling at two sites: (1) the Schaffer lateral branch site: anteroposterior (AP), −1.2 mm from Bregma, mediolateral (ML), −2.2 mm, dorsoventral (DV), 1.3 mm and (2) the granular cell layer site in the CA1 region: AP, −2.0 mm, ML, −1.5 mm, DV, 1.5 mm. Subsequent stimulation was divided into two phases to induce long-term potential. Phase I: Stimulation parameters were adjusted to a frequency of 1/60 Hz, a wave width of 100 s, and a current of 0.3 mA to induce a cluster peak potential. The stimulation electrode and recording electrode were then adjusted to obtain the optimal group spike (PS), and after 30 min of stabilization, the stimulation intensity was adjusted so that the PS was 1/3–1/2 of the maximum value and recorded for 30 min as a baseline; Phase II: the stimulation parameters were adjusted to 5 pulses of 400 Hz, repeated 3 times with 10 s interval, and then the PS was recorded for 120 min after high frequency stimulation (HFS). The slope of the averaged field excitatory postsynaptic potential (fEPSP) recorded for the last 20 min was used for analysis.

Immunofluorescence staining of glial fibrillary acidic protein

Four mice in each group were randomly stained with immunofluorescence on day 11 after tibial fracture to observe the morphological and quantitative changes of astrocytes ($n = 4$). Briefly, paraffin sections were sequentially immersed in xylene and graded concentrations of alcohol to elute the paraffin, and subsequently placed in a modified sodium citrate reagent (P0083, Beyotime, Shanghai, China) and boiled for 20 min, then cooled to room temperature to repair the antigen. After washed thrice in PBS (C0221A, Beyotime, Shanghai, China), the sections were incubated with the quick block solution (P0222, Beyotime, Shanghai, China) for 1 h at room temperature. Sections were then washed again thrice in PBS before incubation with primary polyclonal rabbit antibody against GFAP (1:500, ab1872, Abcam, UK); primary polyclonal rabbit antibody against NEUN (1:200, ET1602-12, HuaBio, Hangzhou, China); primary polyclonal rabbit antibody against Iba-1 (1:200, AF7143, Beyotime, Shanghai, China) and mouse monoclonal antibody mCherry (1:150, K200015M, Solarbio, Beijing, China) overnight at 4°C. After washing thrice with PBS, the secondary antibodies cy3-conjugated goat anti-rabbit IgG (1:200, A5608, Beyotime, Shanghai, China) and FITC-conjugated goat anti-mouse IgG (1:200, A0568, Beyotime, Shanghai, China) was added to incubation for 1 h at room temperature. After washing thrice with PBS, DAPI (P0137, Beyotime, Shanghai, China) was added to stain the cell nuclei for 2 min to show their locations. Images were captured using a laser scanning microscope (Mingmei Photoelectric Technology Co., Ltd., Guangzhou, China). Two fields of visualization were taken from each hippocampal CA1 region on each side of each mouse for analysis, and the number of GFAP-labeled astrocytes under each visual field was counted. The fluorescence area of GFAP under each field of vision was measured using Image J (National Institutes of Health). Three astrocytes with relatively intact structure were selected in each field of view to calculate the fluorescence area.

Statistical analysis

The software GraphPad Prism 9.0.1 (GraphPad Software, Inc.) was used to perform data analysis. The data were tested for normality using the Shapiro test, and normally distributed continuous variables were expressed as mean ± standard deviation. The difference between the C and TF groups were compared by unpaired *t*-tests and multiple comparisons using Bonferroni-corrected *p*-values. Correlation data for the three groups were analyzed using one-way ANOVA with a Tukey *post hoc* test for multiple comparisons. $p < 0.05$ was defined as a statistical difference.

Results

Decreased motor function and cognitive impairment occurred in aged mice after tibial fracture surgery

On day 7 after tibial fracture surgery, we tested the spontaneous mobility of the mice using the open field experiment (Figure 2A). To eliminate the effect of surgical factors, we performed X-ray examinations and did not detect any deformity healing (Supplementary Figure 1). The results of the open filed test showed no significant difference in activity time in the specific regions of the mice in the TF group compared to the C group ($P > 0.05$, Figure 2B), but the total distance traveled was reduced and locomotor speed decreased ($P < 0.05$, Figures 2C,D), indicating that the mice had no significant emotional abnormalities but still had activity limitations 7 days after the anesthesia/surgery. To exclude the effect of postoperative anxiety, we further assessed the anxiety level of the mice with an elevated maze and found no significant difference between the two groups of mice ($P > 0.05$, Figures 2F,G; Supplementary Figure 2). Because of the difference in spontaneous activity between the two groups of mice ($p > 0.05$, Figure 1E), we excluded the usage of the Morris water maze and novel object cognition to assess the memory ability of the mice. We finally chosen the conditioned fear experiment, which is based on the Pavlovian conditioning principle and less dependent on activity ability, to assess memory function (Figure 2H). The results revealed no significant difference in freezing time between the two groups of mice at baseline and in the cue association test ($P > 0.05$, Figure 2I), while freezing time was significantly reduced in the context-related test ($P > 0.05$, Figure 2I). Taken together, these results indicate that tibial fracture surgery in aged mice leads to a hippocampus-dependent decline in cognitive function.

10.3389/fnagi.2022.1040569

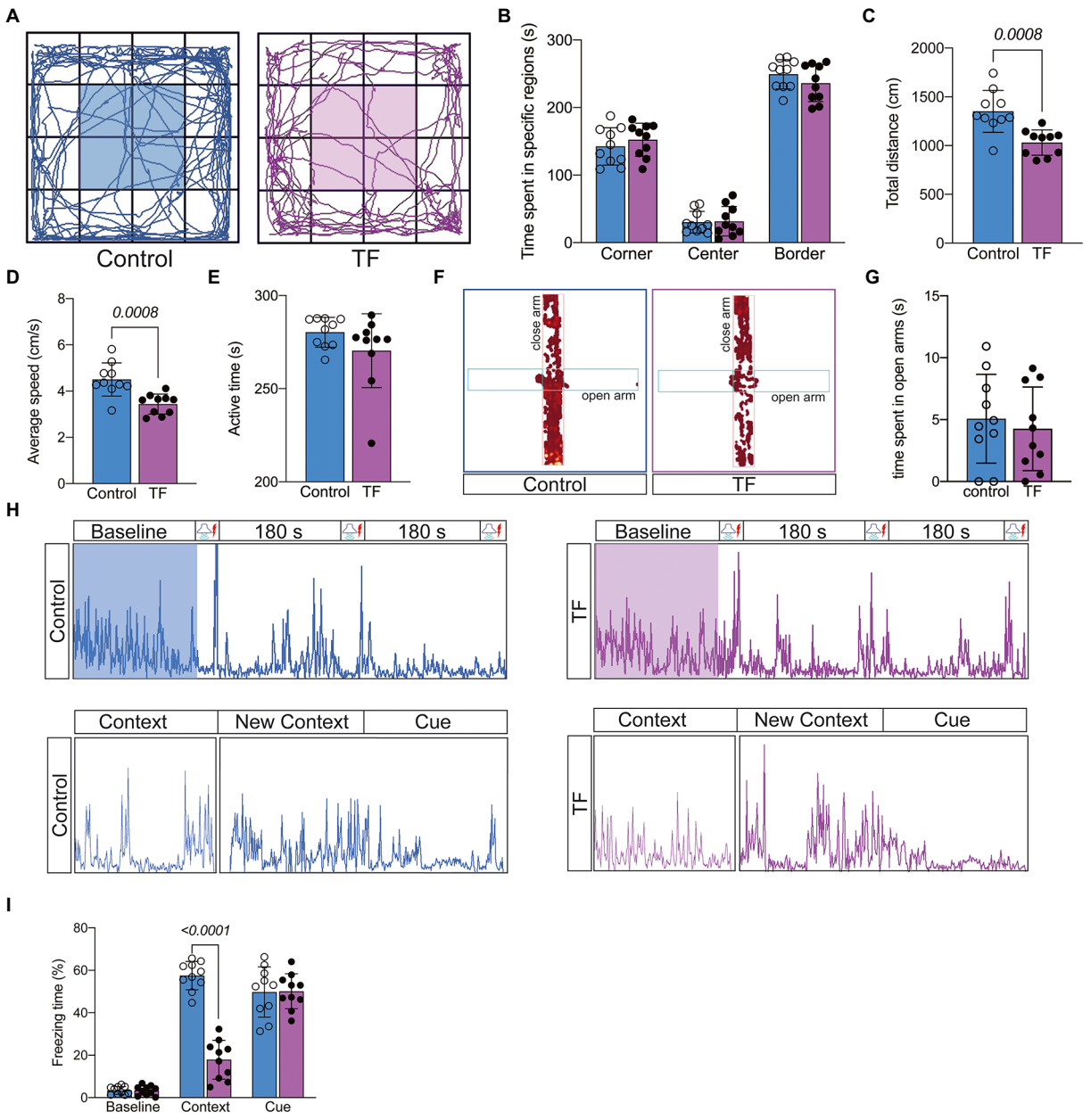

FIGURE 2
Behavioral testing of aged mice after tibial fracture surgery. **(A)** Mobility of aged mice was measured by the open-field test on the 7th day after fracture surgery. **(B–E)** Comparison of the results of the open-field test between the two groups of mice. **(F,G)** Anxiety in aged mice was measured using the elevated plus maze on day 7 after fracture surgery. **(H)** The image above shows the activity of mice trained in 3 cycles of Context (180s)-Cue (30s)-Shock (2s) pairing on day 8 after fracture surgery. The image below shows the activity of the mice during the test phase on day 9 after fracture surgery: Context (180s), Novel Context (180s)-Cue (180s). **(I)** Comparison of the percentage of freezing time in each phase for both groups of mice. Data were expressed as mean±SD and analyzed using two-tailed unpaired *t*-test. The *p*-values are shown in the picture.

Synaptic plasticity is altered in the hippocampal CA1 region of aged mice with POCD

To further determine the memory function in mice, we performed Golgi staining of the hippocampal CA1 brain region responsible for short-term memory to observe the changes in synaptic structure (Figure 3A). The dendritic length, dendritic and dendritic spine density of neurons in the hippocampal CA1 region were quantified by the Sholl analysis method in Image J. The results showed that the total dendritic length ($P < 0.05$, Figure 3B), dendritic spine density ($P < 0.05$, Figure 3C), and the intersection of dendrites with concentric circles ($P < 0.05$, Figure 3D) were reduced in the hippocampal CA1 neurons of the TF group compared with the C group. This indicates that the precise and complex structure of the dendrites of neurons in the

10.3389/fnagi.2022.1040569

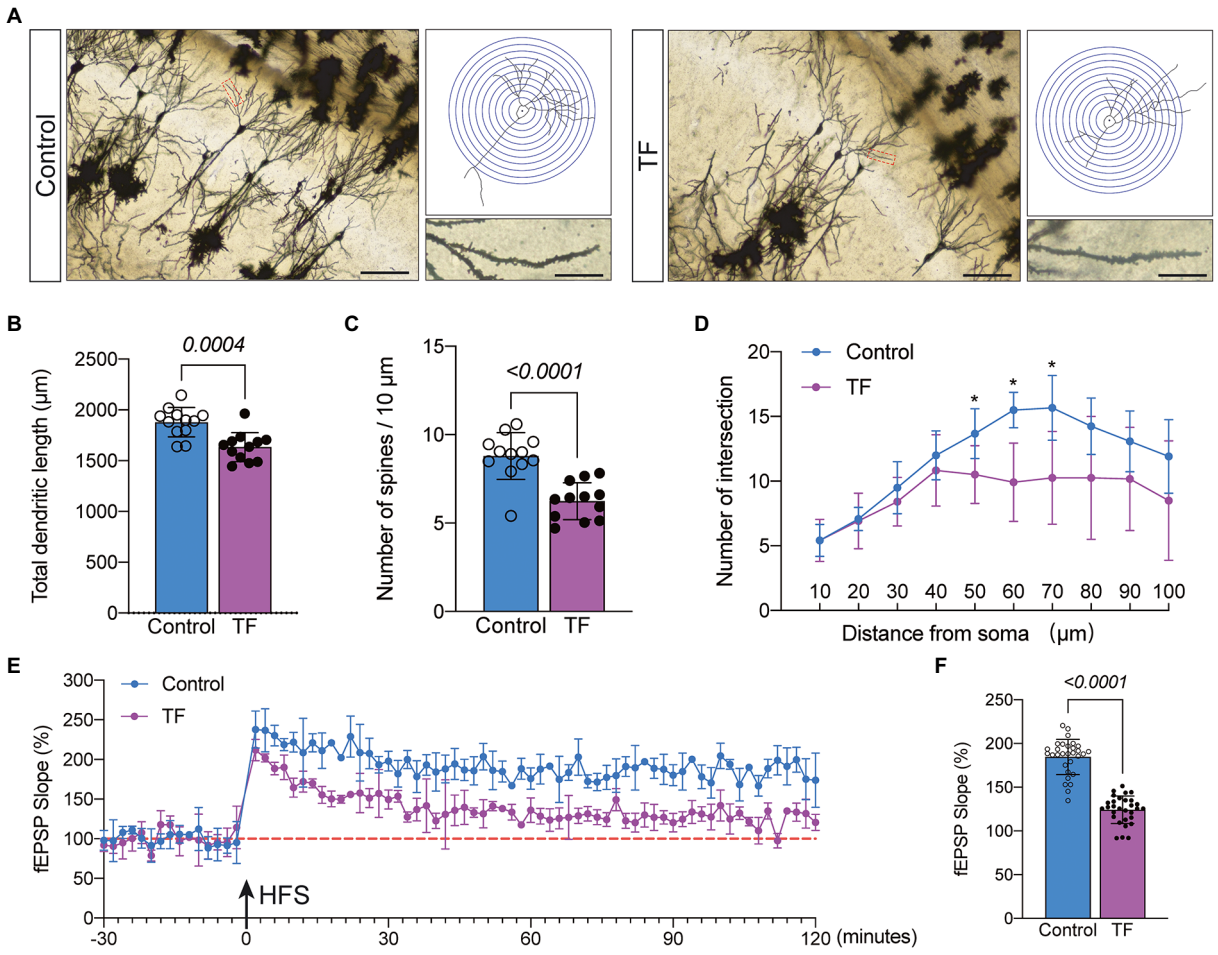

FIGURE 3
Synaptic plasticity in hippocampal CA1 region at day 10 after fracture surgery. **(A)** Golgi staining of the CA1 region of the mouse hippocampus (×200, *n*=3), Sholl analysis and magnification of synapses (×1,000), scale bar=100 or 20 μm. **(B–D)** Quantitative analysis of total synaptic length, synaptic spine density and synaptic number. The Number of intersection was analyzed using unpaired *t*-test with Bonferroni corrected *p*-values. **(E)** Recording and analysis of local field potentials in the CA1 region of the hippocampus in response to stimulation of Schafer's lateral branch fibers (*n*=3). **(F)** Average fEPSP Slop in the last 20min. **p*<0.05, compared with the C group. Data are presented as mean±SD. Data were expressed as mean±SD and analyzed using two-tailed unpaired *t*-test. The *p*-values are shown in the picture.

CA1 region of the hippocampus of mice in the TF group has changed. We further assessed the synaptic plasticity of neurons by examining the slope of mean field excitatory postsynaptic potentials (fEPSP) in the CA1 region of the mouse hippocampus (Figure 3E). The results showed that the decreased LTP in the CA1 brain region of aged mice undergoing tibial fracture surgery indicated that synaptic plasticity was functionally impaired in the TF group of mice ($P < 0.05$, Figure 3F).

Increased abnormal activation of astrocytes in the CA1 region of the hippocampus in POCD-aged mice

To further investigate the possible causes of impaired synaptic plasticity in neurons in the CA1 region of the hippocampus of aged mice with POCD, we observed morphological changes in astrocytes that are actively involved in maintaining synaptic function. We labeled astrocytes with glial fibrillary acidic protein (GFAP) and found increased abnormal activation of astrocytes in the hippocampal CA1 region of aged mice undergoing anesthesia and surgery (Figure 4A). The results of immunofluorescence revealed an increased number of GFAP+ astrocytes in the hippocampal CA1 region of mice in the TF group compared to the C group ($P < 0.05$, Figure 4B), an increased area of GFAP+ fluorescence staining per field of view ($P < 0.05$, Figure 4C), and an increased area of fluorescence of individual glial cells ($P < 0.05$, Figure 4D).

Gq-pathway activation of astrocytes in hippocampal CA1 region can improve cognitive dysfunction caused by anesthesia/surgery

Astrocytes can exchange information with neurons, respond to synaptic activity, and regulate synaptic transmission. Abnormal

10.3389/fnagi.2022.1040569

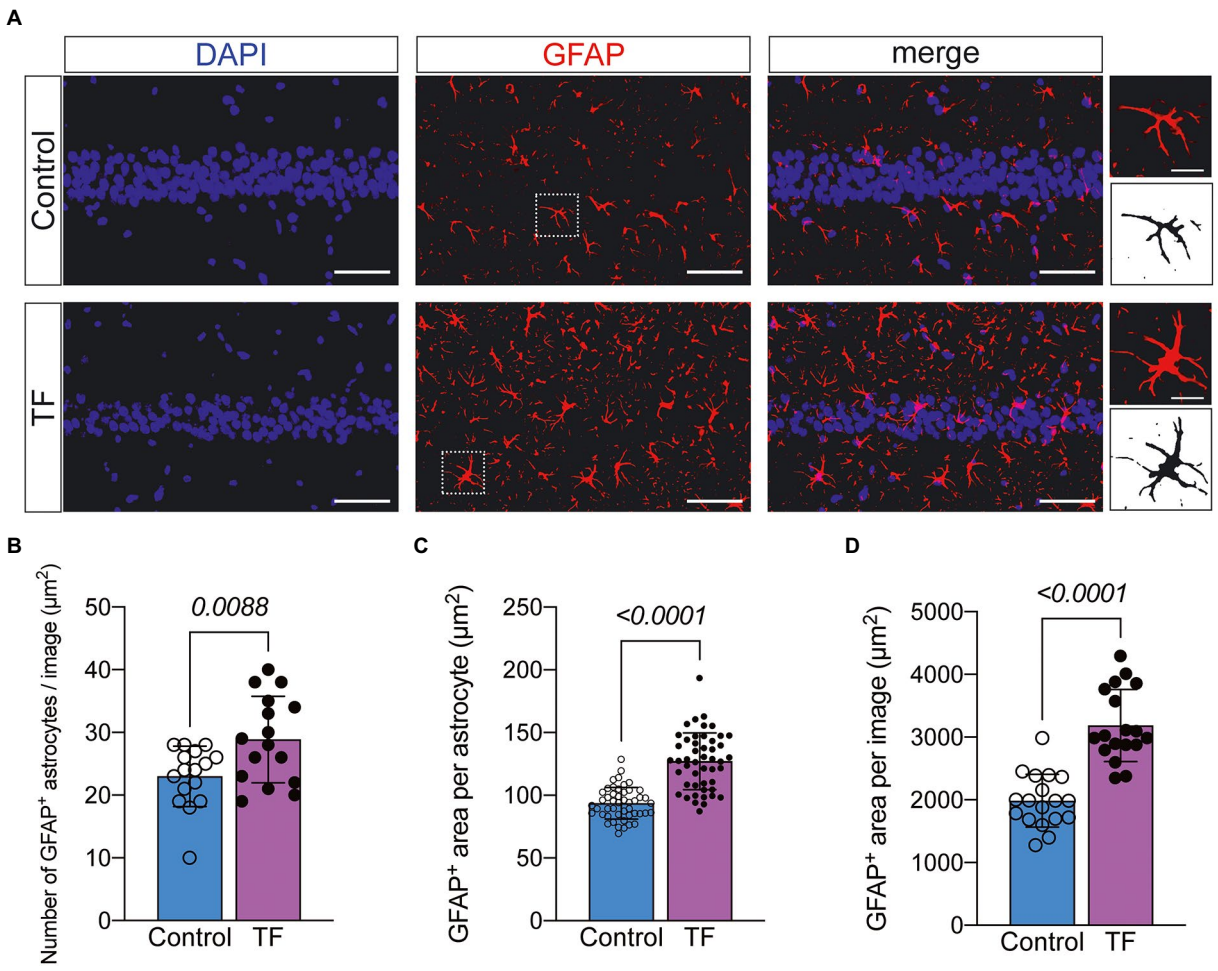

FIGURE 4
Immunofluorescence staining of astrocytes on day 10 after fracture surgery. **(A)** GFAP-labeled astrocytes in the hippocampal CA1 region (n=4). Scale bar=50 μm or 10 μm. **(B–D)** Quantitative analysis of GFAP$^+$ astrocytes. Data were expressed as mean±SD and analyzed using two-tailed unpaired t-test. The p-values are shown in the picture.

activation of astrocytes is often accompanied by functional abnormalities. To verify that abnormal activation and decreased function of astrocytes in the CA1 region are important factors contributing to POCD, we injected the chemical genetic reagent rAAV-GfaABC1D-hM3D(Gq)-mCherry (AAV-hM3D/CNO) into the bilateral hippocampal CA1 region of aged mice 3 weeks before TF surgery to specifically activate hippocampal astrocytes in the CA1 region (Figures 5A,B). At 7 days after TF surgery, the locomotor activity of the mice was detected by open field test, and there was no difference between the three groups ($P > 0.05$, Figures 5C–F). Subsequently, we examined the memory function of the mice with novel object recognition and fear conditioning test. The results showed that mice in the AAV-hM3D/CNO group spent more time exploring the new object and showed more freezing time when recalling context-related fear memories compared to the AAV-mCherry/CNO and AAV-hM3D/Saline groups ($P < 0.05$, Figures 5G–K). In contrast, the total distance of movement and average movement speed did not differ among the 3 groups of mice ($P > 0.05$, Supplementary Figure 3). These results suggest that Gq pathway activation in astrocytes of hippocampal CA1 area can improve cognitive dysfunction induced by anesthesia/surgery.

Gq pathway activation of CA1 area astrocytes ameliorates anesthesia/surgery induced cognitive dysfunction associated with enhanced synaptic plasticity

We hypothesized that activation of the Gq pathway in astrocytes might be associated with improved synaptic plasticity. To confirm this, we observed synaptic structures by Golgi staining (Figure 6A). The results demonstrated that mice in the AAV-hM3D/CNO group had increased total dendritic length, dendritic density and dendritic spine density compared to the AAV-mCherry/CNO and AAV-hM3D/Saline groups ($P<0.05$, Figures 6B–D). We further assessed synaptic function by

10.3389/fnagi.2022.1040569

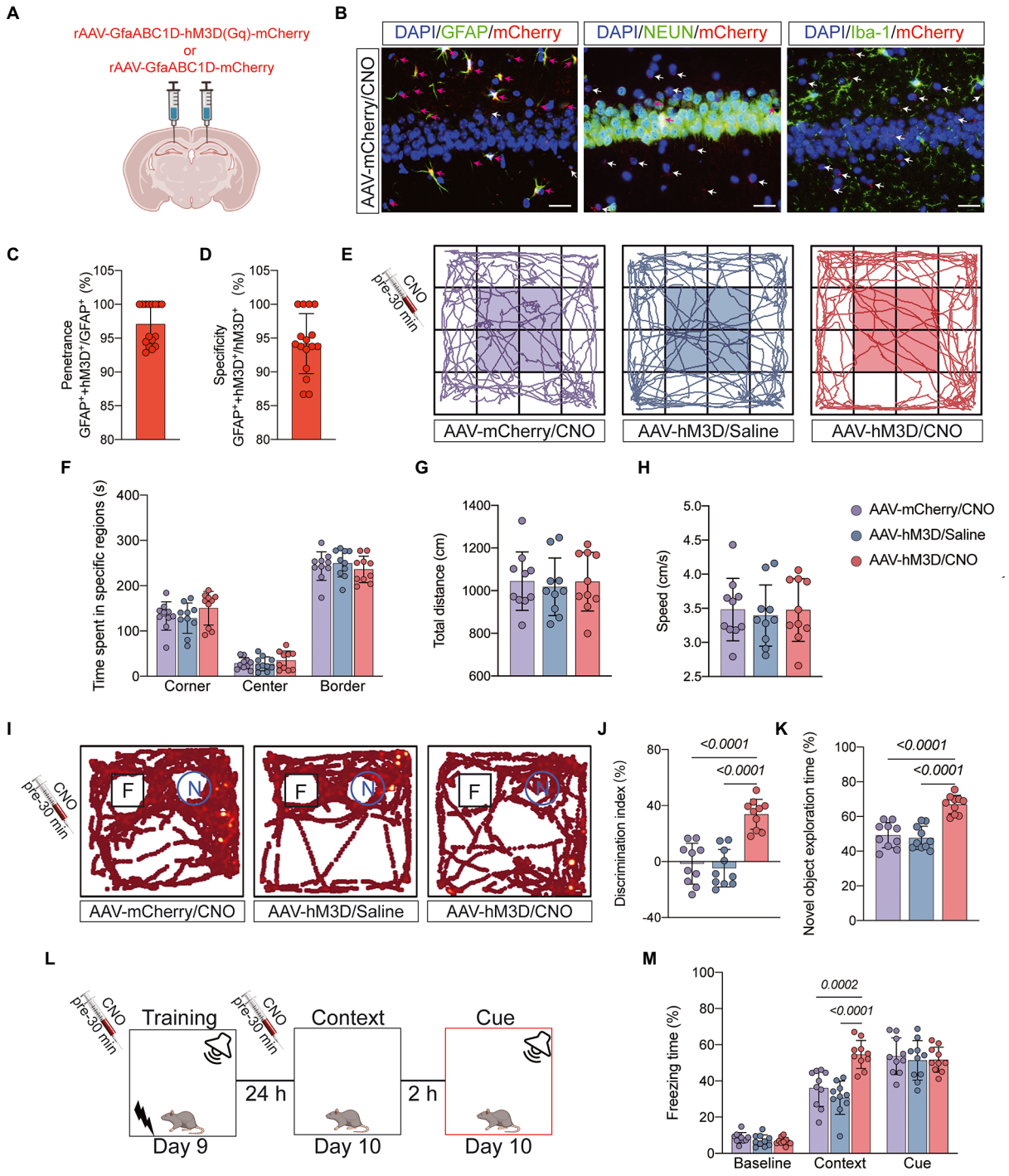

FIGURE 5
Behavioral effects of Gq pathway activation in astrocytes of hippocampal CA1 region. **(A)** Bilateral hippocampal CA1 regions were injected with rAAV-GfaABC1D-hM3D(Gq)-mCherry (n=20) or rAAV-GfaABC1D-mCherry (n=10) 21 days before surgery. **(B)** hM3D(Gq) was specifically expressed in astrocytes. GFAP was used to label astrocytes, NEUN to label neurons, Iba-1 to label microglia, mCherry to label hM3D(Gq), and DAPI to label nuclei, respectively. Red arrows indicate double-staining positivity, while white arrows indicate mCherry single-staining positivity. Scale bar=25 μm. **(C)** The ratio of GFAP and mCherry double-positive cells to GFAP-positive cells is the epistasis rate. **(D)** The ratio of GFAP and mCherry double-positive cells to mCherry-positive cells is the specificity rate. **(E)** Locomotor activity was measured on day 7 after tibial fracture by open-field assay after 30 min of intraperitoneal injection of CNO or saline. **(F–H)** Quantification of total distance travelled, speed of movement, and time spent moving in specific areas in 3 groups of mice. **(I)** Novel object recognition tests were performed on the 7th and 8th day after tibial fracture. **(J,K)** Quantitative analysis of discrimination index and percentage of new object recognition in the 3 groups of mice. **(L,M)** Three cycles of training were performed on postoperative day 9, and the percentage of freezing time was assessed on day 10 in the Context test and the Cue test. Data were expressed as mean±SD and analyzed by *ANOVA* test with a Tukey *post hoc* test. The p-values are shown in the picture.

10.3389/fnagi.2022.1040569

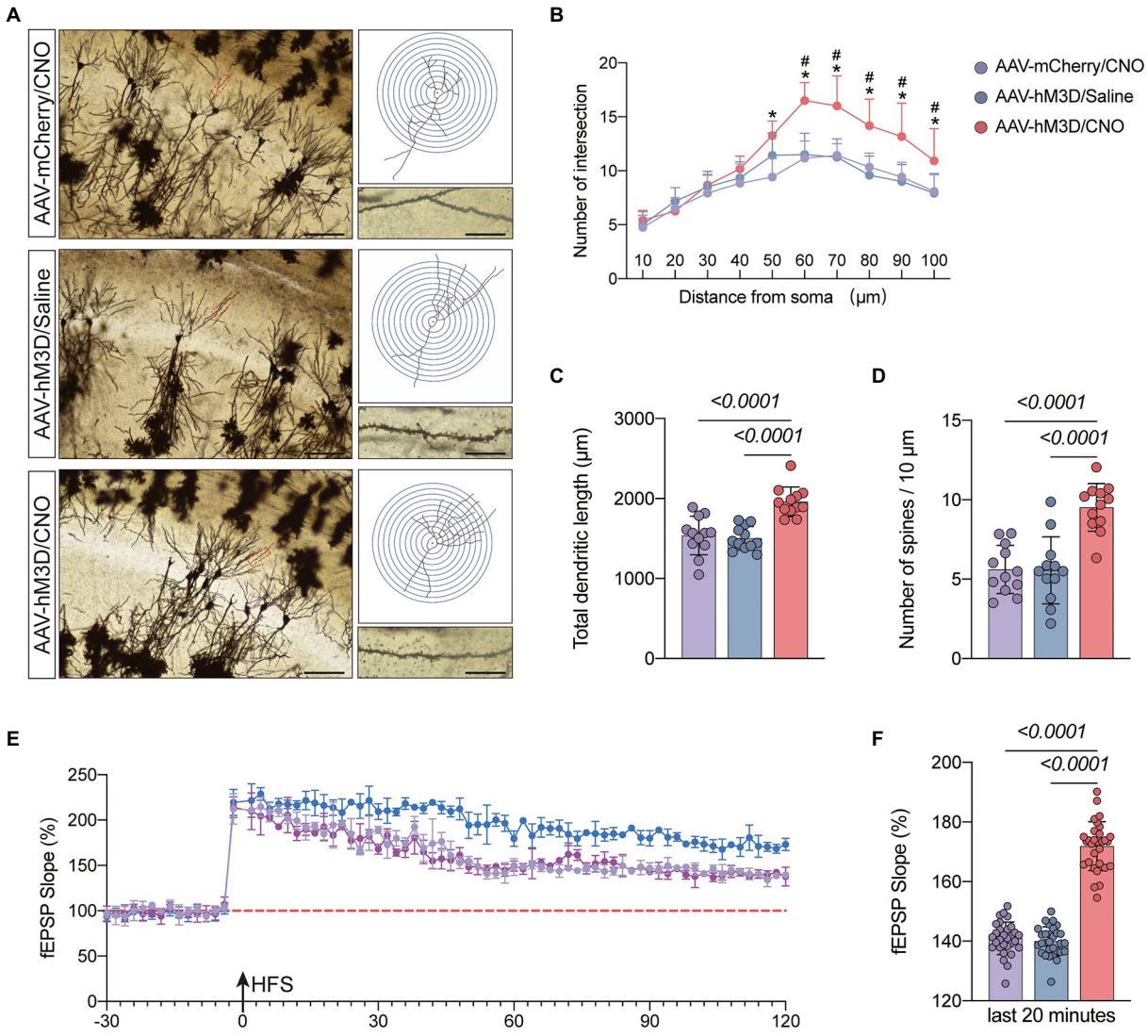

FIGURE 6
Effects of activation of Gq pathways in astrocytes on the structure and function of synaptic plasticity at postoperative day 11. **(A)** Golgi staining of the CA1 region of the mouse hippocampus (×200, *n*=3), Sholl analysis and magnification of synapses (×1,000), scale bar=100 or 20 μm. **(B–D)** Quantitative analysis of total synaptic length, synaptic spine density and synaptic number. **(E)** Recording and analysis of local field potentials in the CA1 region of the hippocampus in response to stimulation of Schafer's lateral branch fibers (*n*=3). **(F)** Average fEPSP Slop in the last 20 min. **p*<0.05, compared with the AVV-mCherry/CNO group. #*p*<0.05, compared with the AVV-hM3D/Saline group. Data were expressed as mean±SD and analyzed by *ANOVA* test with a Tukey *post hoc* test. The *p*-values are shown in the picture.

monitoring fEPSP and found that mice in the AAV-mCherry/CNO group had significantly increased fEPSP compared to the AAV-mCherry/CNO and AAV-hM3D/Saline groups ($P<0.05$, Figures 6E,F). The above results indicate that Gq pathway activation in astrocytes can improve synaptic plasticity of neurons structurally and functionally.

Discussion

Our study aimed to determine that astrocytes are important players in learning memory and that the occurrence of POCD in elderly patients may be related to their abnormal function. Our results suggest that activation of the astrocyte Gq pathway improves learning memory in POCD-aged mice. Astrocytes are known to be active participants in synaptic processing, and their functional state influences synaptic structure and function. Our findings suggest that the occurrence of POCD in aged mice is accompanied by abnormal astrocyte activation and altered synaptic plasticity. In contrast, activation of the Gq pathway in astrocytes using a chemical genetic approach improves learning memory capacity. This was evidenced by increases in dendritic length, number, branching and synaptic spine density; increases in LTP strength; enhanced fear memory in fear conditioning test

and increased time to explore new objects in novel object recognition test. Overall, astrocytes can be used as a target for the prevention and treatment of POCD in elderly patients (Figure 7).

With the aging of the population and the development of medical technology, more and more elderly fracture patients are given the opportunity to undergo surgery (Tzimas et al., 2018). POCD, a common complication after surgery for geriatric fractures, not only prolongs hospitalization and increases treatment costs, but also increases the occurrence of other related complications and even increases the postoperative mortality of patients (Zhu et al., 2021). Therefore, it is important to prevent and reduce the occurrence of POCD. In this study, we used 18-month-old mice to perform tibial osteotomy with intramedullary nail fixation under sevoflurane anesthesia to simulate the anesthetic surgical procedure in clinically aged patients. Postoperatively, we performed x-rays to ensure that the tibial fracture was anatomically repositioned (Supplementary Figure 1). On postoperative day 7, we examined the ability of the mice to move autonomously using the open field test, which showed that although the mice had achieved anatomical repositioning, they still had limited motor function. This may lead to unreliable results in either the Morris water maze or the novel object recognition test. This is inconsistent with the results of Qiu et al.'s (2020) study, which may be caused by our choice of older mice with poorer recovery, but the use of older mice for modeling is more clinically relevant. How to scientifically and correctly detect the memory function of mice after surgery troubled us, so we re-analyzed the results of open field test and found that although the motor speed and motor distance were reduced in older mice after TF surgery, their active time or immobility time was consistent (Figure 1E). Therefore, we chose the fear conditioning test, which is based on the Pavlovian effect and less dependent on motor ability, to test memory function. The results showed that the freezing time baseline in the training phase of the mice in the TF and C groups was consistent. This indicates that it is scientifically feasible to compare the memory function of two groups of mice by fear conditioning test. The results of the recall phase demonstrated that the freezing time associated with the context decreased significantly in the older mice after TF surgery, while there was no difference in the freezing time associated with the cue. Hippocampal-amygdala circuits are the core of contextual fear associated memory (Liu et al., 2012; Lacagnina et al., 2019). Cue-related fear memory is established mainly by auditory cortex and auditory thalamus-amygdala neural circuits (Choi, D. I., et al., 2021). Based on these theories and the results we obtained, it is implied that hippocampus-dependent memory dysfunction occurs in aged mice that have experienced anesthesia and surgery. These results are consistent with the experimental results of Lin et al. (2021). It fully illustrates that sevoflurane anesthesia combined with TF surgery successfully built POCD model.

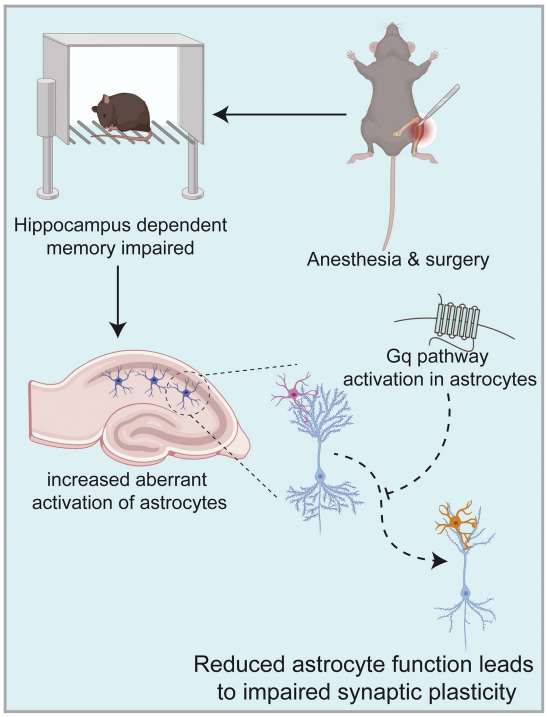

FIGURE 7
Anesthesia/surgery in aged mice can result in hippocampus-dependent cognitive dysfunction accompanied by altered synaptic plasticity in hippocampal CA1 regions. This mechanism may be related to increased aberrant activation of astrocytes in the hippocampus, among which astrocytes are known to be active participants in synaptic processing. In contrast, activation of Gq pathways in hippocampal astrocytes improves hippocampal-dependent cognitive dysfunction. Images were created on the BioRender web platform.

The hippocampus is central to the cognitive functions, and there is growing evidence that POCD is associated with impaired synaptic transmission, reduced neurotransmitters, neuronal apoptosis and altered synaptic plasticity in the hippocampus (Erickson et al., 2011; Chen et al., 2019; Zheng et al., 2019). Reduced dendritic spine and synaptic is characteristic of many neurological disorders, including autism spectrum disorders, schizophrenia, and Alzheimer's disease (Han et al., 2012; Reddy et al., 2018; Stampanoni Bassi et al., 2019). Recent studies have shown that POCD is accompanied by impaired synaptic plasticity in the CA1 region of the hippocampus (Chen et al., 2020). Our Golgi staining results showed reduced synaptic density and reduced number of dendritic spines in the hippocampal CA1 region of POCD mice. The neurophysiological results showed reduced LTP amplitude and frequency in the hippocampal CA1 region of POCD mice. These results support the above theory in terms of synaptic structure and synaptic function. Astrocytes are morphologically complex cells that comprise approximately half of the brain cells and are involved in a variety of structural, metabolic, and homeostatic functions (Chen et al., 2020; Corkrum et al., 2020; Wang, J., et al., 2021). Glial cells are important regulators of synaptic function and plasticity. Astrocytes are a major class of glial cells that respond to neuronal activity by intracellular Ca^{2+} transients and then release gliotransmitters that in turn alter synaptic connections. This reciprocal neuron

astrocyte interaction has led to the concept of the 'tripartite synapse', in which astrocytes are considered active participants in synaptic processing (Lee et al., 2021; Wang, Y., et al., 2021). The fine structure of well-developed astrocytes is highly plastic and activity-dependent (Habib et al., 2020; Choi, M., et al., 2021). They exhibit heterogeneity and morphological diversity in different brain regions, which may be related to astrocyte-neuron spatiotemporal interactions, which also supports the 'tripartite synapse' hypothesis (de Tredern et al., 2021; Sadick et al., 2022). Reactive astrocytes are marked by morphological alterations as well as defects in fine structure, which may drive disease progression and are a common pathological feature of many neurological disorders (Bondi et al., 2021). In the present study we used glial fibrillary acidic protein (GFAP) to label astrocytes and found an increase in GFAP-positive glial cells in the hippocampal CA1 region of POCD-aged mice, with expanded cell body and thickened branches. Study of Wang et al. (2022) had similar results that astrocyte morphology was altered and accompanied by impaired calcium signaling in POCD mice. We hypothesize that the occurrence of POCD is associated with altered morphological and biophysical properties of astrocytes resulting in reduced execution of synaptic modifications. Adamsky et al. (2018) expressed the Gq-coupled receptor hM3Dq in CA1 astrocytes in normal mice by chemical genetic techniques, allowing their activation by CNO. Gq pathway activation in astrocytes was found to lead to enhanced memory recall. Based on this study, we wanted to investigate whether activating astrocytes in POCD mice could improve cognition. We used chemical genetic tools in combination with microinjection of specific brain regions and controlled activation of the Gq-pathway by the GfaABC1D promoter to specifically manipulate astrocytes around hippocampal CA1. The mCherry as a red fluorescent reporter protein, is used for proper visualization of hM3D(Gq). We designed two control groups, the AAV-mCherry/CNO group and the AAV-hM3D/Saline group, in order to exclude the effects of CNO and viral particles. We injected AAV-mCherry or AAV-hM3D in the bilateral hippocampal CA1 region of the mice 21 days before surgery, and on the seventh postoperative day we assessed the motor ability of the mice and found no difference in the motor ability of the three groups. Therefore, we added a novel object recognition test to the memory assessment to make the results more convincing. CNO or saline was injected intraperitoneally 30 min before the training phase and testing phase of novel object recognition test and fear conditioning test. The results showed that the memory function of mice in the AAV-hM3D/CNO group was significantly improved compared with the AAV-mCherry/CNO group and the AAV-hM3D/Saline group. This might be related to the enhanced synaptic plasticity by the activation of Gq pathways in astrocytes. We then used Golgi staining technique and neurophysiological technique to judge synaptic plasticity structurally and functionally, respectively. The results showed a significant increase in dendritic density and number of dendritic spines in the AAV-hM3D/CNO group of mice, and a significant increase in LTP amplitude. This data suggests that the activation of astrocyte Gq pathways improved the function of astrocytes in modifying neuronal synapses, which is consistent with the findings of Van Den Herrewegen et al. (2021) and Kol et al. (2020). The aberrant activation of astrocytes may be the driving force for POCD production. The above results provide a basis for targeting astrocyte cells for clinical prevention and treatment of POCD.

However, there are still some limitations of our study. We only studied memory function between 7 and 11 days after anesthesia/surgery in aged mice and did not verify the effect on their long-term memory. We gave CNO during both the postoperative learning phase and the testing phase, so the specific effects of astrocyte Gq pathway activation on memory formation, memory consolidation or memory extraction remain to be further investigated. In this study, although we detected the expression of hM3D(Gq), no experiments related to the observation of changes in astrocyte calcium activity using two-photon microscopy or miniscop were performed. Direct evidence for Gq pathway activation is lacking. The activation of the Gq pathway in astrocytes involves a wide range of molecular signaling pathways, and the molecular mechanisms that play a major role need to be further investigated.

Conclusion

Overall, our results suggest that tibial fracture surgery in aged mice can lead to recent hippocampal-dependent cognitive dysfunction. Impaired synaptic plasticity due to abnormal activation of astrocytes is an important mechanism for the occurrence of POCD. In contrast, activation of the Gq pathway of astrocytes in the CA1 region of the hippocampus ameliorates POCD in aged mice caused by aging anesthesia/surgery.

Data availability statement

The original contributions presented in the study are included in the article/Supplementary materials, further inquiries can be directed to the corresponding author.

Ethics statement

The animal study was reviewed and approved by Ethics Committee of the Third Hospital of Hebei Medical University.

Author contributions

QW and XW conceived the idea of the study. ZH and FX analyzed the data. JZ and YZ interpreted the results. JY and QZ prepared the model and injected the virus into CA1 brain region. XW wrote the paper. QZ and CY conducted behavioral related

test. All authors contributed to the article and approved the submitted version.

Funding

This work was supported by grants from the *Key project of Precision Medicine Joint Fund of Hebei Natural Science Foundation* (H2021206021), and the *Hebei Provincial government funded the provincial Medical Talents Project*.

Conflict of interest

The authors declare that the research was conducted in the absence of any commercial or financial relationships that could be construed as a potential conflict of interest.

Publisher's note

Supplementary material

The Supplementary material for this article can be found online at: https://www.frontiersin.org/articles/10.3389/fnagi.2022.1040569/full#supplementary-material

References

Adamsky, A., Kol, A., Kreisel, T., Doron, A., Ozeri-Engelhard, N., Melcer, T., et al. (2018). Astrocytic activation generates de novo neuronal potentiation and memory enhancement. *Cells* 174:e14, 59–71. doi: 10.1016/j.cell.2018.05.002

Beishuizen, S. J. E., Van Munster, B. C., De Jonghe, A., Abu-Hanna, A., Buurman, B. M., and De Rooij, S. E. (2017). Distinct cognitive trajectories in the first year after hip fracture. *J. Am. Geriatr. Soc.* 65, 1034–1042. doi: 10.1111/jgs.14754

Bondi, H., Bortolotto, V., Canonico, P. L., and Grilli, M. (2021). Complex and regional-specific changes in the morphological complexity of GFAP astrocytes in middle-aged mice. *Neurobiol. Aging* 100, 59–71. doi: 10.1016/j.neurobiolaging.2020.12.018

Chen, L., Dong, R., Lu, Y., Zhou, Y., Li, K., Zhang, Z., et al. (2019). MicroRNA-146a protects against cognitive decline induced by surgical trauma by suppressing hippocampal neuroinflammation in mice. *Brain Behav. Immun.* 78, 188–201. doi: 10.1016/j.bbi.2019.01.020

Chen, S.-M., Li, M., Xie, J., Li, S., Xiang, S.-S., Liu, H.-Y., et al. (2020). Hydrogen sulfide attenuates postoperative cognitive dysfunction through promoting the pathway of Warburg effect-synaptic plasticity in hippocampus. *Toxicol. Appl. Pharmacol.* 409:115286. doi: 10.1016/j.taap.2020.115286

Choi, D. I., Kim, J., Lee, H., Kim, J.-I., Sung, Y., Choi, J. E., et al. (2021). Synaptic correlates of associative fear memory in the lateral amygdala. *Neuron* 109, 2717–2726.e3. doi: 10.1016/j.neuron.2021.07.003

Choi, M., Lee, S.-M., Kim, D., Im, H.-I., Kim, H.-S., and Jeong, Y. H. (2021). Disruption of the astrocyte-neuron interaction is responsible for the impairments in learning and memory in 5XFAD mice: an Alzheimer's disease animal model. *Mol. Brain* 14:111. doi: 10.1186/s13041-021-00823-5

Corkrum, M., Covelo, A., Lines, J., Bellocchio, L., Pisansky, M., Loke, K., et al. (2020). Dopamine-evoked synaptic regulation in the nucleus accumbens requires astrocyte activity. *Neuron* 105:e5, 1036–1047. doi: 10.1016/j.neuron.2019.12.026

De Tredern, E., Rabah, Y., Pasquer, L., Minatchy, J., Plaçais, P.-Y., and Preat, T. (2021). Glial glucose fuels the neuronal pentose phosphate pathway for long-term memory. *Cell Rep.* 36:109620. doi: 10.1016/j.celrep.2021.109620

Durkee, C. A., and Araque, A. (2019). Diversity and specificity of astrocyte-neuron communication. *Neuroscience* 396, 73–78. doi: 10.1016/j.neuroscience.2018.11.010

Erickson, K. I., Voss, M. W., Prakash, R. S., Basak, C., Szabo, A., Chaddock, L., et al. (2011). Exercise training increases size of hippocampus and improves memory. *Proc. Natl. Acad. Sci. U. S. A.* 108, 3017–3022. doi: 10.1073/pnas.1015950108

Frisoli, A., Paes, A. T., Borges, J., Ingham, S. M., Cartocci, M. M., Lima, E., et al. (2021). The association between low lean mass and osteoporosis increases the risk of weakness, poor physical performance and frailty in Brazilian older adults: data from SARCOS study. *Eur. J. Clin. Nutr.* 75, 446–455. doi: 10.1038/s41430-020-00753-w

Gallagher, J. C. (2004). The effects of calcitriol on falls and fractures and physical performance tests. *J. Steroid Biochem. Mol. Biol.* 89-90, 497–501. doi: 10.1016/j.jsbmb.2004.03.059

Gomez, J. L., Bonaventura, J., Lesniak, W., Mathews, W. B., Sysa-Shah, P., Rodriguez, L. A., et al. (2017). Chemogenetics revealed: DREADD occupancy and activation via converted clozapine. *Science* 357, 503–507. doi: 10.1126/science.aan2475

Habib, N., Mccabe, C., Medina, S., Varshavsky, M., Kitsberg, D., Dvir-Szternfeld, R., et al. (2020). Disease-associated astrocytes in Alzheimer's disease and aging. *Nat. Neurosci.* 23, 701–706. doi: 10.1038/s41593-020-0624-8

Han, S., Tai, C., Westenbroek, R. E., Yu, F. H., Cheah, C. S., Potter, G. B., et al. (2012). Autistic-like behaviour in Scn1a+/− mice and rescue by enhanced GABA-mediated neurotransmission. *Nature* 489, 385–390. doi: 10.1038/nature11356

Holmgaard, F., Vedel, A. G., Rasmussen, L. S., Paulson, O. B., Nilsson, J. C., and Ravn, H. B. (2019). The association between postoperative cognitive dysfunction and cerebral oximetry during cardiac surgery: a secondary analysis of a randomised trial. *Br. J. Anaesth.* 123, 196–205. doi: 10.1016/j.bja.2019.03.045

Kol, A., Adamsky, A., Groysman, M., Kreisel, T., London, M., and Goshen, I. (2020). Astrocytes contribute to remote memory formation by modulating hippocampal-cortical communication during learning. *Nat. Neurosci.* 23, 1229–1239. doi: 10.1038/s41593-020-0679-6

Kontis, V., Bennett, J. E., Mathers, C. D., Li, G., Foreman, K., and Ezzati, M. (2017). Future life expectancy in 35 industrialised countries: projections with a Bayesian model ensemble. *Lancet* 389, 1323–1335. doi: 10.1016/S0140-6736(16)32381-9

Kristek, G., Radoš, I., Kristek, D., Kapural, L., Nešković, N., Škiljić, S., et al. (2019). Influence of postoperative analgesia on systemic inflammatory response and postoperative cognitive dysfunction after femoral fractures surgery: a randomized controlled trial. *Reg. Anesth. Pain Med.* 44, 59–68. doi: 10.1136/rapm-2018-000023

Lacagnina, A. F., Brockway, E. T., Crovetti, C. R., Shue, F., Mccarty, M. J., Sattler, K. P., et al. (2019). Distinct hippocampal engrams control extinction and relapse of fear memory. *Nat. Neurosci.* 22, 753–761. doi: 10.1038/s41593-019-0361-z

Lee, J.-H., Kim, J.-Y., Noh, S., Lee, H., Lee, S. Y., Mun, J. Y., et al. (2021). Astrocytes phagocytose adult hippocampal synapses for circuit homeostasis. *Nature* 590, 612–617. doi: 10.1038/s41586-020-03060-3

Lin, X., Chen, Y., Zhang, P., Chen, G., Zhou, Y., and Yu, X. (2020). The potential mechanism of postoperative cognitive dysfunction in older people. *Exp. Gerontol.* 130:110791. doi: 10.1016/j.exger.2019.110791

Lin, F., Shan, W., Zheng, Y., Pan, L., and Zuo, Z. (2021). Toll-like receptor 2 activation and up-regulation by high mobility group box-1 contribute to post-operative neuroinflammation and cognitive dysfunction in mice. *J. Neurochem.* 158, 328–341. doi: 10.1111/jnc.15368

Liu, X., Ramirez, S., Pang, P. T., Puryear, C. B., Govindarajan, A., Deisseroth, K., et al. (2012). Optogenetic stimulation of a hippocampal engram activates fear memory recall. *Nature* 484, 381–385. doi: 10.1038/nature11028

Liu, Q., Sun, Y.-M., Huang, H., Chen, C., Wan, J., Ma, L.-H., et al. (2021). Sirtuin 3 protects against anesthesia/surgery-induced cognitive decline in aged mice by suppressing hippocampal neuroinflammation. *J. Neuroinflammation* 18:41. doi: 10.1186/s12974-021-02089-z

Papadopoulos, G., Pouangare, M., Papathanakos, G., Arnaoutoglou, E., Petrou, A., and Tzimas, P. (2014). The effect of ondansetron on postoperative delirium and cognitive function in aged orthopedic patients. *Minerva Anestesiol.* 80, 444–451. PMID: 24193238

Qiu, L.-L., Pan, W., Luo, D., Zhang, G.-F., Zhou, Z.-Q., Sun, X.-Y., et al. (2020). Dysregulation of BDNF/TrkB signaling mediated by NMDAR/Ca/calpain might contribute to postoperative cognitive dysfunction in aging mice. *J. Neuroinflammation* 17:23. doi: 10.1186/s12974-019-1695-x

Reddy, P. H., Yin, X., Manczak, M., Kumar, S., Pradeepkiran, J. A., Vijayan, M., et al. (2018). Mutant APP and amyloid beta-induced defective autophagy, mitophagy, mitochondrial structural and functional changes and synaptic damage in hippocampal neurons from Alzheimer's disease. *Hum. Mol. Genet.* 27, 2502–2516. doi: 10.1093/hmg/ddy154

Sadick, J. S., O'dea, M. R., Hasel, P., Dykstra, T., Faustin, A., and Liddelow, S. A. (2022). Astrocytes and oligodendrocytes undergo subtype-specific transcriptional changes in Alzheimer's disease. *Neuron* 110, 1788–1805.e10. doi: 10.1016/j.neuron.2022.03.008

Stampanoni Bassi, M., Iezzi, E., Gilio, L., Centonze, D., and Buttari, F. (2019). Synaptic plasticity shapes brain connectivity: implications for network topology. *Int. J. Mol. Sci.* 20:6193. doi: 10.3390/ijms20246193

Suzuki, A., Stern, S. A., Bozdagi, O., Huntley, G. W., Walker, R. H., Magistretti, P. J., et al. (2011). Astrocyte-neuron lactate transport is required for long-term memory formation. *Cells* 144, 810–823. doi: 10.1016/j.cell.2011.02.018

Tian, H., Xu, Y., Liu, F., Wang, G., and Hu, S. (2015). Effect of acute fentanyl treatment on synaptic plasticity in the hippocampal CA1 region in rats. *Front. Pharmacol.* 6:251. doi: 10.3389/fphar.2015.00251

Tzimas, P., Samara, E., Petrou, A., Korompilias, A., Chalkias, A., and Papadopoulos, G. (2018). The influence of anesthetic techniques on postoperative cognitive function in elderly patients undergoing hip fracture surgery: general vs spinal anesthesia. *Injury* 49, 2221–2226. doi: 10.1016/j.injury.2018.09.023

Van Den Herrewegen, Y., Sanderson, T. M., Sahu, S., De Bundel, D., Bortolotto, Z. A., and Smolders, I. (2021). Side-by-side comparison of the effects of Gq-and Gi-DREADD-mediated astrocyte modulation on intracellular calcium dynamics and synaptic plasticity in the hippocampal CA1. *Mol. Brain* 14:144. doi: 10.1186/s13041-021-00856-w

Wang, Y., Fu, W.-Y., Cheung, K., Hung, K.-W., Chen, C., Geng, H., et al. (2021). Astrocyte-secreted IL-33 mediates homeostatic synaptic plasticity in the adult hippocampus. *Proc. Natl. Acad. Sci. U. S. A.* 118:e2020810118. doi: 10.1073/pnas.2020810118

Wang, J., Li, K.-L., Shukla, A., Beroun, A., Ishikawa, M., Huang, X., et al. (2021). Cocaine triggers astrocyte-mediated synaptogenesis. *Biol. Psychiatry* 89, 386–397. doi: 10.1016/j.biopsych.2020.08.012

Wang, T., Xu, G., Zhang, X., Ren, Y., Yang, T., Xiao, C., et al. (2022). Malfunction of astrocyte and cholinergic input is involved in postoperative impairment of hippocampal synaptic plasticity and cognitive function. *Neuropharmacology* 217:109191. doi: 10.1016/j.neuropharm.2022.109191

Xiao, J.-Y., Xiong, B.-R., Zhang, W., Zhou, W.-C., Yang, H., Gao, F., et al. (2018). PGE2-EP3 signaling exacerbates hippocampus-dependent cognitive impairment after laparotomy by reducing expression levels of hippocampal synaptic plasticity-related proteins in aged mice. *CNS Neurosci. Ther.* 24, 917–929. doi: 10.1111/cns.12832

Zheng, J., Min, S., Hu, B., Liu, Q., and Wan, Y. (2019). Nrdp1 is involved in hippocampus apoptosis in cardiopulmonary bypass-induced cognitive dysfunction via the regulation of ErbB3 protein levels. *Int. J. Mol. Med.* 43, 1747–1757. doi: 10.3892/ijmm.2019.4080

Zhou, Z., Okamoto, K., Onodera, J., Hiragi, T., Andoh, M., Ikawa, M., et al. (2021). Astrocytic cAMP modulates memory via synaptic plasticity. *Proc. Natl. Acad. Sci. U. S. A.* 118:e2016584118. doi: 10.1073/pnas.2016584118

Zhu, J., Wang, W., and Shi, H. (2021). The association between postoperative cognitive dysfunction and cerebral oximetry during geriatric orthopedic surgery: a randomized controlled study. *Biomed. Res. Int.* 2021:5733139. doi: 10.1155/2021/5733139

frontiers | Frontiers in Aging Neuroscience

TYPE Original Research
PUBLISHED 15 November 2022
DOI 10.3389/fnagi.2022.995781

OPEN ACCESS

EDITED BY
Zhongcong Xie,
Massachusetts General Hospital and Harvard Medical School, United States

REVIEWED BY
Zhipeng Xu,
Ningbo University, China
Diansan Su,
Shanghai Jiao Tong University, China

*CORRESPONDENCE
Jianhui Liu
jianhuiliu_1246@163.com

SPECIALTY SECTION
This article was submitted to Neurocognitive Aging and Behavior, a section of the journal Frontiers in Aging Neuroscience

RECEIVED 16 July 2022
ACCEPTED 05 October 2022
PUBLISHED 15 November 2022

CITATION
Zhang J, Basnet D, Du X, Yang J, Liu J, Wu F, Zhang X and Liu J (2022) Does cognitive frailty predict delayed neurocognitive recovery after noncardiac surgery in frail elderly individuals? Probably not. *Front. Aging Neurosci.* 14:995781. doi: 10.3389/fnagi.2022.995781

Does cognitive frailty predict delayed neurocognitive recovery after noncardiac surgery in frail elderly individuals? Probably not

Jingya Zhang, Diksha Basnet, Xue Du, Junjun Yang, Jiehui Liu, Fan Wu, Xiaoqing Zhang and Jianhui Liu*

Department of Anesthesiology, School of Medicine, Tongji Hospital, Tongji University, Shanghai, China

Introduction: Delayed neurocognitive recovery (DNR) is a common post-surgical complication among the elderly. Cognitive frailty (CF) is also an age-related medical syndrome. However, little is known about the association between CF and DNR. Therefore, this study aimed to study whether CF is associated with DNR in elderly patients undergoing elective noncardiac surgery, as well as to explore the potential risk factors for DNR in frail elderly individuals and construct a prediction model.

Methods: This prospective cohort study administered a battery of cognitive and frailty screening instruments for 146 individuals (≥65 years old) scheduled for elective noncardiac surgery. Screening for CF was performed at least one day before surgery, and tests for the presence of DNR were performed seven days after surgery. The association between CF and DNR was investigated. Moreover, the study subjects were randomly divided into a modeling group (70%) and a validation group (30%). Univariate and multivariate logistic regression was performed to analyze the modeling group data and identify the independent risk factors for DNR. The R software was used to construct DNR's nomogram model, verifying the model.

Results: In total, 138 individuals were eligible. Thirty-three cases were diagnosed with DNR (23.9%). No significant difference in the number of patients with CF was observed between the DNR and non-DNR groups ($P > 0.05$). Multivariate analysis after adjusting relevant risk factors showed that only the judgment of line orientation (JLOT) test score significantly affected the incidence of DNR. After internal validation of the constructed DNR prediction model, the area under the curve (AUC) of the forecast probability for the modeling population ($n = 97$) for DNR was 0.801, and the AUC for the validation set ($n = 41$) was 0.797. The calibration curves of both the modeling and validation groups indicate that the prediction model has good stability.

Conclusion: Cognitive frailty is not an independent risk factor in predicting DNR after noncardiac surgery in frail elderly individuals. The preoperative JLOT score is an independent risk factor for DNR in frail elderly individuals. The prediction model has a good degree of discrimination and calibration,

which means that it can individually predict the risk probability of DNR in frail elderly individuals.

KEYWORDS

cognitive frailty, delayed neurocognitive recovery, nomogram, predictive model, frail elderly

Introduction

In China, with the increased life expectancy, approximately 1/3 of elective surgical patients are elderly (≥65 years old) (Culley et al., 2017). Advances in surgical and anesthesia techniques, coupled with better preoperative risk assessment, have resulted in safer operations and lower rates of some serious complications (e.g., hemorrhage, infections) (Kim et al., 2015); however, much less is known about effectively protecting the aging brain from perioperative stress.

Delayed neurocognitive recovery (DNR) is a prevalent post-surgical complication in the elderly, with an incidence of 10–65% in geriatric surgery patients (Androsova et al., 2015; Boone et al., 2020). It is characterized by a temporary disruption in the patient's memory, personality, sleep, or executive function, which can manifest weeks or months following surgery. It may persist for months or even more (Needham et al., 2017). Age, education level, and preoperative cognitive status have been identified as risk factors (Kotekar et al., 2018). It has been proven to be linked with several unfavorable outcomes, including extended hospital stays, increased unanticipated complications, and mortality, which can lead to higher healthcare expenses and degrade patients' quality of life, placing a heavy burden on patients and their families (Monk et al., 2008). However, at present, much less is known about etiopathogenesis and therapies for DNR. There are no effective measures to protect the aging brain from DNR. Therefore, identifying and avoiding its risk factors might be an efficient strategy for therapy (Li et al., 2021).

Moreover, with the advancement of age, the risk of the incidence of frailty increases. The prevalence of frailty in the elderly ranges from 12 to 59% (Collard et al., 2012; O'Caoimh et al., 2021). "Fragile and vulnerable settings" have been listed as one of the top ten global health threats by the WHO since 2019 (Uslu and Canbolat, 2021). Frailty is an age-related medical syndrome that usually leads to a loss of reserve capacity to respond to stressors, deterioration of bodily functions and systems, and dependence on other people for daily activities, eventually leading to death and morbidity (Zaslavsky et al., 2013). Cognitive impairment is also considered a component of frailty. Based on a large body of evidence supporting a significant association between frailty and cognition (Dartigues and Amieva, 2014), the concept of cognitive frailty used in this study was first defined by the International Consensus Group at the International Academy on Nutrition and Aging (I.A.N.A) and the International Association of Gerontology and Geriatrics (I.A.G.G). Cognitive frailty (CF) is a geriatric syndrome characterized by the concurrence of cognitive impairment and physical frailty without dementia (Bu et al., 2021). The prevalence of cognitive frailty in clinical settings is estimated to be 10.7 to 39.7% (Sugimoto et al., 2018). There was more increment in white matter hyperintensity in patients with cognitive frailty than in those without (Sugimoto et al., 2019). Some evidence indicates that WMH causes cognitive decline and increases the risk of dementia (Prins and Scheltens, 2015). Nevertheless, whether cognitive frailty is associated with DNR has not been demonstrated.

To investigate the possible association of the occurrence of DNR with preoperative cognitive frailty and to explore the potential risk factors for DNR in frail elderly patients who undergo elective noncardiac surgery, we implemented a prospective cohort study of senior individuals who were screened for frailty using the FRAIL scale, which is a brief questionnaire that classifies individuals as frail, pre-frail, and robust; we also used the Montreal Cognitive Assessment (MoCA), which is used to identify mild cognitive impairment (MCI) (Aprahamian et al., 2017). This study aims to investigate the association between cognitive frailty and DNR and establish a prediction model for DNR. We hypothesized that cognitive frailty would correlate with cognitive decline in the early stage.

Materials and methods

Study design and participants

We collected 146 frail elderly patients (aged ≥ 65 years) undergoing elective noncardiac surgery at Tongji Hospital, affiliated with Tongji University, between February 2021 and March 2022 (Figure 1). All eligible patients were asked to provide informed consent. The following inclusion criteria were used: (1) aged ≥65 years; (2) each patient was diagnosed as being frail, FRAIL scale scores ≥3; (Aprahamian et al., 2017); (3) Preoperative Mini-Mental State Examination (MMSE) scores ≥ 20 points; (4) patients were scheduled for elective noncardiac surgery under general anesthesia; and (5) ASA classification I-III. The exclusion criteria

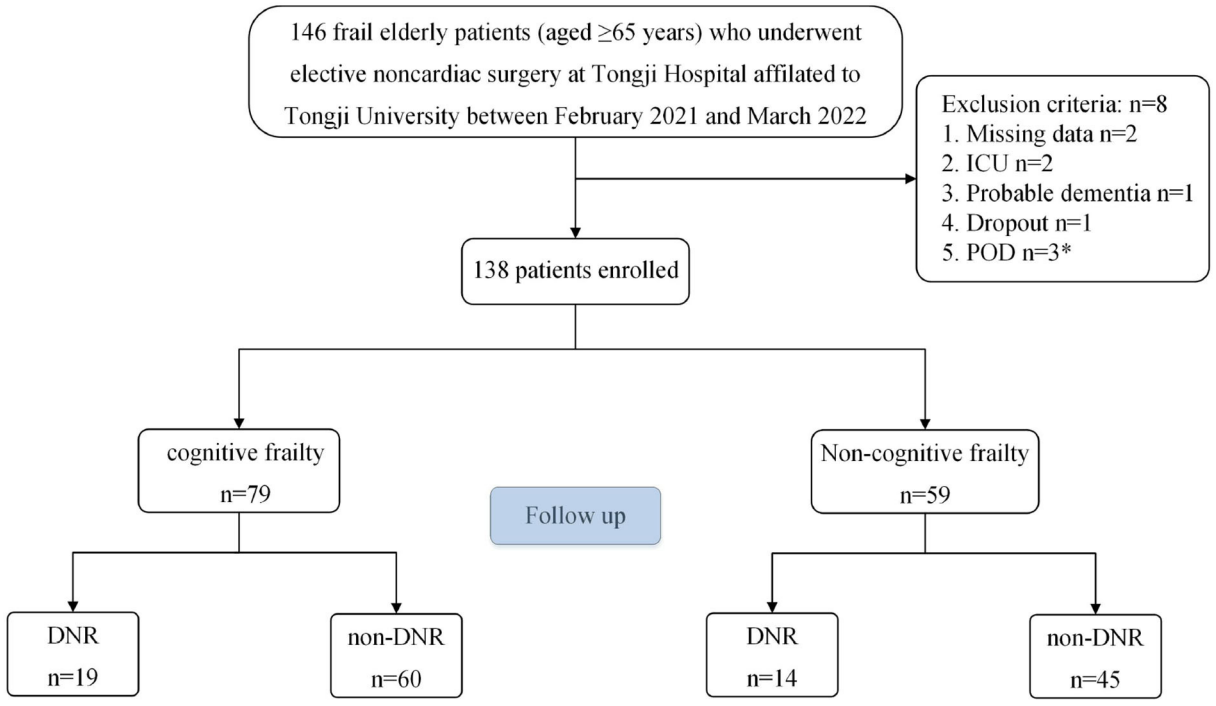

FIGURE 1
Flow diagram of patient selection process. *Including an ICU patient.

were as follows: (1) history of cerebrovascular disease; (2) history of sedatives and antidepressants; (3) history of severe neurological or psychiatric disease; (4) serious audiovisual impairments that impacted assessments; (5) unwillingness to abide by a protocol or withdrawal; (6) Patients admitted to intensive care unit (ICU) after surgery; (7) and patients who developed postoperative delirium (POD). Finally, 138 frail elderly patients were enrolled in this study. All patients were divided into modeling and validation populations using a computer-generated simple randomization list with a 7:3 allocation.

Tongji University's Institutional Review Board approved this study (IRB2021-LCYJ-014), and all subjects participating in the trial obtained written informed consent. The trial was registered before patient enrollment at http://www.chictr.org.cn (ChiCTR2100043475, Principal investigator: Jianhui Liu, registration date: February 19, 2021). All methods were carried out in conformity with the relevant guidelines and regulations. The study subjects gathered data after obtaining written informed consent to participate in the investigation. For the subjects unable to give written informed consent themselves, it was obtained from the legal representatives or guardians of minor subjects.

Data collection

The clinical characteristics, which were used as perioperative variables, consisted of the information obtained from all the patient's medical chart records or interviews: (1) demographics and clinical baseline data, including gender, age, body mass index (BMI), education, MMSE score, MoCA score, comorbidities (hypertension, diabetes, cardiovascular disease, chronic pulmonary diseases, and others); (2) main clinical parameters, including the type of surgeries (spinal, urinary and gastrointestinal), operation time, anesthesia time, VAS scores (1st, 12th, 24th, 48th h after surgery), Resmay sedation scores (1st, 12th, 24th, 48th h after surgery); (3) Results of 11 neuropsychological tests (NPTs), including one day before surgery and 7 days following the surgery.

Frailty assessment

While recruiting the patients, trained research coordinators evaluated physical frailty using the FRAIL scale. The FRAIL scale was validated in diverse groups of patients. A screening tool was easily carried out by various medical professionals or caregivers (Abellan Van Kan et al., 2008a,b). Compared with

other frailty scores, the FRAIL scale has higher sensitivity and has been associated with mortality and complications. In this study, the FRAIL scale was composed of five components: fatigue, resistance, ambulation, illness, and weight loss. The scale defined "fatigue" as the immanent feeling of tiredness "most or all" in the last 4 weeks. If the patient had difficulty or could not climb a flight of stairs, the "resistance" score was positive. If the patient had difficulty walking a block, the "ambulation" score is positive. The presence score for "illnesses" was positive if the patient had five or more comorbidities, including hypertension, diabetes, congestive heart failure, heart attack, angina, chronic pulmonary disease, asthma, arthritis, stroke, cancer, and nephrological disease. If the patient had an unintentional weight loss of more than 5% in the past year, the "loss of weight" score was positive. A score of 1 was set for each positive domain. Participants were classified as frail if they scored three or above, prefrail if they scored 1–2, and a score of 0 was considered robust (Ritt et al., 2017; Aguayo et al., 2018).

Cognitive function assessment

Cognitive frailty measurement

Cognitive frailty was defined as the combination of physical frailty and MCI, which is manifested by evident changes in at least one cognitive domain while maintaining the independence of functional abilities, and excluding concurrent Alzheimer's disease or other forms of dementia (Kelaiditi et al., 2013). In our study, we screened MCI patients with the MoCA scale. Studies have demonstrated that MoCA has advantages in detecting MCI in the elderly (Pinto et al., 2019). The MoCA is an objective neuropsychologic test that assesses a range of cognitive domains supporting independent functioning, including visuospatial/executive, naming, memory, attention, language, abstraction, delayed recall, and orientation to time and place (Freitas et al., 2012; Horton et al., 2015). It is significantly better at detecting MCI among aged people (Pinto et al., 2019). Compared with MMSE, a general cognitive tool, MOCA has higher sensitivity (90 vs. 18%) and considerable specificity (87 vs. 100%). In contrast, participants were considered to have MCI if their MoCA scores were $<$ 26 points (Nasreddine et al., 2005).

Definition of DNR

function assessment was performed at least one day before the surgery (baseline) and on postoperative day 7. Patients were first screened with MMSE and MoCA to eliminate those with dementia and identify those with MCI, respectively. Furthermore, eight tests with 11 subscales were administered, including the Hopkins Verbal Learning Test (HVLT immediate and delayed), Brief Visuospatial Memory Test-revised (BVMT immediate and delayed), Digits Symbol Substitution Test (DSST), Trail Making Test (TMT), Semantic Fluency Test (SFT), Forward and Backward Digit Span Test (DST forward and backward), Stroop Color Word Test (STROOP), and Judgment Of Line Orientation Test (JLOT), mainly focusing on memory, attention force, and executive function, as was the case in our previous study (Du et al., 2021). These measures were not only highly sensitive to the many forms of cognitive impairment but also free of cultural bias. All the tests were conducted in a quiet environment by professionally trained personnel. DNR was defined as a Z score (at least two Z-scores in individual tests, or the composite Z-score of all variables) at $\geq$ 1.96, as described in the International Study of Post-Operative Cognitive Dysfunction (ISPOCD) before (Moller et al., 1998; Du et al., 2021).

Postoperative delirium assessment

Trained members of the study team were assessed for delirium twice daily in the ward (08:00 and 20:00) using the Confusion Assessment Method (CAM) while hospitalized or until day 7. Because POD is a fluctuating state that frequently occurs in the ward and at night, we used chart review to detect any undiagnosed POD episodes (Inouye et al., 2005). Trained researchers reviewed the medical charts. We reviewed the individuals' medical charts to see if the nurse or doctor had any reports of POD (e.g., aggressive or inappropriate behavior, confusion, reports of hallucinations, etc.).

Anesthesia and postoperative analgesia management

We mainly chose major spine, urology, and gastrointestinal surgery operations. No premeditations were administered before surgery. All inpatients received general anesthesia after obtaining informed consent. Patients were intubated under general anesthesia, using etomidate, sufentanil, and cis-atracurium for anesthesia induction; they were then intubated under a visual laryngoscope. For intraoperative anesthetic maintenance, we chose volatile anesthetic sevoflurane and intravenous anesthetic (propofol and remifentanil).

Meanwhile, cis-atracurium was intermittently injected as needed until the end of surgery. In addition to a routine electrocardiogram, arterial blood pressure, end-expiration carbon dioxide, and blood oxygen saturation, anesthesia depth was monitored during the operation to maintain a bispectral index (BIS) between 40 and 60. Intraoperative blood pressure was controlled, and vasoactive agents were used as needed at the discretion of the attending anesthesiologists. A patient-controlled analgesia device (PCA) was used for postoperative pain management. Sufentanil was the main analgesic agent, and the commonly used dose was 100 μg (diluted with 100 mL of normal saline). Postoperative pain was

assessed on a 0–10 visual analog scale (VAS; VAS: 0 = no pain and 10 = worst pain) to keep the VAS below 3 points.

Statistical analysis

Statistical analyses were performed using SPSS statistics version 26.0 (IBM, Inc., Armonk, NY, USA), and the R programming language was used to perform statistical analyses. Several methods were used to analyze all the data.

We first assessed the normality and outliers of the data using the Shapiro-Wilk Normality Test. Patients were divided into two groups based on the occurrence of DNR: the DNR group and the non-DNR group. We applied appropriate statistical tests to compare differences between groups. When comparing the baseline characteristics, we used either the independent sample *t*-test for normally distributed continuous variables (data expressed as mean ± SD) or the Mann–Whitney U-test for non-normally distributed variables [data expressed as median (25, 75 percentile)]. The categorical variables were used in the chi-square test [data reported as counts (%)]. Statistical significance was set as $P < 0.05$ for all analyses.

A univariate and multivariate binary logistic regression was conducted to analyze risk factors and DNR in the modeling population, and the nomogram prediction model was fitted. Relevant factors of *P*-value ≤ 0.15 in univariate analysis and previously suggested risk factors like age, education, and cognitive impairment (Kotekar et al., 2018) were also included in the multivariate binary logistic regression model. The enter method was used. The odds ratio (OR) and its 95% confidence interval (CI) were used to show relative risk. The internal validation method was used mainly to verify the prediction model. We adopted the receiver operating characteristic curve (ROC) analysis to evaluate the resolution of the prediction

TABLE 1 Demographics and clinical data associated with DNR in modeled patients.

Item	DNR ($n = 33$)	non-DNR ($n = 105$)	*P*-value
Male (*n*, %)	23(69.7%)	65(61.9%)	0.417
Age (y), median [Q25, Q75]	69[65, 74]	70[66, 72]	0.872
Education (y), median [Q25, Q75]	9[8, 12]	9[7, 12]	0.476
BMI (kg/m^2), mean ± SD	24.6 ± 3.2	24.4 ± 3.6	0.720
Surgery time (min), median [Q25, Q75]	165[147, 207]	170[135, 217]	0.648
Anesthesia time (min), median [Q25, Q75]	210[183, 240]	205[170, 268]	0.875
BIS, mean ± SD	50.9 ± 5.4	50.3 ± 5.8	0.583
Cognitive frailty	19(57.6%)	60(57.1%)	0.965
Preoperative MMSE scores, median [Q25, Q75]	28[26, 29]	28[26, 29]	0.861
Preoperative MoCA scores, mean ± SD	24.7 ± 3.4	24.0 ± 3.8	0.301
Cognitive frailty (*n*, %)	12(54.5%)	41(54.7%)	0.992
Postoperative VAS scores, median [Q25, Q75]			
1h	2[1, 3]	2[2, 3]	0.010*
12h	1[1, 2]	1[1, 2]	0.337
24h	0[0, 1]	1[0, 1]	0.077
48h	0[0, 0]	0[0, 0]	0.362
Postoperative Resmay scores, median [Q25, Q75]			
1h	1[1,2]	1[1,2]	0.457
12h	3[3,3]	3[3,3]	0.182
Medical history (*n*, %)			
Hypertension	18(54.5%)	55(52.4%)	0.828
Diabetes	6(21.2%)	19(18.1%)	0.690
Cardiovascular Disease	3(9.1%)	22(22.9%)	0.843
Chronic Pulmonary Diseases	1(3.0%)	5(0.1%)	0.724
Surgery category (*n*, %)			
Spine	18(54.5%)	54(52.4%)	0.755
Urinary	10(30.3%)	23(21.9%)	0.324
Gastrointestinal	5(15.2%)	28(26.7%)	0.176

BMI, body mass index; MMSE, mini-mental state examination; MoCA, montreal cognitive assessment; and VAS, visual analog scale.

model. When the area under the curve (AUC) value was ≥ 0.7, the model was considered to have good discrimination ability. The calibration degree of the prediction model was evaluated by the Hosmer-Lemeshow test and calibration curve (Paul et al., 2013), in which we used 100-repetition bootstrapping to draw calibration curves with the test level $\alpha = 0.05$. The cut-off point's value was calculated as per the maximum value of Youden's index.

Results

Demographics and clinical baseline data

The demographic and clinical features of individuals in the DNR and non-DNR groups are outlined in Table 1. The final analysis included 138 frail elderly patients (≥65 years old). Among them, 33 patients were diagnosed with DNR, with an incidence rate of 23.9% (33/138). There was no significant difference in the number of patients with cognitive impairment between the DNR group (57.6%) and the non-DNR group (57.1%; $P > 0.05$).

Risk factors associated with DNR

Table 2 presents the results of univariate and multivariate binary logistic regression analyses for the incidence of DNR in the model population ($n = 97$). The postoperative VAS scores of 1h (OR 0.501, 95%CI 0.267–0.939), the baseline DSST scores (OR 1.057, 95% CI 1.009–1.106), and JLOT scores (OR 1.227, 95% CI 1.016–1.483) were identified as predictors of DNR after surgery. In the multivariate model, the preoperative JLOT score (OR 1.311, 95% CI 1.051–1.636) still significantly influenced DNR even after adjustment for age, education, and cognitive frailty.

Predictive performance analysis of the DNR prediction model

Figure 2 depicts a nomogram showing the risk of DNR in frail elderly patients based on multivariate regression analysis results. To explore the predictive value of the predictive probability for DNR, ROC analysis and the calibration curve were performed. As listed in Figure 3, the AUC of the forecast probability in the modeling population ($n = 97$) for DNR was 0.801 (95% CI: 0.683–0.918; Figure 3A), with a sensitivity of 77.3%, a specificity of 76.0%, and a cut-off value of 0.533. In the validation set ($n = 41$), the AUC of the forecast probability was 0.797 (95% CI: 0.646–0.948; Figure 3B), with a sensitivity of 63.6%, a specificity of 86.7%, and a cut-off value of 0.503. The calibration curves of the model population (Figure 4A) and validation population (Figure 4B) showed that the calibration curves of the prediction model were very close to the standard curves. Goodness-of-fit test results indicated that the prediction model does not deviate much from the actual condition: modeling population ($P = 0.605$) and verification population ($P = 0.484$).

Discussion

As far as we know, this is the first research to investigate the connection between preoperative cognitive frailty and DNR in geriatric patients undergoing elective noncardiac surgery. In this study, contrary to our hypothesis, we did not find an association between the incidence of DNR and cognitive frailty. As noted in previous work, some studies showed no significant difference in the incidence of DNR between MCI and non-MCI patients (Bekker et al., 2010; Trubnikova et al., 2014; Maleva et al., 2020), which indicated that MCI might not be a predictor for DNR. Although some studies have shown that frailty is an essential factor in cognitive dysfunction (Siejka et al., 2022), they are mostly based on community-dwelling elderly samples, and the majority of studies have mainly focused on exploring the relationship between frailty and long-term changes in cognitive function. In our study, we followed up only for a short time for the occurrence of DNR and did not find any association between cognitive frailty and DNR.

DNR is a common postoperative complication following major surgery with unclear specific etiopathogenesis in aging patients (Chan et al., 2013; Eckenhoff et al., 2020). Although methodological issues have plagued the identification of risk factors, numerous prospective, retrospective, and case-control studies have strived to identify risk factors for developing DNR. To explore the risk factors for DNR in frail elderly patients undergoing elective noncardiac surgery, we compared the preoperative data of the DNR group with the non-DNR group (Table 2) and constructed a prediction model for the occurrence of DNR. We calculated a DNR incidence rate of 23.9% (33/138, Table 1), which was within the range of 17–43% reported by Evered et al. (2011). In addition, our findings indicated that the scores of JLOT before surgery were independent risk factors for DNR in frail elderly individuals. The JLOT is one of the most commonly used assessments for evaluating visuospatial perception (Qualls et al., 2000). Generally, JLOT inspects the ability to estimate angular relationships between line segments, a test that requires little or no linguistic mediation and is free of cultural content (Collaer and Nelson, 2002). This study suggested that the assessment of JLOT might improve the accuracy of identification of frail elderly patients at the highest risk of DNR. Thus, our finding supports the possibility of JLOT's role in predicting incident DNR. We highly recommend that the JLOT scores be included in the definition of DNR by a battery of neuropsychological tests.

TABLE 2 Univariate and multivariate logistic regression analysis of incidence of DNR after elective noncardiac surgery in frail elderly modeling population.

	Univariate regression analysis			Multivariate regression analysis[a]		
	OR	95%CI	*p*-value	OR	95%CI	*p*-value
Sex (male)	1.778	0.625–5.059	0.281			
Age (y)	1.05	0.942–1.169	0.378	1.102	0.970–1.253	0.137
Education (y)	1.056	0.898–1.241	0.510	1.048	0.831–1.321	0.692
BMI (kg/m^2)	1.016	0.896–1.152	0.804			
Surgery time (min)	1.002	0.996–1.008	0.562			
Anesthesia time (min)	1	0.994–1.006	0.976			
BIS	0.994	0.913–1.083	0.897			
Preoperative MMSE scores	1.056	0.826–1.351	0.662			
Preoperative MoCA scores	1.004	0.911–1.195	0.536			
Cognitive frailty (n)	1.005	0.387–2.610	0.992	0.296	0.074–1.191	0.087
Postoperative VAS scores						
1h	0.501	0.267–0.939	0.031*	0.559	0.241–1.298	0.176
12h	0.807	0.452–1.440	0.467			
24h	0.16	0.210–1.294	0.16			
48h	0.889	0.262–3.018	0.85			
Postoperative Resmay scores						
1h	1.305	0.493–3.455	0.592			
12h	1.856	0.490–7.035	0.363			
Medical history (n)						
Hypertension	0.943	0.363–2.450	0.904			
Diabetes	0.559	0.184–1.701	0.306			
Cardiovascular Disease	2.784	0.589–13.172	0.197			
Chronic Pulmonary Diseases	1.5	0.166–13.561	0.718			
Surgery category						
spine	1.108	0.427–2.875	0.834			
urinary	2.107	0.753–5.899	0.156			
Gastrointestinal	0.275	0.059–1.284	0.101	1.842	0.306–11.087	0.505
Baseline cognitive tests scores						
HVLT (immediate)	1.075	0.977–1.181	0.137	0.95	0.794–1.137	0.575
HVLT (delayed)	1.177	0.992–1.397	0.062	1.153	0.836–1.591	0.386
BVMT (immediate)	0.988	0.926–1.055	0.724			
BVMT (delayed)	1.047	0.916–1.197	0.503			
DSST	1.057	1.009–1.106	0.019*	1.049	0.986–1.115	0.129
TMT	0.995	0.979–1.013	0.605			
DST (Forward)	0.927	0.783–1.096	0.374			
DST (Backward)	0.966	0.771–1.210	0.763			
SFT	1.066	0.959–1.185	0.238			
STROOP	1.024	0.990–1.059	0.164			
JLOT	1.227	1.016–1.483	0.034*	1.315	1.054–1.640	0.015*

BMI, body mass index; BVMT, brief visuospatial memory test-revised; DDST, digits symbol substitution test; DST, digit span test; HVLT, Hopkins verbal learning test; JLOT, judgment of line orientation test; MMSE, Mini-mental state examination; MoCA, montreal cognitive assessment; SFT, semantic fluency test; STROOP, stroop color word test; TMT, trail making test; and VAS, visual analog scale. [a]Adjusted for age, education, and cognitive frailty. *$P < 0.05$.

Paredes and colleagues analyzed 7 of 24 studies and claimed that increasing age was the most common risk factor for DNR (Paredes et al., 2016). However, in this study, we did not find age to be a potential risk factor for DNR, the reason for which we speculated that the incidence of DNR would increase with increasing age (Olotu, 2020). However, the population age we

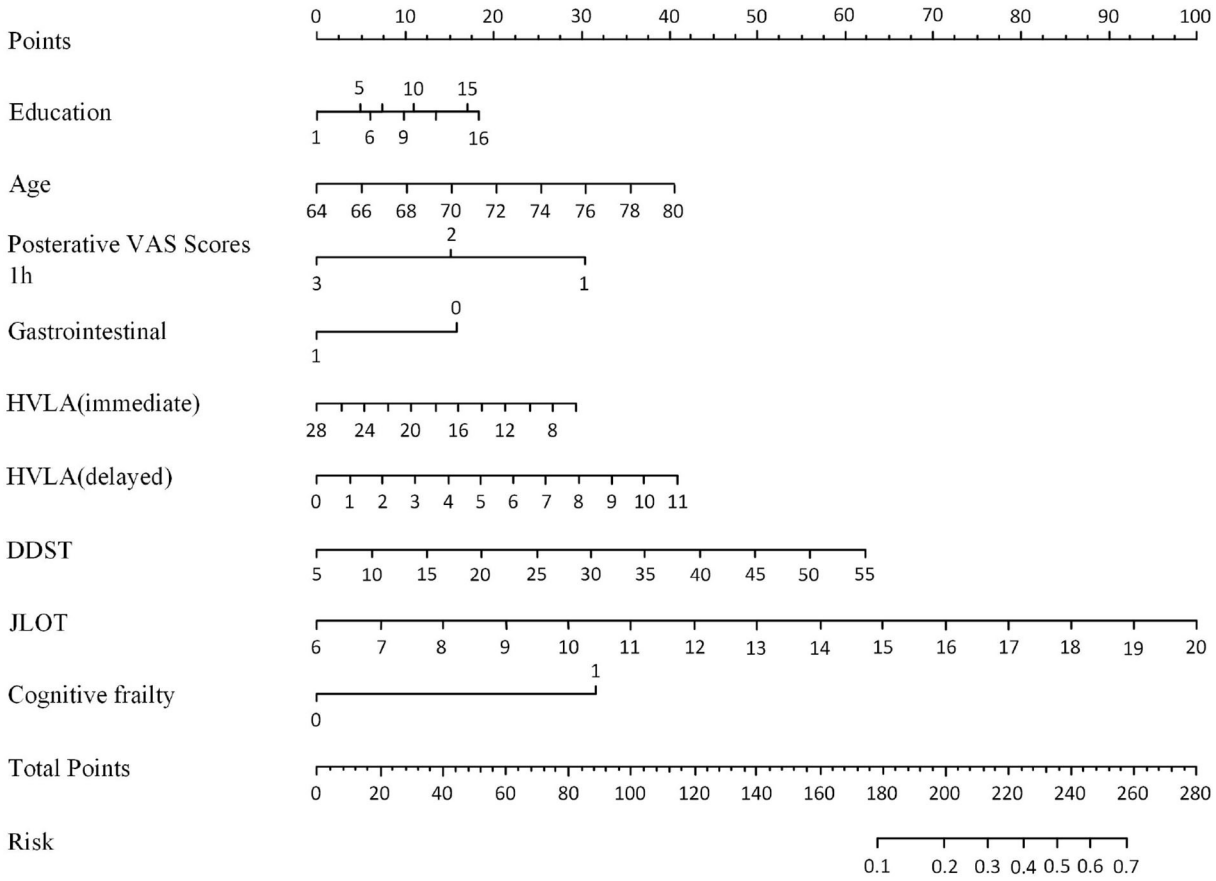

FIGURE 2
Nomogram for DNR risk and its predictive performance in frail elderly patients undergoing elective noncardiac surgery.

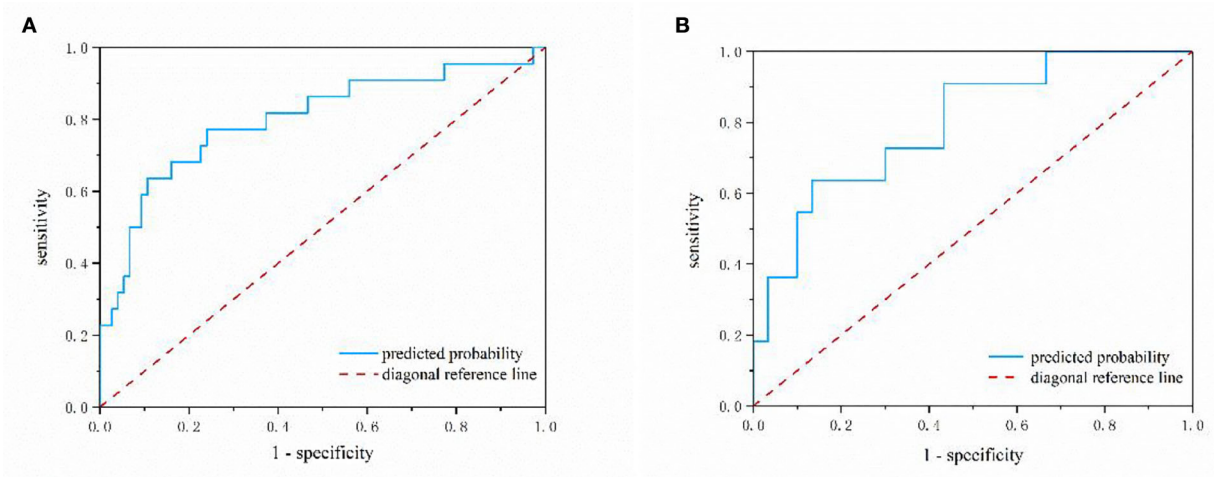

FIGURE 3
The nomogram model predicting the risk of DNR in frail elderly patients by ROC analysis. **(A)** Modeling group **(B)** validation group.

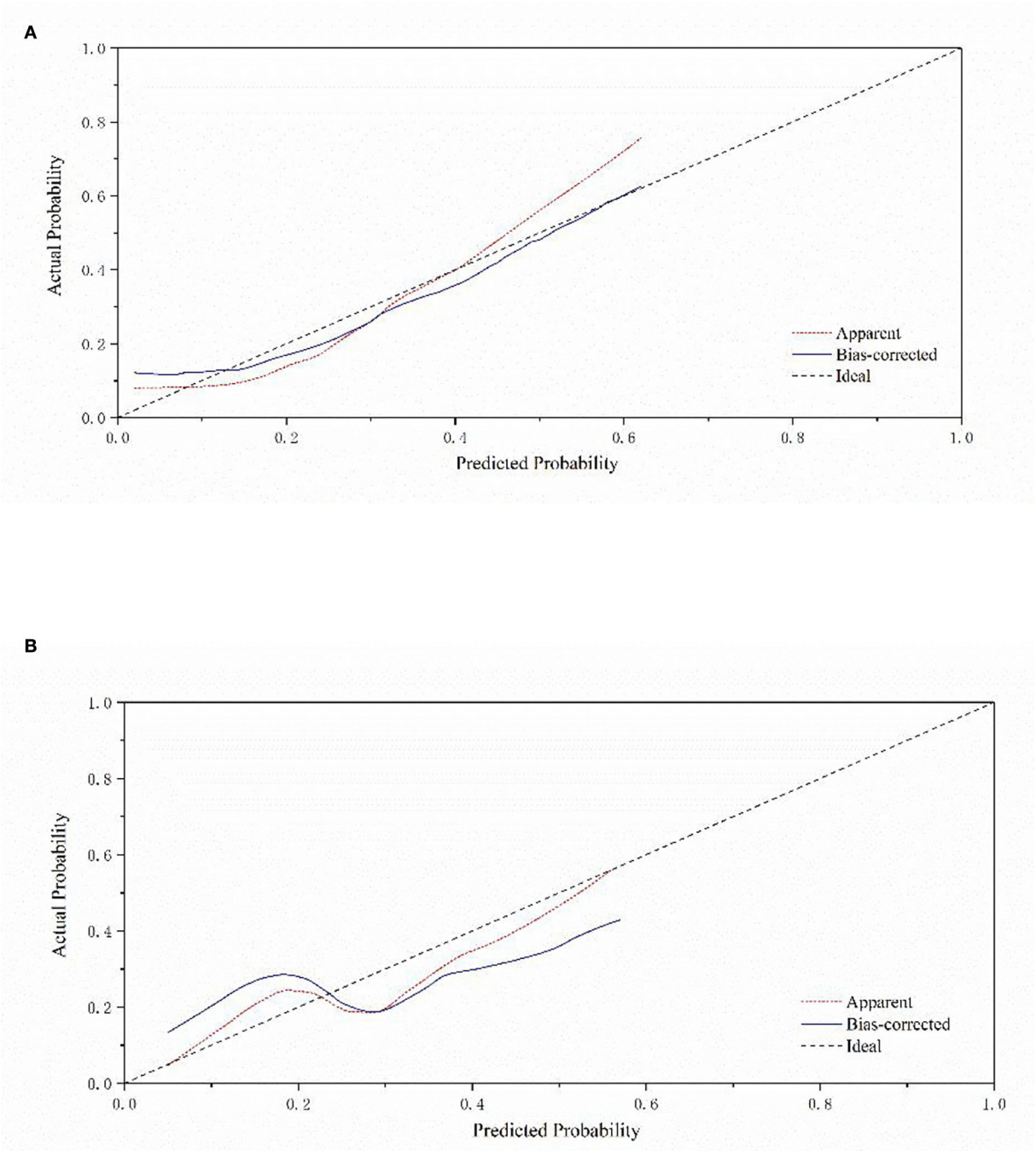

FIGURE 4
Calibration curve of a nomogram model for predicting the risk of DNR in frail elderly patients. **(A)** Modeling group **(B)** validation group.

collected mostly ranged from 65 to 75 years old. The age distribution was relatively concentrated, which weakened the relationship of age with DNR. Studies have revealed that a low education level is also a risk factor for DNR (Moller et al., 1998; Lloyd et al., 2012; Brown and Deiner, 2016). However, the similar mean level of education between groups in this study also weakened the relationship between education and DNR.

Moreover, to our knowledge, this is the first research to propose a nomogram model to predict the risk of DNR in frail elderly patients undergoing elective noncardiac surgery.

The nomogram model is established based on nine effective indicators, which can conveniently calculate the probability of DNR risks in frail elderly patients. The AUC value of the nomogram model in the training set was 0.794, and in the validation set, the AUC value of the nomogram model was 0.797. The geriatric calibration curve showed that the model-predicted probabilities closely matched the actual probabilities on the training and validation sets. These results suggested that the model had sufficient discriminative ability and high accuracy for the prediction of DNR in frail elderly individuals undergoing elective noncardiac surgery.

Above all, the JLOT test is an independent risk factor for DNR. We suggest that among so many neuropsychological tests, preoperative JLOT evaluation may be the most helpful as a promising predictor for DNR occurrence. We believe that the prediction model established may have certain guiding significance for clinical work to predict the occurrence of DNR in frail elderly patients. To our knowledge, DNR, a common postoperative complication, has a higher incidence rate in elderly patients, resulting in more extended hospital stays, higher costs, more significant social burden, and even higher mortality. Therefore, identifying patients with DNR has important clinical significance for anesthesiologists. For frail elderly patients with an increased risk of DNR assessed by predictive nomogram, timely intervention, frequent dynamic cognitive assessment, more comprehensive postoperative care, and long-term cognitive follow-up are recommended to reduce the risk, which also requires the joint participation of multiple disciplines.

Additionally, we compared the baseline data between the cognitive frailty and non-cognitive frailty groups (Supplementary Table S1), and we found that the two potential risk factors—years of education and hypertension—were significantly different between the two groups. Patients with fewer education years were significantly correlated with cognitive frailty. Wongtrakulruang et al. (2020) also linked low education levels (primary school or less) to a greater incidence of physical frailty and MCI (Wongtrakulruang et al., 2020), as the I.A.N.A–I.A.G.G definition stipulates that cognitive frailty is characterized by a reduction in cognitive reserve, which is largely influenced by education level. Education level has been the only measure of cognitive frailty by far (Facal et al., 2019), which parallels our findings. We also found that patients with hypertension were significantly associated with cognitive frailty. It has been proven that frail elderly adults are accompanied by hypertension. Hypertension is connected with an increased incidence of frailty and accelerated functional decline (Woods et al., 2005). Meanwhile, Walker et al. reported that chronic hypertension had a relationship with an increased risk of cognitive decline (Power et al., 2013; Walker et al., 2017), which is consistent with our findings.

Limitation

There are some limitations to our research. The small sample size is a major limitation of the current study. The study was conducted in a single center, and difficulties in patient recruitment have resulted in relatively modest sample sizes, which may lead to potential type II errors. Another limitation was that we could not perform lengthier postoperative follow-ups to assist us in establishing the patient's long-term prognosis, as we only had 7 days of follow-up.

Conclusion

The present study showed that cognitive frailty is not an independent risk factor for predicting delayed neurocognitive recovery after noncardiac surgery in frail elderly individuals. Furthermore, our study demonstrated that the neuropsychological test JLOT is an independent risk factor for early DNR in frail elderly patients. A predictive model for early postoperative DNR in the frail elderly was constructed. The prediction model has a good degree of discrimination and calibration and can individually predict the risk probability of early postoperative DNR in frail elderly patients, which is helpful for medical staff to evaluate quickly and intuitively.

Data availability statement

The original contributions presented in the study are included in the article/Supplementary material, further inquiries can be directed to the corresponding author.

Ethics statement

The studies involving human participants were reviewed and approved by the Tongji University's Institutional Review Board (IRB2021-LCYJ-014). The patients/participants provided their written informed consent to participate in this study.

Author contributions

JZ drafted the manuscript. JiaL conceived and designed the study. JZ, DB, JY, XD, JieL, and FW helped to collect data. JZ and JiaL analyzed the data. DB refined the language. XZ was responsible for quality control. All the authors contributed to the interpretation of the data and the revision of the manuscript and approved the submission of the revision.

Funding

This study was supported by research grants from the National Natural Science Foundation of China (Nos.

82171194 and 81974155 to JiaL), Clinical Research Plan of SHDC (No. SHDC2020CR1005A to Changhong Miao), Shanghai Science and Technology Commission Biomedical Science Project (No. 22S31902600 to JiaL), and Shanghai Tongji Hospital Youth Project (No. ITJ(QN)2008 to JiaL).

Acknowledgments

We would like to extend our heartfelt thanks to the researchers and co-workers from the Spinal Surgery, Urological Surgery, Gastrointestinal Surgery, and Anesthesiology Departments at Tongji Hospital, which is affiliated with Tongji University (Shanghai, China), who provided us with tremendous help on the project in patient recruitment, interviews, and data collection. We would also like to express our sincere gratitude to Dr. Miao Changhong, director of the Department of Anesthesiology, Zhongshan Hospital Affiliated to Fudan University (Shanghai, China), for his financial support.

Conflict of interest

The authors declare that the research was conducted in the absence of any commercial or financial relationships that could be construed as a potential conflict of interest.

Publisher's note

Supplementary material

The Supplementary Material for this article can be found online at: https://www.frontiersin.org/articles/10.3389/fnagi.2022.995781/full#supplementary-material

References

Abellan Van Kan, G., Rolland, Y., Bergman, H., Morley, J. E., Kritchevsky, S. B., and Vellas, B. (2008a). The I.A.N.A task force on frailty assessment of older people in clinical practice. *J. Nut.r Health Aging.* 12, 29–37. doi: 10.1007/BF02982161

Abellan Van Kan, G., Rolland, Y. M., Morley, J. E., and Vellas, B. (2008b). Frailty: toward a clinical definition. *J. Am. Med. Dir. Assoc.* 9, 71–72. doi: 10.1016/j.jamda.2007.11.005

Aguayo, G. A., Vaillant, M. T., Donneau, A. F., Schritz, A., Stranges, S., Malisoux, L., et al. (2018). Comparative analysis of the association between 35 frailty scores and cardiovascular events, cancer, and total mortality in an elderly general population in England: an observational study. *PLoS Med.* 15, e1002543. doi: 10.1371/journal.pmed.1002543

Androsova, G., Krause, R., Winterer, G., and Schneider, R. (2015). Biomarkers of postoperative delirium and cognitive dysfunction. *Front. Aging. Neurosci.* 7, 112. doi: 10.3389/fnagi.2015.00112

Aprahamian, I., Cezar, N. O. C., Izbicki, R., Lin, S. M., Paulo, D. L. V., Fattori, A., et al. (2017). Screening for frailty with the FRAIL Scale: a comparison with the phenotype criteria. *J. Am. Med. Dir. Assoc.* 18, 592–596. doi: 10.1016/j.jamda.2017.01.009

Bekker, A., Lee, C., Santi, D. E, Pirraglia, S., Zaslavsky, E., Farber, A., et al. (2010). Does mild cognitive impairment increase the risk of developing postoperative cognitive dysfunction? *Am. J. Surg.* 199, 782–788. doi: 10.1016/j.amjsurg.2009.07.042

Boone, M. D., Sites, B., Von Recklinghausen, F. M., Mueller, A., Taenzer, A. H., Shaefi, S., et al. (2020). Economic burden of postoperative neurocognitive disorders among US medicare patients. *JAMA Netw. Open* 3, e208931. doi: 10.1001/jamanetworkopen.2020.8931

Brown, C. T., and Deiner, S. (2016). Perioperative cognitive protection. *Br. J. Anaesth.* 117, iii52–iii61. doi: 10.1093/bja/aew361

Bu, Z., Huang, A., Xue, M., Li, Q., Bai, Y., Xu, G., et al. (2021). Cognitive frailty as a predictor of adverse outcomes among older adults: A systematic review and meta-analysis. *Brain Behav.* 11, e01926. doi: 10.1002/brb3.1926

Chan, M. T., Cheng, B. C., Lee, T. M., and Gin, T. (2013). BIS-guided anesthesia decreases postoperative delirium and cognitive decline. *J. Neurosurg. Anesthesiol.* 25, 33–42. doi: 10.1097/ANA.0b013e3182712fba

Collaer, M. L., and Nelson, J. D. (2002). Large visuospatial sex difference in line judgment: possible role of attentional factors. *Brain. Cogn.* 49, 1–12. doi: 10.1006/brcg.2001.1321

Collard, R. M., Boter, H., Schoevers, R. A., and Oude Voshaar, R. C. (2012). Prevalence of frailty in community-dwelling older persons: a systematic review. *J. Am. Geriatr. Soc.* 60, 1487–1492. doi: 10.1111/j.1532-5415.2012.04054.x

Culley, D. J., Flaherty, D., Fahey, M. C., Rudolph, J. L., Javedan, H., Huang, C. C., et al. (2017). Poor performance on a preoperative cognitive screening test predicts postoperative complications in older orthopedic surgical patients. *Anesthesiology* 127, 765–774. doi: 10.1097/ALN.0000000000001859

Dartigues, J. F., and Amieva, H. (2014). Cognitive frailty: rational and definition from an (I.a.N.a./i.a.g.g.) international consensus group. *J. Nutr. Health Aging.* 18, 95. doi: 10.1007/s12603-013-0437-5

Du, X., Gao, Y., Liu, S., Zhang, J., Basnet, D., Yang, J., et al. (2021). Early warning value of ASL-MRI to estimate premorbid variations in patients with early postoperative cognitive dysfunctions. *Front. Aging. Neurosci.* 13, 670332. doi: 10.3389/fnagi.2021.670332

Eckenhoff, R. G., Maze, M., Xie, Z., Culley, D. J., Goodlin, S. J., Zuo, Z., et al. (2020). Perioperative neurocognitive disorder: state of the preclinical science. *Anesthesiology* 132, 55–68. doi: 10.1097/ALN.0000000000002956

Evered, L., Scott, D. A., Silbert, B., and Maruff, P. (2011). Postoperative cognitive dysfunction is independent of type of surgery and anesthetic. *Anesth. Analg.* 112, 1179–1185. doi: 10.1213/ANE.0b013e318215217e

Facal, D., Maseda, A., Pereiro, A. X., Gandoy-Crego, M., Lorenzo-López, L., Yanguas, J., et al. (2019). Cognitive frailty: a conceptual systematic review and an operational proposal for future research. *Maturitas* 121, 48–56. doi: 10.1016/j.maturitas.2018.12.006

Freitas, S., Simões, M. R., Alves, L., and Santana, I. (2012). Montreal Cognitive Assessment: influence of sociodemographic and health variables. *Arch. Clin. Neuropsychol.* 27, 165–175. doi: 10.1093/arclin/acr116

Horton, D. K., Hynan, L. S., Lacritz, L. H., Rossetti, H. C., Weiner, M. F., Cullum, C. M., et al. (2015). An abbreviated montreal cognitive assessment (MoCA) for dementia screening. *Clin. Neuropsychol.* 29, 413–425. doi: 10.1080/13854046.2015.1043349

Inouye, S. K., Leo-Summers, L., Zhang, Y., and Bogardus, S. T. Jr., Leslie, D. L., and Agostini, J. V. (2005). A chart-based method for identification of delirium: validation compared with interviewer ratings using the confusion assessment method. *J. Am. Geriatr. Soc.* 53, 312–318. doi: 10.1111/j.1532-5415.2005.53120.x

Kelaiditi, E., Cesari, M., Canevelli, M., Van Kan, G. A., Ousset, P. J., Gillette-Guyonnet, S., et al. (2013). Cognitive frailty: rational and definition from an (I.A.N.A./I.A.G.G.) international consensus group. *J. Nutr. Health Aging* 17, 726–734. doi: 10.1007/s12603-013-0367-2

Kim, S., Brooks, A. K., and Groban, L. (2015). Preoperative assessment of the older surgical patient: honing in on geriatric syndromes. *Clin. Interv. Aging* 10, 13–27. doi: 10.2147/CIA.S75285

Kotekar, N., Shenkar, A., and Nagaraj, R. (2018). Postoperative cognitive dysfunction - current preventive strategies. *Clin. Interv. Aging* 13, 2267–2273. doi: 10.2147/CIA.S133896

Li, Y. L., Huang, H. F., and Le, Y. (2021). Risk factors and predictive value of perioperative neurocognitive disorders in elderly patients with gastrointestinal tumors. *BMC Anesthesiol.* 21, 193. doi: 10.1186/s12871-021-01405-7

Lloyd, D. G., Ma, D., and Vizcaychipi, M. P. (2012). Cognitive decline after anaesthesia and critical care. *Conti. Educ. Anaesth. Crit. Care Pain* 12, 105–109. doi: 10.1093/bjaceaccp/mks004

Maleva, O. V., Trubnikova, O. A., Syrova, I. D., Solodukhin, A. V., Golovin, A. A., Barbarash, O. L., et al. (2020). [Incidence of postoperative cognitive dysfunction after simultaneous carotid surgery and coronary artery bypass grafting in patients with asymptomatic cerebral atherosclerosis]. *Zh Nevrol Psikhiatr Im S S Korsakova* 120, 5–12. doi: 10.17116/jnevro20201200325

Moller, J. T., Cluitmans, P., Rasmussen, L. S., Houx, P., Rasmussen, H., Canet, J., et al. (1998). Long-term postoperative cognitive dysfunction in the elderly ISPOCD1 study. ISPOCD investigators. International study of post-operative cognitive dysfunction. *Lancet* 351, 857–861. doi: 10.1016/S0140-6736(97)07382-0

Monk, T. G., Weldon, B. C., Garvan, C. W., Dede, D. E., van der Aa, M. T., Heilman, K. M., et al. (2008). Predictors of cognitive dysfunction after major noncardiac surgery. *Anesthesiology* 108, 18–30. doi: 10.1097/01.anes.0000296071.19434.1e

Nasreddine, Z. S., Phillips, N. A., Bédirian, V., Charbonneau, S., Whitehead, V., Collin, I., et al. (2005). The montreal cognitive assessment, MoCA: a brief screening tool for mild cognitive impairment. *J. Am. Geriatr. Soc.* 53, 695–699. doi: 10.1111/j.1532-5415.2005.53221.x

Needham, M. J., Webb, C. E., and Bryden, D. C. (2017). Postoperative cognitive dysfunction and dementia: what we need to know and do. *Br. J. Anaesth.* 119, i115–i125. doi: 10.1093/bja/aex354

O'Caoimh, R., Sezgin, D., O'Donovan, M. R., Molloy, D. W., Clegg, A., Rockwood, K., et al. (2021). Prevalence of frailty in 62 countries across the world: a systematic review and meta-analysis of population-level studies. *Age Ageing* 50, 96–104. doi: 10.1093/ageing/afaa219

Olotu, C. (2020). Postoperative neurocognitive disorders. *Curr. Opin. Anaesthesiol.* 33, 101–108. doi: 10.1097/ACO.0000000000000812

Paredes, S., Cortínez, L., Contreras, V., and Silbert, B. (2016). Post-operative cognitive dysfunction at 3 months in adults after noncardiac surgery: a qualitative systematic review. *Acta. Anaesthesiol. Scand.* 60, 1043–1058. doi: 10.1111/aas.12724

Paul, P., Pennell, M. L., and Lemeshow, S. (2013). Standardizing the power of the Hosmer-Lemeshow goodness of fit test in large data sets. *Stat. Med.* 32, 67–80. doi: 10.1002/sim.5525

Pinto, T. C. C., Machado, L., Bulgacov, T. M., Rodrigues-Júnior, A. L., Costa, M. L. G., Ximenes, R. C. C., et al. (2019). Is the montreal cognitive assessment (moca) screening superior to the mini-mental state examination (MMSE) in the detection of mild cognitive impairment (MCI) and Alzheimer's Disease (AD) in the elderly? *Int. Psychogeriatr.* 31, 491–504. doi: 10.1017/S1041610218001370

Power, M. C., Tchetgen, E. J., Sparrow, D., Schwartz, J., and Weisskopf, M. G. (2013). Blood pressure and cognition: factors that may account for their inconsistent association. *Epidemiology* 24, 886–893. doi: 10.1097/EDE.0b013e3182a7121c

Prins, N. D., and Scheltens, P. (2015). White matter hyperintensities, cognitive impairment and dementia: an update. *Nat. Rev. Neurol.* 11, 157–165. doi: 10.1038/nrneurol.2015.10

Qualls, C. E., Bliwise, N. G., and Stringer, A. Y. (2000). Short forms of the benton judgment of line orientation test: development and psychometric properties. *Arch. Clin. Neuropsychol.* 15, 159–163. doi: 10.1093/arclin/15.2.159

Ritt, M., Ritt, J. I., Sieber, C. C., and Gaßmann, K. G. (2017). Comparing the predictive accuracy of frailty, comorbidity, and disability for mortality: a 1-year follow-up in patients hospitalized in geriatric wards. *Clin. Interv. Aging* 12, 293–304. doi: 10.2147/CIA.S124342

Siejka, T. P., Srikanth, V. K., Hubbard, R. E., Moran, C., Beare, R., Wood, A. G., et al. (2022). Frailty is associated with cognitive decline independent of cerebral small vessel disease and brain atrophy. *J. Gerontol. A. Biol. Sci. Med. Sci.* 9, 1819–1826. doi: 10.1093/gerona/glac078

Sugimoto, T., Ono, R., Kimura, A., Saji, N., Niida, S., Toba, K., et al. (2019). Cross-sectional association between cognitive frailty and white matter hyperintensity among memory clinic patients. *J. Alzheimers. Dis.* 72, 605–612. doi: 10.3233/JAD-190622

Sugimoto, T., Sakurai, T., Ono, R., Kimura, A., Saji, N., Niida, S., et al. (2018). Epidemiological and clinical significance of cognitive frailty: a mini review. *Ageing Res. Rev.* 44, 1–7. doi: 10.1016/j.arr.2018.03.002

Trubnikova, O. A., Mamontova, A. S., Syrova, I. D., Maleva, O. V., and Barbarash, O. L. (2014). Does preoperative mild cognitive impairment predict postoperative cognitive dysfunction after on-pump coronary bypass surgery? *J. Alzheimers Dis.* 42, S45–51. doi: 10.3233/JAD-132540

Uslu, A., and Canbolat, O. (2021). Relationship between frailty and fatigue in older cancer patients. *Semin. Oncol. Nurs.* 37, 151179.doi: 10.1016/j.soncn.2021.151179

Walker, K. A., Power, M. C., and Gottesman, R. F. (2017). Defining the relationship between hypertension, cognitive decline, and dementia: a review. *Curr. Hypertens. Rep.* 19, 24. doi: 10.1007/s11906-017-0724-3

Wongtrakulruang, P., Muangpaisan, W., Panpradup, B., Tawatwattananun, A., Siribamrungwong, M., Tomongkon, S., et al. (2020). The prevalence of cognitive frailty and pre-frailty among older people in Bangkok metropolitan area: a multicenter study of hospital-based outpatient clinics. *J. Frailty Sarcopenia Falls* 5, 62–71. doi: 10.22540/JFSF-05-062

Woods, N. F., LaCroix, A. Z., Gray, S. L., Aragaki, A., Cochrane, B. B., Brunner, R. L., et al. (2005). Frailty: emergence and consequences in women aged 65 and older in the women's health initiative observational study. *J. Am. Geriatr. Soc.* 53, 1321–1330. doi: 10.1111/j.1532-5415.2005.53405.x

Zaslavsky, O., Cochrane, B. B., Thompson, H. J., Woods, N. F., and Herting, J. R., and LaCroix, A. (2013). Frailty: a review of the first decade of research. *Biol. Res. Nurs.* 15, 422–432. doi: 10.1177/1099800412462866

frontiers | Frontiers in Aging Neuroscience

TYPE Original Research
PUBLISHED 17 November 2022
DOI 10.3389/fnagi.2022.1013478

OPEN ACCESS

EDITED BY
Yingwei Wang,
Huashan Hospital of Fudan University, China

REVIEWED BY
Xiao-Qing Tang,
University of South China, China
Changjun Gao,
Fourth Military Medical University, China

*CORRESPONDENCE
Tianlong Wang
w_tl5595@hotmail.com

†These authors have contributed equally to this work and share first authorship

SPECIALTY SECTION
This article was submitted to Neurocognitive Aging and Behavior, a section of the journal Frontiers in Aging Neuroscience

RECEIVED 07 August 2022
ACCEPTED 10 October 2022
PUBLISHED 17 November 2022

CITATION
Liu Y, Feng H, Fu H, Wu Y, Nie B and Wang T (2022) Altered functional connectivity and topology structures in default mode network induced by inflammatory exposure in aged rat: A resting-state functional magnetic resonance imaging study.
Front. Aging Neurosci. 14:1013478.
doi: 10.3389/fnagi.2022.1013478

Altered functional connectivity and topology structures in default mode network induced by inflammatory exposure in aged rat: A resting-state functional magnetic resonance imaging study

Yang Liu[1,2†], Huiru Feng[1†], Huiqun Fu[1], Yan Wu[3], Binbin Nie[4] and Tianlong Wang[1,2*]

[1]Department of Anesthesiology, Xuanwu Hospital, Capital Medical University, Beijing, China, [2]National Clinical Research Center for Geriatric Diseases, Beijing, China, [3]Department of Anatomy, Capital Medical University, Beijing, China, [4]Institute of High Energy Physics, Chinese Academy of Sciences, Beijing, China

Inflammatory stress in anesthesia management and surgical process has been reported to induce long-term cognitive dysfunction in vulnerable aged brain, while few studies focused on the network mechanism. The default mode network (DMN) plays a significant role in spontaneous cognitive function. Changes in topology structure and functional connectivity (FC) of DMN in vulnerable aged brain following inflammatory stress-induced long-term cognitive dysfunction are rarely studied. Eighty-eight aged male rats received intraperitoneal injection of lipopolysaccharide (LPS) as treatment or equal amount of normal saline (NS) as control. Morris Water Maze (MWM) was performed to assess short- (<7 days) and long-term (>30 days) learning and spatial working memory. Enzyme-linked immunosorbent assay (ELISA) was used to measure systemic and hippocampus inflammatory cytokines. Real-time polymerase chain reaction (RT-PCR) was used to measure the changes in gene level. Resting-state functional magnetic resonance imaging (rs-fMRI) was used to exam brain function *prior* to MWM on days 3, 7, and 31 after LPS exposure. Graph theory analysis was used to analyze FC and topology structures in aged rat DMN. Aged rats treated with LPS showed short- and long-term impairment in learning and spatial working memory in MWM test. Graph theory analysis showed temporary DMN intrinsic connectivity increased on day 3 followed with subsequent DMN intrinsic connectivity significantly altered on day 7 and day 31 in LPS-exposed rats as compared with controls. Short- and long-term alterations were observed in FC, while alterations in topology structures were only observed on day 3. Rats with inflammatory stress exposure may cause short- and long-term alterations in intrinsic connectivity in aged rat's DMN while the changes in topology structures only lasted for 3 days. Inflammatory stress has prolonged effects on FC, but not topology structures in venerable aged brain.

KEYWORDS

anesthesia, inflammation, cognitive dysfunction, default mode network, small worldness

Introduction

Cognitive dysfunction following anesthesia and surgery is widely reported in clinical practice (Belrose and Noppens, 2019; Liu et al., 2022). Among the population, elderly patients were shown to be more vulnerable to neuroinflammation induced by anesthesia neurotoxicity and surgical trauma, which may further develop into long-term cognitive dysfunction (Daiello et al., 2019). Surgical trauma is recently believed to be a major source for inflammatory cytokines in clinical practice (Yang T. et al., 2020; Liu et al., 2022). Clinical study has shown that the postoperative cognitive decline is associated with increased mortality (Yang T. et al., 2020; Duprey et al., 2021; Liu et al., 2022). In this case, understanding how the cognitive impaired aged brain functions in such conditions is of great significance for disease prevention and drug target design, as well as a better perioperative outcome for elderly patients.

Traditional neuroscience approaches mainly focused on several localized regions (e.g., hippocampus and prefrontal cortex; Lisman et al., 2017; Le Merre et al., 2021) to make a detailed experiment in particular animal models. However, as none of the cognitive function can be fully understood if taken out of a broad connectionist context (Fuster, 2001) and the brain functions as networks instead of separate regions in living subjects (Avena-Koenigsberger et al., 2017), results from traditional approaches may only provide limited evidence in disease mechanism and development. Recent studies reported the significance of "neural network disease," as the functions of neural network and topology changes contributed largely to disease development and revealed medical treatment outcomes (Zhang et al., 2021; Kukla et al., 2022). These results highly emphasized the importance of understanding how the neural network changes during inflammatory exposure induced cognitive decline in a broad scale in living brain.

Resting-state functional magnetic resonance imaging (rs-fMRI), which measures spontaneous brain activity *via* low frequency fluctuations in blood-oxygen-level-dependent (BOLD) signal, provides a non-invasive method to study brain function in living subjects (Biswal et al., 1995). By abstracting brain networks as graphs, the graph theory method analyzed BOLD signal by dividing the brain networks into different elements (nodes) and their pairwise links (edges). Brain nodes are neurons/entire brain regions and edges are binary/weighted values (Sporns, 2018). Functional connectivity (FC), defined as correlations (edges in the graph) of neuronal activation between different brain regions (nodes in the graph), has been shown to be modulated in various diseases conditions (Ji et al., 2018; Liu et al., 2018; Schumacher et al., 2021). Meanwhile, topology properties and intrinsic connectivity of brain networks may also be altered in disease situations (Lopes et al., 2017; Lee et al., 2019). In this way, by considering topology properties and FC in a whole scale, rs-fMRI and graph theory method provide a detailed understanding of changes in brain networks, indicating an optional choice for studying disease mechanisms.

The default mode network (DMN) is a set of widely distributed brain regions, which often show reductions in activity during attention-demanding tasks but increase their activity across multiple forms of complex cognition. Many of which are linked to memory or abstract thought (Smallwood et al., 2021). Impaired FC in DMN has been characterized as one of the major changes in patients with Alzheimer's disease (AD) and mild cognitive impairment (MCI; Chand et al., 2017; Hohenfeld et al., 2018; Cao et al., 2020), demonstrating a potential use for FC in DMN in cognitive function. Recent data from preclinical experiments have shown that the DMN not only exists across species but also similar in components (Li and Zhang, 2018; Jing et al., 2021; Yeshurun et al., 2021), suggesting that study of DMN in rodent models would be applicable in investigating mechanisms of human diseases. Although there are studies demonstrating changes in DMN in Aβ-induced cognitive decline (Pascoal et al., 2019), few studies focused on the DMN alteration in acute- and long-term after inflammatory stress exposure.

This study is designed to investigate acute and long-term changes in DMN after inflammatory stress exposure in anesthesia process. Inflammatory stress was induced by lipopolysaccharide (LPS) injection, as it is one of the most widely used initiators for inducing systemic inflammatory responses and cognitive decline (Kan et al., 2016; Lakshmikanth et al., 2016; Yang L. et al., 2020) in preclinical experiments. Aged rats were used in this experiment because elderly patients are at highly risk for cognitive dysfunction after anesthesia and surgery (Belrose and Noppens, 2019). The model was adapted from our previous work, which demonstrated that a single intraperitoneal injection of LPS (2 mg/kg) induces a long-term inflammatory response in aged rat hippocampus and impaired behavior performances (Fu et al., 2014; Kan et al., 2016). Systemic levels of inflammatory cytokines, including interleukin-1β (IL-1β) and tumor necrosis factor-alpha (TNFα), were measured by enzyme-linked immunosorbent assay (ELISA) as their levels are highly correlated with sickness behavior after LPS exposure (Oliveira et al., 2020). We hypothesized that the topology structure and FC in the aged rat DMN will both change after inflammatory exposure, which may provide new insights into drug target design and new diagnostic biomarkers.

Materials and methods

Ethics approval

All animal procedures were approved by the Ethical Committee of Capital Medical University as complied with the guide for Care and Use of Laboratory Animals prepared by the Institute of Laboratory Animal Resources and published by the National Institute of Health. All efforts were made to minimize the pain and suffering of the animals.

Animal preparations

A total of 88 adult male Wistar rats (19 months, 650–800 g, Charles-River Animal Technology, Beijing, China) were housed in an animal facility under a 12/12 light–dark cycle at 22 ± 2°C with 50%–60% humidity. Food and water were available *ad libitum*.

Rats were intraperitoneally injected (i.p.) with either lipopolysaccharide (LPS, 055: B5, Sigma-Aldrich, St Louis, MO, United States) or sterilized normal saline (NS, OC90F1, Otsuka Pharmaceutical, Co, Ltd., Beijing, China) and were allocated to either LPS group ($n = 60$, 2 mg/kg, i.p.) or NS group ($n = 28$, same volume with LPS solution injection). The dose for LPS was adapted from our previous work which showed that low-dose LPS injection caused prolonged cognitive dysfunction in aged rat (Figure 1A; Fu et al., 2014; Kan et al., 2016).

Morris water maze

All rats ($n = 12$ in each group) performed MWM test with the protocols adopted from our previous work (Kan et al., 2016). The MWM is a circular tank placed in a quiet and dimly lit room with visual clues around. The inner surface of the tank was painted in black and filled with water (24 ± 1°C) in about 20 cm in depth. A hidden platform was placed in one fixed quadrant hidden in about 1.5 cm below the water surface. On top of the circular tank is a video camera tracking the behavior performance of the rats. Around the circular tank is a series of large support holders with thick curtains to avoid sharp lights if necessary. Briefly, the MWM test contains two sections of spatial acquisition trials (day 1–5 and day 31–35) and probe trials (day 7 and day 37) to assess learning and spatial working memory in both short term (<7 days) and long term (>30 days). For the spatial acquisition trial, the rat was gently placed in one of the quadrants facing the wall of MWM circular pool and then was allowed to swim freely for 60 s to find the hidden platform. If the rat succeeds, it was allowed to stay on the platform for 5 s. Otherwise, it would be manually placed on the platform and allowed to stay for 20 s. Four spatial acquisition trials were performed in each day to let the rat entering the MWM from four different quadrants and the training session lasted for 5 consecutive days. On day 7, a probe trial was performed with the hidden platform removed. Rats were gently placed in the opposite quadrant to the original location of the platform and allowed to swim freely for 30 s. On day 6, the rats were allowed to have a rest. The latency to find the platform in spatial acquisition trials and the time spent and crossovers in platform quadrant in probe trials were recorded and analyzed using an animal behavior tracking system (EthoVision, Noldus Information Technologies, Netherlands). From days 31 to 35, another section of spatial acquisition trials was repeated followed with another probe trial on day 37. After finishing the behavior examination, the rats were sacrificed by over inhalation of isoflurane (ISO) with injection of potassium *via* the femoral vein. The timeline for MWM protocol is summarized in Figures 1B, 2A.

Tissue preparation

On day 0 (before LPS or NS treatment, baseline), and days 3, 7, and 30 after LPS exposure, a cohort of animals ($n = 8$ for each time point each group) was selected for inflammatory cytokine examination. On the day of termination, rats were anesthetized by isoflurane (ISO, Baxter, Lessines, Belgium) prior to *vena cava* blood sampling (5 ml for each time). After 2 h of clotting at 4°C, blood samples were subjected to centrifugation at 1,000*g* for 20 min and the serum was later collected and stored at −80°C.

After decapitation, rat brain was quickly dissected and dividing by half using a chilled cold blade. The left part of the brain was rapidly grinded into small pieces and then homogenized by the RIPA Lysis Buffer (P0013C, Beyotime, Beijing, China) at the concentration of 20 mg tissue/200 μg buffer. Prior to homogenization, PMSF (100 mM, P0100-1, Solarbio, Beijing, China) was added to the RIPA lysis buffer to reach the concentration of 1 mM/ml. After centrifugation (Eppendorf, Centrifuge 5810R, China) at 1,000*g*, 4°C for 20 min, the supernatant was collected and stored at −80°C for further use.

mRNA and RT-PCR

For the same rat, the right part of the brain was used for operating this procedure. Total RNA was extracted from hippocampus by Trizol reagent (Invitrogen, Paisley, United Kingdom) and was purified by the RNase Away Reagent (catalog number 18270466, Invitrogen, Paisley, United Kingdom). Prior the RT-PCR process, the integrity of mRNA was measured by NanoDrop 2000 (Thermo Scientific, Waltham, MA, United States) and the cDNA was synthesized by the M-MLV Reverse Transcriptase Kit according to the manufacturer's instructions. The cDNA amplification was operated by the ABI 7500 Fast Real-Time PCR System (Applied Biosystems, Waltham, MA, United States) for 45 cycles (each for a duration of 2 min at 94°C, annealing for 5 s at 94°C and then for 30 s at 60°C and finally extension for 10 min at 72°C). The primer and amplification

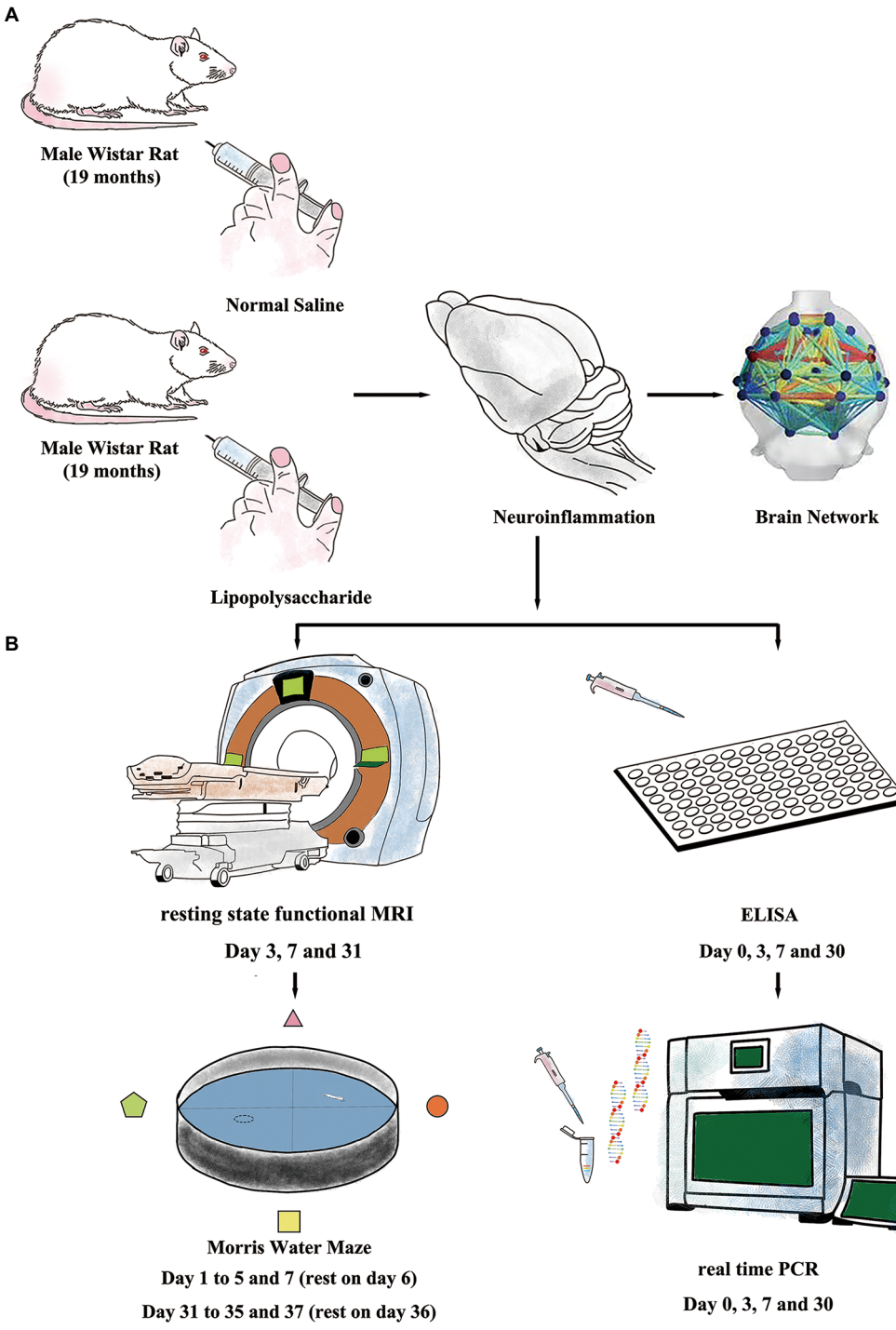

FIGURE 1
Experiment protocols. **(A)** Inflammatory exposure was induced by intraperitoneal injection of lipopolysaccharide (LPS, 2 mg/kg) in aged rat. The LPS further induced short- and long-term neuroinflammation and resulted in impaired brain network. **(B)** Resting-state-functional magnetic resonance imaging (rs-fMRI) and Morris Water Maze (MWM) were used to evaluate changes in neural network and cognitive function. Enzyme-linked immunosorbent assay (ELISA) and real-time polymerase chain reaction (RT-PCR) were performed to study neuroinflammation.

sequences for IL-1β, TNFα, and NF-κB were shown in Table 1. The level of mRNA expression was calculated by the SYBR Green direction method, and all the data were analyzed by the 2ΔΔCt method by the target gene expression in rat cortex corrected by β-actin expression.

Enzyme-linked immunosorbent assay measurements

On day 0 (before LPS or NS treatment), and days 3, 7, and 30 after LPS exposure, a cohort of animals ($n = 8$ for each time point

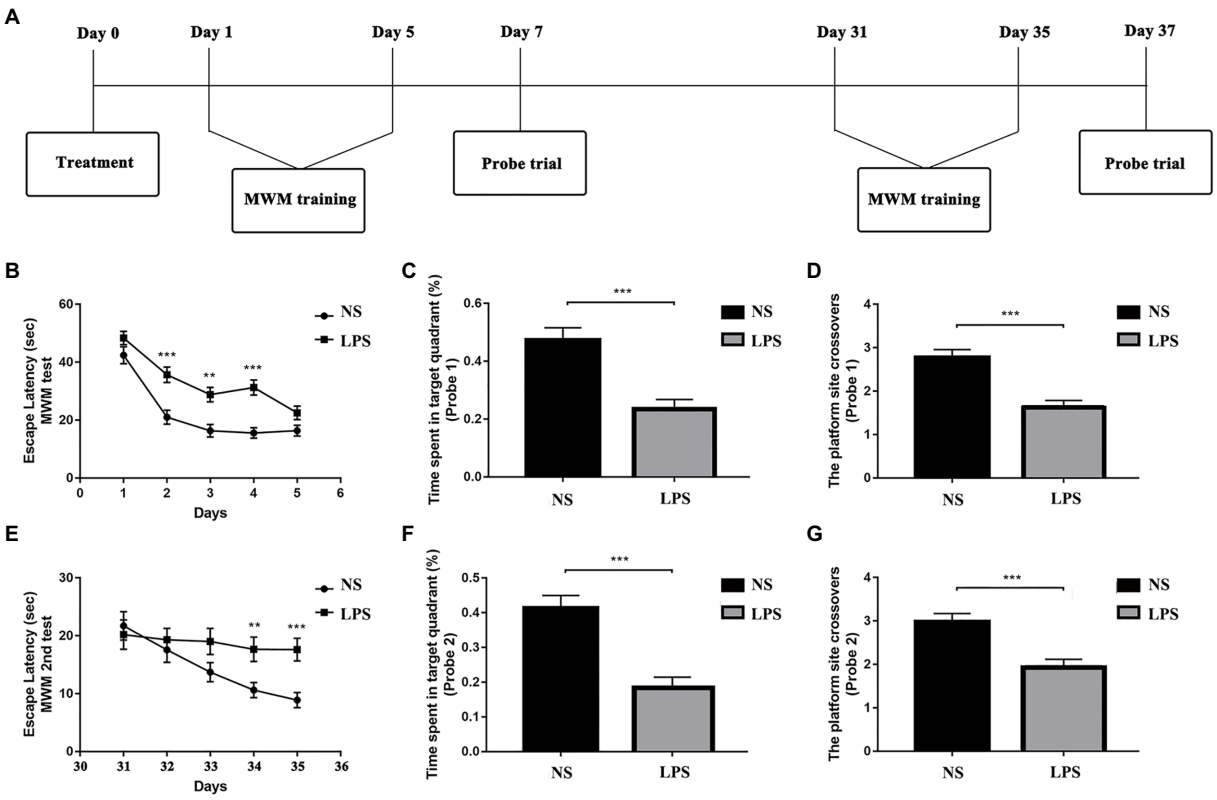

FIGURE 2
Lipopolysaccharide (LPS) exposure caused short- and long-term impaired learning and spatial working memory. **(A)** Morris Water Maze (MWM) test protocol. **(B)** Rats with LPS exposure had longer escape latency compared with those in the control group from day 2 to day 4. **(C,D)** Rats with LPS exposure spent shorter time in the target quadrant and performed fewer platform site crossovers compared with those in the control group. **(E)** Rats with LPS exposure had longer escape latency compared with those in the control group from day 34 to day 35. **(F,G)** Rats with LPS exposure spent shorter time in target quadrant and performed fewer platform site crossovers compared with those in the control group. Escape latency was analyzed by two-way ANOVA for repeated measurement followed by Bonferroni *post hoc* analysis. Time spent in the target quadrant and number of crossovers were analyzed using two-sample *t*-test. Data were presented as mean ± standard error of mean (SEM). **p*<0.05, ***p*<0.01, ****p*<0.001 vs. control group.

TABLE 1 Primer sequences in RT-PCR.

mRNA	Forward primer (5′ → 3′)	Reverse primer (5′ → 3′)
IL-1β	5′-ATGAGAGCATCCAGCTTCAAATC-3′	5′-CACACTAGCAGGTCGTCATCATC-3′
TNFα	5′-CAAGAGCCCTTGCCCTAA-3′	5′-CAGAGCAATGACTCCAAAGTA-3′
NF-κB	5′-AATTTGGCTTCCTTTCTTGGCT-3′	5′-CTGCGATACCTTAATGACAGCG-3
β-actin	5′-CCCATCTATGAGGGTTACGC-3′	5′-TTTAATGTCACGCACGATTTC-3′

each group) was selected for inflammatory cytokine examination (Figure 1). On the day of termination, rats were anesthetized by isoflurane (ISO, Baxter, Lessines, Belgium) prior to *vena cava* blood sampling. After 2 h of clotting at 4°C, the blood was centrifuged at 1,000*g* for 20 min and the serum was later collected and stored at −80°C. IL-1β and TNFα levels were measured using ELISA assay kits (RLB00 and RTA00, R&D Systems, Inc., Minneapolis, MN, United States) according to manufacturer instructions.

Anesthesia on rats

The protocols for anesthesia have been published by Liu et al. elsewhere (Lu et al., 2012). Briefly, all rats were first inducted by ISO at the concentration of 3% followed by intramuscular injection of dexmedetomidine (DEX, Hengrui Medicine Co., Ltd., Jiangsu Province, China, 0.015 mg/kg). During the initial scanning, ISO (1%) in oxygen-enriched air was delivered *via* a customized nose cone with continuous intramuscular infusion of

DEX (0.03 mg/kg/h). After the anatomical localization scans were acquired, the ISO concentration was decreased to 0.20%–0.25% with the respiration rate maintained at 60–85/min. When the respiration rate increased to 90/min, ISO concentration was adjusted to 0.5%. A small animal monitoring system (Model 1025, Small Animal Instruments Inc., New York, NY, United States), including a rectal temperature probe, respiration pneumonic sensor, and fiber optic oximetry sensor or cardiogram electrodes, was adopted for real-time monitoring. The core body temperature was maintained at 37°C *via* a warm water circulation system on the scanning bed.

Magnetic resonance imaging

Animals to perform rs-fMRI ($n = 10–12$ for each group) scanning also performed MWM examination in order to minimize individual variations between rs-fMRI data and behavior performance. The rs-fMRI scanning was performed on days 3, 7, and 31 post-treatment and *prior to* the MWM test. (Figure 1B).

The animal MRI measurements were performed using the 7.0T Bruker PharmaScan System (70/16 PharmaScan, Bruker Biospin GmbH, Germany), operated *via* the ParaVision 5.1 software. The same coils, including a rat brain surface coil and a quadrature resonator volume coil, were adopted in all rats.

Anatomical images (T2WI) were acquired with fast-spin–echo sequence using TurboRARE with the following parameters: repetition time (TR) 5000.0 ms, echo time (TE) 36.0 ms, echo spacing 12 ms, echo-train length 8, field of view 3.50 × 3.50 cm, matrix size 256 × 256, and 28 slices with a thickness of 1.0 mm. For blood-oxygen-level-dependent (BOLD) images, EPI-SE-FOVsat sequence was used with the following parameters: matrix size 64 × 64, flip angle = 90°, resolution = 0.55 mm × 0.55 mm, 28 slices with a thickness of 1.0 mm, slice gap = 0, repetition time (TR) = 2000.0 ms, echo time (TE) = 18.0 ms, and volume = 180.

Data processing and analysis

The data were pre-processed using spmratIHEP software (Nie et al., 2013; Liang et al., 2017) based on the statistical parametric mapping (SPM12; Welcome Department of Imaging Science);[1] and Gretna software[2] based on the Matlab (version 2014a, The MathWorks Inc., Natick, MA, United States). The data were carefully examined for completeness and truncation artifacts. All the functional images post-processing was performed by a single experienced observer, unaware to whom the scans belonged.

The voxel size of the functional datasets of all individuals was first multiplied by a factor of 5 to better approximate human dimensions, and then slice timing and realigning were performed. In the slice-timing section, the difference of slice acquisition times of each subject was corrected. Then, the realignment was done by adjusting the temporal-processed volume of each subject to the first volume in order to remove the head motion. After this, a mean image over the 180 volumes was recreated. In this section, data from subjects were filtered and preserved by which a 1 mm of translation in the *x*, *y*, or *z* axis and a 1° of rotation in each axis were set as criteria. Otherwise, it was eliminated. After spatial normalization into the Paxinos and Watson space, all the normalized images were re-sliced by $1.0 \times 1.5 \times 1.0\ mm^3$ voxels (after zooming). Then the normalized functional series were smoothed with a Gaussian kernel of $2\ mm^3$ Full Width at Half-maximum (FWHM) and the systematic drift or trend was removed using a linear model. Finally, the linear trended images were 0.01–0.08 Hz band-pass filtered and further corrected for the effect of head movement by regressing the translations and rotations of the head estimated during image realignment.

For default mode network (DMN) analysis, 12 regions of interest (ROIs; comprising left/right segmentation) were selected from the rat brain atlas image in Paxinos and Watson space (Nie et al., 2013; Liang et al., 2017). All these ROIs were summarized in Table 2.

These ROIs were defined as nodes and functional connectivity (FC) was defined as the Pearson's correlation coefficients (CCs) between each pair of nodes and calculated in Gretna. Weighted undirected 12 × 12 matrices were constructed for LPS and NS groups for each time point mentioned above, in which the strength of each connection was presented as FC.

Graph theory analysis

Based on the weighted matrix, distance matrices of the above two groups were generated, where the distance between each node was defined as $L_{ij} = 1 - w_{ij}$. The L_{ij} was identified as connection weight in nodes *i* and *j*.

TABLE 2 Region of interest in aged rat brain.

Region of interest (ROI)	ROI index	Short-form
01_Auditory cortex_ Left	1	L_AC
02_ Auditory cortex_ Right	2	R_AC
03_Hippocampus_Left	3	L_Hip
04_ Hippocampus_ Right	4	R_Hip
05_Orbital cortex_ Left	5	L_OC
06_ Orbital cortex_ Right	6	R_OC
07_Parietal association cortex_ Left	7	L_PAC
08_ Parietal association cortex_ Right	8	R_PAC
15_Prelimbic cortex_ Left	9	L_PrC
16_Prelimbic cortex_ Right	10	R_PrC
17_Retrosplenial cortex_ Left	11	L_RSC
18_Retrosplenial cortex_ Right	12	R_RSC

All the ROIs were drawn according to the Paxinos and Watsons space, with 12 ROIs (comprising left/right segmentation) were selected.

1 http://www.fil.ion.ucl.ac.uk/spm

2 https://www.nitrc.org/projects/gretna/

Graph theoretical analysis using Gretna Toolbox[3] was adopted to characterize FC patterns in group LPS and NS. For further analysis, global efficiency (E_{glob}) and local efficiency (E_{loc}) were used to assess network efficiency while nodal efficiency (E_i) and nodal local efficiency (E_{i_local}) were used to assess nodal centralities of the neural network. Based on graph theory, E_{global} is defined as the harmonic mean of the minimum path length between all possible pairs of nodes in neural network. E_{loc} is defined as the local efficiency of sub-graph composed of the neighbors of node *i*. E_i is defined as the ability of a node to propagate information with the other nodes in a network. E_{i_local} is defined as the efficiency of information propagation over a node's direct neighbors (Wang et al., 2010). The mathematical definitions are characterized as the following:

$$E_{\mathrm{glob}}(G)=\frac{1}{N(N-1)}\sum_{i\neq j\in G}\frac{1}{L_{i,j}},E_{\mathrm{loc}}=\frac{1}{N}\sum_{i\in G}E_{glob}(G_i),E_{\mathrm{i}}=\frac{1}{N-1}\sum_{j\neq i\in G}\frac{1}{L_{i,j}}\text{ and }E_{i\_local}=\frac{1}{N_G(N_G-1)}\sum_{j,k\in G}\frac{1}{L_{jk}}$$

where $L_{i,j}$ is the shortest path length between node *i*. *N* is the number of nodes in graph G_i.

Small-worldness analysis

The small-worldness property of neural network is described by the clustering coefficient (C_p) and characteristic path length (L_p). The C_p is defined as the average of clustering coefficients (C_i) of all nodes in the neural network and the L_p is defined as the average of the shortest path length between any pair of nodes in the neural network. The $C_{p\text{-}rand}$ and $L_{p\text{-}rand}$ are defined as the mean C_p and L_p of the matched random network, respectively. The mathematical definitions are characterized as follows:

$$C(i)=\frac{2E_{(i)}}{K_i(K_i-1)}$$

where *E* is the number of existing connections among nodes *i* and *K* is the degree of nodes *i*. The threshold of statistical significance is presented by sparsity ranges of 0.1–0.5, where the step is 0.05. The network would be considered small-world if it meets the following conditions:

$$\gamma=C_{\mathrm{p}}/C_{\mathrm{p-rand}}>1,\lambda=L_{\mathrm{p}}/L_{\mathrm{p-rand}}\approx 1.$$

To identify differences in the FC matrix and topology properties between the two groups, two-sample *t*-test was performed. For multiple comparison correction, results in FC matrices were further corrected based on the network-based analysis (NBS) where the permutation tests were repeated 1,000 times. For results in topology properties, results were further corrected based on false discovery rate (FDR) correction. The value of $p<0.05$ was considered statistically significant.

Statistical analysis

Statistical analyses were conducted using IBM SPSS 25.0 statistics (IBM, Chicago, Illinois, United States). Values were presented as mean ± standard error of mean (SEM). Results in ELISA measurements and RT-PCR were analyzed by one-way ANOVA followed by *Bonferroni post hoc* analysis. Results in MWM probe trials were analyzed by two-sample *t*-test. Results in the MWM spatial acquisition trials were analyzed by repeated measures two-way ANOVA followed by *Bonferroni post hoc* analysis. The value of $p<0.05$ was considered statistically significant. Analysis methods for rs-fMRI data are mentioned in the appropriate subsections above.

Results

Physiological factors during rs-fMRI scanning

Physiological factors during rs-fMRI data acquisition were strictly controlled. No differences were observed in weight, heart rate (HR), respiratory rate (RR) and blood oxygen level (SpO_2) between the two groups ($p=0.838$, $p=0.735$, $p=0.676$, $p=0.283$, respectively, two-sample *t*-test; Table 3).

Lipopolysaccharide exposure caused short- and long-term impaired learning and spatial working memory

The MWM was used to determine the effects of LPS exposure on learning and spatial working memory in both short- (<7 days) and long-term (>30 days). From day 1 to day 5, significant differences were observed in rats exposed to LPS ($F_{(1,51)}=26.309$ for treatment; $F_{(4,204)}=73.179$ for training days, $p<0.001$, repeated measures two-way ANOVA; Figure 2B). A significant difference was also observed for interaction between training treatment and training days ($F_{(4,204)}=2.840$, $p=0.025$). *Post hoc* analysis indicated that LPS caused significantly increased escape latency from day 2 to day 4 ($p<0.001$, $p=0.003$ and $p<0.001$, respectively). For the probe trial on day 7, a shorter time spent in target quadrant and fewer platform crossovers ($p<0.001$ and $p<0.001$, respectively, two-sample *t*-test; Figures 2C,D) were observed in rats

3 https://www.nitrc.org/projects/gretna

TABLE 3 Physiological factors during rs-fMRI data acquisition.

Days	Groups	Weight (g)	HR (/min)	RR (/min)	SpO_2 (%)
3 days	NS	752.2 ± 25.3	295.5 ± 14.8	70.9 ± 2.0	99.0 ± 0.3
	LPS	744.9 ± 24.5	302.8 ± 15.4	72.3 ± 2.4	99.4 ± 0.2
7 days	NS	748.2 ± 25.1	307.5 ± 21.3	72.5 ± 2.6	99.5 ± 0.3
	LPS	702.4 ± 18.0	308.8 ± 19.0	73.6 ± 3.3	98.9 ± 0.4
31 days	NS	772.5 ± 25.8	307.3 ± 25.1	72.1 ± 2.2	99.4 ± 0.3
	LPS	740.1 ± 23.6	306.3 ± 17.0	72.9 ± 2.6	99.2 ± 0.3

Physiological factors were carefully controlled during data acquisition. Data were analyzed by two-sample *t*-test. The value of $p < 0.05$ was considered statistically significant.

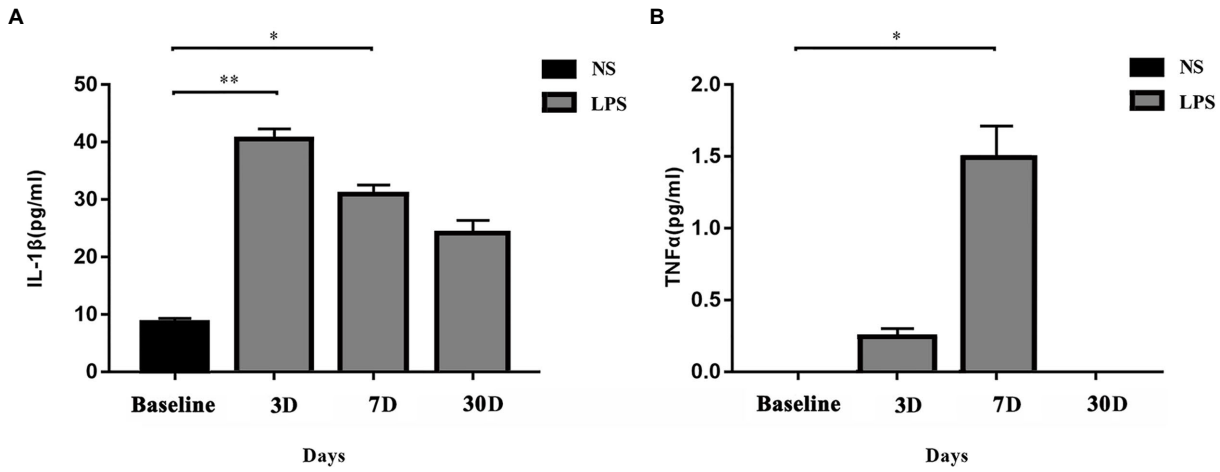

FIGURE 3
Systemic inflammatory responses. **(A)** IL-1β level was significantly elevated on day 3 and day 7 in rats exposed to lipopolysaccharide (LPS) as compared with rats treated with normal saline (NS). **(B)** TNFα level was significantly elevated on day 7 in rats exposed to LPS as compared with rats treated with normal saline NS. Data were presented as mean ± standard error of mean (SEM). *p<0.05, **p<0.01 vs. control group.

exposed to LPS. For the second acquisition trials from day 31 to day 35, significant differences were observed in rats exposed to LPS ($F_{(1,55)} = 0.021$ for treatment; $F_{(4,\ 220)} = 6.109$ for training days, $p = 0.021$ and $p < 0.001$, respectively, repeated measures two-way ANOVA; Figure 2E). A significant difference was also observed for interaction between training treatment and training days ($F_{(4,\ 204)} = 2.704$, $p = 0.031$). *Post hoc* analysis showed that rats exposed to LPS had longer escape latency on day 34 and 35 ($p = 0.009$ and $p < 0.001$, respectively). For the probe trial on day 37, a shorter time spent in the target quadrant and fewer platform crossovers were also observed for rats exposed to LPS ($p < 0.001$ and $p < 0.001$, respectively; Figures 2F,G).

Lipopolysaccharide exposure caused increased systemic inflammatory response

Systemic levels of IL-1β and TNFα were significantly increased in rats exposed to LPS ($p = 0.002$ and $p = 0.009$, respectively; one-way ANOVA). IL-1β level in rats exposed to LPS reached a peak at 3 days and remained elevated at 7 days ($p = 0.001$ and $p = 0.04$, respectively, *Bonferroni post hoc* analysis; Figure 3A). For TNFα level, a significant increase occurred at 7 days ($p = 0.02$, *Bonferroni post hoc* analysis; Figure 3B).

Lipopolysaccharide exposure caused increased inflammatory response in rat brain

To determine whether LPS exposure caused inflammatory responses in aged rat brain, proinflammatory cytokines and mRNA expressions were measured. LPS exposure caused significant increase in IL-1β, TNFα, and NF-κB ($p = 0.005$, 0.005, and $p = 0.043$, respectively; one-way ANOVA; Figure 4). The secretion of IL-1β reached a peak level 3 days, slightly decreased on day 7, and remained significantly higher on day 30 after LPS exposure ($p = 0.006$, 0.023, and 0.026 as compared with control, *Bonferroni post hoc* analysis, Figure 4A). For TNFα and NF-κB, they both reached peak levels on day 3 after

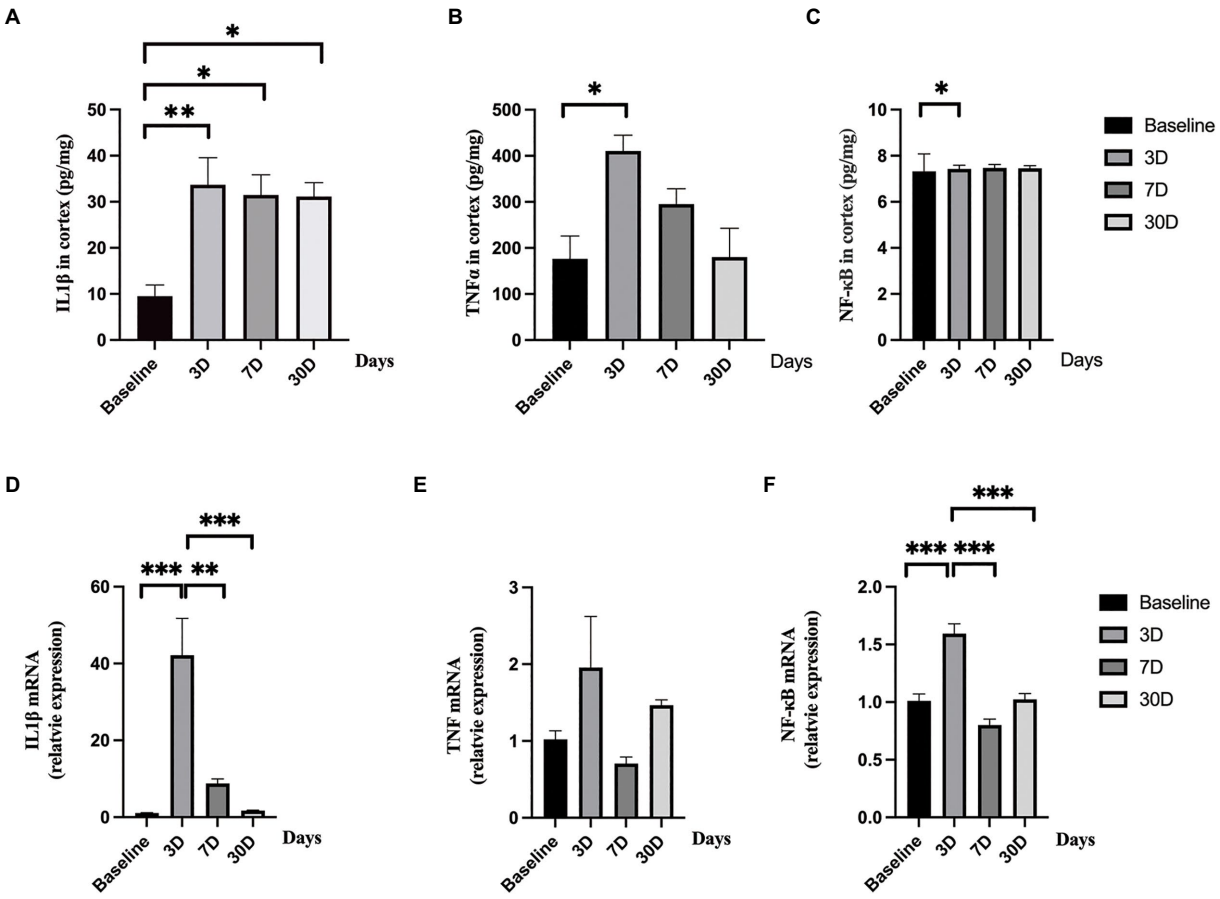

FIGURE 4
Central nerve system inflammatory responses. **(A–C)** The levels of IL-1β, TNFα, and NF-κB significantly elevated after lipopolysaccharide (LPS) exposure as compared with rats treated with normal saline (NS). **(D–F)** The mRNA levels of IL-1β and NF-κB significantly increased after lipopolysaccharide (LPS) exposure while the level of TNFα did not change as compared with rats treated with normal saline (NS). Data were presented as mean±SEM. *p<0.05, **p<0.01, ***p<0.001 vs. control group.

LPS exposure and went back to normal on day 7 and day 30 ($p = 0.013$, 0.477, and 1.000 as compared with control for TNFα; $p = 0.043$, 0.296 and 1.000 as compared with control for NF-κB, *Bonferroni post hoc* analysis, Figures 4B,C). When considering mRNA expression, LPS exposure caused a significant change in IL-1β and NF-κB ($p < 0.001$ and $p < 0.001$, Figures 4D,F) while no significant change was observed in TNFα level ($p = 0.118$, Figure 4E). The mRNA expressions of IL-1β and TNFα reached a peak level on day 3 after LPS exposure and fall back to almost baseline level on day 7 and day 30 ($p < 0.001$ for IL-1β and $p < 0.001$ for NF-κB, *Bonferroni post hoc* analysis).

Lipopolysaccharide exposure caused significant short- and long-term FC alterations In aged rat DMN

After LPS exposure, significant altered FC was temporarily observed with 13 in cortico-cortical connections and 10 in cortical–subcortical connections in LPS group on day 3 (two-sample *t*-test with NBS corrected; Figures 5A,B). One subcortico-subcortical connections were affected (L-Hip and R-Hip). On day 7, significant altered FC was observed in rats exposed to LPS with 7 in cortico-cortical connections and 8 in cortico-subcortical connections (two-sample *t*-test with NBS corrected; Figures 5C,D). On day 31, FC remained significantly altered in rats exposed to LPS with 9 in cortico-cortical connections and 9 in cortico-subcortical connections (two-sample *t*-test with NBS corrected; Figures 5E,F).

Lipopolysaccharide exposure caused short-term instead of long-term topology alterations in aged rat neural network

All rats in both groups showed small-worldness properties for all time points ($\gamma = C_p/C_{p\text{-rand}} > 1$, $\lambda = L_p/L_{p\text{-rand}} \approx 1$; Figure 6A). No significant differences were observed in clustering coefficient

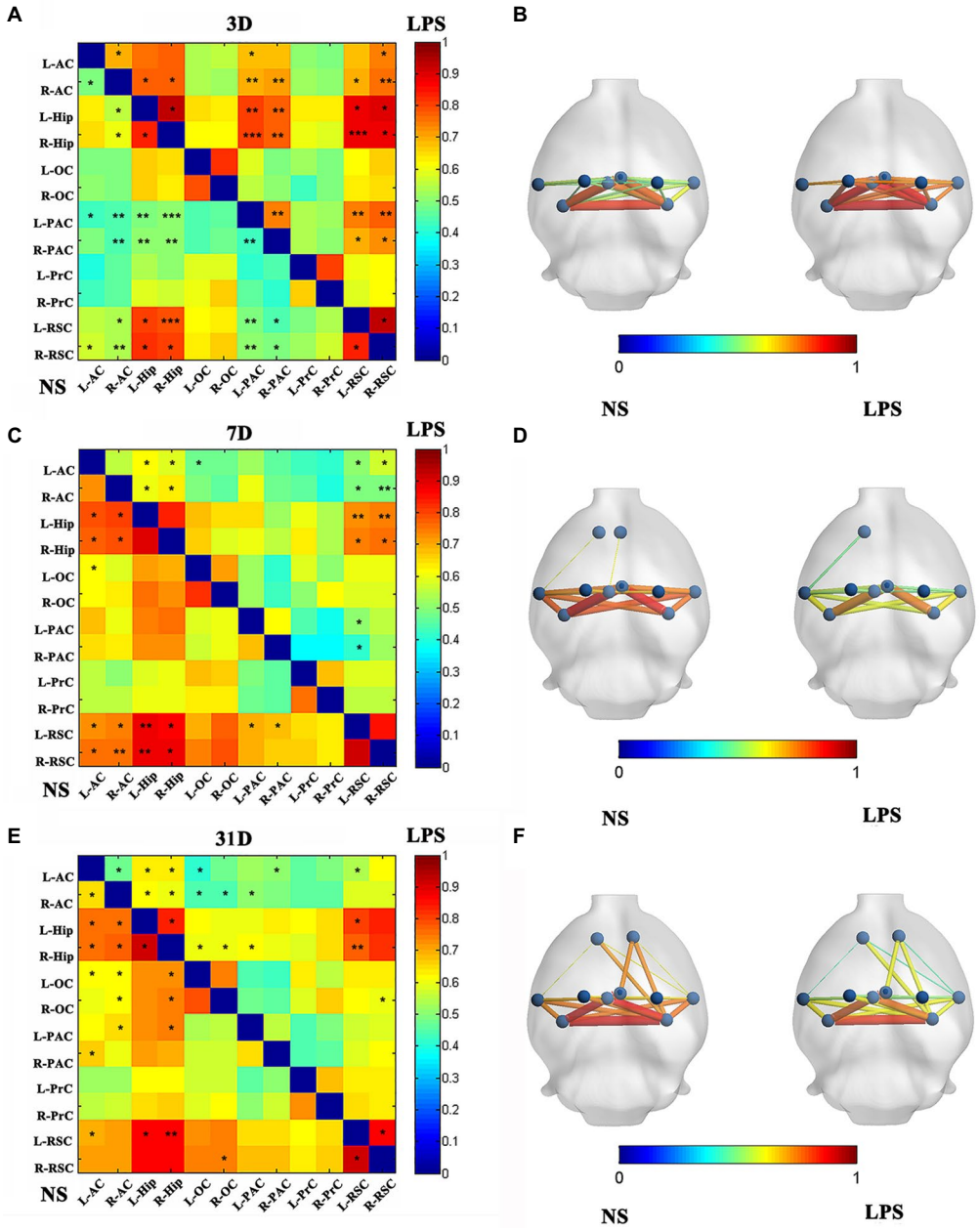

FIGURE 5
Functional connectivity (FC) in rats with lipopolysaccharide (LPS) exposure compared with control group. **(A,B)** FC value, nodes, and edges position in rats receiving LPS exposure (right) and control group (left) on day 3 after LPS exposure. **(C,D)** FC value, nodes, and edges position in rats receiving LPS exposure (right) and control group (left) on day 7 after treatment. **(E,F)** FC value, nodes, and edges position in rats receiving LPS exposure (right) and control group (left) on day 31 after treatment. Data were analyzed using two-sample *t*-test with network-based analysis correction (permutation 1,000 times). *p<0.05, **p<0.01, ***p<0.001 vs. control group.

(Figure 6B) while a significant increased shortest path length was observed in rats exposed to LPS on day 3 ($p = 0.00489$, two-sample *t*-test with FDR corrected; Figure 6C).

Although lower global efficiency was observed at 3 days in rats exposed to LPS ($p = 0.033$, two-sample *t*-test with FDR corrected; Figure 7A), there was no difference between LPS-exposed and control rats in local efficiency (Figure 7B). For local properties, in rats exposed to LPS, E_i was significantly lower in the left and right occipital cortices (L-OC and R-OC) and left and right prelimbic cortices (L-PrC and R-PrC $p = 0.0013$, 0.0031, 0.019, and 0.0013, respectively, two-sample *t*-test with FDR corrected; Figure 5C). E_{i_local} was significantly lower in left and right occipital cortices (L-OC and R-OC; $p = 0.0040$ and 0.012, respectively, two-sample *t*-test with FDR corrected; Figure 5D). However, LPS exposure also caused higher E_i in left-parietal association cortex (L-PAC; $p = 0.0054$, Figure 7C), and higher

10.3389/fnagi.2022.1013478

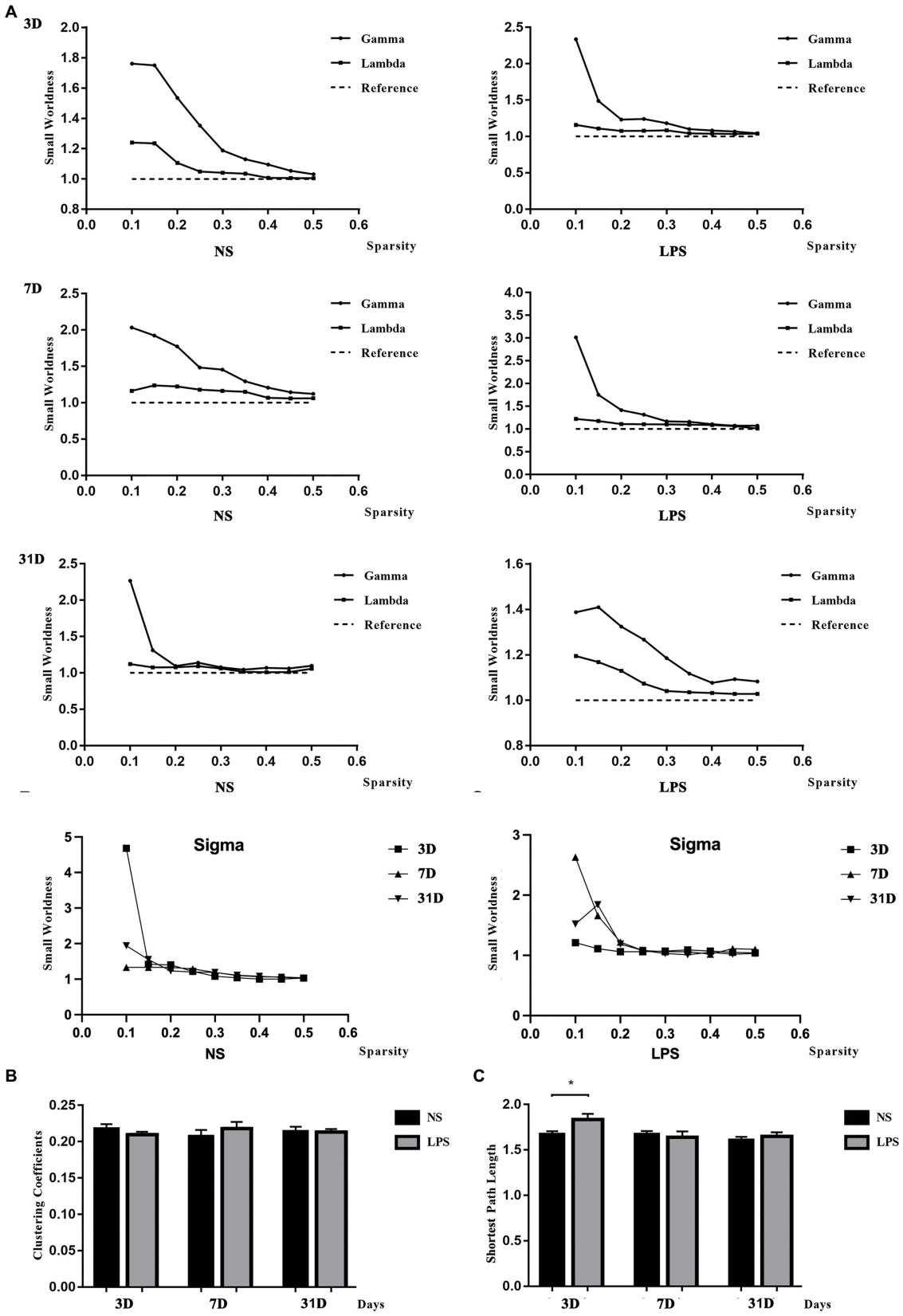

FIGURE 6
Small-worldness in aged rat default mode network (DMN). **(A)** The DMN in lipopolysaccharide (LPS) exposed and control rats showed the small-worldness at all time points. **(B)** LPS exposure caused no alteration in clustering coefficient (C_p). **(C)** LPS exposure caused increased shortest path length (Lp) persisting for 3 days. Data were analyzed using two - sample *t*-test with false discovery rate (FDR) correction. $^{**}p<0.01$ vs. control group.

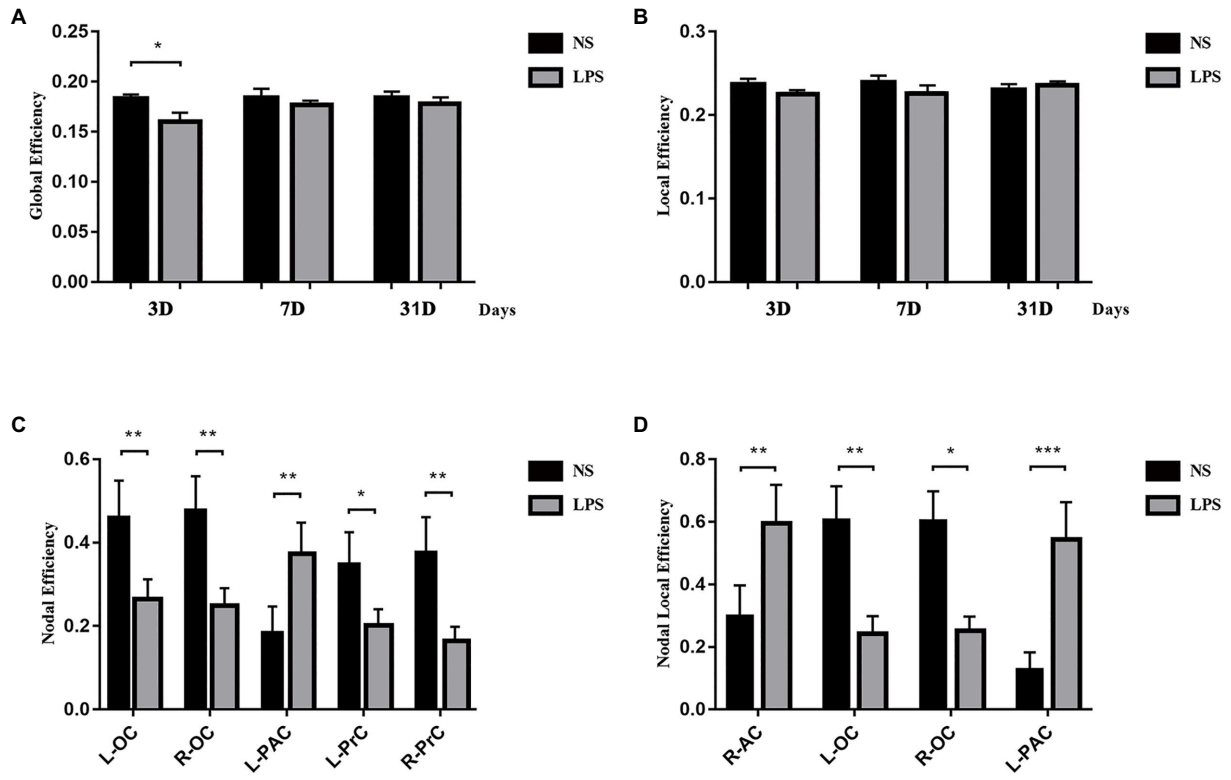

FIGURE 7
Topology structure alterations after lipopolysaccharide (LPS) exposure in aged rat brain. **(A)** Lower global efficiency was observed at 3 days in rats exposed to LPS. **(B)** No differences in local efficiency were observed. **(C)** Higher nodal efficiency in the left parietal association cortex and lower nodal efficiency in bilateral olfactory cortex and prelimbic cortices were observed in rats exposed to LPS. **(D)** Nodal local efficiency was observed higher in the right auditory cortex and left parietal association cortex and lower in bilateral olfactory cortex in rats exposed to LPS. Data were analyzed using two-sample *t*-test with false discovery rate (FDR) correction. *p<0.05, **p<0.01, ***p<0.001 vs. control group.

E_{i_local} in right-auditory cortex (R-AC) and L-PAC ($p = 0.0067$ and 0.0001, Figure 7D). On days 7 and 31 after LPS exposure, no significant topology changes were observed between the two groups.

Discussion

The present study demonstrated that inflammatory stress exposure in anesthesia caused altered intrinsic connectivity of the DMN, short- and long-term impairment in learning and spatial working memory, and altered short-term topology properties in aged rat brain.

Recent studies demonstrated the significance of neuroinflammation in postoperative cognitive decline (Subramaniyan and Terrando, 2019). Systemic inflammation induced by surgical trauma and neurotoxicity induced by anesthetic exposure have been proved to be major contributors (Liu et al., 2022). Our present study showed a significant increase in serum cytokines on day 3 (for IL-1β) and day 7 (for IL-1β and TNFα), demonstrating the occurrence of severe systemic inflammatory response. In central nerve system, significant increases of IL-1β (up to 30 days), TNFα (within 7 days), and NF-κB (within 7 days), indicating the existence of subsequent neuroinflammation. In order to validate the effect of neuroinflammation, the MWM was performed to test cognitive function in aged rats. The present study showed significant longer escape latency, lower time spent, and fewer crossovers in target quadrant in both MWM testing within 7 days and more than 30 days after LPS exposure, indicating that neuroinflammation induced short- and long-term cognitive dysfunction, which is consistent with our previous findings (Fu et al., 2014; Kan et al., 2016).

Altered FC in neural network is a major characteristic in cognitive dysfunction in both clinical practice (Labrenz et al., 2016; Tani et al., 2018) and preclinical experiments (Anckaerts et al., 2019; Passamonti et al., 2019). In the present study, we observed altered intrinsic connectivity in aged rat DMN on day 7 and day 31 after LPS exposure, which is consistent with clinical findings that FC in DMN is decreased in cognitive dysfunction (Qian et al., 2019; Zhao et al., 2020). Contrary to impaired MWM performance, increased intrinsic connectivity within the rat DMN was temporarily observed on day 3 after LPS exposure. Considering the severe systemic inflammation in aged rats, it could be explained by "systemic inflammation induced transient enhancement" as what was reported in

human subjects 3.5 h after inflammatory exposure (Labrenz et al., 2016), which also shown that systemic inflammation began to affect DMN intrinsic connectivity at least 3 days after exposure.

Aside from whole DMN, the Hip and RSC are two most important regions (Raichle, 2015). While both contributing to learning and memory, the Hip plays a more significant role on recent delay while the RSC is more significant in remote delay and trace conditioning (assessed by fear conditioning) in AD related studies (Todd et al., 2019). Although altered RSC-related FC (which corresponds to the post-cingulate gyrus in mankind), which was observed in Aβ-induced cognitive decline in human subjects (Yamashita et al., 2019), was found in our study, the Hip rather than RSC seemed to play a more significant role in the long-term (11 vs. 12 CCs, 8 vs. 10CCs, 10 vs. 5 CCs for 3 days, 7 days and 31 days, respectively). We hypothesize that the reason for this may be a greater sensitivity of the Hip to inflammation in the aged rat as compared with normal adult rats (Barrientos et al., 2015). This result demonstrates that surgery stress and anesthetic neurotoxicity-induced cognitive decline differs from dementia induced by Aβ accumulation, supporting the recent idea that postoperative cognitive dysfunction (POCD) and AD are associated with different transcriptome changes despite their similar clinical manifestations (Wang et al., 2022).

Meanwhile, significant Hip-related FC changes combined with impaired behavior performances existed throughout the experiment period while not all the FCs in the DMN remained changed. This finding indicated that Hip played a significant role not only in neurodegeneration but also in inflammation exposure-induced cognitive dysfunction. Our findings are consistent with previous study that the hippocampus remained severe inflammatory response in long-term cognitive dysfunction (Li et al., 2020). Impaired Hip-related FCs demonstrated neural transmission dysfunction between Hip and other DMN regions, which indicated that impaired correlation between Hip and other DMN regions might be a significant character in inflammatory-induced cognitive dysfunction. Our previous study also showed that there are significant changes in Hip-related FCs in aged rat brain although treatment had already given (Liu et al., 2021). These findings all pointed to the significance of anti-inflammatory treatment in clinical practice, which may help to prevent long-term cognitive dysfunction after anesthesia and inflammation exposure.

Besides intrinsic connectivity (FC in the DMN), topology structure in neural network is also significant in information transmission. Small-worldness, a model combining high C_p and short L_p, is a highly optional choice for studying complex networks in the setting of psychophysiological condition (Bassett and Bullmore, 2017; Miraglia et al., 2020). In the present study, rats with inflammatory exposure showed increased L_p followed with impaired behavior performances, which is similar with clinical findings that AD patients have disrupted small-worldness properties characterized by increased L_p (Dai et al., 2019; Lella and Estrada, 2020). However, it is different that the C_p is not changed in rats with inflammatory exposure-induced cognitive dysfunction as clinical studies reported that AD patients also have decreased C_p (Wu et al., 2019; Rauchmann et al., 2021). Interestingly, a lower E_{global} was observed 3 days after LPS exposure while no change in E_{loc} was also observed in the present study. These results indicated that inflammatory stress-induced cognitive dysfunction mainly relies on causing more steps in information exchange in small-worldness neural network instead of decreasing local interconnectivity between different regions, although they all disrupt small-worldness properties. This also supports the idea that POCD induced by anesthesia and surgery is different from early stage of AD. Whether the POCD develops into AD in the future still needs further studies. For regional properties (E_i, E_{i_local}), LPS exposure caused both increased and decreased changes, which may be a compensation for the decrease in global information transformation. On day 7 and 31 after LPS exposure, no significant differences could be observed in topology properties, while the difference in FC remained, showing that FC alterations, rather than topology changes, may last longer in LPS-induced cognitive impairment.

Based on the results of our study, we presented a background of DMN intrinsic connectivity and topology structures after inflammatory exposure in aged rat brain, indicating short- and long-term changes in functional connectivity and topology structures. Meanwhile, our study also pointed out brain regions that played a significant role in long-term cognitive dysfunction. In the future, a treatment could be given to these rats to evaluate the effect on aged rat DMN and cognitive function in both short- and long-term, providing further evidence for clinical practice. Considering that the DMN exists across species and the components are similar, these results can be used as background data, helping to judge treatment effect and drug-target design.

There are several limitations for the present study. First, the data were collected from aged rats instead of elderly patients. The reason for doing this is that using LPS on senior mankind for inducing sepsis and long-term cognitive dysfunction may cause ethical problem. Fortunately, recent studies reported that the component of DMN in aged rat is similar with those in human beings (Smallwood et al., 2021) and the FC alteration was also observed in various conditions (Serra et al., 2020), making the aged rats an optional choice for mechanism studying. Second, no data from post-mortem subjects were acquired for background comparison. The reason for not doing this is that we have to acquire longitudinal data and the rats have to undergo MWM testing. Third, the anesthesia method may have potential influences on FC patterns in the rat DMN (Paasonen et al., 2018). However, after comparing different methods, the combination of ISO and DEX was selected because it is a proven method for DMN studies and better preserves DMN connectivity as compared with several other anesthetic methods (Lu et al., 2012; Paasonen et al., 2018).

Conclusion

The present study demonstrated inflammatory exposure in anesthesia management impairs intrinsic FC and disrupts small-worldness in aged rat DMN. Alterations in FC may be long-term while disrupted small-worldness may only be temporary. These results offer further insights into drug target design and new biomarkers for cognitive dysfunction induced by anesthesia and inflammatory stress exposure in clinical practice.

Data availability statement

The raw data supporting the conclusions of this article will be made available by the authors, without undue reservation.

Ethics statement

The animal study was reviewed and approved by Ethical Committee of Capital Medical University.

Author contributions

YL, HF (Huiru Feng) and TW: study design. YL and HF (Huiru Feng): study performance. YL, HF (Huiqun Fu) and BN: rs-fMRI data analysis. YL and HF (Huiru Feng): manuscript writing. YW, BN and TW: manuscript revision. Dr. Yang Liu and Dr. Huiru Feng contributed equally to the manuscript and shares first authorship.

Funding

This work was supported by grants from Beijing Municipal Health Commission (Jing 2019-2); Beijing municipal administration of hospitals clinical medicine development of special funding support (Code: ZYLX201706); and Beijing 215 high-level healthcare talent plan academic leader (Code: 008-0027).

Acknowledgments

The authors may express their appreciation to Shengyu Fang from Department of Neurosurgery, Beijing Tiantan Hospital, Capital Medical University for his generous help on data analysis. The authors may also express their appreciation to the staffs of Beijing Area Major Laboratory of Peptide and Small Molecular Drugs, Engineering Research Centre of Endogenous Prophylactic of Ministry of Education of China.

Conflict of interest

The authors declare that the research was conducted in the absence of any commercial or financial relationships that could be construed as a potential conflict of interest.

Publisher's note

References

Anckaerts, C., Blockx, I., Summer, P., Michael, J., Hamaide, J., Kreutzer, C., et al. (2019). Early functional connectivity deficits and progressive microstructural alterations in the TgF344-AD rat model of Alzheimer's disease: a longitudinal MRI study. *Neurobiol. Dis.* 124, 93–107. doi: 10.1016/j.nbd.2018

Avena-Koenigsberger, A., Misic, B., and Sporns, O. (2017). Communication dynamics in complex brain networks. *Nat. Rev. Neurosci.* 19, 17–33. doi: 10.1038/nrn.2017.149

Barrientos, R. M., Kitt, M. M., Watkins, L. R., and Maier, S. F. (2015). Neuroinflammation in the normal aging hippocampus. *Neuroscience* 309, 84–99. doi: 10.1016/j.neuroscience.2015.03.007

Bassett, D. S., and Bullmore, E. T. (2017). Small-world brain networks revisited. *Neuroscientist* 23, 499–516. doi: 10.1177/1073858416667720

Belrose, J. C., and Noppens, R. R. (2019). Anesthesiology and cognitive impairment: a narrative review of current clinical literature. *BMC Anesthesiol.* 19:241. doi: 10.1186/s12871-019-0903-7

Biswal, B., Yetkin, F., Haughton, V., and Hyde, J. (1995). Functional connectivity in the motor cortex of resting human brain using echo-planar MRI. *Magn. Reson. Med.* 34, 537–541. doi: 10.1002/mrm.1910340409

Cao, Y., Yang, H., Zhou, Z., Cheng, Z., and Zhao, X. (2020). Abnormal default-mode network homogeneity in patients with mild cognitive impairment in Chinese communities. *Front. Neurol.* 11:569806. doi: 10.33889/fneur.2020.569806

Chand, G. B., Wu, J., Hajjar, I., and Qiu, D. (2017). Interactions of the salience network and its subsystems with the default-mode and the central-executive networks in normal aging and mild cognitive impairment. *Brain Connect.* 7, 401–412. doi: 10.1089/brain.2017.0509

Dai, Z., Lin, Q., Li, T., Wang, X., Yuan, H., Yu, X., et al. (2019). Disrupted structural and functional brain networks in Alzheimer's disease. *Neurobiol. Aging* 75, 71–82. doi: 10.1016/j.neurobiolaging.2018.11.005

Daiello, L. A., Racine, A. M., Yun Gou, R., Marcantonio, E. R., Xie, Z., Kunze, L. J., et al. (2019). Postoperative delirium and postoperative cognitive dysfunction: overlap and divergence. *Anesthesiology* 131, 477–491. doi: 10.1097/ALN.0000000000002729

Duprey, M. S., Devlin, J. W., van der Hoeven, J. G., Pickkers, P., Briesacher, B. A., Saczynski, J. S., et al. (2021). Association between incident delirium treatment with haloperidol and mortality in critically ill adults. *Crit. Care Med.* 49, 1303–1311. doi: 10.1097/CCM.0000000000004976

Fu, H. Q., Yang, T., Xiao, W., Fan, L., Wu, Y., Terrando, N., et al. (2014). Prolonged neuroinflammation after lipopolysaccharide exposure in aged rats. *PLoS One* 9:e106331. doi: 10.1371/journal.pone.0106331

Fuster, J. (2001). The prefrontal cortex--an update time is of the essence. *Neuron* 30, 319–333. doi: 10.1016/s0896-6273(01)00285-9

Hohenfeld, C., Werner, C. J., and Reetz, K. (2018). Resting-state connectivity in neurodegenerative disorders: is there potential for an imaging biomarker? *Neuroimage Clin.* 18, 849–870. doi: 10.1016/j.nicl.2018.03.013

Ji, M., Xia, J., Tang, X., and Yang, J. (2018). Altered functional connectivity within the default mode network in two animal models with opposing episodic memories. *PLoS One* 13:e0202661. doi: 10.1371/journal.pone.0202661

Jing, W., Xia, Y., Li, M., Cui, Y., Chen, M., Xue, M., et al. (2021). State-independent and state-dependent patterns in the rat default mode network. *NeuroImage* 237:118148. doi: 10.1016/j.neuroimage.2021.118148

Kan, M. H., Yang, T., Fu, H. Q., Fan, L., Wu, Y., Terrando, N., et al. (2016). Pyrrolidine. Dithiocarbamate prevents neuroinflammation and cognitive dysfunction after endotoxemia in rats. *Front. Aging Neurosci.* 8:175. doi: 10.3389/fnagi.2016.00175

Kukla, B., Anthony, M., Chen, S., Turnbull, A., Baran, T. M., and Lin, F. V. (2022). Brain small-worldness properties and perceived fatigue in mild cognitive impairment. *J. Gerontol. A Biol. Sci. Med. Sci.* 77, 541–546. doi: 10.1093/gerona/glab084

Labrenz, F., Wrede, K., Forsting, M., Engler, H., Schedlowski, M., Elsenbruch, S., et al. (2016). Alterations in functional connectivity of resting state networks during experimental endotoxemia – an exploratory study in healthy men. *Brain Behav. Immun.* 54, 17–26. doi: 10.1016/j.bbi.2015.11.010

Lakshmikanth, C. L., Jacob, S. P., Chaithra, V. H., de Castro-Faria-Neto, H. C., and Marathe, G. K. (2016). Sepsis: in search of cure. *Inflamm. Res.* 65, 587–602. doi: 10.1007/s00011-016-0937-y

Le Merre, P., Ahrlund-Richter, S., and Carlen, M. (2021). The mouse prefrontal cortex: unity in diversity. *Neuron* 109, 1925–1944. doi: 10.1016/j.neuron.2021.03.035

Lee, Y. H., Bak, Y., Park, C. H., Chung, S. J., Yoo, H. S., Baik, K., et al. (2019). Patterns of olfactory functional networks in Parkinson's disease dementia and Alzheimer's dementia. *Neurobiol. Aging* 89, 63–70. doi: 10.1016/j.neurobiolaging.2019.12.021

Lella, E., and Estrada, E. (2020). Communicability distance reveals hidden patterns of Alzheimer's disease. *Netw Neurosci.* 4, 1007–1029. doi: 10.1162/netn_a_00143

Li, Z., Wei, M., Lyu, H., Huo, K., Wang, L., Zhang, M., et al. (2020). Fracture shortly before stroke in mice leads to hippocampus inflammation and long-lasting memory dysfunction. *J. Cereb. Blood Flow Metab.* 40, 446–455. doi: 10.1177/0271678X19825785

Li, C. X., and Zhang, X. (2018). Evaluation of prolonged administration of isoflurane on cerebral blood flow and default mode network in macaque monkeys anesthetized with different maintenance doses. *Neurosci. Lett.* 662, 402–408. doi: 10.1016/j.neulet.2017.10.034

Liang, S., Wu, S., Huang, Q., Duan, S., Liu, H., Li, Y., et al. (2017). Rat brain digital stereotaxic white matter atlas with fine tract delineation in Paxinos space and its automated applications in DTI data analysis. *Magn. Reson. Imaging* 43, 122–128. doi: 10.1016/j.mri.2017.07.011

Lisman, J., Buzsáki, G., Eichenbaum, H., Nadel, L., Ranganath, C., and Redish, A. D. (2017). Viewpoints: how the hippocampus contributes to memory, navigation and cognition. *Nat. Neurosci.* 20, 1434–1447. doi: 10.10138/nn.4661

Liu, X., Chen, X., Zheng, W., Xia, M., Han, Y., Song, H., et al. (2018). Altered functional connectivity of insular subregions in Alzheimer's disease. *Front. Aging Neurosci.* 10:107. doi: 10.3389/fnagi.2018.00107

Liu, Y., Fu, H., and Wang, T. (2022). Neuroinflammation in perioperative neurocognitive. Disorders: from bench to the bedside. *CNS Neurosci. Ther.* 28, 484–496. doi: 10.1111/cns.13794

Liu, Y., Fu, H., Wu, Y., Nie, B., Liu, F., Wang, T., et al. (2021). Elamipretide (SS-31) improves functional connectivity in hippocampus and other related regions following prolonged neuroinflammation induced by lipopolysaccharide in aged rats. *Front. Aging Neurosci.* 13:600484. doi: 10.3389/fnagi.2021.600484

Lopes, R., Delmaire, C., Defebvre, L., Moonen, A. J., Duits, A. A., Hofman, P., et al. (2017). Cognitive phenotypes in Parkinson's disease differ in terms of brain-network organization and connectivity. *Hum. Brain Mapp.* 38, 1604–1621. doi: 10.1002/hbm.23474

Lu, H., Zou, Q., Gu, H., Raichle, M. E., Stein, E. A., and Yang, Y. (2012). Rat brains also have a default mode network. *Proc. Natl. Acad. Sci. U. S. A.* 109, 3979–3984. doi: 10.1073/pnas.1200506109

Miraglia, F., Vecchio, F., Marra, C., Quaranta, D., Alu, F., Peroni, B., et al. (2020). Small world index in default mode network predicts progression from mild cognitive impairment to dementia. *Int. J. Neural Syst.* 30:2050004. doi: 10.1143/S0129065720500045

Nie, B., Chen, K., Zhao, S., Liu, J., Gu, X., Yao, Q., et al. (2013). A rat brain MRI template with digital stereotaxic atlas of fine anatomical delineations in paxinos space and its automated application in voxel-wise analysis. *Hum. Brain Mapp.* 34, 1306–1318. doi: 10.1002/hbm.21511

Oliveira, M. K., Dos Santos, R. S., Cabral, L. D. M., Vilela, F. C., and Giusti-Paiva, A. (2020). Simvastatin attenuated sickness behavior and fever in a murine model of endotoxemia. *Life Sci.* 254:117701. doi: 10.1016/j.lfs.2020.117701

Paasonen, J., Stenroos, P., Salo, R. A., Kiviniemi, V., and Grohn, O. (2018). Functional connectivity under six anesthesia protocols and the awake condition in rat brain. *NeuroImage* 172, 9–20. doi: 10.1016/j.neuroimage.2018.01.014

Pascoal, T. A., Mathotaarachchi, S., Kang, M. S., Mohaddes, S., Shin, M., Park, A. Y., et al. (2019). Abeta-induced vulnerability propagates via the brain's default mode network. *Nat. Commun.* 10:2353. doi: 10.1038/s41467-019-10217-w

Passamonti, L., Tsvetanov, K. A., Jones, P. S., Bevan-Jones, W. R., Arnold, R., Borchert, R. J., et al. (2019). Neuroinflammation and functional connectivity in Alzheimer's disease: interactive influences on cognitive performance. *J. Neurosci.* 39, 7218–7226. doi: 10.1523/JNEUROSCI.2574-18.2019

Qian, W., Fischer, C. E., Churchill, N. W., Kumar, S., Rajji, T., and Schweizer, T. A. (2019). Delusions. in Alzheimer disease are associated with decreased default mode network functional connectivity. *Am. J. Geriatr. Psychiatry* 27, 1060–1068. doi: 10.1016/j.jagp.2019.03.020

Raichle, M. E. (2015). The Brain's default mode network. *Annu. Rev. Neurosci.* 38, 433–447. doi: 10.1146/anneurev-neuro-071013-014030

Rauchmann, B. S., Ersoezlue, E., Stoecklein, S., Keeser, D., Brosseron, F., Buerger, K., et al. (2021). Resting-state network alterations differ between Alzheimer's disease atrophy subtypes. *Cereb. Cortex* 31, 4901–4915. doi: 10.10193/cercor/bhab130

Schumacher, J., Gunter, J. L., Przybelski, S. A., Jones, D. T., Graff-Radford, J., Savica, R., et al. (2021). Dementia with Lewy bodies: association of Alzheimer pathology with functional connectivity networks. *Brain* 144, 3212–3225. doi: 10.1093/brain/awab218

Serra, L., Bruschini, M., Di Domenico, C., Mancini, M., Bechi Gabrielli, G., Bonarota, S., et al. (2020). Behavioral psychological symptoms of dementia and functional connectivity changes: a network-based study. *Neurobiol. Aging* 94, 196–206. doi: 10.1016/j.neurobiolaging.2020.06.009

Smallwood, J., Bernhardt, B. C., Leech, R., Bzdok, D., Jefferies, E., and Margulies, D. S. (2021). The default mode network in cognition: a topographical perspective. *Nat. Rev. Neurosci.* 22, 503–513. doi: 10.1038/s41583-021-00474-4

Sporns, O. (2018). Graph theory methods applications in brain networks. *Diagloues Clin Neurosci.* 20, 111–121. doi: 10.31887/DCNS.2018.20.2/osporns

Subramaniyan, S., and Terrando, N. (2019). Neuroinflammation and perioperative neurocognitive disorders. *Anesth. Analg.* 128, 781–788. doi: 10.1213/ANE.0000000000004053

Tani, N., Yaegaki, T., Nishino, A., Fujimoto, K., Hashimoto, H., Horiuchi, K., et al. (2018). Functional connectivity analysis and prediction of cognitive change after carotid artery stenting. *J. Neurosurg.* 131, 1709–1715. doi: 10.3171/2018.7.JNS18404

Todd, T. P., Fournier, D. I., and Bucci, D. J. (2019). Retrosplenial cortex and its role in cue-specific learning and memory. *Neurosci. Biobehav. Rev.* 107, 713–728. doi: 10.1016/j.neurobiorev.2019.04.016

Wang, Y., Wang, L., Yuan, S., Zhang, Y., Zhang, X., and Zhou, L. (2022). Postoperative cognitive dysfunction and Alzheimer's disease: a transcriptome-based comparison of animal models. *Front. Aging Neurosci.* 14:900350. doi: 10.3389/fnagi.2022.900350

Wang, J., Zuo, X., and He, Y. (2010). Graph-based network analysis of resting-state functional MRI. *Front. Syst. Neurosci.* 4:16. doi: 10.3389/fnsys.2010.00016

Wu, Z., Xu, D., Potter, T., and Zhang, Y.Alzheimer's Disease Neuroimaging Initiative (2019). Effects of brain parcellation on the characterization of topological deterioration in Alzheimer's disease. *Front. Aging Neurosci.* 11:113. doi: 10.3389/fnagi.2019.00113

Yamashita, K. I., Uehara, T., Prawiroharjo, P., Yamashita, K., Togao, O., Hiwatashi, A., et al. (2019). Functional connectivity change between posterior cingulate cortex and ventral attention network relates to the impairment of orientation for time in Alzheimer's disease patients. *Brain Imaging Behav.* 13, 154–161. doi: 10.1007/s11682-018-9860-x

Yang, T., Velagapudi, R., and Terrando, N. (2020). Neuroinflammation after surgery: from mechanisms to therapeutic targets. *Nat. Immunol.* 21, 1319–1326. doi: 10.1038/s41590-020-00812-1

Yang, L., Zhou, R., Tong, Y., Chen, P., Shen, Y., Miao, S., et al. (2020). Neuroprotection by dihydrotestosterone in LPS-induced neuroinflammation. *Neurobiol. Dis.* 140:104814. doi: 10.1016/j.nbd.2020.104814

Yeshurun, Y., Nguyen, M., and Hasson, U. (2021). The default mode network: where the idiosyncratic self meets the shared social world. *Nat. Rev. Neurosci.* 22, 181–192. doi: 10.1038/s41583-020-00420-w

Zhang, H., Chiu, P., Ip, I., Liu, T., Wong, G., Song, Y., et al. (2021). Small-world networks and their relationship with hippocampal glutamine/glutamate concentration in healthy adults with varying genetic risk for Alzheimer's disease. *J. Magn. Reson. Imaging* 54, 952–961. doi: 10.1002/jmri.27632

Zhao, T., Quan, M., and Jia, J. (2020). Functional connectivity of default mode network subsystems in the presymptomatic stage of autosomal dominant Alzheimer's disease. *J. Alzheimers Dis.* 73, 1435–1444. doi: 10.3233/JAD-191065

frontiers | Frontiers in Aging Neuroscience

TYPE Original Research
PUBLISHED 01 December 2022
DOI 10.3389/fnagi.2022.1036428

OPEN ACCESS

EDITED BY
Zhongcong Xie,
Massachusetts General Hospital and Harvard Medical School, United States

REVIEWED BY
Mian Peng,
Wuhan University, China
Zhongyong Shi,
Shanghai Jiao Tong University, China

*CORRESPONDENCE
Haixing Zhong
haixing.zhong@139.com

†These authors have contributed equally to this work and share first authorship

SPECIALTY SECTION
This article was submitted to Neurocognitive Aging and Behavior, a section of the journal Frontiers in Aging Neuroscience

RECEIVED 04 September 2022
ACCEPTED 12 October 2022
PUBLISHED 01 December 2022

CITATION
Liu Y, Jia S, Wang J, Wang D, Zhang X, Liu H, Zhou F, Zhang Z, Li Q, Dong H and Zhong H (2022) Endocannabinoid signaling regulates post-operative delirium through glutamatergic mediodorsal thalamus-prelimbic prefrontal cortical projection. *Front. Aging Neurosci.* 14:1036428. doi: 10.3389/fnagi.2022.1036428

Endocannabinoid signaling regulates post-operative delirium through glutamatergic mediodorsal thalamus-prelimbic prefrontal cortical projection

Yang Liu†, Sansan Jia†, Jiajia Wang†, Dan Wang, Xinxin Zhang, Huiqing Liu, Fang Zhou, Zhihao Zhang, Qi Li, Hailong Dong and Haixing Zhong*

Department of Anesthesiology and Perioperative Medicine, Xijing Hospital, The Fourth Military Medical University, Xi'an, China

Background: Post-operative delirium (POD), a common post-operative complication that affects up to 73. 5% of surgical patients, could prolong hospital stays, triple mortality rates, cause long-term cognitive decline and dementia, and boost medical expenses. However, the underlying mechanisms, especially the circuit mechanisms of POD remain largely unclear. Previous studies demonstrated that cannabis use might cause delirium-like behavior through the endocannabinoid system (eCBs), a widely distributed retrograde presynaptic neuromodulator system. We also found that the prelimbic (PrL) and intralimbic (IL) prefrontal cortex, a crucial hub for cognition and emotion, was involved in the eCBs-associated general anesthesia recovery.

Objectives: The present study aimed to investigate the role of eCBs in POD development, and further clarify its neuronal specificity and circuit specificity attributed to POD.

Methods: According to a previous study, 2 h of 1.4% isoflurane anesthesia and simple laparotomy were conducted to establish the POD model in C57/BL6 mice aged 8–12 weeks. A battery of behavioral tests, including the buried food, open field, and Y maze tests, were performed at 24 h before anesthesia and surgery (AS) and 6 and 9 h after AS. The behavioral results were calculated as a composite Z score for the POD assessment. To explore the dynamics of eCBs and their effect on POD regulation, an endocannabinoid (eCB) sensor was microinjected into the PrL, and the antagonists (AM281 and hemopressin) and agonist (nabilone) of type 1 cannabinoid receptor (CB1R), were administered systemically or locally (into PrL). Chemogenetics, combined Cre-loxP and Flp-FRT system, were employed in mutant mice for neuronal specificity and circuit specificity observation.

Results: After AS, the composite Z score significantly increased at 6 and 9 but not at 24 h, whereas blockade of CB1R systemically and intra-PrL could specifically decrease the composite Z score at 6 and 9 h after AS. Results of fiber photometry further confirmed that the activity of eCB in the PrL was enhanced by AS, especially in the Y maze test at 6 h post-operatively. Moreover,

the activation of glutamatergic neurons in the PrL could reduce the composite Z score, which could be significantly reversed by exogenous cannabinoid (nabilone) at 6 and 9 h post-operatively. However, activation of GABAergic neurons only decreased composite Z score at 9 h post-operatively, with no response to nabilone application. Further study revealed the glutamatergic projection from mediodorsal thalamus (MD) to PrL glutamatergic neurons, but not hippocampus (HIP)-PrL circuit, was in charge of the effect of eCBs on POD.

Conclusion: Our study firstly demonstrated the involvement of eCBs in the POD pathogenesis and further revealed that the eCBs may regulate POD through the specific MD^{glu}-PrL^{glu} circuit. These findings not only partly revealed the molecular and circuit mechanisms of POD, but also provided an applicable candidate for the clinical prevention and treatment of POD.

KEYWORDS

post-operative delirium, endocannabinoid signaling, mediodorsal thalamus, type 1 cannabinoid receptor, prelimbic prefrontal cortex

Introduction

With the gradual legalization of cannabis, about 10–20% of the adult population consumes cannabis every year, including 2–3% of the population authorized with medical cannabis (MMP, 2022). Furthermore, it was estimated that 5% of surgical patients might take cannabis in the USA (Davidson et al., 2020). Given the significant psychiatric effects of cannabinoids *via* the type 1 cannabinoid receptor (CB1R), cannabis and its target, the endocannabinoid system (eCBs), may influence post-operative consciousness and cognition (Busquets-Garcia et al., 2015).

Activation of CB1R by cannabis consumption may induce delirium-like behaviors, including delusions, hallucinations, paranoid ideas, impaired memory, and reduced attention spans (Hollister, 1988; Andre et al., 2006; Mack et al., 2012; Kokalj et al., 2016). Furthermore, we previously revealed that general anesthesia may activate eCBs, and blockade of CB1R could accelerate consciousness recovery after general anesthesia (Zhong et al., 2017), indicating eCBs may be associated with delirium after anesthesia and surgery (AS), namely post-operative delirium (POD). As one of the most common perioperative complications, POD affects up to 73.5% of surgical patients (Cui et al., 2020), leading to prolonged hospitalization, 3-fold higher mortality, long-term cognitive decline even dementia, and increased medical costs (Rudolph and Marcantonio, 2011; Daiello et al., 2019; Shi et al., 2019; Labaste et al., 2020). However, the pathogenesis of POD, especially the effect of eCBs on POD, remains largely unclear.

The prefrontal cortex (PFC), a high-order cortex, which plays a vital role in consciousness and cognitive control, is involved in the eCBs associated with recovery from anesthesia (Miller, 2000; Miller and Cohen, 2001; Zhong et al., 2017). Furthermore, the prelimbic prefrontal cortex (PrL), the important part of ventromedial PFC, has been attracting more and more attention in cognition, recognition, learning, and memory (Brockett et al., 2022; Cardoso-Cruz et al., 2022; Garcia-Font et al., 2022). Recent research also showed that increased pro-inflammatory cytokines in the PFC induced by lipopolysaccharide (LPS) led to delirium-like behavior in mice (Zhang et al., 2021). Furthermore, AS decreased excitatory synaptic transmission in PFC pyramidal neurons, but did not change the firing properties of the PFC pyramidal neurons (Matsumoto et al., 2021). Considering the classic retrograde inhibitory effect of CB1R on presynaptic transmitter release, eCBs activated by AS may inhibit the pre-synaptic functions of PFC, resulting in POD.

To verify the hypothesis, especially the POD-associated circuit modulated by the eCBs, we applied chemogenetics, fiber photometry, and behavioral tests. We specifically focused on the PrL (Anastasiades and Carter, 2021), and its upstream brain regions, the mediodorsal thalamus (MD) and hippocampus (HIP). Because the MD-PrL circuit was involved in a wide range of cognitive functions, including working memory, learning, attention, and arousal (Parnaudeau et al., 2018; Sun et al., 2019; Anastasiades et al., 2021), whereas the HIP-PrL circuit plays an essential role in memory encoding and emotion control (Spellman et al., 2015; Sánchez-Bellot and Macaskill, 2020).

In the present study, we confirmed that AS could overexcite the eCB signal in the PrL, which promoted POD through both plasma membrane CB1R (pmCB1R) and mitochondrial CB1R (mtCB1R). Furthermore, the glutamatergic neurons in the PrL innervated by excitatory MD neurons, rather than the HIP-PrL circuit, participated in eCBs-associated POD development. Exogenous cannabinoid nabilone could reverse the protective effect of MD^{glu}-PrL^{glu} circuit activation. Our results, for the first time, revealed that cannabinoids play a

crucial role in POD pathogenesis, and further clarified the neuronal specificity and circuit specificity of eCBs associated with POD development. These findings partly revealed the molecular and circuit mechanisms of POD and provided a new ideal target for POD prevention and treatment.

Materials and methods

Animals

The experimental protocols were approved by the Ethics Committee for Animal Experimentation of the Fourth Military Medical University, and all the experiments were conducted according to the Guidelines for Animal Experimentation of the Fourth Military Medical University (Xi'an, China).

Male C57BL/6 mice, aged 8–12 weeks, were provided by the Experimental Animal Center of the Fourth Military Medical University. Vglut2-Cre mice and Vgat-Cre mice were originated from the Jackson Laboratory. All mice were housed under a 12-h light/dark cycle (lights on from 7:00 to 19:00), 23 ± 1°C temperature, 38–42% humidity, and free access to water and food.

Stereotactic surgeries

Mice were fixed in the stereotaxic frame (RWD, China) under sodium pentobarbital (50 mg/kg) with erythromycin ophthalmic ointment applied for eye protection. After shaving and skin antisepsis, the scalp was sagittal cut. A heating mat was used to keep the mice warm.

For the chemogenetic experiments, 200 nl/side of AAV-DIO-hM3Dq-mCherry (Brain-VTA, China) (hM3Dq) or AAV-DIO-mCherry (Brain-VTA, China) (control) was microinjected into the bilateral PrL [anteroposterior (AP), +1.98 mm; mediolateral (ML), ±0.4 mm; dorsoventral (DV), −1.8 mm], MD (AP, −1.2 mm; ML, ±0.27 mm; DV, −2.75 mm) or HIP (AP, −2.0 mm; ML, ±1.2 mm; DV, −1.5 mm) at a rate of 50 nl/min in Vglut2-Cre or Vgat-Cre mice. For the experiments using combined Cre-loxP with Flp-FRT system, the AAV-DIO-EGFP-FLPO (OBiO, China) was microinjected into the MD, while the AAV-fDIO-hM3Dq-mCherry (OBiO, China) or AAV-fDIO-mCherry (OBiO, China) was administrated into PrL. The injecting glass electrode was left for 10 min and then slowly retrieved.

For fiber photometry, 300 nl of AAV-hsyn-eCB2.0 (WZ Bioscience Inc., China) was microinjected into PrL followed by the optical fiber [2.5 mm in diameter, 200 μm fiber optic cable, numerical aperture (NA) = 0.37, Inper, China] insertion into the PrL.

The dual guide cannulas (0.21 mm in diameter, RWD, China) were inserted into the PrL of mice for pharmacological administration.

Optical fibers and guide cannulas were fixed using methyl methacrylate cement. Animals were allowed to recover for at least 3 weeks after the virus injection, or 5–7 days after cannula implantation before further studies.

POD model establishment and pharmacological intervention

As previously described (Peng et al., 2016), mice in AS group underwent a simple laparotomy under isoflurane anesthesia (1.4% isoflurane delivered with 100% O_2 at 1.0 L/min), whereas mice in the sham group were only placed in the anesthesia chamber with room air without any surgery. The total inhalation time was 2 h in both groups. During the simple laparotomy, the midline abdominal skin, muscles, and peritoneum were longitudinally dissected layer by layer, from the xiphoid to 0.5 cm above the pubic symphysis. An ∼3-cm long segment of the small intestine was exposed outside the abdominal cavity for 2 min. After putting the small intestine back to place, the incision was sutured layer by layer with 5–0 Vicryl. Then, EMLA cream (2.5% lidocaine and 2.5% prilocaine) was applied on the incision wound and then every 8 h for 1 day.

In the pharmacological studies, all drugs, dissolved in a solvent mixture of dimethylsulfoxide (DMSO), Tween 80, and saline (1:1:18), were administrated to mice 15 min before the anesthesia. The selective CB1R antagonists, AM281 and hemopressin (Hemo), were administrated intraperitoneally at a dose of 3 and 1 mg/kg, respectively; or microinjected into the PrL at a dose of 100 ng/200 nl/side. Therefore, AM281 could block CB1R on both the cell membrane and mitochondrial membrane, while the Hemo could only block the plasma membrane CB1R (pmCB1R) (Benard et al., 2012). The synthetic cannabinoid, nabilone, was administrated intraperitoneally at a dose of 1 mg/kg or microinjected into the PrL at a dose of 100 ng/200 nl/side through an injector cannula. All of these agents were obtained from Sigma-Aldrich (USA).

Behavioral tests

The behavioral tests were performed as described in previous studies with modifications (Peng et al., 2016). All mice had multiple behavioral tests in the order of buried food test, open field test (OFT), and Y maze test (YMT) at 24 h before (baseline) the AS and at 6, 9, and 24 h after the AS. All tests were conducted in a quiet and illuminated room. The mice were habituated in the testing room for 1 h before the test. The apparatus was cleaned with 70% ethanol and dried between each test.

Buried food test

In the test cage with 3-cm-high clean bedding, one sweetened cereal was buried 0.5 cm below the surface of the bedding at a random location. The mouse was placed softly in the center of the test cage and allowed to explore for 5 min. The latency was recorded as the duration from the mouse was located in the test cage to its grasped food pellet in the forepaws and/or teeth. If the mouse failed to find the cereal within 5 min, the latency was defined as 300 s.

Open field test

The mouse was gently placed in the corner of a square chamber (40 × 40 × 40 cm) and allowed to move freely for 5 min. The movement was recorded and the total distance moved, time spent in the center, the freezing time, and the latency to the center were analyzed by the Any-Maze animal tracking system software (Stoelting Co., USA).

Y maze test

The standard Y maze used in the study includes the start arm, novel arm, and other arm (8 × 30 × 15 cm) with an angle of 120 degrees between each arm. In the first trial, the mouse was placed in the start arm and allowed to explore the start arm and other arm for 10 min, with the novel arm being blocked. After a 1-h inter-trial interval (ITI), the second trial (retention) was conducted, during which the mouse was placed back in the start arm with free access to all three arms for 5 min. The behavior of mice was monitored, and the number of entries in each arm and the time spent in the novel arm were analyzed by the Any-Maze animal tracking system software.

Chemogenetic experiments

To manipulate the glutamatergic and GABAergic neurons in the PrL, clozapine N-oxide (CNO) (Sigma-Aldrich, USA) at a dose of 1 mg/kg or an equivalent volume of saline was intraperitoneally injected. To explore the function of glutamatergic terminals in the PrL from MD or HIP, 5 μM CNO or saline was microinjected intra the PrL at 0.06 μL/min for 5 min. Thirty min after CNO administration, the anesthesia and surgery were conducted.

Fiber photometry recording

At least 14 days after the viral administration and optic fiber implantation, photometry recording was performed using the commercial photometry system (Thinker Tech, China) in mice during the AS and behavioral tests. The 470 nm LED was used to excite eCB sensors, and the 405 nm LED was used to obtain the isosbestic signal. The photometry data were recorded and exported to MATLAB for further analysis. Account for photobleaching, the raw signals were first adjusted (Dong et al., 2021). For each trial, the averaged baseline signals before stimuli presentation were considered as "F0" and the change of fluorescence (ΔF/F) was calculated as (F–F0)/F0.

Immunohistochemistry

Mice were deep anesthetized and transcardially perfused with 0.9% saline followed by 4% paraformaldehyde (PFA). Brains were post-fixed for 2 h in 4% PFA at 4°C and then dehydrated by 30% sucrose. Subsequently, brains were coronally sectioned at 40 μm using a cryostat microtome (CM1200, Leica, Germany). The sections were washed in phosphate-buffered saline (PBS, pH = 7.4) and then blocked with 5% normal donkey serum in PBS with 0.3% Triton X-100 (PBST) for 2 h at room temperature. Then, the sections were incubated in 2.5% donkey serum with PBST for 24 h at 4°C with guinea pig anti-c-Fos antibody (1:1,000, 226308, Synaptic Systems, Germany), rabbit anti-glutamate antibody (1:500, G6642, Sigma-Aldrich, USA), and rabbit anti-GABA antibody (1:200, GTX125988, GeneTex, USA), respectively. Afterwards, secondary antibodies, including donkey anti-guinea pig Alexa Fluor 488 (1:500, 706-545-148, Jackson ImmunoResearch, USA), donkey anti-guinea pig Alexa Fluor 594 (1:500, 706-585-148, Jackson ImmunoResearch, USA), donkey anti-guinea pig Alexa Fluor 647 (1:500, 706-605-148, Jackson ImmunoResearch, USA), and donkey anti-rabbit Alexa Fluor 488 (1:500, 711-545-152, Jackson ImmunoResearch, USA), were applied for 2 h at room temperature. At last, the slices were washed and mounted in Fluoromount-G (Millipore, USA) and imaged by laser confocal microscopes (FV1200, Olympus, Japan).

Western blot analysis

Mice were decapitated under deep anesthesia, and the PrL was rapidly separated and frozen at −80°C until use. The protein was abstracted using lysate. Protein concentration was estimated using a bicinchoninic acid (BCA) kit (Beyotime, China), and 30 μg samples were loaded onto polyacrylamide-SDS gels. Gels were electrophoresed and then transferred to PVDF membranes. Membranes were blocked with a blocking buffer containing 3% bovine serum albumin (Sigma-Aldrich, USA) for 60 min and probed with antibodies directed toward CNR-1 (1:1,000, Santa Cruz, USA) or GAPDH (1:2,000, ABclonal, China) overnight at 4°C. Primary antibody staining was detected with horseradish peroxidase-conjugated goat anti-rabbit antibodies (1:10,000, Beyotime, China). Each group was immune-blotted in three independent experiments, and average optical density

relative to the internal standard (GAPDH) was reported and analyzed (Bio-Rad, USA).

Statistics

All data were expressed as mean ± standard error of the mean (SEM) and analyzed by the Prism 6 software (GraphPad Software, CA). One-way ANOVA followed by Bonferroni's multiple comparisons was used to assess the differences between groups. Two-way ANOVA followed by Bonferroni's multiple comparisons was applied for photometry analysis. The immunohistochemical stainings were analyzed by unpaired *t*-test. $P < 0.05$ were considered statistically significant.

All the behavior parameters were presented as a percentage of those of the baseline for the same group. The POD-like behavioral impairment was shown by composite Z score (Peng et al., 2016), which was calculated as the sum of Z scores of six behavioral tests normalized with the SD for that sum in the shams, including latency to eat food, time spent in the center, latency to the center, freezing time, entries in the novel arm, and duration in the novel arm. Each Z score of the behavioral parameter was calculated as $Z = [\Delta X_{treatment}\text{-}MEAN(\Delta X)_{sham}]/SD(\Delta X)_{sham}$. In the formula, ΔX_{sham} represents the score differences between after and before sham management in the sham group; $\Delta X_{treatment}$ was the value that the score of post-treatment, including AS and pharmacological interventions, minus baseline; $MEAN(\Delta X)_{sham}$ and $SD(\Delta X)_{sham}$ were the mean and the standard deviation of ΔX_{sham}, respectively. The impairment of cognition was indicated by the reduction, rather than increase, of time spent in the center, freezing time, entries in the novel arm, and duration in the novel arm. The above four parameters were multiplied by −1 before the composite Z score calculation.

Results

Blockade of global CB1R alleviated POD

Firstly, we investigated the involvement of eCBs in POD using the AS model and composite Z score according to the previous studies (Peng et al., 2016; Figure 1A). As shown in Figure 1B, the composite Z score was significantly elevated after AS at both 6 h [$F_{(3, 44)} = 3.010$, $P = 0.0401$; Figure 1B left] and 9 h [$F_{(3, 44)} = 6.850$, $P = 0.0007$; Figure 1B middle], indicating the POD model was successfully established. However, the composite Z score was not changed at 24 h after AS [$F_{(3, 44)} = 2.116$, $P = 0.1118$; Figure 1B right]. Therefore, we only investigated behaviors at 6 and 9 h in the further investigation.

Moreover, systemic application of CB1R selective antagonist, AM281 (3 mg/kg) and Hemo (1 mg/kg) could partly reverse the increased composite Z score induced by AS, particularly at 9 h post-operatively with statistical differences (Figure 1B). Both AM281 and Hemo could reverse the prolonged latency to food after AS [$F_{(3, 44)} = 7.263$, $P = 0.0005$; Figure 1Ca]. The freezing time in OFT significantly increased in the AM281 group compared to the sham and AS groups at 6 h after AS [$F_{(3, 44)} = 4.677$, $P = 0.0064$; Figure 1Cc]. The above results confirmed that the eCB signaling was involved in the POD development. The other parameters shown no significant differences (Figure 1Cb,d–h). The running tracks of the mice in open field and Y maze in groups as shown in Figures 1D,E, respectively.

The PrL was involved in the eCB-associated POD regulation

Then, the involvement of the PFC in the eCB-associated POD regulation was examined by c-Fos staining. Interestingly, the expression of c-Fos in PrL was significantly decreased at 6 and 9 h after AS, which could be reversed by AM281 administration at 9 h after AS (Supplementary Figure 1). On the contrary, the expression of c-Fos in IL (infralimbic cortex) was decreased after AS, but could not be rescued by AM281. Therefore, the PrL was selected in the further experiment.

To reveal the eCB dynamics in PrL before and after AS, a fluorescent sensor for spatiotemporal detection was employed. Two weeks after the microinjection of the eCB sensor intra the PrL and optical fibers implantation (Figure 2A), the eCB signaling was monitored during AS and the behavioral tests, and the expression of the sensor virus was verified (Figure 2B). We found that the eCB signal of PrL was gradually weakened after the initiation of isoflurane anesthesia and boosted during the short operation (Figures 2C,D). Afterward, the signal kept fluctuating until the cessation of anesthesia and gradually recovered to the baseline level at 20 min after anesthesia. However, the eCB signals exhibited an increasing tendency during the behavioral tests mostly without significance. In the YMT, the ΔF/F value of eCB signaling in AS group was significantly higher than in the sham group [$F_{(1, 6)} = 7.184$, $P = 0.0365$; Figures 2E,F] at 6 h, but not 9 h after AS [$F_{(1, 6)} = 1.372$, $P = 0.2859$]. Besides, the expression of the CB1R in the PrL was time-dependently increased after AS, especially at 9 h post-operative (1.000 ± 0.1364 vs. 1.419 ± 0.06338, $P = 0.0360$; Figure 2G).

Next, we bilateral microinjected AM281 (100 ng/200 nl/side) or Hemo (100 ng/200 nl/side) intra the PrL 15 min before AS to verify the role of the PrL CB1R in POD pathogenesis (Figure 3A). The location of the cannulas was confirmed after behavioral tests (Figure 3B). We found that the composite Z score in the AM281 group, but not in the Hemo group, was significantly lower than in the AS group at 6 h [$F_{(3, 36)} = 8.869$, $P = 0.0002$] and 9 h [$F_{(3, 6)} = 6.405$, $P = 0.0014$] post-operatively

10.3389/fnagi.2022.1036428

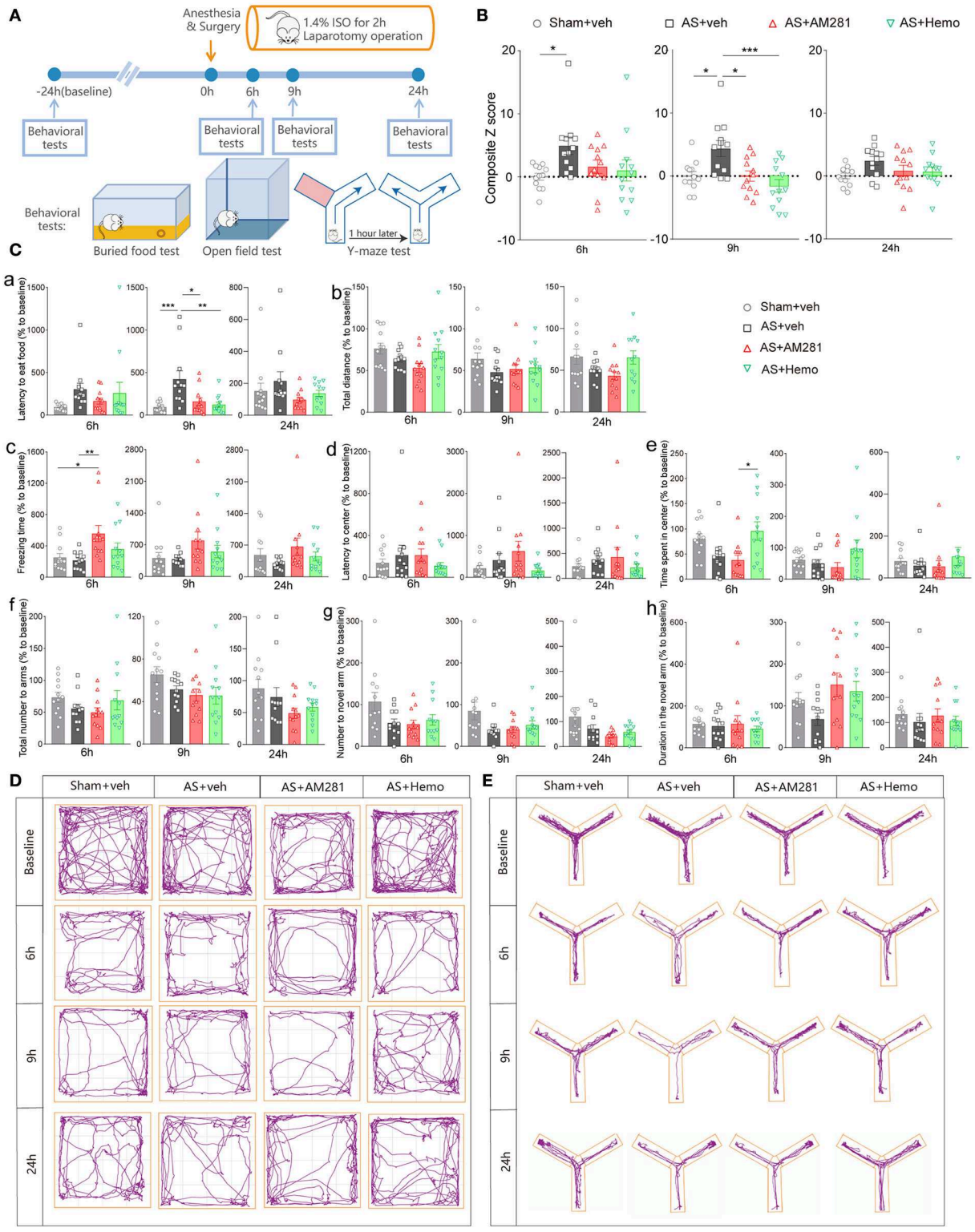

FIGURE 1
Blockade of global CB1R alleviated POD. **(A)** Scheme of the experimental design. **(B)** The composite Z score at 6 h (left), 9 h (middle), and 24 h (right) after AS. **(C)** The latency to eat food in buried food test (a); the total distance (b), the freezing time (c), the latency to center (d), time spent in center (e) in the open field; the total number to arm (f), number to novel arm (g), duration in the novel arm (h) in Y maze at 6 h (left), 9 h (middle), and 24 h (right). **(D,E)** Running tracks of the mice in an open field **(D)** and Y maze **(E)** in groups. Data are shown as mean ± SEM. $N = 12$. $^{*}P < 0.05$, $^{**}P < 0.01$, $^{***}P < 0.001$. ISO, isoflurane; AS, anesthesia and surgery; Hemo, hemopressin.

10.3389/fnagi.2022.1036428

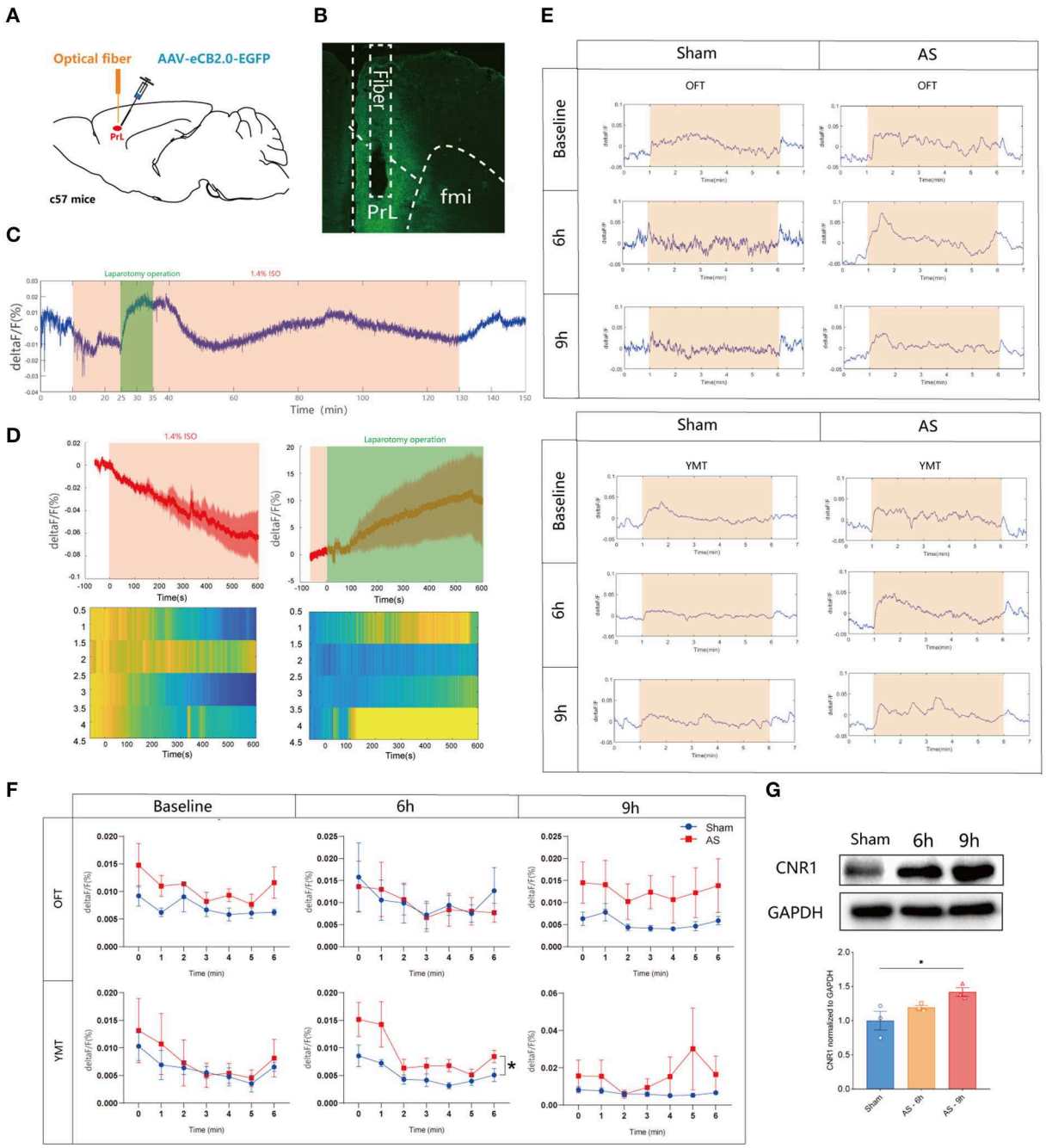

FIGURE 2
The eCB signals in the PrL during AS and behavioral tests. **(A)** Scheme of the viral microinjection and fiber implantation. **(B)** The fiber location and viral expression. **(C,D)** The typical traces **(C)** and analyzed figure **(D)** of the eCB signal during AS. **(E,F)** The typical curves **(E)** and statistical chart **(F)** of the eCB signal during the open field and Y maze tests. **(G)** The expression of CB1R in the PrL after AS. Data are shown as mean ± SEM. $N = 4$. $^*P < 0.05$. AS, anesthesia and surgery; OFT, open field test; YMT, Y maze test.

(Figure 3C), indicating both plasma and mitochondrial CB1R were important in POD regulation. Specifically, the latency to food at 6 h was prolonged in AS group, which was reversed by AM281 [$F_{(3, 36)} = 7.437$, $P = 0.0005$; Figure 3Da]. The other parameters shown no significant differences (Figures 3Db–h). These findings indicated that the eCB signaling in the PrL was associated with POD, presumably through the increased endocannabinoids and CB1R (Riederer et al., 2016).

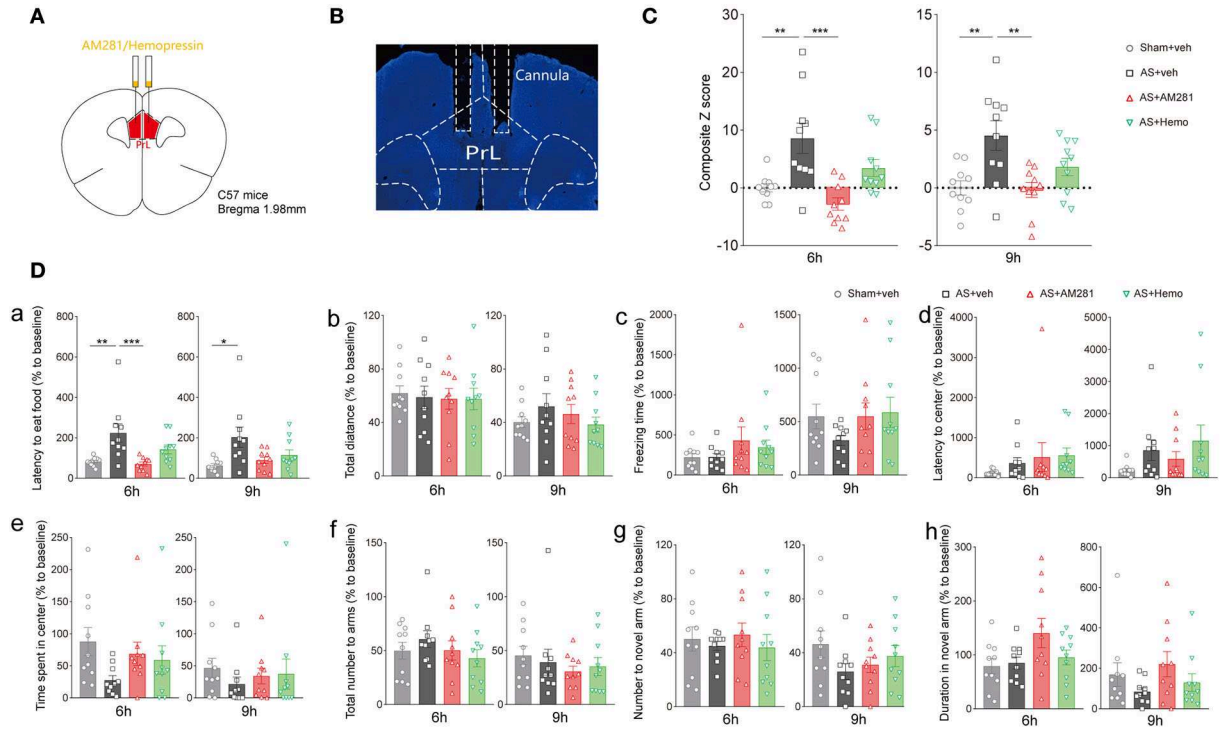

FIGURE 3
Blockade of CB1R in the PrL promoted the composite Z score. **(A)** Scheme of the drug administration. **(B)** The site of the cannula in the PrL. **(C)** The composite Z score at 6 h (left) and 9 h (right) after AS. **(D)** The latency to eat food in buried food test (a); the total distance (b), the freezing time (c), the latency to center (d), time spent in center (e) in the open field; the total number to arm (f), number to novel arm (g), duration in the novel arm (h) in Y maze at 6 h (left) and 9 h (right) after AS. Data are shown as mean ± SEM. $N = 10$. *$P < 0.05$, **$P < 0.01$, ***$P < 0.001$. ISO, isoflurane; AS, anesthesia and surgery; Hemo, hemopressin.

eCB signaling modulated POD through the glutamatergic neurons rather than GABAergic neurons in the PrL

To clarify the neuronal specificity of PrL in POD regulation, we further applied chemogenetics and pharmacological interventions in Vglut2-Cre mice and Vgat-Cre mice (Figure 4A, Supplementary Figure 2A). After 3 weeks of viral expression, the mice were applied with AS followed by behavioral tests. The expression and functions of AAV-DIO-hM3Dq-mCherry (hM3Dq) and AAV-DIO-mCherry (control) viruses were verified, as evidenced by Figure 4B and Supplementary Figure 2B.

We found that activation of PrL glutamatergic neurons in the AS + hM3Dq + CNO group significantly reduced the composite Z score compared with the control (AS + mCherry + CNO) group at both 6 h [$F_{(3, 20)} = 8.079$, $P = 0.0010$] and 9 h [$F_{(3, 20)} = 11.50$, $P = 0.0001$] post-operatively (Figure 4C). However, activation of PrL GABAergic neurons could only relieve the behavioral impairment at 9 h after AS [$F_{(3,20)} = 10.99$, $P = 0.0007$; Supplementary Figure 2C].

Furthermore, activation of CB1R by nabilone (intraperitoneally at a dose of 3 mg/kg) could only reverse the POD-preventing effect induced by activating PrL glutamatergic neurons (Figure 4C) at 6 h, but not by activation of GABAergic neurons at 6 h [$F_{(3, 20)} = 3.356$, $P = 0.0393$; Supplementary Figure 2C]. Nabilone is an exogenous cannabinoid that exerts CB1R-activating effects similar to cannabis consumption. Compared with the sham group, AS and nabilone administration with the activation of glutamatergic neurons significantly reduced the numbers to the novel arm in YMT at 6 h [$F_{(3, 20)} = 7.452$, $P = 0.0015$; Figure 4Dg]. Notably, the nabilone application exhibited significantly longer latency to center in OFT than the other three groups at 9 h post-operatively [$F_{(3, 20)} = 7.754$, $P = 0.0013$; Figure 4Dd], suggesting an enhanced anxiety level induced by nabilone after AS. The other parameters shown no significant differences (Figures 4Da–c,e,f,h). Above findings indicated the PrL glutamatergic neurons, rather than

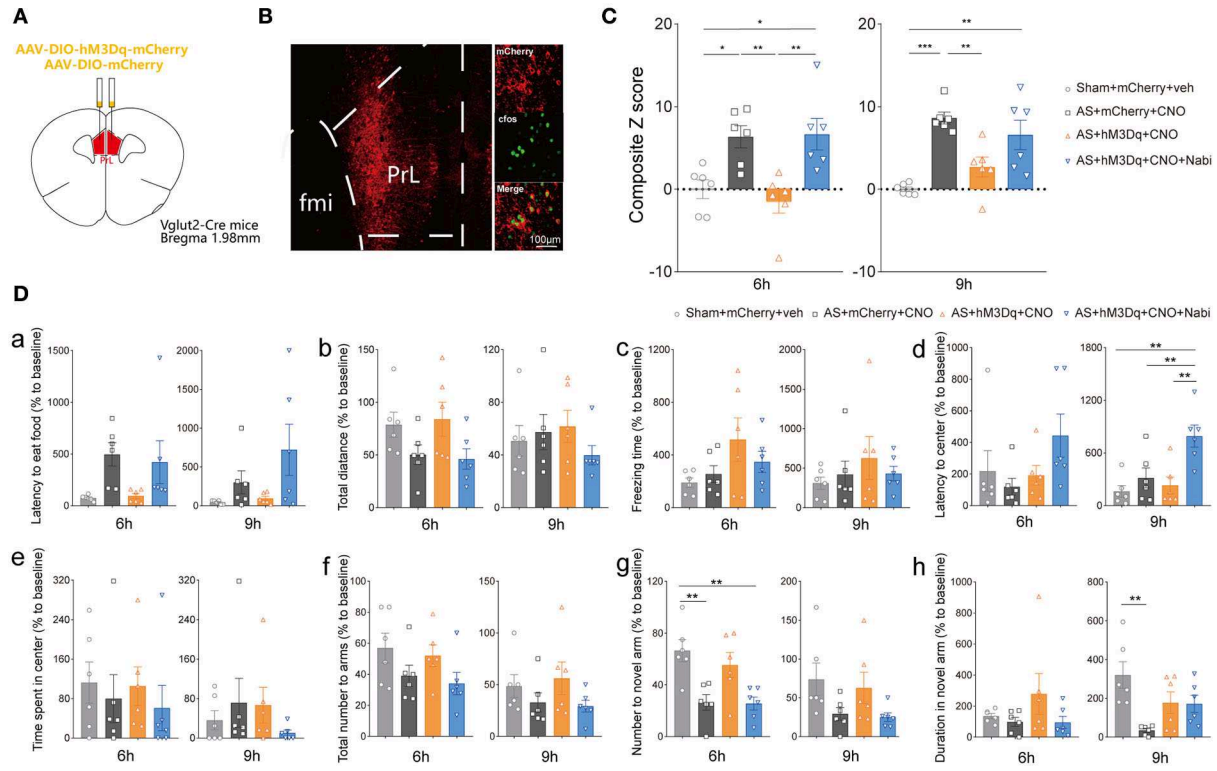

FIGURE 4
eCB signaling modulated POD through the PrL glutamatergic neurons. **(A)** Scheme of hM3Dq or control virus injection into the PrL of Vglut2-Cre mice. **(B)** The injection site (left) and activation efficiency (right). **(C)** The composite Z score at 6 h (left) and 9 h (right) after AS. **(D)** The latency to eat food in buried food test (a); the total distance (b), the freezing time (c), the latency to center (d), time spent in center (e) in the open field; the total number to arm (f), number to novel arm (g), duration in the novel arm (h) in Y maze at 6 h (left) and 9 h (right) after AS. Data are shown as mean ± SEM. $N = 6$. $^*P < 0.05$, $^{**}P < 0.01$, $^{***}P < 0.001$. ISO, isoflurane; AS, anesthesia and surgery; Nabi, nabilone; CNO, clozapine N-oxide; mCherry, AAV-DIO-mCherry; hM3Dq, AAV-DIO-hM3Dq-mCherry.

GABAergic neurons, might play an essential role in the eCBs mediated POD regulation.

The MD^{glu}-PrL^{glu} circuit, but not the HIP^{glu}-PrL circuit, was responsible for the effect of eCB on POD

Given MD-PrL (Parnaudeau et al., 2018) and HIP-PrL (Sánchez-Bellot and Macaskill, 2020) were involved in the regulation of working memory and long-term memory, respectively, we investigated the roles of the two circuits in POD modulation in the further study. The retrograde viruses were used to label the upstream neurons of the PrL glutamatergic neurons in MD and HIP (Supplementary Figure 3A). Two weeks after being injected with the helper viruses (AAV-DIO-H2B-EGFP-T2A-TVA and AAV-DIO-oRVG) and RV-ENVA-NVAdsRed (RV), we co-labeled the glutamatergic and GABAergic neurons in MD and HIP.

Co-expression of the RV and helper viruses in the PrL was verified (Supplementary Figure 3B). As shown in Supplementary Figure 3C, the PrL glutamatergic neurons were innervated by MD glutamatergic neurons more than MD GABAergic neurons (0.47 ± 0.06 vs. 0.29 ± 0.07, $P = 0.0476$; Supplementary Figures 3C,D). However, there were no significant retrograde RV-labeled neurons in the HIP (Supplementary Figure 3E).

Furthermore, we modulated MD^{glu}-PrL and HIP^{glu}-PrL circuits to investigate their roles in POD pathogenesis in Vglut2-Cre mice (Figures 5A,B). Activation of MD^{glu}-PrL could statistically alleviate POD at 6 h [$F_{(3, 20)} = 7.606$, $P = 0.0014$] and 9 h [$F_{(3, 20)} = 9.646$, $P = 0.0004$] compared with AS+mCherry+CNO group (Figure 5C). Meanwhile, nabilone administration (100 ng/200 nl/side) intra the PrL could partly reverse this relieving effect at 6 and 9 h compared with the AS + hM3Dq + CNO group (Figure 5C). It is worth noting that the duration stays in the novel arm in YMT was greatly improved by activation of MD^{glu}-PrL compared to the AS group at 9 h after AS [$F_{(3, 20)} = 9.691$, $P = 0.0004$; Figure 5Dh]. The other

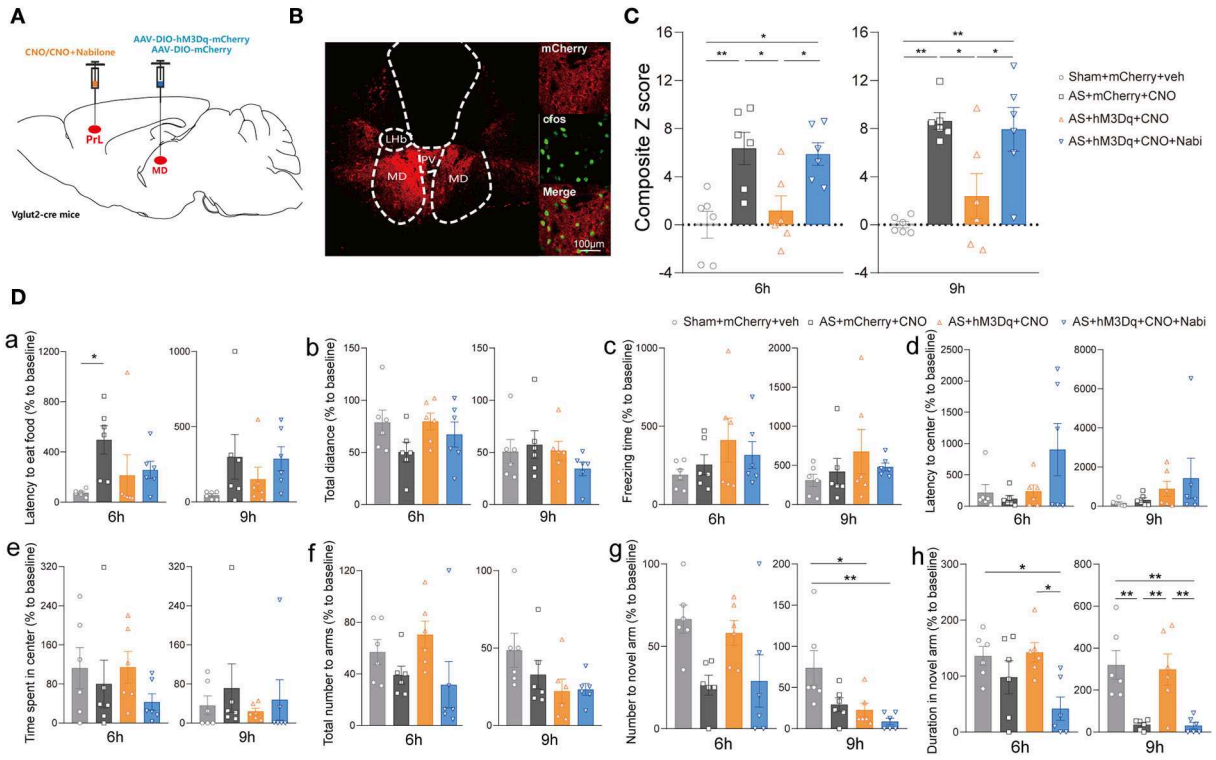

FIGURE 5
The MD^{glu}-PrL circuit was responsible for the effect of eCBs on POD. **(A)** Scheme of viral injection and CNO application. **(B)** The injection site (left) and activation efficiency (right). **(C)** The composite Z score at 6 h (left) and 9 h (right) after AS. **(D)** The latency to eat food in buried food test (a); the total distance (b), the freezing time (c), the latency to center (d), time spent in center (e) in the open field; the total number to arm (f), number to novel arm (g), duration in the novel arm (h) in Y maze at 6 h (left) and 9 h (right) after AS. Data are shown as mean ± SEM. $N = 6$. *$P < 0.05$, **$P < 0.01$. AS, anesthesia and surgery; Nabi, nabilone; CNO, clozapine N-oxide; mCherry, AAV-DIO-mCherry; hM3Dq, AAV-DIO-hM3Dq-mCherry; PrL, prelimbic cortex; MD, mediodorsal thalamus.

parameters shown no significant differences (Figures 5Da–g). However, activation of HIP^{glu}-PrL failed to rescue POD [$F_{(3, 20)} = 2.965$, $P = 0.0567$ at 6 h; $F_{(3, 20)} = 3.664$, $P = 0.0297$ at 9 h; Supplementary Figure 4].

Next, we investigated the effect of the specific MD^{glu}-PrL^{glu} circuit on eCB signaling-related POD regulation using the combined Cre-loxP and Flp-FRT system in Vglut2-Cre mice. Briefly, the AAV-DIO-EGFP-FLPO was microinjected into the MD, while the AAV-fDIO-hM3Dq or AAV-fDIO-mCherry was microinjected into the PrL (Figures 6A,B). Selective activation of the MD^{glu}-PrL^{glu} circuit could decrease the composite Z score, particularly 6 h after AS compared with the AS + mCherry + CNO group while nabilone administration (100 ng/200 nl/side) intra the PrL reversed the protective effect [$F_{(3, 20)} = 8.470$, $P = 0.0008$; Figure 6C]. In the buried food test, the latency to eat food in the AS + mCherry + CNO group was significantly more extended than in the AS + hM3Dq + CNO group [$F_{(3, 20)} = 4.126$, $P = 0.0198$; Figure 6Da] 6 h after AS. The other parameters shown no significant differences (Figures 6Db–h). These findings further confirmed that the MD^{glu}-PrL^{glu} circuit was responsible for the effect of eCB on POD.

Discussion

In this study, we demonstrated the role and underlying circuit mechanisms of eCB signaling in POD regulation for the first time. We found that blockade of CB1R in the PrL could effectively alleviate POD through the glutamatergic neurons rather than GABAergic neurons. Furthermore, the post-operative eCB signaling, activated by AS, may regulate the function of the MD^{glu}-PrL^{glu} circuit, but not HIP^{glu}-PrL projection. Exogenous cannabinoids aggravate POD, which was alleviated by the activation of MD-PrL. Our results suggest the increased eCB signal in the PrL may be a critical factor for POD pathogenesis, which may also be involved in the mechanisms of marijuana smoking-associated POD.

In the present study, we used two antagonists of CB1R: AM281, the classical selective reversal antagonist of CB1R, is lipid-soluble and able to block CB1R on both cell membrane and mitochondrial membrane; while the Hemo could only block the plasma membrane CB1R (pmCB1R) because it is unable to penetrate plasma membranes (Benard et al., 2012). As expected, AM281 showed a significant alleviating effect

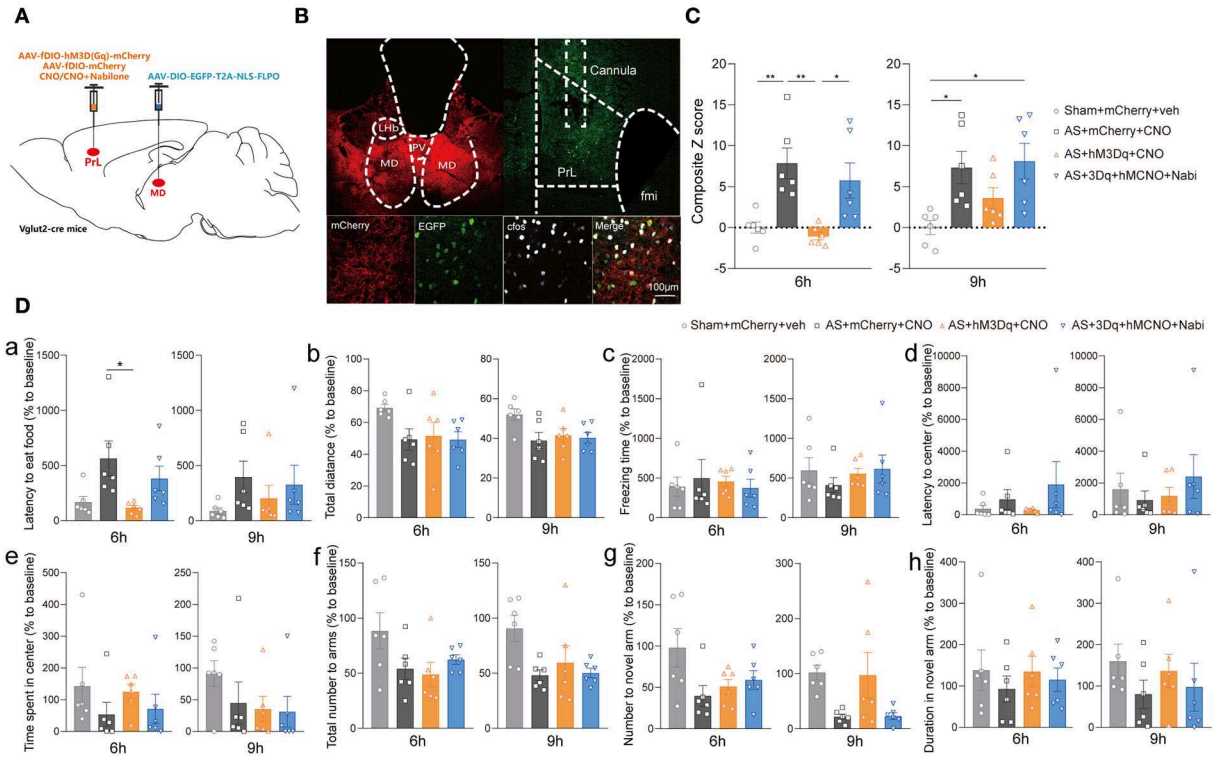

FIGURE 6
The MD^{glu}-PrL^{glu} circuit was involved in the effect of eCB on POD. **(A)** Scheme of viral injection and CNO application. **(B)** The injection site in MD and PrL (above) and activation efficiency (below). **(C)** The composite Z score at 6 h (left) and 9 h (right) after AS. **(D)** The latency to eat food in buried food test (a); the total distance (b), the freezing time (c), the latency to center (d), time spent in center (e) in the open field; the total number to arm (f), number to novel arm (g), duration in the novel arm (h) in Y maze at 6 h (left) and 9 h (right) after AS. Data are shown as mean ± SEM. $N = 6$. $^{*}P < 0.05$, $^{**}P < 0.01$. AS, anesthesia and surgery; Nabi, nabilone; CNO, clozapine N-oxide; mCherry, AAV-fDIO-mCherry; hM3Dq, AAV-fDIO-hM3Dq-mCherry; PrL, prelimbic cortex; MD, mediodorsal thalamus.

on POD rather than Hemo, indicating both the pmCB1R and mitochondrial CB1R (mtCB1R) are necessary for the regulating effect of eCBs on POD. A series of studies have shown that mtCB1R also played an essential role in synaptic function in cognitive and emotional modulation (Cardinal et al., 2012; Djeungoue-Petga and Hebert-Chatelain, 2017). Activation of mtCB1R could decrease mitochondrial ATP production, calcium buffering capacity, ROS generation, and the mobility of neuronal mitochondria to inhibit transmitter release in the synapses (Cardinal et al., 2012; Djeungoue-Petga and Hebert-Chatelain, 2017). Therefore, eCBs may modulate the MD-PrL circuit by the pmCB1R-associated classical retrograde synaptic inhibition (Busquets-Garcia et al., 2015) and mtCB1R-related presynaptic metabolism inhibition.

Within the PrL, we found activation of both glutamatergic and GABAergic neurons could alleviate the POD behavior. However, the influence of PrL glutamatergic neuronal activation was earlier and more prominently than GABAergic neurons, suggesting a temporal sequence for PrL neurons' recovery from AS. The imbalance of PrL glutamatergic and GABAergic neurons recovery could significantly affect the function of the higher cortex, including mood, memory, and states of consciousness (Lacreuse et al., 2018; Dienel et al., 2020; Fogaca et al., 2021; Quinones et al., 2021; Sabihi et al., 2021; Smucny et al., 2021; Yan and Rein, 2021), which may lead to POD. However, activation of PrL GABAergic neurons seemed that they did not further inhibit the local glutamatergic neurons to aggravate cognitive impairments, but alleviated POD probably through other long-range projections as in HIP and amygdala (Alkire et al., 2008; Sun et al., 2019; Guo et al., 2021; Shepherd and Yamawaki, 2021). On the other hand, exogenous cannabinoid only reversed the cognitive relieving effect of glutamatergic neurons, rather than GABAergic neurons, indicating the influence of CB1R on POD in the PrL exhibited cellular specificity. The phenomenon may be attributed to the cardinal effect of glutamatergic neurons in primary information processing, conducting, and amplifying (Sherman, 2016). Otherwise, cannabinoid may selectively act on the pre-synaptic CB1R of glutamatergic neurons in the PrL.

To examine the above hypotheses, we retrogradely traced the PrL glutamatergic neurons and found that MD, instead of the HIP, is the most important upstream nucleus of PrL. PrL

was first defined as the cortex that receives projections from the thalamus, further, MD shares rich reciprocal connections with PrL (Parnaudeau et al., 2013, 2018; Ahrlund-Richter et al., 2019; Lyuboslavsky et al., 2021). However, no RV-labeled neurons were found in the HIP, which may be due to the regional specificity of HIP inputs to the PrL, including strong inputs from multiple layers in the intralimbic area (IL) and weak restricted input from Layer 5 in PrL. Combined with the efficiency and sparse diffusion of viruses, which were predominantly microinjected in Layer 3 in our experiment, the negative result was reasonable (Liu and Carter, 2018). Although the thalamus was believed to be the relay station for integrating various cognitive functions (Wen et al., 2021; Wolff et al., 2021), more and more pieces of evidence confirmed that the thalamus is also engaged in essential and unique computations of cognition through projections to the cortex (Mitchell et al., 2014; Nakajima and Halassa, 2017; Rikhye et al., 2018). The MD projections could sustain PrL activity during working memory maintenance (Bolkan et al., 2017). Inconsistent with the precious results, we confirmed that activation of the MD^{glu}-PrL^{glu} circuit could noticeably improve POD, implying the strength of thalamus-cortex connections was impaired by anesthesia and surgery. Thus, the pyramidal neurons in the PrL were de-excited to maintain normal cognition and emotion, resulting in delirium-like behavior. Combined with the results of the eCBs signaling, the impaired excitatory MD-PrL projection was due to the CB1R-related presynaptic inhibition. These results also supported Yu Matsumoto's findings (Matsumoto et al., 2021) that AS decreased the excitatory presynaptic responses of PrL pyramidal neurons without any changes in the response kinetics.

There are two limitations of the present study. Firstly, we only investigated the MD-PrL and HIP-PrL circuit, however, there are abundant afferent and efferent projections of PrL. Future research is needed to explore other upstream projections and the specific downstream targets mediated emotion and consciousness, such as BLA-PrL (Liu et al., 2020) and DMH-PrL (Zhong et al., 2017). Secondly, we did not further probe the function of PrL GABAergic neurons, which also participated in the POD development. Though activation of PrL GABAergic neurons could not reverse the effect of nabilone, we cannot exclude the involvement of the PrL GABAergic neurons in eCB-associated POD.

In summary, our study, for the first time, demonstrated the involvement of eCB in POD pathogenesis and further revealed that eCB signaling activated by anesthesia and surgery and exogenous cannabinoid could promote POD through the MD^{glu}-PrL^{glu} circuit. These findings not only expanded the understanding of POD from both molecular and circuit aspects but may also provide new applicable therapeutic targets for POD prevention and treatment in the future.

Data availability statement

The original contributions presented in the study are included in the article/Supplementary material, further inquiries can be directed to the corresponding author.

Ethics statement

The animal study was reviewed and approved by Ethics Committee for Animal Experimentation of the Fourth Military Medical University.

Author contributions

YL designed the study, conducted the study, analyzed the data, and wrote the manuscript. SJ and JW conducted the study. DW, XZ, HL, FZ, ZZ, and QL helped conducted the study and analyzed the data. HZ and HD designed the study and polished the manuscript. All authors contributed to the article and approved the submitted version.

Funding

This work was supported by the National Natural Science Foundation of China (Grant Nos. 82071487, 81771427 to HZ and Grant No. 82030038 to HD) and the Natural Science Basic Research Program of Shaanxi province (Grant Nos. 2020JM-313, 2022JC-59 to HZ).

Conflict of interest

The authors declare that the research was conducted in the absence of any commercial or financial relationships that could be construed as a potential conflict of interest.

Publisher's note

Supplementary material

The Supplementary Material for this article can be found online at: https://www.frontiersin.org/articles/10.3389/fnagi.2022.1036428/full#supplementary-material

SUPPLEMENTARY FIGURE 1
The expression of the c-Fos in the PrL after AS. **(A)** The expression of c-Fos (red) in the PrL and IL after AS with vehicle or AM281 administration. **(B)** The changes of c-Fos expression in the PrL. **(C)** The changes of c-Fos expression in the IL. $N \geq 3$. $^{*}P < 0.05$, $^{**}P < 0.01$, $^{***}P < 0.001$. AS, anesthesia & surgery; PrL, prelimbic cortex.

SUPPLEMENTARY FIGURE 2
PrL GABAergic neurons modulated POD without responses to cannabinoid. **(A)** Scheme of viral injection. **(B)** The injection site (left) and activation efficiency (right). **(C)** The composite Z score at 6 h (left) and 9 h (right) after AS. **(D)** The latency to eat food in buried food test (a); the total distance (b), the freezing time (c), the latency to center (d), time spent in center (e) in open field; the total number to arm (f), number to novel arm (g), duration in the novel arm (h) in Y maze at 6 h (left) and 9 h (right) after AS. Data are shown as mean ± SEM. $N = 6$. $^{*}P < 0.05$, $^{**}P < 0.01$, $^{***}P < 0.001$. ISO, isoflurane; AS, anesthesia & surgery; Nabi, nabilone; CNO, clozapine N-oxide; mCherry, AAV–DIO-mCherry; hM3Dq, AAV-DIO-hM3Dq-mCherry; PrL, prelimbic cortex.

SUPPLEMENTARY FIGURE 3
The RV retrograde labeled neurons in the MD and HIP from the PrL glutamatergic neurons. **(A)** Scheme of injection of helper and RV viruses into the PrL of Vglut2-Cre mice. **(B)** The expression of the viruses in the PrL. **(C)** The co-localization of RV-labeled neurons and glutamatergic and GABAergic neurons in the MD. Arrowheads indicate the co-labeled cells. **(D)** The percentage of glutamatergic (blue bar) and GABAergic neurons (red bar) in the RV-labeled neurons. **(E)** The co-localization of RV-labeled neurons and glutamatergic and GABAergic neurons in the HIP. Data are shown as mean ± SEM. $N \geq 3$. $^{*}P < 0.05$, $^{****}P < 0.0001$. RV, RV-ENVA-ΔG-dsRed; Helper, AAV-DIO-H2B-EGFP-T2A-TVA & AAV-DIO-oRVG; PrL, prelimbic cortex; MD, mediodorsal thalamus.

SUPPLEMENTARY FIGURE 4
Activation of HIP^{glu} - PrL circuit did not affect POD. **(A)** Scheme of viral injection and drug application. **(B)** The injection site (left) and activation efficiency (right). **(C)** The composite Z score at 6 h (left) and 9 h (right) after AS. **(D)** The latency to eat food in buried food test (a); the total distance (b), the freezing time (c), the latency to center (d), time spent in center (e) in open field; the total number to arm (f), number to novel arm (g), duration in the novel arm (h) in Y maze at 6 h (left) and 9 h (right) after AS. Data are shown as mean ± SEM. $N = 6$. $^{*}P < 0.05$. AS, anesthesia & surgery; Nabi, nabilone; CNO, clozapine N-oxide; mCherry, AAV-DIO-mCherry; hM3Dq, AAV-DIO-hM3Dq-mCherry; PrL, prelimbic cortex; HIP, hippocampus.

References

Ahrlund-Richter, S., Xuan, Y., Van Lunteren, J. A., Kim, H., Ortiz, C., Pollak Dorocic, I., et al. (2019). A whole-brain atlas of monosynaptic input targeting four different cell types in the medial prefrontal cortex of the mouse. *Nat. Neurosci.* 22, 657–668. doi: 10.1038/s41593-019-0354-y

Alkire, M. T., Hudetz, A. G., and Tononi, G. (2008). Consciousness and anesthesia. *Science* 322, 876–880. doi: 10.1126/science.1149213

Anastasiades, P. G., and Carter, A. G. (2021). Circuit organization of the rodent medial prefrontal cortex. *Trends Neurosci.* 44, 550–563. doi: 10.1016/j.tins.2021.03.006

Anastasiades, P. G., Collins, D. P., and Carter, A. G. (2021). Mediodorsal and ventromedial thalamus engage distinct L1 circuits in the prefrontal cortex. *Neuron* 109, 314–330.e4. doi: 10.1016/j.neuron.2020.10.031

Andre, C., Jaber-Filho, J. A., Bento, R. M., Damasceno, L. M., and Aquino-Neto, F. R. (2006). Delirium following ingestion of marijuana present in chocolate cookies. *CNS Spectr.* 11, 262–264. doi: 10.1017/S1092852900020757

Benard, G., Massa, F., Puente, N., Lourenco, J., Bellocchio, L., Soria-Gomez, E., et al. (2012). Mitochondrial CB(1) receptors regulate neuronal energy metabolism. *Nat. Neurosci.* 15, 558–564. doi: 10.1038/nn.3053

Bolkan, S. S., Stujenske, J. M., Parnaudeau, S., Spellman, T. J., Rauffenbart, C., Abbas, A. I., et al. (2017). Thalamic projections sustain prefrontal activity during working memory maintenance. *Nat. Neurosci.* 20, 987–996. doi: 10.1038/nn.4568

Brockett, A. T., Tennyson, S. S., Debettencourt, C. A., Kallmyer, M., and Roesch, M. R. (2022). Medial prefrontal cortex lesions disrupt prepotent action selection signals in dorsomedial striatum. *Curr. Biol.* 32, 3276–3287.e3. doi: 10.1016/j.cub.2022.06.025

Busquets-Garcia, A., Desprez, T., Metna-Laurent, M., Bellocchio, L., Marsicano, G., and Soria-Gomez, E. (2015). Dissecting the cannabinergic control of behavior: the where matters. *Bioessays* 37, 1215–1225. doi: 10.1002/bies.201500046

Cardinal, P., Bellocchio, L., Clark, S., Cannich, A., Klugmann, M., Lutz, B., et al. (2012). Hypothalamic CB1 cannabinoid receptors regulate energy balance in mice. *Endocrinology* 153, 4136–4143. doi: 10.1210/en.2012-1405

Cardoso-Cruz, H., Laranjeira, I., Monteiro, C., and Galhardo, V. (2022). Altered prefrontal-striatal theta-band oscillatory dynamics underlie working memory deficits in neuropathic pain rats. *Eur. J. Pain* 26, 1546–1568. doi: 10.1002/ejp.1982

Cui, Y., Li, G., Cao, R., Luan, L., and Kla, K. M. (2020). The effect of perioperative anesthetics for prevention of postoperative delirium on general anesthesia: a network meta-analysis. *J. Clin. Anesth.* 59, 89–98. doi: 10.1016/j.jclinane.2019.06.028

Daiello, L. A., Racine, A. M., Yun Gou, R., Marcantonio, E. R., Xie, Z., Kunze, L. J., et al. (2019). Postoperative delirium and postoperative cognitive dysfunction: overlap and divergence. *Anesthesiology* 131, 477–491. doi: 10.1097/ALN.0000000000002729

Davidson, E. M., Raz, N., and Eyal, A. M. (2020). Anesthetic considerations in medical cannabis patients. *Curr. Opin. Anaesthesiol.* 33, 832–840. doi: 10.1097/ACO.0000000000000932

Dienel, S. J., Enwright, J. F. III., Hoftman, G. D., and Lewis, D. A. (2020). Markers of glutamate and GABA neurotransmission in the prefrontal cortex of schizophrenia subjects: disease effects differ across anatomical levels of resolution. *Schizophr. Res.* 217, 86–94. doi: 10.1016/j.schres.2019.06.003

Djeungoue-Petga, M. A., and Hebert-Chatelain, E. (2017). Linking mitochondria and synaptic transmission: the CB1 receptor. *Bioessays* 39, 1700126. doi: 10.1002/bies.201700126

Dong, A., He, K., Dudok, B., Farrell, J. S., Guan, W., Liput, D. J., et al. (2021). A fluorescent sensor for spatiotemporally resolved imaging of endocannabinoid dynamics *in vivo*. *Nat. Biotechnol.* 40, 787–798. doi: 10.1101/2020.10.08.329169

Fogaca, M. V., Wu, M., Li, C., Li, X. Y., Picciotto, M. R., and Duman, R. S. (2021). Inhibition of GABA interneurons in the mPFC is sufficient and necessary for rapid antidepressant responses. *Mol. Psychiatry* 26, 3277–3291. doi: 10.1038/s41380-020-00916-y

Garcia-Font, N., Mitchell-Heggs, R., Saxena, K., Gabbert, C., Taylor, G., Mastroberadino, G., et al. (2022). Ca2+ imaging of self and other in medial prefrontal cortex during social dominance interactions in a tube test. *Proc. Natl. Acad. Sci. U.S.A.* 119, e2107942119. doi: 10.1073/pnas.2107942119

Guo, J., Ran, M., Gao, Z., Zhang, X., Wang, D., Li, H., et al. (2021). Cell-type-specific imaging of neurotransmission reveals a disrupted excitatory-inhibitory cortical network in isoflurane anaesthesia. *EBioMedicine* 65, 103272. doi: 10.1016/j.ebiom.2021.103272

Hollister, L. E. (1988). Cannabis-—1988. *Acta Psychiatr. Scand.* 78, 108–118. doi: 10.1111/j.1600-0447.1988.tb08576.x

Kokalj, A., Rijavec, N., and Tavcar, R. (2016). Delirium with anticholinergic symptoms after a combination of paliperidone and olanzapine pamoate in a patient known to smoke cannabis: an unfortunate coincidence. *BMJ Case Rep.* 2016. doi: 10.1136/bcr-2016-214806

Labaste, F., Porterie, J., Bousquet, P., Marcheix, B., Sanchez-Verlaan, P., Frances, B., et al. (2020). Postoperative delirium is a risk factor of poor evolution three years after cardiac surgery: an observational cohort study. *Clin. Interv. Aging* 15, 2375–2381. doi: 10.2147/CIA.S265797

Lacreuse, A., Moore, C. M., Laclair, M., Payne, L., and King, J. A. (2018). Glutamine/glutamate (Glx) concentration in prefrontal cortex predicts reversal learning performance in the marmoset. *Behav. Brain Res.* 346, 11–15. doi: 10.1016/j.bbr.2018.01.025

Liu, W. Z., Zhang, W. H., Zheng, Z. H., Zou, J. X., Liu, X. X., Huang, S. H., et al. (2020). Identification of a prefrontal cortex-to-amygdala pathway for chronic stress-induced anxiety. *Nat. Commun.* 11, 2221. doi: 10.1038/s41467-020-15920-7

Liu, X., and Carter, A. G. (2018). Ventral hippocampal inputs preferentially drive corticocortical neurons in the infralimbic prefrontal cortex. *J. Neurosci.* 38, 7351–7363. doi: 10.1523/JNEUROSCI.0378-18.2018

Lyuboslavsky, P., Kizimenko, A., and Brumback, A. C. (2021). Two contrasting mediodorsal thalamic circuits target the medial prefrontal cortex. *bioRxiv*. doi: 10.1101/2021.01.20.427526

Mack, D. R., Barbarello-Andrews, L., and Liu, M. T. (2012). Agitated delirium associated with therapeutic doses of sustained-release bupropion. *Int. J. Clin. Pharm.* 34, 9–12. doi: 10.1007/s11096-011-9587-x

Matsumoto, Y., Fujino, Y., and Furue, H. (2021). Anesthesia and surgery induce a functional decrease in excitatory synaptic transmission in prefrontal cortex neurons, and intraoperative administration of dexmedetomidine does not elicit the synaptic dysfunction. *Biochem. Biophys. Res. Commun.* 572, 27–34. doi: 10.1016/j.bbrc.2021.07.065

Miller, E. K. (2000). The prefrontal cortex and cognitive control. *Nat. Rev. Neurosci.* 1, 59–65. doi: 10.1038/35036228

Miller, E. K., and Cohen, J. D. (2001). An integrative theory of prefrontal cortex function. *Annu. Rev. Neurosci.* 24, 167–202. doi: 10.1146/annurev.neuro.24.1.167

Mitchell, A. S., Sherman, S. M., Sommer, M. A., Mair, R. G., Vertes, R. P., and Chudasama, Y. (2014). Advances in understanding mechanisms of thalamic relays in cognition and behavior. *J. Neurosci.* 34, 15340–15346. doi: 10.1523/JNEUROSCI.3289-14.2014

MMP (2022). *Medical Marijuana Patient Numbers*. Marijuana Policy Project (MPP). Available online at: https://www.mpp.org/

Nakajima, M., and Halassa, M. M. (2017). Thalamic control of functional cortical connectivity. *Curr. Opin. Neurobiol.* 44, 127–131. doi: 10.1016/j.conb.2017.04.001

Parnaudeau, S., Bolkan, S. S., and Kellendonk, C. (2018). The mediodorsal thalamus: an essential partner of the prefrontal cortex for cognition. *Biol. Psychiatry* 83, 648–656. doi: 10.1016/j.biopsych.2017.11.008

Parnaudeau, S., O'neill, P. K., Bolkan, S. S., Ward, R. D., Abbas, A. I., Roth, B. L., et al. (2013). Inhibition of mediodorsal thalamus disrupts thalamofrontal connectivity and cognition. *Neuron* 77, 1151–1162. doi: 10.1016/j.neuron.2013.01.038

Peng, M., Zhang, C., Dong, Y., Zhang, Y., Nakazawa, H., Kaneki, M., et al. (2016). Battery of behavioral tests in mice to study postoperative delirium. *Sci. Rep.* 6, 29874. doi: 10.1038/srep29874

Quinones, G. M., Mayeli, A., Yushmanov, V. E., Hetherington, H. P., and Ferrarelli, F. (2021). Reduced GABA/glutamate in the thalamus of individuals at clinical high risk for psychosis. *Neuropsychopharmacology* 46, 1133–1139. doi: 10.1038/s41386-020-00920-4

Riederer, A. M., Campleman, S. L., Carlson, R. G., Boyer, E. W., Manini, A. F., Wax, P. M., et al. (2016). Acute poisonings from synthetic cannabinoids—50 U.S. Toxicology investigators consortium registry sites, 2010-2015. *MMWR Morb. Mortal. Wkly. Rep.* 65, 692–695. doi: 10.15585/mmwr.mm6527a2

Rikhye, R. V., Wimmer, R. D., and Halassa, M. M. (2018). Toward an integrative theory of thalamic function. *Annu. Rev. Neurosci.* 41, 163–183. doi: 10.1146/annurev-neuro-080317-062144

Rudolph, J. L., and Marcantonio, E. R. (2011). Postoperative delirium: acute change with long-term implications. *Anesth. Analg.* 112, 1202–1211. doi: 10.1213/ANE.0b013e3182147f6d

Sabihi, S., Goodpaster, C., Maurer, S., and Leuner, B. (2021). GABA in the medial prefrontal cortex regulates anxiety-like behavior during the postpartum period. *Behav. Brain Res.* 398, 112967. doi: 10.1016/j.bbr.2020.112967

Sánchez-Bellot, C., and Macaskill, A. F. (2020). Two opposing hippocampus to prefrontal cortex pathways for the control of approach and avoidance behavior. *bioRxiv*. doi: 10.1101/2019.12.18.880831

Shepherd, G. M. G., and Yamawaki, N. (2021). Untangling the cortico-thalamo-cortical loop: cellular pieces of a knotty circuit puzzle. *Nat. Rev. Neurosci.* 22, 389–406. doi: 10.1038/s41583-021-00459-3

Sherman, S. M. (2016). Thalamus plays a central role in ongoing cortical functioning. *Nat. Neurosci.* 19, 533–541. doi: 10.1038/nn.4269

Shi, Z., Mei, X., Li, C., Chen, Y., Zheng, H., Wu, Y., et al. (2019). Postoperative delirium is associated with long-term decline in activities of daily living. *Anesthesiology* 131, 492–500. doi: 10.1097/ALN.0000000000002849

Smucny, J., Carter, C. S., and Maddock, R. J. (2021). Medial prefrontal cortex glutamate is reduced in schizophrenia and moderated by measurement quality: a meta-analysis of proton magnetic resonance spectroscopy studies. *Biol. Psychiatry* 90, 643–651. doi: 10.1016/j.biopsych.2021.06.008

Spellman, T., Rigotti, M., Ahmari, S. E., Fusi, S., Gogos, J. A., and Gordon, J. A. (2015). Hippocampal-prefrontal input supports spatial encoding in working memory. *Nature* 522, 309–314. doi: 10.1038/nature14445

Sun, Q., Li, X., Ren, M., Zhao, M., Zhong, Q., Ren, Y., et al. (2019). A whole-brain map of long-range inputs to GABAergic interneurons in the mouse medial prefrontal cortex. *Nat. Neurosci.* 22, 1357–1370. doi: 10.1038/s41593-019-0429-9

Wen, X., Li, W., Liu, Y., Liu, Z., Zhao, P., Zhu, Z., et al. (2021). Exploring communication between the thalamus and cognitive control-related functional networks in the cerebral cortex. *Cogn. Affect. Behav. Neurosci.* 21, 656–677. doi: 10.3758/s13415-021-00892-y

Wolff, M., Morceau, S., Folkard, R., Martin-Cortecero, J., and Groh, A. (2021). A thalamic bridge from sensory perception to cognition. *Neurosci. Biobehav. Rev.* 120, 222–235. doi: 10.1016/j.neubiorev.2020.11.013

Yan, Z., and Rein, B. (2021). Mechanisms of synaptic transmission dysregulation in the prefrontal cortex: pathophysiological implications. *Mol. Psychiatry* 27, 445–465. doi: 10.1038/s41380-021-01092-3

Zhang, J., Ma, L., Wan, X., Shan, J., Qu, Y., and Hashimoto, K. (2021). (R)-Ketamine attenuates LPS-induced endotoxin-derived delirium through inhibition of neuroinflammation. *Psychopharmacology* 238, 2743–2753. doi: 10.1007/s00213-021-05889-6

Zhong, H., Tong, L., Gu, N., Gao, F., Lu, Y., Xie, R. G., et al. (2017). Endocannabinoid signaling in hypothalamic circuits regulates arousal from general anesthesia in mice. *J. Clin. Invest.* 127, 2295–2309. doi: 10.1172/JCI91038

frontiers | Frontiers in Pharmacology

TYPE Clinical Trial
PUBLISHED 20 December 2022
DOI 10.3389/fphar.2022.991581

OPEN ACCESS

EDITED BY
Zhongcong Xie,
Massachusetts General Hospital and Harvard Medical School, United States

REVIEWED BY
Ali Saffaei,
Shahid Beheshti University of Medical Sciences, Iran
Santosh Kumar Swain,
Siksha O Anusandhan University, India

*CORRESPONDENCE
Jiaming Fan,
fjm19890101@sina.com
Wangping Zhang,
zhang650679@163.com

SPECIALTY SECTION
This article was submitted to Neuropharmacology, a section of the journal Frontiers in Pharmacology

RECEIVED 02 August 2022
ACCEPTED 12 December 2022
PUBLISHED 20 December 2022

CITATION
Li Q, Fan J and Zhang W (2022), Low-dose esketamine for the prevention of emergency agitation in children after tonsillectomy: A randomized controlled study.
Front. Pharmacol. 13:991581.
doi: 10.3389/fphar.2022.991581

Low-dose esketamine for the prevention of emergency agitation in children after tonsillectomy: A randomized controlled study

Qi Li[1], Jiaming Fan[2]* and Wangping Zhang[2]*

[1]Department of Anesthesiology, The Second Affiliated Hospital of Jiaxing University, Jiaxing, China, [2]Department of Anesthesiology, Women and Children's Hospital of Jiaxing University, Jiaxing, China

Background: Emergency agitation is a common postoperative complication in pediatric patients after general anesthesia. The aim of this study was to explore the effects of a low dose of esketamine on emergency agitation in children following tonsillectomy.

Materials and Methods: Eighty children were recruited prospectively to this study and divided into the esketamine group and the control group (40 cases in each group). The induction and maintenance of anesthesia were the same in both groups. At the end of surgery, the esketamine group received 0.25 μg/kg esketamine, while the control group received the same volume of normal saline. The extubation time, time to eye opening, Ramsay sedation scale and time to discharge from the post-anesthesia care unit (PACU) were recorded during post-anesthesia care unit. Postoperative complications, such as emergency agitation, respiratory depression, hypertension, tachycardia, nightmares, nausea, and vomiting, were also recorded.

Results: The incidence of emergency agitation was lower in the esketamine group compared with that in the control group (5% *vs*. 27.5%, $p = 0.006$). The time to eye opening was longer in the esketamine group than in the control group (17.2 ± 2.7 *vs*. 15.5 ± 2.3 min, $p = 0.005$). However, the extubation time and time to discharge from PACU were similar between the two groups.

Conclusion: Low-dose of esketamine decreases the incidence of emergency agitation in children after tonsillectomy without delaying extubation time and increasing the postoperative side effects. (www.chictr.org.cn, registration number: ChiCTR2100054178).

KEYWORDS

esketamine, emergency agitation, children, tonsillectomy, general anesthesia

1 Introduction

Emergence agitation is a well-known phenomenon in children after general anesthesia, (Mohkamkar et al., 2014; Cao et al., 2016), especially in those undergoing adenotonsillectomy. (Fattahi-Saravi et al., 2021). The incidence of emergence agitation varies from 0.25% to 90.5%. (Lee and Sung, 2020). Emergence agitation might cause injury, accidental removal of intravenous cannulation, self-extubation, post-operative wound bleeding, and increase the nursing requirements in the post-anesthesia care unit (PACU).. (Zhu et al., 2021).

Intravenous administration of a subhypnotic dose of midazolam, propofol, and ketamine combined with fentanyl is usually performed to decrease the incidence of emergence agitation in children undergoing sevoflurane anesthesia. (Chen et al., 2010). Although intravenous administration of fentanyl at the end of surgery could reduce the incidence of emergence agitation in children undergoing general anesthesia, it was associated with a prolonged PACU stay and an increased incidence of postoperative nausea or vomiting. (Kim et al., 2017). The literature reported that dexmedetomidine decreased the incidence of emergence agitation in children after general anesthesia, but it was accompanied by delayed extubation time. (Yang et al., 2020).

Ketamine is an antagonist of the N-methyl-D-aspartate receptor. In recent years, it has been used widely in clinical anesthesia, pain management, and resistant depression. (Frey et al., 2019; Salloum et al., 2019). Esketamine is a more potent *S*-isomer of ketamine. Its potency is approximately two times higher than that of ketamine, but with fewer side effects. (Jonkman et al., 2018; Wang et al., 2019). Moreover, esketamine offers a shorter recovery time and orientation recovery time compared with ketamine. (Wang et al., 2019). To date, there have been no studies on the use of esketamine to prevent emergency agitation. Therefore, the present study aimed to investigate the efficacy of esketamine in reducing emergency agitation in children undergoing tonsillectomy.

2 Materials and methods

This study was conducted in accordance with the Declaration of Helsinki and was approved by the Ethical Committee of the Jiaxing Children's Hospital (approval number: 201836, Chairman: Prof L. Xia). Written informed consent was obtained from the guardians of the children (www.chictr.org.cn, registration number: ChiCTR2100054178).

From 1 December 2021 to 1 March 2022, a total of 80 children undergoing tonsillectomy with American Society of Anesthesiologists (ASA) stage I–II, weighing between 10 and 50 kg, and aged from 2 to 7 years were included this study. Children with cardiovascular diseases, psychosis, or mental diseases were excluded. The children were randomly divided into the control group and the esketamine group (40 cases in each group). The investigators, anesthesiologists, surgeons, and nurses were blinded to the group allocation.

The children, who did not receive premedication, were fasted for 8 h. After entering the operating center, venous access was established. The electrocardiogram, pulse oxygen saturation (S_PO_2), non-invasive blood pressure, and heart rate (HR) were monitored. Anesthesia was induced using intravenous fentanyl at 3 μg/kg, propofol at 3 mg/kg, and cis-atracurium at 0.12 mg/kg. Endotracheal intubation was performed under direct laryngoscopy. Subsequently, the lungs were ventilated in the pressure-controlled ventilation mode. The ventilation parameters were set as follows: a driving pressure of 15–18 cmH_2O, a breathing rate of 14–20 breaths/min, an oxygen flow rate of 2 L/min, a fraction of inspired oxygen of 0.5, an inspiratory expiratory ratio of 1:1.5, and a positive end-expiratory pressure of zero.

The driving pressure was adjusted to keep the end-tidal carbon dioxide partial pressure ($P_{ET}CO_2$) between 35 and 45 mmHg. Anesthesia was maintained using 2%–4% sevoflurane to keep the systolic blood pressure within a 20% range of baseline. Anesthetics were stopped 5 min before the end of surgery. The esketamine group received 0.25 mg/kg esketamine (Jiangsu Hengrui pharmaceutical company, Jiangsu, China) at the end of surgery and the control group received the same volume of normal saline, after which all the children were transferred to the PACU. These medications were prepared by nurses who were blinded to the grouping.

The systolic blood pressure (SBP), diastolic blood pressure (DBP), and HR were recorded at 3 min after drug administration. The extubation time, time to eye opening, Ramsay sedation scale (RSS) in the PACU, and time to discharge from the PACU were also noted. The adverse events (emergency agitation, respiratory depression, tachycardia, hypotension, nightmares, nausea, and vomiting) were recorded. The endotracheal tube was extubated when the tidal volumes were >6 ml/kg, S_PO_2 was >96%, and $P_{ET}CO_2$ was <45 mmHg during air inhalation. The standards of discharge from the PACU were as follows: ***a.*** Awake. ***b.*** Air breathing SpO_2 > 94%. *c.* Moving the arms, legs, and head with commands. ***d.*** Breathing with a normal respiratory rate. Respiratory depression was defined as SpO_2 < 94% whilst receiving oxygen and a breathing rate <10 times per minute. Hypertension was defined as an SBP above 20% from the baseline values and tachycardia was defined as an HR above 20% from the baseline values. The children were given 1 mg/kg propofol by intravenous injection if emergency agitation occurred.

The level of sedation was assessed using the Ramsay sedation scale (RSS) (1, patients were anxious, agitated, or restless, or both. 2, patients were cooperative, oriented, and tranquil. 3, patients responded to commands only. 4, patients were asleep but had a brisk response to a light glabellar tap or loud auditory stimulus. 5, patients were asleep with a sluggish response to a light glabellar

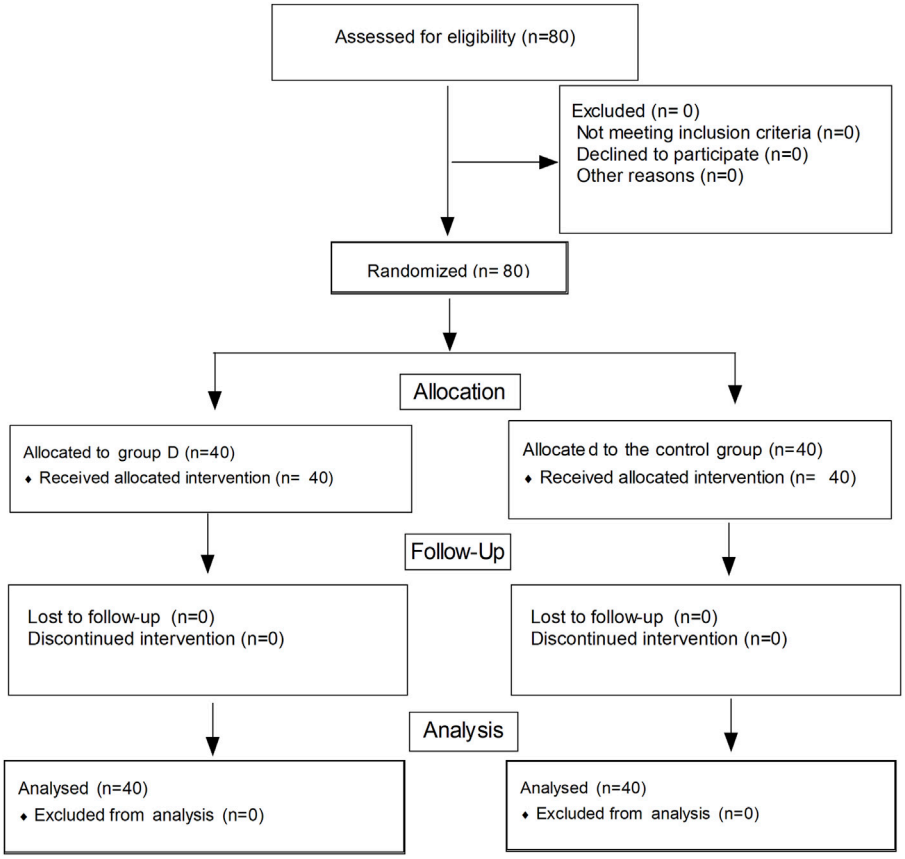

FIGURE 1
Flow diagram of the study.

tap or loud auditory stimulus. 6, patients were asleep and not responsive). Emergency agitation was defined as an RSS value of 1.

2.1 Statistical analysis

In this study, the primary outcome was the incidence of emergency agitation. *A priori* power analysis using two-sided analysis with an α error of 0.05 and a power of 0.8 showed that 32 patients were needed to detect a statistical difference in the incidence of emergency agitation between the two groups for this study. The sample size was increased to 40 to allow for dropout in each group. Data analysis was performed with the SPSS 20.0 statistical software (IBM Corp., Armonk, NY, United States). Data are presented as the mean ± standard deviation. Comparison of the numerical variables between the two groups was performed using a *t*-test for independent samples. The categorical data were compared using a Chi-squared test or Fisher's exact test. *p*-values <0.05 were considered statistically significant.

3 Results

A total of 80 children were enrolled in this trial (Figure 1). There were no significant differences in terms of the age, sex, weight, body mass index, duration of operation, and duration of anesthesia between the two groups ($p > 0.05$) (Table 1). The extubation time and time to discharge from the PACU were similar between the two groups ($p > 0.05$); however, the time to eye opening was longer in the esketamine group than in the control group (17.2 ± 2.7 *vs*.15.5 ± 2.3 min, $p = 0.005$) (Table 1). The SBP and DBP at 3 min after drug administration were similar between the two groups ($p > 0.05$); however, the HR at 3 min after drug administration was greater in the esketamine group than in the control group ($p = 0.042$) (Figure 2).

There were two case of emergency agitation in the esketamine group, while 11 cases of emergency agitation were reported in the control group (5% *vs*. 27.5%, $p = 0.006$). There were no statistical differences in the incidence of respiratory depression, hypotension, tachycardia, nightmare, nausea, and vomiting between the two groups ($p > 0.05$) (Table 2).

TABLE 1 Data of children (n = 40).

Index	Esketaminegroup	Control group	p-Value
Age (year)	4.6 ± 1.0	4.5 ± 1.3	0.622
Gender (male/female)	22/18	21/19	0.823
Weight (kg)	17.2 ± 1.9	16.7 ± 2.1	0.305
Body mass index (kg/m2)	23.4 ± 3.5	23.6 ± 3.2	0.861
Duration of anesthesia (min)	54.9 ± 6.8	56.4 ± 6.3	0.328
Duration of surgery (min)	41.4 ± 7.7	42.4 ± 8.2	0.567
Extubation time (min)	11.5 ± 2.3	10.4 ± 2.4	0.129
Time to eye opening (min)	17.2 ± 2.7	15.5 ± 2.3	0.005
Time to discharge from PACU (min)	40.7 ± 7.8	38.6 ± 7.9	0.223

Data are expressed as the mean +standard deviation or number. PACU: post-anesthesia care unit.

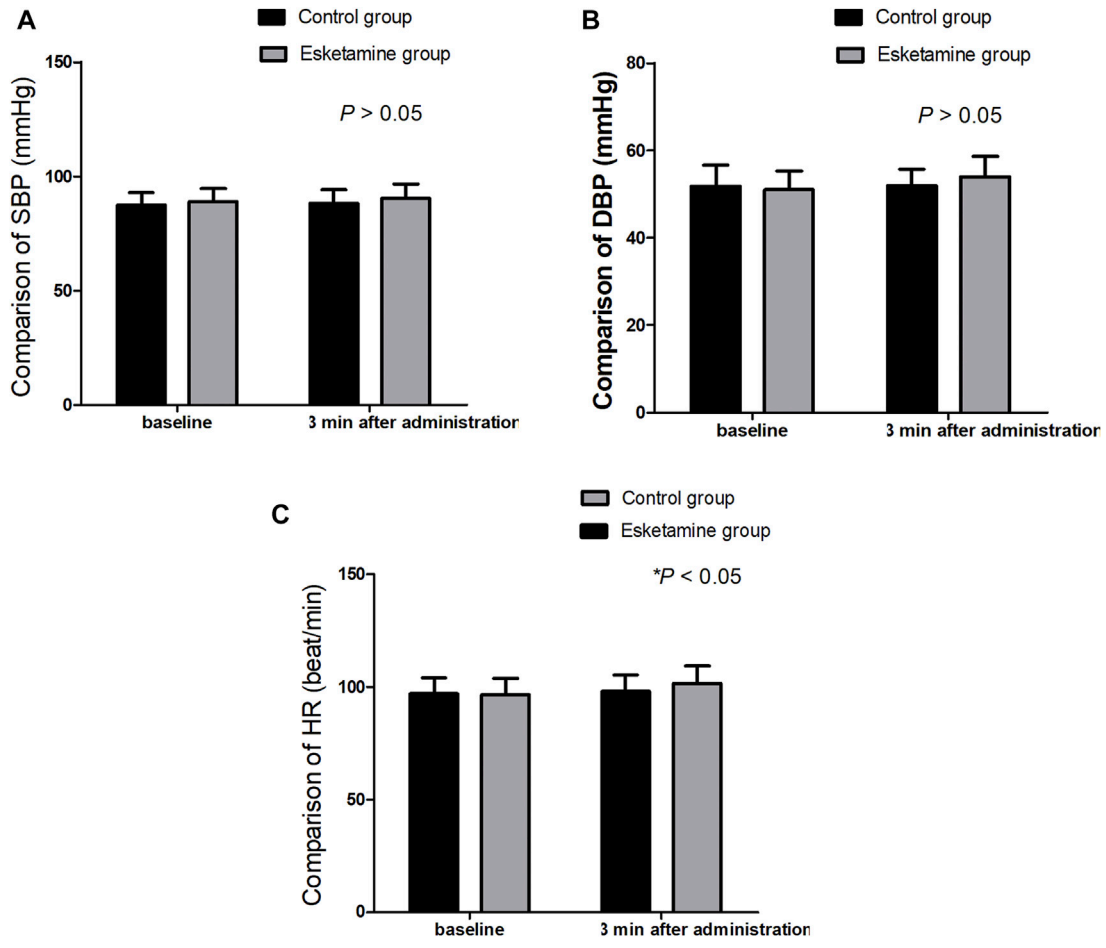

FIGURE 2
(A–C) Comparison of SBP, DBP, and HR between the two groups, *p < 0.05.

TABLE 2 Comparison of side effects in children (n = 40).

Index	Esketamine group	Control group	p-Value
Emergency agitation n)	2 (5%)	11 (27.5%)	0.006
Respiratory depression n)	0	0	—
Hypertension n)	0	0	—
Tachycardia n)	1	0	0.999
Nightmare n)	1	0	0.999
Nausea and vomiting n)	0	1	0.999

Data are expressed as number (percent).

4 Discussion

This study showed that low-dose esketamine reduced the incidence of emergency agitation in children after tonsillectomy without delaying extubation time and increasing postoperative side effects.

Esketamine can produce an analgesic effect by activating the N-methyl-D-aspartate (NMDA) receptor. (Jonkman et al., 2018). In the present study, the incidence of emergency agitation in the PACU was lower in the esketamine group than in the control group. There are many factors related to emergency agitation in patients undergoing general anesthesia, including the use of inhalation anesthetics, rapid recovery, type of surgical procedure, postoperative pain, hypoxia, and airway obstruction. (Kim et al., 2015; Wei et al., 2021). Postoperative pain or discomfort is the main factor in emergency agitation. (Zhong et al., 2018). Esketamine could provide long-term sedation and analgesia, and good sedation and analgesic effects could decrease the incidence of emergency agitation in children after tonsillectomy. Chen, et al. (Chen et al., 2010) reported that low doses of midazolam-fentanyl or propofol-fentanyl were both effective to decrease the incidence of emergency agitation in children undergoing cataract extraction after general anesthesia, without significantly delaying recovery time and time to PACU discharge. Lee, et al. (Lee et al., 2010) found that ketamine was decreased the incidence of emergency agitation in children undergoing tonsillectomy and adenoidectomy after sevoflurane general anesthesia without increasing the extubation time and delivery time from the PACU. Their findings agreed with those of the present study. Ni, et al. (Ni et al., 2015) reported that intravenous dexmedetomidine significantly reduced the incidence of emergency agitation; however, it increased the time to eye-opening and the time to discharge from the PACU.

In the present study, the extubation time and time to discharge from the PACU were similar between the two groups; however, the time to eye opening was longer in the esketamine group compared with that in the control group. A study reported that esketamine countered opioid-induced respiratory depression, (Jonkman et al., 2018), and the clinical dose of esketamine did not cause respiratory depression; therefore, it did not result in prolongation of the extubation time. Low-dose esketamine did not result in extension of the time to discharge from the PACU. This effect was dose-dependent and a high dose of esketamine led to delayed time to PACU discharge. In this study, we found that esketamine increased the time to eye opening, which was associated with the anesthetic effect of esketamine.

No significant differences were observed in the incidence of respiratory depression, hypertension, tachycardia, nightmares, nausea, and vomiting between the two groups in the present study. Hypertension, tachycardia, and nightmares are common side effects of esketamine administration. Low-dose esketamine did not increase the incidence of these side effects. In our study, low-dose esketamine (0.25 mg/kg) did not affect the blood pressure, but led to HR increases ($p < 0.05$).

4.1 Limitations

Nightmares cannot be assessed accurately in children. Furthermore, a large sample study is needed to investigate the side effects of esketamine.

5 Conclusion

This study indicated that low-dose esketamine reduced the incidence of emergency agitation in children undergoing tonsillectomy without delaying extubation time and increasing the postoperative side effects.

Data Availability statement

The original contributions presented in the study are included in the article/supplementary materials, further inquiries can be directed to the corresponding authors.

Ethics statement

The studies involving human participants were reviewed and approved by the Ethical Committee of the Jiaxing Children's Hospital. Written informed consent to participate in this study was provided by the participant's legal guardian/next of kin.

Author contributions

Study design and data analysis: QL, JF and WZ. Patient recruitment and data collection: QL. Writing of the paper: WZ.

Acknowledgments

We would like to thank our colleagues for their valuable contributions.

Conflict of interest

The authors declare that the research was conducted in the absence of any commercial or financial relationships that could be construed as a potential conflict of interest.

Publisher's note

All claims expressed in this article are solely those of the authors and do not necessarily represent those of their affiliated organizations, or those of the publisher, the editors and the reviewers. Any product that may be evaluated in this article, or claim that may be made by its manufacturer, is not guaranteed or endorsed by the publisher.

References

Cao, J. L., Pei, Y. P., Wei, J. Q., and Zhang, Y. Y. (2016). Effects of intraoperative dexmedetomidine with intravenous anesthesia on postoperative emergence agitation/delirium in pediatric patients undergoing tonsillectomy with or without adenoidectomy: A CONSORT-prospective, randomized, controlled clinical trial. *Med. Baltim.* 95 (49), e5566. doi:10.1097/MD.0000000000005566

Chen, J., Li, W., Hu, X., and Wang, D. (2010). Emergence agitation after cataract surgery in children: A comparison of midazolam, propofol and ketamine. *Paediatr. Anaesth.* 20 (9), 873–879. doi:10.1111/j.1460-9592.2010.03375.x

Fattahi-Saravi, Z., Jouybar, R., Haghighat, R., and Asmarian, N. (2021). Comparison of the effect of ketamine, ketamine-midazolam and ketamine-propofol on post-tonsillectomy agitation in children. *Malays J. Med. Sci.* 28 (5), 72–81. doi:10.21315/mjms2021.28.5.7

Frey, T. M., Florin, T. A., Caruso, M., Zhang, N., Zhang, Y., and Mittiga, M. R. (2019). Effect of intranasal ketamine vs fentanyl on pain reduction for extremity injuries in children: The PRIME randomized clinical trial. *JAMA Pediatr.* 173 (2), 140–146. doi:10.1001/jamapediatrics.2018.4582

Jonkman, K., van Rijnsoever, E., Olofsen, E., Aarts, L., Sarton, E., van VelzenM., et al. (2018). Esketamine counters opioid-induced respiratory depression. *Br. J. Anaesth.* 120 (5), 1117–1127. doi:10.1016/j.bja.2018.02.021

Kim, H. J., Kim, D. K., Kim, H. Y., Kim, J. K., and Choi, S. W. (2015). Risk factors of emergence agitation in adults undergoing general anesthesia for nasal surgery. *Clin. Exp. Otorhinolaryngol.* 8 (1), 46–51. doi:10.3342/ceo.2015.8.1.46

Kim, N., Park, J. H., Lee, J. S., Choi, T., and Kim, M. S. (2017). Effects of intravenous fentanyl around the end of surgery on emergence agitation in children: Systematic review and meta-analysis. *Paediatr. Anaesth.* 27 (9), 885–892. doi:10.1111/pan.13181

Lee, S. J., and Sung, T. Y. (2020). Emergence agitation: Current knowledge and unresolved questions. *Korean J. Anesthesiol.* 73 (6), 471–485. doi:10.4097/kja.20097

Lee, Y. S., Kim, W. Y., Choi, J. H., Son, J. H., Kim, J. H., and Park, Y. C. (2010). The effect of ketamine on the incidence of emergence agitation in children undergoing tonsillectomy and adenoidectomy under sevoflurane general anesthesia. *Korean J. Anesthesiol.* 58 (5), 440–445. doi:10.4097/kjae.2010.58.5.440

Mohkamkar, M., Farhoudi, F., Alam-Sahebpour, A., Mousavi, S. A., Khani, S., and Shahmohammadi, S. (2014). Postanesthetic emergence agitation in pediatric patients under general anesthesia. *Iran. J. Pediatr.* 24 (2), 184–190.

Ni, J., Wei, J., Yao, Y., Jiang, X., Luo, L., and Luo, D. (2015). Effect of dexmedetomidine on preventing postoperative agitation in children: A meta-analysis. *PLoS One* 10 (5), e0128450. doi:10.1371/journal.pone.0128450

Salloum, N. C., Fava, M., Freeman, M. P., Flynn, M., Hoeppner, B., Hock, R. S., et al. (2019). Efficacy of intravenous ketamine treatment in anxious versus nonanxious unipolar treatment-resistant depression. *Depress. Anxiety* 36 (3), 235–243. doi:10.1002/da.22875

Wang, J., Huang, J., Yang, S., Cui, C., Ye, L., Wang, S. Y., et al. (2019). Pharmacokinetics and safety of esketamine in Chinese patients undergoing painless gastroscopy in comparison with ketamine: A randomized, open-label clinical study. *Drug Des. Devel Ther.* 13, 4135–4144. doi:10.2147/DDDT.S224553

Wei, B., Feng, Y., Chen, W., Ren, D., Xiao, D., and Chen, B. (2021). Risk factors for emergence agitation in adults after general anesthesia: A systematic review and meta-analysis. *Acta Anaesthesiol. Scand.* 65 (6), 719–729. doi:10.1111/aas.13774

Yang, X., Hu, Z., Peng, F., Chen, G., Zhou, Y., Yang, Q., et al. (2020). Effects of dexmedetomidine on emergence agitation and recovery quality among children undergoing surgery under general anesthesia: A meta-analysis of randomized controlled trials. *Front. Pediatr.* 8, 580226. doi:10.3389/fped.2020.580226

Zhong, H. Y., Deng, X. B., and Wang, Z. (2018). Effects of fascia iliaca compartment block combined with general laryngeal mask airway anesthesia in children undergoing femoral fracture surgery: A randomized trial. *J. Pain Res.* 11, 2821–2826. doi:10.2147/JPR.S177122

Zhu, W., Sun, J., He, J., Zhang, W., and Shi, M. (2021). A randomized controlled study of caudal dexmedetomidine for the prevention of postoperative agitation in children undergoing urethroplasty. *Front. Pediatr.* 9, 658047. doi:10.3389/fped.2021.658047

frontiers | Frontiers in Aging Neuroscience

TYPE Original Research
PUBLISHED 05 January 2023
DOI 10.3389/fnagi.2022.1037904

OPEN ACCESS

EDITED BY
Yingwei Wang,
Huashan Hospital of Fudan University, China

REVIEWED BY
Diansan Su,
Shanghai Jiao Tong University, China
Yanlin Bi,
Qingdao Municipal Hospital, China

*CORRESPONDENCE
Yuan Le
leyuanxy@csu.edu.cn

SPECIALTY SECTION
This article was submitted to Neurocognitive Aging and Behavior, a section of the journal Frontiers in Aging Neuroscience

RECEIVED 06 September 2022
ACCEPTED 24 November 2022
PUBLISHED 05 January 2023

CITATION
Hu L, Luo M, Huang H, Wu L, Ouyang W, Tong J and Le Y (2023) Perioperative probiotics attenuates postoperative cognitive dysfunction in elderly patients undergoing hip or knee arthroplasty: A randomized, double-blind, and placebo-controlled trial.
Front. Aging Neurosci. 14:1037904.
doi: 10.3389/fnagi.2022.1037904

Perioperative probiotics attenuates postoperative cognitive dysfunction in elderly patients undergoing hip or knee arthroplasty: A randomized, double-blind, and placebo-controlled trial

Lin Hu[1,2], Manli Luo[1,2], Huifan Huang[1,2], Lanping Wu[1,2], Wen Ouyang[1,2], Jianbin Tong[1,2] and Yuan Le[1,2]*

[1]Department of Anesthesiology, The Third Xiangya Hospital, Central South University, Changsha, China, [2]Hunan Province Key Laboratory of Brain Homeostasis, The Third Xiangya Hospital, Central South University, Changsha, China

Background: Postoperative cognitive dysfunction (POCD) is a common complication in elderly patients following surgery. The preventive and/or treatment strategies for the incidence remain limited.

Objective: This study aimed to investigate the preventive effect of perioperative probiotic treatment on POCD in elderly patients undergoing hip or knee arthroplasty.

Methods: After obtaining ethical approval and written informed consent, 106 patients (age ≥60 years) were recruited, who scheduled elective hip or knee arthroplasty, from 16 March 2021 to 25 February 2022 for this randomized, double-blind, and placebo-controlled trial. They were randomly assigned with a 1:1 ratio to receive either probiotics or placebo treatment (four capsules, twice/day) from hospital admission until discharge. Cognitive function was assessed with a battery of 11 neuropsychological tests on the admission day and the seventh day after surgery, respectively.

Results: A total of 96 of 106 patients completed the study, and their data were finally analyzed. POCD occurred in 12 (26.7%) of 45 patients in the probiotic group and 29 (56.9%) of 51 patients in the placebo group (relative risk [RR], 0.47 [95% confidence interval [CI], 0.27 to 0.81]; $P = 0.003$). Among them, mild POCD occurred in 11 (24.4%) in the probiotic group and 24 (47.1%) in the placebo group (RR, 0.52 [95% CI, 0.29 to 0.94]; $P = 0.022$). No significant difference in severe POCD incidence was found between the two groups ($P = 0.209$). Compared with the placebo group, the verbal memory domain cognitive function was mainly improved in the probiotic group.

Conclusion: Probiotics may be used perioperatively to prevent POCD development and improve verbal memory performance in elderly patients receiving hip or knee arthroplasty.

Clinical trial registration: www.chictr.org.cn, identifier: ChiCTR2100045620.

KEYWORDS

probiotics, postoperative cognitive dysfunction (POCD), elderly patients, cognitive function, hip or knee arthroplasty

1. Introduction

Postoperative cognitive dysfunction (POCD), characterized by memory, attention, and executive ability impairment (Hood et al., 2018), is highly prevalent in the elderly following orthopedic surgery and is associated with poor clinical outcomes and worst quality of life (Moller et al., 1998; Needham et al., 2017; Deiner et al., 2021). Preventive and/or treatment strategies for POCD development included cognitive and physical exercise (O'Gara et al., 2020; Duan et al., 2022), appropriate depth of anesthesia (Chan et al., 2013), goal-directed fluid therapy (Zhang et al., 2018), effective postoperative analgesia (Kristek et al., 2019), and pharmacologic interventions [e.g., edaravone (Zhang et al., 2020), methylene blue (Deng et al., 2021), dexmedetomidine (Su et al., 2016), and stains (Alam et al., 2018)]. The incidence of POCD in orthopedic patients remains as high as 24.6–75% (Rodriguez et al., 2005; Koch et al., 2007; Ji et al., 2013; Li et al., 2019); thus studying new preventive strategies is urgently needed.

Probiotics are widely used in public and clinically for general health supplements and disease conditions to improve immune function and brain function (Mohajeri et al., 2018; Suez et al., 2019). Recent studies have performed a new insight into the effect of probiotics on postoperative brain function because probiotics have the potential anti-inflammatory capabilities (Zhan et al., 2018; Jiang et al., 2019) and reduce levels of systemic pro-inflammatory cytokines (such as IL-1β, TNF-α, IL-6, IL-10, and IFN-γ) (Schachter et al., 2018; Choi et al., 2020). Our previous study showed that perioperative probiotic treatment has an anti-inflammatory effect and could prevent postoperative cognitive impairment development assessed with Mini-Mental State Examination (MMSE) in the elderly following non-cardiac surgery (Wang et al., 2021). However, MMSE is a broad screening tool and is commonly criticized for its low sensitivity in the diagnosis of POCD. The score of MMSE can be influenced by the education level, leading to false positive indications when patients with a low level of education, or false negative indications when patients with a high level of education (Newman et al., 2007; Malek-Ahmadi et al., 2012). A neuropsychological test battery is wildly recommended to improve study quality (Evered et al., 2018; Borchers et al., 2021). In this study, we further carried out this randomized, double-blind, placebo-controlled trial to investigate the preventive effect of perioperative administration of probiotics on POCD incidence in the elderly undergoing hip or knee arthroplasty using comprehensive neuropsychological battery tests as a cognitive evaluation tool.

2. Methods

2.1. Study design and participants

This prospective trial protocol was established with the compliance of the CONSORT Statement, approved (R21010) by the Ethics Committee, Third Xiangya Hospital, Central South University, Changsha, China, and registered in the Chinese Clinical Trial Registry (ChiCTR2100045620). After the written informed consent was obtained, elderly patients (age ≥60 years) admitted to the Department of Orthopedics, Third Xiangya Hospital, from 16 March 2021 to 25 February 2022, who met the inclusion criteria, were enrolled and randomly assigned to receive either probiotics or placebo (four capsules, twice/day) during the whole hospitalization period. The incidence of POCD was evaluated by a battery of 11 neuropsychological tests on the admission day and the seventh day after surgery.

Patients, who had no history of immune system diseases, psychiatric diseases, and neurodegenerative diseases and were scheduled for elective hip or knee arthroplasty, were eligible to be enrolled in this trial (Figure 1). Patients were excluded when they met any of the following criteria: (1) history of communication disorders (such as severe impairment in speaking, hearing, and vision); myocardial infarctions or poor cardiac function; cerebral hemorrhage, cerebral infarction, brain tumor, and stroke; (2) received more than one surgery during hospital stay; (3) used antibiotics, probiotics, or gastro dynamic drug within 10 days before admission; (4) used complete postoperative parenteral nutrition; (5) mental illness or family history of mental illness; alcoholic or drug addicts; (6) postoperative hospital stay duration was <7 days; (7) participating in other clinical trials; refuse to join the study; not cooperative with the treatment; and (8) for any other reason that is not suitable for this study.

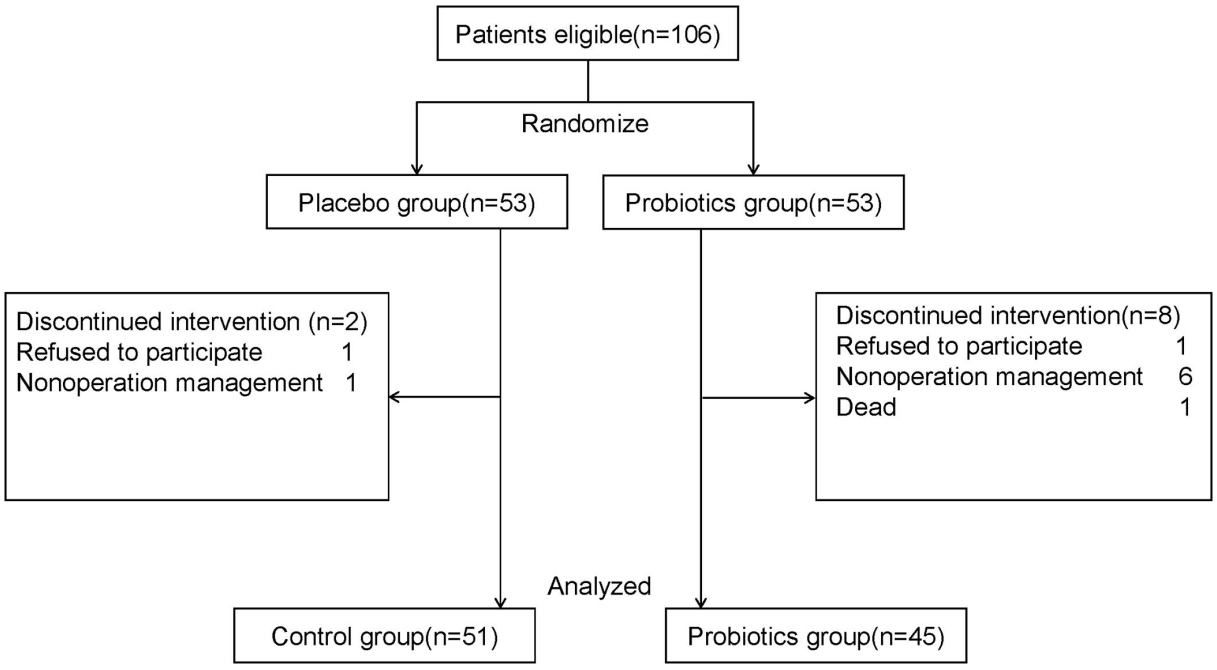

FIGURE 1
Flow chart of study: Participant eligibility and enrollment are performed.

2.2. Blinding and treatment allocation

Patients were randomly divided into the probiotic or placebo groups with concealed allocation by generating random numbers in a 1:1 ratio with SPSS 25.0. Patients and clinicians including surgeons and anesthesiologists and all researchers for pre- and postoperative assessments and data collection were blinded with the trial protocol. However, doctors, who closely looked after patients, can request the unmasking of the treatment assignment or terminate patients' participation if the condition of patients was needed.

2.3. Interventions

Patients were randomly assigned to receive either probiotic or placebo treatment (four capsules, twice a day) during the whole hospitalization period and underwent a battery of 11 neuropsychological tests on the admission day and the seventh day after surgery. The probiotic group received four probiotic capsules (0.84 g) twice a day, from hospital admission until discharge. Each probiotic capsule (BIFICO, Sine Pharmaceuticals, Shanghai, China) contained *Bifidobacterium longum* ($>10^7$ colony-forming unit [CFU]/210mg), *Lactobacillus acidophilus* ($>10^7$ CFU/210 mg), and *Enterococcus faecalis* ($>10^7$ CFU/210 mg). The placebo capsule (also provided by Sine Pharmaceuticals) contained all ingredients except probiotics with an identical size, shape, and smell as probiotic capsules were given to patients in the placebo group in the same way during hospitalization. To fully guarantee the medical treatment and safety of the patients, we did not limit the other clinical treatments of patients.

2.4. Cognitive function assessment

All patients were subjected to cognitive assessments with a battery of 11 neuropsychological tests on the hospital administration (baseline) and the seventh day after surgery by the same assessor who was specifically trained by psychiatrists. The battery tests included the following: Hopkins verbal learning test-revised, delayed recall test, and discrimination index for verbal memory (Lacritz and Cullum, 1998); brief visuospatial memory test-revised (BVMT-R), BVMT-R delayed recall test, and BVMT-R discrimination index for visuospatial memory (Tam and Schmitter-Edgecombe, 2013); number connection test and Benton judgment of line orientation for visuospatial abilities and spatial orientation (Amodio et al., 1999; Boeve et al., 2012); digit span test for attention (Leung et al., 2011); digit symbol substitution test and verbal fluency test for executive function (Jaeger, 2018; Sutin et al., 2019; Juan et al., 2022).

Mild POCD and severe POCD were defined as a decrease of 1–2 standard deviation (SD) or more than 2 SD of two or more neuropsychological tests from the admission baseline to

TABLE 1 Basic characteristics.

	Placebo ($n = 51$)	Probiotics ($n = 45$)	*P*-value
Age (yr)	70 (64,75)	68 (65,73.5)	0.64
Sex			0.55
Male	20 (39.2)	15 (33.3)	
Female	31 (60.8)	30 (66.7)	
Height (cm)	159.76 ± 8.58	159.69 ± 7.11	0.96
Weight (kg)	61.16 ± 10.30	59.90 ± 9.20	0.53
BMI (kg/m^2)	23.97 ± 3.69	23.46 ± 3.06	0.47
Statins	1 (1.96)	2 (4.4)	0.91
Type of operation			0.61
Knee arthroplasty	23 (45.1)	18 (40)	
Hip arthroplasty	28 (54.9)	27 (60)	
ASA classification			0.203
II	26 (51.0)	16 (35.6)	
III	25 (49.0)	28 (62.2)	
IV	0	1 (2.2)	
Education			0.132
Illiteracy	4 (7.8)	7 (15.6)	
Elementary school	21 (41.2)	15 (33.3)	
Middle school	13 (25.5)	5 (11.1)	
High school	11 (21.6)	12 (26.7)	
University	2 (3.9)	6 (13.3)	

BMI, body mass index; ASA, American Society of Anesthesiologists. All data are presented as number (%), median (first quartile, third quartile), or mean ± SD.

the seventh day after surgery (Sachdev et al., 2014; Borchers et al., 2021). The specific value of the standard deviation is shown in Supplementary Table S1. The change scores of each neuropsychological test were calculated by subtracting the postoperative score from the preoperative score, except for the number connection test in which the change scores were defined as a postoperative score minus the baseline score.

2.5. Outcomes and data collection

The primary outcome was the incidence of POCD on the seventh day after surgery. The secondary outcomes included the length of hospital stay, the incidence of hospital death, and 30-day post-hospital death.

The patients' clinical characteristics including laboratory measurements and parameters during anesthesia and surgery including demographics, such as age, sex, height, weight, education, body mass index (BMI), type of operation, American Society of Anesthesiologists (ASA) classification, intraoperative blood loss, type of anesthesia, length of operation, total intraoperative infusion, and type of antibiotics, were collected.

2.6. Sample size

The sample size was determined assuming a POCD rate of 40% in the placebo group and 20% in the probiotic group. The POCD rate of 40% in the control group was based on previous studies (Rodriguez et al., 2005; Wu et al., 2018). Given a significance set at the level of 0.5, power at 70%, and a loss to follow-up rate of 10%, a total of 106 patients ($n_1 = n_2 = 53$) are required to detect a difference, according to the formula as follows:

$$n_1 = n_2 = \frac{\left[Z_\alpha\sqrt{2\bar{p}\left(1-\bar{p}\right)}+Z_\beta\sqrt{p_1\left(1-p_1\right)+p_2\left(1-p_2\right)}\right]^2}{\left(p_1-p_2\right)^2}$$

n_1 and n_2 represent the sample size of two groups, Z_α and Z_β represent the standard normal deviate values of α and β, and P_1 and P_2 represent the incidence of two groups, $\overline{P} = (P_{1+} P_2)/2$.

2.7. Statistical analyses

Normality was tested with the Shapiro–Wilk test. Patients' general characteristics were presented as mean ± standard deviation (SD), or number and percentage, or the median and interquartile range wherever appropriate. Quantitative data with a normal distribution were presented as mean ± standard deviation (SD), or otherwise as the median and interquartile range. Qualitative variables were analyzed with Pearson's chi-square test or Fisher's exact test, and quantitative data were analyzed with a *t*-test or Mann–Whitney U-test where appropriate. The per-protocol (PP) population consisted of all patients who completed the study according to the protocol (Seino et al., 2014). The primary analysis was based on the PP population. The intention-to-treat (ITT) analyses included all randomized patients (Supplementary Tables S2–S6) (Sun et al., 2018). The missing data were calculated using the last observation carried forward imputation method (Lv et al., 2015). All statistical analyses were performed with SPSS software (version 25.0, SPSS, Chicago, United States).

3. Results

3.1. General characteristics of patients studied

A total of 106 patients were enrolled and randomly assigned to receive either probiotic ($n = 53$) or placebo ($n = 53$) treatment; of those, two patients (2 of 53[3.7%] in the placebo group) and eight patients (8 of 53[15.1%] in the probiotic group) were excluded for various reasons, including refusal to continue participating or cancelation of operations, or one death in the probiotic group; the data from 96 patients were included in the

TABLE 2 Results of neuropsychological assessment at baseline.

	Placebo ($n = 51$)	Probiotics (n =45)	*P*-value
HVLT-R	10.02 ± 3.11	9.29 ± 3.79	0.30
HVLT-R delayed recall test	2 (1,3)	2 (0,3.5)	0.78
HVLT-R discrimination index	20 (18,22)	20 (17.5,22)	0.78
BVMT-R	6 (3,10)	5 (3.5,11)	0.99
BVMT-R delayed recall test	2 (1,3)	2 (1,4)	0.79
BVLT-R discrimination index	11 (10,12)	10 (10,12)	0.10
Number connection test	431 (360,502)	427 (322,534)	0.83
Benton judgment of line orientation	14 (12,16)	14 (12,15)	0.57
Digit span test	16.29 ± 3.05	16.31 ± 3.92	0.98
Digit Symbol Substitution Test	16 (11,22)	15 (12,24)	0.87
Verbal fluency test	39.84 ± 10.67	39.33 ± 11.41	0.82

HVLT-R, Hopkins verbal learning test-revised; BVMT-R, brief visuospatial memory test-revised. All data are presented as number (%), median (first quartile, third quartile), or mean ± SD.

final data analysis ($n = 51$ in the placebo group; $n = 45$ in the probiotic group) (Figure 1). There were no statistical differences in the demographics and clinical characteristics of patients (Table 1) and their baseline scores of neuropsychological tests (Table 2) between the two groups.

3.2. Parameters during anesthesia and surgery

Parameters during anesthesia and surgery, including operating time, intraoperative infusion volume, intraoperative blood loss, type of anesthesia, postoperative analgesia regime, perioperative dexmedetomidine use, and intraoperative and postoperative antibiotic treatment, were not statistically different between the placebo and probiotic groups ($P > 0.05$, Table 3).

3.3. Probiotics decreased the incidence of POCD following surgery

Postoperative cognitive dysfunction occurred in 12 (26.7%) of 45 patients in the probiotic group and 29 (56.9%) of 51 patients in the placebo group (RR, 0.47 [95% CI, 0.27 to 0.81]; $P = 0.003$, Table 4). Among them, mild POCD occurred in 11 (24.4%) in the probiotic group and 24 (47.1%) in the placebo group (RR, 0.52 [95% CI, 0.29 to 0.94]; $P = 0.022$, Table 4). No significant differences in severe POCD incidence were found between the two groups ($P = 0.209$). The mild or severe decline of score mainly occurred in the Hopkins verbal learning test-revised test, Hopkins verbal learning test-revised delayed recall test, and Hopkins verbal learning test-revised discrimination index test in two groups (Table 5).

3.4. Probiotics improve performance in verbal tests

To determine which domain of brain function was mainly improved by probiotics, we further compared the incidence of mild and severe decline in each neuropsychological test between the probiotic and placebo groups. The result showed that compared to the placebo group, the incidence of the mild decline of the Hopkins verbal learning test-revised test (11.1 vs. 33.3%, $P = 0.01$) and the Hopkins verbal learning test-revised delayed recall test (13.3 vs. 39.2%, $P = 0.004$) in the probiotic group was significantly lower (Table 5). The incidence of severe decline of the Hopkins verbal learning test-revised test discrimination index in the probiotic group was also lower than that in the placebo group (2.2 vs. 17.6%, $P = 0.018$). These results suggested that probiotics may improve performance mainly in verbal memory.

3.5. Other clinical outcomes

The length of hospital stays, the incidence of hospital death and 30-day post-hospital death, the level of C reactive protein and leukocytes, and the neutrophil percentage did not differ significantly between the placebo and probiotic groups ($P > 0.05$, Table 6).

4. Discussion

In the current randomized, double-blind, and placebo-controlled trial, perioperative probiotic treatment significantly reduced the incidence of POCD in patients who underwent elective hip or knee arthroplasty, which is in line with our previous study of the preventive effect of probiotics on POCD

TABLE 3 Parameters during anesthesia and surgery.

	Placebo ($n = 51$)	Probiotics ($n = 45$)	*P*-value
Intraoperative blood loss (ml)	100 (50,200)	100 (50,200)	0.06
Total intra-operative infusion (ml)	1,200 (1,100, 1,700)	1,300 (1,050,1,700)	0.69
Dexmedetomidine	15	12	0.77
Type of anesthesia			0.36
intravertebral	27 (52.9)	28 (62.2)	
General	24 (47.1)	17 (37.8)	
Length of operation (h)	120.0 (110.0,155.0)	125.00 (95.0,145.0)	0.74
Intra-operative antibiotic			1
β-lactam	47 (92.2%)	42 (93.3%)	
Quinolones	1 (1.1%)	1 (0.9%)	
Polypeptide	3 (2.7%)	2 (2.3%)	
Postoperative antibiotic			0.87
β-lactam	47 (92.2%)	40 (88.9%)	
Quinolones	1 (2.0%)	2 (4.4%)	
Polypeptide	3 (5.9%)	3 (6.7%)	
Postoperative analgesia regime			0.21
Sufentanil	30 (58.8%)	32 (71.1%)	
Sufentanil and dezocine	21 (41.2)	13 (28.9%)	

All data are presented as number (%), median (first quartile, third quartile), or mean ± SD.

TABLE 4 Probiotics decrease the incidence of POCD in elderly patients after joint arthroplasty.

Incidence of cognitive impairment, No./Total (%)	Placebo ($n = 51$)	Probiotics ($n = 45$)	RR (95% CI)	*P*-value
Total	29/51 (56.9)	12/45 (26.7)	0.47 (0.27–0.81)	0.003**
Mild	24/51 (47.1)	11/45 (24.4)	0.52 (0.29–0.94)	0.022*
Severe	5/51 (9.8)	1/45 (2.2)	0.23 (0.03–1.87)	0.209

All data are presented as number (%), median (first quartile, third quartile), or mean ± SD; *$p < 0.5$, **$p < 0.01$.

development assessed with MMSE (Wang et al., 2021). The length of hospital stays, the incidence of hospital death and 30-day post-hospital death, the level of C reactive protein, and blood cell counts were not significantly different between the placebo and probiotic groups. Furthermore, ITT analyses yielded the same conclusions (Supplementary Tables S2–S6). Our study suggests that perioperative probiotic supplements may be potential strategies for preventing POCD development in elderly patients.

Previous studies reported that perioperative peripheral inflammatory responses act as a major mechanism in the pathogenesis of POCD *via* inducing neuroinflammation and, as a result, damaging synapses connectivity (Tanabe et al., 2020; Zhu et al., 2021; Chen et al., 2022) and triggering cognitive decline. Limiting perioperative peripheral inflammatory responses may significantly alleviate POCD in the pre-clinical setting (Cibelli et al., 2010; Terrando et al., 2010). Pharmacologic interventions such as anti-inflammatory drugs, dexmedetomidine (Su et al., 2016), and statins (Alam et al., 2018) have also been reported to have certain effects in preventing POCD clinically. However, preventing POCD remains a clinical challenge. Accumulating evidence showed that gut microbial dysbiosis can affect peripheral inflammation (Fung et al., 2017), the pathogenesis of psychological diseases (Cryan et al., 2019), neurodegenerative diseases (Sun and Shen, 2018), and cognitive impairment following surgery (Xu et al., 2020). Probiotic supplements can significantly alleviate gut microbial dysbiosis and its related pathological effects (O'Mahony et al., 2005; Chunchai et al., 2018). Previous studies also demonstrated that gut microbial dysbiosis promoted peripheral inflammatory response *via* damaging the intestinal wall, changing peripheral metabolites' levels, and modulating HPA axis response (Fung et al., 2017), while probiotic supplements negated all these changes effectively (Suez et al., 2019; Juan et al., 2022). It has been reported that antibiotic administration affects the intestinal microbiota (Dethlefsen and Relman, 2011), which may result

TABLE 5 Incidence of mild and severe decline in each neuropsychological test in different groups.

Incidence of mild and severe decline, No./Total (%)	Mild decline			Major decline		
	Placebo ($n = 51$)	Probiotics ($n = 45$)	*P*-value	Placebo ($n = 51$)	Probiotics ($n = 45$)	*P*-value
HVLT-R	17/51 (33.3)	5/45 (11.1)	0.01*	2/51 (3.9)	1/45 (2.2)	1.000
HVLT-R delayed recall test	20/51 (39.2)	6/45 (13.3)	0.004**	0	0	
HVLT-R discrimination index	8/51 (15.7)	3/45 (6.7)	0.166	9/51 (17.6)	1/45 (2.2)	0.018*
BVMT-R	6/51 (11.8)	5/45 (11.1)	0.920	0	0	
BVMT-R delayed recall test	9/51 (17.6)	7/45 (15.6)	0.784	1/51 (2.0)	1/45 (2.2)	1.000
BVLT-R discrimination index	6/51 (11.8)	4/45 (8.9)	0.746	5/51 (9.8)	3/45 (6.7)	0.719
Number connection test	0	1/45 (2.2)	0.469	0	0	
Benton judgment of line orientation	9/51 (17.6)	7/45 (15.6)	0.784	1/51 (2.0)	0	1.000
Digit span test total	4/51 (7.8)	3/45 (6.7)	1.000	1/51 (2.0)	1/45 (2.2)	1.000
Digit symbol substitution test	4/51 (7.8)	2/45 (4.4)	0.681	0	0	
Verbal fluency test	6/51 (11.8)	6/45 (13.3)	0.817	5/51 (9.8)	0	0.058

HVLT-R, Hopkins verbal learning test-revised; BVMT-R, brief visuospatial memory test-revised. All data are presented as number (%), median (first quartile, third quartile), or mean ± SD; *$p < 0.5$, **$p < 0.01$.

TABLE 6 Other clinical outcomes.

	Placebo ($n = 51$)	Probiotics ($n = 45$)	*P*-value
Length of hospital stays (d)	13 (9,15)	11 (10,14)	0.46
Incidence of hospital death	0	0	1
Incidence of 30-days post-hospital death	0	0	1
Leukocyte ($x10^9$/L)			
Baseline	6.28 (4.56,7.96)	6.05 (5.28,7.24)	0.88
Postoperative day 1	9.95 (2.90)	9.85 (2.55)	0.86
C reactive protein (mg/L)			
Baseline	5.00 (5.00,16.8)	6.64 (5.00,41.97)	0.23
Postoperative day 1	52.11 (22.97,64.19)	47.97 (30.97,77.65)	0.89
Neutrophils (%)			
Baseline	62.61 (11.80)	63.47 (13.20)	0.74
Postoperative day 1	81.50 (78.10,87.40)	81.00 (78.50,87.85)	0.85
Neutrophil count ($x10^9$/L)			
Baseline	3.91 (2.78,5.86)	4.00 (3.02,5.23)	0.83
Postoperative day 1	8.19 (2.76)	8.12 (2.33)	0.89

All data are presented as number (%), median (first quartile, third quartile), or mean ± SD.

in antibiotic-related diarrhea and intestinal complications, such as *Clostridium difficile*-related colitis (De La Cochetière et al., 2005). To exclude the effects of antibiotics on the composition of gut microbiota, subjects who reported antibiotics treatments 10 days before admission were excluded (Wang et al., 2021). No differences were found with respect to the type of intraoperative antibiotic and the type of postoperative antibiotic between the two groups. In this study, we found that perioperative probiotic supplements significantly reduced the incidence of POCD in elderly patients, which further supports our previous findings (Wang et al., 2021) and provides a new strategy for preventing POCD in elderly patients. Further mechanistic investigation showed that perioperative probiotic supplements accelerated the postoperative decrease of inflammatory cytokines and glucocorticoids in peripheral blood (Wang et al., 2021). It is likely that probiotic supplements offered multi-benefits to our surgical patients, and the underlying mechanisms need to be studied further.

Our study had several limitations. First, as a single-center study with a small sample size and simple surgical population, the enrolled patients may not fully represent the patient population. Second, long-term follow-up was not

done, and hence whether the treatment improves long-term outcomes remain unknown. Third, the underlying mechanism for the prevention of POCD using probiotic supplements remains elusive.

5. Conclusion

Our study indicated that a convenient perioperative supplement of probiotics can effectively mitigate postoperative cognitive impairment and improve performance mainly in verbal memory in elderly patients following hip or knee arthroplasty. Furthermore, a large sample-size trial is needed before the strategy can be used clinically to tackle the development of POCD.

Data availability statement

The raw data supporting the conclusions of this article will be made available by the authors, without undue reservation.

Ethics statement

The studies involving human participants were reviewed and approved by the Ethical Committee of the Third Xiangya Hospital of Central South University, China. The patients/participants provided their written informed consent to participate in this study.

Author contributions

YL designed the study. LH, ML, HH, and LW conceived the original data. LH and HH performed the statistical analysis. LH wrote the manuscript. YL, WO, and JT reviewed the manuscript. All authors agree to be accountable for the content of the work.

Funding

This work was supported by the National Natural Science Foundation of China (81771169, 82271235, and 81971028) and the Natural Science Foundation of Hunan Province (2021JJ31008).

Acknowledgments

We authors thank Prof. Daqing Ma, MD, PhD, FRCA, MAE for his critical comments during manuscript preparation. We are grateful to all the participating patients and their families for their contributions during the study.

Conflict of interest

The authors declare that the research was conducted in the absence of any commercial or financial relationships that could be construed as a potential conflict of interest.

Publisher's note

All claims expressed in this article are solely those of the authors and do not necessarily represent those of their affiliated organizations, or those of the publisher, the editors and the reviewers. Any product that may be evaluated in this article, or claim that may be made by its manufacturer, is not guaranteed or endorsed by the publisher.

Supplementary material

The Supplementary Material for this article can be found online at: https://www.frontiersin.org/articles/10.3389/fnagi.2022.1037904/full#supplementary-material

References

Alam, A., Hana, Z., Jin, Z., Suen, K. C., and Ma, D. (2018). Surgery, neuroinflammation and cognitive impairment. *EBioMedicine* 37, 547–556. doi: 10.1016/j.ebiom.2018.10.021

Amodio, P., Del Piccolo, F., Marchetti, P., Angeli, P., Iemmolo, R., Caregaro, L., et al. (1999). Clinical features and survivial of cirrhotic patients with subclinical cognitive alterations detected by the number connection test and computerized psychometric tests. *Hepatology* 29, 1662–1667. doi: 10.1002/hep.510290619

Boeve, B. F., Boylan, K. B., Graff-Radford, N. R., DeJesus-Hernandez, M., Knopman, D. S., Pedraza, O., et al. (2012). Characterization of frontotemporal dementia and/or amyotrophic lateral sclerosis associated with the GGGGCC repeat expansion in C9ORF72. *Brain* 135, 765–783. doi: 10.1093/brain/aws004

Borchers, F., Spies, C. D., Feinkohl, I., Brockhaus, W. R., Kraft, A., Kozma, P., et al. (2021). Methodology of measuring postoperative cognitive dysfunction: a systematic review. *Br. J. Anaesth.* 126, 1119–1127. doi: 10.1016/j.bja.2021.01.035

Chan, M. T., Cheng, B. C., Lee, T. M., and Gin, T. (2013). BIS-guided anesthesia decreases postoperative delirium and cognitive decline. *J. Neurosurg. Anesthesiol.* 25, 33–42. doi: 10.1097/ANA.0b013e3182712fba

Chen, J., Liu, S., Wang, X., Huang, J., Phillips, J., Ma, D., et al. (2022). HDAC6 Inhibition Alleviates Anesthesia and Surgery-Induced Less Medial Prefrontal-Dorsal Hippocampus Connectivity and Cognitive Impairment in Aged Rats. *Mol. Neurobiol.* 59, 6158–6169 doi: 10.1007/s12035-022-02959-4

Choi, S. H., Oh, J. W., Ryu, J. S., Kim, H. M., Im, S. H., Kim, K. P., et al. (2020). IRT5 probiotics changes immune modulatory protein expression in the extraorbital lacrimal glands of an autoimmune dry eye mouse model. *Invest. Ophthalmol. Vis. Sci.* 61, 42. doi: 10.1167/iovs.61.3.42

Chunchai, T., Thunapong, W., Yasom, S., Wanchai, K., Eaimworawuthikul, S., Metzler, G., et al. (2018). Decreased microglial activation through gut-brain axis by prebiotics, probiotics, or synbiotics effectively restored cognitive function in obese-insulin resistant rats. *J. Neuroinflamm.* 15, 11. doi: 10.1186/s12974-018-1055-2

Cibelli, M., Fidalgo, A. R., Terrando, N., Ma, D., Monaco, C., Feldmann, M., et al. (2010). Role of interleukin-1beta in postoperative cognitive dysfunction. *Ann. Neurol.* 68, 360–368. doi: 10.1002/ana.22082

Cryan, J. F., O'Riordan, K. J., Cowan, C. S. M., Sandhu, K. V., Bastiaanssen, T. F. S., Boehme, M., et al. (2019). The microbiota-gut-brain axis. *Physiol. Rev.* 99, 1877–2013. doi: 10.1152/physrev.00018.2018

De La Cochetière, M. F., Durand, T., Lepage, P., Bourreille, A., Galmiche, J. P., and Dor,é, J. (2005). Resilience of the dominant human fecal microbiota upon short-course antibiotic challenge. *J. Clin. Microbiol.* 43, 5588–5592. doi: 10.1128/JCM.43.11.5588-5592.2005

Deiner, S., Liu, X., Lin, H.-., M., Jacoby, R., and Kim, J., et al. (2021). Does postoperative cognitive decline result in new disability after surgery? *Ann. Surg.* 274, e1108–e1114. doi: 10.1097/SLA.0000000000003764

Deng, Y., Wang, R., Li, S., Zhu, X., Wang, T., Wu, J., et al. (2021). Methylene blue reduces incidence of early postoperative cognitive disorders in elderly patients undergoing major non-cardiac surgery: Aa open-label randomized controlled clinical trial. *J. Clin. Anesth.* 68, 110108. doi: 10.1016/j.jclinane.2020.110108

Dethlefsen, L., and Relman, D. A. (2011). Incomplete recovery and individualized responses of the human distal gut microbiota to repeated antibiotic perturbation. *Proc. Natl. Acad. Sci. U. S. A.* 108, 4554–4561. doi: 10.1073/pnas.1000087107

Duan, S., Liao, Y., Tang, Y., Zhang, B., Peng, M., Tong, J., et al. (2022). Short-term perioperative cognitive therapy combined with rehabilitation exercise reduces the incidence of neurocognitive disorder in elderly patients: a randomized controlled trial. *Minerva Anestesiol.* 88, 145–155. doi: 10.23736/S0375-9393.21.15877-8

Evered, L., Silbert, B., Knopman, D. S., Scott, D. A., DeKosky, S. T., Rasmussen, L. S., et al. (2018). Recommendations for the nomenclature of cognitive change associated with anaesthesia and surgery-2018. *Br. J. Anaesth.* 121, 1005–1012. doi: 10.1016/j.bja.2017.11.087

Fung, T. C., Olson, C. A., and Hsiao, E. Y. (2017). Interactions between the microbiota, immune and nervous systems in health and disease. *Nat. Neurosci.* 20, 145–155. doi: 10.1038/nn.4476

Hood, R., Budd, A., Sorond, F. A., and Hogue, C. W. (2018). Peri-operative neurological complications. *Anaesthesia* 73 Suppl 1, 67–75. doi: 10.1111/anae.14142

Jaeger, J. (2018). Digit Symbol Substitution Test: The Case for Sensitivity Over Specificity in Neuropsychological Testing. *J. Clin. Psychopharmacol.* 38, 513–519. doi: 10.1097/JCP.0000000000000941

Ji, M. H., Yuan, H. M., Zhang, G. F., Li, X. M., Dong, L., Li, W. Y., et al. (2013). Changes in plasma and cerebrospinal fluid biomarkers in aged patients with early postoperative cognitive dysfunction following total hip-replacement surgery. *J. Anesth.* 27, 236–242. doi: 10.1007/s00540-012-1506-3

Jiang, X. L., Gu, X. Y., Zhou, X. X., Chen, X. M., Zhang, X., Yang, Y. T., et al. (2019). Intestinal dysbacteriosis mediates the reference memory deficit induced by anaesthesia/surgery in aged mice. *Brain Behav. Immun.* 80, 605–615. doi: 10.1016/j.bbi.2019.05.006

Juan, Z., Chen, J., Ding, B., Yongping, L., Liu, K., Wang, L., et al. (2022). Probiotic supplement attenuates chemotherapy-related cognitive impairment in patients with breast cancer: a randomised, double-blind, and placebo-controlled trial. *Eur. J. Cancer* 161, 10–22. doi: 10.1016/j.ejca.2021.11.006

Koch, S., Forteza, A., Lavernia, C., Romano, J. G., Campo-Bustillo, I., Campo, N., et al. (2007). Cerebral fat microembolism and cognitive decline after hip and knee replacement. *Stroke* 38, 1079–1081. doi: 10.1161/01.STR.0000258104.01627.50

Kristek, G., Rado,š, I., Kristek, D., Kapural, L., and Neškovi,ć, N., Škiljić, S., et al. (2019). Influence of postoperative analgesia on systemic inflammatory response and postoperative cognitive dysfunction after femoral fractures surgery: a randomized controlled trial. *Reg. Anesth. Pain Med.* 44, 59–68. doi: 10.1136/rapm-2018-000023

Lacritz, L. H., and Cullum, C. M. (1998). The Hopkins Verbal Learning Test and CVLT: a preliminary comparison. *Arch. Clin. Neuropsychol.* 13, 623–628. doi: 10.1093/arclin/13.7.623

Leung, J. L., Lee, G. T., Lam, Y. H., Chan, R. C., and Wu, J. Y. (2011). The use of the Digit Span Test in screening for cognitive impairment in acute medical inpatients. *Int. Psychogeriatr.* 23, 1569–1574. doi: 10.1017/S1041610211000792

Li, W. X., Luo, R. Y., Chen, C., Li, X., Ao, J. S., Liu, Y., et al. (2019). Effects of propofol, dexmedetomidine, and midazolam on postoperative cognitive dysfunction in elderly patients: a randomized controlled preliminary trial. *Chin. Med. J. (Engl)* 132, 437–445. doi: 10.1097/CM9.0000000000000098

Lv, Q. W., Zhang, W., Shi, Q., Zheng, W. J., Li, X., Chen, H., et al. (2015). Comparison of Tripterygium wilfordii Hook F with methotrexate in the treatment of active rheumatoid arthritis (TRIFRA): a randomised, controlled clinical trial. *Ann. Rheum. Dis.* 74, 1078–1086. doi: 10.1136/annrheumdis-2013-204807

Malek-Ahmadi, M., Davis, K., Belden, C., Laizure, B., Jacobson, S., Yaari, R., et al. (2012). Validation and diagnostic accuracy of the Alzheimer's questionnaire. *Age Ageing* 41, 396–399. doi: 10.1093/ageing/afs008

Mohajeri, M. H., La Fata, G., Steinert, R. E., and Weber, P. (2018). Relationship between the gut microbiome and brain function. *Nutr. Rev.* 76, 481–496. doi: 10.1093/nutrit/nuy009

Moller, J. T., Cluitmans, P., Rasmussen, L. S., Houx, P., Rasmussen, H., Canet, J., et al. (1998). Long-term postoperative cognitive dysfunction in the elderly: ISPOCD1 study. *Lancet* 351, 857–861. doi: 10.1016/S0140-6736(97)07382-0

Needham, M. J., Webb, C. E., and Bryden, D. C. (2017). Postoperative cognitive dysfunction and dementia: what we need to know and do. *Br. J. Anaes.* 119, i115–i125. doi: 10.1093/bja/aex354

Newman, S., Stygall, J., Hirani, S., Shaefi, S., Maze, M., and Warltier, D. C. (2007). Postoperative cognitive dysfunction after noncardiac surgery: a systematic review. *Anesthesiology* 106, 572–590. doi: 10.1097/00000542-200703000-00023

O'Gara, B. P., Mueller, A., Gasangwa, D. V. I., Patxot, M., Shaefi, S., Khabbaz, K., et al. (2020). Prevention of early postoperative decline: a randomized, controlled feasibility trial of perioperative cognitive training. *Anesth. Analg.* 130, 586–595. doi: 10.1213/ANE.0000000000004469

O'Mahony, L., McCarthy, J., Kelly, P., Hurley, G., Luo, F., Chen, K., et al. (2005). Lactobacillus and bifidobacterium in irritable bowel syndrome: symptom responses and relationship to cytokine profiles. *Gastroenterology* 128, 541–551. doi: 10.1053/j.gastro.2004.11.050

Rodriguez, R. A., Tellier, A., Grabowski, J., Fazekas, A., Turek, M., Miller, D., et al. (2005). Cognitive dysfunction after total knee arthroplasty: effects of intraoperative cerebral embolization and postoperative complications. *J. Arthroplasty* 20, 763–771. doi: 10.1016/j.arth.2005.05.004

Sachdev, P. S., Blacker, D., Blazer, D. G., Ganguli, M., Jeste, D. V., Paulsen, J. S., et al. (2014). Classifying neurocognitive disorders: the DSM-5 approach. *Nat. Rev. Neurol.* 10, 634–642. doi: 10.1038/nrneurol.2014.181

Schachter, J., Martel, J., Lin, C. S., Chang, C. J., Wu, T. R., Lu, C. C., et al. (2018). Effects of obesity on depression: A role for inflammation and the gut microbiota. *Brain Behav. Immun.* 69, 1–8. doi: 10.1016/j.bbi.2017.08.026

Seino, Y., Takami, A., Boka, G., Niemoeller, E., and Raccah, D. (2014). Pharmacodynamics of the glucagon-like peptide-1 receptor agonist lixisenatide in Japanese and Caucasian patients with type 2 diabetes mellitus poorly controlled on sulphonylureas with/without metformin. *Diabetes Obes. Metab.* 16, 739–747. doi: 10.1111/dom.12276

Su, X., Meng, Z. T., Wu, X. H., Cui, F., Li, H. L., Wang, D. X., et al. (2016). Dexmedetomidine for prevention of delirium in elderly patients after non-cardiac surgery: a randomised, double-blind, placebo-controlled trial. *Lancet* 388, 1893–1902. doi: 10.1016/S0140-6736(16)30580-3

Suez, J., Zmora, N., Segal, E., and Elinav, E. (2019). The pros, cons, and many unknowns of probiotics. *Nat. Med.* 25, 716–729. doi: 10.1038/s41591-019-0439-x

Sun, H. B., Li, Y., Liu, X. B., Zhang, R. X., Wang, Z. F., Lerut, T., et al. (2018). Early oral feeding following mckeown minimally invasive esophagectomy: an open-label, randomized, controlled, noninferiority trial. *Ann. Surg.* 267, 435–442. doi: 10.1097/SLA.0000000000002304

Sun, M. F., and Shen, Y. Q. (2018). Dysbiosis of gut microbiota and microbial metabolites in Parkinson's Disease. *Ageing Res. Rev.* 45, 53–61. doi: 10.1016/j.arr.2018.04.004

Sutin, A. R., Stephan, Y., and Terracciano, A. (2019). Verbal fluency and risk of dementia. *Int. J. Geriatr. Psychiatry* 34, 863–867. doi: 10.1002/gps.5081

Tam, J. W., and Schmitter-Edgecombe, M. (2013). The role of processing speed in the Brief visuospatial memory test - revised. *Clin. Neuropsychol.* 27, 962–972. doi: 10.1080/13854046.2013.797500

Tanabe, S., Mohanty, R., Lindroth, H., Casey, C., Ballweg, T., Farahbakhsh, Z., et al. (2020). Cohort study into the neural correlates of postoperative delirium: the role of connectivity and slow-wave activity. *Br J. Anaesth.* 125, 55–66. doi: 10.1016/j.bja.2020.02.027

Terrando, N., Monaco, C., Ma, D., Foxwell, B. M., Feldmann, M., Maze, M., et al. (2010). Tumor necrosis factor-alpha triggers a cytokine cascade yielding postoperative cognitive decline. *Proc. Natl. Acad. Sci. U. S. A.* 107, 20518–20522. doi: 10.1073/pnas.1014557107

Wang, P., Yin, X., Chen, G., Li, L., Le, Y., Xie, Z., et al. (2021). Perioperative probiotic treatment decreased the incidence of postoperative cognitive impairment in elderly patients following non-cardiac surgery: A randomised double-blind and placebo-controlled trial. *Clin. Nutr.* 40, 64–71. doi: 10.1016/j.clnu.2020.05.001

Wu, Z., Zhang, M., Zhang, Z., Dong, W., Wang, Q., Ren, J., et al. (2018). Ratio of β-amyloid protein (Aβ) and Tau predicts the postoperative cognitive dysfunction on patients undergoing total hip/knee replacement surgery. *Exp. Ther. Med.* 15, 878–884. doi: 10.3892/etm.2017.5480

Xu, X., Hu, Y., Yan, E., Zhan, G., Liu, C., Yang, C., et al. (2020). Perioperative neurocognitive dysfunction: thinking from the gut? *Aging (Albany NY)* 12, 15797–15817. doi: 10.18632/aging.103738

Zhan, G., Yang, N., Li, S., Huang, N., Fang, X., Zhang, J., et al. (2018). Abnormal gut microbiota composition contributes to cognitive dysfunction in SAMP8 mice. *Aging* 10, 1257–1267. doi: 10.18632/aging.101464

Zhang, N., Liang, M., Zhang, D. D., Xiao, Y. R., Li, Y. Z., Gao, Y. G., et al. (2018). Effect of goal-directed fluid therapy on early cognitive function in elderly patients with spinal stenosis: A Case-Control Study. *Int. J. Surg.* 54, 201–205. doi: 10.1016/j.ijsu.2018.04.007

Zhang, N. N., Sun, L., Chen, W. T., Yang, Y. L., and Wu, Y. M. (2020). Effects of edaravone on postoperative cognitive function in elderly patients undergoing hip joint. replacement surgery: a randomized controlled trial. *Int. J. Surg.* 80, 13–18. doi: 10.1016/j.ijsu.2020.05.092

Zhu, Y., Zhou, M., Jia, X., Zhang, W., Shi, Y., Bai, S., et al. (2021). Inflammation disrupts the brain network of executive function after cardiac surgery. *Ann. Surg.* doi: 10.1097/SLA.0000000000005041

frontiers | Frontiers in Pharmacology

TYPE Original Research
PUBLISHED 09 January 2023
DOI 10.3389/fphar.2022.1022449

OPEN ACCESS

EDITED BY
Jiaqiang Zhang,
Zhengzhou University, China

REVIEWED BY
Yun Chen,
Nanjing Medical University, China
P. Hemachandra Reddy,
Texas Tech University Health Sciences Center, United States

*CORRESPONDENCE
Dansi Qi,
qidansi@hotmail.com

SPECIALTY SECTION
This article was submitted to Neuropharmacology, a section of the journal Frontiers in Pharmacology

RECEIVED 18 August 2022
ACCEPTED 21 December 2022
PUBLISHED 09 January 2023

CITATION
Zhang X, Lou Y, Zheng D, Lu J and Qi D (2023), Quantitative proteomic analysis reveals the effects of mu opioid agonists on HT22 cells.
Front. Pharmacol. 13:1022449.
doi: 10.3389/fphar.2022.1022449

Quantitative proteomic analysis reveals the effects of mu opioid agonists on HT22 cells

Xutong Zhang[1], Yani Lou[1], Dongxu Zheng[1], Jialin Lu[1] and Dansi Qi[2]*

[1]Department of Anesthesiology, The Second Affiliated Hospital and Yuying Children's Hospital of Wenzhou Medical University, Wenzhou, China, [2]Department of Pathology, Second Affiliated Hospital and Yuying Children's Hospital of Wenzhou Medical University, Wenzhou, China

Introduction: At present, the mu opioid receptor is the most important neuroaesthetics receptor in anesthesiology research, and the damage that it does to the nervous system is unknown.

Methods: We investigated the effects of loperamide, an agonist of the mu opioid receptor, on protein expression in HT22 cells using stable isotope labeling of amino acids in cell culture (SILAC), immobilized metal affinity chromatography (IMAC) enrichment, and high-resolution liquid chromatography-tandem mass spectrometry (LC-MS/MS). A total of 7,823 proteins were identified.

Results and Discussion: Bioinformatic analysis revealed that mu opioid receptor agonism can induce distinct changes in the proteome of HT22 cells. These findings improve our understanding of narcotic drugs.

KEYWORDS

mu opioid agonist, proteomic, loperamide, HT22 cell, nerve injury, LC-MS/MS

Introduction

In the opioid system, mu, delta, and kappa receptors are G protein-coupled receptors that are stimulated by endogenous opioid peptides (Kieffer, 1995). Opioid receptors can also be exogenously activated by alkaloid opioids, the prototypical example of which is morphine. In mice lacking mu opioid receptors, morphine's addictive and analgesic characteristics are eliminated, proving that mu receptors are responsible for both the drug's beneficial and harmful effects (Matthes et al., 1996). The potentiating effects of alcohol, cannabis, and nicotine all work on various receptors and are significantly decreased in these mutant mice, according to many studies (Kieffer and Gaveriaux-Ruff, 2002). Therefore, mu opioid receptor activation has important clinical research significance in nervous system injury (Tiwari et al., 2018). Expanding our understanding of mu receptor function will be of great help as we learn more about the general mechanisms of nerve injury. After direct (morphine) or indirect stimulation (alcohol, cannabinoid, nicotine) of the mu opioid receptors, positive reinforcement occurs, so an understanding of mu receptor function is critical for addiction treatment and the development of neurological damage. A recent study in neurons indicates that mu receptor signaling and modulation are strongly dependent on agonist action. Loperamide is a potent mu opioid agonist which is routinely used to treat diarrhea and as an adjunctive analgesic for oral pain due to mucositis or cancer (Regnard et al., 2011). As loperamide is an effective mu opioid receptor agonist, we used HT22 cells to study the effect of mu opioid receptor agonists on neurons nerve injury and to investigate mu opioid receptor agonists. Actions of opioid receptors. We explored the expression of related proteins in HT22 cells.

Among the brain's most important parts are the hippocampus and it is responsible for the integration of information between short-term and long-term memory. General anesthesia is

known to involve the hippocampus, and therefore, there are concerns that it may inhibit learning and memory. For the research of Alzheimer's disease, Parkinson's disease, Kinson's disease, and the effects of general anesthesia, HT22 cells are frequently employed as a neurobiological cell model. They are produced from HT4 cells, which were initially immortalized from primary mouse hippocampus neuronal cultures (Behl et al., 1995; Behl, 1998; Kulich and Chu, 2001; Schafer et al., 2004; Zhu et al., 2014). Chronic pain is neuropathic for approximately 25%–30% of patients and affects 7%–8% of adults in the general population (Torrance et al., 2014). These individuals frequently endure unpredictable, paroxysmal, and difficult-to-treat pain. However, evoked reflex withdrawal reactions to external stimuli are frequently used to infer neuropathic pain-related behaviors in animal models. Clinically relevant behaviors that are suggestive of persistent pain are more complex and less studied pre-clinically. Therefore, we took a novel approach to examine the proteomic changes caused by the activation of mu opioid receptors in nerve cell injury, to identify relevant clinical markers.

The LC-MS/MS technique is a high-throughput, high-precision proteomic analysis technique that has become a powerful method for analyzing protein expression changes across a variety of species (Edmondson et al., 2002; Bouwmeester et al., 2004; Herring et al., 2015). In this study, we comprehensively compared the proteome of HT22 cells treated with the mu opioid receptor agonist loperamide using an LC-MS/MS-based method. The goal of this study was to reveal the influences of mu opioid receptor activation on proteins related signal transduction in nerve cells, which may help us understand the mechanism of mu opioid receptors in nervous system damage.

Materials and methods

Labeling and drug treatment of HT22 cells

Based on the instructions provided by the manufacturer, HT22 cells were labeled using the Stable Isotope Labeling of Amino Acids in Cell Culture (SILAC) protein quantification kit (Pierce, Thermo Fisher Scientific). Cells were treated with 3.8948 μg/mL loperamide for 8 h and then washed twice with ice-cold phosphate-buffered saline (PBS) and harvested.

Trypsin digestion and fractionation

The solution was digested at 37°C for 16 h with trypsin (Promega) at a ratio of 50:50 (w/w). A final concentration of 5 mM of dithiothreitol (DTT) was added, followed by a 1-h incubation period at 37°C. Incubation at room temperature for 30 min in the dark with iodoacetamide (IAA) at a final concentration of 15 mM was then carried out to alkylate proteins. Adjusting the solution's final cysteine content to 30 mM and letting it sit at room temperature for 30 min stopped the alkylation reaction. Final trypsin: protein ratio of 1:100 (w/w) was added to the solution and incubated at 37°C for 4 h to complete digestion. High pH reverse-phase high-performance liquid chromatography (HPLC) was used to separate the sample using an Agilent 300 Extend C18 column with 5 m particles that had an ID of 4.6 mm and a length of 250 mm. Peptides were initially separated into 80 fractions over 80 min using a gradient of 2%–60% acetonitrile in 10 mM ammonium bicarbonate (pH 10). Following that, the peptides were mixed into 18 fractions and dried using vacuum centrifugation.

IMAC enrichment of phosphopeptides

An immobilized metal affinity chromatography (IMAC) microsphere suspension was first added to the peptide mixtures and incubated under vibration. After centrifugation, phosphopeptide-enriched IMAC microspheres were obtained with the supernatant removed. To remove non-specifically adsorbed peptides from IMAC microspheres, 50% acetonitrile (ACN)/6% trifluoroacetic acid (TFA) was washed sequentially with 30% ACN/0.1% TFA. IMAC microspheres were used to elute the enriched phosphopeptides using an elution buffer containing 10% NH_4OH. For LC-MS/MS analysis, the phosphopeptide-containing supernatant was gathered and lyophilized.

LC-MS/MS analysis

After being dissolved in solvent A [.1% formic acid (FA) in 2% ACN], the peptides were immediately loaded onto a reverse-phase pre-column (Acclaim PepMap 100, Thermo Fisher Scientific). On an EASY-LLC 1000 UPLC system, peptides were separated using a reverse-phase analytical column (Thermo Fisher Scientific, Acclaim PepMap RSLC) with a linear gradient of 4%–22% solvent B (.1% FA in 98% ACN) for 50 min, 22%–35% solvent B for 12 min, 35%–85% solvent B for 4 min, and then 85% solvent B for 3 min. Using a Q Exactive Plus hybrid quadrupole-Orbitrap mass spectrometer, the resultant peptides were examined (Thermo Fisher Scientific).

Peptides were submitted to tandem mass spectrometry (MS) in Q Exactive Plus (Thermo Fisher Scientific) connected to an ultra-performance liquid chromatograph after nanospray ionization (NSI).At a resolution of 70,000, Orbitrap was used to detect intact peptides. The normalized collision energy (NCE) of 30 was used to select peptides for MS/MS analysis and ion fragments were detected using Orbitrap at a resolution of 17,500. Data-dependent procedures were applied to the top 20 precursor ions, alternating between one MS scan and 20 MS/MS scans, with a dynamic exclusion period of 15.0 s. The electrospray voltage that was used was 2.0 kV. Automatic gain control (AGC) targets of 3 106 ions and a maximum injection time of 50 m were used to collect MS1 spectra, whereas an AGC target of 5 104 ions and a maximum injection duration of 200 ms were used to acquire MS2 spectra. The m/z scan range for the MS scans was 350–1,800. Using the dataset identifier PXD004687, mass spectrometry and proteomics data were deposited with the ProteomeXchange Consortium *via* the PRIDE50 partner repository.

Database search and bioinformatics analysis

The obtained MS/MS data were processed using MaxQuant (v.1.4.1.2), which has an integrated Andromeda search engine.

Combining the SwissProt_mouse database with a reverse decoy database, tandem mass spectra were searched. Trypsin/P was defined as cleavage enzyme, and up to two missed cleavages, five modifications per peptide, and five charges were allowed. Ion precursors have a mass error of 10 ppm, while fragments have a mass error of .02 Da. Met oxidation and acetylation were designated as variable modifications, but Cys carbamidomethylation was designated as a permanent modification. Ser, Thr, and Tyr phosphorylations were also designated as variable modifications for the phosphoproteome investigation. The thresholds for false discovery rate (FDR) for proteins, peptides, and modification sites were established at 1%. Seven residues were chosen as the bare minimum for peptide length. To be employed in the next analysis, the other parameters in MaxQuant were set to larger than .75.

The Database for Annotation, Visualization, and Integrated Discovery was used to analyze GO term association and enrichment. Using DAVID's Functional Annotation Tool, domain analysis was carried out on the InterPro database. Protein complexes were analyzed using the hand-maintained CORUM protein complex database. Using Cytoscape, the STRING database system was used to display functional protein-protein interaction networks. A bioinformatics study was conducted, and significant results were defined as adjusted p-values < .05.

Cell growth assay

Measurement of cell growth was done using the CCK8 kit based on the directions provided by the manufacturer (Solarbio, #CA1210). A 5,000-cell density was used in 96-well plates, and loperamide was applied for 8 h to HT22 cells. The cells were then given 10 L of CCK8 to each well, and they were left to react for 4 h. On a plate reader (Heales, #MB-580), the optical densities of the medium in the wells were determined at 450 nm.

RNA isolation and quantitative reverse transcriptase PCR

Using the TRIzol® Plus RNA Purification Kit (Invitrogen, #12183-555), RNA was isolated from HT22 cells in accordance with the manufacturer's instructions. The Loperamide HCl treatment group was used as the experimental group, and the DMSO treatment group was used as the control. A quantitative real-time polymerase chain reaction (RT-PCR) was performed on a StepOnePlus Real-Time PCR System ABI using the One-Step RT-qPCR Kit (Sangon Biotech, B639277). Primer sequences are listed in Supplementary Table S1 and expression levels were normalized to glyceraldehyde-3-phosphate dehydrogenase (GAPDH) was used as the reference for relative quantification.

Statistics

Data are presented as the mean ± standard error of the mean (SEM) and were gathered from at least three different experiments. Using the Student's t-test, statistical significance between the two groups was analyzed. p-values < .05 were used to determine statistical significance for differences. The statistical program GraphPad Prism (GraphPad Software Inc., La Jolla, CA, United States) was used to conduct all tests.

Results

Strategies for quantitative proteome analysis

In this study, we combined SILAC labeling methods, HPLC fractionation, IMAC enrichment, Orbitrap mass spectrometry with high resolution, and a bioinformatics analytic system for quantification. The workflow for the proteome analysis of control and loperamide-treated HT22 cells is shown in Figure 1A. Using this method, we identified 7,820 proteins in HT22 cells (Figure 1B) and a total of 222 differentially expressed proteins were identified in the proteomic analysis of loperamide-treated cells (Figure 1C).

Effects of loperamide on the overall proteome of HT22 cells

Using thresholds of fold-change >1.2 and p-value <.05 (t-test), In HT22 cells treated with loperamide, we found that 105 proteins were upregulated and 117 proteins were downregulated (Supplementary Table S1).

Differentially expressed proteins in the loperamide-treated HT22 cells were analyzed for GO and KEGG enrichment (Figure 2). In the biological process category, loperamide-treated cells showed changes in proteins involved in monocarboxylic acid biosynthetic process, chondrocyte differentiation involved in endochondral bone morphogenesis, inflammatory response, response to external stimuli, methylglyoxal biosynthesis process, among others (Figure 2A). In the cytokine activity category, receptor ligands and molecular functions such as activity, phospholipase inhibitor activity, receptor modulator activity, and sulfur compound binding, were identified, among others (Figure 2B). Additionally, we identified changes in proteins categorized as having functions involving the localization of the extracellular domain, extracellular domain, extracellular space, keratin filament, and intermediate filament, among others (Figure 2C). To show the hierarchical relationship of the enriched GO entries of differential proteins, top GO-directed acyclic graph (DAG) was used to display the top-down defined functional scope, in which the branch represents the inclusion relationship and the lower the branch represents the more specific the defined functional scope is (Figures 2D–F).

To systematically and comprehensively analyze the biological processes, the mechanisms of disease occurrence, and the mechanisms of drug action, it is often necessary to explain the changes in protein levels from the perspective of protein coordination, such as changes in metabolic pathways. Therefore, proteins were annotated using the KEGG pathway database to analyze the cellular pathways affected by loperamide (Figure 3). We found that loperamide treatment significantly changed protein levels in the PI3K-Akt signaling, retrograde endocannabinoid signaling, estrogen signaling, glycolysis/gluconeogenesis, oxidative phosphorylation of AMPK and PPAR signaling pathways (Figure 3A). Specifically, proteins in

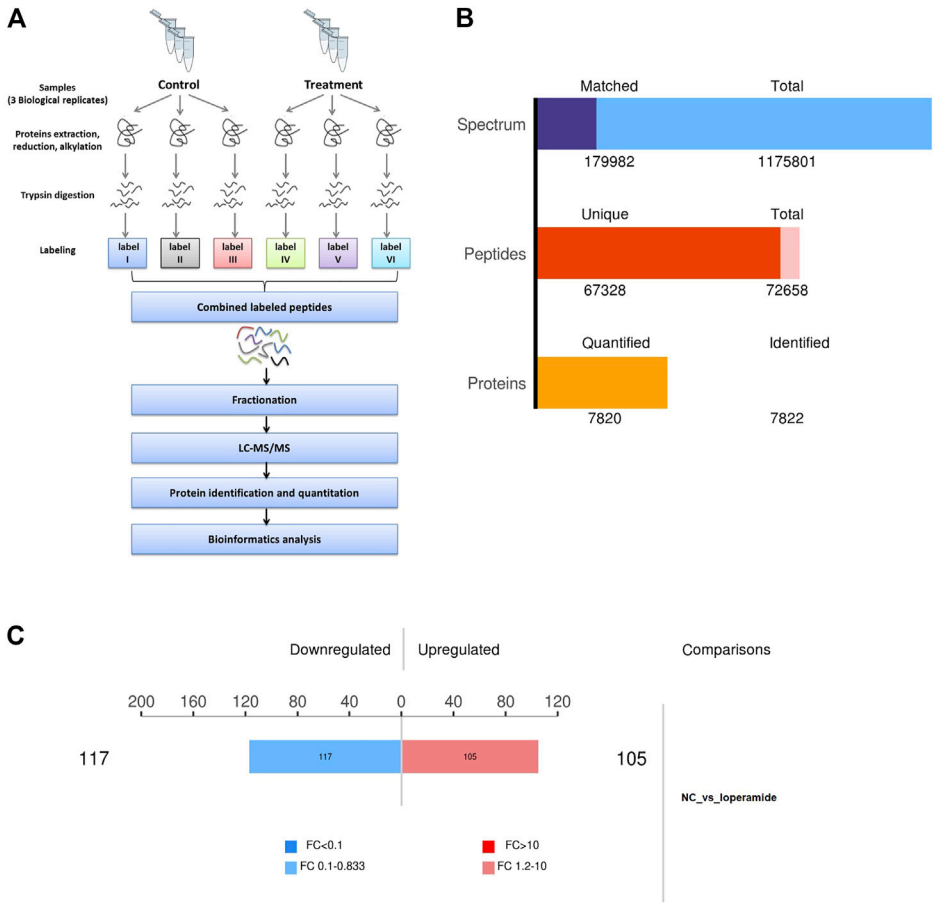

FIGURE 1
Overview of the proteomes of loperamide-treated HT22 cells. **(A)** Systematic workflow of the quantitative proteoome analyses. **(B)** Statistical histogram of identification and quantification results. **(C)** Histogram of differential protein quantification results.

the cytokine-cytokine receptor interaction, JAK-STAT signaling, and TGF-beta signaling pathways were upregulated and glycolysis/gluconeogenesis, HIF−1 signaling, fructose, and mannose metabolism were downregulated (Figure 3B). These results were obtained using Fisher's Exact Test (p-value < .05).

Then, we constructed a protein-protein interaction (PPI) network of the differentially expressed proteins detected following loperamide therapy using Cytoscape software, which is based on protein interaction links in the STRING or IntAct databases (Figure 4A). In the PPI interaction network, highly aggregated proteins often have the same or similar functions and synergistically exert their biological functions. Therefore, based on the principle of topology identification, the highly aggregated proteins in the interaction network were divided into different clusters (Figure 4B). Concurrently, we incorporated correlation analysis and identified the interaction map of key genes affected by loperamide (Figures 4C–F).

Identification of gene expression altered after loperamide treatment by RT-PCR

Based on the results of proteomic sequencing, we analyzed differentially expressed genes. Combined with relevant literature analysis, we determined that loperamide treatment altered the expression of *Pcdhb14*, *Apoc1*, *Nbr1*, *Spp1*, *Ttc3*, *Hes1*, *Thbs1* genes, using RT-PCR analysis (Figure 5).

Discussion

Loperamide is a potent mu opioid agonist which acts as an adjunctive analgesic for oral pain caused by mucositis or cancer (Regnard et al., 2011). Although loperamide is clinically safe, its anesthetic effect, on neuronal cells, is unknown. In this study, we comprehensively compared the proteome of control and loperamide-treated HT22 cells using an LC-MS/MS-based method and identified 7,820 proteins. Comprehensive bioinformatics analysis showed that loperamide treatment affected numerous signaling pathways, including PI3K-Akt, tumor necrosis factor (TNF), and Notch. Based on proteome sequencing and RT-PCR validation, our results show that mu opioid receptor activation can affect the expression of related genes in neural cells, including *Pcdhb14*, *Apoc1*, *Nbr1*, *Spp1*, *Ttc3*, and *Hes1*, and is neurotoxic to HT22 cells. Our findings provide guidance for clinical anesthesia.

Protocadherin Beta 14 (PCDHB14) is a calcium-dependent cell adhesion protein. Protocadherins are a large family of molecules expressed in the central nervous system and have been implicated

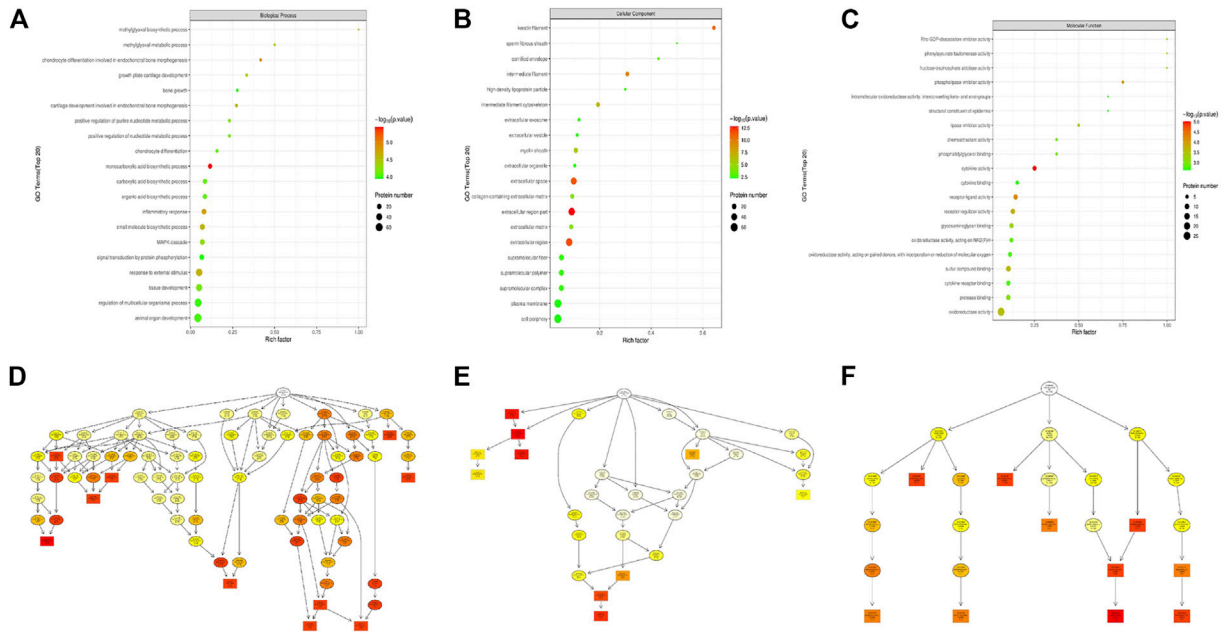

FIGURE 2
KEGG pathway enrichment analysis of differentially expressed proteins in loperamide-treated HT22 cells. **(A)** KEGG pathway annotation statistics for differentially expressed proteins. **(B)** KEGG pathway differential expression analysis map. **(C)** KEGG pathway enrichment bubble map.

in the formation and maintenance of synaptic connections. Several mental functions, including learning and memory, are dependent on it, including neuronal survival and axonal projection. Studies demonstrate that EtOH alters the expression of adhesion molecules, neuronal migration, and neurite outgrowth, hence impairing neuronal development (Liesi, 1997; Vangipuram et al., 2008). EtOH treatment has been reported to decrease *Pcdhb14* expression during neuronal differentiation (Halder et al., 2015); Thus, in line with other research, our results imply that loperamide-induced downregulation of this protocadherin gene may affect synaptic function and hinder the development of the central nervous system (CNS).

Apolipoprotein CI (APOC1) is a candidate Alzheimer's disease (AD) gene, and variants of the gene, such as rs11568822, are associated with AD risk and may be functionally related to AD pathophysiology. A key pathological feature of AD is the production of neuritic plaques, intracellular formation of neurofibrillary tangles, and neuronal loss through extracellular deposition of amyloid beta (Aβ) peptide (Ca Ccamo and Oddo, 2012). Accumulation of mutant APP (mAPP) and Aβ could lead to neuronal dysfunction (Reddy et al., 2018), and mitophagy enhancers resist effectively mAPP and Aβ-induced mitochondrial and synaptic toxicities in AD (Kshirsagar et al., 2022).Apolipoprotein E (APOE) and APOC1 work together to engage in a number of biological processes, including cholesterol metabolism, membrane remodeling, neuronal death, and neuron reconfiguration (Leduc et al., 2010). Accumulating evidence from clinical and pathological studies suggests that the persistent deterioration of cerebral cholesterol metabolism disorders is associated with AD pathophysiology (Leduc et al., 2010; Vestergaard et al., 2010). According to research, frontotemporal dementia and primary progressive aphasia are both caused by APOC1. In Chinese individuals with late-onset Alzheimer's disease, APOC1 H2 may work in concert with APOE4 to raise the risk of cognitive deterioration. Therefore, mu opioid receptor activation appears to influence lipid metabolism in nerve cells.

The eukaryotic kingdom, NBR1 (the neighbor of BRCA1 gene 1) is a widely expressed and highly conserved protein (Yamamoto et al., 2000; Zu et al., 2004; Mardakheh et al., 2009). Only a few ATG8 family members have recently been shown to interact with NBR1, including gamma-aminobutyric acid type A receptor-associated protein (GABARAP), GABARAP-like 1 (GABARAPL1), and 16 kDa Golgi-associated ATPase enhancer (GATE-16 or GABARAPL2) (Zellner et al., 2021). Importantly, the ubiquitin-associated ubiquitin domain of NBR1 interacts with ubiquitin (Walinda et al., 2014). These characteristics have led to the hypothesis that NBR1 might serve as a cargo adapter for the autophagic degradation of ubiquitinated substrates like p62, which can also bind to members of the ATG8 family of proteins (Zhou et al., 2013). Recently, LC3, GABARAP, and GATE-16 have been reported in Parkinson's disease (PD) and dementia with Lewy bodies (DLBs) (Kim et al., 2021). NBR1 may have a role in the development of cytoplasmic inclusions in synucleinopathies because it has been found to localize in Lewy bodies (LBs) in PD and DLB as well as glial cytoplasmic inclusions (GCIs) in multiple system atrophy (MSA) In addition, NBR1 has attracted interest because of its location close to *BRCA1* in the genome. NBR1 may function by interacting with calcium and integrin binding (CIB) and fasciculation and elongation protein zeta-1 (FEZ1) proteins in cellular signaling pathways, and its developmentally-restricted expression suggests a possible role in neurodevelopment (Kirkin et al., 2009). Therefore, activation of mu opioid receptors in HT22 cells may influence autophagy in HT22 cells.

Secreted phosphoprotein 1 (SPP1), also known as osteopontin (OPN) is a multifunctional secreted glycoprotein that affects the adhesion, proliferation, differentiation, migration, and survival of multiple cell types (Jessen and Mirsky, 1999; Stoll and Jander, 1999; Vargas and Barres, 2007; Pegoraro et al., 2011). In the peripheral nervous

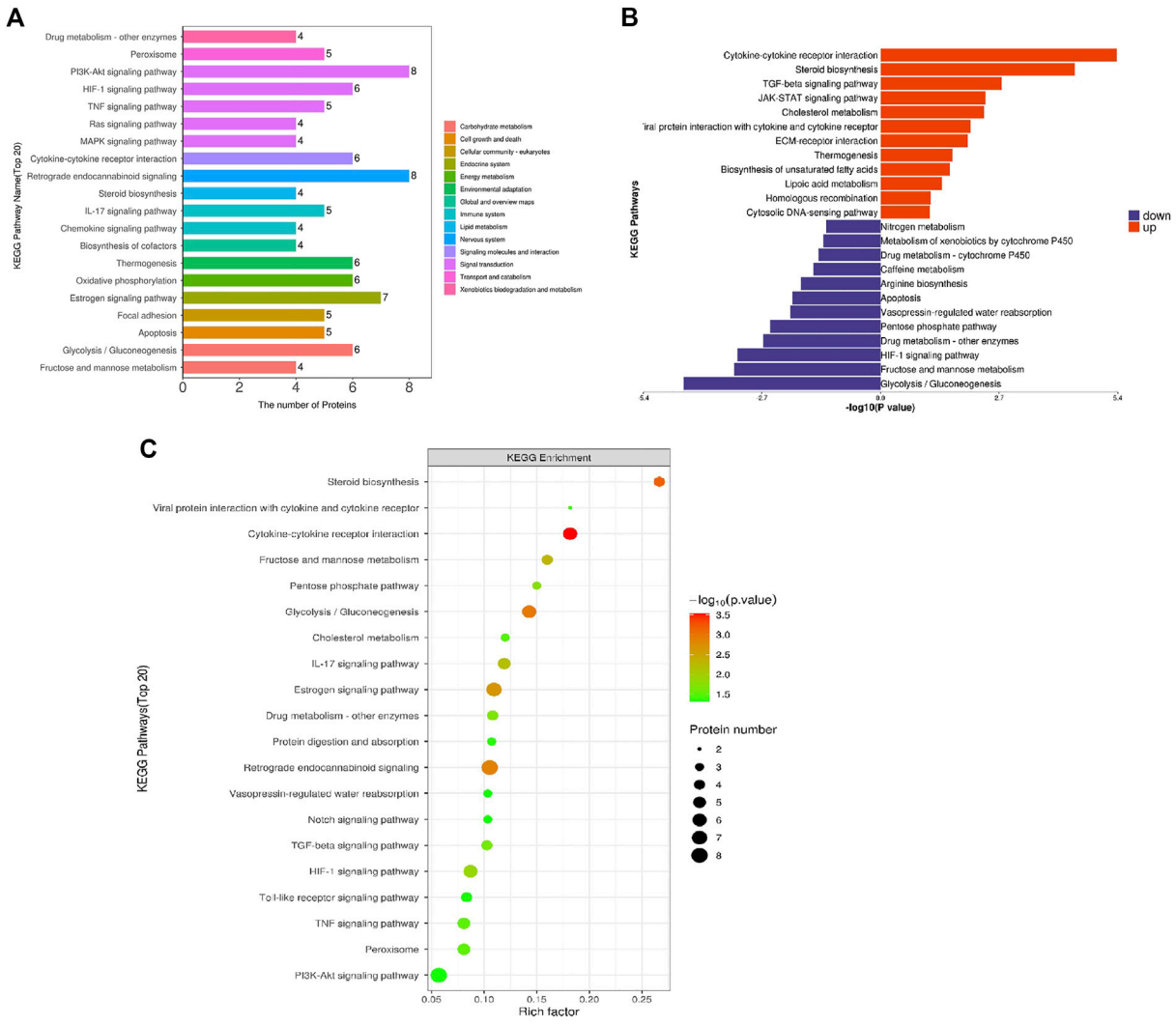

FIGURE 3
KEGG pathway enrichment analysis of differentially expressed proteins in loperamide-treated HT22 cells. **(A)** KEGG pathway annotation statistics for differentially expressed proteins. **(B)** KEGG pathway differential expression analysis map. **(C)** KEGG pathway enrichment bubble map.

system, SPP1 was identified as a novel SC-expressed gene product regulated by axon-derived signaling (Mantuano et al., 2008). SPP1 was found to be upregulated after sciatic nerve transaction and is responsible for motor regeneration in rats (Wang et al., 2011). However, another study reported that the expression of SPP1 was downregulated after sciatic nerve injury in rats (Love and Thompson, 1998). SPP1 promotes Schwann cell (SC) proliferation and inhibits apoptosis through the PKCα signaling pathway by binding to CD44 andαvβ3 (Pegoraro et al., 2011). Thus, it is likely that mu opioid agonist-treated HT22 cells affect their migration and differentiation.

A physiological component of the cell-autonomous pathway of neuronal development is E3 ubiquitin ligase (TTC3).and its knockdown results in increased neurite extension. However, reductions in TTC3 levels are not sufficient to differentiate neurons and alter Golgi organization (Zhou et al., 2021). TTC3's primary role may be to suppress neurite outgrowth by acting on growth cones rather than the Golgi apparatus, which is consistent with the finding that only a tiny portion of TTC3 is linked to the Golgi apparatus. However, TTC3 can express itself above physiological levels in Down's syndrome (DS) and other neurological diseases (Berto et al., 2007), it can disrupt Golgi compactness and impair neurite extension. These findings may be relevant for understanding how elevated TTC3 levels in DS affect the overall intellectual disability phenotype. Mu opioid receptor activation in HT22 cells can affect the expression of TTC3, which may affect the extension of neural synapses and affect the development of a neural function.

The transcription factor Hes1 is a key component of the Notch signaling pathway. The transmembrane protein Notch undergoes membrane-region processing upon activation of Notch signaling, releasing the intracellular domain of Notch. The important Notch signaling mediator Rbpj and this fragment subsequently form a complex in the nucleus, where it stimulates the production of downstream genes including Hes1 and Hes5 (Artavanis-Tsakonas et al., 1999; Hiroshi, 2008). Hes1 and Hes5 suppress the expression of proneural genes and prevent neuronal differentiation (Hiroshi, 2008). Thus, through Notch signaling, differentiating neurons prevent nearby cells from maturing into neurons, retaining neural stem cells (NSCs), a process known as lateral inhibition (Artavanis-Tsakonas et al., 1999; Hiroshi, 2008). Rbpj deletion disrupts Notch signaling, impairing lateral inhibition, and depleting both active and quiescent

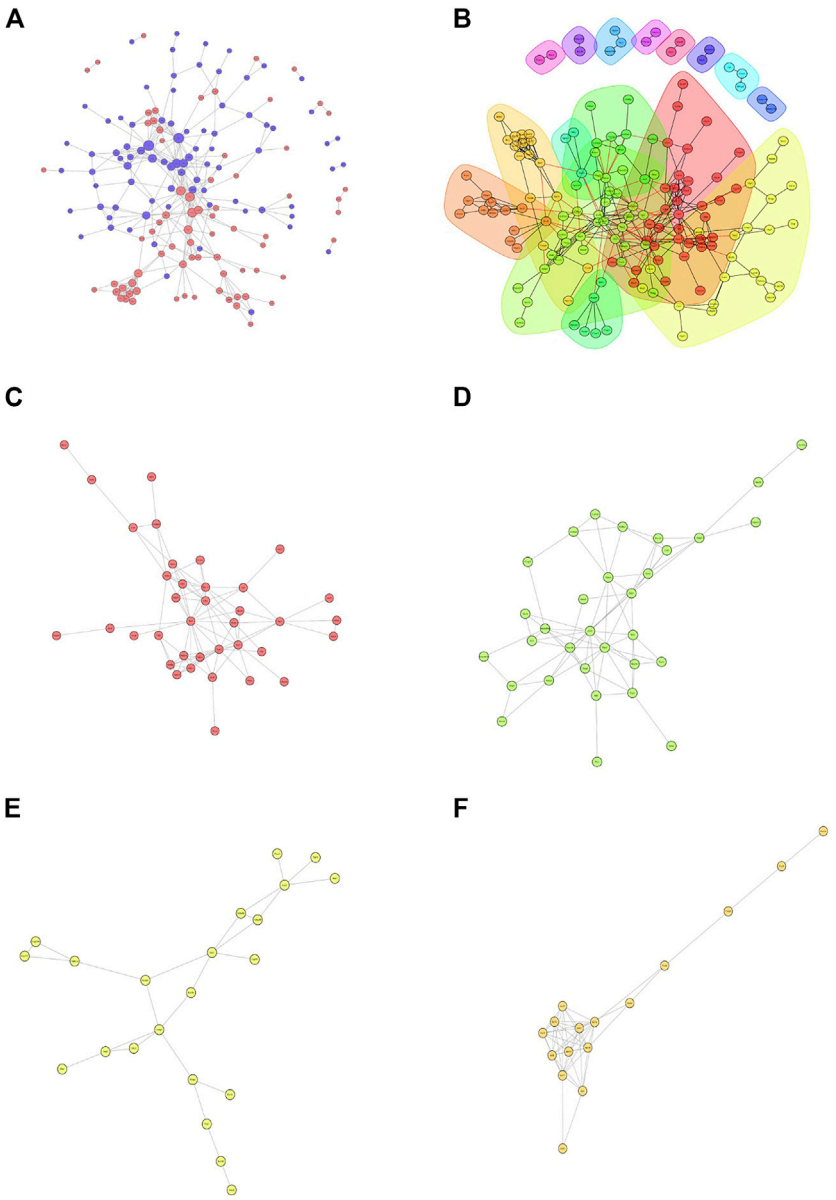

FIGURE 4
Analyses of the protein-protein interaction networks for the differentially expressed proteins in loperamide-treated. **(A)** Group differentially expressed protein interaction network diagram. **(B)** Interaction network diagram for functional classification diagram **(C–F)** interaction network of key genes diagram.

NSCs (Imayoshi et al., 2010). Therefore, loperamide will likely cause the differentiation of neuronal cells HT22 to be affected. There are five members of the thrombospondin (Thbs) stromal cell glycoprotein family (Thbs1–5), and although they are secreted, as intracellular chaperones, they also respond to stress in the endoplasmic reticulum (ER), increase secretory pathway activity, extracellular matrix production, and attachment complex membrane residency (Vanhoutte et al., 2016; Brody et al., 2018; Schips et al., 2019). Thbs proteins from group A form trimers made up of Thbs1 and Thbs2, whereas proteins from group B form pentamers made up of Thbs3, Thbs4, and Thbs5 (Adams and Lawler, 2011). During development, Thbs genes show distinct spatiotemporal expression patterns, but the expression of all five genes after an injury is typically observed only in adults. Single Thbs-null mice have been described as having multiple phenotypes, although our recent discovery that mice with knockout of all five Thbs genes survive into adulthood suggests that these proteins are involved in injury and stress responses. Thbs1 has been demonstrated to induce lethal heart atrophy through PERK-ATF4-regulated autophagy, and so mu opioid receptor agonism may have a role in the regulation of autophagy in HT22 cells.

The phosphatidylinositol-3-kinase (PI3K)/Akt and mammalian target of rapamycin (mTOR) signaling pathways are critical for many aspects of cell growth and survival under physiological and pathological conditions. Protein kinase B (Akt) is also activated by PI3K activation, and Akt then activates mTOR by phosphorylating and deactivating the tuberous sclerosis complex. Cell development in response to advantageous nutrients and other growth stimuli is principally regulated by mTOR. By phosphorylating and

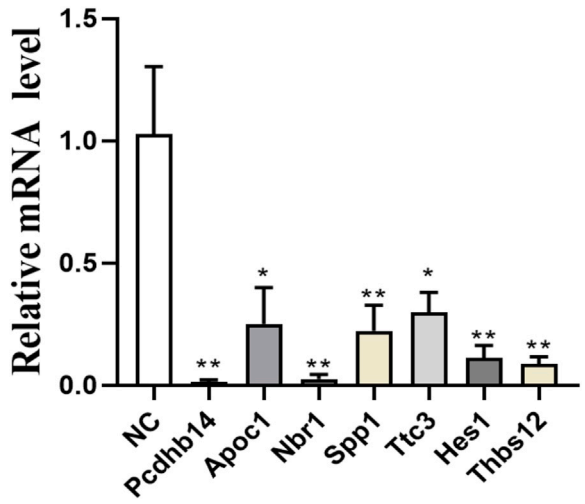

FIGURE 5
Expression of Pcdhb14, Apoc1, Nbr1, Spp1, Ttc3, Hes1, Thbs1 genes after loperamide treatment by QPCR (*p < 0.05; **p < 0.01).

inactivating the tuberous sclerosis complex, protein kinase B (Akt) is also activated in response to PI3K activation. Akt then activates mTOR. While mTOR primarily modulates cell growth in response to growth-promoting foods and other stimuli, it also affects aging and other physiological processes connected to nutrition, such as protein synthesis, ribosome biogenesis, and cell proliferation in adults with very restricted growth (Jacinto and Hall, 2003). mTOR has been linked to numerous neurodevelopmental and neuropsychiatric disorders and is essential for the central nervous system's (CNS) neuronal plasticity, learning, and memory (Costa-Mattioli and Monteggia, 2013). Brain-derived neurotrophic factor (BDNF)-dependent survival requires mTOR activation (Smith et al., 2014). Following CNS damage, conditional deletion of intrinsically negative mTOR regulators such phosphatase and tensin homolog (PTEN) or tuberous sclerosis complex 1 promotes axonal regeneration (Park et al., 2008). Furthermore, activation of mTOR promotes changes in dendritic morphology and the formation of synaptic contacts (Urbanska et al., 2012). Memory reconsolidation and late long-term potentiation (L-LTP) depend on mtor-mediated translational control (Stoica et al., 2011). Our results suggest that mu-opioid receptor agonist treatment of HT22 cells mainly affects the PI3K/AKT signaling pathway, and thus the PI3K/AKT signaling pathway may play an important role as a major regulatory mechanism for the pathological state of HT22 cells. And some studies have also shown that the PI3K/AKT signaling pathway is necessary for mu-opioid receptor activation. Our proteomic sequencing results are consistent with previous studies (Kam et al., 2004).

In summary, we found that mu opioid receptor activation may affect the PI3K/AKT signaling pathway, Notch signaling pathway, neuronal apoptosis, differentiation, autophagy, and lipid metabolism in neurons, Especially the PI3K/AKT signaling pathway. This may be part of the mechanism of the well-known toxic effects of mu opioid receptor activation on nerve cells during the process of medication. In conclusion, our study guides clinical anesthesia and advances our understanding of mu opioid receptor agonist-induced nerve damage. In the future, it will be of interest to combine mu opioid receptor agonists and inhibitors to further study the function and role of mu opioid receptors in nerve cells.

Conclusion

We used mu opioid receptor agonists to study the effect of mu opioid receptor activation on nerve cells. Through proteomic sequencing and RT-PCR, we examined the expression of relevant target genes after mu opioid receptor activation and correlated the results with observed nerve cell damage.

Data availability statement

The original contributions presented in the study are publicly available. This data can be found here: http://proteomecentral.proteomexchange.org/cgi/GetDataset/ PXD004687.

Author contributions

XZ and DQ conceived and designed the research study. YL, DZ and JL collected the data for the study. XZ and YL, DZ and JL analyzed the data and interpreted the results. XZ wrote the first draft of the manuscript. XZ and DQ revised the manuscript. All authors contributed to the article and approved the submitted version.

Funding

This study was funded by the Wenzhou Science and Technology Bureau (Grant No. Y20180067).

Acknowledgments

We wish to acknowledge all the participants in this study.

Conflict of interest

The authors declare that the research was conducted in the absence of any commercial or financial relationships that could be construed as a potential conflict of interest.

Publisher's note

Supplementary material

The Supplementary Material for this article can be found online at: https://www.frontiersin.org/articles/10.3389/fphar.2022.1022449/full#supplementary-material

References

Adams, J. C., and Lawler, J. (2011). The thrombospondins. *Cold Spring Harb. Perspect. Biol.* 3 (10), A009712. doi:10.1101/Cshperspect.A009712

Artavanis-Tsakonas, S., Rand, M. D., and Lake, R. J. (1999). Notch signaling: Cell fate control and signal integration in development. *Science* 284 (5415), 770–776. doi:10.1126/Science.284.5415.770

Behl, C. (1998). Effects of glucocorticoids on oxidative stress-induced hippocampal cell death: Implications for the pathogenesis of Alzheimer's disease. *Exp. Gerontol.* 33 (7-8), 689–696. doi:10.1016/S0531-5565(98)00019-9

Behl, C., Widmann, M., Trapp, T., and HolsboerF. (1995). 17-Beta estradiol protects neurons from oxidative stress-induced cell death in vitro. *Biochem. Biophys. Res. Commun.* 216 (2), 473–482. doi:10.1006/Bbrc.1995.2647

Berto, G., Camera, P., Fusco, C., Imarisio, S., Ambrogio, C., Chiarle, R., et al. (2007). The down syndrome critical region protein Ttc3 inhibits neuronal differentiation via rhoa and citron kinase. *J. Cell Sci.* 120 (11), 1859–1867. doi:10.1242/Jcs.000703

Bouwmeester, T., Bauch, A., Ruffner, H., Angrand, P. O., Bergamini, G., Croughton, K., et al. (2004). A physical and functional map of the human tnf-alpha/nf-kappa B signal transduction pathway. *Nat. Cell Biol.* 6 (2), 97–105. doi:10.1038/Ncb1086

Brody, M. J., Vanhoutte, D., Schips, T. G., Boyer, J. G., Bakshi, C. V., Sargent, M. A., et al. (2018). Defective flux of thrombospondin-4 through the secretory pathway impairs cardiomyocyte membrane stability and causes cardiomyopathy. *Mol. Cell Biol.* 38 (14), E00114. doi:10.1128/Mcb.00114-18

Ca Ccamo, A., and Oddo, S. (2012). P1-271: Inducing autophagy by rapamycin before, but not after, the formation of plaques and tangles ameliorates cognitive deficits. *Alzheimer's. &Amp;. Dement.* 8, 551. doi:10.1016/J.Jalz.2012.05.551

Costa-Mattioli, M., and Monteggia, L. M. (2013). Mtor complexes in neurodevelopmental and neuropsychiatric disorders. *Nat. Neurosci.* 16 (11), 1537–1543. doi:10.1038/Nn.3546

Edmondson, R. D., Vondriska, T. M., Biederman, K. J., Zhang, J., Jones, R. C., Zheng, Y., et al. (2002). Protein kinase C epsilon signaling complexes include metabolism- and transcription/translation-related proteins: Complimentary separation techniques with lc/ms/ms. *Mol. Cell Proteomics* 1 (6), 421–433. doi:10.1074/Mcp.M100036-Mcp200

Halder, D., Mandal, C., Lee, B. H., Lee, J. S., Choi, M. R., Chai, J. C., et al. (2015). Pcdhb14- and gabrb1-like nervous system developmental genes are altered during early neuronal differentiation of nccit cells treated with ethanol. *Hum. Exp. Toxicol.* 34 (10), 1017–1027. doi:10.1177/0960327114566827

Herring, L. E., Grant, K. G., Blackburn, K., Haugh, J. M., and Goshe, M. B. (2015). Development of A tandem affinity phosphoproteomic method with motif selectivity and its application in analysis of signal transduction networks. *J. Chromatogr. B Anal. Technol. Biomed. Life Sci.* 988, 166–174. doi:10.1016/J.Jchromb.2015.02.017

Hiroshi, K. (2008). Cheminform abstract: Spin-ladder iron oxide: Sr3fe2o5 [J]. *Cheminform* 39 (44), 44023. doi:10.1002/chin.200844023

Imayoshi, I., Sakamoto, M., Yamaguchi, M., Mori, K., and Kageyama, R. (2010). Essential roles of Notch signaling in maintenance of neural stem cells in developing and adult brains. *J. Neurosci.* 30 (9), 3489–3498. doi:10.1523/Jneurosci.4987-09.2010

Jacinto, E., and Hall, M. N. (2003). Tor signalling in bugs, brain and brawn. *Nat. Rev. Mol. Cell Biol.* 4 (2), 117–126. doi:10.1038/Nrm1018

Jessen, K. R., and Mirsky, R. (1999). Schwann cells and their precursors emerge as major regulators of nerve development. *Trends Neurosci.* 22 (9), 402–410. doi:10.1016/S0166-2236(98)01391-5

Kam, A. Y., Chan, A. S., and Wong, Y. H. (2004). Phosphatidylinositol-3 kinase is distinctively required for mu-but not kappa-opioid receptor-induced activation of c-Jun N-terminal kinase. *J. Neurochem.* 89 (2), 391–402. doi:10.1111/j.1471-4159.2004.02338.x

Kieffer, B. L., and Gaveriaux-Ruff, C. (2002). Exploring the opioid system by gene knockout. *Prog. Neurobiol.* 66 (5), 285–306. doi:10.1016/S0301-0082(02)00008-4

Kieffer, B. L. (1995). Recent advances in molecular recognition and signal transduction of active peptides: Receptors for opioid peptides. *Cell Mol. Neurobiol.* 15 (6), 615–635. doi:10.1007/BF02071128

Kim, E. J., Koh, S. H., Ha, J., Na, D. L., Seo, S. W., Kim, H. J., et al. (2021). Increased telomere length in patients with frontotemporal dementia syndrome. *J. Neurol. Sci.* 428, 117565. doi:10.1016/J.Jns.2021.117565

Kirkin, V., Lamark, T., Johansen, T., and Dikic, I. (2009). Nbr1 cooperates with P62 in selective autophagy of ubiquitinated targets. *Autophagy* 5 (5), 732–733. doi:10.4161/Auto.5.5.8566

Kshirsagar, S., Sawant, N., Morton, H., Reddy, A. P., and Reddy, P. H. (2022). Protective effects of mitophagy enhancers against amyloid beta-induced mitochondrial and synaptic toxicities in alzheimer disease. *Hum. Mol. Genet.* 31 (3), 423–439. doi:10.1093/Hmg/Ddab262

Kulich, S. M., and Chu, C. T. (2001). Sustained extracellular signal-regulated kinase activation by 6-hydroxydopamine: Implications for Parkinson's disease. *J. Neurochem.* 77 (4), 1058–1066. doi:10.1046/J.1471-4159.2001.00304.X

Leduc, V., Jasmin-Belanger, S., and Poirier, J. (2010). Apoe and cholesterol homeostasis in Alzheimer's disease. *Trends Mol. Med.* 16 (10), 469–477. doi:10.1016/J.Molmed.2010.07.008

Liesi, P. (1997). Ethanol-exposed central neurons fail to migrate and undergo apoptosis. *J. Neurosci. Res.* 48 (5), 439–448. doi:10.1002/(Sici)1097-4547(19970601)48:5<439:Aid-Jnr5>3.0.Co;2-F

Love, F. M., and Thompson, W. J. (1998). Schwann cells proliferate at rat neuromuscular junctions during development and regeneration. *J. Of Neurosci. Official J. Of Soc. Neurosci.* 18 (22), 9376–9385. doi:10.1523/Jneurosci.18-22-09376.1998

Mantuano, E., Inoue, G., Li, X., Takahashi, K., Gaultier, A., Gonias, S. L., et al. (2008). The hemopexin domain of matrix metalloproteinase-9 activates cell signaling and promotes migration of Schwann cells by binding to low-density lipoprotein receptor-related protein. *J. Neurosci.* 28 (45), 11571–11582. doi:10.1523/Jneurosci.3053-08.2008

Mardakheh, F. K., Yekezare, M., Machesky, L. M., and Heath, J. K. (2009). Spred2 interaction with the late endosomal protein Nbr1 down-regulates fibroblast growth factor receptor signaling. *J. Cell Biol.* 187 (2), 265–277. doi:10.1083/Jcb.200905118

Matthes, H. W., Maldonado, R., Simonin, F., Valverde, O., Slowe, S., Kitchen, I., et al. (1996). Loss of morphine-induced analgesia, reward effect and withdrawal symptoms in mice lacking the mu-opioid-receptor gene. *Nature* 383 (6603), 819–823. doi:10.1038/383819a0

Park, K. K., Liu, K., Hu, Y., Smith, P. D., Wang, C., Cai, B., et al. (2008). Promoting axon regeneration in the adult cns by modulation of the pten/mtor pathway. *Science* 322 (5903), 963–966. doi:10.1126/Science.1161566

Pegoraro, E., Hoffman, E. P., Piva, L., Gavassini, B. F., Cagnin, S., ErmaniM., et al. (2011). Spp1 genotype is A determinant of disease severity in duchenne muscular dystrophy. *Neurology* 76 (3), 219–226. doi:10.1212/Wnl.0b013e318207afeb

Reddy, P. H., Yin, X., Manczak, M., Kumar, S., Pradeepkiran, J. A., Vijayan, M., et al. (2018). Mutant app and amyloid beta-induced defective autophagy, mitophagy, mitochondrial structural and functional changes and synaptic damage in hippocampal neurons from Alzheimer's disease. *Hum. Mol. Genet.* 27 (14), 2502–2516. doi:10.1093/Hmg/Ddy154

Regnard, C., Twycross, R., Mihalyo, M., and Wilcock, A. (2011). Loperamide. *J. Pain Symptom Manage* 42 (2), 319–323. doi:10.1016/J.Jpainsymman.2011.06.001

Schafer, M., Goodenough, S., Moosmann, B., and Behl, C. (2004). Inhibition of glycogen synthase kinase 3 beta is involved in the resistance to oxidative stress in neuronal Ht22 cells. *Brain Res.* 1005 (1-2), 84–89. doi:10.1016/J.Brainres.2004.01.037

Schips, T. G., Vanhoutte, D., Vo, A., Correll, R. N., Brody, M. J., Khalil, H., et al. (2019). Thrombospondin-3 augments injury-induced cardiomyopathy by intracellular integrin inhibition and sarcolemmal instability. *Nat. Commun.* 10 (1), 76. doi:10.1038/S41467-018-08026-8

Smith, E. D., Prieto, G. A., Tong, L., Sears-Kraxberger, I., Rice, J. D., Steward, O., et al. (2014). Rapamycin and interleukin-1β impair brain-derived neurotrophic factor-dependent neuron survival by modulating autophagy. *J. Biol. Chem.* 289 (30), 20615–20629. doi:10.1074/Jbc.M114.568659

Stoica, L., Zhu, P. J., Huang, W., Zhou, H., Kozma, S. C., and Costa-Mattioli, M. (2011). Selective pharmacogenetic inhibition of mammalian target of rapamycin complex I (Mtorc1) blocks long-term synaptic plasticity and memory storage. *Proc. Natl. Acad. Sci. U. S. A.* 108 (9), 3791–3796. doi:10.1073/Pnas.1014715108

Stoll, G., and Jander, S. (1999). The role of microglia and macrophages in the pathophysiology of the cns. *Prog. Neurobiol.* 58 (3), 233–247. doi:10.1016/S0301-0082(98)00083-5

Tiwari, V., Anderson, M., Yang, F., Zheng, Q., Tiwari, V., He, S-Q., et al. (2018). Peripherally acting M-opioid receptor agonists attenuate ongoing pain-associated behavior and spontaneous neuronal activity after nerve injury in rats. *Anesthesiology* 128 (6), 1220–1236. doi:10.1097/Aln.0000000000002191

Torrance, N., Lawson, K. D., Afolabi, E., Bennett, M. I., Serpell, M. G., Dunn, K. M., et al. (2014). Estimating the burden of disease in chronic pain with and without neuropathic characteristics: Does the choice between the eq-5d and sf-6d matter? *J. Pain* 155 (10), 1996–2004. doi:10.1016/J.Pain.2014.07.001

Urbanska, M., Gozdz, A., Swiech, L. J., and Jaworski, J. (2012). Mammalian target of rapamycin complex 1 (Mtorc1) and 2 (Mtorc2) control the dendritic arbor morphology of hippocampal neurons. *J. Biol. Chem.* 287 (36), 30240–30256. doi:10.1074/Jbc.M112.374405

Vangipuram, S. D., Grever, W. E., Parker, G. C., and Lyman, W. D. (2008). Ethanol increases fetal human neurosphere size and alters adhesion molecule gene expression. *Alcohol Clin. Exp. Res.* 32 (2), 339–347. doi:10.1111/J.1530-0277.2007.00568.X

Vanhoutte, D., Schips, T. G., Kwong, J. Q., Davis, J., Tjondrokoesoemo, A., Brody, M. J., et al. (2016). Thrombospondin expression in myofibers stabilizes muscle membranes. *J. Elife* 5, E17589. doi:10.7554/Elife.17589

Vargas, M. E., and Barres, B. A. (2007). Why is wallerian degeneration in the cns so slow? [j]. *Annu. Rev. Neurosci.* 30, 153–179. doi:10.1146/Annurev.Neuro.30.051606.094354

Vestergaard, M., Hamada, T., Morita, M., and Takagi, M. (2010). Cholesterol, lipids, amyloid beta, and Alzheimer's. *Curr. Alzheimer Res.* 7 (3), 262–270. doi:10.2174/156720510791050821

Walinda, E., Morimoto, D., Sugase, K., Konuma, T., Tochio, H., and Shirakawa, M. (2014). Solution structure of the ubiquitin-associated (uba) domain of human autophagy

receptor Nbr1 and its interaction with ubiquitin and polyubiquitin. *J. Biol. Chem.* 289 (20), 13890–13902. doi:10.1074/Jbc.M114.555441

Wang, Y., Hu, C., Dong, R., Huang, X., and Qiu, H. (2011). Platelet-derived growth factor-D promotes ovarian cancer invasion by regulating matrix metalloproteinases 2 and 9. *Asian Pac J. Cancer Prev.* 12 (12), 3367–3370. doi:10.1159/000328275

Yamamoto, A., Lucas, J. J., and Hen, R. (2000). Reversal of neuropathology and motor dysfunction in A conditional model of huntington's disease. *Cell* 101 (1), 57–66. doi:10.1016/S0092-8674(00)80623-6

Zellner, S., Schifferer, M., and Behrends, C. (2021). Systematically defining selective autophagy receptor-specific cargo using autophagosome content profiling. *Mol. Cell* 81 (6), 1337–1354.E8. doi:10.1016/J.Molcel.2021.01.009

Zhou, J., Wang, J., Cheng, Y., Chi, Y. J., Fan, B., Yu, J. Q., et al. (2013). Nbr1-Mediated selective autophagy targets insoluble ubiquitinated protein aggregates in plant stress responses. *Plos Genet.* 9 (1), E1003196. doi:10.1371/Journal.Pgen.1003196

Zhou, X., Chen, X., Hong, T., Zhang, M., Cai, Y., and Cui, L. (2021). TTC3-Mediated protein quality control, A potential mechanism for cognitive impairment. *Cell Mol. Neurobiol.* 42, 1659–1669. doi:10.1007/s10571-021-01060-z

Zhu, M., Chen, J., Wen, M., Sun, Z., Sun, X., Wang, J., et al. (2014). Propofol protects against angiotensin ii-induced mouse hippocampal Ht22 cells apoptosis via inhibition of P66shc mitochondrial translocation. *Neuromolecular Med.* 16 (4), 772–781. doi:10.1007/S12017-014-8326-6

Zu, T., Duvick, L. A., Kaytor, M. D., Berlinger, M. S., Zoghbi, H. Y., Clark, H. B., et al. (2004). Recovery from polyglutamine-induced neurodegeneration in conditional Sca1 transgenic mice. *J. Neurosci.* 24 (40), 8853–8861. doi:10.1523/Jneurosci.2978-04.2004

frontiers | Frontiers in Pharmacology

TYPE Original Research
PUBLISHED 10 January 2023
DOI 10.3389/fphar.2022.1066713

OPEN ACCESS

EDITED BY
Jiaqiang Zhang,
Zhengzhou University, China

REVIEWED BY
Francisco Jose Fernandez Gomez,
University of Murcia, Spain
Chun Yang,
Nanjing Medical University, China

*CORRESPONDENCE
Ping Zhao,
zhaop@sj-hospital.org

SPECIALTY SECTION
This article was submitted to Neuropharmacology, a section of the journal Frontiers in Pharmacology

RECEIVED 11 October 2022
ACCEPTED 29 December 2022
PUBLISHED 10 January 2023

CITATION
Wan Y, Wu Z, Li X and Zhao P (2023), Maternal sevoflurane exposure induces neurotoxicity in offspring rats *via* the CB1R/CDK5/p-tau pathway.
Front. Pharmacol. 13:1066713.
doi: 10.3389/fphar.2022.1066713

Maternal sevoflurane exposure induces neurotoxicity in offspring rats *via* the CB1R/CDK5/p-tau pathway

Yuxiao Wan, Ziyi Wu, Xingyue Li and Ping Zhao*

Department of Anesthesiology, Shengjing Hospital of China Medical University, Shenyang, China

Sevoflurane is widely used for maternal anesthesia during pregnancy. Sevoflurane exposure of rats at mid-gestation can cause abnormal development of the central nervous system in their offspring. Sevoflurane is known to increase the expression of cannabinoid 1 receptor (CB1R) in the hippocampus. However, the effect of cannabinoid 1 receptor on fetal and offspring rats after maternal anesthesia is still unclear. At gestational day 14, pregnant rats were subjected to 2-h exposure to 3.5% sevoflurane or air. Rats underwent intraperitoneal injection with saline or rimonabant (1 mg/kg) 30 min prior to sevoflurane or air exposure. cannabinoid 1 receptor, cyclin-dependent kinase 5 (CDK5), p35, p25, tau, and p-tau expression in fetal brains was measured at 6, 12, and 24 h post-sevoflurane/air exposure. Neurobehavioral and Morris water maze tests were performed postnatal days 3–33. The expression of cannabinoid 1 receptor/cyclin-dependent kinase 5/p-tau and histopathological staining of brain tissues in offspring rats was observed. We found that a single exposure to sevoflurane upregulated the activity of cyclin-dependent kinase 5 and the level of p-tau *via* cannabinoid 1 receptor. This was accompanied by the diminished number of neurons and dendritic spines in hippocampal CA1 regions. Finally, these effects induced lower scores and platform crossing times in behavioral tests. The present study suggests that a single exposure to 3.5% sevoflurane of rats at mid-gestation impairs neurobehavioral abilities and cognitive memory in offspring. cannabinoid 1 receptor is a possible target for the amelioration of postnatal neurobehavioral ability and cognitive memory impairments induced by maternal anesthesia.

KEYWORDS

CB1R, learning and memory, hippocampus, rimonabant, sevoflurane, tau

Introduction

In recent years, the mass emergence of fetal treatments, intrauterine diagnoses, and minimally invasive technologies has increased the numbers of women receiving surgical treatments during pregnancy. This has triggered a sharp elevation in women exposed to anesthetics at mid-gestation (Eskandari and Alipour, 2020). Due to their solubility and pharmacokinetics, anesthetics may easily pass through the placental barrier, resulting in a risk of fetal exposure to anesthetics (Reitman and Flood, 2011). Of note, the mid-gestation is an important period of fetal neural development and neuron migration, during which the nervous system is particularly susceptible to the external environment. Clinical research has reported that general anesthesia exposure may elicite the development of abnormal behaviors and learning ability in postnatal fetuses (Creeley and Olney, 2010; Sun, 2010). Sevoflurane is the most widely used inhaled anesthetic and is often used in pregnant women. In 2016, the US Food

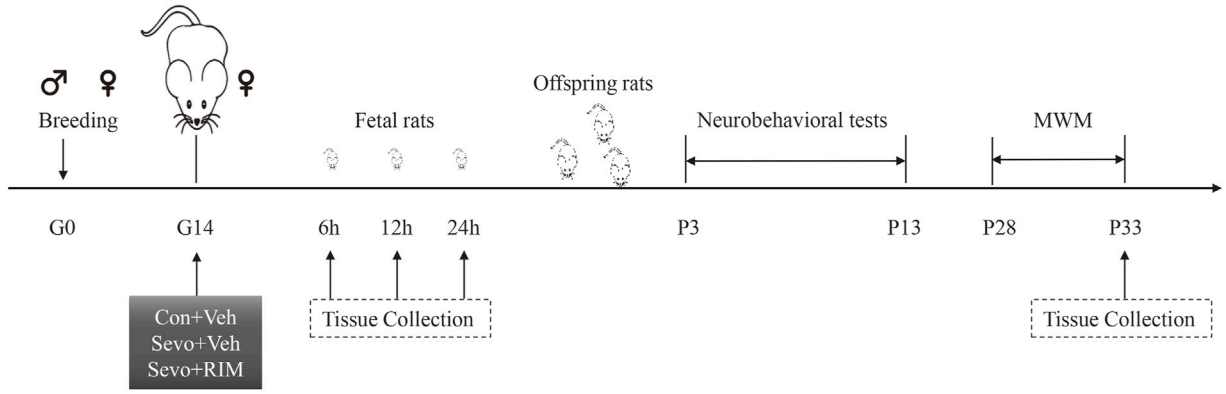

FIGURE 1
Schematic timeline of this research. Pregnant rats received 2-h exposure of 3.5% sevoflurane or air in the day 0 of gestation (G0). Thirty min prior to sevoflurane or air exposure, rats were subjected to intraperitoneal injection with Rimonabant (RIM, 1 mg/kg) or vehicle (Veh). Brain tissues were harvested from fetal rats at 6, 12, or 24 h subsequent to sevoflurane exposure. The offspring rats in each group were employed for neurobehavioral tests and Morris water maze (MWM) tests during P3–33. Next, the hippocampus was harvested 1 h after MWM test.

and Drug Administration announced that repeated or prolonged operations on fetuses and infants may lead to neurotoxicity related to exposure to anesthetics (Stockwell, 2017). Our previous research has shown that repeated exposure to 3% sevoflurane or a single exposure to 3.5% sevoflurane of pregnant rats induced long-term learning and memory impairment in their neonatal rats (Wang et al., 2018; Wu et al., 2018). Therefore, this study continues this exploration. Here, we explored the molecular mechanisms of memory impairments in neonatal rats subsequent to maternal exposure to 3.5% sevoflurane during pregnancy.

Cannabinoid receptor 1 (CB1R) is highly expressed in the presynaptic membrane of nerve endings and assumes a pivotal role in regulating neurotransmitter release, nerve development, synapse formation, learning, and memory (Cristino et al., 2020). Neurodegenerative diseases, such as Alzheimer's disease, multiple sclerosis, and Huntington's disease, are linked to the aberrant expression of CB1R (Aymerich et al., 2018). The pathophysiological manifestations and clinical symptoms of anesthesia-induced neurological abnormalities are similar to these neurodegenerative disorders. However, it is still unclear whether CB1R is involved in sevoflurane anesthesia-related memory impairments.

CB1R can mediate the activation of cyclin-dependent kinase-5 (CDK5) signal transduction, delay synapse maturation, and arouse neurobehavioral deficits (Joshi et al., 2019). CDK5 activity is orchestrated by lipid associated membrane protein (p35) and its cleavage product (p25), and a change in p25/p35 ratio reflects this activity. *In vitro* experiment showed that a sevoflurane-induced increase in CDK5 blocks the dendritic development of cortical neurons in rats (Liao et al., 2021). Additionally, specific inhibition of CDK5 ameliorates the symptoms of cognitive impairment in sevoflurane-stimulated neonatal rats (Liu et al., 2017). Tau protein is involved in facilitating the assembly of microtubules and is essential for maintaining the function, growth, and development of neurons (Stoothoff and Johnson, 2005). Numerous studies have established that the increase in CDK5 activity can cause the hyperphosphorylation of tau (p-tau), responsible for the destruction of neuronal functions (Xiao et al., 2018).

Therefore, the present study explores changes in the learning and memory of neonatal rats when maternal rats are exposed to 3.5% of sevoflurane at mid-gestation and investigates whether the CB1R/CDK5/tau pathway participates in this process.

Materials and methods

Animals

All Sprague Dawley rats were fed in a room at 23°C ± 1°C with a 12-h/12-h light/dark cycle and water and food *ad libitum*. All experiments were implemented under the ratification from the Laboratory Animal Care Committee of China Medical University (P2019PS198K). All procedures followed NIH Guidelines for the Care and Use of Laboratory Animals. Every effort was taken to minimize the number of used rats and their suffering.

Experimental design and treatment groups

The experimental protocol is shown in Figure 1. One male rat was caged with three female rats for mating. The female rats were thought to be in day 0 of gestation (G0) if sperm or vaginal emboli was detected. In total, 36 pregnant rats were randomly allocated into controls + vehicle (Con + Veh), sevoflurane + vehicle (Sevo + Veh), and sevoflurane + rimonabant, a selective antagonist of CB1R (Sevo + RIM) groups (n = 12 rats per group). 10 mg RIM was dissolved into 500 μL 5% DNSO to make stock solution. 10 μL stock solution was added into 80 μL 40% PEG300, 10 μL 5% Tween 80 and 100 μL saline. Vehicle solution was prepared as mentioned above, but without RIM. On G14, rats in the Sevo + Veh and Sevo + RIM groups were exposed to 3.5% sevoflurane with 30% oxygen in a specially constructed plastic chamber for 2 h. Animal facility rearing with 30% oxygen only was performed on control animals (Con + Veh) (Wang Y et al., 2018; Li XY et al., 2017). A solution of saline or rimonabant (1 mg/kg) was injected intraperitoneally 30 min before oxygen or sevoflurane exposure, respectively. The dose selection of rimonabant was based on

previous reports (Shivakumar et al., 2020) and our preliminary study. Cesarean sections (3 dams/group at each time point) were conducted at 6, 12, or 24 h after modeling. The fetal brains in each group (six offspring rats, two pups/dam) were extracted for molecular study. The remaining dams (n = 3 per group) were allowed to deliver naturally. The behavioral testing was performed on twelve offspring rats from each group (four pups/dam) during postnatal days P3–33. The brain tissues were collected 1 h after the Morris water maze (MWM) test.

Behavioral tests

Neonatal neurobehaviors can be used as an early sensitive index to reflect the functional development of brain in newborn. It is reported that the behavioral outcomes in the present study mature in neonatal rats after P7 (George et al., 2015).

Surface righting reflex

To evaluate the coordination of the offspring rats (pups), they were placed on their backs on a horizontal table. The time required for flipping to right themselves in position was recorded. This time was measured three times a day during P3–7 for each pup (Naik AA et al., 2015; Zhang Y et al., 2010; McDonnell-Dowling K et al., 2014).

Negative geotaxis reflex

The vestibular and proprioceptive functions of pups were evaluated by placing them on a 30° mesh incline in a head-down position. The time taken for pups to turn 180° to an upright position was recorded for a maximum of 60 s. Each pup performed this test three times a day during P3–7 (Naik AA et al., 2015; Zhang Y et al., 2010; McDonnell-Dowling K et al., 2014).

Forelimb grip test

This test was performed to evaluate the forelimb sensation, muscle strength, and reactivity of the pups. The pups grasped the horizontal rod of a suspension hanger (.5 cm in diameter) using their forelimbs on P7, 9, 11, and 13. The time duration when each pup was able to remain suspended before falling down to the sponge below was measured three times in 1 day and the average value was calculated (McDonnell-Dowling K et al., 2014; Adedara IA et al., 2017).

Cliff avoidance test

To evaluate the integration of exteroceptive input and locomotor output during P3–7, pups were put on a table with their head and forepaws over the edge. A positive result was recorded if the pups retreated or turned around, otherwise it was negative. The total observation time was 60 s and the observed data reflected the rate of positive responses (Naik AA et al., 2015; Khalki L et al., 2013).

Sensory reflexes

To evaluate the development of sensory ability, including ear-edge reflex and eyelid reflex, the eyelid and ear edge of the pups was touched with a sterile cotton swab during P6–13. If the corresponding reflex appeared, the trial was deemed positive. The results were expressed as the positive rate of each group (Horvath G et al., 2013).

MWM test

This behavioral test was conducted as documented in our previous research (Fan et al., 2021). Briefly, the maze (height: 60 cm, diameter: 180 cm) was divided into four quadrants. In the center of the second quadrant, a circular platform was submerged to a depth of 1.5 cm underneath the water surface. During P28–32, all rats completed four sessions each day attempting to locate the hidden platform. Each rat was allowed to swim 90 s without the platform On P33. A Noldus Ethovision XT video analysis system (Netherlands) was adopted for recording escape latency, the times of crossing the platform, and time spent in each quadrant.

Nissl staining

The procedures for this evaluation were performed as in our previous study. Briefly, three pups in each group were chosen for perfusion with saline and 4% paraformaldehyde. Afterwards, the whole brain of pups were collected and placed into 4% paraformaldehyde overnight at 4°C. After paraffin embedding, 4-μm-thick coronal slices were subjected to Nissl staining. Pyramidal cell layers in the CA1 area of the brain were photographed with a digital microscope. Nissl-positive neurons were counted using the ImageJ software.

Golgi staining

Golgi staining was carried out following the protocols of the FD rapid GolgiStain™ kit (#pk401A, FD NeuroTechnologies, Inc. Columbia, MD, United States); the rats (3 rats per group) underwent transcardial perfusion of phosphate buffered saline (PBS), and then, their brains were collected and fixed in kit solutions A and B for 2 weeks. Thereafter, brain tissues were transferred to kit solution C for 72-h incubation. The staining was conducted on a 150-μm-thick brain section using kit solutions D and E. As a final step, spine density was tested for each neuron using ImageJ software (number of spines per 10 m).

Immunofluorescence staining

The rats (3 rats in each group) received transcardial perfusion with PBS before 4% paraformaldehyde treatment. Post-fixation with 4% paraformaldehyde and dehydration in 30% sucrose were performed at 4°C for 24 h. Ten-micron-thick coronal sections of the hippocampus were obtained with a cryostat. Samples were probed with primary antibodies against CBR1 (1:1000, #93815, CST, Danvers, MA, United States), CDK5 (1:1000, #14145, CST), and Nestin (1:200,

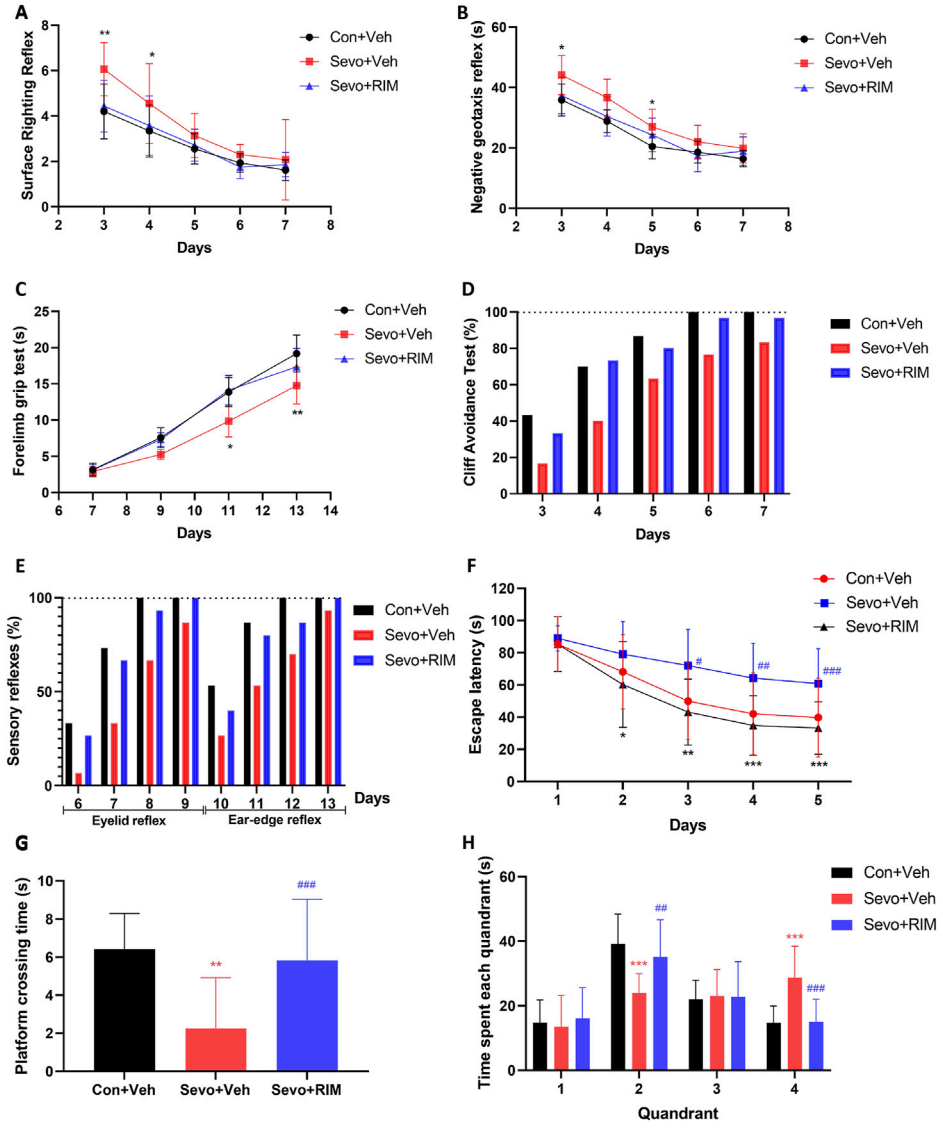

FIGURE 2
Maternal sevoflurane exposure caused dysfunction in neurobehaviors and cognitive memory in neonatal rats. Neurobehavioral tests (n = 12 per group) were performed during P3–13 and included surface righting reflex **(A)**, negative geotaxis reflex **(B)**, forelimb grip test **(C)**, cliff avoidance test **(D)**, and sensory reflexes **(E)**. The MWM tests (n = 12 per group) were carried out during P28–33. Escape latency **(F)**, the times of crossing the platform **(G)**, and time spent in each quadrant **(H)** were recorded. Data are depicted as mean ± S.E.M. *p < .05, **p < .01, vs. the Con + Veh group; #p < .05, vs. the Sevo + Veh group.

#11306, Abcam, Cambridge, England). After 24 h, samples were incubated with secondary antibodies. Nuclei were counterstained with DAPI stain solution (#AR1177, Boster Biological Technology, Pleasanton, CA, United States).

Western blotting

Western blotting was performed on fetal brain tissue and offspring hippocampus according to the method as previously described by our research group (Wu ZY et al., 2018; Li XY et al., 2017). The whole brains of fetuses were removed immediately when the female rats were under cesarean section. Hippocampus of offspring rats was harvested at P33 after the behavior tests. Fetal brain tissue and hippocampus homogenates (n = 3 per group) were prepared for determination of CB1R, CDK5, p35, p25, tau, p-tau, and GAPDH levels. Protein levels were examined by incubating hippocampus homogenates with antibodies to CB1R (1:1000, Cell Signaling Technology, 93,815, United States), CDK5 (1:1000, Cell Signaling Technology, 14,145, United States), p35 (1:1000, Cell Signaling Technology, 2,680, United States), p25 (1:1000, Cell Signaling Technology, 2,680, United States), tau (1:1000, Cell Signaling Technology, 46,687, United States), p-tau (1:1000, Cell Signaling Technology, 20,194, United States), and GAPDH (1:1000, Cell Signaling Technology, 2,118, United States). If the target protein is phosphorylation index (tau,p-tau), phosphatase inhibitors should be added in addition to PMSF. Visualization of the bands was performed with enhanced chemiluminescence and quantification was carried out with ImageJ (NIH Image, United States).

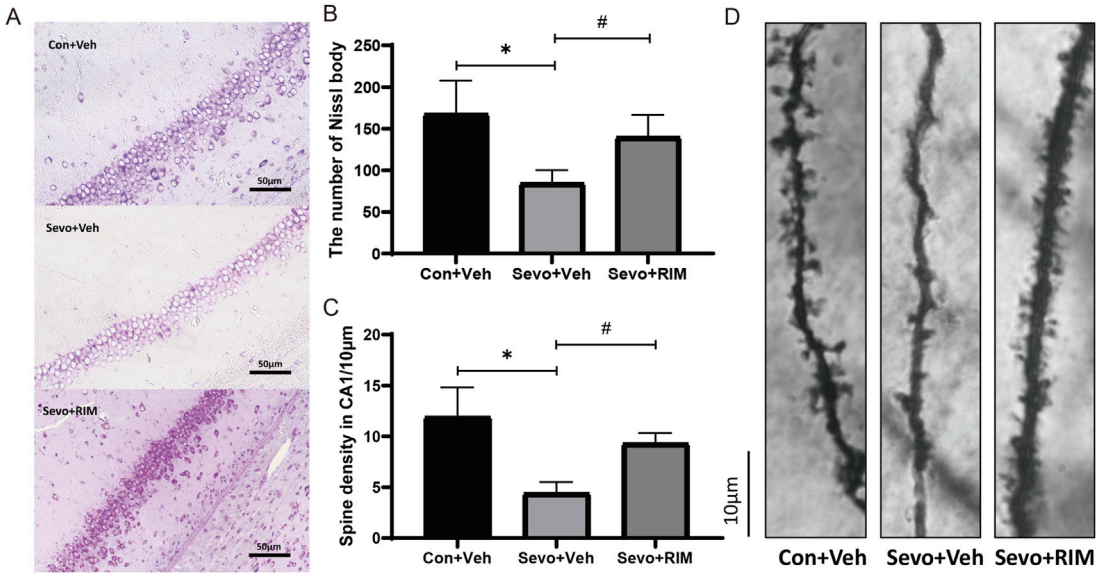

FIGURE 3
Functions of maternal sevoflurane exposure in neuronal density and dendritic spine density in the hippocampal CA1 area of neonatal rats. Nissl staining under ×400 **(A)** and neuronal density ratio changes **(B)** in each group (n = 3). Golgi staining under ×1000 **(D)** and histograms of spine density/10 μm **(C)** in each group (n = 3). Data are displayed as mean ± S.E.M. $^{**}p < .01$, vs. the Con + Veh group; $\#p < .05$, $\#\#\#p < .001$, vs. the Sevo + Veh group.

Statistical analysis

All data were manifested as mean ± S.E.M and processed using SPSS 17.0 (SPSS Inc., United States). Additionally, all data underwent one-way ANOVA using Tukey's *post-hoc* multiple comparison tests that were only conducted if F reached a statistical significance of $p < .05$.

Results

Maternal sevoflurane exposure triggered impairments in neurobehaviors and cognitive memory in offspring rats

Neurobehavioral and MWM tests were conducted during P3–33 in offspring rats to investigate the function of maternal exposure to sevoflurane in neurological functions and cognitive memory, Figure 2. Compared to the Con + Veh group, rats in the Sevo + Veh group took longer time to turn to right ($p < .01$; Figure 2A) and turn around ($p < .05$; Figure 2B) on P3 and spent shorter time hanging from the suspension hanger in the forearm grip strength test on P13 ($p < .01$; Figure 2C). Cliff avoidance tests or sensory reflexes were not different between the Con + Veh and Sevo + Veh groups (Figures 2D, E). Escape latency of rats were longer in the Sevo + Veh group than in the Con + Veh group for the MWM test during P30–32 ($p < .05$; Figure 2F), accompanied by fewer times of crossing the platform ($p < .01$; Figure 2G) and shorter time in the second quadrant on P33 ($p < .01$; Figure 2H).

RIM pretreatment markedly shortened the time for pups to right themselves ($p < .05$; Figure 2A) and prolonged the time they were able to grasp the hanger ($p < .05$; Figure 2C) versus the Sevo + Veh group. Additionally, in the MWM test, treatment with RIM decreased the escape latency during P30–32 ($p < .05$; Figure 2F) and enhanced the times of crossing the platform ($p < .05$; Figure 2G) and time in the second quadrant on P33 ($p < .05$; Figure 2H) in contrast to the Sevo + Veh group.

Impacts of maternal sevoflurane exposure on neuronal and dendritic spine densities in the hippocampal CA1 area of neonatal rats

Sevoflurane exposure dramatically decreased the number of neurons ($p < .05$; Figures 3A,B) and dendritic spines ($p < .01$; Figures 3C,D) in the hippocampal CA1 areas in offspring rats of the Sevo + Veh group relative to the Con + Veh group. RIM pretreatment significantly increased the number of neurons ($p < .001$; Figures 3A,B) and dendritic spines ($p < .05$; Figures 3C,D) in the hippocampal CA1 areas of offspring rats belonging to the Con + Veh group versus the Sevo + Veh group.

Sevoflurane upregulated p-tau expression in the fetal brains *via* the CB1R/CDK5/p25 pathway

To determine how maternal sevoflurane exposure impairs neurological functions and cognitive memory, we determined CB1R, CDK5, p35, p25, tau, and p-tau expression. As shown in Figures 4A–D, sevoflurane time-dependently increased CB1R expression (12 h, $p < .05$; 24 h, $p < .01$), p25 (12 h, $p < .05$; 24 h,

10.3389/fphar.2022.1066713

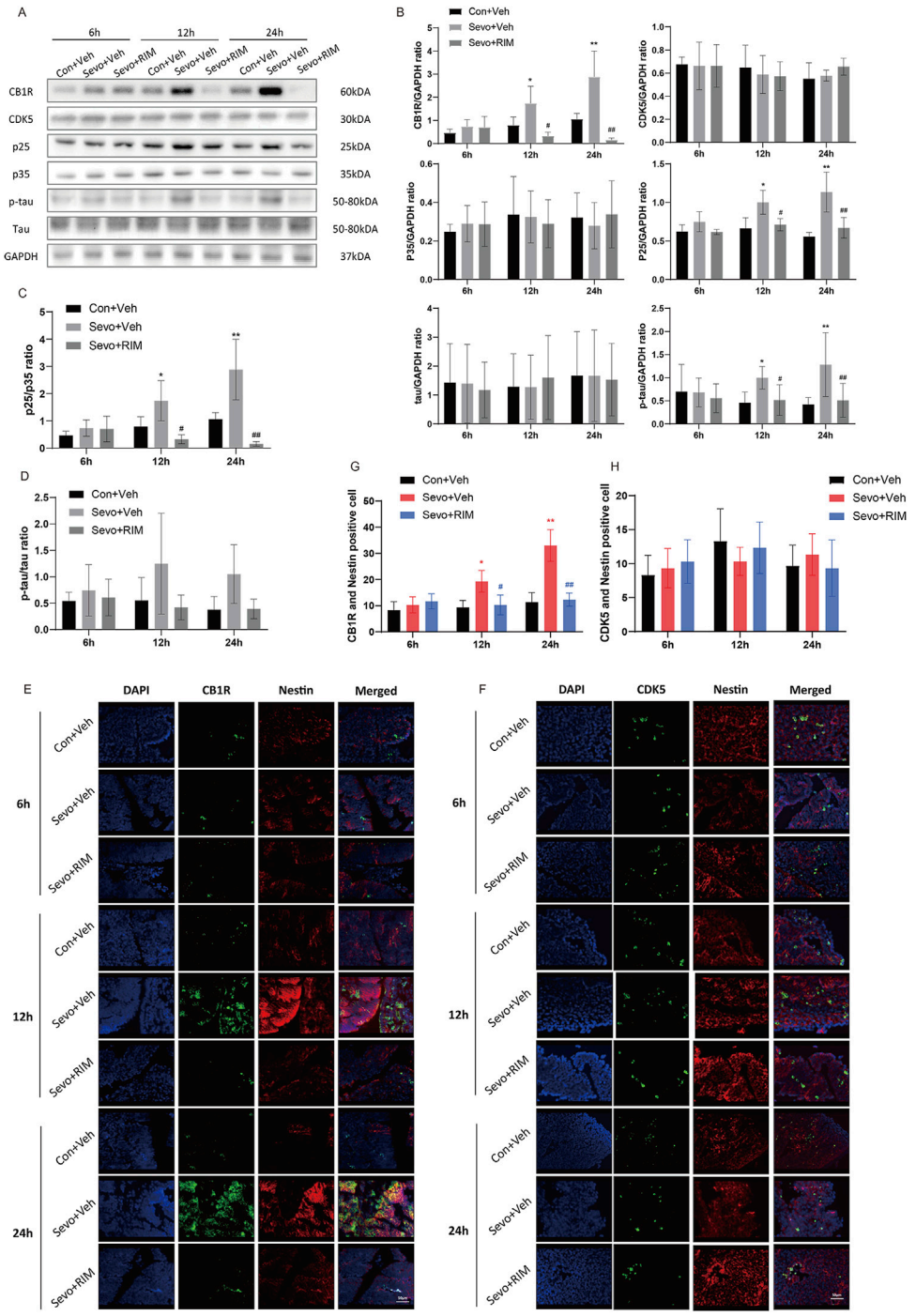

FIGURE 4
Sevoflurane upregulated p-tau in the fetal brains *via* the CB1R/CDK5/p25 pathway. Assays of western blotting (n = 3) demonstrating the expression of CB1R, CDK5, p35, p25, tau, and p-tau **(A,B)** and the value of p25/p35 **(C)** and p-tau/tau **(D)**. Immunofluorescence double staining of CB1R and Nestin (**E**, n = 3) and CDK5 and Nestin (**F**, n = 3) in the fetal rat brains. Quantification of CB1R/Nestin-positive cells **(G)** and CDK5/Nestin-positive cells **(H)**. Data are manifested as mean ± S.E.M. *p < .05, **p < .01, vs. the Con + Veh group; #p < .05, ##p < .01, vs. the Sevo + Veh group.

p < .01) and tau phosphorylation (12 h, p < .05; 24 h, p < .01) in the brain of offspring rats of the Sevo + Veh group relative to the Con + Veh group. A higher number of CB1R/Nestin-positive cells (12 h, p < .05; 24 h, p < .01; Figures 4E,G) were observed in the Sevo + Veh group than in the Con + Veh group. CDK5-, p35-, tau-, and CDK5/Nestin-positive cells did (Figures 4F,H) not differ between the Sevo + Veh and Con + Veh groups. RIM pretreatment negated sevoflurane-stimulated increases in CB1R (12 h, p < .05; 24 h, p < .01), p25 (12 h, p < .05; 24 h, p < .0112, 24 h, p < .05), and p-tau (12 h, p < .05; 24 h, p < .01) expression and the number of CB1R/Nestin-positive cells (12 h, p < .05; 24 h, p < .01).

10.3389/fphar.2022.1066713

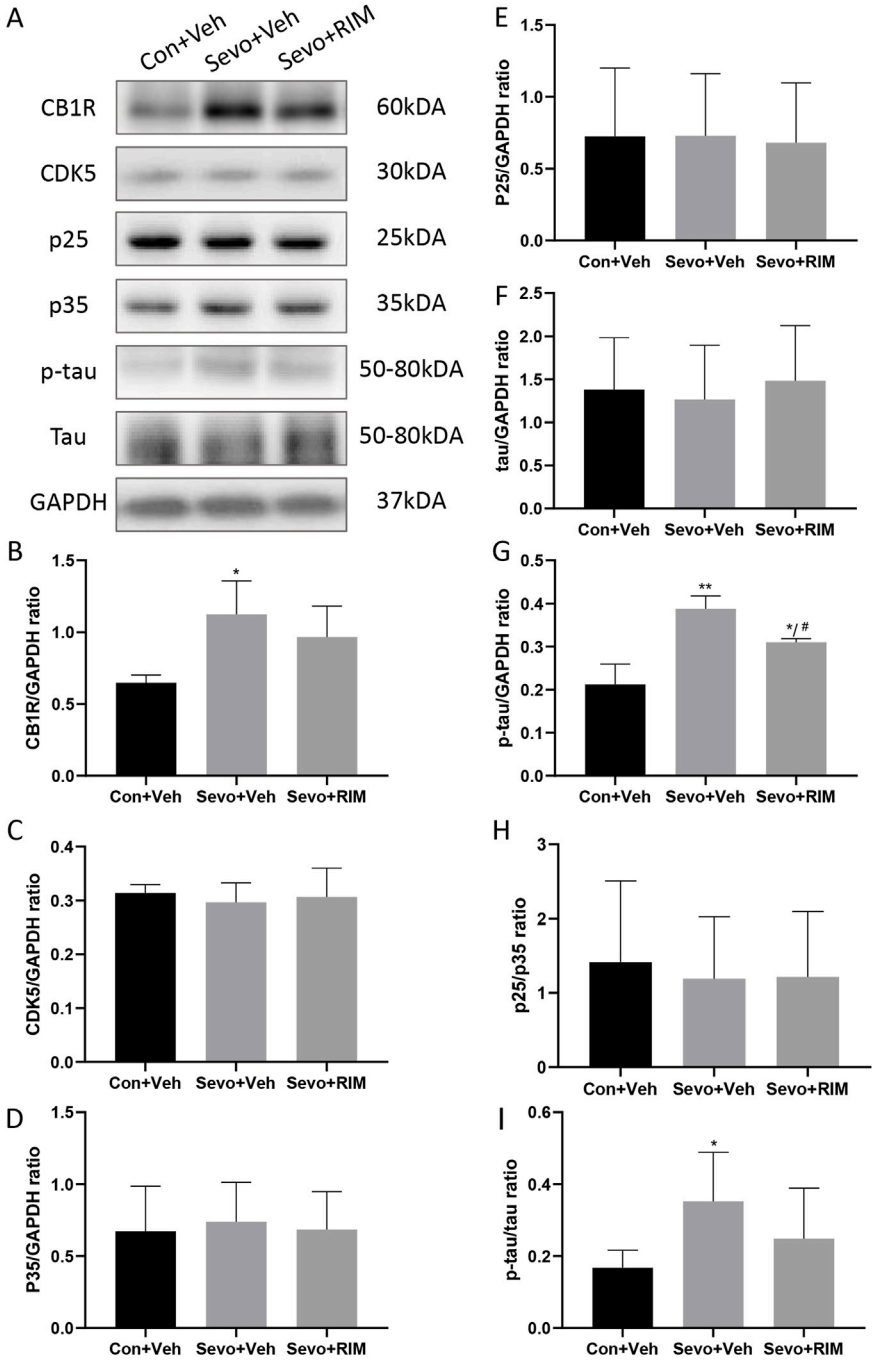

FIGURE 5
Sevoflurane augmented p-tau expression in the hippocampus of offspring rats. Representative western blots **(A)** and quantitation **(B–I)** of western blotting assays (n = 3 rats/group) showing CB1R, p35, CDK5, p25, tau, and p-tau expression in the hippocampus. Data are summarized as mean ± S.E.M. *p < .05, **p < .01, vs. the Con + Veh group; #p < .05, vs. the Sevo + Veh group.

Sevoflurane increased p-tau expression in the hippocampus of offspring rats

To ascertain whether sevoflurane activated the CB1R/p25/p-tau pathway in offspring rats, CB1R, CDK5, p35, p25, tau, and p-tau expression was tested in the hippocampus (Figure 5A). Sevoflurane substantially augmented CB1R (p < .05) and p-tau (p < .01) expression in the Sevo + Veh group versus the Con + Veh group (Figures 5B,G,I). No considerable alteration was noted in CDK5, p35, p25, and tau expression between the Con + Veh and Sevo + Veh groups (Figures 5C,D,E,F,H). The RIM pretreatment may interfere with sevoflurane's effects on p-tau expression (p < .05).

Discussion

Our research unveiled that a single exposure of rats at mid-gestation to 3.5% sevoflurane impaired neurobehavioral abilities

and long-term cognitive memory accompanied by increased p-tau expression in the hippocampus of offspring rats and fetuses. We first found that rimonabant, a selective antagonist of CB1R, can block the activation of the CB1R/CDK5/p-tau pathway, improve neurobehavioral abilities, and alleviate cognitive memory loss induced by sevoflurane.

Former research has mostly concentrated on the function of sevoflurane in ethology during adolescence or adulthood. The eight arm maze, MWM, Y maze, and open field tests have often been used to evaluate learning and memory of rodents (Xu et al., 2016; Yang et al., 2020). In our study, neurobehavioral tests were used for the first time to comprehensively evaluate the sensory, motor, coordination, and cognitive abilities to accurately reflect the functional development of the brain in offspring rats. Our results showed that the time it took pups in the Sevo + Veh group to right themselves and to turn around was evidently prolonged in the Sevo + Veh group relative to the Con + Veh group on P3. This indicates that coordination, vestibular, and proprioceptive functions were damaged in the offspring rats. In the forelimb grip test, suspension time of the Sevo + Veh group was prominently shortened versus the Con + Veh group on P11 and P13, indicating that the forelimb sensation, muscle strength, and reactivity of offspring rats were impeded subsequent to maternal sevoflurane exposure. Although there were no significant differences in the cliff avoidance and sensory reflex experiments between the two groups, the Sevo + Veh group displayed lower positive rates than the Con + Veh group on the same day. This demonstrated that maternal sevoflurane exposure may decrease the risk assessment ability and sensory functions of offspring rats. The MWM test depicted higher escape latency, fewer times of crossing the platform, and shorter time in the second quadrant on P28–33, suggesting that maternal exposure to sevoflurane resulted in cognitive memory dysfunction in the offspring rats. After exposure to RIM, the behavioral abnormalities were reversed in the Sevo + Veh group. These data demonstrate the crucial involvement of CB1R in maternal sevoflurane exposure-stimulated neurobehavioral and cognitive impairments in the offspring rats.

Tau, belonging to the family of microtubule-associated proteins, participates in cell homeostasis, cell movement, and axon signal transmission (Liu et al., 2015). A previous study has shown the stimulating impacts of sevoflurane anesthesia on p-tau expression and cognitive abnormalities in neonatal mice (Liao et al., 2021). Nonetheless, the impacts of maternal sevoflurane exposure on tau in the offspring rats are still unknown. Our results demonstrated that p-tau (Ser404) expression in the hippocampus of fetal and postnatal rats noticeably increased in the Sevo + Veh group versus the Con + Veh group. Previous studies also reported that cognitive dysfunction caused by sevoflurane was related to the phosphorylation of Ser396/404 epitope of tau protein (Freche et al., 2012; Zhang YH et al., 2021). Tau expression did not change significantly as tau widely exists in the central nervous system under physiological conditions (Richetin et al., 2020). Although a part of tau is hyperphosphorylated, the total amount of tau does not obviously decrease. P-tau expression was markedly augmented in the Sevo + Veh group in contrast to the Con + Veh group on P33, while the upstream expression of CDK5/p25 returned to normal, indicating that the hyperphosphorylation of tau is not easy to reverse rapidly after maternal sevoflurane exposure.

CB1R is located in the presynaptic membrane of nerve terminals and regulates the release of neurotransmitters (Di Marzo and Piscitelli, 2015). Isoflurane treatment of mouse hippocampal neural stem cells leads to the dose-dependent increase in CB1R mRNA levels (Zhou et al., 2016). Repeated sevoflurane exposure increases the levels of endogenous cannabinoid and activates extracellular signal-regulated kinases (Zheng et al., 2015; Zhang et al., 2016). In the current research, the data established that 3.5% sevoflurane could time-dependently upregulate the expression of CB1R in fetal and offspring rats. During the development of synapses, CB1R can mediate the activation of CDK5 and cause neurological deficits (Roufayel and Murshid, 2019). An increase in CDK5 activity can cause the hyperphosphorylation of tau (p-tau) followed by a series of pathological changes of nervous system, such as neuronal injury (Liu et al., 2017). However, the expression of CDK5 did not change in our study. This is because, similar to other CDK family proteins, CDK5 does not have enzymatic activity in a monomeric state except for the binding of its specific regulatory units, like p35 and p25. In addition, its activity can be reflected by the ratio of p35 and p25 (Roufayel and Murshid, 2019). The abnormal activity of CDK5/p25 can elicit neurological abnormalities and a variety of neurodegenerative diseases (Bu et al., 2002; Ba et al., 2017; Zeb et al., 2019). Our data elucidated that p25 in fetal brains, but not in offspring rats, is remarkably upregulated in the Sevo + Veh group relative to the Con + Veh group, suggesting that sevoflurane could activate CDK5/p25 in fetal rats. P25, a cleavage product of p35, possesses longer half-life than p35, which, therefore, can observably prolong the activation of CDK5. This may be the reason why p35 has not changed significantly in the current research.

It was previously elaborated that hippocampal, peripheral, and systemic blockade of CB1R abolishes the stress-stimulated memory abnormalities (Busquets-Garcia et al., 2016). Intra-medial prefrontal cortex or systemic administration of rimonabant enhances extinction of cocaine-stimulated conditioned place preference memory but impairs consolidation of low-dose cocaine-stimulated conditioned place preference memory (Hu et al., 2015). The data obtained from our research demonstrated that 3.5% sevoflurane exposure of maternal rats activated CB1R/CDK5/p25/p-tau pathway in the hippocampus of fetuses and offspring rats, resulting in diminishment in neuron and dendritic spine densities in the hippocampal CA1 area. These alterations indicated neurotoxicity occurrence in offspring rats and the potential role of CB1R pathway in sevoflurane exposure. We also found that a CB1R antagonist could markedly block the activation of the CB1R/CDK5/p25/p-tau pathway. Subsequently, it reversed sevoflurane-induced decrease in neuron density and dendritic spine density in the CA1 region. Finally, it ameliorated neurobehavioral and cognitive impairments in sevoflurane-treated rats. The present study indicates that CB1R critically manipulates sevoflurane-stimulated neurotoxicity in fetal and offspring rats. Therefore, our research provides an important theoretical basis for the development of new drugs targeting CB1R.

There is two limitations in the present study: 1) We did not perform Control + RIM group to evaluate deleterious possible effects in offspring. That is because the toxicological effects of rimonabant in clinic is clear, including tremor, dyskinesia, anxiety and hyperexcitability (Christensen et al., 2007). Data from FDA in the United States showed that rimonabant could increase the risk of suicide of users (Vinod and Hungund, 2006). However, it is necessary to explore the deleterious effects in offspring as well. 2) Tau protein have more than eighty epitopes to be phosphorylated (Freche et al., 2012). However, we only explore the expression of p-tau (Ser404) in sevoflurane-treated rats.

Data availability statement

The raw data supporting the conclusion of this article will be made available by the authors, without undue reservation.

Ethics statement

The animal study was reviewed and approved by Medical Ethics Committee Shengjing Hospital of China Medical University.

Author contributions

YW designed the study and wrote the manuscript. ZW analyzed data and revised the manuscript. XL performed the research. PZ supervised the study.

Funding

This research is supported by grant from the National Natural Science Foundation of China (Nos 81870838, Nos 82071215), Liaoning Province Distinguished Professor Support Program (No. XLYC1802096), Shenyang Clinical Medicine Research Center of Anesthesiology (No. 19-110-4-24, No. 20-204-4-44), and Outstanding Scientific Fund of Shengjing Hospital (No. 201708).

Conflict of interest

The authors declare that the research was conducted in the absence of any commercial or financial relationships that could be construed as a potential conflict of interest.

Publisher's note

All claims expressed in this article are solely those of the authors and do not necessarily represent those of their affiliated organizations, or those of the publisher, the editors and the reviewers. Any product that may be evaluated in this article, or claim that may be made by its manufacturer, is not guaranteed or endorsed by the publisher.

References

Adedara, I. A., Abolaji, A. O., Idris, U. F., Olabiyi, B. F., Onibiyo, E. M., Ojuade, T. D., et al. (2017). Neuroprotective influence of taurine on fluoride-induced biochemical and behavioral deficits in rats. *Chem. Biol. Interact.* 261, 1–10. doi:10.1016/j.cbi.2016.11.011

Aymerich, M. S., Aso, E., Abellanas, M. A., Tolon, R. M., Ramos, J. A., Ferrer, I., et al. (2018). Cannabinoid pharmacology/therapeutics in chronic degenerative disorders affecting the central nervous system. *Bio Pharm.* 157, 67–84. doi:10.1016/j.bcp.2018.08.016

Ba, L., Li, Z. J., Bu, B. T., Wang, W., and Zhang, M. (2017). Aberrant activation of Cdc2/cyclin B1 is involved in initiation of cytoskeletal pathology in murine Niemann-Pick disease type C. *J. Huazhong Univ. Sci. Technol. Med. Sci.* 37 (5), 732–739. doi:10.1007/s11596-017-1796-7

Bu, B., Li, J., Davies, P., and Vincent, I. (2002). Deregulation of cdk5, hyperphosphorylation, and cytoskeletal pathology in the Niemann-Pick type C murine model. *J. Neurosci.* 22 (15), 6515–6525. doi:10.1523/JNEUROSCI.22-15-06515.2002

Busquets-Garcia, A., Gomis-González, M., Srivastava, R. K., Cutando, L., Ortega-Alvaro, A., Ruehle, S., et al. (2016). Peripheral and central CB1 cannabinoid receptors control stress-induced impairment of memory consolidation. *Pro Natl. Acad. Sci. U. S. A.* 113 (35), 9904–9909. doi:10.1073/pnas.1525066113

Christensen, R., Kristensen, P. K., Bartels, E. M., Bliddal, H., and Astrup, A. (2007). Efficacy and safety of the weight-loss drug rimonabant: A meta-analysis of randomised trials. *Lancet* 370 (9600), 1706–1713. doi:10.1016/S0140-6736(07)61721-8

Creeley, C. E., and Olney, J. W. (2010). The young:Neuroapoptosis induced by anesthetics and what to do about it. *Anesth. Analg.* 110, 442–448. doi:10.1213/ANE.0b013e3181c6b9ca

Cristino, L., Bisogno, T., and Di Marzo, V. (2020). Cannabinoids and the expanded endocannabinoid system in neurological disorders. *Nat. Rev. Neurol.* 16 (1), 9–29. doi:10.1038/s41582-019-0284-z

Di Marzo, V., and Piscitelli, F. (2015). The endocannabinoid system and its modulation by phytocannabinoids. *Neurotherapeutics* 12 (4), 692–698. doi:10.1007/s13311-015-0374-6

Eskandari, A., and Alipour, S. (2020). Aspects of anesthesia for breast surgery during pregnancy. *Adv. Exp. Med. Biol.* 1252, 107–114. doi:10.1007/978-3-030-41596-9_14

Fan, X. Y., Shi, G., and Zhao, P. (2021). Neonatal sevoflurane exposure impairs learning and memory by the hypermethylation of hippocampal synaptic genes. *Mol. Neurobiol.* 58 (3), 895–904. doi:10.1007/s12035-020-02161-4

Freche, H. L., Brouillette, J., Fernandez-Gomez, F., Patin, P., Caillierez, R., Zommer, N., et al. (2012). Tau phosphorylation and sevoflurane anesthesia: An association to postoperative cognitive impairment. *Anesthesiology* 116 (4), 779–787. doi:10.1097/ALN.0b013e31824be8c7

George, J. M., Boyd, R. N., Colditz, P. B., Rose, S. E., Pannek, K., Fripp, J., et al. (2015). Ppremo: A prospective cohort study of preterm infant brain structure and function to predict neurodevelopmental outcome. *BMC Pediatr.* 15, 123. doi:10.1186/s12887-015-0439-z

Horvath, G., Reglodi, D., Vadasz, G., Farkas, J., and Kiss, P. (2013). Exposure to enriched environment decreases neurobehavioral deficits induced by neonatal glutamate toxicity. *Int. J. Mol. Sci.* 14 (9), 19054–19066. doi:10.3390/ijms140919054

Hu, S. S., Liu, Y. W., and Yu, L. (2015). Medial prefrontal cannabinoid CB1 receptors modulate consolidation and extinction of cocaine-associated memory in mice. *Psychopharmacology* 232 (10), 1803–1815. doi:10.1007/s00213-014-3812-y

Joshi, V., Subbanna, S., Shivakumar, M., and Basavarajappa, B. S. (2019). CB1R regulates CDK5 signaling and epigenetically controls Rac1 expression contributing to neurobehavioral abnormalities in mice postnatally exposed to ethanol. *Neuropsychopharmacology* 44 (3), 514–525. doi:10.1038/s41386-018-0181-y

Khalki, L., M'hamed, S. B., Sokar, Z., Bennis, M., Vinay, L., Bras, H., et al. (2013). Prenatal exposure to fenugreek impairs sensorimotor development and the operation of spinal cord networks in mice. *PLoS One* 8 (11), e80013. doi:10.1371/journal.pone.0080013

Li, X. Y., Wu, Z. Y., Zhang, Y., Xu, Y., Han, G., and Zhao, P. (2017). Activation of autophagy contributes to sevoflurane-induced neurotoxicity in fetal rats. *Front. Mol. Neurosci.* 10, 432. doi:10.3389/fnmol.2017.00432

Liao, Z., Huang, Z., Li, J., Li, H., Miao, L., Liu, Y., et al. (2021). Regulation of CRMP2 by Cdk5 and GSK-3β participates in sevoflurane-induced dendritic development abnormalities and cognitive dysfunction in developing rats. *Toxicol. Lett.* 341, 68–79. doi:10.1016/j.toxlet.2021.01.023

Liu, Y., Lin, D., Liu, C., Zhao, Y., Shen, Z., Zhang, K., et al. (2017). Cyclin-dependent kinase 5/Collapsin response mediator protein 2 pathway may mediate sevoflurane-induced dendritic development abnormalities in rat cortical neurons. *Neurosci. Lett.* 651, 21–29. doi:10.1016/j.neulet.2017.04.040

Liu, Y. H., Xia, S. X., Liu, Y. F., Kiy, C. L., and Juan, L. Y. (2015). Role of Cdk5-CRMP pathway in sevoflurane-induced dendritic developmental disorder of neurons in prefrontal cortex of neonatal rats. *Chin. J. Pathophysiol.* 31 (10), 1729–1736. doi:10.3969/j.issn.1000-4718.2015.10.001

McDonnell-Dowling, K., Donlon, M., and Kelly, J. P. (2014). Methamphetamine exposure during pregnancy at pharmacological doses produces neurodevelopmental and behavioural effects in rat offspring. *Int. J. Dev. Neurosci.* 35, 42–51. doi:10.1016/j.ijdevneu.2014.03.005

Naik, A. A., Patro, I. K., and Patro, N. (2015). Slow physical growth, delayed reflex ontogeny, and permanent behavioral as well as cognitive impairments in rats following intra-generational protein malnutrition. *Front. Neurosci.* 9, 446. doi:10.3389/fnins.2015.00446

Reitman, E., and Flood, P. (2011). Anaesthetic considerations for non-obstetric surgery during pregnancy. *Br. J. Anaesth.* 107 (1), i72–i78. doi:10.1093/bja/aer343

Richetin, K., Steullet, P., Pachoud, M., Perbet, R., Parietti, E., Maheswaran, M., et al. (2020). Tau accumulation in astrocytes of the dentate gyrus induces neuronal dysfunction and memory deficits in Alzheimer's disease. *Nat. Neurosci.* 23 (12), 1567–1579. doi:10.1038/s41593-020-00728-x

Roufayel, R., and Murshid, N. (2019). CDK5: Key regulator of apoptosis and cell survival. *Biomedicines* 7 (4), 88. doi:10.3390/biomedicines7040088

Shivakumar, M., Subbanna, S., Joshi, V., and Basavarajappa, B. S. (2020). Postnatal ethanol exposure activates HDAC-mediated histone deacetylation, impairs synaptic plasticity gene expression and behavior in mice. *Int. J. Neuropsychopharmacol.* 23 (5), 324–338. doi:10.1093/ijnp/pyaa017

Stockwell, S. (2017). FDA anesthesia warning for pregnant women, children. *Am. J. Nurs.* 117 (4), 18. doi:10.1097/01.NAJ.0000515223.23086.fc

Stoothoff, W. H., and Johnson, G. V. (2005). Tau phosphorylation:physiological and pathological consequences. *Biochim. Biophys. Acta* 1739 (2-3), 280–297. doi:10.1016/j.bbadis.2004.06.017

Sun, L. (2010). Early childhood general anaesthesia exposure and neurocognitive development. *Br. J. Anaesth.* 105, i61–i68. doi:10.1093/bja/aeq302

Vinod, K. Y., and Hungund, B. L. (2006). Role of the endocannabinoid system in depression and suicide. *Trends Pharmacol. Sci.* 27 (10), 539–545. doi:10.1016/j.tips.2006.08.006

Wang, Y., Yin, S. W., Xue, H., Zhang, N., and Zhao, P. (2018). Mid-gestational sevoflurane exposure inhibits fetal neural stem cell proliferation and impairs postnatal learning and memory function in a dose-dependent manner. *Dev. Biol.* 435 (2), 185–197. doi:10.1016/j.ydbio.2018.01.022

Wu, Z. Y., Li, X. Y., Zhang, Y., Tong, D. Y., Wang, L. L., and Zhao, P. (2018). Effects of sevoflurane exposure during mid-pregnancy on learning and memory in offspring rats: Beneficial effects of maternal exercise. *Front. Cell Neurosc* 12, 122. doi:10.3389/fncel.2018.00122

Xiao, N., Zhang, F., Zhu, B., Liu, C., Lin, Z., Wang, H., et al. (2018). CDK5-mediated tau accumulation triggers methamphetamine-induced neuronal apoptosis via endoplasmic reticulum-associated degradation pathway. *Toxicol. Lett.* 292, 97–107. doi:10.1016/j.toxlet.2018.04.027

Xu, Y., Tian, Y., Tian, Y., Li, X., and Zhao, P. (2016). Autophagy activation involved in hypoxic-ischemic brain injury induces cognitive and memory impairment in neonatal rats. *J. Neurochem.* 139 (5), 795–805. doi:10.1111/jnc.13851

Yang, M., Tan, H., Zhang, K., Lian, N. Q., Yu, Y., and Yu, Y. H. (2020). Protective effects of Coenzyme Q10 against sevoflurane-induced cognitive impairment through regulating apolipoprotein E and phosphorylated Tau expression in young mice. *Int. J. Dev. Neurosci.* 80, 418–428. doi:10.1002/jdn.10041

Zeb, A., Son, M., Yoon, S., Kim, J. H., Park, S. J., and Lee, K. W. (2019). Computational simulations identified two candidate inhibitors of cdk5/p25 to abrogate tau-associated neurological disorders. *Comput. Struct. Biotechnol. J.* 17, 579–590. doi:10.1016/j.csbj.2019.04.010

Zhang, H., Li, L., Sun, Y., Zhang, X., Zhang, Y., Xu, S., et al. (2016). Sevoflurane prevents stroke-induced depressive and anxiety behaviors by promoting cannabinoid receptor subtype I-dependent interaction between β-arrestin 2 and extracellular signal-regulated kinases 1/2 in the rat hippocampus. *J. Neurochem.* 137 (4), 618–629. doi:10.1111/jnc.13613

Zhang, Y., Li, N., Yang, J., Zhang, T., and Yang, Z. (2010). Effects of maternal food restriction on physical growth and neurobehavior in newborn Wistar rats. *Brain Res. Bull.* 83 (1-2), 1–8. doi:10.1016/j.brainresbull.2010.06.005

Zhang, Y. H., Gao, Q. S., Wu, Z. Y., Xue, H., and Zhao, P. (2021). Sevoflurane postconditioning ameliorates neuronal migration disorder through Reelin/Dab1 and improves long-term cognition in neonatal rats after hypoxic-ischemic injury. *Neurotox. Res.* 39 (5), 1524–1542. doi:10.1007/s12640-021-00377-3

Zheng, L., Wu, X., Dong, X., Ding, X., and Song, C. (2015). Effects of chronic alcohol exposure on the modulation of ischemia-induced glutamate release via cannabinoid receptors in the dorsal hippocampus. *Alcohol Clin. Exp. Res.* 39 (10), 1908–1916. doi:10.1111/acer.12845

Zhou, C. H., Ting, G. U., Chen, Y. C., Wang, X. X., Wang, H. N., and Zhang, Y. H. (2016). Effect of isoflurane on the expression of endocannabinoid system related genes and cell viability of neural stem cells. *Prog. Mod. Biomed.* 16 (34), 6606–6609.

frontiers | Frontiers in Aging Neuroscience

TYPE Original Research
PUBLISHED 18 January 2023
DOI 10.3389/fnagi.2022.1076393

OPEN ACCESS

EDITED BY
Zhongcong Xie,
Harvard Medical School,
United States

REVIEWED BY
Yajing Si,
Xinxiang Medical University,
China
M. Bruce MacIver,
Stanford University,
United States

*CORRESPONDENCE
Susanne Koch
✉ susanne.koch@charite.de

SPECIALTY SECTION
This article was submitted to Neurocognitive Aging and Behavior, a section of the journal Frontiers in Aging Neuroscience

RECEIVED 21 October 2022
ACCEPTED 05 December 2022
PUBLISHED 18s January 2023

CITATION
Leroy S, Major S, Bublitz V, Dreier JP and Koch S (2023) Unveiling age-independent spectral markers of propofol-induced loss of consciousness by decomposing the electroencephalographic spectrum into its periodic and aperiodic components. *Front. Aging Neurosci.* 14:1076393. doi: 10.3389/fnagi.2022.1076393

Unveiling age-independent spectral markers of propofol-induced loss of consciousness by decomposing the electroencephalographic spectrum into its periodic and aperiodic components

Sophie Leroy[1], Sebastian Major[2,3,4], Viktor Bublitz[1], Jens P. Dreier[2,3,4,5,6] and Susanne Koch[1]*

[1]Department of Anesthesiology and Operative Intensive Care Medicine (CCM, CVK), Charité—Universitätsmedizin Berlin, Corporate Member of Freie Universität Berlin, Humboldt-Universität zu Berlin, Berlin, Germany, [2]Center for Stroke Research Berlin, Charité—Universitätsmedizin Berlin, Corporate Member of Freie Universität Berlin, Humboldt-Universität zu Berlin, Berlin, Germany, [3]Department of Experimental Neurology, Charité—Universitätsmedizin Berlin, Corporate Member of Freie Universität Berlin, Humboldt-Universität zu Berlin, Berlin, Germany, [4]Department of Neurology, Charité—Universitätsmedizin Berlin, Corporate Member of Freie Universität Berlin, Humboldt-Universität zu Berlin, Berlin, Germany, [5]Bernstein Center for Computational Neuroscience Berlin, Berlin, Germany, [6]Einstein Center for Neurosciences Berlin, Berlin, Germany

Background: Induction of general anesthesia with propofol induces radical changes in cortical network organization, leading to unconsciousness. While perioperative frontal electroencephalography (EEG) has been widely implemented in the past decades, validated and age-independent EEG markers for the timepoint of loss of consciousness (LOC) are lacking. Especially the appearance of spatially coherent frontal alpha oscillations (8–12 Hz) marks the transition to unconsciousness. Here we explored whether decomposing the EEG spectrum into its periodic and aperiodic components unveiled markers of LOC and investigated their age-dependency. We further characterized the LOC-associated alpha oscillations by parametrizing the adjusted power over the aperiodic component, the center frequency, and the bandwidth of the peak in the alpha range.

Methods: In this prospective observational trial, EEG were recorded in a young (18–30 years) and an elderly age-cohort (≥70 years) over the transition to propofol-induced unconsciousness. An event marker was set in the EEG recordings at the timepoint of LOC, defined with the suppression of the lid closure reflex. Spectral analysis was conducted with the multitaper method. Aperiodic and periodic components were parametrized with the FOOOF toolbox. Aperiodic parametrization comprised the exponent and the offset. The periodic parametrization consisted in the characterization of the peak in the alpha range with its adjusted power, center frequency and bandwidth. Three time-segments were defined: preLOC (105 – 75 s before LOC), LOC (15 s before to 15 s after LOC), postLOC (190 – 220 s after LOC). Statistical significance was determined with a repeated-measures ANOVA.

Results: Loss of consciousness was associated with an increase in the aperiodic exponent (young: p=0.004, elderly: p=0.007) and offset (young: p=0.020, elderly: p=0.004) as well as an increase in the adjusted power (young: p<0.001, elderly p=0.011) and center frequency (young: p=0.008, elderly: p<0.001) of the periodic alpha peak. We saw age-related differences in the aperiodic exponent and offset after LOC as well as in the power and bandwidth of the periodic alpha peak during LOC.

Conclusion: Decomposing the EEG spectrum over induction of anesthesia into its periodic and aperiodic components unveiled novel age-independent EEG markers of propofol-induced LOC: the aperiodic exponent and offset as well as the center frequency and adjusted power of the power peak in the alpha range.

KEYWORDS

loss of consciousness, propofol, anesthesia induction, Electroencephalography, aperiodic activity, periodic activity, ageing, 1/f

Introduction

General anesthesia is commonly induced with an opiate followed by a bolus of propofol, a positive modulator of $GABA_A$-receptor mediated inhibition (Trapani et al., 2000). Until today, to recognize the timepoint of loss of consciousness (LOC) anesthesiologists rely on clinical signs like the suppression of brain stem reflexes or missing response to verbal or pain stimuli. Spectral dynamics of propofol-induced LOC have been extensively described in the frontal electroencephalograms (EEG) of non-geriatric patients (Kuizenga et al., 2001; Boly et al., 2012; Purdon et al., 2013). However, a major share of general anesthesia is conducted on elderly and vulnerable patients, who are most prone to develop neurocognitive complications (Staheli and Rondeau, 2022).

Although still insufficiently understood, the transition to unconsciousness represents a key moment for the postoperative outcome of elderly patients (Koch et al., 2021; Windmann et al., 2022). Propofol causes a non-physiological disbalance in the inhibitory inputs of GABAergic neurons on pyramidal cells. Subcortical circuits induce a radical re-organization in cortical networks (Ching et al., 2010; Hutt and Longtin, 2010; Brown et al., 2011; Moody et al., 2021). A switch occurs from a high frequency low amplitude spectrogram to high amplitude low frequency oscillations (Purdon et al., 2015b). Alpha oscillations migrate in the scalp EEG from the occipital to the frontal channels in a process called anteriorization. High-density EEG recordings demonstrate that propofol-induced frontal alpha waves are spatially coherent, possibly due to the anesthetics' effect on thalamocortical loops (Ching et al., 2010; Cimenser et al., 2011). Overall, the predominance of spatially coherent frontal alpha oscillations superimposed on delta and slow waves is a recurrently proposed spectral power distribution to recognize the unconscious state (Cantero et al., 1999; Gugino et al., 2001; Purdon et al., 2013).

The EEG spectrum can be decomposed into a periodic and an aperiodic component. The superimposed periodic component corresponds to coordinated rhythmic activity around a frequency value, often summarized in classical power bands: sub-delta, delta, theta, alpha, beta, and gamma. Periodic oscillations detectable by scalp EEG arise from cortical neural populations synchronized by common, subcortical generators (Pascual-Marqui et al., 2009).The underlying aperiodic component corresponds to asynchronous spectrum-wide neural rhythms(Miller et al., 2009; Donoghue et al., 2020). Long considered as noise, aperiodic activity delivers information about cerebral activity states with clinical correlates. Changes in aperiodic activity have been described in physiological processes like sleep (Lendner et al., 2020) and ageing (Voytek et al., 2015) but also in neurological (Lanzone et al., 2022; Zhang et al., 2022) and psychiatric disorders (Arnett et al., 2022; Manyukhina et al., 2022). Aperiodic parametrization has been undertaken in non-geriatric patients under general anesthesia: propofol-induced unconsciousness engenders an increase in the aperiodic activity (Brake et al., 2021).

In this explorative analysis we decomposed the EEG spectrum around propofol-induced loss of consciousness into its periodic and aperiodic components in a young and an elderly cohort. Our goal was to find markers of the dynamic transition to unconsciousness in the EEG. Furthermore, we examined cohort differences in the spectral properties to shed light on the age-dependent divergences.

Materials and methods

Trial protocol

This analysis is a subproject of the ACDC-Trial (NCT04320082), which was approved by the local ethics

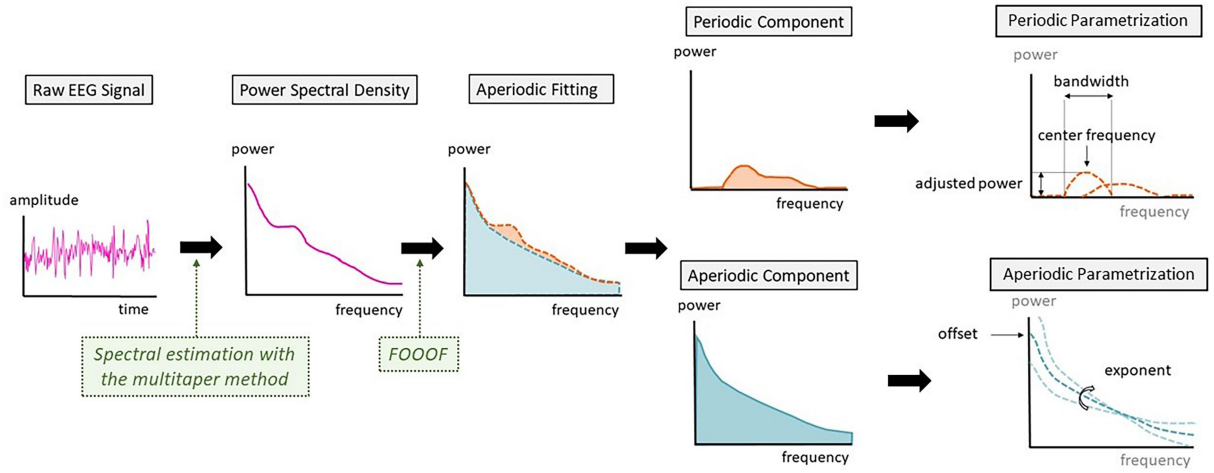

FIGURE 1
Schematic representation of the steps between raw electroencephalography (EEG) signal and the parametrization into periodic and aperiodic components.

committee (Charité Universitätsmedizin Berlin, EA2/029/20). Written approval was obtained from all participants according to the Declaration of Helsinki. Ethical and scientific quality standards were respected following the ICH-GCP guidelines. Patients undergoing general anesthesia for elective orthopedic surgery lasting more than 60 min at the Charité Universitätsmedizin Berlin, Campus Virchow Klinikum were enrolled in this prospective observational trial. Patients with preexisting psychiatric or neurological diseases as well as patients taking centrally acting medication were excluded.

Two age cohorts were formed: a young cohort including 9 patients between 18 and 30 years old, and an elderly cohort with 14 patients over 70 years old. Clinical data were collected including age, sex, height, weight, physical status in the classification system of the American Society of Anesthesiologists (ASA-Score), concomitant diseases, and medication.

Premedication and anesthesia were conducted following the standard operation procedures of the clinic (Spies, 2005). Anesthesia was induced intravenously with a fentanyl bolus followed by a bolus of propofol. The anesthetic doses were individually defined by the anesthesiologist following the clinical presentation of the patients (age, weight, sex, and concomitant diseases). Propofol was infused manually, without a syringe driver, by a nurse anesthetist. During induction of anesthesia the lid closure reflex was regularly tested to estimate the timepoint of LOC. A non-depolarizing neuromuscular blocker was given to relax the airways if endotracheal intubation was indicated. After a stable sedated state was reached patients were either intubated with an endotracheal tube or a laryngeal mask airway was introduced. Patients with early postoperative neurocognitive disorders were excluded from this analysis.

Data analysis

Twenty-one Ag/AgCl electrodes (EasyCap GmbH, Woerthsee-Etterschlag, Germany) were placed preoperatively following the 10/20-system on the scalp. The reference and ground electrodes were placed at AFz and FCz, respectively. A full-band, direct current (DC)/alternating current (AC)-EEG reaching from 0 to 5,000 Hz was recorded with a BrainAmp DC amplifier and BrainVision Recorder (Brain Products GmbH, Gilching, Germany). Impedances were kept below 5 kOhm. An event marker was set in the EEG recordings at LOC, defined as the loss of lid closure reflex. Event markers were also set at the start of propofol infusion and at intubation.

EEG recordings were aligned at the LOC event and cut to six-minute episodes from 120 s before to 240 s after LOC. 30 s EEG segments were defined for statistical analysis: preLOC (105–75 s before LOC), LOC (15 s before to 15 s after LOC), postLOC (190–220 s after LOC, Figure 1). The segmentation of the EEG was based on the clinical markers of anesthesia. The preLOC segment represented the time shortly before propofol induction. The LOC segment comprised the 30 s around the loss of lid closure reflex. The postLOC segment depicted the very early sedation state around the start of mechanic ventilation.

Spectral analysis

Spectral analysis was performed with the Chronux toolbox (version 2.12 v03)[1] in MATLAB (MATLAB R2022a, MathWorks

1 http://chronux.org/

Inc.; Partha Mitra, 2009). Preprocessing of the EEG included trendline removal, down-sampling to 500 Hz and bandpass filtering (0.1–45 Hz). EEGs were visually inspected regarding the occurrence of burst-suppression patterns. Power spectrum was estimated using the multitaper method with the following parameters: moving window length of 2 s and shift 0.1 s, time-bandwidth product of 2 and number of tapers of 3. The frequency bands were defined as followed: sub-delta (0.1–1.5 Hz), delta (1.5–4 Hz), theta (4–8 Hz), alpha (8–12 Hz), beta (12–30 Hz) and gamma (30–45 Hz). A spectrogram was computed and normalized by the total power at each timepoint of the spectrogram for one frontal channel (Fp1). Power Spectral Density (PSD) arrays were computed for each time-segment (preLOC, LOC, and postLOC) from the non-normalized spectra of the respective age-group.

The analysis of the aperiodic components in the spectral power distribution was computed at each timepoint with the Fitting Oscillations and One-Over-f (FOOOF) toolbox (version 1.0.0, Donoghue et al., 2020) in MATLAB and averaged over the time segments with the following settings: peak width limit 0.5–12 Hz, infinite maximum number of peaks, minimum peak height of 0 μV^2, peak threshold of 2 standard deviations and a fixed aperiodic mode without a knee parameter.

Characterization of the aperiodic activity comprises the offset and exponent, respectively the y-intercept and the slope of the decay (Donoghue et al., 2020). A flatter exponential curve corresponds to a smaller exponent value and a steeper curve to a greater exponent value.

By deducting the aperiodic fit to the raw PSD, the periodic power peaks over the aperiodic fit were extracted for both age groups. These periodic power peaks were represented in spectrograms. When negative values were reached due to aperiodic overfitting, values were replaced with zeros for the power peak spectrograms.

The FOOOF toolbox also parametrizes the periodic peaks detected by the algorithm. Given the dynamics of alpha oscillations over the transition to unconsciousness, we analyzed the characteristics of the alpha peak. For every patient, we searched if a peak of power with a center frequency between 8 and 12 Hz was present. These were defined as alpha peaks and were further described by differentiating their center frequency, the adjusted power over and above the aperiodic component and the bandwidth of the oscillation peak (Figure 1).

Statistical analysis

Statistical analysis was carried out in IBM SPSS Statistics (Version: 28.0.1.0). Statistical significance in clinical data was assessed with the appropriated test (Chi-squared test, *t*-test, or Mann–Whitney-*U* test). Except for the assessment of differences in the population demographics, results were not interpreted as significant or not significant given the unavoidable multiple testing in an explorative pilot study design. To minimize type I and type II errors in statistical interpretation, we defined a reporting level of $p \leq 0.05$ without correcting for multiple testing.

The following EEG parameters were averaged over the time-segments: aperiodic parameters (exponent, offset), alpha peak characteristics (center frequency, adjusted power, and bandwidth). We assessed differences between the groups in these parameters with a repeated-measures ANOVA with timepoints and EEG parameters as within-subjects factors and the age group as between-subjects factor.

Using a custom-written MATLAB code, we assessed differences in the density spectral array with a Mann–Whitney-*U* test at each sampling point and each frequency bin in the raw spectrogram and plotted the results in a three-dimensional space. Only results with $p \leq 0.05$ were displayed, in blue when the power was higher in the young patients and in red when the power was higher in the elderly. A similar method was applied in a paper by Obert and colleagues (Obert et al., 2020). The same procedure was applied to the spectrograms of the aperiodic activity. We visually compared these plots of differences between the raw spectrograms and the aperiodic activity spectrograms.

Results

Study population, demographic data, clinical data

Out of the 23 patients included in this analysis, 14 were over 70 years old and 9 were between 18 and 30 years old. The mean age in the young cohort was 25.7 years while the mean age in the elderly cohort amounted to 80.1 years. The BMI was significantly higher in the elderly patients ($p = 0.037$). The patients of the young cohort had significantly smaller ASA-scores ($p < 0.001$). Both groups received similar doses of fentanyl preoperatively ($p = 0.968$). Elderly patients received around half the doses per kg of propofol administered to young patients for induction of anesthesia ($p < 0.001$). The time between the start of the propofol injection and the LOC ($p = 0.075$) as well as the time between LOC and intubation ($p = 0.710$) was similar in the elderly compared to the young cohort (Table 1). Two young and four elderly patients exhibited burst-suppression patterns after induction of anesthesia.

Descriptive spectral analysis

Young patients exhibited a burst in alpha, beta, and low gamma power at LOC in the spectrogram (Figure 2A, upper panel). Inspection of individual spectrograms of this age-group showed that the power burst was present in each patients' spectrogram and had a uniform dynamic: it appeared in the low gamma, spread to the beta, and finally reached the alpha range. During the early sedation state, increased power values for all frequencies under 30 Hz remained, and strong slow and alpha bands established. The elderly cohort had more heterogeneous raw spectral signatures

TABLE 1 Characteristics of the study population.

Cohort	Young (value±SD)	Elderly (value±SD)	*p*-Value
Age (years)	23.7 ± 3.0	80.1 ± 3.5	–
Sex male/female (%)[1]	100/0	71.4/28.6	0.078
BMI (kg/m2) [2]	**23.4 ± 3.0**	**28.1 ± 6.6**	**0.037**
ASA-Score I/II/III/IV/V[1]	**8/1/0/0/0**	**0/5/7/2/0**	**<0.001**
Dose fentanyl for induction (μg)[2]	227.8 ± 44.1	228.6 ± 46.9	0.968
Dose propofol for induction (mg/kg)[2]	**3.41 ± 0.63**	**1.78 ± 0.66**	**<0.001**
Time between start propofol injection & LOC[3] (s)	68.9 ± 14.9	52.6 ± 18.9	0.075
Time between LOC and Intubation/LMA[3] (s)	151.0 ± 105.2	183.0 ± 120.2	0.71

[1]Chi-squared test.
[2]*t*-test.
[3]Mann–Whitney-*U*-test.
Results with *p*-values below 0.05 were represented bold.

during the transition to unconsciousness (Figure 2A, middle panel). Upon individual spectrogram analysis, four elderly patients appeared to develop the power burst around LOC like the young patients. The remaining patients either showed an attenuated power increase or no differentiable high frequency power bursts.

Overall, the young patients developed higher power values than elderly in all frequencies around LOC in the raw spectrum (Figure 3, left column). Clusters of differences with higher power were unveiled: in the gamma, beta to alpha frequencies around LOC and in the alpha and slow bands after LOC (Figure 2A, lower panel).

Aperiodic components of the EEG spectrum

We decomposed the spectral activity in its periodic and aperiodic components. With the obtained exponent and offset we built the slope of the aperiodic component (Figure 3, middle column).

Overall, the transition to unconsciousness was associated with an increase in the aperiodic exponent in both age groups (young: $p = 0.004$, elderly: $p = 0.007$). However, the elderly cohort already showed the increase between preLOC and LOC ($p < 0.001$) while it occurred between postLOC and LOC in the young cohort ($p = 0.002$; Figure 4A). Upon individual patient plot analysis, 8 of the 9 young patients (89%) as well as 5 of the 14 (36%) elderly patients had a drop in the exponent between preLOC and LOC. The aperiodic offset increased between preLOC and LOC in both groups (young: $p = 0.020$, elderly: $p = 0.004$). The value further increased between LOC and postLOC in the young patients ($p = 0.001$). The exponent and the offset were higher in the young than elderly patients with a statistically discernable difference solely at postLOC (Table 2; Figure 4; Supplementary Table S1).

Periodic components of the EEG spectrum

By subtracting the aperiodic slope to the raw PSD, we unveiled the periodic component of the power spectrum (Figure 3, right column). We computed group spectrograms of solely the periodic activity (Figure 2B, upper and middle panel). Most of the clusters of differences from the raw spectrograms did not appear. Solely a cluster in the low gamma, beta and alpha bands around LOC and a cluster through the alpha range after LOC remained frankly discriminable (Figure 2B, lower panel).

To explore the group difference in the periodic oscillations in the alpha range, we undertook the further characterization of the peak. Both cohorts showed an acceleration in the center frequency of the alpha peak from around 10 to 11 Hz during the transition to unconsciousness (young: $p = 0.008$, elderly: $p < 0.001$). There were no group differences in the center frequency of the alpha peak. The adjusted power of the alpha peak increased in both cohorts between preLOC and postLOC (young: $p < 0.001$, elderly $p = 0.011$). This power rise started between preLOC and LOC in the young ($p = 0.002$) whereas it appeared between LOC and postLOC in the elderly ($p = 0.001$). Young patients exhibited a higher adjusted alpha power at LOC ($p = 0.002$) and postLOC ($p = 0.039$) than the elderly. The peaks' bandwidth enlarged with induction of anesthesia in young patients ($p = 0.002$). No clear effect was obvious in the elderly cohort regarding the bandwidth of the alpha peak. Young patients exhibited a larger peak bandwidth than elderly patients solely at LOC ($p = 0.019$; Table 2; Figure 5; Supplementary Table S1).

Discussion

By decomposing the frontal EEG during the transition to propofol-induced unconsciousness into its periodic and aperiodic components, we unveiled age-independent markers of LOC: an increase in the aperiodic exponent and offset, an acceleration in the center frequency of the periodic alpha peak and an increase in the adjusted power of the alpha peak. We depicted age-related differences in both aperiodic parameters after LOC as well as in the power and bandwidth of the periodic alpha peak during the transition to unconsciousness.

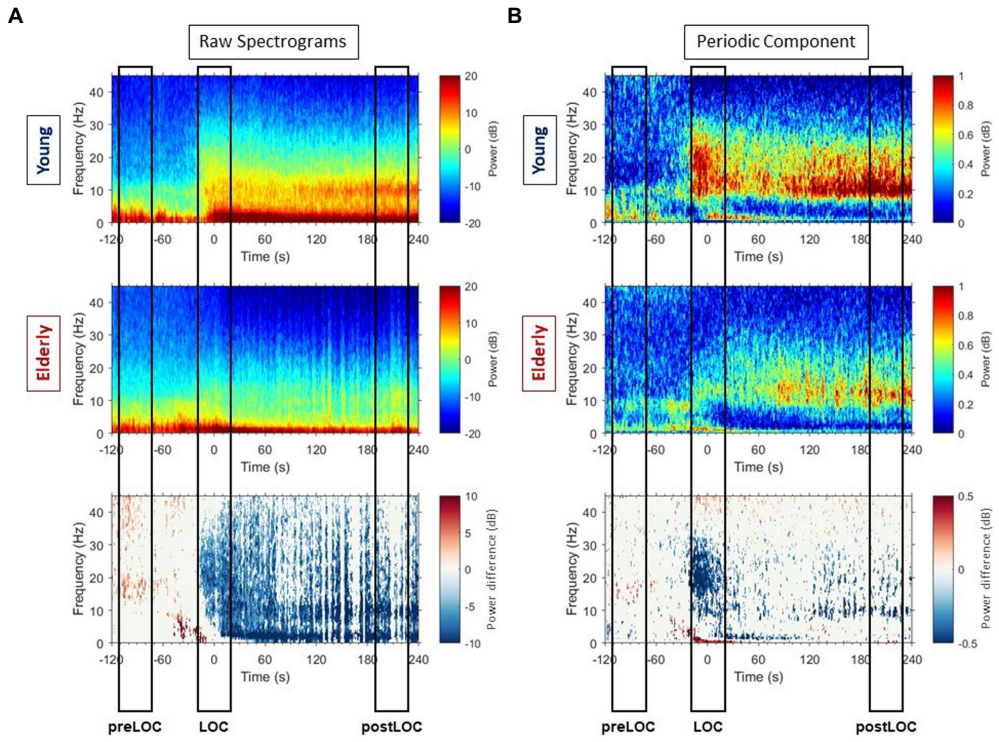

FIGURE 2
Raw spectrograms and spectrograms of periodic components with group differences. **(A)** Group-averaged raw median spectrograms at Fp1 for the young (upper panel) and elderly (middle panel) cohort with representation of the differences with $p \leq 0.05$, calculated with Mann–Whitney-*U* test at each timepoint and each frequency bin, in blue when the power is higher in the young patients and red when the power is higher in the elderly. **(B)** Group-averaged median periodic component spectrograms at Fp1 for the young (upper panel) and elderly (middle panel) cohort with representation of the differences with $p \leq 0.05$, calculated with Mann–Whitney-*U* test at each timepoint and each frequency bin, in blue when the power is higher in the young patients and red when the power is higher in the elderly.

Electroencephalography-derived markers of LOC

Anesthesia induction resulted age-independently in an increase of the aperiodic exponent. Recent work suggests that the exponent reflects the cortical balance between excitation and inhibition (Bédard and Destexhe, 2009; Gao et al., 2017). The increase possibly reflects the predominance of inhibitory synaptic currents due to the massive propofol-mediated GABAergic activation (Hutt and Longtin, 2010). LOC was also characterized by an increase of periodic activity in the low gamma, beta, and alpha frequencies in both cohorts. This corresponds to the previously described phenomenon of a "traveling peak" (Purdon et al., 2013). Both cohorts exhibited an increase in the adjusted power and an acceleration in the center frequency of the alpha peak during LOC.

It is notable that most young patients as well as some elderly patients exhibited a drop in the exponent between shortly before LOC. This transduces in a flatter slope, possibly induced by a rise of excitatory synaptic activity. Especially young patients frequently developed so-called "paradoxical excitation" during early propofol-induced anesthesia or at low propofol doses for light sedation with preserved brainstem reflexes (Lee et al., 2019). The exact neurophysiological mechanism behind this phenomenon is not sufficiently understood but the exponent value could be an EEG marker of this process.

Age-induced changes in the power spectrum

Due to neurophysiological and neuroanatomical alterations including brain atrophy (Lee and Kim, 2022), cortical thinning (McGinnis et al., 2011; Fjell et al., 2014), and neurotransmitter disbalance (Mora et al., 2007), EEG recordings undergo characteristic changes with growing age. Elderly patients under general anesthesia are known to exhibit a decreased power in the EEG due to an amplitude reduction of 2- to 3-fold compared to young adults (Purdon et al., 2015a). We did not correct for this effect to discern whether difference arose from changes in periodic or aperiodic components.

When adjusting by the aperiodic fit, elderly patients exhibited similar spectrograms than young patients with an anesthesia-induced increase in the low gamma, beta, and

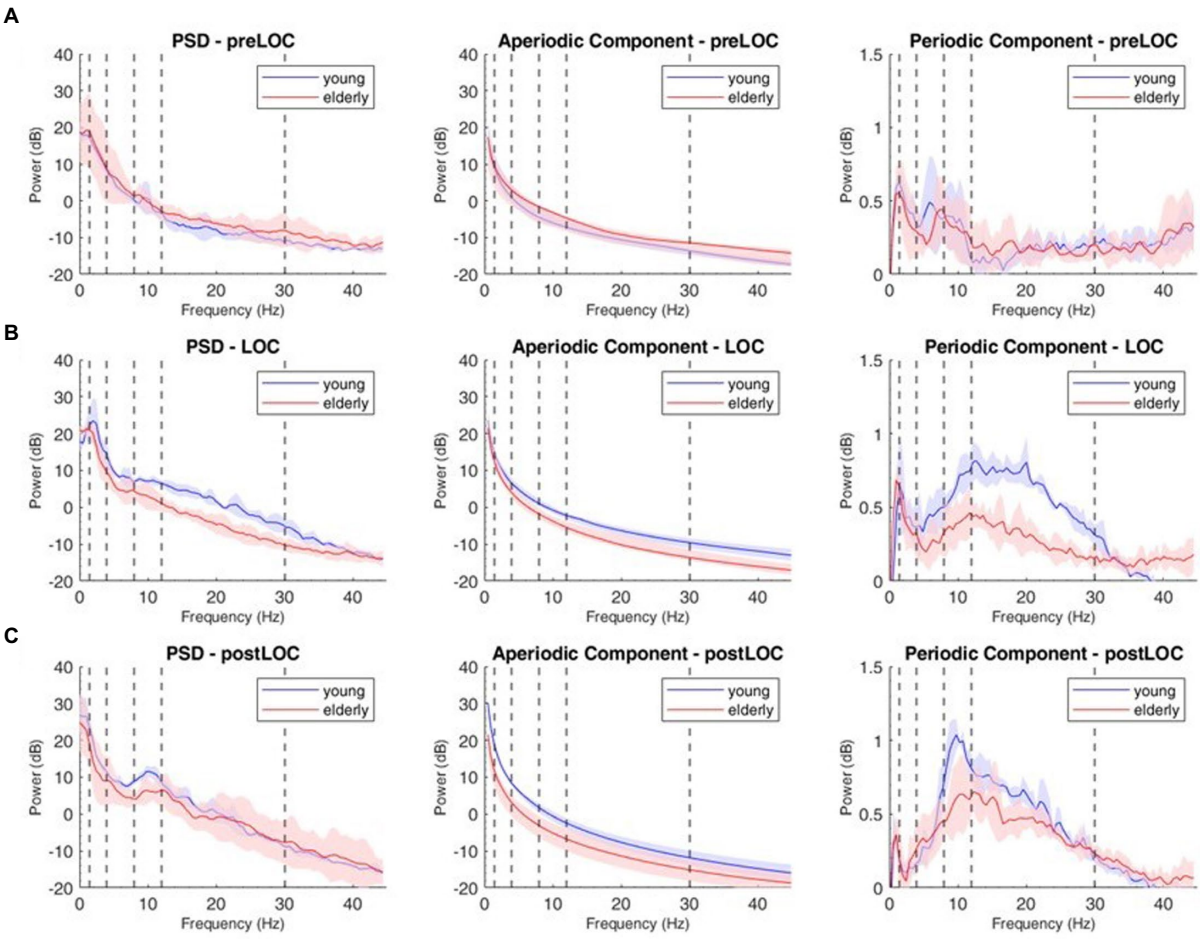

FIGURE 3
Decomposition of the power spectral density (PSD) array in its periodic and aperiodic components for the young (blue, *n*=9) and elderly (red, *n*=14) cohort at Fp1. Left column: raw PSD, Middle column: aperiodic component of the PSD. Right column: periodic component of the PSD at preLOC **(A)**, LOC **(B)**, postLOC **(C)**. Shaded Areas correspond to the interquartile range. Vertical dashed lines mark the limits of the frequency bands.

alpha power. This finding implies that a major element of the age-related difference in the power distribution arises from the differences in the aperiodic neural rhythms. According to the neural noise hypothesis, due to a desynchronization of spiking, ageing is associated with an increase in neural background noise activity—measured as a flattening of the slope, a smaller exponent—inducing deficits in neural communication (Hong and Rebec, 2012; Voytek et al., 2015). The resulting decrease in the effective signal-to-noise ratio has been linked to age-related cognitive decline (Salthouse and Lichty, 1985; Voytek et al., 2015).

We also unveiled differences in the overlayed synchronized periodic activity. Elderly patients exhibited a reduced adjusted alpha power already in the first minutes of anesthesia, at a very early sedation state. Decreased alpha power during intraoperative stable sedation is associated with preoperative cognitive impairment (Koch et al., 2019), intraoperative occurrence of burst suppression patterns (Shao et al., 2020) as well as the emergence of a postoperative delirium (Koch et al., 2021).

Anesthesia induction in the elderly

Despite the commonly carried out reduction of anesthesia doses in geriatric patients, drug overdosing occurs often and mostly during anesthesia induction (Phillips et al., 2015; Akhtar et al., 2016). In our investigation, elderly patients received about half of the propofol doses given to the young adults, as recommended (Rivera and Antognini, 2009). Nevertheless, they were more likely to develop burst-suppression patterns. Burst suppression patterns are an EEG marker of excessive anesthesia depth, pathophysiologically linked to drug-induced hypotension (Georgii et al., 2022). Higher age and ASA physical status ≥ 3 are predictors of hypotension after induction of anesthesia (Reich et al., 2005). Burst suppression patterns are associated with the emergence of postoperative delirium (Soehle et al., 2015; Fritz et al., 2016). We would like to further emphasize the crucial importance of a risk minimization during anesthesia induction. Especially in geriatric and multimorbid patients,

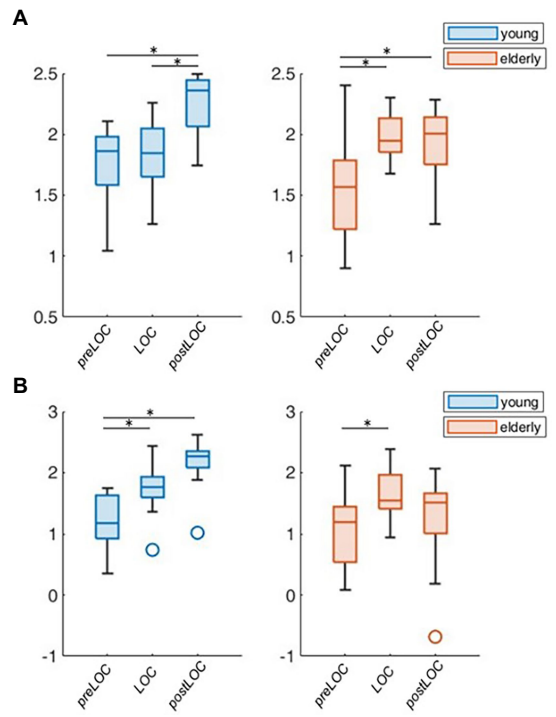

FIGURE 4
Group-wise boxplots of aperiodic parameters over loss of consciousness (LOC). **(A)** Aperiodic exponent. **(B)** Aperiodic offset. *p*-values ≤0.05 were marked with a *.

care should be given regarding the choice of anesthetic agents, drug doses, and speed of injection (Obert et al., 2020).

Reliable EEG-derived indices parametrizing the highly dynamic transition during LOC are still lacking. Common clinical monitoring devices are not specifically trained for this purpose and are inherently based on algorithms that are updated with a lag of over 30 s (Ferreira et al., 2019). This is sufficient to monitor episodes of steady state anesthesia but not for anesthesia induction. Neuromonitoring-based anesthesia titration has led to a significant decrease in postoperative neurocognitive complications (Radtke et al., 2013). The future of intraoperative neuromonitoring lies in the further evolution towards a personalized precision medicine with real-time EEG-derived indices allowing prompt adjustment of anesthesia.

Limitations

Due to a high inter-investigator variability and difficult objectification without electromyographic recordings, care should be given when interpreting the event of loss of lid closure reflex. To facilitate the readability of our findings, we called LOC the timepoint of loss of lid closure reflex. This event does not reliably represent the precise timepoint, further underlining the need for an EEG-based objectification of LOC.

TABLE 2 Difference between age cohorts at each time-segment with *p*-values computed with repeated-measures ANOVA.

Parameter	Time point	Mean young cohort [95% confidence interval]	Mean elderly cohort [95% confidence interval]	*p*-Value
Aperiodic parametrization				
Exponent	preLOC	1.766 [1.501 2.031]	1.564 [1.352 1.777]	0.231
(μV^2/Hz)	LOC	1.828 [1.632 2.024]	2.003 [1.846 2.160]	0.161
	postLOC	**2.237 [2.031 2.442]**	**1.917 [1.752 2.081]**	**0.019**
Offset	preLOC	1.212 [0.834 1.589]	1.097 [0.795 1.400]	0.628
(μV^2)	LOC	1.733 [1.414 2.052]	1.631 [1.375 1.887]	0.609
	postLOC	**2.141 [1.690 2.593]**	**1.279 [0.917 1.641]**	**0.005**
Periodic parametrization of the alpha peak (8–12Hz)				
Center frequency	preLOC	10.,068 [9.498 10.638]	9.999 [9.541 10.456]	0.845
(Hz)	LOC	10.962 [10.443 11.481]	11.034 [10.618 11.450]	0.824
	postLOC	10.872 [10.355 11.389]	11.037 [10.623 11.452]	0.610
Adjusted power	preLOC	0.803 [0.667 0.939]	0.795 [0.686 0.904]	0.925
(μV^2)	LOC	**1.060 [0.936 1.186]**	**0.794 [0.694 0.894]**	**0.002**
	postLOC	**1.277 [1.115 1.438]**	**1.058 [0.929 1.188]**	**0.039**
Bandwidth	preLOC	2.217 [1.830 2.604]	2.358 [2.048 2.669]	0.559
(Hz)	LOC	**2.985 [2.663 3.306]**	**2.482 [2.225 2.740]**	**0.019**
	postLOC	3.267 [2.844 3.690]	2.775 [2.435 3.114]	0.073

Results with p-values below 0.05 were represented bold.

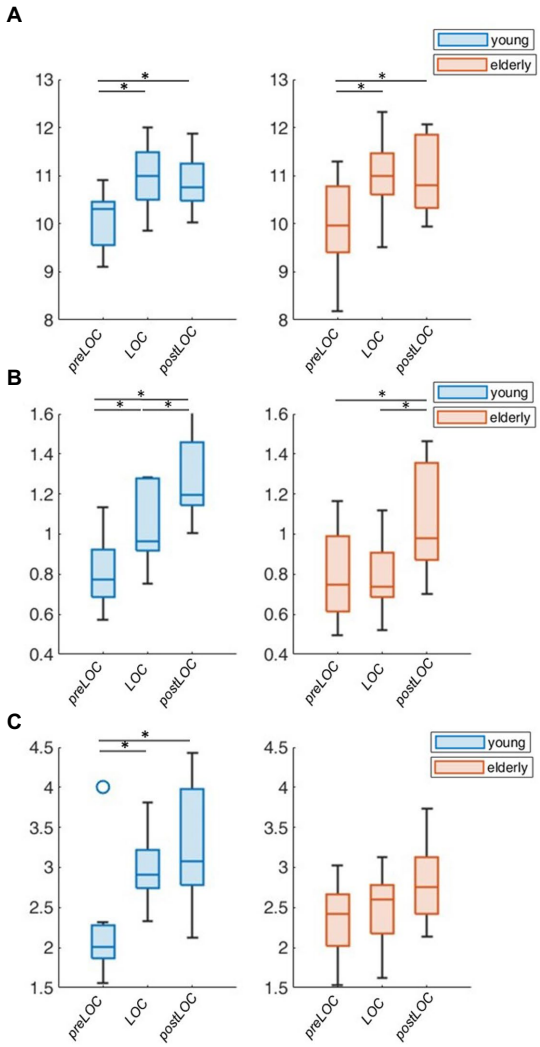

FIGURE 5
Group-wise boxplots of alpha peak characteristics over LOC. **(A)** Center frequency. **(B)** Adjusted power. **(C)** Bandwidth. *p*-Values ≤0.05 were marked with a *.

We used the FOOOF toolbox to parametrize aperiodic activity. It is established and commonly used to this end (Arnett et al., 2022; Brookshire, 2022; Shuffrey et al., 2022). The FOOOF toolbox delivers an accurate aperiodic parametrization in "easy" PSDs without plateau or major peak overlap (Gerster et al., 2022). We noticed that the aperiodic curve was overfitted in the gamma range of the young patients as negative values were reached in the power peaks. The results of our investigation regarding the aperiodic activity depend on the accuracy of the FOOOF toolbox parametrization.

Given the explorative character of this study and associated unavoidable multiple testing, *p*-values were calculated and listed but not interpreted as significant but rather as statistical aids for interpretation, requiring further studies to confirm the findings (Bender and Lange, 2001). The intention here was to describe these dynamics in a hypothesis-generating manner instead of directly implementable parameters (Hollenbeck and Wright, 2016).

Conclusion

In this study we identified several age-independent EEG-derived features that concur with propofol induced loss of consciousness. These features can potentially be used to assess the moment of loss of consciousness more precisely and reliably in an age-independent fashion. This may provide tools for an optimization of EEG-based anesthesia induction, a procedure known to pose significant risk to the elderly. The role of age-dependent alterations in the periodic and aperiodic spectral signatures of anesthesia-induced LOC needs to be further examined.

Data availability statement

The raw data supporting the conclusions of this article will be made available by the authors, without undue reservation.

Ethics statement

The studies involving human participants were reviewed and approved by Ethikkommission der Charité—Universitätsmedizin Berlin. The patients/participants provided their written informed consent to participate in this study.

Author contributions

SL, SM, JD, and SK conceived and designed the trial. SL conducted the experiments and wrote the first draft of the manuscript. SL, VB, and SM analyzed the data. All authors contributed to the article and approved the submitted version.

Funding

JD was supported by Deutsche Forschungsgemeinschaft (DFG DR 323/10-1), and Era-Net Neuron EBio2, with funds from BMBF (01EW2004). SL was financially supported by the Berlin Institute of Health (BIH) with a research stipend. SK was funded by the Deutsche Forschungsgemeinschaft (DFG, German Research Fundation) – Project number KO 4249/3-1).

Conflict of interest

SK is an inventor on patents, sold to Medtronic, and received speaker's honoraria from Medtronic.

The remaining authors declare that the research was conducted in the absence of any commercial or financial relationships that could be construed as a potential conflict of interest.

Publisher's note

All claims expressed in this article are solely those of the authors and do not necessarily represent those of their affiliated organizations, or those of the publisher, the editors and the reviewers. Any product that may be evaluated in this article, or claim that may be made by its manufacturer, is not guaranteed or endorsed by the publisher.

Supplementary material

The Supplementary material for this article can be found online at: https://www.frontiersin.org/articles/10.3389/fnagi.2022.1076393/full#supplementary-material

References

Akhtar, S., Heng, J., Dai, F., Schonberger, R. B., and Burg, M. M. (2016). A retrospective observational study of anesthetic induction dosing practices in female elderly surgical patients: are we overdosing older patients? *Drugs Aging* 33, 737–746. doi: 10.1007/s40266-016-0394-x

Arnett, A. B., Rutter, T. M., and Stein, M. A. (2022). Neural markers of methylphenidate response in children with attention deficit hyperactivity disorder. *Front. Behav. Neurosci.* 16:887622. doi: 10.3389/fnbeh.2022.887622

Bédard, C., and Destexhe, A. (2009). Macroscopic models of local field potentials and the apparent 1/F noise in brain activity. *Biophys. J.* 96, 2589–2603. doi: 10.1016/j.bpj.2008.12.3951

Bender, R., and Lange, S. (2001). Adjusting for multiple testing—when and how? *J. Clin. Epidemiol.* 54, 343–349. doi: 10.1016/S0895-4356(00)00314-0

Boly, M., Moran, R., Murphy, M., Boveroux, P., Bruno, M. A., Noirhomme, Q., et al. (2012). Connectivity changes underlying spectral Eeg changes during Propofol-induced loss of consciousness. *J. Neurosci.* 32, 7082–7090. doi: 10.1523/JNEUROSCI.3769-11.2012

Brake, N., Duc, F., Rokos, A., Arseneau, F., Shahiri, S., Khadra, A., et al. (2021). Aperiodic EEG activity masks the dynamics of neural oscillations during loss of consciousness from propofol. bioRXiv [Preprint]. doi: 10.1101/2021.10.12.464109

Brookshire, G. (2022). Putative rhythms in Attentional switching can be explained by aperiodic temporal structure. *Nat. Hum. Behav.* 6, 1280–1291. doi: 10.1038/s41562-022-01364-0

Brown, E. N., Purdon, P. L., and Van Dort, C. J. (2011). General anesthesia and altered states of arousal: a systems neuroscience analysis. *Annu. Rev. Neurosci.* 34, 601–628. doi: 10.1146/annurev-neuro-060909-153200

Cantero, J. L., Atienza, M., Salas, R. M., and Gómez, C. M. (1999). Alpha Eeg coherence in different brain states: an electrophysiological index of the arousal level in human subjects. *Neurosci. Lett.* 271, 167–170. doi: 10.1016/S0304-3940(99)00565-0

Ching, S., Cimenser, A., Purdon, P. L., Brown, E. N., and Kopell, N. J. (2010). Thalamocortical model for a Propofol-induced alpha-rhythm associated with loss of consciousness. *Proc. Natl. Acad. Sci. U. S. A.* 107, 22665–22670. doi: 10.1073/pnas.1017069108

Cimenser, A., Purdon, P. L., Pierce, E. T., Walsh, J. L., Salazar-Gomez, A. F., Harrell, P. G., et al. (2011). Tracking brain states under general anesthesia by using global coherence analysis. *Proc. Natl. Acad. Sci. U. S. A.* 108, 8832–8837. doi: 10.1073/pnas.1017041108

Donoghue, T., Haller, M., Peterson, E. J., Varma, P., Sebastian, P., Gao, R., et al. (2020). Parameterizing neural power spectra into periodic and aperiodic components. *Nat. Neurosci.* 23, 1655–1665. doi: 10.1038/s41593-020-00744-x

Ferreira, A. L., Mendes, J. G., Nunes, C. S., and Amorim, P. (2019). Evaluation of Bispectral index time delay in response to anesthesia induction: an observational study. *Braz. J. Anesthesiol. (English Edition)* 69, 377–382. doi: 10.1016/j.bjan.2019.03.008

Fjell, A. M., Westlye, L. T., Grydeland, H., Amlien, I., Espeseth, T., Reinvang, I., et al. (2014). Accelerating cortical thinning: unique to dementia or universal in aging? *Cereb. Cortex* 24, 919–934. doi: 10.1093/cercor/bhs379

Fritz, B. A., Kalarickal, P. L., Maybrier, H. R., Muench, M. R., Dearth, D., Chen, Y., et al. (2016). Intraoperative electroencephalogram suppression predicts postoperative delirium. *Anesth. Analg.* 122, 234–242. doi: 10.1213/ANE.0000000000000989

Gao, R., Peterson, E. J., and Voytek, B. (2017). Inferring synaptic excitation/inhibition balance from field potentials. *NeuroImage* 158, 70–78. doi: 10.1016/j.neuroimage.2017.06.078

Georgii, M. T., Kreuzer, M., Fleischmann, A., Schuessler, J., Schneider, G., and Pilge, S. (2022). Targeted interventions to increase blood pressure and decrease anaesthetic concentrations reduce intraoperative burst suppression: a randomised interventional clinical trial. *Front. Syst. Neurosci.* 16:786816. doi: 10.3389/fnsys.2022.786816

Gerster, M., Waterstraat, G., Litvak, V., Lehnertz, K., Schnitzler, A., Florin, E., et al. (2022). Separating neural oscillations from aperiodic 1/F activity: challenges and recommendations. *Neuroinformatics* 20, 991–1012. doi: 10.1007/s12021-022-09581-8

Gugino, L. D., Chabot, R. J., Prichep, L. S., John, E. R., Formanek, V., and Aglio, L. S. (2001). Quantitative EEG changes associated with loss and return of consciousness in healthy adult volunteers anaesthetized with Propofol or Sevoflurane. *Br. J. Anaesth.* 87, 421–428. doi: 10.1093/bja/87.3.421

Hollenbeck, J. R., and Wright, P. M. (2016). Harking, sharking, and Tharking: making the Case for post hoc analysis of scientific data. *J. Manag.* 43, 5–18. doi: 10.1177/0149206316679487

Hong, S. L., and Rebec, G. V. (2012). A new perspective on behavioral inconsistency and neural noise in aging: compensatory speeding of neural communication. *Front. Aging Neurosci.* 4:27. doi: 10.3389/fnagi.2012.00027

Hutt, A., and Longtin, A. (2010). Effects of the anesthetic agent Propofol on neural populations. *Cogn. Neurodyn.* 4, 37–59. doi: 10.1007/s11571-009-9092-2

Koch, S., Feinkohl, I., Chakravarty, S., Windmann, V., Lichtner, G., Pischon, T., et al. (2019). Cognitive impairment is associated with absolute intraoperative frontal A-band power but not with baseline A-band power: a pilot study. *Dement. Geriatr. Cogn. Disord.* 48, 83–92. doi: 10.1159/000502950

Koch, S., Windmann, V., Chakravarty, S., Kruppa, J., Yürek, F., Brown, E. N., et al. (2021). Perioperative electroencephalogram spectral dynamics related to postoperative delirium in older patients. *Anesth. Analg.* 133, 1598–1607. doi: 10.1213/ANE.0000000000005668

Kuizenga, K., Wierda, J. M., and Kalkman, C. J. (2001). Biphasic Eeg changes in relation to loss of consciousness during induction with thiopental, Propofol, Etomidate, midazolam or Sevoflurane. *Br. J. Anaesth.* 86, 354–360. doi: 10.1093/bja/86.3.354

Lanzone, J., Colombo, M. A., Sarasso, S., Zappasodi, F., Rosanova, M., Massimini, M., et al. (2022). EEG spectral exponent as a synthetic index for the longitudinal assessment of stroke recovery. *Clin. Neurophysiol.* 137, 92–101. doi: 10.1016/j.clinph.2022.02.022

Lee, J., and Kim, H. J. (2022). Normal aging induces changes in the brain and Neurodegeneration Progress: review of the structural, biochemical, metabolic, cellular and molecular changes. *Front. Aging Neurosci.* 14:931536. doi: 10.3389/fnagi.2022.931536

Lee, S. H., Lee, G. M., Lee, D. R., and Lee, J. U. (2019). Factors related to paradoxical reactions during Propofol-induced sedated endoscopy. *Scand. J. Gastroenterol.* 54, 371–376. doi: 10.1080/00365521.2019.1585938

Lendner, J. D., Helfrich, R. F., Mander, B. A., Romundstad, L., Lin, J. J., Walker, M. P., et al. (2020). An electrophysiological marker of arousal level in humans. *elife* 9:E55092. doi: 10.7554/eLife.55092

Manyukhina, V. O., Prokofyev, A. O., Galuta, I. A., Goiaeva, D. E., Obukhova, T. S., Schneiderman, J. F., et al. (2022). Globally elevated excitation-inhibition ratio in children with autism Spectrum disorder and below-average intelligence. *Mol. Autism.* 13:20. doi: 10.1186/s13229-022-00498-2

Mcginnis, S. M., Brickhouse, M., Pascual, B., and Dickerson, B. C. (2011). Age-related changes in the thickness of cortical zones in humans. *Brain Topogr.* 24, 279–291. doi: 10.1007/s10548-011-0198-6

Miller, K. J., Sorensen, L. B., Ojemann, J. G., and Den Nijs, M. (2009). Power-law scaling in the brain surface electric potential. *PLoS Comput. Biol.* 5:E1000609. doi: 10.1371/journal.pcbi.1000609

Moody, O. A., Zhang, E. R., Vincent, K. F., Kato, R., Melonakos, E. D., Nehs, C. J., et al. (2021). The neural circuits underlying general anesthesia and sleep. *Anesth. Analg.* 132, 1254–1264. doi: 10.1213/ANE.0000000000005361

Mora, F., Segovia, G., and Del Arco, A. (2007). Aging, plasticity and environmental enrichment: structural changes and neurotransmitter dynamics in several areas of the brain. *Brain Res. Rev.* 55, 78–88. doi: 10.1016/j.brainresrev.2007.03.011

Obert, D. P., Sepúlveda, P., Kratzer, S., Schneider, G., and Kreuzer, M. (2020). The influence of induction speed on the frontal (processed) EEG. *Sci. Rep.* 10:19444. doi: 10.1038/s41598-020-76323-8

Partha Mitra, H. B. (2009). *Observed Brain Dynamics*. Oxford: Oxford University Press.

Pascual-Marqui, R. D., Sekihara, K., Brandeis, D., and Michel, C. M. (2009). "Imaging the electric neuronal generators of EEG/MEG," in *Electrical Neuroimaging*. eds. C. M. Michel, D. Brandeis, J. Wackermann, L. R. R. Gianotti and T. Koenig (Cambridge: Cambridge University Press)

Phillips, A. T., Deiner, S., Mo Lin, H., Andreopoulos, E., Silverstein, J., and Levin, M. A. (2015). Propofol use in the elderly population: prevalence of overdose and association with 30-day mortality. *Clin. Ther.* 37, 2676–2685. doi: 10.1016/j.clinthera.2015.10.005

Purdon, P. L., Pavone, K. J., Akeju, O., Smith, A. C., Sampson, A. L., Lee, J., et al. (2015a). The ageing brain: age-dependent changes in the electroencephalogram during Propofol and Sevoflurane general anaesthesia. *Br. J. Anaesth.* 115, I46–I57. doi: 10.1093/bja/aev213

Purdon, P. L., Pierce, E. T., Mukamel, E. A., Prerau, M. J., Walsh, J. L., Wong, K. F., et al. (2013). Electroencephalogram signatures of loss and recovery of consciousness from Propofol. *Proc. Natl. Acad. Sci. U. S. A.* 110, E1142–E1151. doi: 10.1073/pnas.1221180110

Purdon, P. L., Sampson, A., Pavone, K. J., and Brown, E. N. (2015b). Clinical electroencephalography for anesthesiologists: part I: background and basic signatures. *Anesthesiology* 123, 937–960. doi: 10.1097/ALN.0000000000000841

Radtke, F. M., Franck, M., Lendner, J., Krüger, S., Wernecke, K. D., and Spies, C. D. (2013). Monitoring depth of anaesthesia in a randomized trial decreases the rate of postoperative delirium but not postoperative cognitive dysfunction. *Br. J. Anaesth.* 110, I98–I105. doi: 10.1093/bja/aet055

Reich, D. L., Hossain, S., Krol, M., Baez, B., Patel, P., Bernstein, A., et al. (2005). Predictors of hypotension after induction of general anesthesia. *Anesth. Analg.* 101, 622–628. doi: 10.1213/01.ANE.0000175214.38450.91

Rivera, R., and Antognini, J. F. (2009). Perioperative drug therapy in elderly patients. *Anesthesiology* 110, 1176–1181. doi: 10.1097/ALN.0b013e3181a10207

Salthouse, T. A., and Lichty, W. (1985). Tests of the neural noise hypothesis of age-related cognitive change. *J. Gerontol.* 40, 443–450. doi: 10.1093/geronj/40.4.443

Shao, Y. R., Kahali, P., Houle, T. T., Deng, H., Colvin, C., Dickerson, B. C., et al. (2020). Low frontal alpha power is associated with the propensity for burst suppression: an electroencephalogram phenotype for a "vulnerable brain". *Anesth. Analg.* 131, 1529–1539. doi: 10.1213/ANE.0000000000004781

Shuffrey, L. C., Pini, N., Potter, M., Springer, P., Lucchini, M., Rayport, Y., et al. (2022). Aperiodic electrophysiological activity in preterm infants is linked to subsequent autism risk. *Dev. Psychobiol.* 64:E22271. doi: 10.1002/dev.22271

Soehle, M., Dittmann, A., Ellerkmann, R. K., Baumgarten, G., Putensen, C., and Guenther, U. (2015). Intraoperative burst suppression is associated with postoperative delirium following cardiac surgery: a prospective, observational study. *BMC Anesthesiol.* 15:61. doi: 10.1186/s12871-015-0051-7

Spies, W. K. A. C. (2005). *Check-Up Anästhesiologie, Standards Anästhesie-Intensivmedizin-Schmerztherapie-Notfallmedizin*., Heidelberg: Springer Medizin Verlag.

Staheli, B., and Rondeau, B. (2022). "Anesthetic Considerations," in *The Geriatric Population*. StatPearls. Treasure Island (FL): StatPearls Publishing. Copyright © 2022, StatPearls Publishing LLC.

Trapani, G., Altomare, C., Liso, G., Sanna, E., and Biggio, G. (2000). "Propofol in anesthesia. Mechanism of action, structure-activity relationships and drug delivery. *Curr. Med. Chem.* 7, 249–271. doi: 10.2174/0929867003375335

Voytek, B., Kramer, M. A., Case, J., Lepage, K. Q., Tempesta, Z. R., Knight, R. T., et al. (2015). Age-related changes in 1/F neural electrophysiological noise. *J. Neurosci.* 35, 13257–13265. doi: 10.1523/JNEUROSCI.2332-14.2015

Windmann, V., Dreier, J. P., Major, S., Spies, C., Lachmann, G., and Koch, S. (2022). Increased direct current-electroencephalography shifts during induction of anesthesia in elderly patients developing postoperative delirium. *Front. Aging Neurosci.* 14:921139. doi: 10.3389/fnagi.2022.921139

Zhang, J., Villringer, A., and Nikulin, V. V. (2022). Dopaminergic modulation of local non-oscillatory activity and global-network properties in Parkinson's disease: an Eeg study. *Front. Aging Neurosci.* 14:846017. doi: 10.3389/fnagi.2022.846017

frontiers | Frontiers in Aging Neuroscience

TYPE Original Research
PUBLISHED 01 February 2023
DOI 10.3389/fnagi.2023.1067268

OPEN ACCESS

EDITED BY
Jiaqiang Zhang,
Zhengzhou University,
China

REVIEWED BY
Ana Cervera-Ferri,
University of Valencia,
Spain
Cheng Ni,
Cancer Hospital,
Chinese Academy of Medical Sciences,
Peking Union Medical College,
China

*CORRESPONDENCE
Susanne Koch
✉ susanne.koch@charite.de

†These authors have contributed equally to this work

SPECIALTY SECTION
This article was submitted to Neurocognitive Aging and Behavior, a section of the journal Frontiers in Aging Neuroscience

RECEIVED 11 October 2022
ACCEPTED 09 January 2023
PUBLISHED 01 February 2023

CITATION
Koch S, Blankertz B, Windmann V, Spies C, Radtke FM and Röhr V (2023) Desflurane is risk factor for postoperative delirium in older patients' independent from intraoperative burst suppression duration.
Front. Aging Neurosci. 15:1067268.
doi: 10.3389/fnagi.2023.1067268

Desflurane is risk factor for postoperative delirium in older patients' independent from intraoperative burst suppression duration

Susanne Koch[1]*, Benjamin Blankertz[2], Victoria Windmann[1], Claudia Spies[1], Finn M. Radtke[3†] and Vera Röhr[2†]

[1]Department of Anaesthesiology and Operative Intensive Care Medicine, Charité – Universitätsmedizin Berlin, Berlin, Germany, [2]Neurotechnology Group, Technische Universität Berlin, Berlin, Germany, [3]Department of Anesthesia, Hospital of Nykobing, University of Southern Denmark, Odense, Denmark

Background: Postoperative Delirium (POD) is the most frequent neurocognitive complication after general anesthesia in older patients. The development of POD is associated with prolonged periods of burst suppression activity in the intraoperative electroencephalogram (EEG). The risk to present burst suppression activity depends not only on the age of the patient but is also more frequent during propofol anesthesia as compared to inhalative anesthesia. The aim of our study is to determine, if the risk to develop POD differs depending on the anesthetic agent given and if this correlates with a longer duration of intraoperative burst suppression.

Methods: In this secondary analysis of the SuDoCo trail [ISRCTN 36437985] 1277 patients, older than 60 years undergoing general anesthesia were included. We preprocessed and analyzed the raw EEG files from each patient and evaluated the intraoperative burst suppression duration. In a logistic regression analysis, we assessed the impact of burst suppression duration and anesthetic agent used for maintenance on the risk to develop POD.

Results: 18.7% of patients developed POD. Burst suppression duration was prolonged in POD patients (POD 27.5 min ± 21.3 min vs. NoPOD 21.4 ± 16.2 min, p <0.001), for each minute of prolonged intraoperative burst suppression activity the risk to develop POD increased by 1.1% (OR 1.011, CI 95% 1.000–1.022, p = 0.046). Burst suppression duration was prolonged under propofol anesthesia as compared to sevoflurane and desflurane anesthesia (propofol 32.5 ± 20.3 min, sevoflurane 17.1 ± 12.6 min and desflurane 20.1 ± 16.0 min, p <0.001). However, patients receiving desflurane anesthesia had a 1.8fold higher risk to develop POD, as compared to propofol anesthesia (OR 1.766, CI 95% 1.049–2.974, p = 0.032).

Conclusion: We found a significantly increased risk to develop POD after desflurane anesthesia in older patients, even though burst suppression duration was shorter under desflurane anesthesia as compared to propofol anesthesia. Our finding might help to explain some discrepancies in studies analyzing the impact of burst suppression duration and EEG-guided anesthesia on the risk to develop POD.

KEYWORDS

burst suppression EEG, intraoperative EEG monitoring, desflurane anesthesia, propofol anesthesia, elderly, postoperative delirium

Highlights

- **Question:** Does propofol, with its higher tendency to trigger intraoperative burst suppression activity, trigger POD in older patients at a higher rate than sevoflurane or desflurane?
- **Findings:** Desflurane is associated with a higher risk to develop POD in older patients as compared to propofol or sevoflurane, even though propofol shows prolonged intraoperative burst suppression activity.
- **Meaning:** In older patients desflurane anesthesia maintenance should be used with caution, since it is associated with a higher risk to develop POD as compared to propofol or sevoflurane anesthesia maintenance.

Introduction

Postoperative Delirium (POD) is the most frequent neurocognitive complication after general anesthesia in older patients, being associated with a higher mortality and increased morbidity (Aldecoa et al., 2017). POD is a multifactorial syndrome being related to preexisting risk factors as an age above 60 years, preoperative lower cognitive abilities, the presence of comorbidities, alcohol-related disorders and precipitating risk factors as prolonged preoperative fluid fasting, abdominal and cardiothoracic surgeries, surgery duration, intraoperative bleeding, the anticholinergic load of drug given and prolonged periods of too deep anesthesia (Chan et al., 2013; Radtke et al., 2013; Soehle et al., 2015; Fritz et al., 2016; Aldecoa et al., 2017). Periods of too deep anesthesia can be identified with intraoperative electroencephalographic (EEG) recording, were burst suppression activity is the typical signature (Brown et al., 2010; Purdon et al., 2015b). Burst suppression activity in general is an isoelectric line with intermittened bursts of alpha oscillations, indicating a highly reduced cerebral metabolism (Brown et al., 2010).

Here we like to assess the impact of different anesthetic agents on the risk to develop POD and if this is correlated to the intraoperative duration of burst suppression activity. The risk to develop intraoperative burst suppression activity is related to the dosage of the anesthetic agents given. But importantly it has been shown that the risk to present intraoperative burst suppression activity also increases with the age of the patient and shows differences depending on which anesthetic agent was given (Purdon et al., 2015a,b). Propofol has a higher tendency to induce burst suppression activity as compared to sevoflurane anesthesia (Purdon et al., 2015a). But there seems to be no EEG-slowing effect when comparing desflurane with sevoflurane (Rehberg et al., 1999).

Based on the knowledge of these former studies, we expected that older patients receiving a total intravenous anesthesia (TIVA) with propofol have (1) a higher risk to present intraoperative burst suppression activity, showing a prolonged intraoperative burst suppression duration and an increased burst suppression ratio, when compared to patients undergoing general anesthesia with either sevoflurane or desflurane. Additionally, (2) we expected to see a higher incidence of POD in older patients receiving a TIVA with propofol compared to volatile anesthetics such as sevoflurane or desflurane.

Hence, the aim of our study was first to analyze the incidence of POD in older patients in relation to the given anesthetic agent – propofol, sevoflurane or desflurane – and second to evaluate the burst suppression activity if patients who received either propofol, sevoflurane or desflurane for maintenance of general anesthesia. Finally, we wanted to know if the development of burst suppression activity in the intraoperative EEG with respect to the different anesthetic agents given intraoperatively is related to the development of POD.

Materials and methods

The initial single center SuDoCo study was conducted as a randomized controlled trail at the Charité-Universitätsmedizin Berlin, Germany, Department of Anaesthesiology and operative intensive care medicine between March 2009 and August 2010. The ethical commission at the Charité approved the study (EA1/242/08) and all patients gave written informed consent. Data privacy and security regulations were followed and the study was registered under ISRCTN 36437985. In this secondary analysis of the single-center SuDoCo trail, we analyzed the initially 1,277 included patients. The inclusion criteria for the SuDoCo study were an age older than 60 years, the conduction of a surgery planned to last at least 60 min and the need for general anesthesia. Pre-operatively the Mini-Mental State Examination (MMSE) was performed, and patients with a MMSE score < 24 or patients who had a history of neurologic deficits were excluded (Radtke et al., 2013).

Patients' data assessment

Characteristics of the patients, intraoperative and postoperative data were assessed during the initial study period at the Charité from 2009 until 2010. The preoperative patient characteristics (age, American Society of Anesthesiologists' physical status (ASA status), sex, body mass index (BMI) and Mini-Mental State Examination (MMSE)) were included in our analysis.

All patients received general anesthesia according to the standard operation procedures (SOPs) of the Charité-Universitätsmedizin Berlin (Kox and Spies, 2005). Anesthesia was induced with bolus application of thiopental, propofol, or etomidate in combination with fentanyl or remifentanil, followed by neuromuscular block to facilitate tracheal intubation. For anesthesia maintenance, patients received either total intravenous anesthesia with propofol, or inhalational anesthesia with sevoflurane or desflurane. The anesthetic agent given was chosen by the anesthesiologist in charge and was not controlled by the regime of the SuDoCo study.

POD was assessed twice daily by trained study personnel from the day of surgery until postoperative day seven by using the Diagnostic and Statistical Manual of Mental Disorders (DSM IV).

Intraoperative EEG recording was performed using the BIS monitor (Covidien, Boulder, CO, United States). EEG electrodes (electrode position Fp1, Fp2, F7 and F8) were placed in the forehead of the patient

before induction of anesthesia. Bispectral Index (BIS) values indicate depth of anesthesia ranging from 0 (isoelectric line in EEG) to 100 (fully awake). BIS values between 40 and 60 indicate adequate depth of anesthesia.

EEG data analysis

Each recorded EEG file was separately preprocessed. Periods of artifacts were excluded. Such artifacts included high amplitude artifacts, based on the 99% quantile of the data amplitude, and frequency artifacts below 0.5 Hz or above 50 Hz activity. EEG artifacts were mostly seen during anesthesia induction, caused by intubation and correct placement of the patient for surgery. After the artefact removal, the data was re-referenced by the mean. Then we determined intraoperative signatures of burst suppression activity by calculating a burst suppression probability for each time point. This probability is calculated as the ratio of time points within a second surrounding the given point that have an amplitude value below the 60% quantile of the data amplitudes. For each amplitude artifact that was removed in the first step, the second around the artifact was removed after this stage. If the probability surpassed 80% the point was marked as a suppression point. Using this as a basis, we calculated the overall burst suppression duration (min) per EEG file. The burst suppression ratio was calculated by using the fraction of burst suppression activity and the artifact-free EEG duration. All data analysis was performed with self-written scripts written in the programming languages Python and Julia using standard toolboxes and packages (PosDefManifold and PosDefManifoldML).

Statistics

Statistical analyses were performed with SPSS, Version 26 (Copyright SPSS, Inc., Chicago, IL 60606, United States). Patients were divided into a POD and NoPOD group, according to the DSM IV results. Data are expressed as mean with standard deviation, median with 95% CI or as frequencies (%). Values were considered significant if $p < 0.05$.

Significant differences in patient characteristics were calculated by using for continuous data either the student *t*-test for age and BMI or the Mann–Whitney U-Test for MMSE, surgery duration, Burst suppression duration and burst suppression ratio. Categorical data were assessed by either the Fisher's exact test (sex and Midazolam given) or the Pearson chi-square test (ASA status, surgical specialty, outcome, and anesthetic agent given). Differences between the anesthetic agent groups were calculated by using the Kruskal-Wallis test and the Pearson chi-square test. We also assessed the outcome parameters (days on the ward, days on ICU) and in-hospital mortality within the different anesthetic agent groups with the Kruskal-Wallis test and the Pearson chi-square test.

In a binominal logistic regression, we analyzed the independent impact of burst suppression duration and anesthetic agent used for maintenance on the risk to develop POD. We adjusted the logistic regression analysis for all predescribed POD risk factors that significantly correlated with POD in our study group.

Results

After analyzing and preprocessing the raw electroencephalographic data files (EEG), we had to exclude 110 data files because of missing EEG raw data files or the presence of too many artifacts in the raw data files. We excluded all EEG files, where we could not at least analyze 20 min of clean raw EEG. Additionally, from 9 patients the anesthetic agent used for anesthesia maintenance was not given. Finally, we could include 1,058 patients in our analysis.

Patients' characteristics for POD and NoPOD

198 (18.7%) patients developed POD and 860 (81.3%) did not (NoPOD). Patients' characteristics are given in Table 1 (detailed information see Supplementary material). POD patients had significantly prolonged burst suppression duration (POD 27.5 ± 21.3 min vs. NoPOD 21.4 ± 16.2 min, $p < 0.001$) and received more frequently desflurane for anesthesia maintenance and less frequently sevoflurane or propofol (desflurane 50.5%, sevoflurane 30.3%, propofol 19.2%, $p < 0.001$). Average and minimum BIS level of sedation did not differ between POD and NoPOD patients.

In spearman correlation analyses we found a high correlation of POD with age, ASA status, MMSE score, surgery duration, surgery specialization, burst suppression duration and anesthetic agent given for maintenance (Supplementary material).

Patients' characteristics for propofol, sevoflurane and desflurane anesthesia

When comparing the patients' characteristics between patients who received either propofol, sevoflurane or desflurane for anesthesia maintenance, we found differences in sex, BMI, surgery duration and surgical specialty. But we found no differences in age, ASA status, preoperative MMSE score and average and minimum BIS level of sedation between the patients' groups receiving either propofol, sevoflurane or desflurane (Table 2; Supplementary material). However, we found a higher incidence of POD in the desflurane group (25.4%) compared to propofol (12.9%) or sevoflurane group (16.2%) (Table 2; Figure 1).

As expected, burst suppression duration was prolonged under propofol anesthesia (32.5 ± 20.3 min) and shorter under sevoflurane (17.1 ± 12.6 min) and desflurane (20.2 ± 16.0 min) anesthesia and burst suppression ratio was highest under propofol anesthesia (0.25 ± 0.08) as compared to sevoflurane (0.16 ± 0.09) and desflurane (0.18 ± 0.12) (Table 2).

Anesthetic agent, burst suppression activity and the impact on POD

In our binominal logistic regression analysis (including anesthetic agents given for maintenance (propofol vs. sevoflurane and propofol vs. desflurane), burst suppression duration (min), age (years), ASA status (I, II, III, IV), MMSE score (25 to 30), surgery duration (min) and surgery specialty (general surgery, orthopedics, urology, gynecology, other)) we found a significant association with POD for age, preoperative ASA score, preoperative MMSE score, surgery duration desflurane versus propofol and burst suppression duration (Table 3). Overall, we found that each minute of prolonged intraoperative burst suppression activity the risk to develop POD

10.3389/fnagi.2023.1067268

TABLE 1 Patients characteristics for patients with postoperative delirium (POD) and without (NoPOD).

	All patients (*n* =1,058)	NoPOD (*n* =860)	POD (*n* =198)	Value of *p*
Age (years)	69.7 ± 6.3	69.2 ± 6.1	72.1 ± 6.5	0.000
Sex male/female (%)	54 / 46	54 / 46	53.5 / 46.5	n.s.
BMI	27.1 ± 5.0	27.3 ± 5.2	26.4 ± 4.7	0.020
ASA status (%)				0.000
1	3.1	3.8	0	
2	49.1	51.4	39.4	
3	45.8	43.4	56.6	
4	1.9	1.4	4.0	
MMSE preoperative	28.9 ± 1.4	29.0 ± 1.3	28.6 ± 1.6	0.000
Midazolam premedication yes/no (%)	5/95	5/95	7/93	n.s.
Surgical specialty (%)				0.001
General surgery	49.1	46.1	62.4	
Orthopedics	29.7	31.4	22.3	
Urology	8.1	8.1	8.1	
Gynecology	10.6	11.8	5.6	
Other	2.5	2.7	1.5	
Surgery duration (min)	170 ± 101	157 ± 92	235 ± 117	0.000
Anesthetic agents maintenance (%)				0.000
Propofol	27.8	29.8	19.2	
Sevoflurane	35.1	36.2	30.3	
Desflurane	37.1	34.1	50.5	
Depth of anesthesia				
Average BIS (0–100)	40.6 ± 7.3	40.6 ± 7.1	40.1 ± 7.8	n.s.
Minimum BIS (0–100)	32.1 ± 13.6	32.2 ± 13.4	31.2 ± 14.7	n.s.
Burst suppression duration (min)	22.5 ± 17.7	21.4 ± 16.2	27.5 ± 21.3	0.000
Burst suppression ratio	0.19 ± 0.1	0.19 ± 0.1	0.2 ± 0.11	n.s.
Outcome/discharge (%)				0.000
Home	88.9	92.5	73.6	
Other hospital	8.9	6.5	18.8	
Died	2.2	1.0	7.6	

POD patients were significant older, had lower BMI scores, lower MMSE scores, elevated ASA scores, prolonged surgery duration, prolonged burst suppresion duration and more frequently a desflurane anaesthesia. We found no significant differences in sex, premedication with midazolam, depth of anesthesia index assessed with the bispectral index (BIS) in average or minimum levels and burst suppression ratio. Sex, ASA status and anaesthetic agents used were compared by Chi-Square test. Continuious data were compared by independent *t*-test.

TABLE 2 Outcome parameter for the anesthetic agent given throughout anesthesia maintenance.

	All Patients (*n* =1,058)	Propofol (*n* =294)	Sevoflurane (*n* =371)	Desflurane (*n* =393)	Value of *p*
Burst suppression duration (min)*	22.6 ± 17.4	32.5 ± 20.3	17.1 ± 12.6	20.2 ± 16.0	0.000
Burst suppression ratio*	0.19 ± 0.1	0.25 ± 0.08	0.16 ± 0.09	0.18 ± 0.12	0.000
Depth of anesthesia					
Average BIS (0–100)	40.6 ± 7.3	40.3 ± 7.2	40.8 ± 7.4	40.8 ± 7.2	0.649
Minimum BIS (0–100)	32.1 ± 13.6	36.3 ± 6.8	36.6 ± 6.9	36.7 ± 6.9	0.633
POD yes/no (%)*	18.7/81.3	12.9/87.1	16.2/83.8	25.4/74.6	0.000
Days on the ward*	13.8 ± 11.8	13 ± 13.3	13.0 ± 10.0	15.2 ± 12.0	0.003
Days on ICU	1.5 ± 7.3	1.3 ± 7.1	1.1 ± 6.0	2.0 ± 8.6	0.527
In-hospital mortality (%)	2.2	0.3	2.2	3.6	0.001

POD and In-hospital mortality were compared by Chi-Square test. Continuious data were compared by Kruska Wallis test. *indicates $p < 0.05$.

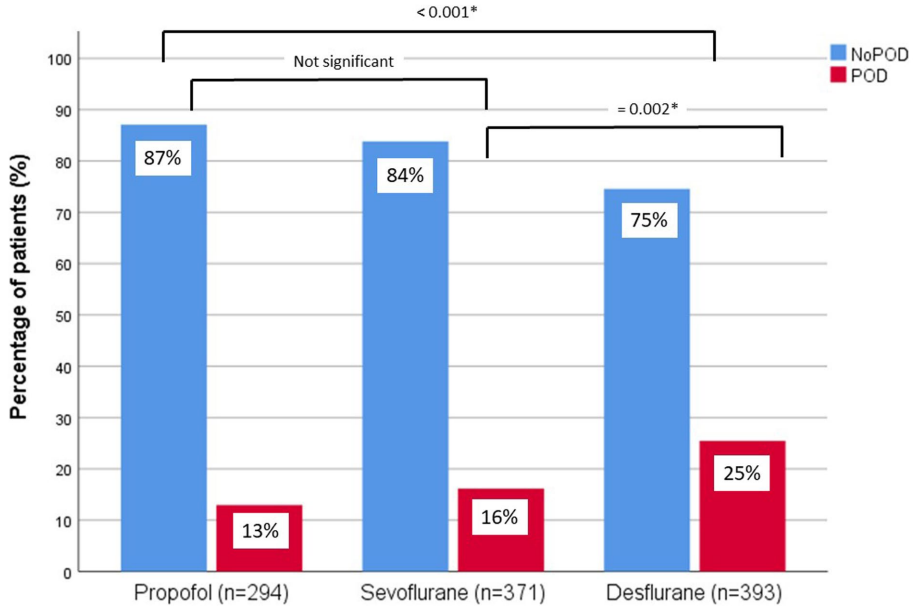

FIGURE 1
Incidence of POD and NoPOD for each anesthetic agent (propofol, sevoflurane, desflurane) in percentage of patients (%). Differences were calculated by Chi-Square test.

TABLE 3 Binominal logistic regression analyzing the impact on postoperative delirium (POD), including the anesthetic agent given (propofol vs. sevoflurane and propofol vs. desflurane), burst suppression duration (min), age (years), ASA status (I, II, III, IV), MMSE score (25–30), surgery duration (min), and surgery specialty (general surgery, orthopedics, urology, gynecology, other).

	Exp (B)	95% Confidence interval	Value of *p*
Sevoflurane vs. propofol	1.316	0.768–2.258	0.318
Desflurane vs. propofol*	1.766	1.049–2.974	0.032
Burst suppression duration (min)*	1.011	1.000–1.022	0.046
Age (years)*	1.084	1.053–1.115	0.000
Pre-operative ASA score*	1.574	1.146–2.163	0.005
Pre-operative MMSE score*	0.830	0.738–0.932	0.002
Surgery duration (min)*	1.000	1.000–1.000	0.000
Surgery specialty	0.852	0.711–1.022	0.085

*indicates a significant impact.

increased by 1.1% (OR 1.011, CI 95% 1.000–1.022, $p = 0.046$) (Table 3). Importantly, in our binominal logistic regression analysis, we found that patients had a 1.8-fold risk to develop POD after desflurane anesthesia, compared to propofol anesthesia (OR 1.766, CI 95% 1.049–2.974, $p = 0.032$), but there was no difference between propofol and sevoflurane anesthesia.

However, the risk to develop POD related to duration of burst suppression differed significantly depending to the anesthetic agent used. POD patients receiving propofol anesthesia had significantly longer burst suppression activity as compared to sevoflurane or desflurane anesthesia (Burst suppression duration of POD patients: propofol: 44.1 + 25.0 min; sevoflurane: 23.9 + 15.4 min; desflurane: 23.5 + 20.0 min; $p = 0.025$; Figure 2; Supplementary material). Additionally, patients after desflurane anesthesia stayed longer in hospital and had a higher in-hospital mortality (Table 2; Supplementary material).

Discussion

We found a significantly increased risk to develop POD in older patients after desflurane anesthesia compared to propofol anesthesia or sevoflurane anesthesia. Interestingly this finding was independent of intraoperative burst suppression duration. Even though in general prolonged burst suppression duration was associated with a higher risk to develop POD and burst suppression duration was longest under propofol anesthesia and shortest under desflurane anesthesia, the risk to trigger POD in relation to burst suppression duration was higher under desflurane anesthesia.

Propofol seems to reduce the risk to develop POD in older patients when compared to desflurane general anesthesia, even though inducing prolonged burst suppression activity.

POD is the most frequent brain dysfunction seen after anesthesia procedures, most frequently occurring in elderly patients, where

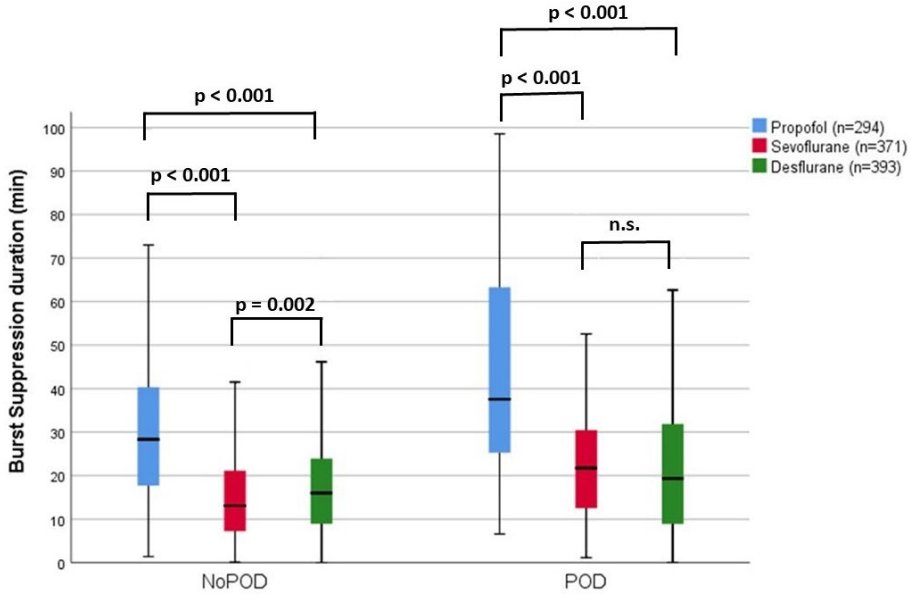

FIGURE 2
Intraoperative burst suppression duration (min) within the NoPOD and POD group within for different anesthetic agents given during anesthesia maintenance. Burst suppression duration were within the propofol group in NoPOD patients: 30.8 + 18.9 min, range 1.4 to 132.8 min and POD patients: 44.1 + 25 min, range 6.6 to 98.5 min; within the sevoflurane group in NoPOD patients: 15.8 + 11.5 min, range 0.1 to 64.1 min and POD patients: 23.9 + 15.4 min, range 1.1 to 80.7 min; within the desflurane group NoPOD patients: 19.1 + 14.2 min, range 0 to 73.6 min and POD patients: 23.3 + 20.0 min, range 0 to 133 min.

prolonged periods of too deep anesthesia are a known risk factor. It is today common sense, that EEG guidance of depth of anesthesia can reduce the risk to develop POD in elderly patients (Chan et al., 2013; Radtke et al., 2013; Whitlock et al., 2014; Punjasawadwong et al., 2018; Chan et al., 2020; Sumner et al., 2022) by avoiding too deep anesthesia (Evered et al., 2021) and prolonged periods of burst suppression (Soehle et al., 2015; Fritz et al., 2016; Xu et al., 2021). However, in recent years some randomised control trials failed to prove the advantage of EEG guidance (Zhou et al., 2018; Wildes et al., 2019; Tang et al., 2020; Wang et al., 2022). Hence, a more detailed EEG data analysis may help to improve the advantage of intraoperative EEG guidance.

Burst suppression activity in the brain presents a clear reduction of brain metabolism (Brown et al., 2010), which is discussed to be the pathophysiological reason for the higher risk to develop POD in older patients. Since it was shown that propofol has a higher ability to induce intraoperative burst suppression activity compared to sevoflurane (Purdon et al., 2015a), we would have expected a higher risk to develop POD in patients receiving propofol anesthesia. Surprisingly, we found the contrary in our study group. Patients who received propofol showed a POD incidence of 13%, after sevoflurane general anesthesia the POD rate was 16% and in patients who received a desflurane anesthesia the POD incidence was highest with 25%.

On the other hand, our data are in line with the study from Purdon et al. (2015a) showing that propofol has a higher ability to trigger burst suppression activity compared to sevoflurane. We could expand these findings by showing that desflurane also has a lower risk to trigger intraoperative burst suppression activity compared to propofol anesthesia. Importantly, we found, that the incidence of POD in relation to intraoperative burst suppression duration significantly differs between propofol and inhalative anesthetic agents. 10% of elderly patients develop POD, when presenting ~12 min of burst suppression activity under desflurane anesthesia, compared to 19 min of burst suppression activity under sevoflurane anesthesia and more than 30 min of intraoperative burst suppression under propofol anesthesia. These results indicate that a simple correlation between intraoperative burst suppression duration and the risk to develop POD in elderly patients could fail, when not including the anesthetic agent given in the analysis.

In 2011, the first study comparing the risk of developing POD between propofol and desflurane anesthesia was conducted (Royse et al., 2011). The propofol group had a slightly lower incidence of POD (7.9%) compared with the desflurane group (13.2%), but this was not significant. POD assessment was not the primary endpoint (Royse et al., 2011). In another study from 2017, 100 patients receiving either desflurane or propofol anesthesia were assessed for risk of developing POD (Tanaka et al., 2017). However, in this study, only one patient in the propofol group developed POD and no patient in the desflurane group. However, the POD surveys took place only on the first and second postoperative days, which must be considered insufficient from today's perspective (Aldecoa et al., 2017). On the other hand, one patient in the desflurane group developed a "confused state," but this was not designated as POD. Both studies were funded by Baxter. A more recent, larger randomized clinical trial (n = 684) compared propofol with volatile anesthesia (desflurane and sevoflurane) and the effects on the development of POD (Jiang et al., 2022). In the volatile anesthetics group, 18.7% developed POD, compared with 22.4% in the propofol group. On the other hand, this study did not distinguish between sevoflurane and desflurane. Since the significantly higher greenhouse effect of desflurane compared with sevoflurane has been discussed in recent years, it could be that the proportion of sevoflurane in the volatile group is higher than that of desflurane (Koch et al., 2022). Because we also found no difference between propofol and sevoflurane in inducing POD, this would be consistent with our data.

In the studies by Royse et al. (2011) and Jiang et al. (2022), the patients were also younger compared to our patients cohort (Royse:

~62 years; Jiang: ~54 years), which may also have contributed to the different results. For example, one might speculate that older patients have a lower ability to respond to the cerebral changes induced by desflurane administration than younger patients do.

The different anesthetic agents induce distinct intraoperative EEG signatures (Purdon et al., 2015b). Propofol shows a high, coherent alpha and slow-delta band power, whereas sevoflurane and desflurane presents additionally a theta coherent signature (Akeju et al., 2014; Purdon et al., 2015b). The pathophysiological basis behind this finding is not clear. But as propofol is a primary $GABA_A$ agonist, this is the reason for it's higher tendency to induce burst suppression activity. In contrast sevoflurane and desflurane also show GABAergic activation as well as a blockade of 2-pore potassium channels, HCN channels and they block the glutamate release by binding to NMDA receptors (Hemmings et al., 2005). Desflurane has a major inhibitory effect on voltage-gated potassium channels, whereas propofol and sevoflurane show only a lower inhibitory effect here. Propofol and sevoflurane have a major trigger effect on Glycine receptors, which is not seen under desflurane (Alkire et al., 2008). These distinct receptor affinities of the different anesthetic agents are most likely the underlying causes for their different EEG signatures (Purdon et al., 2015b) and their different ability to induce burst suppression activity (Purdon et al., 2015a). Since in preschool children, elevated neuronal excitability is related to the occurrence of emergence delirium (Martin et al., 2014; Koch et al., 2018), but not the presence of burst suppression activity (Faulk et al., 2010; Frederick et al., 2016; Koch et al., 2019), it is obvious, that there are different pathophysiological neuronal states being related to delirious symptoms. Moreover, it has been shown in molecular studies that volatile anesthetics can mediate inflammatory responses or may show neurotoxic effects (Jiang and Jiang, 2015; Yuki and Eckenhoff, 2016). Hence, one can speculate that the different receptor affinities as well as the induced neurotoxic and inflammatory effects on the cellular level of desflurane may be the underlying cause to trigger POD to a higher extent than propofol or sevoflurane do.

Limitations

Our study is a secondary analysis and the questions we raised here were not considered the primary endpoint of the study. Moreover, the sub-groups of patients receiving either propofol, sevoflurane or desflurane differed concerning sex, BMI, surgery duration and surgery specialty, which might have biased our results. Nevertheless, since we adjusted our final analysis for the known risk factors for POD (as age, ASA status, MMSE score, and surgery duration (min) and surgery specialty) we think that our results are reliable. The patients in our study were older than 65 years; hence, our results cannot be extended to younger patients. We did not include the drugs administered for induction of anesthesia in our model. Since in most cases the first 15 min of EEG data recording could not be evaluated due to artifacts, we assume that the effect of the anesthetic administered for induction of anesthesia had already worn off by the time we could start the EEG data evaluation and thus this had no influence on the results of our evaluation.

Conclusion

We show that propofol induces prolonged burst suppression activity in elderly patients as compared to desflurane or sevoflurane; however, this was not associated with an increased risk to develop POD. In contrast, desflurane was associated with a higher incidence of POD in our elderly cohort, independent from intraoperative burst suppression activity.

Our findings were unexpected but therefore might help to explain some discrepancies in studies analyzing the impact of burst suppression duration or the advantage of EEG neuromonitoring on the risk to develop POD. In the future, the impact of anesthetic agents on POD should be more respected and the recommendation to administer desflurane in older patients should be questioned.

Data availability statement

The data analyzed in this study is subject to the following licenses/restrictions: Due to the nature of this research, participants of the original study did not agree for their data to be shared publicly, so supporting data is not available. Requests to access these datasets should be directed to SK, susanne.koch@charite.de. Request to access the data analysis code should be directed to VR, v.roehr@tu-berlin.de.

Ethics statement

The studies involving human participants were reviewed and approved by Ethical commission at the Charité, Universitätsmedizin Berlin – Campus Virchow Klinikum, Augustenburger Platz 1, 13,533 Berlin. The patients/participants provided their written informed consent to participate in this study.

Author contributions

SK conceived and designed the study, analyzed the data, wrote and revised the manuscript, and supervised the overall study. BB supervised data analysis and revised the manuscript. VW analyzed the data and revised the manuscript. CS conceived and designed the study, helped to interpret the data, and revised the manuscript. FMR conceived and designed the study, performed the experiments, helped to interpret the data, and revised the manuscript. VR performed the experiments, analyzed the data, and revised the manuscript. All authors contributed to the article and approved the submitted version.

Funding

The research leading to these results was supported by Charité – Universitätsmedizin Berlin. The initial study has received funding from Aspect Medical Systems, now Medtronic. SK was funded by the Deutsche Forschungsgemeinschaft (DFG, German Research Foundation) – Project number KO 4249/3-1). VR acknowledges the financial support from the Research Training Group (RTG 2433) DAEDALUS (Differential Equation- and Data-driven Models in Life Sciences and Fluid Dynamics) funded by Deutsche Forschungsgemeinschaft (DFG, German Research Foundation). We acknowledge support from the German Research Foundation and the Open Access Publication Fund of TU Berlin.

Conflict of interest

SK is an inventor on patents, sold to Medtronic. She reports a grant during the conduct of the study by the German Research Society. CS is an inventor on patents, she reports grants during the conduct of a study from European Commission, from Aridis Pharmaceutical Inc., B. Braun Melsung, Drägerwerk AG & Co. KGaA, German Research Society, German Aerospace Center, Einstein Foundation Berlin, European Society of Anesthesiology, Federal Joint committee, and Inner University grants. Grants promoting Science and Education from WHOCC, Baxter Deutschland GmbH, Cytosorbents Europe GmbH, Edwars Lifesciences Germany GmbH, Fresenius Medical Care, Grünenthal GmbH, Masimo Europe Ltd. Phizer Pharma PFE GmbH. Personal fees from Georg Thieme Verlag, Dr. F. Köhler Chemie GmbH, Sintetica GmbH, European commission, Stifterverband für die deutsche Wissenschaft e.V. /Philips, Stiftung Charite, AGUETTANT Deutschland GmbH, AbbVie Deutschland GmbH & Co. KG, Amomed Pharma GmbH, Touch Health, Copra System GmbH, Correvio GmbH, Max-Planck-Gesellschaft zur Förderung der Wissenschaft e.V., Deutsche Gesellschaft für Anästhesiologie & Intensivmedizin (DGAI), Medtronic, Philips Electronics Nederland BV, BMG and BMBF.

The remaining authors declare that the research was conducted in the absence of any commercial or financial relationships that could be construed as a potential conflict of interest.

Publisher's note

Supplementary material

The Supplementary material for this article can be found online at: https://www.frontiersin.org/articles/10.3389/fnagi.2023.1067268/full#supplementary-material

References

Akeju, O., Westover, M. B., Pavone, K. J., Sampson, A. L., Hartnack, K. E., Brown, E. N., et al. (2014). Effects of sevoflurane and propofol on frontal electroencephalogram power and coherence. *Anesthesiology* 121, 990–998. doi: 10.1097/ALN.0000000000000436

Aldecoa, C., Bettelli, G., Bilotta, F., Sanders, R. D., Audisio, R., Borozdina, A., et al. (2017). European society of anaesthesiology evidence-based and consensus-based guideline on postoperative delirium. *Eur. J. Anaesthesiol.* 34, 192–214. doi: 10.1097/EJA.0000000000000594

Alkire, M. T., Hudetz, A. G., and Tononi, G. (2008). Consciousness and anesthesia. *Science* 322, 876–880. doi: 10.1126/science.1149213

Brown, E. N., Lydic, R., and Schiff, N. D. (2010). General anesthesia, sleep, and coma. *N. Engl. J. Med.* 363, 2638–2650. doi: 10.1056/NEJMra0808281

Chan, M. T., Cheng, B. C., Lee, T. M., and Gin, T.Group CT (2013). BIS-guided anesthesia decreases postoperative delirium and cognitive decline. *J. Neurosurg. Anesthesiol.* 25, 33–42. doi: 10.1097/ANA.0b013e3182712fba

Chan, M. T. V., Hedrick, T. L., Egan, T. D., Garcia, P. S., Koch, S., Purdon, P. L., et al. (2020). American Society for Enhanced Recovery and Perioperative Quality Initiative Joint Consensus Statement on the role of Neuromonitoring in Perioperative outcomes: electroencephalography. *Anesth. Analg.* 130, 1278–1291. doi: 10.1213/ANE.0000000000004502

Evered, L. A., Chan, M. T. V., Han, R., Chu, M. H. M., Cheng, B. P., Scott, D. A., et al. (2021). Anaesthetic depth and delirium after major surgery: a randomised clinical trial. *Br. J. Anaesth.* 127, 704–712. doi: 10.1016/j.bja.2021.07.021

Faulk, D. J., Twite, M. D., Zuk, J., Pan, Z., Wallen, B., and Friesen, R. H. (2010). Hypnotic depth and the incidence of emergence agitation and negative postoperative behavioral changes. *Paediatr. Anaesth.* 20, 72–81. doi: 10.1111/j.1460-9592.2009.03191.x

Frederick, H. J., Wofford, K., de Lisle, D. G., and Schulman, S. R. (2016). A randomized controlled trial to determine the effect of depth of anesthesia on emergence agitation in children. *Anesth. Analg.* 122, 1141–1146. doi: 10.1213/ANE.0000000000001145

Fritz, B. A., Kalarickal, P. L., Maybrier, H. R., Muench, M. R., Dearth, D., Chen, Y., et al. (2016). Intraoperative electroencephalogram suppression predicts postoperative delirium. *Anesth. Analg.* 122, 234–242. doi: 10.1213/ANE.0000000000000989

Hemmings, H. C. Jr., Akabas, M. H., Goldstein, P. A., Trudell, J. R., Orser, B. A., and Harrison, N. L. (2005). Emerging molecular mechanisms of general anesthetic action. *Trends Pharmacol. Sci.* 26, 503–510. doi: 10.1016/j.tips.2005.08.006

Jiang, J., and Jiang, H. (2015). Effect of the inhaled anesthetics isoflurane, sevoflurane and desflurane on the neuropathogenesis of Alzheimer's disease (review). *Mol. Med. Rep.* 12, 3–12. doi: 10.3892/mmr.2015.3424

Jiang, J. L., Zhang, L., He, L. L., Yu, H., Li, X. F., Dai, S. H., et al., (2022). *Volatile versus Total intravenous anesthesia on postoperative delirium in adult patients undergoing cardiac valve surgery: A randomized clinical trial. Anesth Analg*

Koch, S., Rupp, L., Prager, C., Wernecke, K. D., Kramer, S., Fahlenkamp, A., et al. (2018). Emergence delirium in children is related to epileptiform discharges during anaesthesia induction: an observational study. *Eur. J. Anaesthesiol.* 35, 929–936. doi: 10.1097/EJA.0000000000000867

Koch, S., Samwer, C., Rossaint, R., Coburn, M., Pecher, S., Schuster, M., et al. (2022). Survey regarding routine use of anaesthetic techniques and knowledge of their environmental impact in Germany 2020. *Eur. J. Anaesthesiol.* 39, 282–284. doi: 10.1097/EJA.0000000000001537

Koch, S., Stegherr, A. M., Rupp, L., Kruppa, J., Prager, C., Kramer, S., et al. (2019). Emergence delirium in children is not related to intraoperative burst suppression – prospective, observational electrography study. *BMC Anesthesiol.* 19:146. doi: 10.1186/s12871-019-0819-2

Kox, W. J., and Spies, C. D. (2005). *Check-up Anästhesiologie*, Standards Anästhesie-Intensivmedizin-Schmerztherapie-Notfallmedizin. Springer Medizin Verlag Berlin, Heidelberg.

Martin, J. C., Liley, D. T., Harvey, A. S., Kuhlmann, L., Sleigh, J. W., and Davidson, A. J. (2014). Alterations in the functional connectivity of frontal lobe networks preceding emergence delirium in children. *Anesthesiology* 121, 740–752. doi: 10.1097/ALN.0000000000000376

Punjasawadwong, Y., Chau-In, W., Laopaiboon, M., Punjasawadwong, S., and Pin-On, P. (2018). Processed electroencephalogram and evoked potential techniques for amelioration of postoperative delirium and cognitive dysfunction following non-cardiac and non-neurosurgical procedures in adults. *Cochrane Database Syst. Rev.* 2018:CD011283. doi: 10.1002/14651858.CD011283.pub2

Purdon, P. L., Pavone, K. J., Akeju, O., Smith, A. C., Sampson, A. L., Lee, J., et al. (2015a). The ageing brain: age-dependent changes in the electroencephalogram during propofol and sevoflurane general anaesthesia. *Br. J. Anaesth.* 115, i46–i57. doi: 10.1093/bja/aev213

Purdon, P. L., Sampson, A., Pavone, K. J., and Brown, E. N. (2015b). Clinical electroencephalography for anesthesiologists: part I: background and basic signatures. *Anesthesiology* 123, 937–960. doi: 10.1097/ALN.0000000000000841

Radtke, F. M., Franck, M., Lendner, J., Kruger, S., Wernecke, K. D., and Spies, C. D. (2013). Monitoring depth of anaesthesia in a randomized trial decreases the rate of postoperative delirium but not postoperative cognitive dysfunction. *Br. J. Anaesth.* 110, i98–i105. doi: 10.1093/bja/aet055

Rehberg, B., Bouillon, T., Zinserling, J., and Hoeft, A. (1999). Comparative pharmacodynamic modeling of the electroencephalography-slowing effect of isoflurane, sevoflurane, and desflurane. *Anesthesiology* 91, 397–405. doi: 10.1097/00000542-199908000-00013

Royse, C. F., Andrews, D. T., Newman, S. N., Stygall, J., Williams, Z., Pang, J., et al. (2011). The influence of propofol or desflurane on postoperative cognitive dysfunction in patients undergoing coronary artery bypass surgery. *Anaesthesia* 66, 455–464. doi: 10.1111/j.1365-2044.2011.06704.x

Soehle, M., Dittmann, A., Ellerkmann, R. K., Baumgarten, G., Putensen, C., and Guenther, U. (2015). Intraoperative burst suppression is associated with postoperative delirium following cardiac surgery: a prospective, observational study. *BMC Anesthesiol.* 15:61. doi: 10.1186/s12871-015-0051-7

Sumner, M., Deng, C., Evered, L., Frampton, C., Leslie, K., Short, T., et al. (2022). Processed electroencephalography-guided general anaesthesia to reduce postoperative delirium: a systematic review and meta-analysis. *Br. J. Anaesth.* doi: 10.1016/j.bja.2022.01.006

Tanaka, P., Goodman, S., Sommer, B. R., Maloney, W., Huddleston, J., and Lemmens, H. J. (2017). The effect of desflurane versus propofol anesthesia on postoperative delirium in elderly obese patients undergoing total knee replacement: a randomized, controlled, double-blinded clinical trial. *J. Clin. Anesth.* 39, 17–22. doi: 10.1016/j.jclinane.2017.03.015

Tang, C. J., Jin, Z., Sands, L. P., Pleasants, D., Tabatabai, S., Hong, Y., et al. (2020). ADAPT-2: a randomized clinical trial to reduce intraoperative EEG suppression in older surgical patients undergoing major noncardiac surgery. *Anesth. Analg.* 131, 1228–1236. doi: 10.1213/ANE.0000000000004713

Wang, E., Wang, L., Ye, C., Luo, N., Zhang, Y., Zhong, Y., et al. (2022). Effect of electroencephalography spectral edge frequency (SEF) and patient state index (PSI)-guided Propofol-remifentanil anesthesia on delirium after laparoscopic surgery: the eMODIPOD randomized controlled trial. *J. Neurosurg. Anesthesiol.* 34, 183–192. doi: 10.1097/ANA.0000000000000823

Whitlock, E. L., Torres, B. A., Lin, N., Helsten, D. L., Nadelson, M. R., Mashour, G. A., et al. (2014). Postoperative delirium in a substudy of cardiothoracic surgical patients in the BAG-RECALL clinical trial. *Anesth. Analg.* 118, 809–817. doi: 10.1213/ANE.0000000000000028

Wildes, T. S., Mickle, A. M., Ben Abdallah, A., Maybrier, H. R., Oberhaus, J., Budelier, T. P., et al. (2019). Effect of electroencephalography-guided anesthetic administration on postoperative delirium among older adults undergoing major surgery: the ENGAGES randomized clinical trial. *JAMA* 321, 473–483. doi: 10.1001/jama.2018.22005

Xu, N., Li, L. X., Wang, T. L., Jiao, L. Q., Hua, Y., Yao, D. X., et al. (2021). Processed multiparameter electroencephalogram-guided general anesthesia management can reduce postoperative delirium following carotid endarterectomy: a randomized clinical trial. *Front. Neurol.* 12:666814. doi: 10.3389/fneur.2021.666814

Yuki, K., and Eckenhoff, R. G. (2016). Mechanisms of the immunological effects of volatile anesthetics: a review. *Anesth. Analg.* 123, 326–335. doi: 10.1213/ANE.0000000000001403

Zhou, Y., Li, Y., and Wang, K. (2018). Bispectral index monitoring during anesthesia promotes early postoperative recovery of cognitive function and reduces acute delirium in elderly patients with colon carcinoma: a prospective controlled study using the attention network test. *Med. Sci. Monit.* 24, 7785–7793. doi: 10.12659/MSM.910124

frontiers | Frontiers in Aging Neuroscience

TYPE Original Research
PUBLISHED 09 March 2023
DOI 10.3389/fnagi.2023.1084462

OPEN ACCESS

EDITED BY
Yingwei Wang,
Fudan University, China

REVIEWED BY
Ce Zhang,
Xiamen University, China
Fuzhou Hua,
Second Affiliated Hospital of Nanchang University, China
Jianhui Liu,
Tongji Hospital Affiliated to Tongji University, China

*CORRESPONDENCE
Jun Zeng
✉ 525726540@qq.com
Lihong Hou
✉ 909723907@qq.com
Jun Zhang
✉ snapzhang@aliyun.com
Yongyu Si
✉ siyongyu@vip.sina.com
Kexuan Liu
✉ liukexuan705@163.com
Mingjun Wang
✉ jfj301@vip.sina.com
Hong Li
✉ LH78553@163.com

†These authors have contributed equally to this work and share first authorship

SPECIALTY SECTION
This article was submitted to Neurocognitive Aging and Behavior, a section of the journal Frontiers in Aging Neuroscience

RECEIVED 30 October 2022
ACCEPTED 21 February 2023
PUBLISHED 09 March 2023

CITATION
Zhan J, Chen F, Wu Z, Duan Z, Deng Q, Zeng J, Hou L, Zhang J, Si Y, Liu K, Wang M and Li H (2023) Consistency of the anesthesia consciousness index versus the bispectral index during laparoscopic gastrointestinal surgery with sevoflurane anesthesia: A prospective multi-center randomized controlled clinical study.
Front. Aging Neurosci. 15:1084462.
doi: 10.3389/fnagi.2023.1084462

Consistency of the anesthesia consciousness index versus the bispectral index during laparoscopic gastrointestinal surgery with sevoflurane anesthesia: A prospective multi-center randomized controlled clinical study

Jian Zhan[1,2†], Feng Chen[1†], Zhuoxi Wu[1], Zhenxin Duan[1], Qiangting Deng[3], Jun Zeng[4*], Lihong Hou[5*], Jun Zhang[6*], Yongyu Si[7*], Kexuan Liu[8*], Mingjun Wang[9*] and Hong Li[1*]

[1]Department of Anesthesiology, Second Affiliated Hospital of Army Medical University, Chongqing, China, [2]Department of Anesthesiology, Affiliated Hospital of Southwest Medical University, Luzhou, Sichuan, China, [3]Editorial Office of Journal of Army Medical University, Army Medical University, Chongqing, China, [4]Department of Anesthesiology, West China Hospital of Sichuan University, Chengdu, Sichuan, China, [5]Department of Anesthesiology, Xijing Hospital of Air Force Military Medical University, Xi'an, Shanxi, China, [6]Department of Anesthesiology, Fudan University Shanghai Cancer Center, Shanghai, China, [7]Department of Anesthesiology, Second Affiliated Hospital of Kunming Medical University, Kunming, China, [8]Department of Anesthesiology, Nanfang Hospital of Southern Medical University, Guangzhou, China, [9]Department of Anesthesiology, Chinese People's Liberation Army General Hospital, Beijing, China

Background: This study aimed to compare the consistency of anesthesia consciousness index (Ai) with that of bispectral index (BIS) in monitoring the depth of anesthesia (DOA) during sevoflurane anesthesia, to reveal the optimal cutoff values in different states of consciousness, and explore the stability of DOA monitoring during intraoperative injurious stimulation.

Methods: We enrolled 145 patients (97 men and 48 women) from 10 medical centers. General anesthesia was induced using intravenous anesthetics and maintained with sevoflurane. Ai and BIS values were recorded.

Results: The mean difference between the Ai and BIS was -0.1747 (95% confidence interval, −0.6660 to 0.3166; p=0.4857). The regression equation of Ai and BIS from the Deming regression analysis was y=5.6387+0.9067x (y is BIS, x is Ai), and the slope and intercept were statistically significant. Meanwhile, the receiver operating characteristic curve analysis of anesthesia-induced unconsciousness, loss of consciousness, and recovery of consciousness revealed that the accuracy of Ai and BIS were similar. In addition, the optimal cutoff values of the different states of consciousness were not sensitive to age, and both Ai and BIS had no correlation with hemodynamics.

Conclusion: We conclude that Ai and BIS show no systematic deviation in readings with high consistency, similar accuracy, and good stability; these insights provide more data for clinical application.

KEYWORDS

depth of anesthesia, anesthesia consciousness index, bispectral index, sevoflurane, consistency

Introduction

To prevent intraoperative awareness of patients under general anesthesia, an accurate monitoring of the depth of anesthesia (DOA) is crucial, thereby maintaining an appropriate DOA, reducing the number of anesthetics and anesthesia-related complications, and accelerating postoperative recovery (Myles et al., 2004; Radtke et al., 2013; Lewis et al., 2019). Electroencephalogram (EEG) signals reflect the effects of general anesthetics on the central nervous system and accurately monitor changes in the patient's state of consciousness (Brown et al., 2010, 2011). Various anesthesia depth indices have been developed based on EEG signals. The bispectral index (BIS) is the first anesthesia depth index certified by the United States Food and Drug Administration and is thus often used as a reference standard for evaluating the accuracy of anesthesia depth monitoring (Myles et al., 2004; Powers et al., 2005; Brown et al., 2010, 2011; Radtke et al., 2013; Lewis et al., 2019). However, advanced age, the performance of response to stress diverges, neurovascular diseases, and intracranial pathology are some potential interference factors, and many anesthetic drugs produce characteristic effects on the EEG. Further research revealed important limitations of this technology (Katoh et al., 1999; Bowdle, 2006; Bennett et al., 2008; Leece et al., 2008); therefore, an effective DOA monitor is needed to guide anesthetic titration for optimal clinical care and minimal hospitalization costs.

The anesthesia consciousness index (Ai) is a new quantitative index that assesses brain waves from an awake state to the deepest state of anesthesia based on sample entropy (Liu et al., 2015). Entropy measures the randomness or irregularity of the signals. Increasing anesthesia depth correlates with decreased randomness, with the EEG signals displaying more regularity, implying a more stable and predictable system (Fahy and Chau, 2018). It has been reported that BIS cannot predict the exact moment of consciousness recovery (Johansen, 2006), whereas Ai can better reflect the altered state of consciousness (Shalbaf et al., 2012; Jiang et al., 2015). Therefore, although it has been established that the accuracy of Ai in monitoring propofol-induced depth is not significantly different from that of BIS (Fu et al., 2019), Ai may perform better than BIS in monitoring the DOA.

However, an accurate parameter for anesthesia depth monitoring under inhalational anesthetics has not been reported, and whether it is affected by intraoperative hemodynamics remains unclear. Therefore, this study aimed to evaluate the consistency and accuracy of Ai and BIS in monitoring the DOA during sevoflurane administration, to explore the stability of these indices in monitoring the DOA during intraoperative noxious stimulation, and to reveal the optimal cutoff values of different consciousness levels to provide a data reference for clinical application.

Materials and methods

Participants

This study was registered in the China Clinical Trial Registration Center (ChiCTR2000034839) and approved by the Medical Ethics Committee of the Second Affiliated Hospital of Army Medical University (2020-Research No. 062–01). Informed consents were signed by patients or their guardians. We enrolled 152 patients aged 18–75 years who underwent elective laparoscopic gastrointestinal surgery under general anesthesia (American Standards Association state I or II, body mass index 18.5–24.9 kg/m^2). No patient had a history of mental or neurological disease, sedative or analgesic drug therapy or abuse, or contraindications for or allergies to sedative or analgesic drugs; language or hearing impairment; or serious heart, lung, kidney, or liver dysfunction.

All patients were randomly assigned to the Second Affiliated Hospital of Army Medical University, West China Hospital of Sichuan University, Nanfang Hospital of Southern Medical University, Chinese People's Liberation Army General Hospital, the Second Affiliated Hospital of Kunming Medical University, Xijing Hospital of Air Force Military Medical University, Fudan University Shanghai Cancer Center, the First Hospital of Shanxi Medical University, the Fourth Hospital of Hebei Medical University, and Shandong Yantai Yuhuangding Hospital.

Experimental procedures

The side of the forehead was randomized, the EEG electrode strips for Ai (Conview YY-106, Zhejiang Puke Medical Technology Co., Ltd.) were positioned, and the BIS (VISTA™ monitoring system, Covidien LLC, One Upland Road Norwood, MA 02062, USA) electrodes were placed on the opposite side. Moreover, non-invasive blood pressure, pulse oxygen saturation, electrocardiogram, heart rate, and end-tidal carbon dioxide partial pressure were monitored. The peripheral veins of the upper extremities were opened. Oxygen was provided using a mask without premedication.

Conscious patients were instructed to remain calm with their eyes closed (but not to fall asleep) (Nieuwenhuijs et al., 2002)and to keep their facial muscles completely relaxed(Bruhn et al., 2000). Recordings were started after verifying a sustained low electromyography activity and a signal quality index above 95%. During the induction of anesthesia, patients were instructed to open their eyes, and continuous verbal communication with the anesthetists was maintained. Concurrently, the patient's state of consciousness was assessed. Loss of consciousness (LOC) was defined as the absence of a response to calling commands (i.e., no response to the "name, name, open eyes" command) (Russell, 2006). Recovery of consciousness (ROC) was defined as a

TABLE 1 Characteristics of patients at baseline.

	N (%) or $\bar{x} \pm s$
Men (%)	97(66.9%)
Women (%)	48(33.1%)
Age (years)	56.48 ± 10.38
Height (cm)	164.70 ± 7.60
Weight (kg)	61.86 ± 13.10
BMI (kg/m^2)	22.71 ± 4.11
ASA status (%)	
I	11(7.6%)
II	134(92.4%)
BIS electrode sticking position	
Left forehead (%)	72(49.7%)
Right forehead (%)	73(50.3%)
Operation time (min)	198.99 ± 89.37
Anesthesia time (min)	225.89 ± 91.01

response to the name command (i.e., a response to the "name, name, open eyes" command [eyes open]) (Russell, 2006).

Intravenous injection of propofol (1.5–2.5 mg/kg), followed by sufentanil (0.3–0.5 μg/kg) and cisatracurium (0.15–0.2 mg/kg) were administered after LOC. Anesthesia was maintained with sevoflurane to maintain the DOA at a BIS of 40–60, with further intermittent or continuous administration of sufentanil, remifentanil, and cisatracurium. No other sedatives or analgesics were administered during the surgery. Blood pressure was maintained within 20% of the baseline blood pressure (baseline blood pressure was calculated by taking the average of three non-invasive blood pressure measurements before anesthesia induction) (Bijker et al., 2007; Monk et al., 2015). The end-tidal carbon dioxide partial pressure was 35–45 mmHg and the core temperature was >36°C. Thirty minutes before the end of the surgery, sufentanil (0.1 μg/kg) was intravenously injected as the first dose of postoperative analgesia, and additional muscle relaxants were stopped. Sevoflurane was stopped at the end of the surgery. When awakening from anesthesia, the patient's state of consciousness was assessed every minute. Tracheal extubation was performed after the patient awakened from anesthesia and met the indications for extubation.

Data collection

Ai and BIS values were recorded at rest with eyes closed (baseline data) and at the start of induction, LOC, tracheal intubation, surgical skin incision, establishment of pneumoperitoneum, peritoneal irrigation and removal of the endoscope, ROC, and tracheal extubation. Postoperative follow-up was performed on the first and seventh days after the surgery. The researchers followed up the patients and evaluated the occurrence of intraoperative awareness using a modified Brice questionnaire (Mashour et al., 2013).

Statistical analysis

SPSS 26.0 and MedCalc 15.2 statistical software were used for analysis. Count data and grade data were expressed as frequencies and composition ratios. Continuous variable data are presented as the mean ± standard deviation ($\bar{x} \pm s$). Bland–Altman consistency analysis and Deming regression analysis were used to analyze the consistency of Ai and BIS. The receiver operating characteristic curve was used to analyze the accuracy and optimal cutoff values of the two indices in judging the state of consciousness. Spearman's rank correlation analysis was used to analyze the correlation between the two indices and hemodynamics for reflecting the stability. Differences were considered statistically significant at $p < 0.05$.

Bland–Altman consistency analysis of Ai and BIS was the main observation index used to determine the sample size of this study. The Bland–Altman agreement test suggested a sample size of over 100 (Fu et al., 2019). An α of 0.05 and a power ($1-\beta$) of 0.9 was set for this study. Based on pre-experimental data, the mean of the difference between Ai and BIS was-2.93, and the standard deviation of the difference was 9.28. The difference in various anesthesia depth index values is considered statistically significant if the difference is greater than or equal to 10 (Aho et al., 2015). Based on the Bland–Altman consistency sample size calculation formula, the requisite sample size was 121 cases. Setting a dropout rate of 20%, the total sample size was set at 152 cases.

Results

Demographic

Among the 152 patients, seven were excluded, including five whose procedure was converted to laparotomy and two who were lost to follow-up. The sex, age, height, weight, body mass index, American Standards Association classification, BIS electrode sticking position, operation time, and anesthesia time of the participants are shown in Table 1. No intraoperative awareness was observed in any of the subjects.

Consistency comparison of Ai and BIS

Bland–Altman consistency analysis was used to compare the differences between Ai and BIS, and the results showed that the mean difference between the two indices was-0.1747 (95% confidence interval, −0.6660 to 0.3166), $p = 0.4857$. The ±1.96 standard deviation range of the two indices was (−29.6 to 29.3%). Overall, the difference between Ai and BIS scores was not statistically significant (Figure 1).

Deming regression analysis was used to compare the consistency between Ai and BIS. The results show that the Deming regression equation $y = 5.6387 + 0.9067x$ (y is BIS, x is Ai), the slope, and intercept are statistically significant (Figure 2). Moreover, the residuals were calculated according to the predicted values of the Deming regression equation, and the distribution of the residuals obeyed the normal distribution, with zero as the mean and 8.6 as the standard deviation (Figure 3).

Accuracy comparison in judging the anesthesia-induced unconsciousness, LOC, and ROC between Ai and BIS

Receiver operating characteristic curve analysis was used to compare the accuracy of Ai and BIS in judging anesthesia-induced

10.3389/fnagi.2023.1084462

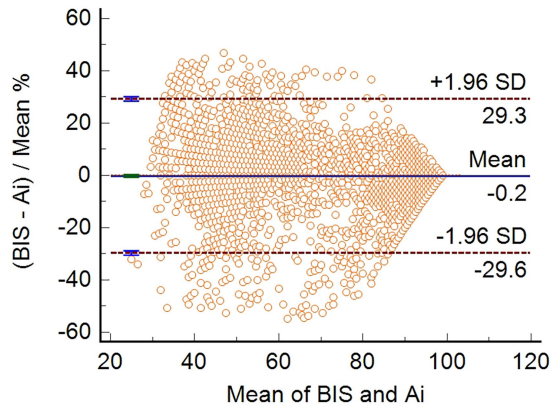

FIGURE 1
Bland–Altman consistency analysis between Ai and BIS. The bias (mean difference) between the Ai and BIS was-0.1747 (95% CI, −0.6660 to 0.3166) (n=3,600).

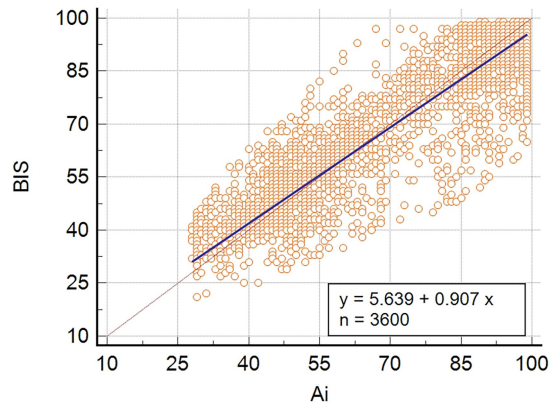

FIGURE 2
Deming regression analysis of Ai and BIS. The valve of BIS ranged from 21 to 98, and the value of Ai ranged from 29 to 99.

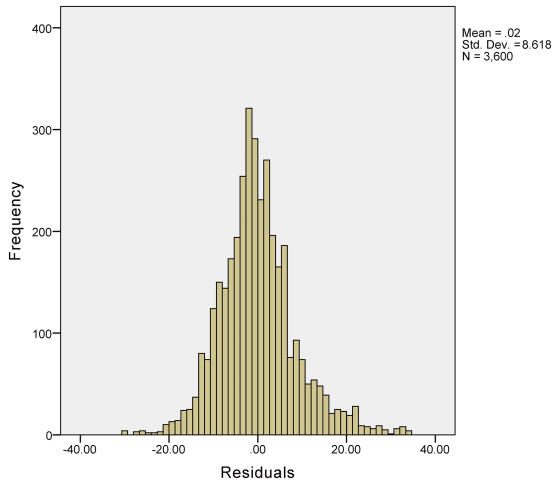

FIGURE 3
Deming regression-predicted residual values distribution.

unconsciousness (from LOC to ROC). The results showed that the area under the curve (AUC) of BIS in distinguishing anesthesia-induced unconsciousness was 0.943, and the AUC of Ai was 0.941 (p=0.4705), with no statistical difference (Table 2; Figure 4A). To compare the optimal cutoff values of consciousness states for Ai and BIS, the Youden index method of determining the cutoff value on the receiver operating characteristic curve was adopted. The value range was 0–1, and the optimal cutoff for the index monitoring was defined as the maximum value of the index. The optimal cutoff values for anesthesia-induced unconsciousness of the Ai and BIS were 71.5 and 72.5, respectively, and those for the Youden index were 0.798 and 0.814, respectively (Table 2; Figure 5).

To compare the accuracy and optimal cutoff values of Ai and BIS in distinguishing LOC, the receiver operating characteristic curve analysis showed that the AUC of BIS in discriminating the LOC was 0.953, and the AUC of Ai was 0.965 (p=0.0013), with a statistical difference (Table 2; Figure 4B). The optimal cutoff values for the LOC of the two indices were both 79.5, while those of the Youden index were 0.882 and 0.855, respectively (Table 2).

To compare the accuracy and optimal cutoff value of Ai and BIS in judging ROC, receiver operating characteristic curve analysis revealed that the AUC of BIS in discriminating the ROC was 0.936, and the AUC of Ai was 0.934 (p=0.5271), with no statistical difference (Table 2; Figure 4C). The optimal cutoff values for the ROC of the two indices were 71.5 and 70.5, respectively, and those of the Youden index were 0.799 and 0.778, respectively (Table 2).

The receiver operating characteristic curve analysis was used to compare the accuracy and optimal cutoff values of Ai and BIS in distinguishing the anesthesia-induced unconsciousness, LOC, and ROC in patients below and over 60 years of age. The results showed that Ai and BIS discriminated the different states of consciousness similarly. However, the optimal cutoff values for patients aged 60 years and above were slightly lower than that of patients below 60 years old, but the difference was not significant (Table 3).

Stability comparison of Ai and BIS during noxious stimulation

Spearman's rank correlation analysis was used to compare the correlation between Ai and BIS and the hemodynamics during noxious stimulation. This analysis showed that there was no correlation between Ai and BIS with blood pressure (systolic arterial pressure and diastolic arterial pressure) and heart rate during noxious stimulation (tracheal intubation, surgical skin incision, establishment of pneumoperitoneum, peritoneal irrigation, and endoscope removal) under anesthesia (Table 4).

Discussion

Our study evaluated the consistency, accuracy, and stability of the Ai and BIS in monitoring the DOA during sevoflurane anesthesia under prospective multi-center randomized controlled conditions. The Ai (ConView YY-105), a new anesthesia depth monitor, differs from the BIS in terms of the underlying algorithm. BIS monitors the mixed information obtained by fast Fourier transform and bispectral analysis of the power and frequency of the EEG and classifies this

TABLE 2 Comparison of the accuracy and optimal cutoff values in judging the anesthesia-induced unconsciousness, LOC, and ROC between Ai and BIS.

States of consciousness	Index	AUC	SE	95%CI	Cutoff value	Yd
Anesthesia-induced	Ai	0.941	0.00401	0.933–0.948	71.5	0.789
Unconsciousness	BIS	0.943	0.00412	0.935–0.950	72.5	0.814
LOC	Ai	0.953	0.00437	0.944–0.960	79.5	0.882
	BIS	0.965	0.00424	0.957–0.971	79.5	0.855
ROC	Ai	0.936	0.00456	0.927–0.944	70.5	0.799
	BIS	0.934	0.00479	0.925–0.942	71.5	0.778

AUC, Area under the curve; SE, Standard error; CI: Confidence interval; Cutoff, Optimal Cutoff value; Yd, Youden index.

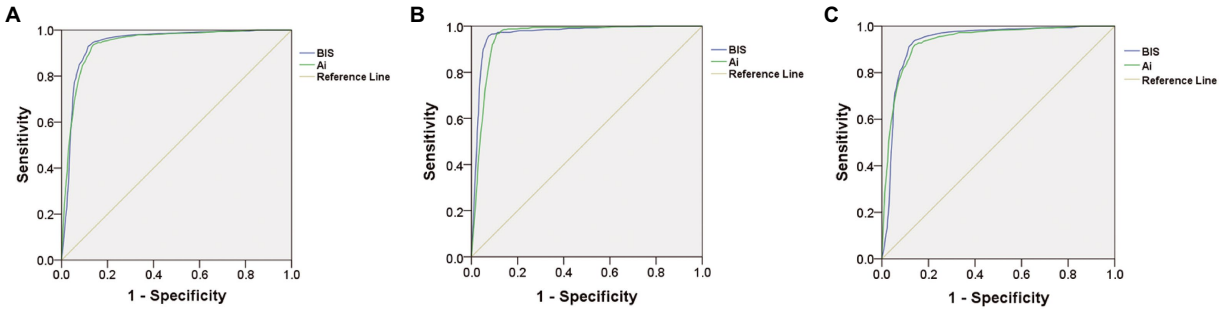

FIGURE 4
Comparison of receiver operating characteristic curve showing the accuracy in judging the anesthesia-induced unconsciousness **(A)**, LOC **(B)**, or ROC **(C)** between Ai and BIS.

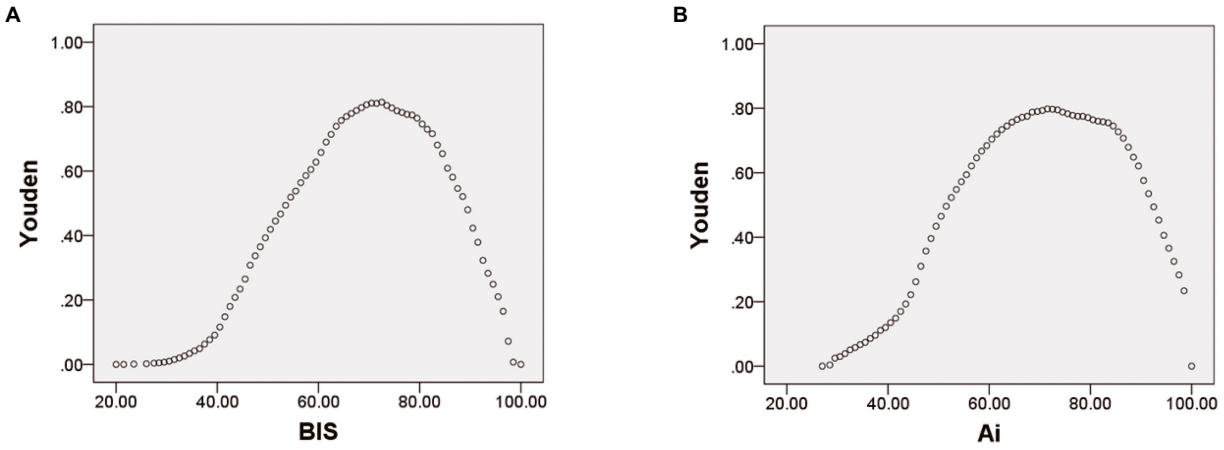

FIGURE 5
BIS with the Youden index **(A)** and Ai with the Youden index **(B)**.

information as an optimal number on a scale of 0–100, with zero indicating no EEG signal and 100 indicating awakeness. The changes in these values can reflect the functional status of the cerebral cortex (Vretzakis et al., 2005). Conversely, after anesthesia, Ai classified EEG signals using a decision tree classifier, and anesthesia awareness index was obtained through the least squares method (Liu et al., 2015). The design process of the Ai defines the appropriate anesthesia depth at 40–60, which is consistent with that of the BIS (Liu et al., 2015).

A study reported that under general anesthesia with propofol, Ai exhibits a good correlation with BIS, which is widely used in clinical practice (Fu et al., 2019). However, compared with propofol, inhalation anesthetics have different effects on EEG, including biphasic changes, which may be related to the increased activity of hormones, such as dopamine, in the body (Boisseau et al., 2002). As an ideal inhalation anesthetic, sevoflurane has a low blood gas partition coefficient, which makes the onset and recovery of anesthesia faster, allowing the DOA to be well controlled. The BIS correlates with the DOA produced by most anesthetics and is reliable for monitoring DOA with sevoflurane (Ibrahim et al., 2001). Therefore, in this study, we maintained a BIS of 40–60 as the appropriate DOA under sevoflurane while monitoring

TABLE 3 Comparison of the efficacy of Ai and BIS in monitoring the different states of consciousness of patients in different age groups.

States of consciousness	Index	Age (years)	AUC	SE	95% CI	Cutoff value
Anesthesia-induced unconsciousness	Ai	<60	0.947	0.004779	0.852, 0.942	71.5
		≥60	0.932	0.006998	0.866, 0.938	70.5
	BIS	<60	0.947	0.005216	0.879, 0.937	72.5
		≥60	0.939	0.006647	0.892, 0.919	72.5
LOC	Ai	<60	0.958	0.005202	0.889, 0.967	78.5
		≥60	0.945	0.007534	0.882, 0.977	75.5
	BIS	<60	0.969	0.005027	0.929, 0.967	79.5
		≥60	0.960	0.007158	0.917, 0.953	77.5
ROC	Ai	<60	0.943	0.005514	0.852, 0.923	71.5
		≥60	0.926	0.007846	0.863, 0.922	69.5
	BIS	<60	0.937	0.006133	0.862, 0.942	70.5
		≥60	0.930	0.007623	0.869, 0.929	69.5

AUC, Area under the curve; SE, Standard error; CI, Confidence interval; Cutoff, Optimal cutoff value.

TABLE 4 Correlation analysis of Ai and BIS with hemodynamics during noxious stimulation.

Index	Hemodynamics (during noxious stimulation)	Correlation coefficient	*p* value
BIS	SAP	−0.004	0.906
	DAP	0.010	0.754
	HR	0.011	0.736
Ai	SAP	−0.019	0.556
	DAP	0.009	0.788
	HR	0.028	0.385

SAP, Systolic arterial pressure; DAP, Diastolic arterial pressure; HR, Heart rate.

Ai synchronously in the same patient. This allowed us to observe the consistency between Ai and BIS.

Bland–Altman analysis (Bland and Altman, 1986; Bland and Altman, 2007) showed that the mean difference between Ai and BIS was not significant (−0.1747, 95% confidence interval (−0.6660 to 0.3166), $p = 0.4857$), indicating that Ai and BIS monitoring have high consistency and both can accurately reflect the DOA of patients. The results of the Bland–Altman consistency evaluation of Ai and BIS were similar to those reported by Fu et al. (2019).

Previous studies have identified Deming regression analysis as a valid method to analyze the agreement between clinical monitoring methods, and it can be used to assess whether there is a fixed or proportional bias between the two monitoring methods (Haji et al., 2015; Nasr et al., 2019). In this study, the Deming regression analysis was $y = 5.6387 + 0.9067x$ (y is BIS, s is Ai), and the slope and intercept were both statistically significant. This revealed similar DOA values for Ai and BIS monitoring, with high consistency and no systematic deviation in the readings. We further demonstrated that both Ai and BIS can objectively monitor the DOA of patients under sevoflurane.

Receiver operating characteristic curve analysis is a commonly used and effective clinical judgment method. Researchers have used it to judge the success rate of weaning in elderly high-risk heart disease patients (Bouhemad et al., 2020) and to judge acute kidney injury after cardiac surgery (Coulson et al., 2021). Thus, the receiver operating characteristic curve analysis is also applicable in evaluating the accuracy of Ai and BIS for discriminating the DOA. In addition, the Youden index was used to determine the optimal cutoff value on the receiver operating characteristic curve, and the range of values was 0–ss1. The maximum index value was the optimal cutoff value for the monitoring method.

In this study, the receiver operating characteristic curve was used to compare the accuracy and optimal cutoff values of Ai and BIS in evaluating anesthesia-induced unconsciousness. The optimal cutoff values for Ai and BIS for anesthesia-induced unconsciousness were 71.50 and 72.50, respectively. Previous studies have reported that the difference between various anesthesia depth index values is significant if the difference is greater than or equal to 10 (Aho et al., 2015). Therefore, the difference in the optimal cutoff value of anesthesia-induced unconsciousness between Ai and BIS is not clinically significant. The results of this study show that the accuracy of Ai and BIS in judging the level of consciousness is consistent, and the optimal cutoff values of anesthesia-induced unconsciousness are similar.

The receiver operating characteristic curve was used to further analyze the accuracy and optimal cutoff values of Ai and BIS in distinguishing LOC and ROC. Our results showed that the AUC of BIS for distinguishing LOC was 0.953, and the AUC of Ai was 0.965 ($p < 0.05$), suggesting that the accuracy of BIS was slightly higher than that of Ai in judging the LOC in adults, although the difference in AUC was 0.012, which is very small. Statistically, when the sample size is large enough, a small difference may show a significant statistical difference, but the clinical significance of this difference will be small; therefore, it can be considered that the accuracies of Ai and BIS in distinguishing LOC are similar. However, there was no statistically significant difference in the AUC between Ai and BIS, and the accuracies were the same. In this study, Ai and BIS had the same optimal cutoff value for LOC (79.5), whereas the optimal cutoff value for ROC in Ai (71.5) was different from that of BIS (70.5), but the difference was not clinically significant.

A study reported that when propofol induced unconsciousness, the mean values of Ai and BIS were 60.76 and 62.18, respectively, at LOC and 73.9 and 75.66, respectively, at ROC (Bouhemad et al.,

2020). Compared with the results of this study, the mean value of LOC during anesthesia induction with Ai and BIS was lower than our optimal cutoff value, which may be related to the inconsistent interval of consciousness judgment during anesthesia induction. In this study, during induction, patients were instructed to open their eyes, and verbal communication with the patient continued while the anesthetists assessed their state of consciousness.In previous studies, the time interval for assessing the level of consciousness during anesthesia induction was 30 s (Bouhemad et al., 2020). A possible reason is that it takes a certain amount of time to obtain an Ai or BIS through the acquisition of EEG signals and proprietary algorithms, resulting in a significant time delay for Ai or BIS to display visible values (Li and Li, 2014).

It was reported that under the same concentration of sevoflurane, the decreased magnitude of BIS of patients in the elderly group (age > 60 years) is greater than that in the young group (age 20–40 years), which may be related to the decline in nervous system function and increase in sensitivity to anesthetic drugs in elderly patients (Katoh et al., 1993). Receiver operating characteristic curve analysis was used to identify any differences in the accuracy and optimal cutoff values of Ai and BIS for different age groups. We found that Ai and BIS had similar accuracies and optimal critical values in discriminating anesthesia-induced unconsciousness, LOC, and ROC in young and middle-aged or elderly patients, and there was no statistical difference. Therefore, the results of this study show that the accuracy and optimal cutoff values of the two indices for distinguishing anesthesia-induced unconsciousness, LOC, and ROC are insensitive to age.

Many studies have investigated the effect of Ai in monitoring the DOA in patients under non-noxious stimulation (Liu et al., 2015; Fu et al., 2019). However, the influence of hemodynamic fluctuations on Ai and BIS during intraoperative noxious stimulation remains unclear. In this study, surgeries, such as tracheal intubation, surgical skin incision, establishment of pneumoperitoneum, peritoneal irrigation, and endoscope removal under anesthesia, were considered strong external noxious stimuli (Chen et al., 2010). We aimed to evaluate the stability of DOA monitoring by comparing the correlation between Ai and BIS with hemodynamics during noxious stimulation. The results revealed that Ai and BIS were not correlated with blood pressure and heart rate during noxious stimulation, indicating that the stability of Ai monitoring of anesthesia depth was similar to that of BIS and was not affected by hemodynamic fluctuations.

Our study has several limitations. First, the anti-jamming capabilities of Ai and BIS were not evaluated. The duration of intraoperative interference, such as electrosurgical interference, is relatively short, and real-time observation and recording are required for comparison. However, we mainly compared the changes in the level of consciousness of Ai and BIS during anesthesia, especially during anesthesia induction and awakening. No obvious abnormal interference occurred because of the short observation time. Furthermore, relevant interference times and events were not recorded. Previous studies have reported that opioid analgesics have no effect on BIS (Lysakowski et al., 2001). Therefore, this study did not consider the effect of opioid analgesics on the DOA index. Moreover, muscle relaxants reportedly have no direct effect on EEG signals, but can suppress electrical activity in the frontal muscles, which may interfere with the accuracy of the DOA index. To avoid the possible influence of muscle relaxants on the DOA index, cisatracurium was administered only after LOC was assessed during anesthesia induction, and additional muscle relaxants were stopped 30 min before the end of the surgery to minimize the effect of muscle relaxants on anesthesia. Minimize the effect of muscle relaxants on EEG signal acquisition and analysis. In this study, the effect of noxious stimulation intensity on the anesthesia depth index was evaluated only by monitoring changes in blood pressure and heart rate. The measurement of catecholamines in the blood of patients should be assessed to further reflect patient intraoperative stress, to provide more accurate evidence for changes in the DOA index.

In our study, Ai and BIS showed high consistency, similar accuracies, and good stability in DOA monitoring of sevoflurane anesthesia in 10 medical centers. In addition, Ai-based DOA monitoring results are insensitive to age and not affected by hemodynamic fluctuations during intraoperative noxious stimulation which provide broader prospects for clinical research.

Data availability statement

The original contributions presented in the study are included in the article/supplementary material, further inquiries can be directed to the corresponding authors.

Ethics statement

The studies involving human participants were reviewed and approved by the Medical Ethics Committee of the Second Affiliated Hospital of Army Medical University (NO. 2020-Research No. 062–01). The patients/participants provided their written informed consent to participate in this study.

Author contributions

LH, JZhan and QD: conceived and designed the experiments. FC, ZW, ZD, JZeng, LH, JZhang, YS, KL, and MW: performed the experiments. JZhan, ZD, FC and ZW: collected data. QD, JZhan, and FC: analyzed data. HL, JZhan, FC, QD and ZW: wrote the paper. All authors contributed to the article and approved the submitted version.

Funding

This study is supported by the National Key R&D Program of China (2018YFC0117200) and the Clinical Research Project of Army Medical University (CX2019LC114).

Acknowledgments

We thank 10 medical centers who participated in the clinical data collection during the study.

Conflict of interest

The authors declare that the research was conducted in the absence of any commercial or financial relationships that could be construed as a potential conflict of interest.

The handling editor YW declared a shared parent affiliation with the author JZ at the time of review.

Publisher's note

References

Aho, A. J., Kamata, K., Jäntti, V., Kulkas, A., Hagihira, S., Huhtala, H., et al. (2015). Comparison of bispectral index and entropy values with electroencephalogram during surgical anaesthesia with sevoflurane. *Br. J. Anaesth.* 115, 258–266. doi: 10.1093/bja/aev206

Bennett, R. C., Fancy, S. P., Walsh, C. M., Brown, A. J., and Taylor, P. M. (2008). Comparison of sevoflurane and isoflurane in dogs anaesthetised for clinical surgical or diagnostic procedures. *J. Small Anim. Pract.* 49, 392–397. doi: 10.1111/j.1748-5827.2008.00586.x

Bijker, J. B., van Klei, W. A., Kappen, T. H., van Wolfswinkel, L., Moons, K. G., and Kalkman, C. J. (2007). Incidence of intraoperative hypotension as a function of the chosen definition: literature definitions applied to a retrospective cohort using automated data collection. *Anesthesiology* 107, 213–220. doi: 10.1097/01.anes.0000270724.40897.8e

Bland, J. M., and Altman, D. G. (1986). Statistical methods for assessing agreement between two methods of clinical measurement. *Lancet* 327, 307–310. doi: 10.1016/S0140-6736(86)90837-8

Bland, J. M., and Altman, D. G. (2007). Agreement between methods of measurement with multiple observations per individual. *J. Biopharm. Stat.* 17, 571–582. doi: 10.1080/10543400701329422

Boisseau, N., Madany, M., Staccini, P., Armando, G., Martin, F., Grimaud, D., et al. (2002). Comparison of the effects of sevoflurane and propofol on cortical somatosensory evoked potentials. *Br. J. Anaesth.* 88, 785–789. doi: 10.1093/bja/88.6.785

Bouhemad, B., Mojoli, F., Nowobilski, N., Hussain, A., Rouquette, I., Guinot, P. G., et al. (2020). Use of combined cardiac and lung ultrasound to predict weaning failure in elderly, high-risk cardiac patients: a pilot study. *Intensive Care Med.* 46, 475–484. doi: 10.1007/s00134-019-05902-9

Bowdle, T. A. (2006). Depth of anesthesia monitoring. *Anesthesiol. Clin.* 24, 793–822. doi: 10.1016/j.atc.2006.08.006

Brown, E. N., Lydic, R., and Schiff, N. D. (2010). General anesthesia, sleep, and coma. *N. Engl. J. Med.* 363, 2638–2650. doi: 10.1056/NEJMra0808281

Brown, E. N., Purdon, P. L., and Van Dort, C. J. (2011). General anesthesia and altered states of arousal: a systems neuroscience analysis. *Annu. Rev. Neurosci.* 34, 601–628. doi: 10.1146/annurev-neuro-060909-153200

Bruhn, J., Bouillon, T. W., and Shafer, S. L. (2000). Electromyographic activity falsely elevates the bispectral index. *Anesthesiology* 92, 1485–1487. doi: 10.1097/00000542-200005000-00042

Chen, X., Thee, C., Gruenewald, M., Wnent, J., Illies, C., Hoecker, J., et al. (2010). Comparison of surgical stress index-guided analgesia with standard clinical practice during routine general anesthesia: a pilot study. *Anesthesiology* 112, 1175–1183. doi: 10.1097/ALN.0b013e3181d3d641

Coulson, T., Bailey, M., Pilcher, D., Reid, C. M., Seevanayagam, S., Williams-Spence, J., et al. (2021). Predicting acute kidney injury after cardiac surgery using a simpler model. *J. Cardiothorac. Vasc. Anesth.* 35, 866–873. doi: 10.1053/j.jvca.2020.06.072

Fahy, B. G., and Chau, D. F. (2018). The technology of processed electroencephalogram monitoring devices for assessment of depth of anesthesia. *Anesth. Analg.* 126, 111–117. doi: 10.1213/ANE.0000000000002331

Fu, Y., Xu, T., Xie, K., Wei, W., Gao, P., Nie, H., et al. (2019). Comparative evaluation of a new depth of anesthesia index in conview® system and the bispectral index during total intravenous anesthesia: a multicenter clinical trial. *Biomed. Res. Int.* 2019, 1–7. doi: 10.1155/2019/1014825

Haji, K., Royse, A., Tharmaraj, D., Haji, D., Botha, J., and Royse, C. (2015). Diaphragmatic regional displacement assessed by ultrasound and correlated to subphrenic organ movement in the critically ill patients--an observational study. *J. Crit. Care* 30, 437–439. doi: 10.1016/j.jcrc.2014.10.028

Ibrahim, A. E., Taraday, J. K., and Kharasch, E. D. (2001). Bispectral index monitoring during sedation with sevoflurane, midazolam, and propofol. *Anesthesiology* 95, 1151–1159. doi: 10.1097/00000542-200111000-00019

Jiang, G. J., Fan, S. Z., Abbod, M. F., Huang, H. H., Lan, J. Y., Tsai, F. F., et al. (2015). Sample entropy analysis of eeg signals via artificial neural networks to model patients' consciousness level based on anesthesiologists experience. *Biomed. Res. Int.* 2015:343478, 1–8. doi: 10.1155/2015/343478

Johansen, J. W. (2006). Update on bispectral index monitoring. *Best Pract. Res. Clin. Anaesthesiol.* 20, 81–99. doi: 10.1016/j.bpa.2005.08.004

Katoh, T., Kobayashi, S., Suzuki, A., Iwamoto, T., Bito, H., and Ikeda, K. (1999). The effect of fentanyl on sevoflurane requirements for somatic and sympathetic responses to surgical incision. *Anesthesiology* 90, 398–405. doi: 10.1097/00000542-199902000-00012

Katoh, T., Suguro, Y., Ikeda, T., Kazama, T., and Ikeda, K. (1993). Influence of age on awakening concentrations of sevoflurane and isoflurane. *Anesth. Analg.* 76, 348–352.

Leece, E. A., Corletto, F., and Brearley, J. C. (2008). A comparison of recovery times and characteristics with sevoflurane and isoflurane anaesthesia in horses undergoing magnetic resonance imaging. *Vet. Anaesth. Analg.* 35, 383–391. doi: 10.1111/j.1467-2995.2008.00399.x

Lewis, S. R., Pritchard, M. W., Fawcett, L. J., and Punjasawadwong, Y. (2019). Bispectral index for improving intraoperative awareness and early postoperative recovery in adults. *Cochrane Database Syst. Rev.* 9:D3843. doi: 10.1002/14651858.CD003843.pub4

Li, T. N., and Li, Y. (2014). Depth of anaesthesia monitors and the latest algorithms. *Asian Pac J Trop Med* 7, 429–437. doi: 10.1016/S1995-7645(14)60070-5

Liu, J., Zhou, Y., Chen, S., Xu, T., Chen, X., and Xie, F. (2015). Study on the evaluation index of depth of anesthesia awareness based on sample entropy and decision tree. *Sheng Wu Yi Xue Gong Cheng Xue Za Zhi* 32, 434–439.

Lysakowski, C., Dumont, L., Pellegrini, M., Clergue, F., and Tassonyi, E. (2001). Effects of fentanyl, alfentanil, remifentanil and sufentanil on loss of consciousness and bispectral index during propofol induction of anaesthesia. *Br. J. Anaesth.* 86, 523–527. doi: 10.1093/bja/86.4.523

Mashour, G. A., Kent, C., Picton, P., Ramachandran, S. K., Tremper, K. K., Turner, C. R., et al. (2013). Assessment of intraoperative awareness with explicit recall: a comparison of 2 methods. *Anesth. Analg.* 116, 889–891. doi: 10.1213/ANE.0b013e318281e9ad

Monk, T. G., Bronsert, M. R., Henderson, W. G., Mangione, M. P., Sum-Ping, S. T., Bentt, D. R., et al. (2015). Association between intraoperative hypotension and hypertension and 30-day postoperative mortality in noncardiac surgery. *Anesthesiology* 123, 307–319. doi: 10.1097/ALN.0000000000000756

Myles, P. S., Leslie, K., McNeil, J., Forbes, A., and Chan, M. T. (2004). Bispectral index monitoring to prevent awareness during anaesthesia: the b-aware randomised controlled trial. *Lancet* 363, 1757–1763. doi: 10.1016/S0140-6736(04)16300-9

Nasr, V. G., Bergersen, L. T., Lin, H. M., Benni, P. B., Bernier, R. S., Anderson, M. E., et al. (2019). Validation of a second-generation near-infrared spectroscopy monitor in children with congenital heart disease. *Anesth. Analg.* 128, 661–668. doi: 10.1213/ANE.0000000000002796

Nieuwenhuijs, D., Coleman, E. L., Douglas, N. J., Drummond, G. B., and Dahan, A. (2002). Bispectral index values and spectral edge frequency at different stages of physiologic sleep. *Anesth. Analg.* 94, 125–129. doi: 10.1097/00000539-200201000-00024

Powers, K. S., Nazarian, E. B., Tapyrik, S. A., Kohli, S. M., Yin, H., van der Jagt, E. W., et al. (2005). Bispectral index as a guide for titration of propofol during procedural sedation among children. *Pediatrics* 115, 1666–1674. doi: 10.1542/peds.2004-1979

Radtke, F. M., Franck, M., Lendner, J., Krüger, S., Wernecke, K. D., and Spies, C. D. (2013). Monitoring depth of anaesthesia in a randomized trial decreases the rate of postoperative delirium but not postoperative cognitive dysfunction. *Br. J. Anaesth.* 110, i98–i105. doi: 10.1093/bja/aet055

Russell, I. F. (2006). The narcotrend 'depth of anaesthesia' monitor cannot reliably detect consciousness during general anaesthesia: an investigation using the isolated forearm technique. *Br. J. Anaesth.* 96, 346–352. doi: 10.1093/bja/ael017

Shalbaf, R., Behnam, H., Sleigh, J., and Voss, L. (2012). Measuring the effects of sevoflurane on electroencephalogram using sample entropy. *Acta Anaesthesiol. Scand.* 56, 880–889. doi: 10.1111/j.1399-6576.2012.02676.x

Vretzakis, G., Ferdi, E., Argiriadou, H., Papaziogas, B., Mikroulis, D., Lazarides, M., et al. (2005). Influence of bispectral index monitoring on decision making during cardiac anesthesia. *J. Clin. Anesth.* 17, 509–516. doi: 10.1016/j.jclinane.2004.12.018

frontiers | Frontiers in Aging Neuroscience

TYPE Original Research
PUBLISHED 16 May 2023
DOI 10.3389/fnagi.2023.1060186

OPEN ACCESS

EDITED BY
Jiaqiang Zhang,
Zhengzhou University, China

REVIEWED BY
Afzal Misrani,
Guangzhou Panyu Central Hospital, China
Aniruddha Das,
Lerner Research Institute,
Cleveland Clinic, United States
Shruthi Shanmukha,
Johns Hopkins University, United States

*CORRESPONDENCE
Matthew B. Friese
✉ mfriese@gmail.com
Gregory Crosby
✉ gcrosby@bwh.harvard.edu

†PRESENT ADDRESSES
Matthew B. Friese,
Sanofi US, Boston, MA, United States
Taranjit S. Gujral,
Division of Human Biology,
Fred Hutchinson Cancer Research Center,
Seattle, WA, United States
Arvind Palanisamy,
Department of Anesthesiology,
Washington University,
St. Louis, MO, United States
Brittany Hemmer,
Nash Family Department of Neuroscience,
Icahn School of Medicine at Mount Sinai,
New York, NY, United States
Deborah J. Culley,
Department of Anesthesiology and Critical Care, Perelman School of Medicine,
University of Pennsylvania,
Philadelphia, PA, United States

RECEIVED 02 October 2022
ACCEPTED 17 April 2023
PUBLISHED 16 May 2023

CITATION
Friese MB, Gujral TS, Palanisamy A, Hemmer B, Culley DJ and Crosby G (2023) Anesthetics inhibit phosphorylation of the ribosomal protein S6 in mouse cultured cortical cells and developing brain.
Front. Aging Neurosci. 15:1060186.
doi: 10.3389/fnagi.2023.1060186

Anesthetics inhibit phosphorylation of the ribosomal protein S6 in mouse cultured cortical cells and developing brain

Matthew B. Friese[1*†], Taranjit S. Gujral[2†], Arvind Palanisamy[1†], Brittany Hemmer[1†], Deborah J. Culley[1†] and Gregory Crosby[1*]

[1]Laboratory for Aging Neuroscience, Department of Anesthesiology, Perioperative and Pain Medicine, Harvard Medical School and Brigham and Women's Hospital, Boston, MA, United States, [2]Department of Systems Biology, Harvard Medical School, Boston, MA, United States

Introduction: The development and maintenance of neural circuits is highly sensitive to neural activity. General anesthetics have profound effects on neural activity and, as such, there is concern that these agents may alter cellular integrity and interfere with brain wiring, such as when exposure occurs during the vulnerable period of brain development. Under those conditions, exposure to anesthetics in clinical use today causes changes in synaptic strength and number, widespread apoptosis, and long-lasting cognitive impairment in a variety of animal models. Remarkably, most anesthetics produce these effects despite having differing receptor mechanisms of action. We hypothesized that anesthetic agents mediate these effects by inducing a shared signaling pathway.

Methods: We exposed cultured cortical cells to propofol, etomidate, or dexmedetomidine and assessed the protein levels of dozens of signaling molecules and post-translational modifications using reverse phase protein arrays. To probe the role of neural activity, we performed separate control experiments to alter neural activity with non-anesthetics. Having identified anesthetic-induced changes *in vitro*, we investigated expression of the target proteins in the cortex of sevoflurane anesthetized postnatal day 7 mice by Western blotting.

Results: All the anesthetic agents tested *in vitro* reduced phosphorylation of the ribosomal protein S6, an important member of the mTOR signaling pathway. We found a comparable decrease in cortical S6 phosphorylation by Western blotting in sevoflurane anesthetized neonatal mice. Using a systems approach, we determined that propofol, etomidate, dexmedetomidine, and APV/TTX all similarly modulate a signaling module that includes pS6 and other cell mediators of the mTOR-signaling pathway.

Discussion: Reduction in S6 phosphorylation and subsequent suppression of the mTOR pathway may be a common and novel signaling event that mediates the impact of general anesthetics on neural circuit development.

KEYWORDS

anesthetic neurotoxicity, mTOR, activity dependent cell signaling, developmental neurotoxicity, reverse phase protein array

1. Introduction

The development and maintenance of neural circuits is highly sensitive to neural activity. General anesthetics, as befits their ability to produce unconsciousness, have profound effects on neural activity. As such, there is concern that these agents, by disrupting neural homeostasis, may alter cellular integrity and interfere with brain wiring, such as when exposure occurs during the vulnerable period of brain development (Perouansky and Hemmings, 2009; Lei et al., 2014). Thus, data from a variety of animal models including rats, mice, *C. elegans*, guinea pigs, pigs, sheep, and non-human primates indicate that anesthetic exposure during early neurodevelopment is associated with widespread apoptosis, changes in dendritic spine density, synaptic strength, and number, and long-lasting cognitive impairment (Rizzi et al., 2008; Liang et al., 2010; Gentry et al., 2013; Olutoye et al., 2015; Whitaker et al., 2016; Coleman et al., 2017; Walters and Paule, 2017). The implications of these data for use of anesthetics in children is a matter of debate (Sun et al., 2016; McCann et al., 2019) but concerns remain that long or multiple general anesthetics may have deleterious long-term consequences (Davidson and Sun, 2018).

One of the most striking and consistent observations of studies thus far is that the deleterious effects of anesthesia on the developing brain do not appear to be limited to specific agents or agents of a particular class. Most general anesthetics work, at least in part, through γ-Aminobutyric acid A ($GABA_A$) receptor agonism or NMDA receptor antagonism but agents that act on either or neither of these systems induce neurodevelopmental effects. For instance, agents with strong $GABA_A$ receptor agonist properties such as isoflurane, sevoflurane, desflurane, propofol, etomidate, and midazolam cause neuroapoptosis and/or alterations in synapse number, morphology or strength in animals, but so too does ketamine, an agent with only minor effects on $GABA_A$ receptors that acts mainly by antagonizing NMDA receptor-mediated neural excitation (Young et al., 2005; Slikker et al., 2007; Brambrink et al., 2010, 2012; Liang et al., 2010; Kodama et al., 2011; Creeley et al., 2013; Zheng et al., 2013; Coleman et al., 2017). While controversial, dexmedetomidine, an α2-adrenergic receptor agonist with little or no effect on either $GABA_A$ or NMDA receptors, has also been shown to cause neuroapoptosis in developing neurons (Liu et al., 2016). The fact that these neurodevelopmental effects occur across a broad range of anesthetic/sedative agents with diverse receptor mechanisms of action implies they are mediated by a common, but unidentified, intracellular signaling pathway.

To test that hypothesis, we exposed cortical cells *in vitro* to anesthetics with differing mechanisms of action and quantified signaling pathway responses with a semi-hi-throughput protein quantification assay. The most consistent signaling event was a reduction in phosphorylation of the ribosomal protein S6, which we confirmed also occurs in the brain of neonatal mice anesthetized with sevoflurane. pS6 is a well-known member of the mTOR pathway, and mTOR signaling plays many important roles in brain development and neural homeostasis. Therefore, suppression of this pathway is a potential mechanism for the adverse effects of anesthetics on the developing brain.

2. Materials and methods

2.1. Mice and anesthesia

The Harvard/BWH Institutional Animal Care and Use Committee approved the protocol and all experiments were conducted according to regulations set forth by the Harvard Medical School and Brigham and Women's Hospital Standing Committee on Animals.

For *in vitro* experiments, E16 timed pregnant female C57BL/6 mice were purchased from Charles River Laboratory (Wilmington, MA, United States), and cortical cells were isolated as described by others (Kim et al., 2010). Briefly, we grossly dissected the cortex and incubated it for 4 min at 37°C in a solution of 1x Hanks Balanced Salt Solution (HBSS) supplemented with papain (Worthington, NJ, United States) and cysteine (0.3 mg/mL). Protease digestion with papain was terminated with 2x washes in 1x HBSS supplemented with trypsin inhibitor (Sigma, MO, United States) and the cells were then mechanically triturated using a sterile pipette. The cells were counted with a Countess Cell Counter (Invitrogen, CA, United States) and diluted to 1×10^6 cells/mL. 5×10^5 cells were plated in each well of a 24-well culture dish pre-coated with poly-ornithine (Sigma; 30 μg/mL). The cortical cell cultures were maintained in Neurobasal media (ThermoFisher) supplemented with B27 (1:50; ThermoFisher), GlutaMax (1:100; ThermoFisher) and penicillin–streptomycin (1:100; ThermoFisher) and fed with fresh media on the fourth and sixth days *in vitro*.

For *in vivo* experiments, timed pregnant female C57BL/6 mice were purchased from Charles River Laboratory (Wilmington, MA) and housed in individual cages until delivery. A total of 12 neonatal mice (both sexes) remained with their mother until postnatal day 7 (P7) at which time 6 randomly assigned neonatal mice underwent general anesthesia in three independent experiments, with 2 animals undergoing anesthesia and 2 control animals per experiment. The anesthesia exposure consisted of 2.0% sevoflurane in 30% oxygen (2 L/min) for 6 h, mirroring clinically relevant conditions and comparable to other preclinical rodent experiments where developmental neurotoxicity was observed (Zheng et al., 2013). The mice were kept at 37–38°C by placing the anesthetizing chamber in a warm water bath, and skin temperature and sevoflurane concentration were measured at 5-min increments. The remaining six mice served as controls and were treated identically except that they received only 30% oxygen for 6 h. Animals were sacrificed by decapitation at the end of the experiment, with control mice anesthetized briefly prior to sacrifice. We then grossly dissected the cortex and homogenized it at room temperature in a solution containing 1 mL of RPPA buffer [2% sodium dodecyl sulfate (SDS), 50 mM Tris–HCl, 5% glycerol, 5 mM ethylenediaminetetraacetic acid (EDTA), 1 mM sodium fluoride, 10 mM β-glycerol phosphate, 1 mM phenylmethylsulfonyl fluoride (PMSF), 1 mM sodium orthovanadate (Na_3VO_4), and 1 mM dithiothreitol (DTT)] and supplemented with protease and phosphatase inhibitor cocktail (ThermoFisher, MA, United States). After homogenization, the samples were centrifuged and the supernatants frozen at −80°C.

2.2. Cortical cell anesthesia exposure

Starting on DIV7 and continuing through DIV8, cortical cultures were exposed to propofol, etomidate, or dexmedetomidine. The initial

dose in the screening experiments were selected to be supratherapeutic in order to maximize the chance of detecting a signal and then conducted a dose–response study to confirm the results at clinically relevant concentrations of the agents. In brief, neurobasal media was removed and replaced with conditioned media (from sister cultures) that contained one of the following: propofol (2–6 diisopropylphenol; 100 μM; Sigma), etomidate (100 μm; Tocris, MS, United States), or dexmedetomidine (1 μM; Tocris) dissolved to a final concentration of 0.1% dimethyl sulfoxide (DMSO; Sigma). As anesthetics cause profound changes in neural activity, we performed separate experiments to alter neural activity with non-anesthetics. Thus, we treated cells with bicuculline (10 μM; Tocris), a $GABA_A$ antagonist that blocks inhibitory signaling and increases neural activity, or a combination of tetrodotoxin (TTX, 1 μM; Tocris), an inhibitor of voltage-gated sodium channels, and 2-amino-5-phosphonopentanoic acid (APV, 100 μM; Tocris), an NMDA receptor antagonist, that completely block action potentials and reduce neural activity. All drugs were dissolved in 0.1% DMSO and cells treated with DMSO alone served as a vehicle control. Cells were treated with each agent for 1, 6, or 24 h, after which they were washed twice with PBS at 4°C, lysed in RPPA buffer, and stored at −80°C. Experimental results are from a total of at least four independent biological replicates (i.e., independent dissections performed on different days). For dose response experiments, cortical cells were treated for 6 h but the dose of etomidate and propofol were varied from 2 to 100 μM ($N = 4$, as indicated), and otherwise treated as above. For all agents, the final concentration of DMSO was 0.1%.

2.3. Reverse phase protein arrays

To measure the state of signaling proteins in cultured cortical cells exposed to various IV anesthetics and sedatives, whole cell lysates were subjected to reverse phase protein arrays analysis as described previously (Luckert et al., 2012). Reverse-phase protein arrays are an automated and miniaturized dot-blot assay for protein quantification (Figure 1B). As the system requires only small amounts of protein sample it can be easily scaled up, to test multiple protein samples in a high throughput manner. Briefly, cells were lysed in RPPA buffer. Protein lysates were filter cleared using AcroPrep™ Advance 96-Well Filter Plates (Pall Corporation, NY, United States) by centrifuging at 1,962 × g for 4–6 h at room temperature. Total protein amount in lysates was quantified using BCA protein assay kit (ThermoFisher) using manufacturer's instructions.

Protein microarrays were printed and processed as described in detail previously (Luckert et al., 2012). Protein lysates were printed onto 16-pad nitrocellulose-coated slides (Grace Biolabs, OR, United States) using Aushon 2470 microarrayer (Aushon BioSystems, MA, United States). A total of 6 slides were printed allowing probing with 96 previously validated antibodies (Supplementary Table S1). Slides were stored at −20°C until processing.

2.4. Array processing and probing

RPPA slides were washed with 1 M Tris–HCl (pH 9.0) for 2–4 days to remove SDS. Slides were then washed 2–3 times with phosphate-buffered saline (PBS) for 5 min each and blocked with Odyssey Blocking Buffer (OBB, Licor, NE, United States) for 1 h at RT. After blocking, arrays were incubated with primary antibodies in OBB at 4°C overnight. The following day, arrays were washed three times with PBS and incubated with IRDye labeled secondary antibodies in OBB for 1 h at room temperature. Arrays were washed again three times in PBS and once in ddH_2O and spun dry.

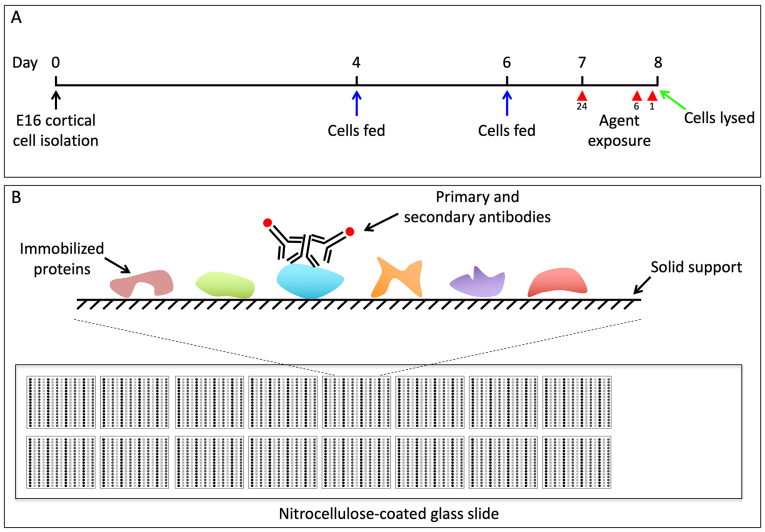

FIGURE 1
(A) Schematic of experimental design. We dissected the brains from pups of timed pregnant C57BL/6 mice at E16.5. The cortical neurons from all pups were pooled and 5×10^5 cells were plated at a density of 1×10^6 cells/mL on 24 well dishes. On DIV4 and DIV6 the media was replenished. On DIV7 we began the 24-h pharmacological exposures, and subsequently began the 6 and 1h treatments on DIV8. All cells were simultaneously lysed in RPPA buffer on DIV8. **(B)** Outline of RPPA experiments. Each glass microscope slide is embedded with 16 approximately 1cm×1cm nitrocellulose squares. A small amount of protein lysate is dot blotted, or "printed," onto each of the nitrocellulose squares in replicate, and each nitrocellulose square has the capacity for 225 separate protein lysate dots. Each nitrocellulose square is then blotted with antibodies to the protein of interest, as well as antibodies to actin, which serves as a loading control (Gujral and MacBeath, 2009).

2.5. Signal quantification and data analysis

The RPPA slides treated with IR-labeled secondary antibodies were scanned using Licor Odyssey CLX Scanner (LiCOR, NE, United States). Total signal intensity from each spot was quantified using Array-Pro analyzer software package (Media Cybernetics, MD, United States). The measurement of a specific protein from individual sample was then normalized to total β-actin (Sigma).

2.6. Western blots

Protein samples were thawed to room temperature and amount of total protein quantified using a BCA protein assay (ThermoFisher). Fifty microgram of total protein was separated by SDS-PAGE (Bio-Rad, CA, United States) and transferred to polyvinylidene difluoride membranes (Bio-Rad) using a semi-dry electrotransfer system (Bio-Rad). The chemiluminescence (ECL) HRP substrate membranes were then blocked in 3% bovine serum albumin (BSA; Sigma) in 0.1% Tween-20 in TBS (TBS-T) for 1 h at room temperature. The blot was then cut into separate pieces based upon the size distribution and the appropriate gel section blotted overnight at 4°C in 3% BSA in TBS-T with the following antibodies: beta-actin (Cell Signaling Technology, MA, United States; Cat #13E5; 1:1,000), pS6 Ser 235/236 (Cell Signaling Technology; Cat #2211; 1:1,000) and cleaved caspase 3 (CC3; Cell Signaling Technology; Cat # 5A1E; 1:200). The following day the blots were washed 3 × 5 min in TBS-T and subsequently blotted with anti-rabbit secondary (Jackson Immuno Research Laboratories, PA, United States; 1:5,000) in 3% BSA in TBS-T for 1 h at room temperature. The blots were washed 3 × 5 min in TBS-T and incubated with SuperSignal West Dura chemiluminescence substrate (ThermoFisher), imaged on ChemiDoc XRS+ imager (Bio-Rad) and analyzed using the Quantity One software package (Bio-Rad).

2.7. Data analysis and statistics

Raw data were imported and processed in R (v3.5.1)[1] or Excel (Mircosoft, WA, United States). In brief, for each pharmacological condition we calculated the $\log_2$ of the fold-change compared to controls (baseline, unstimulated cortical cells). We then calculated *p*-values using a one-sample *t*-test and subsequently adjusted for the false-discovery rate using the method of Benjamini and Hochberg (1995). Western blot quantification was performed using a 2-sample *t*-test in Excel. Correlation matrix plots were made using the corrplot package for R.

3. Results

After correcting for the false discovery rate, we identified signaling events in the *in vitro* experiments that were significantly altered by agent exposure; 6 of these involved changes in phosphorylation of the ribosomal protein S6 (pS6). Propofol and dexmedetomidine reduced pS6 at 6 h ($p = 0.002$ and 0.049, respectively; $N = 4$; Figures 2B, 3A). Likewise, etomidate ($p = 0.027$; $N = 4$) and APV/TTX (noted with two separate antibodies to distinct phosphorylation sites; $p = 0.033$ and 0.040; $N = 4$; Figures 2B, 3A), caused a significant reduction in pS6 at 24 h. In contrast, bicuculline, which increases neural activity (Arnold et al., 2005), increased both pS6 and pyruvate dehydrogenase after 1 and 24 h of treatment ($p = 0.032$ and 0.032, respectively; $N = 4$; Figures 2B, 3A). Given that anesthetics suppress pS6 similar to APV/TTX, whereas bicuculline increases it, these data suggest that anesthetics might be inhibiting pS6 levels by reducing neural activity.

1 cran.r-project.org

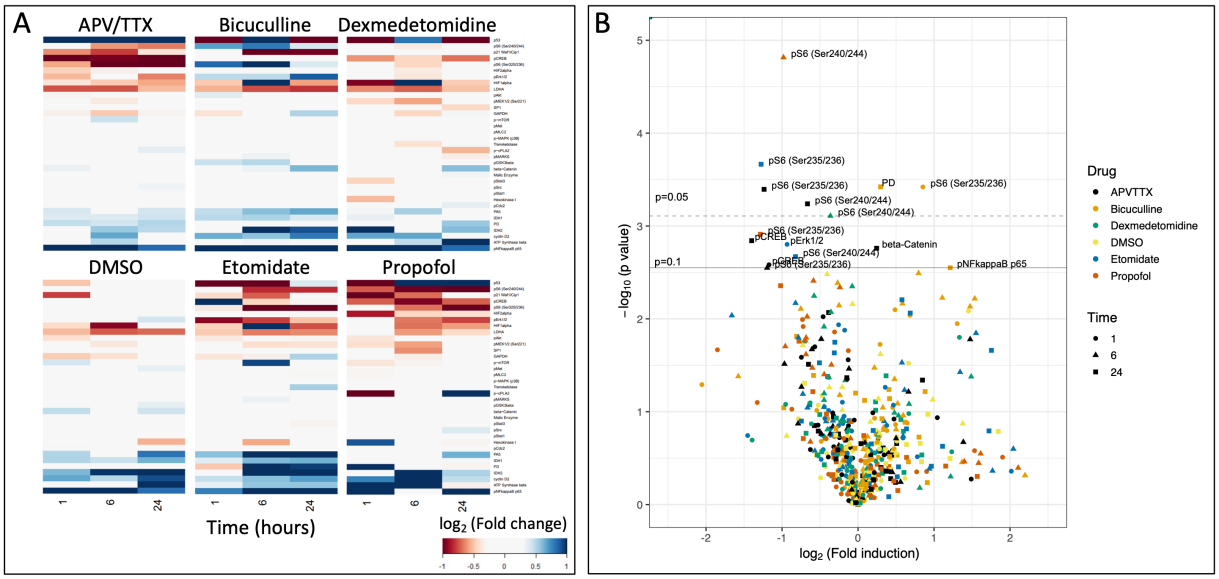

FIGURE 2
(A) Heatmap of raw data from RPPA experiment showing $\log_2$(fold change) of protein in comparison to baseline after 1, 6, and 24 h of pharmacological exposure. **(B)** Volcano plot of $-\log_{10}$(*p*-value) as a function of the $\log_2$(fold change). Solid line indicates an adjusted $p = 0.1$, and dashed line indicates and adjusted $p = 0.05$ (Benjamini and Hochberg, 1995). There are seven data points that reach the level of significance, six of which are phosphorylation of the ribosomal protein S6.

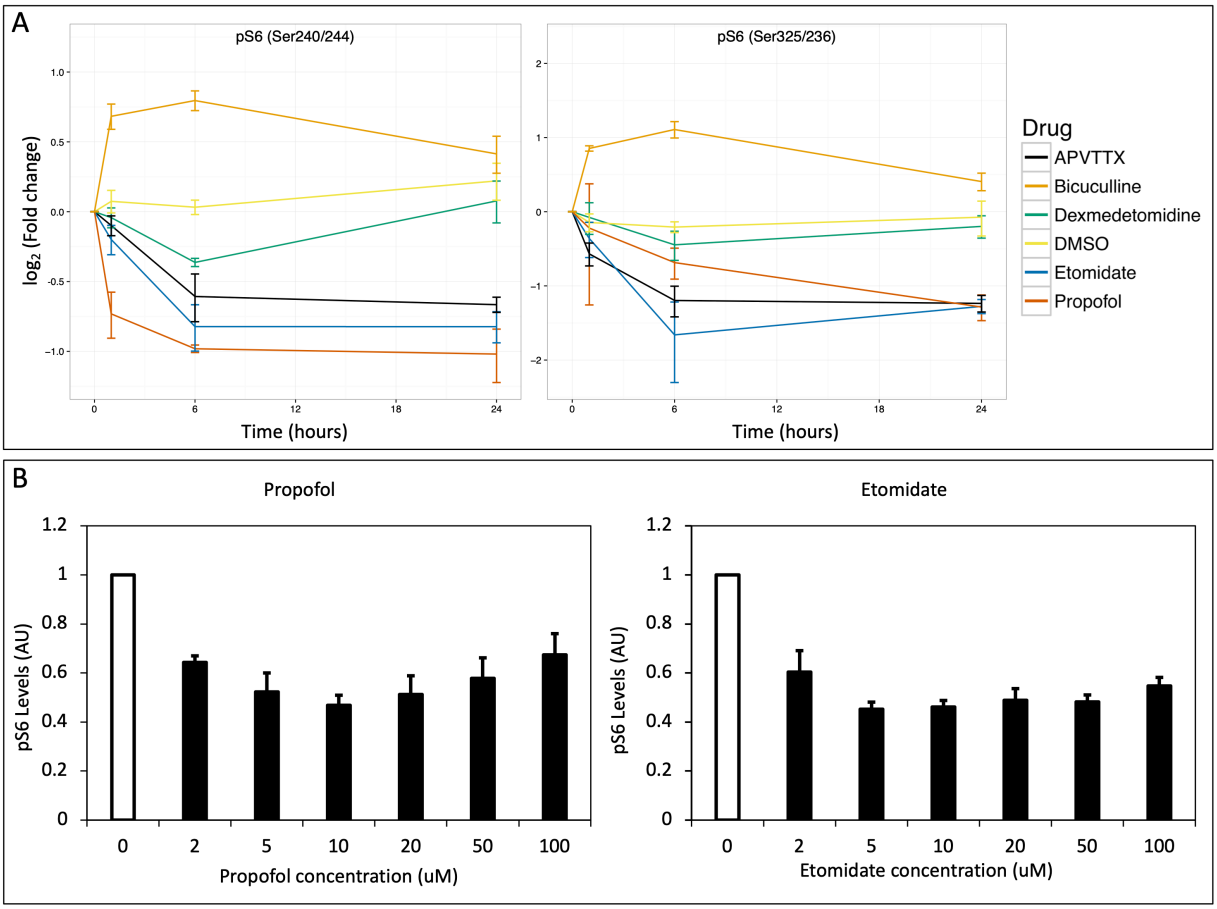

FIGURE 3
(A) Change in pS6 over time. The $\log_2$(fold change) vs. time is plotted for two antibodies against pS6 that recognize distinct phosphorylation sites (Ser 240/244 and Ser325/326 respectively) and show strikingly similar profiles. Propofol, etomidate, dexmedetomidine and APV/TTX all potently suppress phosphorylation of S6, whereas bicuculline potentiates phosphorylation of S6 and DMSO exhibits no effect on pS6. **(B)** Inhibition of pS6 as a function of concentration for propofol and etomidate. Cortical cells were stimulated for 6h while varying the concentration of propofol and etomidate from 2 to 100μM with 0.1% DMSO in neurobasal media. Both propofol and etomidate lead to maximum suppression of pS6 in the range or 2–10μM. Error bars indicate standard error of mean in both figures.

We intentionally used supra-therapeutic anesthetic concentrations in these initial experiments to demonstrate proof-of-concept. Therefore, we next tested a range of clinically relevant concentrations of propofol and etomidate, ranging from 2 to 100 μM propofol or etomidate for 6 h. Propofol produced a significant reduction in pS6 at 2 μM ($p = 0.005$; $N = 4$), 10 μM ($p = 0.006$; $N = 4$), and 20 μM ($p = 0.047$; $N = 4$), and etomidate produced a significant reduction in pS6 at 5 μM ($p = 0.002$; $N = 4$), 10 μM ($p = 0.002$; $N = 4$), 20 μM ($p = 0.01$; $N = 4$), 50 μM ($p = 0.002$; $N = 4$), and 100 μM ($p = 0.006$; $N = 4$) indicating that the decrease in pS6 occurs at brain concentrations of these agents reported to cause clinical effect (Gredell et al., 2004; Benkwitz et al., 2007).

To determine if similar changes in pS6 occur *in vivo* during anesthesia, we anesthetized postnatal day 7 (P7) mice with 2% sevoflurane for 6 h and measured pS6 in the brain by Western blot. Sevoflurane is a commonly used volatile anesthetic in children and is reported to produce neuroapoptosis and synaptic abnormalities in neonatal rodents. Compared to control animals that received only oxygen, there was a significant decrease in pS6 in the brain of the sevoflurane anesthetized mice ($p = 0.00015$, $N = 6$ animals per group; Figure 4). Furthermore, there was a significant increase in cleaved caspase 3 in the brain of the anesthetized mice ($p = 3.21 \times 10^{-6}$, $N = 6$; Figure 4). These data indicate an anesthetic-induced decrease in pS6 occurs in the brain of neonatal animals at a concentration of sevoflurane that also triggers an increase in a marker of apoptosis.

Finally, we used a systems-based approach to further evaluate the data from the RPPA experiments. For each signaling event assayed using every time point and pharmacological treatment, we computed a Pearson correlation coefficient for every other assay in a pairwise manner. These correlation coefficients were then clustered using a pairwise clustering algorithm to develop a correlation matrix (Figure 5A), where only statistically significant correlations are shown ($p < 0.05$). This correlation matrix allows us to identify potential signaling modules that may mediate anesthetic-induced signaling. A highly correlated signaling module (identified in Figure 5A and highlighted in Figure 5B) includes pS6 and other cell mediators of the mTOR-signaling pathway (Figure 5C). A correlation matrix comparing how the module highlighted in Figures 5A,B is related across different pharmacological treatments,

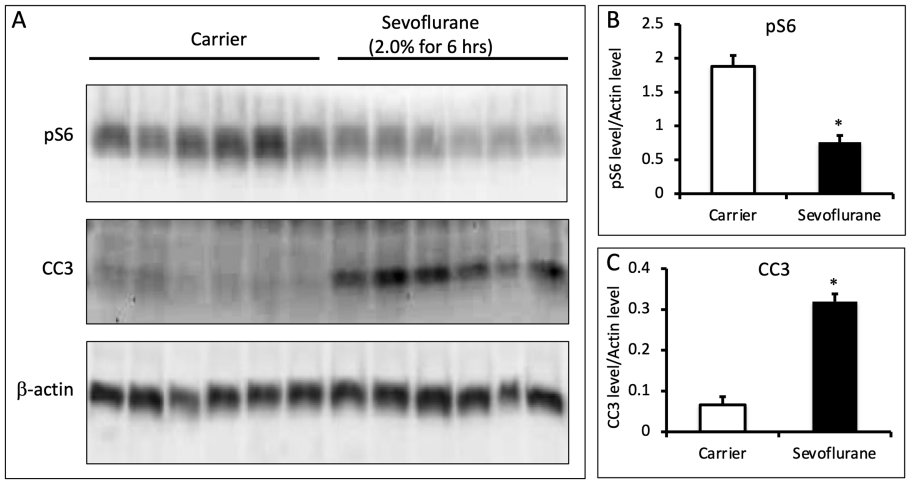

FIGURE 4
(A) Sevoflurane inhibits phosphorylation of S6 in the brains of P7 mice. P7 C57BL/6 mice were anesthetized with 2.0% sevoflurane for 6h, while control animals were treated identically and received carrier gas but no sevoflurane (n=6 per group). Whole brain lysates were analyzed via quantitative western blots and assayed for the amount of pS6, CC3, and b-actin. **(B,C)** Sevoflurane anesthesia leads to a decrease in pS6 levels and an increase in CC3 (p=0.00015 for pS6 and p=3.2e-6 for CC3; N=6 animals per group; 2 sample t-test; error bars indicate SEM; * indicates $p < 0.05$).

indicates that propofol, etomidate, dexmedetomidine, and APV/TTX all similarly modulate this pathway (Figure 5D).

4. Discussion

Using a hi-throughput protein quantification assay, we demonstrate that clinically relevant concentrations of propofol, etomidate and dexmedetomidine, agents with different mechanisms of action, all suppress S6 phosphorylation in early stage cultured cortical cells. We also extended and validated these results in an vivo model and show that 6 h of sevoflurane anesthesia at clinically relevant concentrations leads to a reduction in pS6 as well as an increase in the apoptosis marker cleaved caspase 3. Phosphorylation of S6 is a well-known component of the mTOR-signaling pathway, and a systems-based approach to analyze the RPPA results further supports our hypothesis by showing that many signaling molecules involved in the mTOR pathway function in a highly correlated signaling module. The activation of this module was correlated between propofol, etomidate, dexmedetomidine and APV/TTX, suggesting that alterations in neural activity level may be responsible for mediating changes in the mTOR pathway. Consistent with this possibility, there was a small but statistically significant increase in expression of pyruvate dehydrogenase, a component of cellular respiration, in cells exposed for 24 h to bicuculline, a drug that increases neural activity. The fact that pyruvate dehydrogenase suppression was not observed with drugs that reduce neural activity suggests a floor in its expression, driven perhaps by ongoing basal, non-activity driven cellular metabolism.

The highly conserved mTOR pathway is involved in many aspects of neural development and homeostasis, making it an intriguing potential target for mediating neurodevelopmental effects of anesthetics (Lipton and Sahin, 2014). Interestingly, the mTOR pathway is implicated in isoflurane and propofol-induced synaptic and behavioral changes, albeit via an aberrant increase in mTOR signaling (Kang et al., 2017; Xu et al., 2018). In that work, the authors exposed older animals (P18) to 4 h of 1.5% isoflurane anesthesia and found 12 days after exposure (P30) that there was an increase in pS6 staining in the dentate gyrus. This increase in pS6 staining was associated with an increase in dendritic length, a reduction in the number of dendritic spines, and later spatial learning defects. Inhibiting the isoflurane-induced activation of the mTOR pathway with rapamycin rescued both the spine loss and behavioral defects, implicating the mTOR pathway in the neurodevelopmental effects of isoflurane, a prototypical volatile anesthetic. Further studies using primary cortical neurons harvested from E18 rats, and exposed to isoflurane between 3 and 7 DIV, showed a similar increase in the number of pS6 positive cells 3+ days after exposure to isoflurane (Kang et al., 2017; Xu et al., 2018).

Our experiments appear to be at odds with the results reported above, inasmuch as we report that propofol, etomidate, and dexmedetomidine reduce pS6 in cultured cells and that sevoflurane produces a similar reduction in the developing brain. However, others have reported that sevoflurane reduces pS6 in the developing brain (Tan et al., 2015; Xu et al., 2018) and that a decrease in mTor signaling, as induced by the mTor inhibitor rapamycin, is associated with apoptosis as identified by markers such as CC3 (Bowling et al., 2018). In addition, there are two important differences between our study and the one mentioned above. First, our anesthesia exposure occurred in DIV8 cortical cells (isolated from E16.5 mice) or P7 animals whereas the prior investigators exposed mice on P18. This is potentially important because the effects of anesthesia on the brain appear to be exquisitely sensitive to developmental age. For instance, apoptosis is first detectable in rodents when anesthesia exposure occurs around birth, reaches a peak when animals are exposed at P7, and then rapidly declines such that it is almost non-existent when exposure occurs on P14 (Yon et al., 2005). Further, others have reported that propofol anesthesia will lead to a loss of dendritic spines when exposure occurs at P5-P10 but that exposure a week later leads to an increase in spines, indicating that in rodents anesthesia has

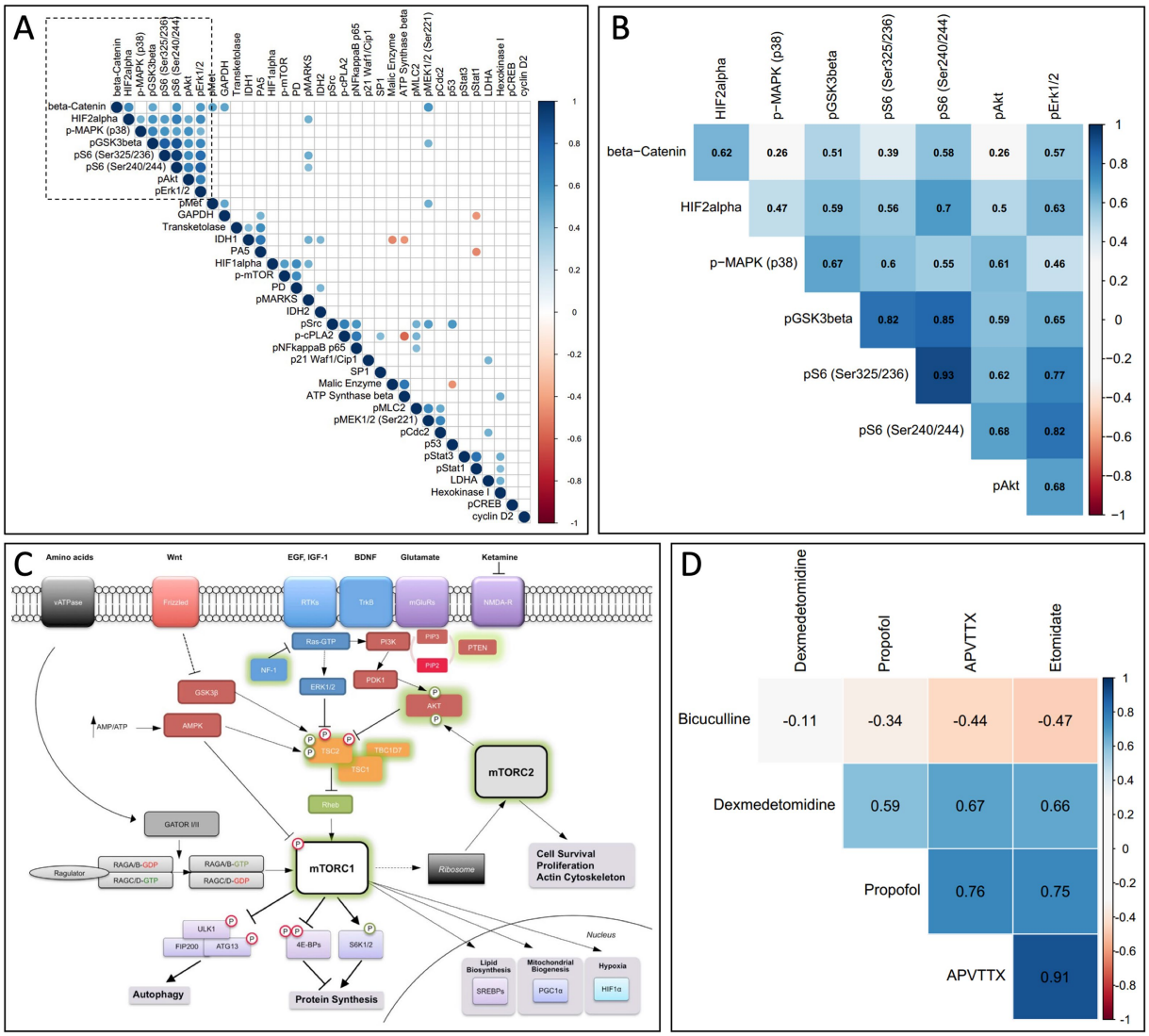

FIGURE 5
(A) Correlation matrix comparing all assays used in RPPA. For each assay on the RPPA matrix we calculated a correlation coefficient for every other assay against all pharmacological conditions and time points, and only significant correlations are shown ($p<0.05$). The data was clustered using a non-supervised clustering algorithm to identify potential signaling modules. **(B)** A higher magnification of the signaling module outlined by the dashed box in **(A)**, now superimposed with the corresponding correlation coefficient. **(C)** mTOR signaling pathway. A diagram from the mTOR signaling pathway showing that multiple members of the signaling module from **(A,B)** are involved in the mTOR pathway (from Lipton and Sahin, 2014, with permission). **(D)** Correlation matrix comparing the signaling module indicated in **(A,B)** across different pharmacological treatments. Propofol, etomidate, APV/TTX and dexmedetomidine modulate the signaling module from **(A,B)** in a correlated manner. Bicuculline activity on the signaling module indicated in **(A,B)** is anti-correlated with propofol, etomidate and APV/TTX.

opposite effects depending on developmental age (Briner et al., 2011). Taken together, these data suggest that differences in the mTOR signaling response may underlie some of the age-dependent effects of anesthetic agents on neuronal viability and dendritic spines.

Another potential reason for inhibition of pS6 in our study versus an increase in another may be differences in the post-anesthetic interval, as we assayed pS6 immediately after anesthesia whereas other investigators did so 12 days after exposure in mice, or 3+ days after exposure in rat primary cortical cultures (Kang et al., 2017; Xu et al., 2018). Phosphorylation of S6 corresponds to the activity state of neurons; thus, like other activity-regulated immediate early genes such as Fos, Npas4, and Arc, a change in neuronal action potential firing leads to a corresponding change in phosphorylation of S6 (Kim et al., 2010). Indeed, pS6 is frequently used as an indirect assay for neural activity (Kim et al., 2010; Renier et al., 2016). As such, one would expect phosphorylation of S6 to be low at the end of a prolonged anesthetic, when neural activity levels are generally reduced. Using the same logic, a decrease in pS6 following sevoflurane anesthesia suggests the agent is inhibiting neural activity in the cortex of P7 animals, whereas others have suggested that it does so by increasing excitation (Zhao et al., 2011). On the other hand, increased pS6 days or weeks later might be secondary to, or a marker of, compensatory post-anesthetic neuronal hyperexcitability. Indeed, in the offspring of mice exposed to sevoflurane on post-natal D 16/17, there was an increase in mTor phosphorylation in the brain 24 h later (Ju, 2020). Homeostatic synaptic scaling and several other

well-described mechanisms predict that perturbations in neural activity, such as the decrease that typically occurs during general anesthesia, will induce compensatory synaptic changes and a period of neuronal hyperexcitability subsequently (Turrigiano et al., 1998; Turrigiano, 2012; Hengen et al., 2016). Therefore, to the extent pS6 is an activity-regulated immediate early gene, an increase in cortical pS6 days after exposure to general anesthesia with sevoflurane may be a homeostatic response to an earlier period of anesthetic-induced neuronal depression.

Strengths of our study include use of *in vitro* and *in vivo* models, a multiplexed assay system, several anesthetic classes, and non-anesthetic *in vitro* controls. This work also has important limitations. While we identified a common cell-signaling module that is altered similarly across a wide variety of both intravenous and inhalational anesthetics, we have not directly linked this pathway to the central nervous system complications observed after early developmental exposure to these agents. As others have reported neurotoxicity in older animals with an increase in mTOR signaling, the conditions under which an acute change in pS6 is physiologic or detrimental remains to be determined. We did not investigate anesthetic-induced CC3 changes in the *in vitro* experiments because the reagent had not been validated for the RPPA platform, and thus we cannot confirm that propofol, etomidate and dexmedetomidine produced apoptosis-like changes in the *in vitro* model. However, there was an increase in CC3 in the brain of neonatal mice exposed to sevoflurane, suggesting that the pS6 changes are associated with apoptotic events. Finally, this study was largely performed using soluble agents in a tissue culture model. This limits generalizability and requires that results obtained *in vitro* for propofol, etomidate and dexmedetomidine be replicated *in vivo*. Notably, however, we confirmed the results *in vivo* with a widely used inhalational anesthetic (sevoflurane) at a clinically relevant dose.

We conducted these experiments in order to determine whether exposure of cortical cells to anesthetics of different classes alters similar signaling pathways, and thus to provide insight into how agents with different mechanisms of action may mediate similar changes within developing neurons. Here, we find that at clinically relevant concentrations, the intravenous anesthetics propofol, etomidate, and dexmedetomidine suppress pS6 levels in cultured cortical cells, and sevoflurane has a similar effect in the developing mouse brain. The fact that these effects are similar to those seen with the neural activity blockers APV/TTX and opposite those of the neural activity enhancer bicuculline suggest that pS6 is changing in response to alterations in neural activity. Because pS6 is a well-established member of the mTOR signaling pathway, our results suggest that some aspects of anesthetic actions on developing neurons are triggered by reductions in neural activity and subsequent perturbations in this important signaling pathway.

Data availability statement

The raw data supporting the conclusions of this article will be made available by the authors, without undue reservation.

Author contributions

MF, TG, DC, and GC conceived and designed the experiments. MF, TG, AP, and BH performed the experiments. MF analyzed the data and drafted the manuscript. All authors revised and approved the final manuscript.

Funding

This work was funded by the Harvard Anesthesia Training Program (GM007592), a Foundation for Anesthesia Education and Research GEMSSTAR Award, and NIA AG053280 to MF, NIA AG048522 to DC, and NIA AG051812 to GC.

Conflict of interest

The authors declare that the research was conducted in the absence of any commercial or financial relationships that could be construed as a potential conflict of interest.

Publisher's note

Supplementary material

The Supplementary material for this article can be found online at: https://www.frontiersin.org/articles/10.3389/fnagi.2023.1060186/full#supplementary-material

References

Arnold, F. J. L., Hofmann, F., Bengtson, C. P., Wittmann, M., Vanhoutte, P., and Bading, H. (2005). Microelectrode array recordings of cultured hippocampal networks reveal a simple model for transcription and protein synthesis-dependent plasticity. *J. Physiol.* 564, 3–19. doi: 10.1113/jphysiol.2004.077446

Benjamini, Y., and Hochberg, Y. (1995). Controlling the false discovery rate: a practical and powerful approach to multiple testing. *J. R. Stat. Soc. Ser. B Methodol.* 57, 289–300. doi: 10.1111/j.2517-6161.1995.tb02031.x

Benkwitz, C., Liao, M., Laster, M. J., Sonner, J. M., Eger, E. I., and Pearce, R. A. (2007). Determination of the EC50 amnesic concentration of etomidate and its diffusion profile in brain tissue: implications for *in vitro* studies. *Anesthesiology* 106, 114–123. doi: 10.1097/00000542-200701000-00020

Bowling, S., di Gregorio, A., Sancho, M., Pozzi, S., Aarts, M., Signore, M., et al. (2018). P53 and mTOR signalling determine fitness selection through cell competition during early mouse embryonic development. *Nat. Commun.* 9:1763. doi: 10.1038/s41467-018-04167-y

Brambrink, A. M., Evers, A. S., Avidan, M. S., Farber, N. B., Smith, D. J., Martin, L. D., et al. (2012). Ketamine-induced neuroapoptosis in the fetal and neonatal rhesus macaque brain. *Anesthesiology* 116, 372–384. doi: 10.1097/ALN.0b013e318242b2cd

Brambrink, A. M., Evers, A. S., Avidan, M. S., Farber, N. B., Smith, D. J., Zhang, X., et al. (2010). Isoflurane-induced neuroapoptosis in the neonatal rhesus macaque brain. *Anesthesiology* 112, 834–841. doi: 10.1097/ALN.0b013e3181d049cd

Briner, A., Nikonenko, I., de Roo, M., Dayer, A., Muller, D., and Vutskits, L. (2011). Developmental stage-dependent persistent impact of propofol anesthesia on dendritic spines in the rat medial prefrontal cortex. *Anesthesiology* 115, 282–293. doi: 10.1097/ALN.0b013e318221fbbd

Coleman, K., Robertson, N. D., Dissen, G. A., Neuringer, M. D., Martin, L. D., Cuzon Carlson, V. C., et al. (2017). Isoflurane anesthesia has long-term consequences on motor and behavioral development in infant rhesus macaques. *Anesthesiology* 126, 74–84. doi: 10.1097/ALN.0000000000001383

Creeley, C., Dikranian, K., Dissen, G., Martin, L., Olney, J., and Brambrink, A. (2013). Propofol-induced apoptosis of neurones and oligodendrocytes in fetal and neonatal rhesus macaque brain. *Br. J. Anaesth.* 110, i29–i38. doi: 10.1093/bja/aet173

Davidson, A. J., and Sun, L. S. (2018). Clinical evidence for any effect of anesthesia on the developing brain. *Anesthesiology* 128, 840–853. doi: 10.1097/ALN.0000000000001972

Gentry, K. R., Steele, L. M., Sedensky, M. M., and Morgan, P. G. (2013). Early developmental exposure to volatile anesthetics causes behavioral defects in *Caenorhabditis elegans*. *Anesth. Analg.* 116, 185–189. doi: 10.1213/ANE.0b013e31826d37c5

Gredell, J. A., Turnquist, P. A., MacIver, M. B., and Pearce, R. A. (2004). Determination of diffusion and partition coefficients of propofol in rat brain tissue: implications for studies of drug action *in vitro*. *Br. J. Anaesth.* 93, 810–817. doi: 10.1093/bja/aeh272

Gujral, T. S., and MacBeath, G. (2009). Emerging miniaturized proteomic technologies to study cell signaling in clinical samples. *Sci. Signal.* 2:pe65. doi: 10.1126/scisignal.293pe64

Hengen, K. B., Torrado Pacheco, A., McGregor, J. N., Van Hooser, S. D., and Turrigiano, G. G. (2016). Neuronal firing rate homeostasis is inhibited by sleep and promoted by wake. *Cells* 165, 180–191. doi: 10.1016/j.cell.2016.01.046

Ju, X. (2020). The mTOR inhibitor rapamycin prevents general anesthesia-induced changes in synaptic transmission and mitochondrial respiration in late postnatal mice. *Front. Cell. Neurosci.* 14:4. doi: 10.3389/fncel.2020.00004

Kang, E., Jiang, D., Ryu, Y. K., Lim, S., Kwak, M., Gray, C. D., et al. (2017). Early postnatal exposure to isoflurane causes cognitive deficits and disrupts development of newborn hippocampal neurons via activation of the mTOR pathway. *PLoS Biol.* 15:e2001246. doi: 10.1371/journal.pbio.2001246

Kim, T. K., Hemberg, M., Gray, J. M., Costa, A. M., Bear, D. M., Wu, J., et al. (2010). Widespread transcription at neuronal activity-regulated enhancers. *Nature* 465, 182–187. doi: 10.1038/nature09033

Kodama, M., Satoh, Y., Otsubo, Y., Araki, Y., Yonamine, R., Masui, K., et al. (2011). Neonatal desflurane exposure induces more robust neuroapoptosis than do isoflurane and sevoflurane and impairs working memory. *Anesthesiology* 115, 979–991. doi: 10.1097/ALN.0b013e318234228b

Lei, S. Y., Hache, M., and Loepke, A. W. (2014). Clinical research into anesthetic neurotoxicity: does anesthesia cause neurological abnormalities in humans? *J. Neurosurg. Anesthesiol.* 26, 349–357. doi: 10.1097/ANA.0000000000000117

Liang, G., Ward, C., Peng, J., Zhao, Y., Huang, B., and Wei, H. (2010). Isoflurane causes greater neurodegeneration than an equivalent exposure of sevoflurane in the developing brain of neonatal mice. *Anesthesiology* 112, 1325–1334. doi: 10.1097/ALN.0b013e3181d94da5

Lipton, J. O., and Sahin, M. (2014). The neurology of mTOR. *Neuron* 84, 275–291. doi: 10.1016/j.neuron.2014.09.034

Liu, J. R., Yuki, K., Baek, C., Han, X. H., and Soriano, S. G. (2016). Dexmedetomidine-induced Neuroapoptosis is dependent on its cumulative dose. *Anesth. Analg.* 123, 1008–1017. doi: 10.1213/ANE.0000000000001527

Luckert, K., Gujral, T. S., Chan, M., Sevecka, M., Joos, T. O., Sorger, P. K., et al. (2012). A dual array-based approach to assess the abundance and posttranslational modification state of signaling proteins. *Sci. Signal.* 5:pl1. doi: 10.1126/scisignal.2002372

McCann, M. E., de Graaff, J. C., Dorris, L., Disma, N., Withington, D., Bell, G., et al. (2019). Neurodevelopmental outcome at 5 years of age after general anaesthesia or awake-regional anaesthesia in infancy (GAS): an international, multicentre, randomised, controlled equivalence trial. *Lancet* 393, 664–677. doi: 10.1016/S0140-6736(18)32485-1

Olutoye, O. A., Lazar, D. A., Akinkuotu, A. C., Adesina, A., and Olutoye, O. O. (2015). Potential of the ovine brain as a model for anesthesia-induced neuroapoptosis. *Pediatr. Surg. Int.* 31, 865–869. doi: 10.1007/s00383-015-3751-7

Perouansky, M., and Hemmings, H. C. (2009). Neurotoxicity of general anesthetics: cause for concern? *Anesthesiology* 111, 1365–1371. doi: 10.1097/ALN.0b013e3181bf1d61

Renier, N., Adams, E. L., Kirst, C., Wu, Z., Azevedo, R., Kohl, J., et al. (2016). Mapping of brain activity by automated volume analysis of immediate early genes. *Cells* 165, 1789–1802. doi: 10.1016/j.cell.2016.05.007

Rizzi, S., Carter, L. B., Ori, C., and Jevtovic-Todorovic, V. (2008). Clinical anesthesia causes permanent damage to the fetal guinea pig brain. *Brain Pathol.* 18, 198–210. doi: 10.1111/j.1750-3639.2007.00116.x

Slikker, W., Zou, X., Hotchkiss, C. E., Divine, R. L., Sadovova, N., Twaddle, N. C., et al. (2007). Ketamine-induced neuronal cell death in the perinatal rhesus monkey. *Toxicol. Sci.* 98, 145–158. doi: 10.1093/toxsci/kfm084

Sun, L. S., Li, G., Miller, T. L. K., Salorio, C., Byrne, M. W., Bellinger, D. C., et al. (2016). Association between a single general anesthesia exposure before age 36 months and neurocognitive outcomes in later childhood. *JAMA* 315, 2312–2320. doi: 10.1001/jama.2016.6967

Tan, H., Li, J., Chen, L., Chen, X., Zhang, S., Ke, L., et al. (2015). Sevoflurane inhibits the phosphorylation of ribosomal protein S6 in neonatal rat brain. *Int. J. Clin. Exp. Med.* 8, 21830–21832.

Turrigiano, G. (2012). Homeostatic synaptic plasticity: local and global mechanisms for stabilizing neuronal function. *Cold Spring Harb. Perspect. Biol.* 4:a005736. doi: 10.1101/cshperspect.a005736

Turrigiano, G. G., Leslie, K. R., Desai, N. S., Rutherford, L. C., and Nelson, S. B. (1998). Activity-dependent scaling of quantal amplitude in neocortical neurons. *Nature* 391, 892–896. doi: 10.1038/36103

Walters, J. L., and Paule, M. G. (2017). Review of preclinical studies on pediatric general anesthesia-induced developmental neurotoxicity. *Neurotoxicol. Teratol.* 60, 2–23. doi: 10.1016/j.ntt.2016.11.005

Whitaker, E. E., Bissonnette, B., Miller, A. D., Koppert, T. L., Tobias, J. D., Pierson, C. R., et al. (2016). A novel, clinically relevant use of a piglet model to study the effects of anesthetics on the developing brain. *Clin. Transl. Med.* 5:2. doi: 10.1186/s40169-015-0079-9

Xu, J., Mathena, R. P., Xu, M., Wang, Y., Chang, C., Fang, Y., et al. (2018). Early developmental exposure to general anesthetic agents in primary neuron culture disrupts synapse formation via actions on the mTOR pathway. *Int. J. Mol. Sci.* 19:2183. doi: 10.3390/ijms19082183

Yon, J. H., Daniel-Johnson, J., Carter, L. B., and Jevtovic-Todorovic, V. (2005). Anesthesia induces neuronal cell death in the developing rat brain via the intrinsic and extrinsic apoptotic pathways. *Neuroscience* 135, 815–827. doi: 10.1016/j.neuroscience.2005.03.064

Young, C., Jevtovic-Todorovic, V., Qin, Y. Q., Tenkova, T., Wang, H., Labruyere, J., et al. (2005). Potential of ketamine and midazolam, individually or in combination, to induce apoptotic neurodegeneration in the infant mouse brain. *Br. J. Pharmacol.* 146, 189–197. doi: 10.1038/sj.bjp.0706301

Zhao, Y. L., Xiang, Q., Shi, Q. Y., Li, S. Y., Tan, L., Wang, J. T., et al. (2011). GAB aergic excitotoxicity injury of the immature hippocampal pyramidal neurons' exposure to isoflurane. *Anesth. Analg.* 113, 1152–1160. doi: 10.1213/ANE.0b013e318230b3fd

Zheng, S. Q., An, L. X., Cheng, X., and Wang, Y. J. (2013). Sevoflurane causes neuronal apoptosis and adaptability changes of neonatal rats. *Acta Anaesthesiol. Scand.* 57, 1167–1174. doi: 10.1111/aas.12163

Frontiers in
Aging Neuroscience

Explores the mechanisms of central nervous system aging and age-related neural disease

The third most-cited journal in the field of geriatrics and gerontology, with a focus on understanding the mechanistic processes associated with central nervous system aging.

Discover the latest Research Topics

See more →

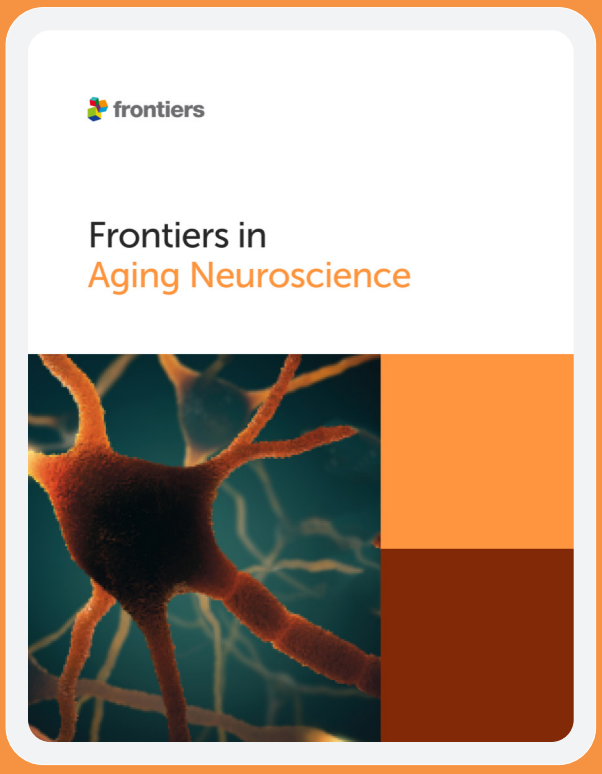

Frontiers

Avenue du Tribunal-Fédéral 34
1005 Lausanne, Switzerland
frontiersin.org

Contact us

+41 (0)21 510 17 00
frontiersin.org/about/contact